Научном већу Института за физику у Београду Београд, 08. октобар 2018.

ИНСТИТУТ ЗА ФИЗИКУ

ПРИМЉЕНО: 08. 10. 2018			
Рад.јед.	б р о ј	Арх.шифра	Прилог
0801	1407/1		

ПРЕДМЕТ:

Молба за покретање поступка за стицање звања виши научни сарадник

Молим Научно веће Института за физику у Београду да, у складу с Правилником о поступку и начину вредновања и квантитативном исказивању научно-истраживачких резултата истраживача, покрене поступак за мој избор у звање виши научни сарадник.

У прилогу достављам:

1. Мишљење руководиоца пројекта са предлогом чланова комисије
2. Биографске податке
3. Преглед научне активности
4. Елементе за квалитативну оцену научног доприноса
5. Елементе за квантитативну оцену научног доприноса
6. Списак објављених радова и њихове копије
7. Податке о цитираности
8. Фотокопију решења о претходном избору у звање
9. Додатне прилоге

С поштовањем,

Милан Радоњић

др Милан Радоњић
научни сарадник,
Институт за физику у Београду

Научном већу Института за физику у Београду

Предмет: Мишљење руководиоца пројекта о избору др Милана Радоњића у звање виши научни сарадник

Др Милан Радоњић је запослен у Лабораторији за примену рачунара у науци, у оквиру Националног центра изузетних вредности за изучавање комплексних система Института за физику у Београду и ангажован је на пројекту основних истраживања Министарства просвете, науке и технолошког развоја Републике Србије ОН171017, под називом "Моделирање и нумеричке симулације сложених вишечестичних физичких система". На поменутом пројекту ради на темама везаним за проучавање Бозе-Ајнштајн кондензације, утицаја динамичког неуређења и отворених квантних система. С обзиром да испуњава све предвиђене услове у складу са Правилником о поступку, начину вредновања и квантитативном исказивању научноистраживачких резултата истраживача МПНТР, сагласан сам са покретањем поступка за избор др Милана Радоњића у звање виши научни сарадник.

За састав комисије за избор др Милана Радоњића у звање виши научни сарадник предлажем:

(1) др Антун Балаж, научни саветник, Институт за физику у Београду
(2) др Ивана Васић, виши научни сарадник, Институт за физику у Београду
(3) др Јована Петровић, виши научни сарадник, Институт за нуклеарне науке "Винча"
(4) др Бранислав Јеленковић, научни саветник у пензији, дописни члан САНУ

Руководилац пројекта

др Антун Балаж
научни саветник

2. Биографски подаци кандидата

Милан Радоњић је рођен 14. јула 1983. године у Смедеревској Паланци. Завршио је Прву крагујевачку гимназију 2002. године као матурант генерације и освајач бронзане медаље на 33. Међународној олимпијади из физике. Основне студије на Физичком факултету у Београду, смер Теоријска и експериментална физика, завршио је 2007. године као студент генерације просечном оценом 10.00, одбранивши дипломски рад на тему *"Квантни Холов ефекат у графену"* под руководством др Милице Миловановић. Током студија био је стипендиста Министарства науке и технологије Републике Србије. Докторску дисертацију под насловом *"Electromagnetically induced coherent effects in laser excited Raman resonances in rubidium vapor"* урадио је под руководством др Бранислава Јеленковића и одбранио 2013. године на Физичком факултету Универзитета у Београду. Добитник је и годишње награде Института за физику у Београду за најбољу докторску дисертацију одбрањену током календарске године. У периоду од септембра 2015. до децембра 2017. године, Милан Радоњић је радио као постдокторски истраживач у групи проф. др Филипа Валтера на Факултету за физику Универзитета у Бечу. Од јануара 2018. године започео је даље постдокторско усавршавање у групи проф. др Себастијана Егерта на Одсеку за физику Техничког универзитета у Кајзерслаутерну у Немачкој.

Током 2008. године Милан Радоњић је као докторанд-стипендиста Министарства науке и технологије Републике Србије учествовао у раду Центра за фотонику Института за физику у Београду. Од 1. јануара 2009. запослен је у истом центру као истраживач-приправник. Фебруара 2010. године је изабран у звање истраживач-сарадник. Од 2009. године до 2011. године кандидат ради у оквиру пројекта Министарства науке и технолошког развоја бр. 141003 "Квантна и оптичка интерферометрија", под руководством др Бранислава Јеленковића. Током наредног пројектног циклуса, од јануара 2011. до децембра 2017. године, био је запослен на пројектима Министарства просвете и науке бр. ИИИ45016 "Продукција и карактеризација нано-фотоничних функционалних структура у био-медицини и информатици" (руководилац др Бранислав Јеленковић) и бр. ОН171038 "Холографски методи за генерисање специфичних таласних фронтова за ефикасну контролу квантних кохерентних ефеката у интеракцији атома и ласера" (руководилац др Дејан Пантелић) са по 6 истраживач-месеци. У звање научног сарадника изабран је 26. фебруара 2014. године. Почевши од 20. децембра 2017. године др Милан Радоњић ради у Лабораторији за примену рачунара у науци у оквиру Центра за изучавање комплексних система Института за физику у Београду, у оквиру пројекта бр. ОН171017 "Моделирање и нумеричке симулације сложених вишечестичних система" (руководилац др Антун Балаж). Кандидат је такође учествовао у пројектима *NAI-DBEC, IBEC* и *BEC-L* билатералне сарадње Министарства просвете, науке и технололошког развоја Републике Србије и Немачке агенције за академску размену (*DAAD*) током периода 2013-2014, 2015-2016. и 2017-2018. године, респективно, којима је руководио др Антун Балаж. Осим тога, био је и учесник билатералног истраживачког *SCOPES* пројекта бр. IZ73Z0_152511 између Института за физику у Београду и Лабораторије за временске и фреквентне стандарде Универзитета у Нојшателу у Швајцарској током 2014. и 2015. године.

Главне научне теме кандидата су проучавање кохерентних и нелинеарних ефеката у квантној оптици, Бозе-Ајнштајн кондензата фотона, отворених квантних система, хибридних квантно-класичних система и макроскопских квантних система. У тренутку подношења овог извештаја, Милан Радоњић је коаутор укупно 47 радова у међународним часописима са ISI листе, од којих 16 у категорији М21а, 11 у категорији М21, 4 у категорији М22, 4 у категорији М23 и 12 у категорији М33. Укупан број цитата радова кандидата је 166 (100 не рачунајући самоцитате), са Хиршовим индексом 8. Др Милан Радоњић научну сарадњу са групама из Немачке и Аустрије. Био је ментор за израду докторске дисертације Мађити Анђела (Maggitti Angelo), одбрањене 2016. године на Физичком факултету Универзитета у Београду.

3. ПРЕГЛЕД НАУЧНЕ АКТИВНОСТИ

Научно-истраживачка активност кандидата обухвата проучавање:

- кохерентних и нелинеарних ефеката у квантној оптици,
- хибридних квантно-класичних система,
- отворених квантних система,
- макроскопских квантних система,
- Бозе-Ајнштајн кондензата фотона.

У наредним одељцима укратко су приказани главни научни резултати добијени у оквиру набројаних тема.

3.1 Кохерентни и нелинеарни ефекти у квантној оптици

Приликом интеракције атома са сложеном структуром енергијских нивоа и ласерске светлости могу се испољити различити нелинеарни и кохерентни ефекти. Током рада на својој докторској дисертацији кандидат је проучавао и бавио се теоријско-нумеричким моделирањем електромагнетски индуковане транспаренције, електромагнетски индуковане апсорпције, нелинеарне магнето-оптичке ротације и Штарковог брзог адијабатског прелаза. Испитиван је утицај профила интензитета ласерског снопа на поменуте ефекте у термалним атомским парама рубидијума. Узимајући у обзир детаље сложене хиперфине структуре рубидијума и реалистичне параметре система кандидат је развио теоријски модел који је успешно описао и разјаснио експерименте урађене у Центру за фотонику Института за физику. Развијени модел је омогућио увид у различите типове кохерентне еволуције атома приликом интеракције са ласерским сноповима различитих профила. Такође је успешно примењен у каснијим истраживањима просторно и временски одвојених ласерских побуда у тзв. Рамзијевој конфигурацији. Претходно поменути резултати су садржај радова:

- **M. Radonjić**, D. Arsenović, Z. Grujić, and B. M. Jelenković, *Coherent population trapping linewidths for open transitions: Cases of different transverse laser intensity distribution*, Phys. Rev. A **79**, 023805 (2009),
- A. J. Krmpot, S. M. Ćuk, S. N. Nikolić, **M. Radonjić**, D. G. Slavov, and B. M. Jelenković, *Dark Hanle resonances from selected segments of the Gaussian laser beam cross-section*, Opt. Express **17**, 22491 (2009),
- A. J. Krmpot, S. M. Ćuk, S. N. Nikolić, **M. Radonjić**, Z. D. Grujić, and B. M. Jelenković, *Laser Beam Profile Influence on Dark Hanle Resonances in Rb Vapor*, Acta Phys. Pol. A **116**, 563 (2009),
- M. M. Mijailović, Z. D. Grujić, **M. Radonjić**, D. Arsenović, and B. M. Jelenković, *Nonlinear magneto-optical rotation narrowing in vacuum gas cells due to interference between atomic dark states of two spatially separated laser beams*, Phys. Rev. A **80**, 053819 (2009),
- Z. Grujić, D. Arsenović, **M. Radonjić**, M. Mijailović, and B. Jelenković, *Numerical simulation of Raman resonance due to the Ramsey interference induced by thermal motion of atoms*, Phys. Scr. **T135**, 014026 (2009),
- S. M. Ćuk, **M. Radonjić**, A. J. Krmpot, S. N. Nikolić, Z. D. Grujić, and B. M. Jelenković, *Influence of laser beam profile on electromagnetically induced absorption*, Phys. Rev. A **82**, 063802 (2010),
- A. J. Krmpot, **M. Radonjić**, S. M. Ćuk, S. N. Nikolić, Z. D. Grujić, and B. M. Jelenković, *Evolution of dark state of an open atomic system in constant intensity laser field*, Phys. Rev. A **84**, 043844 (2011),

- Z. D. Grujić, M. M. Lekić, **M. Radonjić**, D. Arsenović, and B. M. Jelenković, *Ramsey effects in coherent resonances at closed transition $F_g = 2 \rightarrow F_e = 3$ of ^{87}Rb*, J. Phys. B **45**, 245502 (2012),
- S. N. Nikolić, V. Djokić, N. M. Lučić, A. J. Krmpot, S. M. Ćuk, **M. Radonjić**, and B. M. Jelenković, *The connection between electromagnetically induced transparency in the Zeeman configuration and slow light in hot rubidium vapor*, Phys. Scr. **T149**, 014009 (2012),
- S. N. Nikolić, A. J. Krmpot, N. M. Lučić, B. V. Zlatković, **M. Radonjić**, and B. M. Jelenković, *Effects of laser beam diameter on electromagnetically induced transparency due to Zeeman coherences in Rb vapor*, Phys. Scr. **T157**, 014019 (2013),
- S. N. Nikolić, **M. Radonjić**, A. J. Krmpot, N. M. Lučić, B. V. Zlatković, and B. M. Jelenković, *Effects of a laser beam profile on Zeeman electromagnetically induced transparency in the Rb buffer gas cell*, J. Phys. B **46**, 075501 (2013),
- S. M. Ćuk, A. J. Krmpot, **M. Radonjić**, S. N. Nikolić, and B. M. Jelenković, *Influence of a laser beam radial intensity distribution on Zeeman electromagnetically induced transparency line-shapes in the vacuum Rb cell*, J. Phys. B **46**, 175501 (2013),
- S. N. Nikolić, **M. Radonjić**, N. M. Lučić, A. J. Krmpot, and B. M. Jelenković, *Optical Ramsey fringes observed during temporal evolution of Zeeman coherences in Rb buffer gas cell*, Phys. Scr. **T162**, 014038 (2014),
- S. N. Nikolić, **M. Radonjić**, N. M. Lučić, A. J. Krmpot, and B. M. Jelenković, *Transient development of Zeeman electromagnetically induced transparency during propagation of Raman-Ramsey pulses through Rb buffer gas cell*, J. Phys. B **48**, 045501 (2015),
- Ivan S. Radojičić, **Milan Radonjić**, Marina M. Lekić, Zoran D. Grujić, Dragan Lukić, and Branislav Jelenković, *Raman-Ramsey electromagnetically induced transparency in the configuration of counterpropagating pump and probe in vacuum Rb cell*, J. Opt. Soc. Am. B **32**, 426 (2015).

Кандидат је уопштио постојећу теорију Штарковог брзог адијабатског прелаза у системима са два или три енергијска нивоа на случај када ти нивои могу имати произвољан број поднивоа. Коришћени приступ представља генерализацију Морис-Шорове трансформације на случајеве када уклоњена дегенерација поднивоа доводи до раздешавања дво-фотонске Раманове резонанце. На основу тога су детаљно испитане могућности преноса популације међу нивоима и показано да је могућ веома ефикасан пренос када је почетно стање погодно изабрана суперпозиција стања која одговарају поднивоима. То је предмет радова:

- **M. Radonjić** and B. M. Jelenković, *Stark-chirped rapid adiabatic passage among degenerate-level manifolds*, Phys. Rev. A **80**, 043416 (2009),
- **M. Radonjić** and B. M. Jelenković, *Stark-Chirped Rapid Adiabatic Passage in a Multilevel Atom*, Acta Phys. Pol. A **116**, 476 (2009).

Четвороталасно мешање је још један нелинеарни квантно-оптички феномен који је био истраживан од стране кандидата. Користећи термалну пару калијума побуђивану двама ласерским сноповима у Λ-конфигурацији, добијени су веома велики квантни приноси у двама накнадно генерисаним светлосним сноповима. На основу квалитативног теоријског описа то је доведено у везу са великом сусцептибилношћу атома калијума, која је последица малог хиперфиног цепања основног стања. Претходно је садржај рада:

- B. Zlatković, A. J. Krmpot, N. Šibalić, **M. Radonjić**, and B. M. Jelenković, *Efficient parametric non-degenerate four wave mixing in hot potassium vapor*, Laser Phys. Lett. **13**, 015205 (2016).

У току менторства при изради докторске тезе Анђела Мађитија кандидат је радио на генерализацијама поларитона тамних стања. У питању су сложене ексцитације које су суперпозиција атомских и фотонских стања и настају у атомским медијумима побуђиваним ласерским пољима у условима електромагнетски индуковане транспаренције. Једна од њихових примена је спора или заустављена светлост. Прво уопштење се тиче атома чији

побуђивани енергијски нивои поседују дегенерацију. У зависности од поларизације коришћених побудних поља, одређене су дисперзионе релације и састав тамних поларитона и предложена примена тих сазнања. Претходно је приказано је у раду:

- A. Maggitti, **M. Radonjić**, and B. M. Jelenković, *Dark-state polaritons in a degenerate two-level system*, Laser Phys. **23**, 105202 (2013).

Друго уопштење се односи на низове спрегнутих микрорезонатора у којима се налази по један атом, односно на једнодимензионални Џејнс-Камингс-Хабардов модел са додатном модификацијом. Разматран је случај две ексцитације и нађено да оне могу образовати две различите врсте везаних парова тамних поларитона, који су просторно локализовани и са енергијама у процепима између енергијских трака делокализованих стања. Додатно је показана могућност да везани пар поларитона буде основно стање и да се може користити као квантна меморија. Испитивани систем поседује велику подесивост и ова истраживања су тек први корак у откривању његових даљих потенцијала. За више детаља погледати рад:

- A. Maggitti, **M. Radonjić**, and B. M. Jelenković, *Dark-polariton bound pairs in the modified Jaynes-Cummings-Hubbard model*, Phys. Rev. A **93**, 013835 (2016).

3.2 Хибридни квантно-класични системи

Један од постулата квантне механике је мерни постулат којим се описује пробабилистички колапс стања квантног система приликом интеракције са класичним мерним апаратом. Међутим, не постоји доследан динамички опис мерног процеса. Разлози су у различитим особинама квантних и класичних система и у различитим формализмима којима се описују. Квантна механика се најчешће изражава у терминима Хилбертових простора, док је класична механика формулисана на фазном простору. Теорија хибридних квантно-класичних система има за циљ превазилажење ових препрека и конзистентно динамичко моделовање процеса мерења квантног система. Кандидат је развио и анализирао приступ заснован на формализму Хамилтонових динамичких система. Полазећи од квантно-механичког описа оба система, на један од њих је наметнута веза која осигурава да је његова динамика ограничена на многострукост кохерентних стања, која у макроскопском лимиту постају класична. Овај приступ је основа следећих радова:

- **Milan Radonjić**, Slobodan Prvanović, and Nikola Burić, *System of classical nonlinear oscillators as a coarse-grained quantum system*, Phys. Rev. A **84**, 022103 (2011),
- **M. Radonjić**, S. Prvanović, and N. Burić, *Emergence of classical behavior from the quantum spin*, Phys. Rev. A **85**, 022117 (2012),
- **M. Radonjić**, Slobodan Prvanović, and Nikola Burić, *Alternative routes to equivalent classical models of a quantum system*, Chin. Phys. B **21**, 120301 (2012),
- **M. Radonjić**, S. Prvanović, and N. Burić, *Hybrid quantum-classical models as constrained quantum systems*, Phys. Rev. A **85**, 064101 (2012),
- N. Burić, I. Mendaš, D. B. Popović, **M. Radonjić**, and S. Prvanović, *Statistical ensembles in the Hamiltonian formulation of hybrid quantum-classical systems*, Phys. Rev. A **86**, 034104 (2012),
- **Milan Radonjić**, Slobodan Prvanović, and Nikola Burić, *Constrained quantum dynamics and coarse-grained description of a quantum system of nonlinear oscillators*, Phys. Scr. **T149**, 014011 (2012),
- N. Burić, D. B. Popović, **M. Radonjić**, and S. Prvanović, *Hybrid quantum-classical model of quantum measurements*, Phys. Rev. A **87**, 054101 (2013),
- N. Burić, D. B. Popović, **M. Radonjić**, and S. Prvanović, *Hamiltonian Formulation of Statistical Ensembles and Mixed States of Quantum and Hybrid Systems*, Found. Phys. **43**, 1459

(2013),

- N. Burić, D. B. Popović, **M. Radonjić**, and S. Prvanović, *Orbits of hybrid systems as qualitative indicators of quantum dynamics*, Phys. Lett. A **378**, 1081 (2014),
- N. Burić, D. B. Popović, **M. Radonjić**, and S. Prvanović, *Unified Treatment of Geometric Phases for Statistical Ensembles of Classical, Quantum and Hybrid Systems*, Int. J. Theor. Phys. **53**, 1046 (2014),
- D. Arsenović, N. Burić, D. B. Popović, **M. Radonjić**, and S. Prvanović, *Cloning in nonlinear Hamiltonian quantum and hybrid mechanics*, Phys. Rev. A **90**, 042115 (2014),
- N. Burić, D. B. Popović, **M. Radonjić**, and S. Prvanović, *A quantum-classical theory with nonlinear and stochastic dynamics*, Phys. Scr. **T163**, 014003 (2014),
- Nikola Burić, Duška B. Popović, **Milan Radonjić**, and Slobodan Prvanović, *Phase space theory of quantum-classical systems with nonlinear and stochastic dynamics*, Ann. Phys. (N.Y.) **343**, 16 (2014),
- D. Arsenović, N. Burić, D. B. Popović, **M. Radonjić**, and S. Prvanović, *Positive-operator-valued measures in the Hamiltonian formulation of quantum mechanics*, Phys. Rev. A **91**, 062114 (2015).

Комплементаран приступ хибридним системима помоћу Купман-фон Нојмановог унитарног описа класичних система у Хилбертовом простору такође је био предмет истраживања кандидата. Уведени су апстрактни системи који интерполирају између класичних и квантних система и размотрена је физичка конзистентност описа два таква система чија је интеракција потенцијална, што је представљено у раду:

- **M. Radonjić**, D. B. Popović, S. Prvanović, and N. Burić, *Ehrenfest principle and unitary dynamics of quantum-classical systems with general potential interaction*, Phys. Rev. A **89**, 024104 (2014).

3.3 Отворени квантни системи

Сваки квантни систем се неизбежно налази под утицајем окружења – отворен је. Услед тога долази до ефеката декохеренције и дисипације, па је еволуција отвореног квантног система неунитарна. Стога је уопштење разултата који су познати у случају унитарне квантне еволуције на неунитарни сценарио врло нетривијално. Најједноставнији тип окружења не поседује меморију о својој прошлости. Тада је динамика отвореног квантног система описана Линдбладовом мастер једначином. Еволуција атомских система поменутих у одељку 3.1 је управо моделирана таквим једначинама.

Кандидат је анализирао могућност дефинисања геометријске фазе отвореног квантног система помоћу ансамбла таласних функција чија стохастичко-дифузна еволуција у средњем репродукује еволуцију задату Линдбладовом једначином. Показано је да постоји погодна дефиниција која је инваријантна на унитарну групу симетрија ансамбла и указано на ограничења приступа такве врсте, што се може видети у радовима:

- Nikola Burić and **Milan Radonjić**, *Uniquely defined geometric phase of an open system*, Phys. Rev. A **80**, 014101 (2009),
- N. Burić and **M. Radonjić**, *Geometric Phase of an Open System*, Acta Phys. Pol. A **116**, 483 (2009).

Геометријска фаза побуђиваног квантног система са два нивоа је аналитички израчуната у раду:

- I. Mendaš, N. Burić, D. B. Popović, S. Prvanović, and **M. Radonjić**, *Geometric Phase for Analytically Solvable Driven Time-Dependent Two-Level Quantum Systems*, Acta Phys. Pol. A **126**, 670 (2014).

Даље, испитивана је динамика дво-модног ласеру сличног система проширујући дво-модни Тејвис-Камингсов модел дисипативним процесима и некохерентном побудом атомског медијума. Аналитички су нађена четири могућа неравнотежна стационарна стања (фиксне тачке еволуције) и одређен је одговарајући фазни дијаграм. Могуће фазе се разликују по броју фиксних тачака и по њиховој стабилности. Додатно, проучена су три сценарија увођења Пирагасове контролне повратне спреге са кашњењем. У зависности од времена кашњења и јачине контроле показано је да се може постићи стабилизација нестабилних фиксних тачака или избор конкретне моде која ће садржати макроскопски број фотона. Више детаља садржи рад:

- Wassilij Kopylov, **Milan Radonjić**, Tobias Brandes, Antun Balaž, and Axel Pelster, *Dissipative two-mode Tavis-Cummings model with time-delayed feedback control*, Phys. Rev. A **92**, 063832 (2015).

3.4 Макроскопски квантни системи

Позната је чињеница да се суперпозиције веома различитих квантних стања макроскопских система не реализују у свету око нас. Парадокс Шредингерове живо-мртве мачке управо говори о томе. С тим у вези, кандидат је проучавао које врсте макроскопских суперпозиција (не)могу природно бити јединствена основна стања локалних, физички релевантних многочестичних Хамилтонијана са коначним енергијским процепом. Изведена је горња граница величине процепа произвољног физичког Хамилтонијана под претпоставком да је његово основно стање суперпозиција два добро различива макроскопска стања. За веома велику класу таквих стања показано је да енергијски процеп Хамилтонијана мора тежити нули у термодинамичком лимиту. Последица тога је да припрема таквих стања једноставним поступком хлађења у основно стање није експериментално изводљива, јер би водила мешаном стању уместо чистом. Коришћени методи и добијени резултати су од ширег значаја и могу послужити нпр. расветљавању неких аспеката квантних маргиналних проблема. Више о томе видети у раду:

- Borivoje Dakić and **Milan Radonjić**, *Macroscopic Superpositions as Quantum Ground States*, Phys. Rev. Lett. **119**, 090401 (2017).

3.5 Бозе-Ајнштајн кондензати фотона

Системима у којима је остварена Бозе-Ајнштајн кондензација 2010. године су прибројани и фотони. Основу изведбе чини микрорезонатор испуњен молекулима органских боја који се могу побуђивати фотонима резонаторских мода. Димензије резонатора и ширина апсорпционог спектра молекула обезбеђују динамичку битност само једне лонгитудиналне моде. Додавши претходном закривљеност огледала резонатора, фотони у њему ефективно постају масени и у дводимензионалном хармонијском потенцијалу. Термализација је обезбеђена реапсорпцијом и емисијом од стране молекула органских боја. Кондензат се постиже довољно снажном некохерентном побудом молекула.

Полазећи од Линдбладове мастер једначине поменутог система кандидат је развио детаљни микроскопски модел као уопштење постојећег неравнотежног модела, који осим дисипативног укључује и кохерентни допринос динамици. На тај начин модел успешно интерполира између два дијаметрално супротна физичка случаја – Бозе-Ајнштајн кондензата фотона, када дисипација доминира динамиком, и стања сличног ласеру, када су кохерентни ефекти довољно изражени. У случају фотонског кондензата показано је да кохерентни процеси воде појави ефективне фотон-фотон интеракције која се преноси преко молекула органских боја. Процењена је јачина интеракције и добијено добро слагање са литературом. Такође је испитана њена зависност од параметара система. Све то је садржано у раду:

- **M. Radonjić**, W. Kopylov, A. Balaž, and A. Pelster, *Interplay of coherent and dissipative dynamics in condensates of light*, New J. Phys. **20**, 055014 (2018).

4. ЕЛЕМЕНТИ ЗА КВАЛИТАТИВНУ ОЦЕНУ НАУЧНОГ ДОПРИНОСА КАНДИДАТА

4.1 Квалитет научних резултата

4.1.1 Научни ниво и значај резултата, утицај научних радова

Др Милан Радоњић је у свом досадашњем раду објавио 47 радова у међународним часописима са ISI листе, од којих 16 у категорији М21а, 11 у категорији М21, 4 у категорији М22, 4 у категорији М23 и 12 у категорији М33.

У периоду након одлуке Научног већа о предлогу за стицање претходног научног звања, др Милан Радоњић је објавио 26 радова у међународним часописима са ISI листе и саопштења на међународним конференцијама, од којих 4 у категорији М21а, 8 у категорији М21, 4 у категорији М22, 1 у категорији М23, 1 у категорији М32, 4 у категорији М33 и 4 у категорији М34.

Као пет најзначајнијих радова кандидата могу се узети:

1. **M. Radonjić**, D. Arsenović, Z. Grujić, and B. M. Jelenković, *Coherent population trapping linewidths for open transitions: Cases of different transverse laser intensity distribution*, Phys. Rev. A **79**, 023805 (2009), цитиран 15 пута,
2. **M. Radonjić**, S. Prvanović, and N. Burić, *Hybrid quantum-classical models as constrained quantum systems*, Phys. Rev. A **85**, 064101 (2012), цитиран 23 пута,
3. Wassilij Kopylov, **Milan Radonjić**, Tobias Brandes, Antun Balaž, and Axel Pelster, *Dissipative two-mode Tavis-Cummings model with time-delayed feedback control*, Phys. Rev. A **92**, 063832 (2015), цитиран 12 пута,
4. Borivoje Dakić and **Milan Radonjić**, *Macroscopic Superpositions as Quantum Ground States*, Phys. Rev. Lett. **119**, 090401 (2017), цитиран 1 пут,
5. **M. Radonjić**, W. Kopylov, A. Balaž, and A. Pelster, *Interplay of coherent and dissipative dynamics in condensates of light*, New J. Phys. **20**, 055014 (2018), цитиран 0 пута.

Први рад је био полазна основа докторске дисертације кандидата. У њему је уведен детаљни теоријски модел временски зависне ласер-атом интеракције, који узима у обзир комплексну хиперфину структуру атома алкалних метала. Користећи развијени метод успешно су описани и физички интерпретирани експерименти у вези са квантно-оптичким кохерентним и нелинеарним ефектима. Модел је омогућио да се прецизно испита временска еволуција атома рубидијума приликом интеракције са ласерским пољима различитих профила интензитета и да се схвате сасвим различити физички феномени у разматраним случајевима.

Други рад уводи оригинални конзистентни опис хибридних интерагујућих квантно-класичних система преко Хамилтоновог формализма. Приступ је надаље резултовао бројним публикацијама на ту тему. Дираков формализам система са везама, познат у класичној механици, искоришћен је у контексту хибридних система и резултовао тзв. описом у смислу средњег поља. Наиме, класични системи су описани као макроскопски квантни са динамиком ограниченом на многострукост кохерентних стања. Тиме је омогућен унифициран третман класичних и квантних система на компатибилан начин.

Трећи рад садржи анализу дисипативног дво-модног Тејвис-Камингсовог модела интеракције атомског ансамбла и светлости. Основу чини теорија средњег поља примењена

на Линдбладову мастер једначину система. Разматрана су могућа стационарна стања система када постоји спољашња побуда и утврђена њихова стабилност. Рад заправо садржи доста поједностављени модел потпуног микроскопског описа кондензата светлости, без механизма термализације. Међутим, добијени резултати ипак одговарају карактеристичним особинама реалистичних система. Такође су разматране могућности које нуди контрола преко повратне спреге са кашњењем.

Четврти рад се бави питањем да ли макроскопске квантне суперпозиције могу бити јединствена основна стања локалних Хамилтонијана. Под претпоставком да таква суперпозиција јесте основно стање, показано је да у термодинамичком лимиту енергијски процеп мора тежити нули. Физичка последица тога је да хлађење макроскопског квантног система води препарацији мешаног стања, а не чистог. Такав резултат делимично расветљује парадокс Шредингерове мачке и има импликације на квантни маргинални проблем, као и на адијабатско квантно рачунање које користи основна стања квантних система.

Пети рад излаже детаљни микроскопски модел кондензата светлости и добијање Линдбладове мастер једначине система. За разлику од постојеће литературе, конзистентно је урачунат допринос кохерентне динамике, поред дисипативне. То је омогућило да се истим моделом интерполира између два потпуно различита физичка сценарија – стања сличног ласеру и Бозе-Ајнштајн кондензата фотона. У првом случају кохерентни ефекти су знатни и воде усаглашавању фаза светлости и активног медијума. У другом режиму дисипативни ефекти доминирају и воде термализацији светлости. Кохерентни ефекти тада узрокују појаву слабе ефективне фотон-фотон интеракције која се преноси путем активног медијума и чије понашање у зависности од параметара система је проучено.

4.1.2 Позитивна цитираност научних радова кандидата

Према бази података *Web of Science* на дан 1. октобра 2018. године, радови кандитата су цитирани укупно 166 пута, односно 100 пута не рачунајући самоцитате. Према истој бази, Хиршов индекс кандидата је 8. Релевантни подаци о цитираности са интернет странице *Web of Science* базе су дати након списка свих радова (одељак 6).

4.1.3 Параметри квалитета часописа

Битан елемент за процену квалитета научних резултата је и квалитет часописа у којима су радови објављени, односно њихов импакт фактор – ИФ. У категоријама М21а, М21, М22, М23 и М33 кандидат је објавио радове у следећим часописима, при чему су подвучени случајеви у који се односе на период након одлуке Научног већа о предлогу за стицање претходног научног звања:

- 1 рад у *Physical Review Letters* (ИФ = 8,839),
- 1 рад у *Optics Express* (ИФ = 3,880),
- 1 рад у *New Journal of Physics* (ИФ = 3,786),
- 1 рад у *Laser Physics* (ИФ = 3,605),
- 1 рад у *Annals of Physics (N.Y.)* (ИФ = 3,318),
- 11 + 5 радова у *Physical Review A* (ИФ = 3,042 за 4 рада, ИФ = 2,878 за 2 рада, ИФ = 2,866 за 1 рад, ИФ = 2,908 за 4 рада, ИФ = 3,042 за 2 рада, ИФ = 2,991 за 2 рада, ИФ = 2,925 за 1 рад),
- 1 рад у *Laser Physics Letters* (ИФ = 2,964),
- 2 + 2 рада у *Journal of Physics B* (ИФ = 2,031 за 2 рада, ИФ = 2,031 за 1 рад, ИФ = 1,975 за 1 рад),

- 1 рад у *Journal of the Optical Society of America B* (ИФ = 1,970),
- 1 рад у *Physics Letters A* (ИФ = 1,766),
- 1 рад у *Chinese Physics B* (ИФ = 1,631),
- 3 + 3 рада у *Physica Scripta* (ИФ = 1,204 за 2 рада, ИФ = 1,088 за 1 рад, ИФ = 1,296 за 1 рад, ИФ = 1,296 за 2 рада),
- 1 рад у *International Journal of Theoretical Physics* (ИФ = 1,186),
- 1 рад у *Foundations of Physics* (ИФ = 1,170),
- 3 + 1 рад у *Acta Physica Polonica A* (ИФ = 0,433 за 3 рада, ИФ = 0,604 за 1 рад),
- 3 + 1 рад у *Proceedings of SPIE* (без ИФ),
- 2 рада у *Journal of Physics: Conference Series* (без ИФ).

Укупан фактор утицаја радова кандидата је 98,883, а у периоду након одлуке Научног већа о предлогу за стицање претходног научног звања тај фактор је 52,093. Часописи у којима је кандидат објављивао су по свом угледу веома цењени у областима којима припадају. Међу њима се посебно истичу: *Physical Review Letters*, *Optics Express*, *New Journal of Physics*, *Physical Review A* и *Annals of Physics*.

Додатни библиометријски показатељи у вези са објављеним радовима кандидата након одлуке Научног већа о предлогу за стицање претходног научног звања дати су у доњој табели. Она садржи импакт факторе (ИФ) радова, М бодове радова по српској категоризацији научноистраживачких резултата, као и импакт фактор нормализован по импакту цитирајућег чланка (СНИП). У табели су дате укупне вредности, као и вредности свих фактора усредњених по броју чланака и по броју аутора по чланку, за радове објављене у категоријама М20.

	ИФ	М	СНИП
Укупно	48,205	127	21,359
Усредњено по чланку	2,836	7,471	1,256
Усредњено по аутору	13,811	32,683	5,671

4.1.4 Степен самосталности и степен учешћа у реализацији радова у научним центрима у земљи и иностранству

Кандидат је водећи аутор 11 радова, други аутор 12 радова, трећи аутор 11 радова, четврти аутор 10 радова, пети аутор 2 рада и шести аутор 1 рада, од укупно 47 радова. На радовима који су објављени у периоду након одлуке Научног већа о предлогу за стицање претходног звања, кандидат је водећи аутор 2 рада, други аутор 7, трећи аутор 6 радова, четврти аутор 4 рада и пети аутор 2 рада, од укупно 21 рада. У другом назначеном периоду кандидат је на 2 рада други аутор, док је први аутор студент Анђело Мађити чијом израдом докторске тезе је кандидат руководио.

При изради поменутих радова др Милан Радоњић је учествовао у осмишљавању, формулацији и дискусији проблема, изведби релевантних нумеричких симулација, анализи добијених података (и поређењу са експериментима у одређеним случајевима), развоју аналитичких метода и аналитичким прорачунима, као и самом писању радова.

Током израде докторске дисертације у Центру за фотонику Института за физику у Београду, кандидат је развио теоријско-нумерички модел интеракције ласерског зрачења и атома алкалних метала који је био кључан за опис и разумевање експеримената урађених у поменутом Центру на тему кохерентних и нелинеарних ефеката у квантној оптици. Током завршне године израде докторске дисертације кандидат је започео плодотворну сарадњу са др Николом Бурићем и разрадио оригинални приступ конзистентном третману хибридних

интерагујућих квантно-класичних система. Такође, започео је и водио истраживање поларитона тамних стања који су били тема докторске дисертације студента Анђела Мађитија. Након завршетка своје докторске дисертације кандидат је наставио са истраживањима на претходно поменуте теме и уз др Антуна Балажа успоставио сарадњу са др Акселом Пелстером са Техничког универзитета у Кајзерслаутерну на истраживањима Бозе-Ајнштајн кондензата фотона. Током постдокторског усавршавања у групи проф. др Филипа Валтера на Универзитету у Бечу кандидат је радио на теоријским проблемима макроскопских квантних стања и осмишљавању фотоничких симулатора. Експерименти у вези са последњом темом су у фази израде. Кандидат се тренутно бави и проучавањем ефеката динамичког неуређења на Бозе-Ајнштајн кондензате у оквиру постдокторског ангажмана на Техничком универзитету у Кајзерслаутерну.

Кандидат учествује у раду Центра за изучавање комплексних система и Центра за фотонику Института за физику у Београду. Такође, има међународну сарадњу са групом проф. др Филипа Валтера у Бечу, са др Боривојем Дакићем у Бечу, са др Акселом Пелстером у Кајзерслаутерну и др Василијем Копиловим у Берлину. Скорашњи радови настали као резултат међународне сарадње су видни у листи публикација кандидата, док је неколико радова тренутно у фази припреме.

4.1.5 Награде

Кандидат је добитник Студентске награде Института за физику у Београду 2014. године за најбољу докторску дисертацију урађену током претходне године.

Прилог: диплома Студентске награде Института за физику у Београду.

4.2 Ангажованост у формирању научних кадрова

Кандидат др Милан Радоњић је био ментор доктората студента Физичког факултета у Београду Анђела Мађитија, на тему поларитона тамних стања и дво-поларитонских везаних стања у низовима атома и оптичких микрорезонатора. Током рада на изради поменутог доктората урађени су следећи радови:

- A. Maggitti, **M. Radonjić**, and B. M. Jelenković, *Dark-state polaritons in a degenerate two-level system*, Laser Phys. **23**, 105202 (2013),
- A. Maggitti, **M. Radonjić**, and B. M. Jelenković, *Dark-polariton bound pairs in the modified Jaynes-Cummings-Hubbard model*, Phys. Rev. A **93**, 013835 (2016),

који су део докторске дисертације:

- Анђело Мађити (Angelo Maggitti), *Formation of dark-state polaritons and two-polariton bound states in arrays of atoms and optical cavities*, Физички факултет Универзитета у Београду, октобар 2015. године

  Ментор: др Милан Радоњић, коментор: др Бранислав Јеленковић.

Прилог: одговарајући записник са седнице Наставно-научног већа Физичког факултета, одговарајућа страница интернет портала НаРДуС (Национални Репозиторијум Дисертација у Србији) и уводне странице дисертације Анђела Мађитија.

4.3 Нормирање броја коауторских радова, патената и техничких решења

21 радова кандидата, објављених након одлуке Научног већа о предлогу за стицање претходног научног звања, спадају у следеће категорије:

- у категорију теоријских радова у природно-математичким наукама који се признају са пуним бројем М бодова до три коаутора спадају радови [1,2,3,4,18,21,30,31,32,38] и нормирани су у складу са Правилником,
- у категорију радова са нумеричким симулацијама који се признају са пуним бројем М бодова до пет коаутора спадају радови [17,20,23,29,36,49,50,51,52] и нормирани су у складу са Правилником,
- у категорију експерименталних радова у природно-математичким наукама који се признају са пуним бројем М бодова до седам коаутора спадају радови [19,22,24,28,37, 39,40] и нормирани су у складу са Правилником.

Након нормирања према Правилнику, број М бодова које је кандидат остварио након одлуке Научног већа о предлогу за стицање претходног научног звања се мења са 134,5 на 125, односно нормирање не утиче на значајан начин на број бодова, а кандидат свакако има вишеструко већи број бодова од захтеваног.

4.4 Руковођење пројектима, потпројектима и пројектним задацима

Кандидат руководи потпројектом "Утицај динамичког неуређења на особине Бозе-Ајнштајн кондензата" у оквиру пројекта ОН171017 "Моделирање и нумеричке симулације сложених вишечестичних система" којим руководи др Антун Балаж.

Прилог: потврда руководиоца пројекта о руковођењу потпројектом.

Такође, током постдокторског рада на Факултету за физику Универзитета у Бечу кандидат је руководио пројектним задатком у оквиру европског QUCHIP пројекта са темом теоријског дизајна квантног кола за симулацију бензена помоћу шест фотона. Експеримент који се бави реализацијом дизајнираног кола је у току.

Прилог: потврдно писмо о руковођењу пројектним задатком.

4.5 Активност у научним и научно-стручним друштвима

Кандидат је рецензент у следећим научним часописима: *Physical Review Letters*, *Optics Communications*, *Optical and Quantum Electronics* и *International Journal of Modern Physics B*.

Прилог: писма уредништва часописа рецензенту.

4.6 Утицајност научних резултата

Утицајност научних резултата кандидата је наведена у одељку 4.1 овог документа. Пун списак радова је дат у одељку 6, а подаци о цитираности са интернет странице *Web of Science* базе су дати након списка свих радова кандидата.

4.7 Конкретан допринос кандидата у реализацији радова у научним центрима у земљи и иностранству

Кандидат је значајно допринео сваком раду у чијој припреми је учествовао. Сви радови објављени у периоду након одлуке Научног већа Института за физику о предлогу за стицање претходног научног звања су урађени у сарадњи са колегама из земље и иностранства. Др Радоњић је имао кључни допринос публикацијама на којима је први аутор (2 рада) и други

аутор (7 радова). Током израде ових радова, он је битно утицао на сам ток истраживања, радио на развоју и извођењу одговарајућих нумеричких симулација, анализи релевантних података, на теоријским и аналитичким прорачунима, методима и техникама приступа проблемима, писању радова, а такође је учествовао и у комуникацији са рецензентима приликом припреме радова за објављивање.

4.8 Уводна предавања на конференцијама и друга предавања

У периоду након одлуке Научног већа о предлогу за стицање претходног звања, кандидат је одржао следеће предавање по позиву на међународном скупу, које је штампано у изводу (категорија М32):

- **M. Radonjić**, W. Kopylov, A. Balaž, and A. Pelster, *Interplay of coherent and dissipative dynamics in condensates of light*, 659. WE-Heraeus-Seminar on "Condensates of Light", 14-17. January 2018, Physikzentrum Bad Honnef, Germany.

Поред тога, одржао је и следећа саопштења на међународним конференцијама, која су штампана у изводу (категорија М34):

- **M. Radonjić**, W. Kopylov, T. Brandes, A. Balaž, and A. Pelster, *Microscopic Model of Photon Condensation*, 616. WE-Heraeus-Seminar on "Ultracold Quantum Gases – Current Trends and Future Perspectives", 9-13. May 2016, Physikzentrum Bad Honnef, Germany,
- **Milan Radonjić** and Philip Walther, *Photonic simulation of open quantum systems with various exchange statistics*, PHOTONICA2017 The Sixth International School and Conference on Photonics, 28. August - 1. September 2017, Belgrade, Serbia,
- **M. Radonjić**, W. Kopylov, A. Balaž, and A. Pelster, *Modeling Dye-Mediated Photon-Photon Interaction in Condensates of Light*, 82nd Annual Conference of the DPG and DPG Spring Meeting, 4-9. March 2018, Erlangen, Germany,
- **M. Radonjić**, W. Kopylov, A. Balaž, and A. Pelster, *Interplay of coherent and dissipative dynamics in condensates of light*, 49th Annual DAMOP Meeting, 28. May - 1. June 2018, Ft. Lauderdale, Florida, USA.

У оквиру међународне сарадње, др Радоњић је одржао следећа предавања на иностраним универзитетима и институтима:

- **Milan Radonjić**, *Microscopic Model of Photon Condensation*, 19. November 2015, Department of Physics, Technical University of Kaiserslautern, Germany,
- **M. Radonjić**, *Hamiltonian Formulation of Hybrid Quantum-classical Systems*, Nikola Burić Memorial Workshop, 9. December 2016, Institute of Physics Belgrade, Serbia,

Прилог: позивна писма, апстракти излагања са пропратним материјалом.

5. ЕЛЕМЕНТИ ЗА КВАНТИТАТИВНУ ОЦЕНУ НАУЧНОГ ДОПРИНОСА КАНДИДАТА

Остварени резултати у периоду након одлуке Научног већа о предлогу за стицање претходног научног звања:

Категорија	М бодова по раду	Број радова	Укупно М бодова	Нормирани број М бодова
M21a	10	4	40	35,48
M21	8	8	64	61,72
M22	5	4	20	18,33
M23	3	1	3	2,14
M32	1,5	1	1,5	1,5
M33	1	4	4	3,83
M34	0,5	4	2	2

Поређење са минималним квантитативним условима за избор у звање виши научни сарадник:

Минимални број М бодова		Остварено, М бодова без нормирања	Остварено, нормирани број М бодова
Укупно	50	**134,5**	**125**
M10+M20+M31+M32+M33+M41+M42+M90	40	**132,5**	**123**
M11+M12+M21+M22+M23	30	**127**	**117,67**

Према бази података *Web of Science* на дан 1. октобра 2018. године, радови кандитата су цитирани укупно 166 пута, односно 100 пута не рачунајући самоцитате. Према истој бази, Хиршов индекс кандидата је 8.

6. СПИСАК РАДОВА ДР МИЛАНА РАДОЊИЋА

6.1 Радови у међународним часописима изузетних вредности (М21а)

Радови објављени након претходног избора у звање:

1. Borivoje Dakić and **Milan Radonjić**, *Macroscopic Superpositions as Quantum Ground States*, Phys. Rev. Lett. **119**, 090401 (2017) (ИФ = 8,839 за 2017. годину),
2. D. Arsenović, N. Burić, D. B. Popović, **M. Radonjić**, and S. Prvanović, *Cloning in nonlinear Hamiltonian quantum and hybrid mechanics*, Phys. Rev. A **90**, 042115 (2014) (ИФ = 3,042 за 2012. годину),
3. **M. Radonjić**, D. B. Popović, S. Prvanović, and N. Burić, *Ehrenfest principle and unitary dynamics of quantum-classical systems with general potential interaction*, Phys. Rev. A **89**, 024104 (2014) (ИФ = 3,042 за 2012. годину),

Радови објављени после одлуке Научног већа о предлогу за стицање претходног научног звања:

4. A. Maggitti, **M. Radonjić**, and B. M. Jelenković, *Dark-state polaritons in a degenerate two-level system*, Laser Phys. **23**, 105202 (2013) (ИФ = 3,605 за 2011. годину),

Радови објављени пре претходног избора у звање:

5. N. Burić, D. B. Popović, **M. Radonjić**, and S. Prvanović, *Hybrid quantum-classical model of quantum measurements*, Phys. Rev. A **87**, 054101 (2013) (ИФ = 3,042 за 2012. годину),
6. N. Burić, I. Mendaš, D. B. Popović, **M. Radonjić**, and S. Prvanović, *Statistical ensembles in the Hamiltonian formulation of hybrid quantum-classical systems*, Phys. Rev. A **86**, 034104 (2012) (ИФ = 3,042 за 2012. годину),
7. **M. Radonjić**, S. Prvanović, and N. Burić, *Hybrid quantum-classical models as constrained quantum systems*, Phys. Rev. A **85**, 064101 (2012) (ИФ = 3,042 за 2012. годину),
8. **M. Radonjić**, S. Prvanović, and N. Burić, *Emergence of classical behavior from the quantum spin*, Phys. Rev. A **85**, 022117 (2012) (ИФ = 3,042 за 2012. годину),
9. A. J. Krmpot, **M. Radonjić**, S. M. Ćuk, S. N. Nikolić, Z. D. Grujić, and B. M. Jelenković, *Evolution of dark state of an open atomic system in constant intensity laser field*, Phys. Rev. A **84**, 043844 (2011) (ИФ = 2,878 за 2011. годину),
10. **Milan Radonjić**, Slobodan Prvanović, and Nikola Burić, *System of classical nonlinear oscillators as a coarse-grained quantum system*, Phys. Rev. A **84**, 022103 (2011) (ИФ = 2,878 за 2011. годину),
11. S. M. Ćuk, **M. Radonjić**, A. J. Krmpot, S. N. Nikolić, Z. D. Grujić, and B. M. Jelenković, *Influence of laser beam profile on electromagnetically induced absorption*, Phys. Rev. A **82**, 063802 (2010) (ИФ = 2,908 за 2008. годину),
12. M. M. Mijailović, Z. D. Grujić, **M. Radonjić**, D. Arsenović, and B. M. Jelenković, *Nonlinear magneto-optical rotation narrowing in vacuum gas cells due to interference between atomic dark states of two spatially separated laser beams*, Phys. Rev. A **80**, 053819 (2009) (ИФ = 2,908 за 2008. годину),
13. A. J. Krmpot, S. M. Ćuk, S. N. Nikolić, **M. Radonjić**, D. G. Slavov, and B. M. Jelenković, *Dark Hanle resonances from selected segments of the Gaussian laser beam cross-section*, Opt. Express **17**, 22491 (2009) (ИФ = 3,880 за 2008. годину),

14. **M. Radonjić** and B. M. Jelenković, *Stark-chirped rapid adiabatic passage among degenerate-level manifolds*, Phys. Rev. A **80**, 043416 (2009) (ИФ = 2,908 за 2008. годину),
15. Nikola Burić and **Milan Radonjić**, *Uniquely defined geometric phase of an open system*, Phys. Rev. A **80**, 014101 (2009) (ИФ = 2,908 за 2008. годину),
16. **M. Radonjić**, D. Arsenović, Z. Grujić, and B. M. Jelenković, *Coherent population trapping linewidths for open transitions: Cases of different transverse laser intensity distribution*, Phys. Rev. A **79**, 023805 (2009) (ИФ = 2,908 за 2008. годину).

6.2 Радови у врхунским међународним часописима (М21)

Радови објављени након претходног избора у звање:

17. **M. Radonjić**, W. Kopylov, A. Balaž, and A. Pelster, *Interplay of coherent and dissipative dynamics in condensates of light*, New J. Phys. **20**, 055014 (2018) (ИФ = 3,786 за 2016. годину),
18. A. Maggitti, **M. Radonjić**, and B. M. Jelenković, *Dark-polariton bound pairs in the modified Jaynes-Cummings-Hubbard model*, Phys. Rev. A **93**, 013835 (2016) (ИФ = 2,925 за 2016. годину),
19. B. Zlatković, A. J. Krmpot, N. Šibalić, **M. Radonjić**, and B. M. Jelenković, *Efficient parametric non-degenerate four wave mixing in hot potassium vapor*, Laser Phys. Lett. **13**, 015205 (2016) (ИФ = 2,964 за 2013. годину, рад објављен 30.11.2015),
20. Wassilij Kopylov, **Milan Radonjić**, Tobias Brandes, Antun Balaž, and Axel Pelster, *Dissipative two-mode Tavis-Cummings model with time-delayed feedback control*, Phys. Rev. A **92**, 063832 (2015) (ИФ = 2,991 за 2013. годину),
21. D. Arsenović, N. Burić, D. B. Popović, **M. Radonjić**, and S. Prvanović, *Positive-operator-valued measures in the Hamiltonian formulation of quantum mechanics*, Phys. Rev. A **91**, 062114 (2015) (ИФ = 2,991 за 2013. годину),
22. S. N. Nikolić, **M. Radonjić**, N. M. Lučić, A. J. Krmpot, and B. M. Jelenković, *Transient development of Zeeman electromagnetically induced transparency during propagation of Raman-Ramsey pulses through Rb buffer gas cell*, J. Phys. B **48**, 045501 (2015) (ИФ = 1,975 за 2014. годину),
23. Nikola Burić, Duška B. Popović, **Milan Radonjić**, and Slobodan Prvanović, *Phase space theory of quantum-classical systems with nonlinear and stochastic dynamics*, Ann. Phys. (N.Y.) **343**, 16 (2014) (ИФ = 3,318 за 2012. годину).

Радови објављени после одлуке Научног већа о предлогу за стицање претходног научног звања:

24. S. M. Ćuk, A. J. Krmpot, **M. Radonjić**, S. N. Nikolić, and B. M. Jelenković, *Influence of a laser beam radial intensity distribution on Zeeman electromagnetically induced transparency line-shapes in the vacuum Rb cell*, J. Phys. B **46**, 175501 (2013) (ИФ = 2,031 за 2012. годину).

Радови објављени пре претходног избора у звање:

25. S. N. Nikolić, **M. Radonjić**, A. J. Krmpot, N. M. Lučić, B. V. Zlatković, and B. M. Jelenković, *Effects of a laser beam profile on Zeeman electromagnetically induced transparency in the Rb buffer gas cell*, J. Phys. B **46**, 075501 (2013) (ИФ = 2,031 за 2012. годину),
26. **M. Radonjić**, Slobodan Prvanović, and Nikola Burić, *Alternative routes to equivalent classical models of a quantum system*, Chin. Phys. B **21**, 120301 (2012) (ИФ = 1,631 за 2010. годину),

27. Z. D. Grujić, M. M. Lekić, **M. Radonjić**, D. Arsenović, and B. M. Jelenković, *Ramsey effects in coherent resonances at closed transition $F_g = 2 \rightarrow F_e = 3$ of ^{87}Rb*, J. Phys. B **45**, 245502 (2012) (ИФ = 2,031 за 2012. годину).

6.3 Радови у истакнутим међународним часописима (М22)

Радови објављени након претходног избора у звање:

28. Ivan S. Radojičić, **Milan Radonjić**, Marina M. Lekić, Zoran D. Grujić, Dragan Lukić, and Branislav Jelenković, *Raman-Ramsey electromagnetically induced transparency in the configuration of counterpropagating pump and probe in vacuum Rb cell*, J. Opt. Soc. Am. B **32**, 426 (2015) (ИФ = 1,970 за 2014. годину),
29. N. Burić, D. B. Popović, **M. Radonjić**, and S. Prvanović, *Orbits of hybrid systems as qualitative indicators of quantum dynamics*, Phys. Lett. A **378**, 1081 (2014) (ИФ = 1,766 за 2012. годину).

Радови објављени после одлуке Научног већа о предлогу за стицање претходног научног звања:

30. N. Burić, D. B. Popović, **M. Radonjić**, S. Prvanović, *Unified Treatment of Geometric Phases for Statistical Ensembles of Classical, Quantum and Hybrid Systems*, Int. J. Theor. Phys. **53**, 1046 (2014) (ИФ = 1,186 за 2013. годину),
31. N. Burić, D. B. Popović, **M. Radonjić,** and S. Prvanović, *Hamiltonian Formulation of Statistical Ensembles and Mixed States of Quantum and Hybrid Systems*, Found. Phys. **43**, 1459 (2013) (ИФ = 1,170 за 2012. годину).

6.4 Радови у међународним часописима (М23)

Радови објављени након претходног избора у звање:

32. I. Mendaš, N. Burić, D. B. Popović, S. Prvanović, and **M. Radonjić**, *Geometric Phase for Analytically Solvable Driven Time-Dependent Two-Level Quantum Systems*, Acta Phys. Pol. A **126**, 670 (2014) (ИФ = 0,604 за 2013. годину).

Радови објављени пре претходног избора у звање:

33. A. J. Krmpot, S. M. Ćuk, S. N. Nikolić, **M. Radonjić**, Z. D. Grujić, and B. M. Jelenković, *Laser Beam Profile Influence on Dark Hanle Resonances in Rb Vapor*, Acta Phys. Pol. A **116**, 563 (2009) (ИФ = 0,433 за 2013. годину),
34. N. Burić and **M. Radonjić**, *Geometric Phase of an Open System*, Acta Phys. Pol. A **116**, 483 (2009) (ИФ = 0,433 за 2013. годину),
35. **M. Radonjić** and B. M. Jelenković, *Stark-Chirped Rapid Adiabatic Passage in a Multilevel Atom*, Acta Phys. Pol. A **116**, 476 (2009) (ИФ = 0,433 за 2013. годину).

6.5 Предавања по позиву с међународних скупова штампана у изводу (М32)

Саопштења објављена након претходног избора у звање:

36. **M. Radonjić**, W. Kopylov, A. Balaž, and A. Pelster, *Interplay of coherent and dissipative dynamics in condensates of light*, 659. WE-Heraeus-Seminar on "Condensates of Light", 14-17. January 2018, Physikzentrum Bad Honnef, Germany.

6.6 Саопштења са међународних скупова штампана у целини (М33)

Саопштења објављена након претходног избора у звање:

37. B. Zlatković, A. J. Krmpot, N. Šibalić, **M. Radonjić**, and B. M. Jelenković, *Parametric non-degenerate four wave mixing in hot potassium vapor*, Proc. SPIE **9447**, 944706 (2015),
38. N. Burić, D. B. Popović, **M. Radonjić**, and S. Prvanović, *A quantum-classical theory with nonlinear and stochastic dynamics*, Phys. Scr. **T163**, 014003 (2014) (ИФ = 1,296 за 2013. годину),
39. S. N. Nikolić, **M. Radonjić**, N. M. Lučić, A. J. Krmpot, and B. M. Jelenković, *Optical Ramsey fringes observed during temporal evolution of Zeeman coherences in Rb buffer gas cell*, Phys. Scr. **T162**, 014038 (2014) (ИФ = 1,296 за 2013. годину).

Саопштења објављена после одлуке Научног већа о предлогу за стицање претходног научног звања:

40. S. N. Nikolić, A. J. Krmpot, N. M. Lučić, B. V. Zlatković, **M. Radonjić**, and B. M. Jelenković, *Effects of laser beam diameter on electromagnetically induced transparency due to Zeeman coherences in Rb vapor*, Phys. Scr. **T157**, 014019 (2013) (ИФ = 1,296 за 2013. годину).

Саопштења објављена пре претходног избора у звање:

41. N. Burić, I. Mendaš, D. B. Popović, **M. Radonjić**, and S. Prvanović, *Hybrid dynamics as a constrained quantum system*, J. Phys. Conf. Ser. **442**, 012027 (2013),
42. N. Burić, S. Prvanović, and **M. Radonjić**, *Coarse-grained quantum systems and symmetries*, J. Phys. Conf. Ser. **343**, 012018 (2012),
43. **Milan Radonjić**, Slobodan Prvanović, and Nikola Burić, *Constrained quantum dynamics and coarse-grained description of a quantum system of nonlinear oscillators*, Phys. Scr. **T149**, 014011 (2012) (ИФ = 1,204 за 2011. годину),
44. S. N. Nikolić, V. Djokić, N. M. Lučić, A. J. Krmpot, S. M. Ćuk, **M. Radonjić**, and B. M. Jelenković, *The connection between electromagnetically induced transparency in the Zeeman configuration and slow light in hot rubidium vapor*, Phys. Scr. **T149**, 014009 (2012) (ИФ = 1,204 за 2011. годину),
45. A. J. Krmpot, S. N. Nikoilić, S. M. Ćuk, **M. Radonjić**, and B. M. Jelenković, *Dark Hanle resonance narrowing by blocking the central part of the Gaussian laser beam*, Proc. SPIE **7747**, 77470E (2011),
46. Zoran Grujić, Dusan Arsenović, **Milan Radonjić**, Marina Mijailović, and Branislav Jelenković, *Numerical simulation of Raman resonance due to the Ramsey interference induced by thermal motion of atoms*, Phys. Scr. **T135**, 014026 (2009) (ИФ = 1,088 за 2009. годину),
47. **M. Radonjić**, D. Arsenović, Z. Grujić, and B. M. Jelenković, *Line shapes and widths of CPT resonances: effect of laser beam profile in open atomic system*, Proc. SPIE **7027**, 70270N (2008),
48. B. M. Jelenković, D. Arsenović, Z. Grujić, **M. Radonjić**, and M. Mijailović, *Open system CPT with spatially separated pump and probe beams*, Proc. SPIE **7027**, 70270D (2008).

6.7 Саопштења са међународних скупова штампана у изводу (М34)

Саопштења објављена након претходног избора у звање:

49. **M. Radonjić**, W. Kopylov, A. Balaž, and A. Pelster, *Interplay of coherent and dissipative dynamics in condensates of light*, 49th Annual DAMOP Meeting, 28. May - 1. June 2018, Ft. Lauderdale, Florida, USA,
50. **M. Radonjić**, W. Kopylov, A. Balaž, and A. Pelster, *Modeling Dye-Mediated Photon-Photon Interaction in Condensates of Light*, 82nd Annual Conference of the DPG and DPG Spring Meeting, 4-9. March 2018, Erlangen, Germany,
51. **Milan Radonjić** and Philip Walther, *Photonic simulation of open quantum systems with various exchange statistics*, PHOTONICA2017 The Sixth International School and Conference on Photonics, 28. August - 1. September 2017, Belgrade, Serbia,
52. **M. Radonjić**, W. Kopylov, T. Brandes, A. Balaž, and A. Pelster, *Microscopic Model of Photon Condensation*, 616. WE-Heraeus-Seminar on "Ultracold Quantum Gases – Current Trends and Future Perspectives", 9-13. May 2016, Physikzentrum Bad Honnef, Germany.

Citation report for 47 results from Web of Science Core Collection between 2008 and 2018 Go

You searched for: **AUTHOR:** (Radonjic Milan OR Radonjic M)
Refined by: WEB OF SCIENCE CATEGORIES: (OPTICS OR PHYSICS ATOMIC MOLECULAR CHEMICAL OR PHYSICS MULTIDISCIPLINARY OR PHYSICS MATHEMATICAL) AND **DOCUMENT TYPES:** (ARTICLE OR PROCEEDINGS PAPER)
Timespan: 2008-2018. **Indexes:** SCI-EXPANDED, CPCI-S, CPCI-SSH, BKCI-S, ESCI.
...Less

This report reflects citations to source items indexed within Web of Science Core Collection. Perform a Cited Reference Search to include citations to items not indexed within Web of Science Core Collection.

Export Data: Save to Excel File

Total Publications	*h*-index	Sum of Times Cited	Citing articles
47 Analyze	8	166	110 Analyze
1999 – 2018	Average citations per item: 3.53	Without self citations: 100	Without self citations: 80 Analyze

Sum of Times Cited per Year

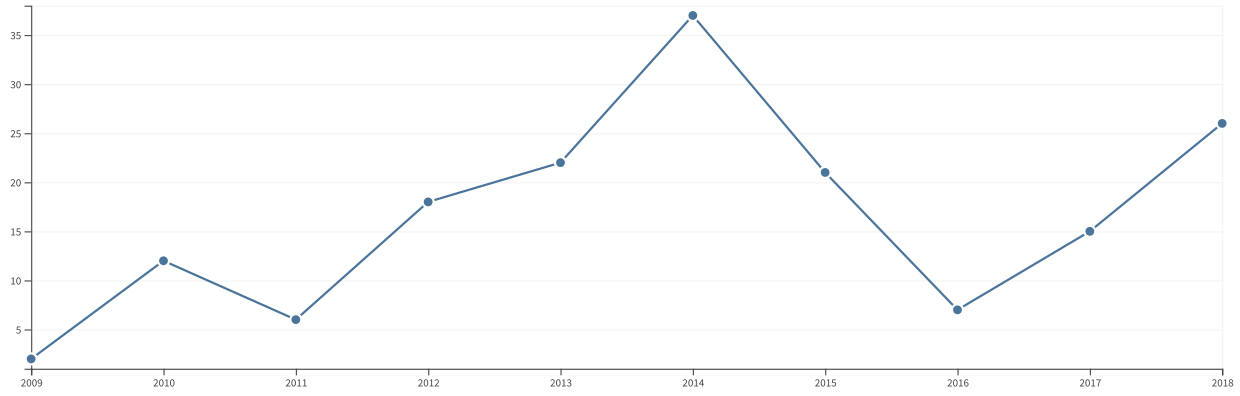

Sort by: Times Cited Date More

Page 1 of 5

		2015	2016	2017	2018	2019	Total	Average Citations per Year
Use the checkboxes to remove individual items from this Citation Report		21	7	15	26	0	166	16.60
or restrict to items published between 2008 and 2018 Go								
☐	1. Interplay of coherent and dissipative dynamics in condensates of light By: Radonjic, Milan; Kopylov, Wassilij; Balaz, Antun; et al. NEW JOURNAL OF PHYSICS Volume: 20 Article Number: 055014 Published: MAY 31 2018	0	0	0	0	0	0	0.00
☐	2. Macroscopic Superpositions as Quantum Ground States By: Dakic, Borivoje; Radonjic, Milan PHYSICAL REVIEW LETTERS Volume: 119 Issue: 9 Article Number: 090401 Published: SEP 1 2017	0	0	0	1	0	1	0.50
☐	3. Dark-polariton bound pairs in the modified Jaynes-Cummings-Hubbard model By: Maggitti, A.; Radonjic, M.; Jelenkovic, B. M. PHYSICAL REVIEW A Volume: 93 Issue: 1 Article Number: 013835 Published: JAN 19 2016	0	0	2	0	0	2	0.67
☐	4. Efficient parametric non-degenerate four-wave mixing in hot potassium vapor By: Zlatkovic, B.; Krmpot, A. J.; Sibalic, N.; et al. LASER PHYSICS LETTERS Volume: 13 Issue: 1 Article Number: 015205 Published: JAN 2016	0	1	3	7	0	11	3.67
☐	5. Dissipative two-mode Tavis-Cummings model with time-delayed feedback control By: Kopylov, Wassilij; Radonjic, Milan; Brandes, Tobias; et al. PHYSICAL REVIEW A Volume: 92 Issue: 6 Article Number: 063832 Published: DEC 21 2015	0	3	3	6	0	12	3.00

6. **Positive-operator-valued measures in the Hamiltonian formulation of quantum mechanics** By: Arsenovic, D.; Buric, N.; Popovic, D. B.; et al. PHYSICAL REVIEW A Volume: 91 Issue: 6 Article Number: 062114 Published: JUN 12 2015	0	0	0	0	0	0	0.00
7. **Raman-Ramsey electromagnetically induced transparency in the configuration of counterpropagating pump and probe in vacuum Rb cell** By: Radojicic, Ivan S.; Radonjic, Milan; Lekic, Marina M.; et al. JOURNAL OF THE OPTICAL SOCIETY OF AMERICA B-OPTICAL PHYSICS Volume: 32 Issue: 3 Pages: 426-430 Published: MAR 2015	0	0	0	0	0	0	0.00
8. **Transient development of Zeeman electromagnetically induced transparency during propagation of Raman-Ramsey pulses through Rb buffer gas cell** By: Nikolic, S. N.; Radonjic, M.; Lucic, N. M.; et al. JOURNAL OF PHYSICS B-ATOMIC MOLECULAR AND OPTICAL PHYSICS Volume: 48 Issue: 4 Article Number: 045501 Published: FEB 28 2015	0	0	0	2	0	2	0.50
9. **Parametric non-degenerate four wave mixing in hot potassium vapor** By: Zlatkovic, Bojan; Krmpot, Aleksandar J.; Sibalic, Nikola; et al. Conference: 18th International School on Quantum Electronics (ISQE) - Laser Physics and Applications Location: Sozopol, BULGARIA Date: SEP 29-OCT 03, 2014 Sponsor(s): Bulgarian Acad Sci, Inst Elect; European Phys Soc; Minist Educ & Sci; Natl Tech Univ Athens, Sch Appl Math & Phys Sci 18TH INTERNATIONAL SCHOOL ON QUANTUM ELECTRONICS: LASER PHYSICS AND APPLICATIONS Book Series: Proceedings of SPIE Volume: 9447 Published: 2015	0	0	0	0	0	0	0.00
10. **A quantum-classical theory with nonlinear and stochastic dynamics** By: Buric, N.; Popovic, D. B.; Radonjic, M.; et al. Conference: 15th Vaxjo conference on Quantum Foundations Location: Vaxjo, SWEDEN Date: JUN 10-13, 2013 PHYSICA SCRIPTA Volume: T163 Article Number: 014003 Published: DEC 2014	0	0	0	0	0	0	0.00

Select Page | Save to Excel File

Sort by: Times Cited **Date** More

Page 1 of 5

47 records matched your query of the 26,083,729 in the data limits you selected.
Key: = Structure available.

Citation report for 47 results from Web of Science Core Collection between 2008 and 2018 Go

You searched for: **AUTHOR:** (Radonjic Milan OR Radonjic M)
Refined by: WEB OF SCIENCE CATEGORIES: (OPTICS OR PHYSICS ATOMIC MOLECULAR CHEMICAL OR PHYSICS MULTIDISCIPLINARY OR PHYSICS MATHEMATICAL) AND **DOCUMENT TYPES:** (ARTICLE OR PROCEEDINGS PAPER)
Timespan: 2008-2018. **Indexes:** SCI-EXPANDED, CPCI-S, CPCI-SSH, BKCI-S, ESCI.
...Less

This report reflects citations to source items indexed within Web of Science Core Collection. Perform a Cited Reference Search to include citations to items not indexed within Web of Science Core Collection.

Use the checkboxes to remove individual items from this Citation Report

or restrict to items published between 2008 and 2018 Go

	2015	2016	2017	2018	2019	Total	Average Citations per Year
	21	7	15	26	0	166	16.60
11. Cloning in nonlinear Hamiltonian quantum and hybrid mechanics By: Arsenovic, D.; Buric, N.; Popovic, D. B.; et al. PHYSICAL REVIEW A Volume: 90 Issue: 4 Article Number: 042115 Published: OCT 21 2014	0	0	0	0	0	0	0.00
12. Optical Ramsey fringes observed during temporal evolution of Zeeman coherences in Rb buffer gas cell By: Nikolic, S. N.; Radonjic, M.; Lucic, N. M.; et al. Conference: 4th International School and Conference on Photonics Location: Belgrade, SERBIA Date: AUG 26-30, 2013 PHYSICA SCRIPTA Volume: T162 Article Number: 014038 Published: SEP 2014	0	0	0	0	0	0	0.00
13. Geometric Phase for Analytically Solvable Driven Time-Dependent Two-Level Quantum Systems By: Mendas, I.; Buric, N.; Popovic, D. B.; et al. ACTA PHYSICA POLONICA A Volume: 126 Issue: 3 Pages: 670-672 Published: SEP 2014	0	0	0	1	0	1	0.20
14. Phase space theory of quantum-classical systems with nonlinear and stochastic dynamics By: Buric, Nikola; Popovic, Duska B.; Radonjic, Milan; et al. ANNALS OF PHYSICS Volume: 343 Pages: 16-26 Published: APR 2014	0	0	0	0	0	1	0.20
15. Orbits of hybrid systems as qualitative indicators of quantum dynamics By: Buric, N.; Popovic, D. B.; Radonjic, M.; et al. PHYSICS LETTERS A Volume: 378 Issue: 16-17 Pages: 1081-1084 Published: MAR 14 2014	0	0	0	0	0	0	0.00
16. Unified Treatment of Geometric Phases for Statistical Ensembles of Classical, Quantum and Hybrid Systems By: Buric, N.; Popovic, D. B.; Radonjic, M.; et al. INTERNATIONAL JOURNAL OF THEORETICAL PHYSICS Volume: 53 Issue: 3 Pages: 1046-1055 Published: MAR 2014	0	0	0	0	0	0	0.00
17. Ehrenfest principle and unitary dynamics of quantum-classical systems with general potential interaction By: Radonjic, M.; Popovic, D. B.; Prvanovic, S.; et al. PHYSICAL REVIEW A Volume: 89 Issue: 2 Article Number: 024104 Published: FEB 28 2014	1	1	0	0	0	2	0.40
18. Hamiltonian Formulation of Statistical Ensembles and Mixed States of Quantum and Hybrid Systems By: Buric, N.; Popovic, D. B.; Radonjic, M.; et al. FOUNDATIONS OF PHYSICS Volume: 43 Issue: 12 Pages: 1459-1477 Published: DEC 2013	2	0	0	1	0	4	0.67
19. Effects of laser beam diameter on electromagnetically induced transparency due to Zeeman coherences in Rb vapor By: Nikolic, S. N.; Krmpot, A. J.; Lucic, N. M.; et al. Conference: 3rd International Conference on the Physics of Optical Materials and Devices Location: Belgrade, SERBIA Date: SEP 02-06, 2012 PHYSICA SCRIPTA Volume: T157 Article Number: 014019 Published: NOV 2013	0	0	0	0	0	0	0.00
20. Dark-state polaritons in a degenerate two-level system By: Maggitti, A.; Radonjic, M.; Jelenkovic, B. M. LASER PHYSICS Volume: 23 Issue: 10 Article Number: 105202 Published: OCT 2013	0	1	0	1	0	2	0.33

Select Page Save to Excel File

47 records matched your query of the 26,083,729 in the data limits you selected.
Key: = Structure available.

Citation report for 47 results from Web of Science Core Collection between 2008 and 2018 Go

You searched for: **AUTHOR:** (Radonjic Milan OR Radonjic M)
Refined by: WEB OF SCIENCE CATEGORIES: (OPTICS OR PHYSICS ATOMIC MOLECULAR CHEMICAL OR PHYSICS MULTIDISCIPLINARY OR PHYSICS MATHEMATICAL) AND **DOCUMENT TYPES:** (ARTICLE OR PROCEEDINGS PAPER)
Timespan: 2008-2018. **Indexes:** SCI-EXPANDED, CPCI-S, CPCI-SSH, BKCI-S, ESCI.
...Less

This report reflects citations to source items indexed within Web of Science Core Collection. Perform a Cited Reference Search to include citations to items not indexed within Web of Science Core Collection.

Use the checkboxes to remove individual items from this Citation Report

or restrict to items published between 2008 and 2018 Go

	2015	2016	2017	2018	2019	Total	Average Citations per Year
	21	7	15	26	0	166	16.60
21. Influence of a laser beam radial intensity distribution on Zeeman electromagnetically induced transparency line-shapes in the vacuum Rb cell By: Cuk, S. M.; Krmpot, A. J.; Radonjic, M.; et al. JOURNAL OF PHYSICS B-ATOMIC MOLECULAR AND OPTICAL PHYSICS Volume: 46 Issue: 17 Article Number: 175501 Published: SEP 14 2013	0	0	1	0	0	1	0.17
22. Hybrid quantum-classical model of quantum measurements By: Buric, N.; Popovic, D. B.; Radonjic, M.; et al. PHYSICAL REVIEW A Volume: 87 Issue: 5 Article Number: 054101 Published: MAY 31 2013	1	0	0	0	0	3	0.50
23. Effects of a laser beam profile on Zeeman electromagnetically induced transparency in the Rb buffer gas cell By: Nikolic, S. N.; Radonjic, M.; Krmpot, A. J.; et al. JOURNAL OF PHYSICS B-ATOMIC MOLECULAR AND OPTICAL PHYSICS Volume: 46 Issue: 7 Article Number: 075501 Published: APR 14 2013	1	0	2	1	0	4	0.67
24. Hybrid dynamics as a constrained quantum system By: Buric, N.; Mendas, I.; Popovic, D. B.; et al. Conference: 6th International Workshop on Decoherence, Information, Complexity and Entropy (DICE) Location: Castiglioncello, ITALY Date: SEP 17-21, 2012 Sponsor(s): Univ Pisa; Domus Galilaeana; Centro Interdisciplinare Studio Sistemi Complessi (CISSC); Univ Salerno, Dipartimento Ingn Industriale; Ist Italiano Studi Filosofici (IISF); Solvay Italia SA; Inst Phys Publishing (IOP); Springer Verlag; Hungarian Sci Res Fund (OTKA) 6TH INTERNATIONAL WORKSHOP DICE2012 SPACETIME - MATTER - QUANTUM MECHANICS: FROM THE PLANCK SCALE TO EMERGENT PHENOMENA Book Series: Journal of Physics Conference Series Volume: 442 Article Number: UNSP 012027 Published: 2013	0	0	0	0	0	0	0.00
25. Ramsey effects in coherent resonances at closed transition F-g=2 -> F-e=3 of Rb-87 By: Grujic, Z. D.; Lekic, M. M.; Radonjic, M.; et al. JOURNAL OF PHYSICS B-ATOMIC MOLECULAR AND OPTICAL PHYSICS Volume: 45 Issue: 24 Article Number: 245502 Published: DEC 28 2012	1	0	0	1	0	2	0.29
26. Alternative routes to equivalent classical models of a quantum system By: Radonjic, M.; Prvanovic, Slobodan; Buric, Nikola CHINESE PHYSICS B Volume: 21 Issue: 12 Article Number: 120301 Published: DEC 2012	0	0	0	0	0	1	0.14
27. Statistical ensembles in the Hamiltonian formulation of hybrid quantum-classical systems By: Buric, N.; Mendas, I.; Popovic, D. B.; et al. PHYSICAL REVIEW A Volume: 86 Issue: 3 Article Number: 034104 Published: SEP 27 2012	3	0	0	1	0	21	3.00
28. Hybrid quantum-classical models as constrained quantum systems By: Radonjic, M.; Prvanovic, S.; Buric, N. PHYSICAL REVIEW A Volume: 85 Issue: 6 Article Number: 064101 Published: JUN 4 2012	3	0	1	1	0	23	3.29
29. The connection between electromagnetically induced transparency in the Zeeman configuration and slow light in hot rubidium vapor By: Nikolic, S. N.; Djokic, V.; Lucic, N. M.; et al. Conference: 3rd International School and Conference on Photonics Location: Belgrade, SERBIA Date: AUG 29-SEP 02, 2011 PHYSICA SCRIPTA Volume: T149 Article Number: 014009 Published: APR 2012	0	0	0	0	0	0	0.00
30. Constrained quantum dynamics and coarse-grained description of a quantum system of nonlinear oscillators By: Radonjic, Milan; Prvanovic, Slobodan; Buric, Nikola Conference: 3rd International School and Conference on Photonics Location: Belgrade, SERBIA Date: AUG 29-SEP 02, 2011 PHYSICA SCRIPTA Volume: T149 Article Number: 014011 Published: APR 2012	0	0	0	0	0	0	0.00

Select Page Save to Excel File

Citation report for 47 results from Web of Science Core Collection between 2008 and 2018 Go

You searched for: **AUTHOR:** (Radonjic Milan OR Radonjic M)
Refined by: WEB OF SCIENCE CATEGORIES: (OPTICS OR PHYSICS ATOMIC MOLECULAR CHEMICAL OR PHYSICS MULTIDISCIPLINARY OR PHYSICS MATHEMATICAL) AND **DOCUMENT TYPES:** (ARTICLE OR PROCEEDINGS PAPER)
Timespan: 2008-2018. **Indexes:** SCI-EXPANDED, CPCI-S, CPCI-SSH, BKCI-S, ESCI.
...Less

This report reflects citations to source items indexed within Web of Science Core Collection. Perform a Cited Reference Search to include citations to items not indexed within Web of Science Core Collection.

Use the checkboxes to remove individual items from this Citation Report

or restrict to items published between 2008 and 2018 Go

	2015	2016	2017	2018	2019	Total	Average Citations per Year
	21	7	15	26	0	166	16.60
31. **Emergence of classical behavior from the quantum spin** By: Radonjic, M.; Prvanovic, S.; Buric, N. PHYSICAL REVIEW A Volume: 85 Issue: 2 Article Number: 022117 Published: FEB 13 2012	2	0	0	0	0	9	1.29
32. **Coarse-grained quantum systems and symmetries** By: Buric, N.; Prvanovic, S.; Radonjic, M. Conference: 7th International Conference on Quantum Theory and Symmetries (QTS) Location: Prague, CZECH REPUBLIC Date: AUG 07-13, 2011 Sponsor(s): Czech Tech Univ, Fac Nucl Sci & Phys Engn, Dept Math & Phys; Bogoliubov Lab Theoret Phys Joint Inst Nucl Res; Acad Sci, Inst Phys 7TH INTERNATIONAL CONFERENCE ON QUANTUM THEORY AND SYMMETRIES (QTS7) Book Series: Journal of Physics Conference Series Volume: 343 Article Number: 012018 Published: 2012	0	0	0	0	0	0	0.00
33. **Evolution of dark state of an open atomic system in constant intensity laser field** By: Krmpot, A. J.; Radonjic, M.; Cuk, S. M.; et al. PHYSICAL REVIEW A Volume: 84 Issue: 4 Article Number: 043844 Published: OCT 25 2011	1	0	1	0	0	4	0.50
34. **System of classical nonlinear oscillators as a coarse-grained quantum system** By: Radonjic, Milan; Prvanovic, Slobodan; Buric, Nikola PHYSICAL REVIEW A Volume: 84 Issue: 2 Article Number: 022103 Published: AUG 2 2011	2	0	0	0	0	15	1.88
35. **Dark Hanle resonance narrowing by blocking the central part of the Gaussian laser beam** By: Krmpot, A. J.; Nikolic, S. N.; Cuk, S. M.; et al. Conference: 16th International School on Quantum Electronics - Laser Physics and Applications Location: Nessebar, BULGARIA Date: SEP 20-24, 2010 Sponsor(s): SPIE; Inst Elect, Bulgarian Acad Sci; Opt Soc Amer; European Phys Soc; Natl Techn Univ Athens, Sch Appl Math & Phys Sci; European Opt Soc; VIVACOM 16TH INTERNATIONAL SCHOOL ON QUANTUM ELECTRONICS: LASER PHYSICS AND APPLICATIONS Book Series: Proceedings of SPIE Volume: 7747 Article Number: 77470E Published: 2011	0	0	0	0	0	0	0.00
36. **Influence of laser beam profile on electromagnetically induced absorption** By: Cuk, S. M.; Radonjic, M.; Krmpot, A. J.; et al. PHYSICAL REVIEW A Volume: 82 Issue: 6 Article Number: 063802 Published: DEC 1 2010	0	0	0	0	0	2	0.22
37. **Dark Hanle resonances from selected segments of the Gaussian laser beam cross-section** By: Krmpot, A. J.; Cuk, S. M.; Nikolic, S. N.; et al. OPTICS EXPRESS Volume: 17 Issue: 25 Pages: 22491-22498 Published: DEC 7 2009	0	0	0	0	0	6	0.60
38. **Nonlinear magneto-optical rotation narrowing in vacuum gas cells due to interference between atomic dark states of two spatially separated laser beams** By: Mijailovic, M. M.; Grujic, Z. D.; Radonjic, M.; et al. PHYSICAL REVIEW A Volume: 80 Issue: 5 Article Number: 053819 Published: NOV 2009	0	0	0	0	0	1	0.10
39. **Stark-Chirped Rapid Adiabatic Passage in a Multilevel Atom** By: Radonjic, M.; Jelenkovic, B. M. Conference: International School and Conference on Photonics (PHOTONICA09) Location: Belgrade, SERBIA Date: AUG 24-28, 2009 ACTA PHYSICA POLONICA A Volume: 116 Issue: 4 Pages: 476-478 Published: OCT 2009	0	0	0	0	0	0	0.00
40. **Geometric Phase of an Open System** By: Buric, N.; Radonjic, M. Conference: International School and Conference on Photonics (PHOTONICA09) Location: Belgrade, SERBIA Date: AUG 24-28, 2009 ACTA PHYSICA POLONICA A Volume: 116 Issue: 4 Pages: 483-485 Published: OCT 2009	0	0	0	0	0	1	0.10

Select Page Save to Excel File

Citation report for 47 results from Web of Science Core Collection between 2008 and 2018 Go

You searched for: **AUTHOR:** (Radonjic Milan OR Radonjic M)
Refined by: WEB OF SCIENCE CATEGORIES: (OPTICS OR PHYSICS ATOMIC MOLECULAR CHEMICAL OR PHYSICS MULTIDISCIPLINARY OR PHYSICS MATHEMATICAL) AND **DOCUMENT TYPES:** (ARTICLE OR PROCEEDINGS PAPER)
Timespan: 2008-2018. **Indexes:** SCI-EXPANDED, CPCI-S, CPCI-SSH, BKCI-S, ESCI.
...Less

This report reflects citations to source items indexed within Web of Science Core Collection. Perform a Cited Reference Search to include citations to items not indexed within Web of Science Core Collection.

Sort by: Times Cited Date More Page 5 of 5

Use the checkboxes to remove individual items from this Citation Report

or restrict to items published between 2008 and 2018 Go

	2015	2016	2017	2018	2019	Total	Average Citations per Year
	21	7	15	26	0	166	16.60
41. Laser Beam Profile Influence on Dark Hanle Resonances in Rb Vapor By: Krmpot, A. J.; Cuk, S. M.; Nikolic, S. N.; et al. Conference: International School and Conference on Photonics (PHOTONICA09) Location: Belgrade, SERBIA Date: AUG 24-28, 2009 ACTA PHYSICA POLONICA A Volume: 116 Issue: 4 Pages: 563-565 Published: OCT 2009	0	0	0	0	0	0	0.00
42. Stark-chirped rapid adiabatic passage among degenerate-level manifolds By: Radonjic, M.; Jelenkovic, B. M. PHYSICAL REVIEW A Volume: 80 Issue: 4 Article Number: 043416 Published: OCT 2009	0	0	1	0	0	3	0.30
43. Numerical simulation of Raman resonance due to the Ramsey interference induced by thermal motion of atoms By: Grujic, Zoran; Arsenovic, Dusan; Radonjic, Milan; et al. Conference: 15th Central European Workshop on Quantum Optics Location: Belgrade, SERBIA Date: MAY 29-JUN 03, 2008 PHYSICA SCRIPTA Volume: T135 Article Number: 014026 Published: JUL 2009	0	0	0	0	0	0	0.00
44. Uniquely defined geometric phase of an open system By: Buric, Nikola; Radonjic, Milan PHYSICAL REVIEW A Volume: 80 Issue: 1 Article Number: 014101 Published: JUL 2009	2	0	1	1	0	16	1.60
45. Coherent population trapping linewidths for open transitions: Cases of different transverse laser intensity distribution By: Radonjic, M.; Arsenovic, D.; Grujic, Z.; et al. PHYSICAL REVIEW A Volume: 79 Issue: 2 Article Number: 023805 Published: FEB 2009	2	0	0	2	0	15	1.50
46. Open system CPT with spatially separated pump and probe beams By: Jelenkovic, B. M.; Arsenovic, D.; Grujic, Z.; et al. Conference: Conference of the 15th International School on Quantum Electronics - Laser Physics and Applications Location: Bourgas, BULGARIA Date: SEP 15-19, 2008 Sponsor(s): Bulgarian Acad Sci, Inst Elect; ASO Sofia - Austrian Sci & Res Liaison off; HORIBA Jobin Yvon GmbH; Optella Ltd; Coherent Inc 15TH INTERNATIONAL SCHOOL ON QUANTUM ELECTRONICS: LASER PHYSICS AND APPLICATIONS Book Series: Proceedings of SPIE Volume: 7027 Article Number: 70270D Published: 2008	0	1	0	0	0	1	0.09
47. Line-shapes and widths of CPT resonances: Effect of laser beam profile in open atomic system By: Radonjic, M.; Arsenovic, D.; Grujic, Z.; et al. Conference: Conference of the 15th International School on Quantum Electronics - Laser Physics and Applications Location: Bourgas, BULGARIA Date: SEP 15-19, 2008 Sponsor(s): Bulgarian Acad Sci, Inst Elect; ASO Sofia - Austrian Sci & Res Liaison off; HORIBA Jobin Yvon; Optella Ltd; Coherent Inc 15TH INTERNATIONAL SCHOOL ON QUANTUM ELECTRONICS: LASER PHYSICS AND APPLICATIONS Book Series: Proceedings of SPIE Volume: 7027 Article Number: 70270N Published: 2008	0	0	0	0	0	0	0.00

Select Page Save to Excel File

Sort by: Times Cited Date More Page 5 of 5

47 records matched your query of the 26,083,729 in the data limits you selected.
Key: = Structure available.

Република Србија
МИНИСТАРСТВО ПРОСВЕТЕ, НАУКЕ И ТЕХНОЛОШКОГ РАЗВОЈА
Комисија за стицање научних звања

Број:660-01-00194/342
26.02.2014. године
Б е о г р а д

На основу члана 22. става 2. члана 70. став 5. Закона о научноистраживачкој делатности ("Службени гласник Републике Србије", број 110/05 и 50/06 – исправка и 18/10), члана 2. става 1. и 2. тачке 1 – 4.(прилози) и члана 38. Правилника о поступку и начину вредновања и квантитативном исказивању научноистраживачких резултата истраживача ("Службени гласник Републике Србије", број 38/08) и захтева који је поднео

Институт за физику у Београду

Комисија за стицање научних звања на седници одржаној 26.02.2014. године, донела је

ОДЛУКУ
О СТИЦАЊУ НАУЧНОГ ЗВАЊА

Др Милан Радоњић
стиче научно звање
Научни сарадник

у области природно-математичких наука - физика

О Б Р А З Л О Ж Е Њ Е

Институт за физику у Београду

утврдио је предлог број 1173/1 од 24.09.2013. године на седници научног већа Института и поднео захтев Комисији за стицање научних звања број 1219/1 од 07.10.2013. године за доношење одлуке о испуњености услова за стицање научног звања ***Научни сарадник***.

Комисија за стицање научних звања је по претходно прибављеном позитивном мишљењу Матичног научног одбора за физику на седници одржаној 26.02.2014. године разматрала захтев и утврдила да именовани испуњава услове из члана 70. став 5. Закона о научноистраживачкој делатности ("Службени гласник Републике Србије", број 110/05 и 50/06 – исправка и 18/10), члана 2. става 1. и 2. тачке 1 – 4.(прилози) и члана 38. Правилника о поступку и начину вредновања и квантитативном исказивању научноистраживачких резултата истраживача ("Службени гласник Републике Србије", број 38/08) за стицање научног звања ***Научни сарадник***, па је одлучила као у изреци ове одлуке.

Доношењем ове одлуке именовани стиче сва права која му на основу ње по закону припадају.

Одлуку доставити подносиоцу захтева, именованом и архиви Министарства просвете, науке и технолошког развоја у Београду.

ПРЕДСЕДНИК КОМИСИЈЕ
др Станислава Стошић-Грујичић,
научни саветник

МИНИСТАР
Проф. др Томислав Јовановић

Institut za fiziku u Beogradu

Na osnovu obrazloženog predloga Naučnog saveta dodeljuje

STUDENTSKU NAGRADU INSTITUTA ZA FIZIKU ZA 2014. GODINU

dr Milanu M. Radonjiću

za doktorsku disertaciju „Elektromagnetski indukovani koherentni efekti u laserski pobuđivanim Ramanovim rezonancama u parama rubidijuma".

B. Marinković

dr Bratislav Marinković
predsednik
Naučnog saveta

ИНСТИТУТ ЗА ФИЗИКУ

Beograd
7. maj 2014.

dr Aleksandar Belić
direktor
Instituta za fizik

З А П И С Н И К

са IX седнице Изборног и Наставно-научног већа Физичког факултета
одржане у среду 1. јула 2015. године

Седници присуствује 49 чланова Изборног и Наставно-научног већа.

Службено одсутни: проф. др Петар Аџић
Мирослав Поповић

Оправдано одсутни: проф. др Владимир Милосављевић
проф. др Јован Пузовић
проф. др Владан Вучковић
доц. др Зоран Борјан
доц. др Владимир Миљковић
доц. др Иван Виденовић
мр Саша Ивковић
Весна Ковачевић
Биљана Николић

Декан Факултета проф. др Јаблан Дојчиловић, отворио је седницу у 11:15 и предложио следећи

Д н е в н и р е д

1. Усвајање Записника са VIII седнице Изборног и Наставно-научног већа.

Изборно веће

2. Утврђивање предлога за избор директора Института за физику и Института за метеорологију Физичког факултета за мандатни период 2015-2018 година
3. Усвајање Извештаја Комисије за избор наставника Физичког факултета и то:
   a) једног редовног професора за ужу научну област Нуклеарна физика
   b) једног редовног професора за ужу научну област Примењена физика
   c) једног асистента за ужу научну област Физика честица и поља

Наставно-научно веће

4. Одређивање Комисије за оцену испуњености услова и оправданост предложене теме за израду докторске дисертације за:
   a) МИЛОША ДРАЖИЋА, дипломираног физичара, који је пријавио докторску дисертацију под називом: „ТЕОРИЈА НЕРАВНОТЕЖНОГ, ВРЕМЕНСКИ ЗАВИСНОГ ЕЛЕКТРОНСКОГ ТРАНСПОРТА КРОЗ КВАНТНЕ ТАЧКЕ И МОЛЕКУЛЕ“
5. Усвајање Извештаја Комисије за оцену испуњености услова и оправданост предложене теме за израду докторске дисертације и одређивање ментора за:
   a) АНЂЕЛА МАЂИТИЈА, дипломираног физичара, који је пријавио докторску дисертацију под називом: „FORMATION OF DARK-STATE POLARITONS AND TWO-POLARITON BOUND STATES IN ARRAYS OF ATOMS AND OPTICAL CAVITIES“ (Формирање тамних поларитона и дво-поларитонских везаних стања у низовима атома и оптичких микрорезонатора)
   b) МАРИЈУ МАРЈАНОВИЋ, дипломираног физичара, која је пријавила докторску дисертацију под називом: „ПОТРАГА ЗА СУПЕРСИМЕТРИЧНИМ ЧЕСТИЦАМА ПРОДУКОВАНИМ ЈАКОМ ИНТЕРАКЦИЈОМ ПОМОЋУ *АТЛАС* ДЕТЕКТОРА И ИНТЕРПРЕТАЦИЈА РЕЗУЛТАТА У ОКВИРУ *pMSSM* МОДЕЛА“
   c) ИРИНЕЛА ТАПАЛАГУ, дипломираног физичара, који је пријавио докторску дисертацију под називом: „ИСПИТИВАЊЕ РЕГУЛАРНОСТИ ШТАРКОВОГ ШИРЕЊА КОД ИЗОЕЛЕКТРОНСКИХ НИЗОВА ЛИТИЈУМА И НАТРИЈУМА“
6. Одређивање Комисије за преглед и оцену докторске дисертације за:

др Радомир Жикић, научни саветник ИФ

5. тачка

Усвојен је Извештај Комисије за оцену испуњености услова и оправданост предложене теме за израду докторске дисертације и одређен ментор за:

a) АНЂЕЛА МАЂИТИЈА, дипломираног физичара, који је пријавио докторску дисертацију под називом: „FORMATION OF DARK-STATE POLARITONS AND TWO-POLARITON BOUND STATES IN ARRAYS OF ATOMS AND OPTICAL CAVITIES“ (Формирање тамних поларитона и дво-поларитонских везаних стања у низовима атома и оптичких микрорезонатора)
Ментор: др Милан Радоњић, научни сарадник ИФ

b) МАРИЈУ МАРЈАНОВИЋ, дипломираног физичара, која је пријавила докторску дисертацију под називом: „ПОТРАГА ЗА СУПЕРСИМЕТРИЧНИМ ЧЕСТИЦАМА ПРОДУКОВАНИМ ЈАКОМ ИНТЕРАКЦИЈОМ ПОМОЋУ *АТЛАС* ДЕТЕКТОРА И ИНТЕРПРЕТАЦИЈА РЕЗУЛТАТА У ОКВИРУ *pMSSM* МОДЕЛА“
Ментор: др Марија Врањеш-Милосављевић

c) ИРИНЕЛА ТАПАЛАГУ, дипломираног физичара, који је пријавио докторску дисертацију под називом: „ИСПИТИВАЊЕ РЕГУЛАРНОСТИ ШТАРКОВОГ ШИРЕЊА КОД ИЗОЕЛЕКТРОНСКИХ НИЗОВА ЛИТИЈУМА И НАТРИЈУМА“
Ментор: проф. др Иван Дојчиновић

6. тачка

Одређена је Комисија за преглед и оцену докторске дисертације за:

a) ГОРАНА СРЕТЕНОВИЋА, дипломираног физичара, који је предао докторску дисертацију под називом: „СПЕКТРОСКОПСКА ИСТРАЖИВАЊА ДИНАМИКЕ РАЗВОЈА СТРИМЕРА У ХЕЛИЈУМУ“
Комисија: др Милорад Кураица, редовни професор ФФ
др Братислав Обрадовић, ванредни професор ФФ
др Невена Пуач, виши научни сарадник ИФ

b) МИРЈАМ ВУЈАДИНОВИЋ, дипломираног метеоролога, која је предала докторску дисертацију под називом: „МОДЕЛИРАЊЕ ХИДРОЛОШКОГ ЦИКЛУСА У ИНТЕГРИСАНОМ ГЕОФИЗИЧКОМ СИСТЕМУ“
Комисија: др Боривој Рајковић, ванредни професор ФФ у пензији
др Владимир Ђурђевић, доцент ФФ
др Ана Вуковић, доцент Пољопривредног факултета

c) АЛЕКСАНДРА ТОМОВИЋА, дипломираног физичара, који је предао докторску дисертацију под називом: „ЕЛЕКТРОНСКЕ ОСОБИНЕ И МОРФОЛОГИЈА ТАНКИХ

Formation of dark-state polaritons and two-polariton bound states in arrays of atoms and optical cavities

Формирање тамних поларитона и дво-поларитонских везаних стања у низовима атома и оптичких микрорезонатора.

(/bitstream/handle/123456789/7258/Disertacija.pdf?sequence=1&isAllowed=y)

Отварање

Disertacija.pdf (3.200Mb) (/bitstream/handle/123456789/7258/Disertacija.pdf?sequence=1&isAllowed=y)
Angelo_Maggitti_referat_disertacija_FIF.pdf (253.3Kb) (/bitstream/handle/123456789/7258/Angelo_Maggitti_referat_disertacija_FIF.pdf?sequence=5&isAllowed=y)

Докторанд:
Maggitti, Angelo

Факултет:
Универзитет у Београду, Физички факултет

Датум одбране дисертације:
07-04-2016

Ментор:
Radonjić, Milan (http://orcid.org/0000-0002-2972-2969)

Чланови комисије:
Jelenković, Branislav (http://orcid.org/0000-0001-8276-1169)
Kuraica, Milorad (http://orcid.org/0000-0001-8201-8500)
Konjević, Nikola (http://orcid.org/0000-0002-2507-9099)
Damnjanović, Milan (http://orcid.org/0000-0003-2806-253X)

Метаподаци
Приказ свих података о дисертацији (/handle/123456789/7258?show=full)

Остали линкови:

http://eteze.bg.ac.rs/application/showtheses?thesesId=4224 (http://eteze.bg.ac.rs/application/showtheses?thesesId=4224)

https://fedorabg.bg.ac.rs/fedora/get/o:13925/bdef:Content/download (https://fedorabg.bg.ac.rs/fedora/get/o:13925/bdef:Content/download)

http://vbs.rs/scripts/cobiss?command=DISPLAY&base=70036&RID=48203023 (http://vbs.rs/scripts/cobiss?command=DISPLAY&base=70036&RID=48203023)

http://nardus.mpn.gov.rs/123456789/7258 (http://nardus.mpn.gov.rs/123456789/7258)

Сажетак:

This thesis covers a theoretical analysis of non-interacting and interacting quasi particles, called polaritons. Polaritons are composites, based on photonic and atomic excitations in a tunable and controlled manner. Dark-state polaritons, as a subclass of polaritons, are very curious objects, as they can act as a quantum memory of photons within an ensemble of alkali-metal atoms in -type conguration which admit electromagnetically induced transparency (EIT). This thesis focus on the formation of dark-state polaritons in degenerate two-level systems, where two light elds, a quantum probe and a classical driving eld, couple the same transition between the ground state and excited state manifold. An algorithm is going to be derived in order to determine the dispersion relation and inherent composition of the dark-state polaritons in the degenerate two-level system. The algorithm is based on a microscopic equation of motion technique and provides an extension of the non-degenerate case. Depending Више

Ova teza predstav a teorijsku analizu neinteragujuih i interagujuih kvazi-qestica, tzv. polaritona. Polaritoni su kombinacije fotonskih i atom-skih ekscitacija u kontrolisano promen ivom odnosu. Vrsta polaritona, tamni polaritoni, su veoma neobiqni objekti budui da mogu da slue kao kvantna memorija za fotone unutar ansambla atoma alkalnih metala u - konfiguraciji, a u vezi sa efektom elektromagnetno indukovane transparen- cije (EIT). Teza se fokusira na prouqavae formiraa tamnih polaritona u sistemima sa dva nivoa, osnovnim i pobuenim, koji poseduju mnogostrukosti degenerisanih podnivoa i spregnuti su kvantnim probnim i klasiqnim kon- trolnim laserskim po em. Bie izveden algoritam za dobijae disperzione relacije i odgovarajueg sastava tamnih polaritona u sistemima sa dva-nivoa i degeneracijom. Algoritam je zasnovan na tehnici mikroskopskih jednaqina kretaa i predstav a proxiree sluqaja bez degeneracije. Bie pokazano da u zavisnosti od polarizacije po a mogu postojati jedan ili dva tamna Више

Кључне речи:

EIT, dark-state polaritons, cavity QED arrays, interacting darkpolaritons, dark-polariton bound pairs, quantum memory of light and disorder; elektromagnetno indukovana transparencija (EIT), tamni polaritoni, niz kvantno-elektrodinamiqkih mikrorezonatora, interagujui tamni polaritoni, vezani parovi tamnih polaritona, kvantna memorija za fo- tone i neureee

UNIVERSITY OF BELGRADE
FACULTY OF PHYSICS

Angelo Maggitti

FORMATION OF DARK-STATE POLARITONS AND TWO-POLARITON BOUND STATES IN ARRAYS OF ATOMS AND OPTICAL CAVITIES

Doctoral Dissertation

Belgrade, 2015.

УНИВЕРЗИТЕТ У БЕОГРАДУ
ФИЗИЧКИ ФАКУЛТЕТ

Анђело Мађити

ФОРМИРАЊЕ ТАМНИХ ПОЛАРИТОНА И ДВО-ПОЛАРИТОНСКИХ ВЕЗАНИХ СТАЊА У НИЗОВИМА АТОМА И ОПТИЧКИХ МИКРОРЕЗОНАТОРА

Докторска дисертација

Београд, 2015.

Committee members

dr Milan Radonjić, Thesis advisor
Research Associate
Photonics Center, Institute of Physics Belgrade, University of Belgrade

dr Branislav Jelenković, Thesis co-advisor
Principal Research Fellow
Photonics Center, Institute of Physics Belgrade, University of Belgrade

dr Milorad Kuraica
Full Professor
Faculty of Physics, University of Belgrade

dr Nikola Konjević
Full Professor Emeritus
Faculty of Physics, University of Belgrade

dr Milan Damnjanović
Full Professor
Faculty of Physics, University of Belgrade

Захвалница

На пруженој подршци током истраживања, а и ван сарадње на изради доктората, дубоко бих се захвалио ментору др Милану Радоњићу и коментору др Бранимиру Јеленковићу који су бројним дискусијама и саветима допринели стварању ове тезе и проширењу мог знања превашодно из области квантне оптике, али и из физике уопште.

Даље бих се захвалио колегама са Института за физику и Физичког факултета у Београду који су ми пружили подршку и пријатељство током целог доктората. Опуштена дружења и разговори који нису били непосредно везани за физику допринели су свеукупној позитивној атмосфери.

Такође желим да се захвалим пријатељима ван студијског програма који су ми улепшали тренутке упознавањем дивне архитектуре и културне баштине града Београда са једне стране, а са друге стране и богатог опуштајућег ноћног живота.

Својим дивним родитељима, мајци Гордани и оцу Алфреду желим најискреније да се захвалим на пруженој љубави и подршци, не само током доктората него и током целог свог живота.

Београд, 25. децембар 2015.

УНИВЕРЗИТЕТ У БЕОГРАДУ
ИНСТИТУТ ЗА ФИЗИКУ | БЕОГРАД
ИНСТИТУТ ОД НАЦИОНАЛНОГ ЗНАЧАЈА ЗА РЕПУБЛИКУ СРБИЈУ
Прегревица 118, 11080 Земун - Београд, Република Србија
Телефон: +381 11 3713000, Факс: +381 11 3162190, www.ipb.ac.rs
ПИБ: 100105980, Матични број: 07018029, Текући рачун: 205-66984-23

ПОТВРДА О РУКОВОЂЕЊУ ПОТПРОЈЕКТОМ

Овим потврђујем да научни сарадник **др Милан Радоњић** за кога се покреће избор у звање виши научни сарадник, у оквиру Лабораторије за примену рачунара у науци Националног центра изузетних вредности за изучавање комплексних система Института за физику у Београду, односно у оквиру пројекта ОН171017 „Моделирање и нумеричке симулације сложених вишечестичних система“ руководи потпројектом: „Утицај динамичког неуређења на особине Бозе-Ајнштајн кондензата“. На поменутом потпројекту су ангажовани следећи истраживачи: др Милан Радоњић, др Ивана Васић, др Владимир Лончар, др Антун Балаж, Владимир Вељић, Ана Худомал, Душан Вудраговић.

др Антун Балаж
научни саветник
Руководилац пројекта ОН171017
Руководилац Центра за изучавање комплексних
система Института за физику у Београду

Univ.Prof. DI Dr. Philip Walther
Quantum Information Science & Quantum Computing

Vice-Dean of the Faculty of Physics &
Speaker of the Quantum Optics, Quantum Nanophysics and Quantum Information Group &
Speaker of the Research Platform TURIS

Faculty of Physics & VCQ
Boltzmanngasse 5, A-1090 Vienna, Austria

Tel: +43 (1) 4277 72560
Email: philip.walther@univie.ac.at
Web: http://walther.quantum.at
http://turis.univie.ac.at

To whom it may concern

Vienna, September 21th, 2018

Dear ladies and gentlemen,

it is my great pleasure to write a letter of recommendation for Milan Radonjić, who has been part of my research group at the University of Vienna as a postdoctoral researcher. During his research he was the prime person in charge of managing the task of theoretical design of the quantum circuit for the six-photon benzene simulation within the European QUCHIP project, in which he proved himself very valuable regarding the efforts of the group as well as the project.

Milan Radonjić's results and achievements were of importance for ongoing experiments. Through his work he could demonstrate that he possesses a great creativity and a scientific insight in solving physical problems.

In conclusion, I give Milan Radonjić my high recommendation without any reservation.
Please send an e-mail or call me if you have any further questions.

With kind regards,

Philip Walther

Subject **Review_request RADONJIC** [redacted]
From <prl@aps.org>
To <milanr@ipb.ac.rs>
Date 2015-03-18 18:48

Re: [redacted]

Dear Dr. Radonjic,

We would appreciate your review of this manuscript, which has
been submitted to Physical Review Letters.

Comments from the editor:

> We sent this referral first to another referee, who now informs us
> that it has been passed to you. Since you will need personalized
> access to the referee server, we send you this electronic referral
> with pertinent instructions.We welcome you as a referee for the
> APS journals and thank you for any help you can give us. Since you
> are new, we would appreciate your checking and updating your
> record via our referee server (https://referees.aps.org/);
> particularly your contact information and expertise/interests. See
> http://journals.aps.org/referee-information for more information
> about reviewing for the Physical Review journals.
>
> Please be aware that to access our referee server you will need to
> have an active APS Journal account. For more information and to
> create an account please go to https://journals.aps.org/signup.

Thank you for your help.

Yours sincerely,

Daniel Ucko
Associate Editor
Physical Review Letters
Email: prl@aps.org
http://journals.aps.org/prl/

IMPORTANT: Editorial "Review Changes"
http://journals.aps.org/prl/edannounce/PhysRevLett.111.180001

We ask that you download the manuscript and return your report via:

[redacted]

Alternatively, you may send your completed Referee Response Form
by email to prl@aps.org. If you use email, either reply to this
message or give as the subject "Report RADONJIC [redacted]".

ABSTRACT:

[redacted]

FORMS AND MEMOS:

Please see the following:

> http://journals.aps.org/prl/referees/advice-referees-physical-review-letters

Subject **Review_request RADONJIć** [redacted]
From <prl@aps.org>
To <milanr@ipb.ac.rs>
Date 2015-12-18 05:23

Re: [redacted]

Dear Dr. Radonjić,

We would appreciate your review of this manuscript, which has
been submitted to Physical Review Letters.

Comments from the editor:

    This might be publishable science, but does it meet the Physical
    Review Letters criteria of impact, innovation, and interest?
    Please comment on this in your report.

Thank you for your help.

Yours sincerely,

Mu Wang
Associate Editor
Physical Review Letters
Email: prl@aps.org
http://journals.aps.org/prl/

IMPORTANT: Editorial "Review Changes"
http://journals.aps.org/prl/edannounce/PhysRevLett.111.180001

We ask that you download the manuscript and return your report via:

[redacted]

Alternatively, you may send your completed Referee Response Form
by email to prl@aps.org. If you use email, either reply to this
message or give as the subject "Report RADONJIć [redacted]".

ABSTRACT:

[redacted]

FORMS AND MEMOS:

Please see the following:

    http://journals.aps.org/prl/referees/advice-referees-physical-review-letters
      Advice to referees for Physical Review Letters

Physical Review Letters - REFEREE RESPONSE FORM

Insert X in the parentheses in the response form as appropriate.

 Referee: Dr. Radonjić,

 Manuscript Number: [redacted]

 Author: [redacted]

 Title: [redacted]

PRL aims to publish innovative work of significant impact and interest.
Your report and recommendation should address the basic question about
any possible Letter: Why should this paper be published in PRL, rather
than in the Physical Review, which also publishes papers that
significantly advance physics?

Subject **Review_request RADONJIć** [redacted]
From <prl@aps.org>
To <milanr@ipb.ac.rs>
Date 2017-05-03 15:48

Re: [redacted]

Dear Dr. Radonjić,

We would appreciate your review of this manuscript, which has
been submitted to Physical Review Letters.

Comments from the editor:

    This might be publishable science, but does it meet the Physical
    Review Letters criteria of impact, innovation, and interest?
    Please comment on this in your report.

Thank you for your help.

Yours sincerely,

Mu Wang
Associate Editor
Physical Review Letters
Email: prl@aps.org
http://journals.aps.org/prl/

IMPORTANT: Editorial "Review Changes"
http://journals.aps.org/prl/edannounce/PhysRevLett.111.180001

We ask that you download the manuscript and return your report via:

[redacted]

Alternatively, you may send your completed Referee Response Form
by email to prl@aps.org. If you use email, either reply to this
message or give as the subject "Report RADONJIć [redacted]".

ABSTRACT:

[redacted]

FORMS AND MEMOS:

Please see the following:

    http://journals.aps.org/prl/referees/advice-referees-physical-review-letters
      Advice to referees for Physical Review Letters

Physical Review Letters - REFEREE RESPONSE FORM

Insert X in the parentheses in the response form as appropriate.

 Referee: Dr. Radonjić,

 Manuscript Number: [redacted]

 Author: [redacted]

 Title: [redacted]

PRL aims to publish innovative work of significant impact and interest.
Your report and recommendation should address the basic question about
any possible Letter: Why should this paper be published in PRL, rather
than in the Physical Review, which also publishes papers that
significantly advance physics?

Subject **Manuscript [redacted] Optics Communications Review Request**
From Min Qiu <optcomm@zju.edu.cn>
Sender <ees.optics.631e.38f280.5e28d6e6@eesmail.elsevier.com>
To <milan.radonjic@ipb.ac.rs>
Date 2016-04-29 08:21

Dear Dr. Radonjić,

The following manuscript has been submitted for publication in Optics Communications:

Title: [redacted]
Authors: [redacted]
Manuscript: Please see web link below for access to manuscript PDF file and reviewing process.

Optics Communications has recently set stricter, higher standards for manuscript submissions, while still maintaining its aim to provide short publication times to authors. Submissions should offer clear evidence of novelty and significance. Papers devoted, for the most part, to mathematical and computational issues, with limited direct connection to current trends of optics research, are generally not suitable for publication in the Journal. Similarly, small technical advances, or papers concerned only with engineering applications or issues of materials science should not be considered favourably. Full guidelines for reviewers and authors can be found at:

http://www.elsevier.com/wps/find/journaldescription.cws_home/505711/authorinstructions

I would very much appreciate your opinion on the suitability of this paper for publication in Optics Communications. The report should be written constructively and tactfully, and be suitable for direct transmission to the author. You should state whether:

-the manuscript meets the acceptance criteria outlined above.
-the authors have properly acknowledged related research.
-the contents are expressed clearly, concisely and in proper English

If you accept this invitation, your comments will be due within 15 days. If you are unable to act as a reviewer at this time, I would greatly appreciate your suggestions for alternate reviewers.

For your convenience, below are the direct links to the individual functions for downloading the PDF file and accepting or declining the review. Make sure that you are NOT logged into the Elsevier Editorial System at the same time. The PDF file can only be downloaded once in this manner, but can also be retrieved the normal way by logging in to your reviewer homepage.

To accept the reviewer invitation please click the link below:
[redacted]

In order to view the PDF of the submission, please go to
[redacted]

However if you wish to decline it, please click the link below:
[redacted]

Please see the instructions below for submitting your review. If you need more time for your review, please let me know by replying to this email optcomm@zju.edu.cn

To submit your review (upload your review) -- please log into your EES reviewer homepage at:

http://ees.elsevier.com/optics/
Your username is: [redacted]

If you need to retrieve password details, please go to: http://ees.elsevier.com/OPTICS/automail_query.asp.

To update your personal classifications and keywords, please proceed to the following link:
[redacted]

As a reviewer you are entitled to complimentary access to Scopus and ScienceDirect for 30 days. Full instructions and details will be provided upon accepting this invitation to review.

In addition to accessing our subscriber content, you can also use our Open Access content. Read more about Open Access here: http://www.elsevier.com/openaccess

Upon submission of your review report to the system, you will get access to your personalized Elsevier reviews profile page as well as the possibility of creating a public page listing your reviews across all publishers in just a few steps! See http://www.reviewerrecognition.elsevier.com and http://www.reviewerpage.com for more information.

Sincerely,

Min Qiu, Ph.D.
Editor of Optics Communications

Reviewer Guidelines are now available to help you with your review:
http://www.elsevier.com/wps/find/reviewershome.reviewers/reviewersguidelines

Subject **Manuscript [redacted] Optics Communications Review Request**
From Myungshik Kim <eesserver@eesmail.elsevier.com>
Sender <eesserver@eesmail.elsevier.com>
To <milan.radonjic@ipb.ac.rs>
Reply-To Myungshik Kim <optcomm-editor@imperial.ac.uk>
Date 2018-04-15 09:08

Dear Dr. Radonjić,

The following manuscript has been submitted for publication in Optics Communications:

Title: [redacted]
Authors: [redacted]
Manuscript: Please see web link below for access to manuscript PDF file and reviewing process.

Optics Communications has recently set stricter, higher standards for manuscript submissions, while still maintaining its aim to provide short publication times to authors. Submissions should offer clear evidence of novelty and significance. Papers devoted, for the most part, to mathematical and computational issues, with limited direct connection to current trends of optics research, are generally not suitable for publication in the Journal. Similarly, small technical advances, or papers concerned only with engineering applications or issues of materials science should not be considered favourably. Full guidelines for reviewers and authors can be found at:

http://www.elsevier.com/wps/find/journaldescription.cws_home/505711/authorinstructions

I would very much appreciate your opinion on the suitability of this paper for publication in Optics Communications. The report should be written constructively and tactfully, and be suitable for direct transmission to the author. You should state whether:

-the manuscript meets the acceptance criteria outlined above.
-the authors have properly acknowledged related research.
-the contents are expressed clearly, concisely and in proper English

If you accept this invitation, your comments will be due within 15 days. If you are unable to act as a reviewer at this time, I would greatly appreciate your suggestions for alternate reviewers.

For your convenience, below are the direct links to the individual functions for downloading the PDF file and accepting or declining the review. Make sure that you are NOT logged into the Elsevier Editorial System at the same time. The PDF file can only be downloaded once in this manner, but can also be retrieved the normal way by logging in to your reviewer homepage.

To accept the reviewer invitation please click the link below:
[redacted]

In order to view the PDF of the submission, please go to
[redacted]

However if you wish to decline it, please click the link below:
[redacted]

Please see the instructions below for submitting your review. If you need more time for your review, please let me know by replying to this email optcomm-editor@imperial.ac.uk;m.kim@imperial.ac.uk

To submit your review (upload your review) -- please log into your EES reviewer homepage at:

https://ees.elsevier.com/optics/
Your username is: [redacted]

If you need to retrieve password details, please go to: http://ees.elsevier.com/OPTICS/automail_query.asp.

To update your personal classifications and keywords, please proceed to the following link:
https://ees.elsevier.com/optics/l.asp?i=452137&l=WNS4L1RJ

As a reviewer you are entitled to complimentary access to Scopus and ScienceDirect for 30 days. Full instructions and details will be provided upon accepting this invitation to review.

In addition to accessing our subscriber content, you can also use our Open Access content. Read more about Open Access here: http://www.elsevier.com/openaccess

Upon submission of your review report to the system, you will get access to your personalized Elsevier reviews profile page as well as the possibility of creating a public page listing your reviews across all publishers in just a few steps! See http://www.reviewerrecognition.elsevier.com and http://www.reviewerpage.com for more information.
Please also note that authors have been invited to convert their supplementary material into a Data in Brief article (a data description article). You may notice this change alongside the revised manuscript. You do not need to review this, but may need to look at the files in order to confirm that any supporting information you requested is present there.

Sincerely,

Myungshik Kim
Editor of Optics Communications

Reviewer Guidelines are now available to help you with your review:
http://www.elsevier.com/wps/find/reviewershome.reviewers/reviewersguidelines

Subject **Manuscript [redacted] for review**

From Optical and Quantum Electronics (OQEL) <em@editorialmanager.com>

Sender <em.oqel.0.57a73b.28f1493f@editorialmanager.com>

To Milan Radonjic <milan.radonjic@ipb.ac.rs>

Reply-To Optical and Quantum Electronics (OQEL) <sarvagnan.subramanian@springer.com>

Date 2017-12-03 20:13

Dear Dr. Radonjic,

In view of your expertise I would be very grateful if you could review the following manuscript which has been submitted to Optical and Quantum Electronics.

Manuscript Number: [redacted]

Title: [redacted]

Abstract: [redacted]

In case you are willing to review this submission please click on this link:

[redacted]

If you can not, or do not feel qualified, please click on this link:

[redacted]

We hope you are willing to review the manuscript. If so, would you be so kind as to return your review to us within
21 days of agreeing to review? Thank you.

You are requested to submit your review online by using the Editorial Manager.

Your username is: [redacted]
If you forgot your password, you can click the 'Send Login Details' link on the EM Login page at
http://oqel.edmgr.com/

IN ORDER TO KEEP DELAYS TO A MINIMUM, PLEASE ACCEPT OR DECLINE THIS ASSIGNMENT ONLINE AS SOON AS POSSIBLE!

If you have any questions, please do not hesitate to contact us. We appreciate your assistance.

With kind regards,
Guest Editors of S.I. : Photonica 2017
Springer Journals Editorial Office

Subject **[IJMPB] [redacted] Reviewer Invitation**
From Int. J. Mod. Phys. B (IJMPB) <em@editorialmanager.com>
Sender <em.ijmpb.0.5d7063.dc3d1c4f@editorialmanager.com>
To Milan Radonjic <milan.radonjic@ipb.ac.rs>
Reply-To Int. J. Mod. Phys. B (IJMPB) <ijmpb@wspc.com>
Date 2018-08-24 03:49

Journal Title: International Journal of Modern Physics B
Submission No.: [redacted]
Submission Title: [redacted]
Corresponding Author: [redacted]

Dear Prof Radonjic,

You are invited to help kindly referee the above paper.
The abstract of the paper is here:

[redacted]

To download the PDF of the paper, please click this link:
[redacted]

We look forward to receiving a response to this review request within the next three weeks. Please recommend rejection if the paper is not of acceptable quality.

****
To accept the review request, please click this link:
[redacted]
(The comments can be submitted online through the link. There you will find spaces for confidential comments to the editor, comments for the author and a blank report form. As it is desirable for scientific papers to be published in a timely manner, it will be ideal if the comments can be received in 25 days.)

To decline the review request, please click this link:
[redacted]
(We would be very much grateful if you can suggest the names of two possible referees with their email addresses so that this paper can get reviewed)

Please note that you will need to be logged off from the online review system (Editorial Manager) for the above links to function properly. If there are problems in the above links, please access Editorial Manager directly here:
https://ijmpb.editorialmanager.com/

Your username: [redacted]
Your password:
****

We hope you will accept our review request and we thank you in advance for your contribution, also on behalf of the authors.

Thank you for your contribution to the growth of quality scientific literature.

Best regards,

IJMPB Editor
WSPC Journal Office
International Journal of Modern Physics B
www.worldscinet.com/ijmpb

UNIVERSITY OF BELGRADE
INSTITUTE OF PHYSICS BELGRADE
Pregrevica 118, 11080 Zemun – Belgrade, Serbia
Tel: +381 11 3713000, Fax: +381 11 3162190, www.ipb.ac.rs

Dr Milan Radonjić
Assistant Research Professor
Photonics Center,
Center for Complex Systems,
Institute of Physics Belgrade,
Pregrevica 118, 11080 Belgrade,
Serbia

Belgrade, 21 November 2016

LETTER OF INVITATION

Dear Dr Radonjić,

On behalf of the Institute of Physics Belgrade, I cordially invite you to hold a talk in the forthcoming conference "Nikola Burić Memorial Workshop" that will be organized at the Institute of Physics Belgrade, Serbia, on 9-12 December 2016. Given your outstanding expertise in the field of hybrid quantum-classical systems, I am sure that the conference will significantly benefit from your impact. Please let us know whether you accept our invitation and provide us the preliminary title of your talk.

Sincerely yours,

Dr Igor Franović
Assistant Research Professor
E-mail: franovic@ipb.ac.rs
Scientific Computing Laboratory
Center for the Study of Complex Systems
Institute of Physics Belgrade

NIKOLA BURIĆ MEMORIAL WORKSHOP

9 December 2016, Institute of Physics Belgrade, Serbia

Book of Abstracts

Workshop chair

Antun Balaž

Co-chairs

Igor Franović

Slobodan Prvanović

Webpage: http://nbmw.scl.rs

Morning Session: Foundations of Quantum Mechanics and Quantum Complexity

9:45-10:00	**Opening of the Workshop**	**Antun Balaž Đorđe Šijački Branislav Jelenković**
10:00-10:30	**Quantum-to-classical Transition Through Coarse-grained Measurements**	**Časlav Brukner**
10:30-11:00	**Full Symmetry Implementation in Condensed Matter and Molecular Physics – Modified Group Projector Technique**	**Milan Damnjanović**
11:00-11:30	**Exploring the Boundaries of Quantum Mechanics**	**Hans-Thomas Elze**
11:30-11:45	**COFFEE BREAK**	
11:45-12:15	**Quantum Cryptography Beyond Key Distribution: Bit Commitment and Secure Multiparty Computation**	**Nikola Paunković**
12:15-12:45	**Hamiltonian Formulation of Hybrid Quantum-classical Systems**	**Milan Radonjić**
12:45-13:15	**Benefits of Generalizations in Different Topics**	**Dušan Arsenović**

LUNCH BREAK 13:15-14:30

Hamiltonian Formulation of Hybrid Quantum-classical Systems

Milan Radonjić[1,2,a)]

[1]*Scientific Computing Laboratory, Center for the Study of Complex Systems, Institute of Physics Belgrade, University of Belgrade, Pregrevica 118, 11080 Belgrade, Serbia*
[2]*Faculty of Physics, University of Vienna, Boltzmanngasse 5, 1090 Vienna, Austria.*

[a)]Corresponding author: milan.radonjic@ipb.ac.rs

In this talk an overview of the dynamical description of interacting quantum-classical systems will be given, based on a novel approach recently introduced by N. Burić and co-workers. General constrained Hamiltonian framework is applied to quantum systems in order to tackle the emergence of classical systems and their consistent joint treatment. Some results and emerging issues will be presented by following the development time-line of the approach.

Subject **Re: 'Condensates of Light' Heraeus Workshop: HOT TOPIC TALK?**

From Martin Weitz <weitz@uni-bonn.de>

To Milan Radonjić <milan.radonjic@ipb.ac.rs>

Cc <pelster@zedat.fu-berlin.de>, <r.nyman@imperial.ac.uk>, <jmjk@st-andrews.ac.uk>, <steinseifer@iap.uni-bonn.de>

Date 2018-01-08 08:17

Dear Dr. Radonjic,

thank you very much, we are looking forward to your talk.
(which will probably be Tuesday early afternoon).

Best regards,
  Martin Weitz

On Sun, 07 Jan 2018 21:29:59 +0100
 Milan Radonjić <milan.radonjic@ipb.ac.rs> wrote:

> Dear Prof. Weitz,
>
> thank you very much for the opportunity to deliver a hot topic talk. I am quite glad to accept it. The title is "Interplay of Coherent and Dissipative Dynamics in Condensates of Light" and the abstract you may find in the attachment.
>
> Best wishes,
> Milan Radonjic
>
> On 2018-01-05 18:40, Martin Weitz wrote:
>> Dear Dr. Radonjic,
>>
>> this email is to inquite whether you would be willing to deliver a hot
>> topic talk on a topic related to your recent preprint arXiv:1801.00155
>> on the upcoming condensates of light conference. If you accept this invitation,
>> please also send me a title of your talk very shortly (and best also
>> an abtract),
>> because we have to complete the program. The title could very well
>> id´dentical to
>> that of your preprint. We would be looking forward to your talk.
>>
>> Best regards,
>>   Martin Weitz
>>
>> ====================================
>> Prof. Dr. Martin Weitz
>>
>> Institut für Angewandte Physik der Universität Bonn
>> Wegeler Str. 8
>> 53115 Bonn
>> Germany
>> Tel: +49-(0)228-73-4837/4836
>> Fax: +49-(0)228-73-4835
>> e-mail: martin.Weitz@uni-bonn.de
>>
>> https://www.qo.uni-bonn.de/
>> ====================================
>
> ---
> Милан Радоњић
> Научни сарадник
> Центар за фотонику,
> Центар за изучавање комплексних система,
> Институт за физику Београд,
> Прегревица 118, 11080 Београд, Србија
> http://www.scl.rs/milan/
> ---
> Milan Radonjić
> Assistant Research Professor
> Photonics Center,
> Center for Complex Systems,
> Institute of Physics Belgrade,
> Pregrevica 118, 11080 Belgrade, Serbia
> http://www.scl.rs/milan/

WILHELM UND ELSE HERAEUS-STIFTUNG

WE-Heraeus-Stiftung, Postfach 15 53, D-63405 Hanau

Telefon (06181) 92325-0
Fax (06181) 92325-15
Internet www.we-heraeus-stiftung.de

Bearbeitung Elisabeth Nowotka
Durchwahl (06181) 92325-12
E-Mail nowotka@we-heraeus-stiftung.de

Teilnahme-Bestätigung-mTitel_e-Std.doc

CERTIFICATION

October 2017

This is to certify that

Dr. Milan Radonjic
Institute of Physics Belgrade /Serbia

has participated in our seminar

659. WE-Heraeus-Seminar on

'Condensates of Light'

January 14 – 17, 2018 at the Physikzentrum Bad Honnef (Germany)

and has contributed to the scientific program with a hot topic talk, entitled
"Interplay of Coherent and Dissipative Dynamics in Condensates of Light

and a poster, entitled
"Modeling dye-mediated contribution to photon-photon interaction in condensates of light".

Nowotka

Elisabeth Nowotka
(Seminar Organization)

Interplay of Coherent and Dissipative Dynamics in Condensates of Light

M. Radonjić[1,3], W. Kopylov[2], A. Balaž[1], and A. Pelster[3]

[1]*Center for the Study of Complex Systems, Institute of Physics Belgrade, University of Belgrade, Serbia*
[2]*Institute for Theoretical Physics, Technische Universität Berlin, Germany*
[3]*Physics Department and Research Center OPTIMAS, Technische Universität Kaiserslautern, Germany*
E-mail: milan.radonjic@ipb.ac.rs, radonjic@rhrk.uni-kl.de

Based on the Lindblad master equation approach, we obtain a detailed microscopic model of photons in a dye-filled cavity, which features condensation of light [1-3]. To this end, we generalize a recent non-equilibrium approach of Kirton and Keeling [4], such that the dye-mediated contribution to the photon-photon interaction in the photon condensate is accessible due to an interplay of coherent and dissipative dynamics [5]. We describe the steady-state properties of the system by analyzing the resulting equations of motion of both photonic and matter degrees of freedom. In particular, we discuss the existence of two limiting cases for steady states: photon Bose-Einstein condensate and laser-like regime. In the former case, we determine the corresponding dimensionless photon-photon interaction strength by relying on realistic experimental data and find a good agreement with previous theoretical estimates [6]. Furthermore, we investigate how the dimensionless interaction strength depends on the respective system parameters.

References

[1] J. Klaers, J. Schmitt, F. Vewinger, and M. Weitz, Nature **468**, 545 (2010).
[2] R. A. Nyman and M. H. Szymanska, Phys. Rev. A **89**, 033844 (2014).
[3] S. Greveling, K. L. Perrier, D. van Oosten, arXiv:1712.07888 (2017).
[4] P. Kirton and J. Keeling, Phys. Rev. Lett. **111**, 100404 (2013).
[5] M. Radonjić, W. Kopylov, A. Balaž, A. Pelster, arXiv:1801.00155 (2017).
[6] E. C. I. van der Wurff, A.-W. de Leeuw, R. A. Duine, and H. T. C. Stoof, Phys. Rev. Lett. **113**, 135301 (2014).

WILHELM UND ELSE HERAEUS-STIFTUNG

WE-Heraeus-Stiftung, Postfach 15 53, D-63405 Hanau

Telefon (06181) 92325-0
Fax (06181) 92325-15
Internet www.we-heraeus-stiftung.de

Bearbeitung Elisabeth Nowotka
Durchwahl (06181) 92325-12
E-Mail nowotka@we-heraeus-stiftungde

Teilnahme-Bestätigung-mTitel_e-Std.doc

CERTIFICATION

May 2016

This is to certify that

Dr. Milan Radonjic
University of Vienna/Austria

has participated in our seminar

616. WE-Heraeus-Seminar on

**Ultracold Quantum Gases -
Current Trends and Future Perspectives**

**9 – 13 May 2016
at the Physikzentrum Bad Honnef (Germany)**

and has contributed to the scientific program with a contributed talk, entitled

"Microscopic Model of Photon Condensation".

Nowotka

Elisabeth Nowotka
(Seminar Organization)

Microscopic Model of Photon Condensation

M. Radonjić[1,3], W. Kopylov[2], T. Brandes[2], A. Balaž[3], and A. Pelster[4]

[1]Faculty of Physics, University of Vienna, Austria
[2]Institute for Theoretical Physics, Technische Universität Berlin, Germany
[3]Institute of Physics Belgrade, University of Belgrade, Serbia
[4]Physics Department and Research Center OPTIMAS, Technische Universität Kaiserslautern, Germany
E-mail: milan.radonjic@univie.ac.at

Convincing evidence of macroscopic occupation of the lowest mode for a gas of photons confined in a dye-filled optical microcavity has been first presented in a seminal experiment in Bonn [1] and recently also in London [2]. Thermal relaxation of the dye molecules due to interaction with solvent gives rise to a Bose-Einstein distribution of the microcavity photons in the experiment. These equilibrium properties could recently be understood within the framework of a non-equilibrium description [3,4]. We critically analyze and extend this description by including coherent coupling between the dye molecules and the microcavity photons, influenced by the solvent, in addition to a dissipative coupling that leads to thermalization. Interestingly, we find that strong interaction of the dye molecules with the solvent favors the thermalization dynamics and makes possible Bose-Einstein condensation of photons. On the other hand, weak solvent influence promotes the coherent dynamics and enables the formation of a laser-like state. Depending on the values of experimental parameters different optical cavity modes may become macroscopically occupied. The onset of the latter behavior has recently been noticed in a simplistic two-mode laser model [5] that can be seen as a minimalistic precursor of the detailed model of photon condensation.

References

[1] J. Klaers, J. Schmitt, F. Vewinger, and M. Weitz, Nature (London) **468**, 545 (2010)
[2] J. Marelic and R. A. Nyman, Phys. Rev. A **91**, 033813 (2015)
[3] P. Kirton and J. Keeling, Phys. Rev. Lett. **111**, 100404 (2013)
[4] P. Kirton and J. Keeling, Phys. Rev. A **91**, 033826 (2015)
[5] W. Kopylov, M. Radonjić, T. Brandes, A. Balaž, and A. Pelster, Phys. Rev. A **92**, 063832 (2015)

Book of abstracts

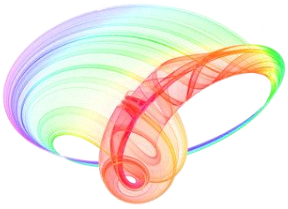

PHOTONICA2017

The Sixth International School and Conference on Photonics

& COST actions: MP1406 and MP1402

&H2020-MSCA-RISE-2015 CARDIALLY workshop

28 August – 1 September 2017

Belgrade, Serbia

Editors

Marina Lekić and Aleksandar Krmpot

Institute of Physics Belgrade, Serbia

Belgrade, 2017

Progress reports

1. Quantum optics and ultracold systems

Photonic simulation of open quantum systems with various exchange statistics

Milan Radonjić[1, 2] and Philip Walther[1]
[1]*Faculty of Physics, University of Vienna,*
Vienna, Austria
[2]*Institute of Physics Belgrade,*
Belgrade, Serbia
e-mail: milan.radonjic@univie.ac.at, milan.radonjic@ipb.ac.rs

Photonic quantum technology has reached a point where it is almost viable to use photonic setups to simulate the behavior of other quantum systems. Realistic quantum systems are inevitably influenced by the external environment – they are open. When the environment introduces pronounced memory effects, one speaks of non-Markovianity. The need to understand and the possibility of exploiting this phenomenon as a potential resource for quantum information tasks has spurred an increasing interest in generating and manipulating non-Markovian quantum dynamics using various experimental platforms, including photonic setups.

The essentially distinct dynamical behavior of quantum entities obeying different exchange statistics (e.g., bosonic, fermionic or anyonic) has to leave a marked signature on non-Markovianity. We will describe the project that ultimately aims to emphasize and to explore theoretically the versatility of photonic setups for simulating and studying the interplay between various exchange statistics and quantum non-Markovianity, with the ultimate goal of identifying and experimentally validating the benefits for quantum information applications.

Verhandlungen der Deutschen Physikalischen Gesellschaft e.V.

Erlangen 2018 – scientific program

Q: Fachverband Quantenoptik und Photonik

Q 37: Quantum Gases (Bosons) IV

Tuesday, March 6, 2018, 14:00–16:00, K 2.020

Selection status for this session: not selected

⊕ 14:00 Q 37.1 Fluctuation-dissipation relations and finite compressibility of a grand canonical Bose-Einstein condensate — •Fahri Emre Ozturk, Tobias Damm, David Dung, Christian Kurtscheid, Erik Busley, Frank Vewinger, Julian Schmitt, and Martin Weitz

⊖ 14:15 Q 37.2 Modeling Dye-Mediated Photon-Photon Interaction in Condensates of Light — •Milan Radonjić, Wassilij Kopylov, Antun Balaž, and Axel Pelster

selection status for this contribution: according to the sessions' setting

Modeling Dye-Mediated Photon-Photon Interaction in Condensates of Light — •Milan Radonjić[1], Wassilij Kopylov[2], Antun Balaž[1], and Axel Pelster[3] — [1]Institute of Physics Belgrade, University of Belgrade, Serbia — [2]Department of Physics, Technische Universität Berlin, Germany — [3]Department of Physics and Research Center OPTIMAS, Technische Universität Kaiserslautern, Germany

Based entirely on the Lindblad master equation approach we obtain a microscopic description of photons in a dye-filled cavity, which features condensation of light [1,2]. To this end we generalize the nonequilibrium approach of Ref. [3] such that the dye-mediated contribution to the photon-photon interaction in the light condensate is accessible. We describe the dynamics of the system by analyzing the resulting equations of motion. In particular, we discuss the existence of two limiting cases for steady states: photon BEC and laser-like. In the former case, we determine the corresponding dimensionless interaction strength relying on realistic experimental data and find a good agreement with the previous theoretical estimate [4]. Furthermore, we investigate how the dimensionless interaction strength depends on the respective system parameters such as the effective temperature of the dye and the number of the dye molecules.

[1] J. Klaers et al., Nature **468**, 545 (2010)

[2] R. A. Nyman and M. H. Szymanska, Phys. Rev. A **89**, 033844 (2014)

[3] P. Kirton and J. Keeling, Phys. Rev. Lett. **111**, 100404 (2013)

[4] E. C. I. van der Wurff et al., Phys. Rev. Lett. **113**, 135301 (2014)

⊕ 14:30 Q 37.3 Photon Condensates in Microstructured Trapping Potentials — •Christian Kurtscheid, David Dung, Erik Busley, Julian Schmitt, Tobias Damm, Frank Vewinger, Jan Klärs, and Martin Weitz

⊕	14:45	Q 37.4	QED treatment of the photon BEC in arbitrary geometries: Coupled dissipative dynamics of dye molecules — •Yaroslav Gorbachev, Robert Bennett, and Stefan Yoshi Buhmann
⊕	15:00	Q 37.5	Mode selection in a system of photons in a dye-filled microcavity — •Martina Vlaho, Daniel Vorberg, Alexander Leymann, and André Eckardt
⊕	15:15	Q 37.6	Towards photon Bose-Einstein condensation in a quantum dot microcavity — •Thilo vom Hövel, Christian Kurtscheid, David Dung, Erik Busley, Tobias Damm, Hadiseh Alaeian, Frank Vewinger, and Martin Weitz
⊕	15:30	Q 37.7	Collective Frequencies of Trapped Photon Bose-Einstein Condensate — •Enrico Stein and Axel Pelster
⊕	15:45	Q 37.8	Towards a Photon Bose-Einstein Condensate in the Vacuum-Ultraviolet Spectral Regime — •Christian Wahl, Marvin Hoffmann, Frank Vewinger, and Martin Weitz

Bulletin of the American Physical Society

49th Annual Meeting of the APS Division of Atomic, Molecular and Optical Physics APS Meeting
Monday–Friday, May 28–June 1 2018; Ft. Lauderdale, Florida

Session V03: Bose-Einstein Condensates
10:30 AM–12:30 PM, Friday, June 1, 2018
Room: Grand B

Chair: Robert Smith, University of Oxford

Abstract: V03.00002 : Interplay of Coherent and Dissipative Dynamics in Condensates of Light*
10:42 AM–10:54 AM

Preview Abstract

← Abstract →

Authors:
Milan Radonjic
(Technical University of Kaiserslautern, Germany)

Wassilij Kopylov
(Technical University of Berlin, Germany)

Antun Balaz
(Institute of Physics Belgrade, Serbia)

Axel Pelster
(Technical University of Kaiserslautern, Germany)

Based on the Lindblad master equation approach we obtain a detailed microscopic model of photons in a dye-filled cavity, which features condensation of light. To this end we generalise a recent non-equilibrium approach of Kirton and Keeling such that the dye-mediated contribution to the photon-photon interaction in the light condensate is accessible due to an interplay of coherent and dissipative dynamics. We describe the steady-state properties of the system by analysing the resulting equations of motion of both photonic and matter degrees of freedom. In particular, we discuss the existence of two limiting cases for steady states: photon Bose-Einstein condensate and laser-like. In the former case, we determine the corresponding dimensionless photon- photon interaction strength by relying on realistic experimental data and find a good agreement with previous theoretical estimates. Furthermore, we investigate how the dimensionless interaction strength depends on the respective system parameters.

*DAAD, DFG via SFB 910, SFB/TR49, SFB/TR185, EU via QUCHIP, grant No. 641039

Dear members of the SFB/TR49,

we would like to draw your attention to our TR49 colloquium in **Kaiserslautern**.

Thursday
November 19th, 2015
15:30

Fachbereich Physik
TU Kaiserslautern
Erwin-Schroedinger-Str.
Gebäude 46
Raum 46-576

Dr. Milan Radonjić
University of Vienna, AUSTRIA and
Institute of Physics Belgrade, SERBIA

"Microscopic model of photon condensation"

For more detailed information please see the leaflet attached.

With kind regards,
Dietlinde Gebauer

Dietlinde Gebauer
Sekretariat SFB/TR 49
"Condensed Matter Systems with Variable Many-Body Interactions"

Physikalisches Institut
Johann Wolfgang Goethe-Universitaet Frankfurt
Campus Riedberg
Max-von-Laue-Str. 1
60438 Frankfurt am Main | Germany
Tel.: +49 (0)69-798-47248
Fax: +49 (0)69-798-47249
E-Mail: Gebauer@Physik.uni-frankfurt.de
www.tr49.de

Einladung zum

SFB/TR 49 KOLLOQUIUM
Kaiserslautern

Donnerstag,
19. November 2015
15:30 Uhr

Fachbereich Physik
TU Kaiserslautern
Erwin-Schroedinger-Str.
Gebäude 46
Raum 46-576

Dr. Milan Radonjić
University of Vienna, AUSTRIA and
Institute of Physics Belgrade, SERBIA

Microscopic model of photon condensation

Convincing evidence of macroscopic occupation of the lowest mode for a gas of photons confined in a dye-filled optical microcavity has been first presented in a seminal experiment in Bonn [1] and recently also in London [2]. Thermal relaxation of the dye molecules due to interaction with the solvent gives rise to a Bose-Einstein distribution of the microcavity photons in the experiment.

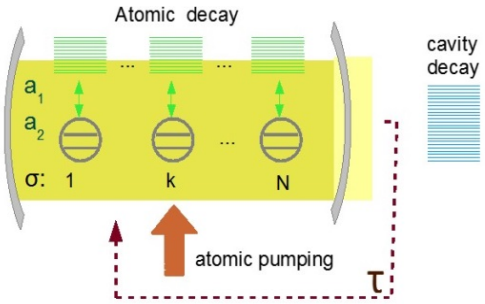

These equilibrium properties could recently be understood within the frame- work of a non-equilibrium description [3]. We will critically analyze and extend this description by including coherent coupling between dye molecules and microcavity photons, influenced by the solvent, in addition to a dissipative coupling that leads to the thermalization. Interestingly, our prelimnary results indicate that the strong interaction of the dye molecules with the solvent favors the thermalization dynamics and makes possible Bose-Einstein condensation of photons.

On the other hand, weak solvent influence promotes the coherent dynamics and enables the formation of a laser-like state. Depending on the values of experimental parameters different optical cavity modes may become macroscopically occupied. The onset of the latter behavior has recently been noticed in a simplistic two-mode laser model [4] that can be seen as a minimalistic precursor of the detailed model of photon condensation.

References

[1] J. Klaers, J. Schmitt, F. Vewinger, and M. Weitz, Nature (London) **468**, 545 (2010)
[2] J. Marelic and R. A. Nyman, Phys. Rev. A **91**, 033813 (2015)
[3] P. Kirton and J. Keeling, Phys. Rev. Lett. **111**, 100404 (2013); Phys. Rev. A **91**, 033826 (2015)
[4] W. Kopylov, M. Radonjić, T. Brandes, A. Balaž, and A. Pelster, *arXiv:1507.01811*

New Journal of Physics
The open access journal at the forefront of physics

Deutsche Physikalische Gesellschaft DPG
IOP Institute of Physics

Published in partnership with: Deutsche Physikalische Gesellschaft and the Institute of Physics

OPEN ACCESS

RECEIVED
30 December 2017

REVISED
16 April 2018

ACCEPTED FOR PUBLICATION
4 May 2018

PUBLISHED
31 May 2018

PAPER

Interplay of coherent and dissipative dynamics in condensates of light*

Milan Radonjić[1,2,3], **Wassilij Kopylov**[4], **Antun Balaž**[1] **and Axel Pelster**[3]

[1] Scientific Computing Laboratory, Center for the Study of Complex Systems, Institute of Physics Belgrade, University of Belgrade, Serbia
[2] Faculty of Physics, University of Vienna, Austria
[3] Physics Department and Research Center OPTIMAS, Technische Universität Kaiserslautern, Germany
[4] Institute for Theoretical Physics, Technische Universität Berlin, Germany

E-mail: milan.radonjic@ipb.ac.rs

Keywords: photon Bose–Einstein condensate, photon–photon interaction, open dissipative quantum systems

Abstract

Based on the Lindblad master equation approach we obtain a detailed microscopic model of photons in a dye-filled cavity, which features condensation of light. To this end we generalise a recent non-equilibrium approach of Kirton and Keeling such that the dye-mediated contribution to the photon–photon interaction in the light condensate is accessible due to an interplay of coherent and dissipative dynamics. We describe the steady-state properties of the system by analysing the resulting equations of motion of both photonic and matter degrees of freedom. In particular, we discuss the existence of two limiting cases for steady states: photon Bose–Einstein condensate and laser-like. In the former case, we determine the corresponding dimensionless photon–photon interaction strength by relying on realistic experimental data and find a good agreement with previous theoretical estimates. Furthermore, we investigate how the dimensionless interaction strength depends on the respective system parameters.

1. Introduction

Within the last decades open dissipative many-body quantum systems have emerged as a promising research direction for both basic research and applications. In particular, this is due to the development of exquisite technologies to coherently manipulate and control the internal and external degrees of freedom of atomic and photonic matter, as well as their interaction. A prominent example at the immediate interface of quantum optics and condensed matter physics is provided by the laser as a coherent light source which has contributed not only to our modern understanding of non-equilibrium phase transitions in general but even to many useful applications in our everyday life [1–4].

Another more modern prominent object of research is the Bose–Einstein condensate (BEC) of light, which has so far been realised in a dye-filled microcavity at room temperature in Bonn [5], in London [6], and quite recently also in Utrecht [7]. One of the key ingredients is the possibility of photons to acquire an effective mass by trapping them in a cavity in two dimensions—without this, the photons would just disappear according to the Planck law upon lowering the temperature. In the experiment, this is achieved via a curved-mirror cavity, which changes the dispersion relation of the photons from linear to quadratic. Along the resonator axis the frequency of the mode is quantised according to the resonance condition. Simultaneously, the curved mirrors create a harmonic trapping potential for the photons in the transverse direction. The next crucial element is given by dye molecules in the resonator, which are pumped incoherently. The multiple absorption and emission events between the cavity photons and the dye molecules lead to a thermalisation of the light [8], so the resulting photon BEC emerges from an equilibrium phase transition [9–11]. Photon thermalisation was also shown to be possible in much simpler but periodically driven systems, such as double quantum dots [12], or a collection of

* This paper is dedicated to the memory of Tobias Brandes

harmonic modes [13], both coupled to some environment. Recently, an elaborate theoretical proposal for a BEC of light in nanofabricated semiconductor micro-cavities has been put forward [14].

The usual atomic BEC as a thermal equilibrium phase transition occurs for temperatures below some critical value [15, 16] when the resulting ground-state condensate acquires macroscopic occupation, while the populations of the higher energy levels obey the Bose–Einstein distribution even before the transition. Phase transition into a macroscopically occupied mode emerges as well in a controllable way in the laser case, but—in contrast to the BEC—this transition depends on the rate of the loss and the pumping channels, which makes it a non-equilibrium paradigm. The two transitions, which *a priori* seem to be incompatible with each other due to their different nature, can thus be regarded as two sides of the same coin within a single non-equilibrium setup [17]. Several studies concerning the similarities and differences of condensate and lasing states and their appearance in different systems exist [18–23]. The investigation of systems and conditions under which a complex equilibrium state can be realized within a non-equilibrium setup has developed into an attractive topic, both in experiment and theory.

Apart from photonic systems, condensation effects of bosonic quasi-particles have also been observed in solid-state physics for magnons [24–28] and exciton polaritons [29–34]. The latter quasi-particles can be created in semiconductor micro-cavities using strong coupling between photons and particle-hole excitations [29]. A non-equilibrium BEC of polaritons has been observed in various experiments in polymers [35, 36]. Surprisingly, the transition therein is not always restricted to a mode with the lowest momentum [37].

The first microscopic model of a photon condensate was developed by Kirton and Keeling [38, 39], which has recently been further extended by the same authors [40, 41]. They considered a dye-filled cavity with multiple optical modes together with additional incoherent pump and loss channels and derived a Markovian quantum master equation of the Lindblad type [42, 43]. Using an adiabatic elimination of the degrees of freedom of the dye molecules, Kirton and Keeling obtained a mean-field equation for the occupation of the cavity modes. The resulting steady-state turned out to have different physical properties depending on the values of the respective system parameters. Provided that the relaxation time towards equilibrium is much shorter than the life time of the photons in the cavity, the steady-state is given by a Bose–Einstein distribution, otherwise a laser-like state occurs having macroscopic occupation of a higher energy mode. Inspired by such a behaviour, a minimal two-mode laser model with a Dicke-like interaction was investigated [44]. Different phases with up to four possible and up to two stable fixed points were found, some of which have an analogy to the laser-to-condensate-like transition. However, this analogy is only quite limited due to the absence of a temperature scale in the model. Quite recently, by considering the full spatial dynamics of light [40] a rich non-equilibrium phase diagram featuring Bose–Einstein condensation, multimode condensation and lasing has been demonstrated [45]. On the other side, by using the Schwinger–Keldysh formalism a Langevin field equation describing the dynamics of photons in a dye-filled cavity was obtained [46] and later utilised to study phase fluctuations [47] and phase diffusion [48] in such systems. Moreover, a quantum Langevin model for non-equilibrium condensation of photons in planar microcavity devices was developed in [49] and recently extended to address pseudo-thermalisation in driven-dissipative non-Markovian open quantum systems [50]. A theoretical description of a photon condensate based on three-dimensional Maxwell equations, which are mapped via a paraxial approximation to a two-dimensional Schrödinger equation, was suggested as well [51]. We also note that a unified theory for excited-state, fragmented and equilibrium-like Bose condensation in pumped photonic many-body systems has recently been introduced in [52].

The theoretical modelling of dissipative condensates usually strives for a reduced description in terms of a mean-field approximation in the form of a complex-valued Gross–Pitaevskii equation, which explicitly takes into account gains and losses. It describes the system around this phase transition even in non-equilibrium [53–55]. Within equilibrium, a real-valued Gross–Pitaevskii equation is a standard tool to describe condensation effects [15, 16, 56–59]. At the present stage, the Gross–Pitaevskii-like equation for a photon condensate can only be obtained by including a nonlinear self-interaction into the model on a phenomenological level [5, 49, 51]. A more detailed investigation shows that this nonlinear self-interaction of photons is mediated via the change of the refractive index of the dye molecules due to the mutual presence of the optical Kerr and the thermo-optical effect [60]. Due to dimensional reasons the effective photon–photon interaction strength g in two spatial dimensions corresponds to a dimensionless number $\tilde{g} = gm/\hbar^2$ [61], which turns out to be of the order of $10^{-9} - 10^{-8}$ for the Kerr and 10^{-4} for the thermo-optic effect, respectively [60]. Based on the observed momentum- and position-resolved spectra and images of the photoluminescence from thermalised and condensed dye-microcavity photons, the upper bound $\tilde{g} \lesssim 10^{-3}$ was obtained [62]. In addition, a theoretical investigation of the influence of photon–photon interaction on the number fluctuations in a BEC of light [63] successfully explained the measurements [64] and estimated the range $\tilde{g} \sim 10^{-8} - 10^{-7}$. Surprisingly, even a much higher value for the interaction $\tilde{g} \sim 10^{-2}$ was recently measured [65].

In this paper we generalise the microscopic model of the photon BEC by Kirton and Keeling [38, 39] such that the dye-mediated contribution to the photon–photon interaction strength becomes microscopically

accessible due to an interplay of coherent and dissipative dynamics. To this end, in section 2 we work out in detail the underlying model and discuss its improvements in comparison to [38, 39]. Based on the corresponding Lindblad master equation, we derive the resulting equations of motion of expectation values of the relevant system operators. In section 3 we determine the realistic model parameters in relation to current experiments. We then proceed in section 4 to analyse the steady-state properties of the system and identify the two limiting cases: a photon BEC and a laser-like regime. The latter one is novel and accessible precisely due to the inclusion of the coherent dynamics. For the former case, in section 5 we determine the dye-mediated dimensionless photon–photon interaction strength from realistic experimental data and, in particular, how it depends on the respective system parameters. Section 6 presents our concluding remarks.

2. Model

Let us now introduce a physical system which encompasses both laser and photon BEC as the possible limiting cases. This is going to be done in close correspondence with the actual experimental setups of photon BEC experiments. We consider N identical non-interacting two-level systems (TLS) inside an optical cavity. The transition between the two levels has the frequency Δ and it is nearly resonant with M modes of the cavity. The dipole coupling between the TLS and the cavity modes has the strength g and it is assumed to be sufficiently weak so that the rotating wave approximation (RWA) holds. In the photon BEC experiments, the TLS were actually dye molecules dissolved in a solvent. The dye molecules have very broad rovibrational absorption and emission spectra, which can be modelled as an on-site phonon coupled to its own thermal bath [38, 39]. In addition, due to frequent collisions with the solvent particles the dye molecules experience rapid dephasing. Hence, we take that each of the TLS is coupled to its own reservoir of $R \gg 1$ harmonic oscillators. This can be thought of as a compound reservoir consisting of a phonon and its bath. The reservoirs are supposed to be independent and of identical properties. The collisional dephasing rate of each TLS is denoted by γ_ϕ. We also assume that the TLS are incoherently pumped to the excited-state with the rate $\gamma_\uparrow$ and decay to the ground-state with the rate $\gamma_\downarrow$ via spontaneous emission of photons outside of the cavity. The decay rate of all cavity modes is abbreviated by κ. A conceptually similar system has previously been treated by Kirton and Keeling [38, 39] using a mixture of the master equation and the Schwinger–Keldysh formalisms, but without accounting for the dephasing quantitatively. Our approach, instead, is based entirely on the master equation formalism and we improve several aspects of their model. Later on we underline those specific points and our enhancements that enable us to have access to a completely different regime of physical parameters.

In reality, the coupling between TLS and some cavity mode will also depend on the spatial mode function. A tractable model that incorporates the spatial dynamics was devised by Keeling and Kirton [40]. It has led to the successful understanding of the recent experiments [6, 17]. However, the spatial dynamics introduces yet another level of complexity to the theoretical description. It could be implemented in our approach as well, but that would make the numerical calculations an order of magnitude more challenging. Thus, in the present work we make two additional simplifying assumptions: (*i*) all TLS are at exactly the same position and (*ii*) all cavity modes have the same intensity at the position of the TLS. This means that all TLS can be considered to evolve in an equivalent manner. Later on we will indicate how these assumptions may influence some of our results.

2.1. Master equation

Due to the above mentioned assumptions we consider the system Hamiltonian ($\hbar = 1$)

$$H = \sum_{m=1}^{M} \omega_m a_m^\dagger a_m + \sum_{j=1}^{N} H_{\downarrow\uparrow,\mathrm{R}}^{(j)} + V_{\downarrow\uparrow,\mathrm{C}}, \tag{1a}$$

$$H_{\downarrow\uparrow,\mathrm{R}}^{(j)} = \frac{\Delta}{2}\sigma_j^z + \sum_{r=1}^{R}[w_r b_{j,r}^\dagger b_{j,r} + \lambda_r(b_{j,r}^\dagger + b_{j,r})\sigma_j^z], \tag{1b}$$

$$V_{\downarrow\uparrow,\mathrm{C}} = g\sum_{m=1}^{M}\sum_{j=1}^{N}(a_m^\dagger \sigma_j^- + a_m \sigma_j^+), \tag{1c}$$

where ω_m denote the cavity-mode frequencies and a_m ($a_m^\dagger$) the bosonic annihilation (creation) operators of the cavity modes. The Hamiltonian $H_{\downarrow\uparrow,\mathrm{R}}^{(j)}$ describes the jth TLS and its reservoir, with $\sigma_j^\pm$ and σ_j^z being its Pauli spin operators. Bosonic annihilation (creation) operators and frequencies of the reservoir oscillators are $b_{j,r}$ ($b_{j,r}^\dagger$) and w_r, respectively, while λ_r are the appropriate interaction strengths. Since the experimental spectra of the dye molecules are very broad, we are led to assume that the TLS-reservoir coupling is strong. In order to treat it non-perturbatively to all orders, we perform the polaron transformation $\tilde{H} = UHU^\dagger$ with

$$U = \exp\left[\sum_{j=1}^{N}\sigma_j^z\sum_{r=1}^{R}\frac{\lambda_r}{w_r}(b_{j,r}^\dagger - b_{j,r})\right], \tag{2}$$

and find

$$\tilde{H} = \sum_{m=1}^{M}\omega_m a_m^\dagger a_m + \sum_{j=1}^{N}\frac{\Delta}{2}\sigma_j^z + \tilde{V}_{\downarrow\uparrow,\mathrm{C}} + \sum_{j=1}^{N}H_{\mathrm{R}}^{(j)}, \tag{3a}$$

$$\tilde{V}_{\downarrow\uparrow,\mathrm{C}} = g\sum_{m=1}^{M}\sum_{j=1}^{N}(a_m^\dagger\sigma_j^- D_j^- + a_m\sigma_j^+ D_j^+), \quad H_{\mathrm{R}}^{(j)} = \sum_{r=1}^{R}w_r b_{j,r}^\dagger b_{j,r}, \tag{3b}$$

up to constant terms, where

$$D_j^\pm = \otimes_{r=1}^{R}\exp\left[\pm\frac{2\lambda_r}{w_r}(b_{j,r}^\dagger - b_{j,r})\right] \tag{4}$$

are the polaron displacement operators of the jth TLS. In this way, $\tilde{V}_{\downarrow\uparrow,\mathrm{C}}$ captures the coupling of the TLS and the cavity modes which is dressed by the reservoir oscillators.

In order to proceed further, we assume that the oscillators in the polaron frame represent a bath in a thermal state at temperature T

$$\rho_\beta = Z_\beta^{-1}\otimes_{j=1}^{N}\exp[-\beta H_{\mathrm{R}}^{(j)}], \tag{5}$$

where Z_β stands for the canonical partition function and $\beta = 1/(k_{\mathrm{B}}T)$ [66]. We consider such initial conditions that the subsystem TLS-cavity is uncorrelated with the bath in the polaron frame, i.e., $\rho_{\mathrm{total}} = \rho_{\downarrow\uparrow,\mathrm{C}}\otimes\rho_\beta$. Since the coupling strength g is supposed to be weak, the bath influence can be incorporated by means of a master equation, i.e., by treating $\tilde{V}_{\downarrow\uparrow,\mathrm{C}}$ as a perturbation up to the second order [67, 68]. The first order contributes to the coherent unitary evolution through the thermal-averaged term

$$\langle\tilde{V}_{\downarrow\uparrow,\mathrm{C}}\rangle_\beta = g\sum_{m=1}^{M}\sum_{j=1}^{N}(a_m^\dagger\sigma_j^-\langle D_j^-\rangle_\beta + a_m\sigma_j^+\langle D_j^+\rangle_\beta), \tag{6}$$

where we introduced the notation $\langle X\rangle_\beta \equiv \mathrm{Tr}[X\rho_\beta]$ for a bath expectation value. Using the result

$$\langle\exp[\alpha b^\dagger - \alpha^* b]\rangle_\beta = \exp\left[-\frac{|\alpha|^2}{2}\coth\frac{\beta\omega}{2}\right], \tag{7}$$

for a harmonic oscillator of frequency ω in a thermal state, we find for the bath expectation value of the polaron displacement operators (4)

$$\langle D_j^\pm\rangle_\beta = \exp\left[-2\sum_{r=1}^{R}\frac{\lambda_r^2}{w_r^2}\coth\frac{\beta w_r}{2}\right]. \tag{8}$$

Hence, one can naturally introduce a bath-dressed TLS-cavity coupling strength $g_\beta = g\langle D_j^\pm\rangle_\beta$. Obviously, due to (8) we have $0 < g_\beta/g < 1$, so that the influence of the bath in the first order is to effectively reduce the TLS-cavity interaction

$$\langle\tilde{V}_{\downarrow\uparrow,\mathrm{C}}\rangle_\beta = g_\beta\sum_{m=1}^{M}\sum_{j=1}^{N}(a_m^\dagger\sigma_j^- + a_m\sigma_j^+). \tag{9}$$

At this point we note that the previous first-order term was omitted by Kirton and Keeling [38, 39], based on the implicit assumption that it is irrelevant due to the rapid collisional dephasing [69]. As we will demonstrate below, its influence deep in the photon BEC regime turns out to be negligible, so this regime can be described satisfactorily even if it is not taken into account. However, in the opposite laser-like regime such a term does play a major role, even in the presence of a fast sub-picosecond dephasing. Anyhow, on formal grounds, it should be a part of the proper treatment.

We continue by applying the Born–Markov approximation as well as RWA, by tracing out the bath degrees of freedom and by taking into account the cavity losses along with the pumping and the decay of the TLS, similarly as [38, 39]. As already mentioned, we additionally account for the dephasing of the individual TLS. Incoherent pumping can be formally described as coupling each TLS to a bath of inverted harmonic oscillators [70]. With this we find that the reduced density matrix $\rho_{\downarrow\uparrow,\mathrm{C}}$ of the TLS-cavity subsystem obeys the following master equation

$$\dot{\rho}_{\downarrow\uparrow,\mathrm{C}} = -\mathrm{i}\left[\sum_{m=1}^{M}\delta_m a_m^\dagger a_m + g_\beta\sum_{m=1}^{M}\sum_{j=1}^{N}(a_m^\dagger\sigma_j^- + a_m\sigma_j^+),\ \rho_{\downarrow\uparrow,\mathrm{C}}\right] - \left\{\sum_{m=1}^{M}\frac{\kappa}{2}L[a_m] + \sum_{j=1}^{N}\left(\frac{\gamma_\uparrow}{2}L[\sigma_j^+] + \frac{\gamma_\downarrow}{2}L[\sigma_j^-] + \frac{\gamma_\phi}{2}L[\sigma_j^z]\right) + \sum_{m=1}^{M}\sum_{j=1}^{N}\left(\frac{\gamma_m^+}{2}L[a_m\sigma_j^+] + \frac{\gamma_m^-}{2}L[a_m^\dagger\sigma_j^-]\right)\right\}\rho_{\downarrow\uparrow,\mathrm{C}}\,, \tag{10}$$

where $\mathcal{L}[X]\rho = \{X^\dagger X,\ \rho\} - 2X\rho X^\dagger$ and we have moved into the frame rotating with the frequency Δ, so that $\delta_m = \omega_m - \Delta$ stands for the detuning of the cavity mode from the TLS transition. The thermal fluctuations of $\tilde{V}_{\downarrow\uparrow,\mathrm{C}}$ give rise in the second order of perturbation theory to the incoherent transitions described by the dissipative Lindblad terms contained in the last double-sum of (10). The terms proportional to γ_m^+ correspond to the absorption of the cavity photons by the TLS, while those with the prefactor γ_m^- represent the stimulated emission into the cavity modes. The previous approach should be satisfactory whenever $\tilde{V}_{\downarrow\uparrow,\mathrm{C}}$ has small fluctuations around its thermal average and when the characteristic time scale, in which the bath modes undergo a displacement in order to adjust themselves to the instantaneous state of the TLS-cavity subsystem, is very short in comparison with the time scale of the subsystem relaxation. Note that the additional Lamb shifts due to the presence of the bath have been neglected as in [38, 39]. Due to the dynamical influence of the bath, the corresponding rates $\gamma_m^\pm = \gamma(\pm\delta_m)$ turn out to be frequency-dependent and are obtained along the lines of [38, 39, 71] as

$$\gamma(\delta) = 2\,g^2\,\mathrm{Re}\int_0^\infty \mathrm{e}^{-\frac{1}{2}(\gamma_\uparrow+\gamma_\downarrow)t}\,\mathcal{C}_\beta(t)\,\mathrm{e}^{\mathrm{i}\delta t}\mathrm{d}t, \tag{11}$$

with

$$\mathcal{C}_\beta(t) = \langle D_j^-(t)D_j^+\rangle_\beta - \langle D_j^-(t)\rangle_\beta\langle D_j^+\rangle_\beta \tag{12}$$

being the retarded connected correlation function of the bath displacement operators. One can notice that the pumping and the decay of the TLS yield an exponentially decaying factor in (11), i.e., they introduce an additional level broadening [71]. The time evolution of $D_j^-(t)$ is generated by the free Hamiltonian $H_\mathrm{R}^{(j)}$, starting from $D_j^-(0) \equiv D_j^-$. Having in mind the result (7), one gets $\langle D_j^-(t)\rangle_\beta = \langle D_j^-\rangle_\beta$ and

$$\langle D_j^-(t)D_j^+\rangle_\beta = \exp\left\{-4\sum_{r=1}^{R}\frac{\lambda_r^2}{w_r^2}\left[(1-\cos w_r t)\coth\frac{\beta w_r}{2} + \mathrm{i}\sin w_r t\right]\right\}. \tag{13}$$

Note that in the long-time limit the many oscillatory terms from the above sum simply add up to zero, such that, recalling (8), one finds $\lim_{t\to\infty}\langle D_j^-(t)D_j^+\rangle_\beta = \langle D_j^-\rangle_\beta\langle D_j^+\rangle_\beta$ and $\lim_{t\to\infty}\mathcal{C}_\beta(t) = 0$, i.e., the two displacement operators of very distant moments in time become uncorrelated. In the Kirton–Keeling's approach [38, 39], the definition of the quantity (11) was actually without the last term of (12), i.e., $\mathcal{C}_\beta(t)$ had a finite long-time limit. On formal grounds, if both $\gamma_\uparrow$ and $\gamma_\downarrow$ are zero, that leads to a divergence of the absorption and emission rates of resonant light, i.e., $\gamma(\delta = 0) \to \infty$. We trace this shortcoming back to the very absence of the first-order coherent term (9) from their treatment. Thus, the two improvements we have made to their approach come in pair.

The full master equation (10) is notoriously difficult to solve. However, its structure already reveals some general features of the system dynamics. Namely, one can clearly distinguish the coherent and the dissipative influence of the oscillator bath. The former one comes from the TLS-cavity coupling of the reduced strength g_β — in a typical laser-like fashion, while the latter one is realised through the terms containing $\gamma_m^\pm$, which were shown to lead to thermalisation of light and emergence of photon BEC [38, 39]. In the following we will demonstrate that precisely their interplay determines these two limiting stationary behaviours, i.e., a photon BEC or a laser.

2.2. Equations of motion approach

In order to be able to perform a quantitative analysis, we proceed to obtain the equations of motion for the mean values of the system observables $\langle X\rangle \equiv \mathrm{Tr}[X\rho_{\downarrow\uparrow,\mathrm{C}}]$, e.g., the populations of the cavity modes, the population inversion of the TLS etc from the master equation (10). Since this procedure yields an infinite hierarchy of coupled equations, we use the cumulant expansion method [72–75] to truncate the hierarchy at the second level, i.e., we will keep the cumulants up to the second order only. If one wants to calculate higher-order correlation functions, a higher level of truncation will be necessary. However, due to the presence of coherent terms in the master equation, the situation becomes considerably more involved than in [38, 39], even at this second-order truncation level.

We note that the system possesses a $U(1)$ gauge symmetry: $a_m \to a_m e^{-i\phi}$, $a_m^\dagger \to a_m^\dagger e^{i\phi}$, $\sigma_j^- \to \sigma_j^- e^{-i\phi}$ and $\sigma_j^+ \to \sigma_j^+ e^{i\phi}$, $\phi \in \mathbb{R}$. In a single experimental run a coherent field with a particular spontaneously chosen phase ϕ can build up. However, since the density matrix describes an average over many such realisations, the following equalities hold $\langle a_m \rangle = \langle a_m^\dagger \rangle = \langle \sigma_j^- \rangle = \langle \sigma_j^+ \rangle = 0$ and similarly for all other gauge non-invariant operators [73]. In particular, it means that $\langle a_m \sigma_1^+ \rangle = \langle a_m \sigma_1^+ \rangle_c$, $\langle a_k^\dagger a_m \rangle = \langle a_k^\dagger a_m \rangle_c$ etc., since $\langle XY \rangle = \langle XY \rangle_c + \langle X \rangle \langle Y \rangle$, where the index c denotes connected correlation functions. For instance, one has

$$\begin{aligned}\langle a_k^\dagger a_m \sigma_1^z \rangle = \langle a_k^\dagger a_m \sigma_1^z \rangle_c + \langle a_k^\dagger a_m \rangle_c \langle \sigma_1^z \rangle + \langle a_k^\dagger \sigma_1^z \rangle_c \langle a_m \rangle + \langle a_m \sigma_1^z \rangle_c \langle a_k^\dagger \rangle \\ + \langle a_k^\dagger \rangle \langle a_m \rangle \langle \sigma_1^z \rangle \approx \langle a_k^\dagger a_m \rangle \langle \sigma_1^z \rangle. \end{aligned} \tag{14}$$

Due to the two simplifying assumptions mentioned in the beginning, we assume that all the TLS are mutually equivalent such that, e.g., $\langle \sigma_i^z \rangle = \langle \sigma_1^z \rangle$ and $\langle \sigma_i^+ \sigma_j^- \rangle = \langle \sigma_1^+ \sigma_2^- \rangle$ for all $i, j = 1, \ldots, N$ and $i \neq j$. The resulting equations of motion for the cavity mode occupations $\langle n_m \rangle \equiv \langle a_m^\dagger a_m \rangle$ read

$$\begin{aligned}\frac{\mathrm{d}}{\mathrm{d}t}\langle n_m \rangle = -\kappa \langle n_m \rangle + iN g_\beta (\langle a_m \sigma_1^+ \rangle - \langle a_m^\dagger \sigma_1^- \rangle) - \frac{N}{2}\gamma_m^+ \langle n_m \rangle (1 - \langle \sigma_1^z \rangle) \\ + \frac{N}{2}\gamma_m^- (\langle n_m \rangle + 1)(1 + \langle \sigma_1^z \rangle), \end{aligned} \tag{15}$$

whereas for the TLS population inversion $\langle \sigma_1^z \rangle$ we obtain

$$\begin{aligned}\frac{\mathrm{d}}{\mathrm{d}t}\langle \sigma_1^z \rangle = \gamma_\uparrow (1 - \langle \sigma_1^z \rangle) - \gamma_\downarrow (1 + \langle \sigma_1^z \rangle) + 2i g_\beta \sum_{m=1}^{M} (\langle a_m^\dagger \sigma_1^- \rangle - \langle a_m \sigma_1^+ \rangle) \\ + \sum_{m=1}^{M} [\gamma_m^+ \langle n_m \rangle (1 - \langle \sigma_1^z \rangle) - \gamma_m^- (\langle n_m \rangle + 1)(1 + \langle \sigma_1^z \rangle)]. \end{aligned} \tag{16}$$

These equations are exactly like those of Kirton and Keeling [38, 39], apart from the coherent terms proportional to g_β which introduce the additional coupling to the mixed-type terms $\langle a_m \sigma_1^+ \rangle = \langle a_m^\dagger \sigma_1^- \rangle^*$. They measure the correlation between TLS and cavity photons and evolve according to

$$\begin{aligned}\frac{\mathrm{d}}{\mathrm{d}t}\langle a_m \sigma_1^+ \rangle = \left(-i\delta_m - \frac{\gamma_\uparrow + \gamma_\downarrow + 4\gamma_\phi + \kappa}{2} \right) \langle a_m \sigma_1^+ \rangle \\ - i g_\beta \left[\frac{1 + \langle \sigma_1^z \rangle}{2} + \langle \sigma_1^z \rangle \sum_{k=1}^{M} \langle a_k^\dagger a_m \rangle + (N-1) \langle \sigma_1^+ \sigma_2^- \rangle \right] \\ - \frac{\gamma_m^+}{4}(N-1)\langle a_m \sigma_1^+ \rangle (1 - \langle \sigma_1^z \rangle) + \frac{\gamma_m^-}{4}(N-1)\langle a_m \sigma_1^+ \rangle (1 + \langle \sigma_1^z \rangle) \\ - \sum_{k=1}^{M} \left\{ \frac{\gamma_k^+}{2} [\langle a_m \sigma_1^+ \rangle \langle n_k \rangle + \langle a_k \sigma_1^+ \rangle \langle a_m a_k^\dagger \rangle] \right. \\ \left. + \frac{\gamma_k^-}{2} [\langle a_m \sigma_1^+ \rangle (\langle n_k \rangle + 1) + \langle a_k \sigma_1^+ \rangle \langle a_k^\dagger a_m \rangle] \right\}, \end{aligned} \tag{17}$$

where now the additional quantities $\langle a_k^\dagger a_m \rangle$ and $\langle \sigma_1^+ \sigma_2^- \rangle$ appear. The former represent the correlations between different cavity modes, whose evolution is governed by

$$\begin{aligned}\frac{\mathrm{d}}{\mathrm{d}t}\langle a_k^\dagger a_m \rangle = [-\kappa + i(\delta_k - \delta_m)] \langle a_k^\dagger a_m \rangle + iN g_\beta (\langle a_m \sigma_1^+ \rangle - \langle a_k^\dagger \sigma_1^- \rangle) \\ + \frac{N}{4}(\gamma_k^- + \gamma_m^-) \langle a_m a_k^\dagger \rangle (1 + \langle \sigma_1^z \rangle) - \frac{N}{4}(\gamma_k^+ + \gamma_m^+) \langle a_k^\dagger a_m \rangle (1 - \langle \sigma_1^z \rangle), \end{aligned} \tag{18}$$

and the latter the correlations between dipoles of different TLS following from

$$\begin{aligned}\frac{\mathrm{d}}{\mathrm{d}t}\langle \sigma_1^+ \sigma_2^- \rangle = -(\gamma_\uparrow + \gamma_\downarrow + 4\gamma_\phi) \langle \sigma_1^+ \sigma_2^- \rangle + i g_\beta \langle \sigma_1^z \rangle \sum_{m=1}^{M} (\langle a_m \sigma_1^+ \rangle - \langle a_m^\dagger \sigma_1^- \rangle) \\ - \sum_{m=1}^{M} \{ \gamma_m^+ [\langle \sigma_1^+ \sigma_2^- \rangle \langle n_m \rangle + \langle a_m^\dagger \sigma_1^- \rangle \langle a_m \sigma_1^+ \rangle] \\ + \gamma_m^- [\langle \sigma_1^+ \sigma_2^- \rangle (\langle n_m \rangle + 1) + \langle a_m \sigma_1^+ \rangle \langle a_m^\dagger \sigma_1^- \rangle] \}. \end{aligned} \tag{19}$$

It is important to notice that the quantities $\langle a_m \sigma_1^+ \rangle$, $\langle a_k^\dagger a_m \rangle$ and $\langle \sigma_1^+ \sigma_2^- \rangle$ can reach non-zero stationary values precisely due to the coherent part of the evolution, which we have introduced in addition to [38, 39].

At this point, one additional specialisation is in order. Namely, based on the photon BEC experiments, we consider the photon modes as being transverse, arising from a two-dimensional effective harmonic potential [5]. We thus consider regularly spaced cavity levels $\omega_\ell = \omega_1 + (\ell - 1)\Omega$ with $\ell = 1, \ldots, L$, such that the energy

Table 1. Parameters of the model adjusted to current experimental setup of photon BEC [5]. The first four parameters are obtained from the fit to the absorption spectrum of the dye. The remaining parameters are taken from [17, 64, 81].

w_c	η	g	Δ	κ	δ_1	δ_L	T	N
20.5 THz	0.6	2.46 GHz	3487 THz	3.5 GHz	−260 THz	−120 THz	300 K	10^9

level ω_ℓ has the degeneracy $d_\ell = 2\ell$, where the factor 2 comes from the two independent polarisations of light. The lowest frequency ω_1 represents the cavity cutoff. Since degenerate cavity modes evolve in the same manner, we have

$$\sum_{m=1}^{M} f(a_m, a_m^\dagger, \ldots) = \sum_{\ell=1}^{L} d_\ell f(a_\ell, a_\ell^\dagger, \ldots), \tag{20}$$

for any arbitrary function f, where from each level ω_ℓ we have chosen a representative mode described by a_ℓ and $a_\ell^\dagger$.

2.3. Bath model

In the following we analyse the stationary solutions of the equations (15)–(19) in the two regimes: a photon BEC and a laser-like regime. To this end, we specialise the model by choosing the bath spectral density, defined by $J(w) = \sum_{r=1}^{R} \lambda_r^2\, \delta(w - w_r)$, to be super-ohmic with an exponential cutoff [76, 77]

$$J(w) = \frac{\eta}{w_c^2} w^3 \exp(-w/w_c), \tag{21}$$

where η represents a dimensionless parameter measuring the coupling strength of the TLS to the bath and w_c is the cutoff frequency of the bath. This allows us to obtain for (8) and (13) the closed-form expressions

$$\langle D_j^{\pm}\rangle_\beta = \exp\left\{2\eta\left[1 - \frac{2\psi'\left(\frac{1}{\beta w_c}\right)}{(\beta w_c)^2}\right]\right\}, \tag{22a}$$

$$\langle D_j^{-}(t) D_j^{+}\rangle_\beta = \exp\left\{4\eta\left[1 - \frac{1}{(1 - \mathrm{i}w_c t)^2} + \frac{\psi'\left(\frac{1 - \mathrm{i}w_c t}{\beta w_c}\right) + \psi'\left(\frac{1 + \mathrm{i}w_c t}{\beta w_c}\right) - 2\psi'\left(\frac{1}{\beta w_c}\right)}{(\beta w_c)^2}\right]\right\}, \tag{22b}$$

where $\psi(z) = \Gamma'(z)/\Gamma(z)$ denotes a logarithmic derivative of the gamma function. In relation to the experiments, both parameters η and w_c characterise the impact of the used solvent on the spectral properties of the dye molecules. Below we discuss in detail that they change the absorption and the emission spectra $\gamma(\pm\delta)$ drastically. Furthermore, they turn out to have an impact upon the resulting bath-dressed coupling strength g_β.

3. Determination of realistic model parameters

In order to apply our theory to the current experimental setups, we have to fix the model parameters in the experimentally accessible regimes. One of the key ingredients for the thermalisation of photons are the spectral properties of the dye molecules [17, 50]. Whereas the Einstein rate coefficient for absorption $B_{12}(\omega)$ is usually measured, the stimulated emission rate $B_{21}(\omega)$ is determined via the Kennard–Stepanov relation [78–80]

$$\frac{B_{21}(\omega)}{B_{12}(\omega)} \sim \exp\left(-\frac{\hbar\omega}{k_B T}\right), \tag{23}$$

where the spectral (rovibrational) temperature T of the dye molecules is $T = 300$ K [17]. Comparing the rate equation from the supplemental material of [17] with our equation (15), we can interpret the rates $\gamma_m^+ = \gamma(\delta_m)$ and $\gamma_m^- = \gamma(-\delta_m)$ as the absorption and the emission rates $B_{12}(\omega_m)$ and $B_{21}(\omega_m)$, respectively. Therefore, we fit the expression $\gamma(\omega - \Delta)$ from (11), using equations (22*a*) and (22*b*) as well, to the experimentally measured absorption spectrum $B_{12}(\omega)$ of the used Rhodamine 6G dye dissolved in ethylene glycol [81], by taking into account the absolute value $B_{12}(\omega = 3300\ \mathrm{THz}) = 1.3$ kHz [17]. The fitting allows then to fix the parameters of our bath model, namely the dimensionless coupling strength η of the TLS and the bath, the cutoff frequency of the bath w_c, as well as the TLS-cavity coupling strength g and the TLS transition frequency Δ, which physically corresponds to the zero-phonon-line frequency of the dye. The obtained values are listed in table 1. Thus, the fitted value for $\eta = 0.6$ leads to a rather small bath-dressed TLS-cavity coupling strength $g_\beta = 8.3 \times 10^{-3} g$, as expected, since this corresponds to the BEC regime.

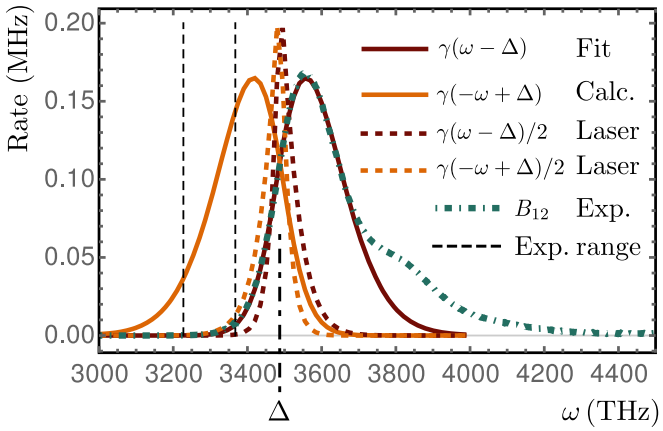

Figure 1. Absorption rate $\gamma(\omega - \Delta)$ (brown/dark) fitted to measured data from [17, 81] (dash–dotted). Emission rate $\gamma(-\omega + \Delta)$ (orange/light) for same parameters. Absorption and emission rates are also shown for lasing regime with $\eta = 0.1$ (dashed).

Figure 1 shows the resulting fit for $\gamma(\omega - \Delta)$ and the experimentally provided data. Note, that we do not fit the absorption curve for $\omega > 3700$ THz, since most of the relevant cavity modes are not influenced by the departure from the actual spectrum, as is indicated by the vertical dashed lines. If one wants to also fit this higher-frequency region, the inclusion of another bath would be necessary since the experimental spectrum displays the presence of another peak. A corresponding physical motivation in terms of another dye-molecule active phonon coupled to a thermal environment was discussed in [39]. With the fitted values our theory provides the emission rate curve $\gamma(-\omega + \Delta)$ as well, which is shown in the same figure. The curves $\gamma(\omega - \Delta)$ and $\gamma(-\omega + \Delta)$ cross at the frequency Δ. We checked that the Kennard–Stepanov relation (23) is valid in the BEC regime for the relevant range of the cavity mode frequencies. For comparison, in the laser regime where η is small, the absorption and emission curves become squeezed towards the zero-phonon-line frequency Δ, see the dotted curves in figure 1. However, the Kennard–Stepanov relation (23) in this regime is no longer granted for frequencies highly detuned from Δ. The corresponding experimental number of dye molecules is taken to be $N = 10^9$, based on the extensive discussion in [64]. The loss rate $\gamma_\downarrow$ can be fixed to 0.25 GHz [81]. Furthermore, the pumping of the TLS $\gamma_\uparrow$ is considered as a control parameter which is tuned to cross the boundary of the phase transition. Knowing that dye molecules experience at least 10^{12} collisions per second with solvent molecules [82], we will consider here $\gamma_\phi = 0.1$ THz as a referent value. Since there is an uncertainty about the exact order of magnitude of this rate, we will later analyse how its variation in a broad range of values influences our results.

In the experiment the cavity cutoff wavelength, corresponding to the mode of frequency ω_1, can be tuned from 570 to 610 nm. The frequency separation of the cavity modes is 0.26 THz [5]. For the simulation we choose ω_1 to correspond to 585 nm, thus we get for the highest detuning $\delta_1 = \omega_1 - \Delta = -260$ THz. Our simulations cover the same spectral range as in [5], but due to computational complexity we choose a higher value $\Omega = 1.4$ THz, if not stated otherwise. The photon loss rate κ is frequency-dependent [17], so we take a mean value $\kappa = 3.5$ GHz. For the sake of clarity the used spectral range is marked in figure 1 by vertical dashed lines.

4. Two regimes: photon BEC and laser-like state

Having discussed the realistic values of the model parameters, in this section we take: $N = 10^9$, $w_c = 20.5$ THz, $T = 300$ K, $g = 2.3$ GHz, $\gamma_\downarrow = 0.25$ GHz, $\gamma_\uparrow = 0.1$ GHz, $\kappa = 3.5$ GHz and $\delta_1 = -260$ THz. The results will be presented for two values of the dephasing rate, $\gamma_\phi = 0.1$ THz estimated from the literature [82] and a much larger one, $\gamma_\phi = 10$ THz, for the sake of comparison. Here we take $\Omega = 10$ THz and consider $L = 20$ energy levels of the cavity. In the following we distinguish two limiting regimes:

(i) $\eta \gtrsim 1$. In this case one has $g_\beta/g = \langle D_j^\pm \rangle_\beta \ll 1$, meaning that the coherent contribution of the bath is highly suppressed and the evolution is dominated by the dissipative influence which leads to a thermalisation of light and an emergence of photon BEC;

(ii) $\eta \ll 1$. Here one finds $g_\beta/g \approx 1$, so that the bath has a pronounced coherent influence. In addition, the rates $\gamma_m^\pm$ of the highly detuned cavity modes acquire orders of magnitude smaller values in comparison with the previous regime, so that the dissipative influence becomes overwhelmed, but is still relevant. Hence, we expect that the non-equilibrium stationary state is then highly coherent and laser-like.

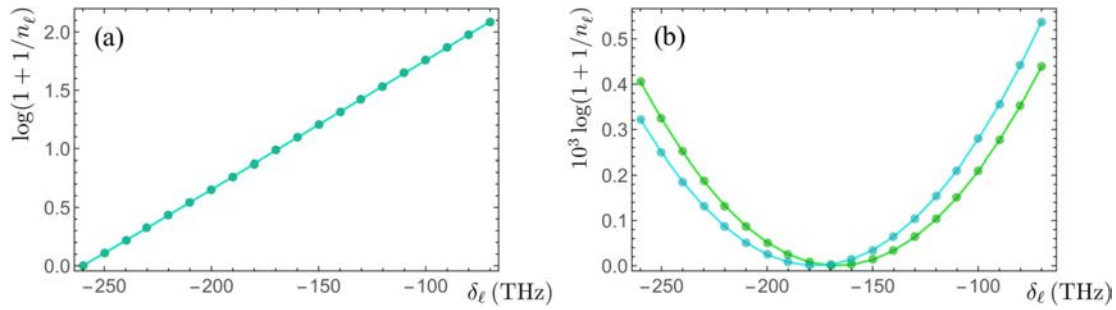

Figure 2. Stationary occupations n_ℓ of cavity modes $\ell = 1, \ldots, 20$ when (a) $\eta = 1.5$ and (b) $\eta = 0.05$. Cyan colour corresponds to $\gamma_\phi = 0.1$ THz, while green is used for $\gamma_\phi = 10$ THz. For other used parameters see main text. Note that in (a) the two cases are visually indistinguishable.

For the regime (*i*) we choose $\eta = 1.5$, yielding $g_\beta/g = 6.2 \times 10^{-6}$. The resulting steady-state solution yields the distribution of occupations of the cavity modes n_ℓ for $\ell = 1, \ldots, 20$ as shown in figure 2(a). It is noticeable that the results (almost) do not depend on the value of dephasing rate. This is predictable since the coherent evolution is anyhow largely suppressed in this regime. The lowest energy level is macroscopically occupied with about 2.84×10^7 photons. The straight line corresponds to a Bose–Einstein distribution $\log(1 + 1/n_\ell) = \beta(\delta_\ell - \mu)$, where μ denotes the chemical potential. Such a state was already analysed in detail in [38, 39] and it was shown to correspond to a photon BEC. Our approach enables us to additionally characterise the stationary states by their photonic correlations. Namely, we have access to the quantities

$$c_{\ell,\ell'} = \frac{|\langle a_\ell^\dagger a_{\ell'}\rangle|}{\sqrt{n_\ell\, n_{\ell'}}}, \quad 1 \leqslant \ell < \ell' \leqslant L, \tag{24}$$

which provide a measure of correlations between representative cavity modes related to different energy levels. Their values belong to the interval [0,1], where values close to 1 (0) correspond to a high (low) degree of correlation. In case (*i*) we find $c_{\ell,\ell'} < 4 \times 10^{-7}$, i.e., the photon BEC state has almost no correlation between the modes of different frequencies. This is expected since the correlations build up through the coherent evolution which is highly ineffective in this regime.

In the opposite regime (*ii*), we take $\eta = 0.05$, which gives $g_\beta/g = 0.67$. The distribution of stationary populations of the representative cavity modes is presented in figure 2(b) for two values of γ_ϕ, namely 0.1 and 10 THz. In the former case, the cavity level $\ell = 9$ acquires macroscopic occupation of almost 1.90×10^7 photons, but the distribution is quite distinct from the Bose–Einstein one. In this case we find $c_{\ell,\ell'} > 0.996$, which demonstrates that the stationary state contains a quite high degree of correlations among the cavity modes of different energies. This is expected since the coherent influence of the bath is very pronounced. The stationary state is laser-like with some dissipative bath influence. For the larger value of the dephasing rate, the level $\ell = 10$ becomes macroscopically occupied with 1.76×10^7 photons, while $c_{\ell,\ell'} > 0.986$. Interestingly, in the considered parameter regime the results for $\gamma_\phi = 0$ would be almost indistinguishable from those for $\gamma_\phi = 0.1$ THz. This means that there is a certain dephasing threshold below which the coherent system dynamics is robust to the dephasing. Moreover, if one considered the full spatial structure of the cavity modes as in [40], the aforementioned correlations would decrease due to only partial overlap among different modes. However, this would not alter the present conclusions. We note that similar states supporting macroscopic occupations of optical modes of higher energies were also observed in [38, 39] and, indeed, we can also reproduce such behaviour in the regime (*i*). However, the steady-state we have just presented features near-unity correlations of light, which represents a crucial difference and indicates that it is of an entirely different nature. Moreover, for different values of the cavity decay rate even the lowest level can acquire macroscopic occupation, while the populations of other cavity levels strongly depart from the Bose–Einstein distribution. Hence, the stationary states in the two regimes (*i*) and (*ii*) differ completely regarding the correlations and the distribution of photons among the cavity levels, as a consequence of different influences of the bath.

5. Properties of photon BEC

In the following, we focus on interesting properties of the photon BEC. At first, we determine from our model the equation of state. This allows then to extract the dimensionless effective photon–photon interaction strength in the photon BEC regime and study its dependence on various model parameters, which could be tuned

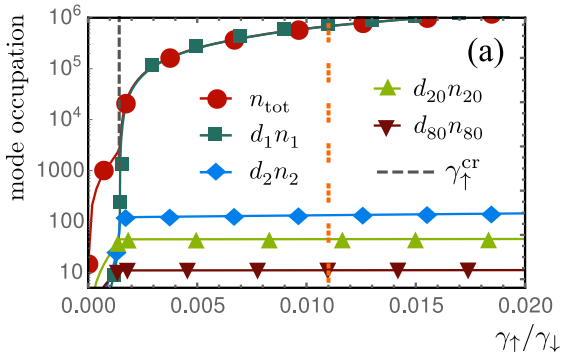

Figure 3. (a) Occupation of 1st, 2nd and some higher cavity levels as well as total occupation of all modes as function of pumping $\gamma_\uparrow$ reveals condensation for $\gamma_\uparrow > \gamma_\uparrow^{\rm cr}$ (vertical dashed line) for $L = 101$. Further increase of $\gamma_\uparrow$ mainly populates the lowest level. Orange triple-dashed vertical line marks the value $\gamma_\uparrow = 0.011\ \gamma_\downarrow$. (b) Zoom around $\gamma_\uparrow^{\rm cr}$ shows onset of condensation in the lowest energy level (green squares). Onset of condensation in total number of photons (red circles) becomes smoothened for higher number of levels (red circles versus dashed and dotted lines). Transition is also visible in occupation of higher levels (blue rhombi). Parameters are listed in table 1.

experimentally. We will adopt the terminology in accordance with the experiments and, for instance, instead of TLS refer to dye molecules.

5.1. Equation of state

In this section we apply our theory to experimentally realistic values and determine at first the steady-state of the equations of motion (15)–(19) for different pumping rates $\gamma_\uparrow$ and evaluate the dependence of the chemical potential μ on the total photon number $n_{\rm tot}$, i.e., we obtain the equation of state $\mu(n_{\rm tot})$. In the following we present and discuss this procedure in detail by using the specific parameters from table 1, if not stated otherwise.

In figure 3(a) we show the occupation of different energy levels of the cavity in the BEC regime for the increasing pump rate $\gamma_\uparrow$ with all other parameters being fixed. The onset of the condensation starts at the critical value $\gamma_\uparrow^{\rm cr}$. A zoom around $\gamma_\uparrow^{\rm cr}$ is shown in figure 3(b). Clearly, the occupation of the lowest level d_1n_1 shows a sudden increase at the critical point and becomes macroscopic afterwards. Further increase of $\gamma_\uparrow$ mainly populates the lowest level, while the population of higher energy levels does not change significantly after the transition. At the critical value of the pumping parameter $\gamma_\uparrow^{\rm cr}$ the total number of photons $n_{\rm tot} = \sum_{\ell=1}^{L} d_\ell n_\ell$ amounts to $n_{\rm tot}(\gamma_\uparrow^{\rm cr}) \approx 2800$, which is quite close to the expected critical photon number for the condensation onset in the case of non-interacting interacting bosons in two dimensions [15, 16] and at $T = 300$ K

$$n^{\rm cr} = \frac{\pi^2}{3}\left(\frac{k_{\rm B}T}{\hbar\Omega}\right)^2 = 2640, \tag{25}$$

where the existence of two independent polarisations of light has been taken into account. Note that the rise of the total photon number $n_{\rm tot}$ around the transition point becomes smoothened when the number of cavity levels L in the considered frequency range is increased, as is seen in figure 3(b). This can be explained with the significant contribution of degeneracies d_ℓ of the energy levels with high ℓ to $n_{\rm tot}$.

The mode occupation n_ℓ for a fixed $\gamma_\uparrow$ is shown in a logarithmic representation in figure 4(a), along the triple-dashed vertical line of figure 3(a). The linear behaviour indicates that the modes are distributed according to Bose–Einstein statistics

$$n_\ell = \frac{1}{\exp[\beta(\delta_\ell - \mu)] - 1}. \tag{26}$$

Fitting a linear function to $\log(1 + 1/n_\ell)$ yields the inverse temperature β and the chemical potential μ due to equation (26). For a non-interacting BEC condensate, i.e., $g_\beta = 0$, the temperature obtained by fitting to a thermal cloud coincides with the spectral temperature of the dye and the chemical potential is locked to the value δ_1 above the threshold [38]. However, here g_β is non-zero but small, which induces additional small corrections of the occupation. As a consequence, the effective thermalisation temperature of the thermal cloud differs generically from the spectral temperature of the dye. This behaviour depends on all system parameters, and especially a high pumping rate $\gamma_\uparrow$ can significantly change the temperature. For a choice of parameters outside of a certain region the non-equilibrium properties of the model are dominating the tendency to thermalise and the distribution is, in general, not thermal any more. This happens even in the case $g_\beta = 0$ [39]. Therefore, we restrict our further analysis only to the cases where a thermal cloud does exist. We have observed that a few of the lowest modes do not follow the linear dependency in figure 4(a), thus they are not considered in our fitting

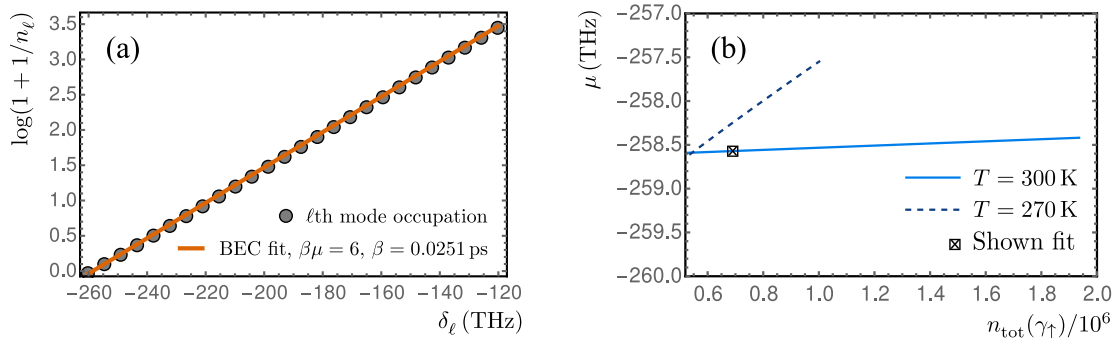

Figure 4. (a) Occupation n_ℓ of every fourth mode for $\gamma_\uparrow = 0.011\gamma_\downarrow$, i.e., vertical triple-dashed line in figure 3(a), shows linear behaviour in logarithmic representation indicating thermalisation. Fitted μ value shown as crossed square on the right. (b) Chemical potential μ as function of total photon number n_{tot} reveals non-zero slope for two different temperatures. We use $L = 101$, other parameters are given in table 1.

procedure. Additionally, we drop some of the highest modes as well, as they hold relatively small occupation and can, therefore, have large relative numerical error. The resulting value of μ from figure 4(a) is shown by a crossed square symbol in figure 4(b). We repeat the procedure for different values of the pumping rate $\gamma_\uparrow$ and obtain a linear equation of state $\mu = \mu(n_{\mathrm{tot}})$, as presented in figure 4(b).

5.2. Photon–photon interaction strength

The slope $\partial\mu / \partial n_{\mathrm{tot}}$ of the equation of state $\mu = \mu(n_{\mathrm{tot}})$ in figure 4(b) is a consequence of the dye-mediated effective photon–photon interaction (see the appendix), which is measured by the dimensionless interaction strength

$$\tilde{g} = \frac{2\pi}{\hbar\Omega}\frac{\partial\mu}{\partial n_{\mathrm{tot}}}. \tag{27}$$

Thus, we infer from figure 4(b) the resulting interaction strength $\tilde{g} = 5.2 \times 10^{-7}$, which agrees quite well with the range $\tilde{g} \sim 10^{-8} - 10^{-7}$ given in [63]. Note that, as mentioned in the introduction, the thermo-optical effect dominates the photon–photon interaction. Therefore, this value cannot be directly compared with the measured values [5, 62, 65], since we only model one of the respective contributions.

Now we investigate how $\tilde{g}$ depends on the parameters of our model. First, we vary those that could be tuned in experimental setups: the number of cavity levels L in the experimentally relevant range of 140 THz above δ_1, the number of dye molecules N, the spectral temperature of the dye T and the cavity decay rate κ. Next, it is instructive to think of g_β as being an independent parameter. In this way, by tuning g_β from zero to its experimental value g_β^{exp}, we are able to examine how the coherent terms of our model give rise to the effective photon–photon interaction strength. Finally, since the dephasing rate γ_ϕ is only approximately known in the experiments, we also investigate its influence on $\tilde{g}$ for various values of other parameters. The corresponding results are presented in figure 5. The number of equations increases quadratically with the number of levels L. We have chosen $L = 101$ due to computational constraints. Figure 5(a) shows that the interaction strength $\tilde{g}$ depends non-monotonously on L. In case of up to 200 levels, the interaction $\tilde{g}$ increases nearly exponentially with the number of cavity levels. However, after reaching the maximum at $L \approx 200$ the dimensionless interaction strength $\tilde{g}$ starts to decrease. The value of $\tilde{g}$ in the case of the experimental number of levels $L = 501$ is then comparable with the value for $L = 101$ levels, which we used in our simulations.

According to figure 5(b), a larger number of dye molecules N increases $\tilde{g}$ dramatically, since more dye molecules mediating an effective coupling between the photons are present. In addition, much larger photon–photon interaction can also be achieved by lowering the temperature, see figure 5(c). In contrast, figure 5(d) reveals that increasing the decay rate κ decreases only slightly the interaction strength $\tilde{g}$. An intuitive explanation of the last two results is as follows. Increasing either the temperature or the photon decay rate reduces the total number of photons in the system, thus there are less photons available to modify the dye medium and $\tilde{g}$ decreases correspondingly.

In figure 5(e) we investigate the dependency of $\tilde{g}$ on the coherent coupling g_β, which we vary artificially from zero to the experimental value g_β^{ext}. Quite expectedly, in the limit $g_\beta \to 0$ the dimensionless interaction strength $\tilde{g}$ practically vanishes, the latter corresponding to the case of the Kirton–Keeling model [38, 39]. The increase of $\tilde{g}$ is nonlinear and in the considered range an even polynomial in g_β yields a good fit (red line). We observe that the quadratic term is almost negligible compared to quartic and higher-order terms, akin to the consideration of a photon–photon interaction corresponding to the box Feynman diagram analysed in the work [63]. In our

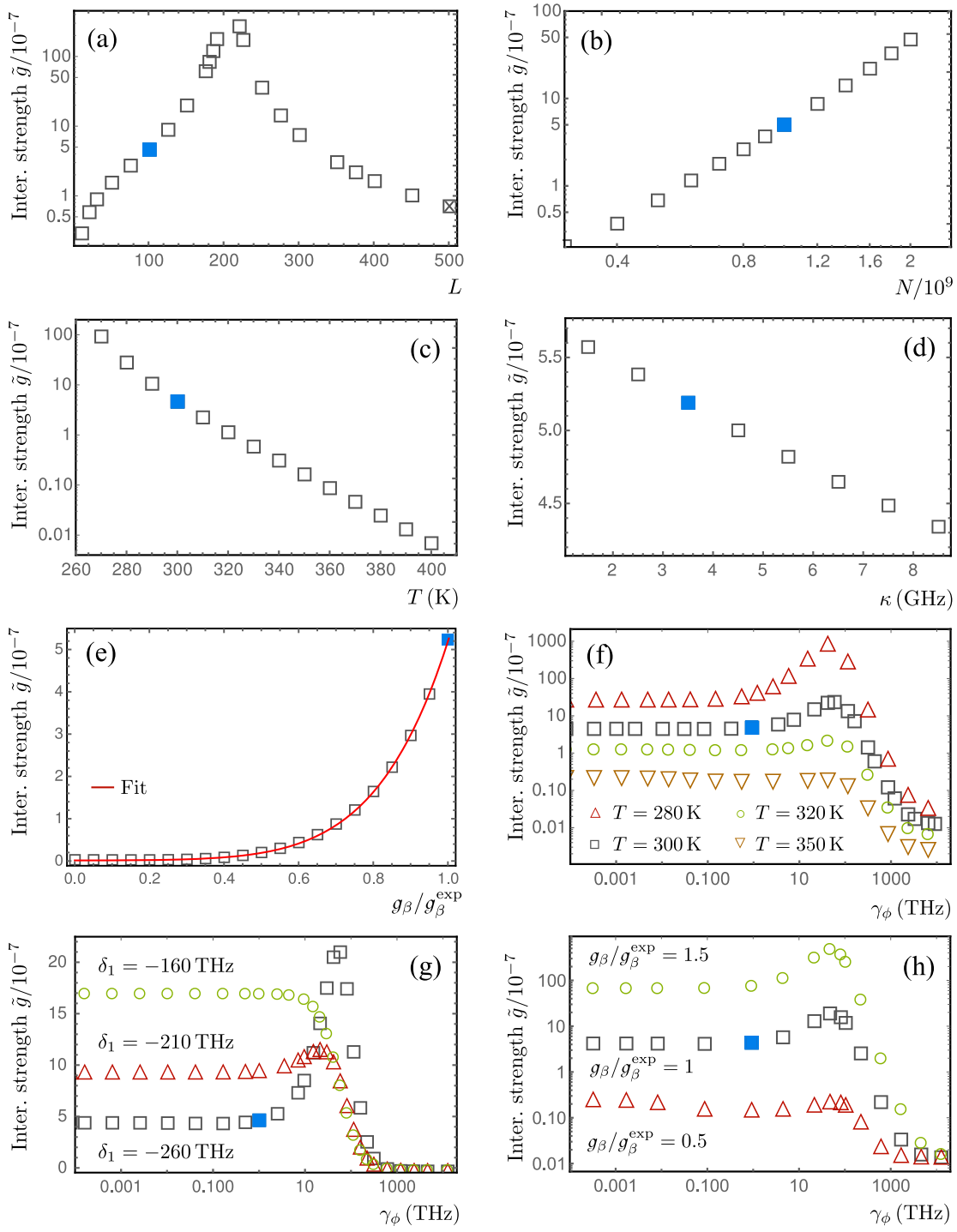

Figure 5. Dependence of dimensionless effective photon–photon interaction strength $\tilde{g}$ on: (a) number of cavity levels L, (b) number of dye molecules N, (c) temperature T, (d) cavity decay rate κ and (e) rescaled dressed dye-cavity coupling strength $g_\beta/g_\beta^{\rm exp}$, using a fixed $\gamma_\phi = 0.1$ THz. Influence of dephasing rate for various: (f) temperatures, (g) cavity cutoffs δ_1, (h) ratios $g_\beta/g_\beta^{\rm exp}$. From (a) we see that the number of cavity levels (i.e., the value of Ω) in our model has a non-monotonous effect on the interaction strength $\tilde{g}$: the maximum is located around $L \approx 200$, where $L = 501$ (crossed square) corresponds to the experimental regime. Blue filled squares in all panels show results in the case of experimentally chosen values (see table 1), apart from $L = 101$ which is used in (b)–(h). As we see, increase of N or decrease of T significantly increases $\tilde{g}$, whereas κ and γ_ϕ affect its value only slightly in the vicinity of experimentally realistic values. Fit (red line) in (e) indicates the dependence of $\tilde{g}$ on g_β in the form of an even polynomial.

framework, such a dependence could easily be understood via a simple perturbative expansion of the expectation values $\langle X\rangle = \sum_{p=0}^{\infty}\langle X\rangle^{(p)}$, where $\langle X\rangle^{(p)} \propto g_\beta^p$, for an arbitrary system operator X in the equations (15)–(19), with the time derivatives set to zero. In such a way, higher perturbation orders can be systematically calculated from the lower ones. The zeroth order solutions for $\langle n_m\rangle^{(0)}$ and $\langle\sigma_1^z\rangle^{(0)}$ are exactly those

from the work of Kirton and Keeling [38, 39]. It turns out that $\langle n_m \rangle = \langle n_m \rangle^{(0)} + \langle n_m \rangle^{(2)} + \langle n_m \rangle^{(4)} + \ldots$, so that we have an expansion $\tilde{g} = \tilde{g}^{(2)} + \tilde{g}^{(4)} + \ldots$ in even powers of g_β.

Next, we analyse the effect of the dephasing on $\tilde{g}$ and the sensitivity of the obtained dependence on other system parameters. Figures 5(f)–(h) show that, quite generically, $\tilde{g}$ is affected insignificantly when the dephasing rate γ_ϕ is varied from zero to few THz. Such a result could be attributed to the presence of a large detuning in (17), of the order of 100 THz, which anyhow strongly suppresses the coherent evolution on its own. Further increase of γ_ϕ may lead to the appearance of a resonance-like peak, followed by a polynomial decay for dephasing rates above several hundreds of THz. The latter is expected to happen when the dephasing rate becomes larger than $|\delta_1|$. The resonance-like peak becomes more pronounced as g_β is increased or the temperature decreased, as is seen in figures 5(f) and (h). This observation indicates that the peak is of coherent origin. On the other hand, the resonance-like peak can completely disappear when the cavity cutoff frequency is shifted towards the zero-phonon line, which is demonstrated in figure 5(g).

6. Conclusions

Here we presented a model which can interpolate between two different kinds of states of light in a microcavity, namely between a nearly non-interacting photon BEC and a laser-like state. Our model is based on a master equation approach, with an interplay between coherent and dissipative dynamics. The dominance of the former or the latter leads either to a coherent lasing state or to an equilibrated BEC state, respectively. We demonstrated that in the BEC case the lowest cavity energy level is macroscopically occupied and cavity modes of different energies are almost uncorrelated, whereas in the lasing case some cavity level becomes macroscopically occupied with strong correlations being present in the system. Afterwards, we showed how to fix the parameters of our theory in an experimentally realistic regime. We emphasised that the coherent part of the master equation is then overwhelmed by the dissipative effects, but still significant enough to lead to an additional effective photon–photon interaction. As a consequence, the chemical potential depends linearly on the total number of photons, as is expected from a perturbative solution of a Gross–Pitaevskii equation for the condensate wave function. This dependency allowed us to determine the dimensionless interaction strength $\tilde{g}$ to be of the order of 10^{-7} for experimentally realistic parameters.

We also investigated the dependency of $\tilde{g}$ on different model parameters, which can feasibly be tuned in the photon BEC experiments. Our numerics showed that increasing the number of dye molecules or decreasing the spectral dye temperature can significantly increase the $\tilde{g}$ value, whereas it is not much influenced by the cavity loss rate κ. However, this value cannot be directly connected to the current experimental values [5, 62, 65]. The reason is that in the experimental setups the dominating photon–photon interaction is of thermo-optical origin, whereas our theory has no spatial degrees of freedom and, thus, cannot capture such diffusive effects. Instead, in our case the effective photon–photon interaction could be compared with the dye-mediated photon–photon scattering. And indeed, our value is in the range of the expected estimate [63].

Another currently disputed feature of the photon condensate concerns its possible polarisation. Whereas no significant polarisation of the photon BEC was found in the original Bonn experiment [5], recent systematic measurements of the Stokes parameters in Utrecht [83] indicate that the polarisation of the photon BEC correlates with the polarisation of the pump pulse. These new experimental results together with the recent theoretical investigation in the BEC case [41] offer the prospect that the polarisation dependency could be investigated on the basis of an extension of our microscopic model during the whole crossover from the photon BEC to the laser-like phase.

Acknowledgments

We acknowledge H Haken, J Keeling, P Kirton, J Klärs, R Nyman, D van Oosten, G Schaller, J Schmitt, E Stein, F Vewinger and M Weitz for inspiring discussions. This work was supported in part by the Ministry of Education, Science and Technological Development of the Republic of Serbia under projects ON171017, ON171038, III45016 and BEC-L, by the German Academic and Exchange Service (DAAD) under project BEC-L, by the German Research Foundation (DFG) via the Collaborative Research Centers SFB 910, SFB/TR49 and SFB/TR185 and grant BR 1528/9-1 and by the European Commission through the project QUCHIP, grant No. 641039.

Appendix. Interaction dependence of equation of state

Here we derive relation (27), which allows to determine the dimensionless photon–photon interaction strength $\tilde{g}$ from the slope $\partial\mu/\partial n_{\rm tot}$ of the equation of state $\mu(n_{\rm tot})$. To this end we follow [5] and assume that the photon BEC is described by a condensate wave function $\Psi(\mathbf{x})$, which obeys a two-dimensional time-independent Gross–Pitaevskii equation:

$$\left[-\frac{\hbar^2}{2m}\Delta + \frac{1}{2}m\Omega^2\mathbf{x}^2 + g\,|\Psi(\mathbf{x})|^2\right]\Psi(\mathbf{x}) = \mu\Psi(\mathbf{x}). \tag{A.1}$$

Here, g denotes the photon–photon interaction strength, m stands for the photon mass, Ω is the trapping frequency and μ represents the chemical potential. As the photon–photon interaction strength g is supposed to be small, we solve equation (A.1) perturbatively. At first we neglect the interaction g, so equation (A.1) can be solved exactly. The ground-state wave function $\Psi^{(0)}(\mathbf{x})$, which is normalised to the total number of photons $n_{\rm tot}$, reads

$$\Psi^{(0)}(\mathbf{x}) = \sqrt{\frac{n_{\rm tot}}{\pi l^2}}\,\exp\left(-\frac{\mathbf{x}^2}{2l^2}\right), \tag{A.2}$$

with the oscillator length $l = \sqrt{\hbar/m\Omega}$ and the chemical potential $\mu^{(0)} = \hbar\Omega$ coincides with the zero-point energy of the two-dimensional harmonic oscillator. For a non-vanishing interaction strength g we assume a perturbative correction in first order for both the condensate wave function and the chemical potential:

$$\Psi(\mathbf{x}) = \Psi^{(0)}(\mathbf{x}) + \Psi^{(1)}(\mathbf{x}) + \ldots, \tag{A.3}$$

$$\mu = \mu^{(0)} + \mu^{(1)} + \ldots. \tag{A.4}$$

With this ansatz the Gross–Pitaevskii equation (A.1) reduces to

$$\left[-\frac{\hbar^2}{2m}\Delta + \frac{1}{2}m\Omega^2\mathbf{x}^2 - \mu^{(0)}\right]\Psi^{(1)}(\mathbf{x}) = \mu^{(1)}\Psi^{(0)}(\mathbf{x}) - g\Psi^{(0)}(\mathbf{x})^3, \tag{A.5}$$

which determines both interaction corrections $\Psi^{(1)}(\mathbf{x})$ and $\mu^{(1)}$. In our context it is sufficient to calculate the latter one, which follows from the Fredholm alternative [84]. To this end we multiply equation (A.5) with $\Psi^{(0)}(\mathbf{x})$ and integrate over $\mathbf{x}$, so we get due to (A.2) with the dimensionless interaction parameter [61]

$$\tilde{g} = \frac{gm}{\hbar^2} \tag{A.6}$$

the equation of state

$$\mu = \hbar\Omega + \frac{\tilde{g}\hbar\Omega}{2\pi}n_{\rm tot} + \ldots. \tag{A.7}$$

Thus, for small interactions $\tilde{g}$ the chemical potential μ changes linearly with the photon number $n_{\rm tot}$. The slope $\partial\mu/\partial n_{\rm tot}$ of the equation of state $\mu(n_{\rm tot})$ depends then via $\partial\mu/\partial n_{\rm tot} = \tilde{g}\hbar\Omega/(2\pi)$ linearly on the dimensionless interaction strength $\tilde{g}$, which leads to relation (27).

References

[1] Haken H 1970 *Laser Theory, Encyclopedia of Physics* (Berlin: Springer)
[2] Sargent M, Scully M O and Lamb W E 1978 *Laser Physics* (New York: Perseus)
[3] Siegman A E 1986 *Lasers* (Mill Valley, CA: University Science Books)
[4] Meschede D 2017 *Optics, Light, and Lasers: The Practical Approach to Modern Aspects of Photonics and Laser Physics* 3rd edn (Weinheim: Wiley)
[5] Klärs J, Schmitt J, Vewinger F and Weitz M 2010 *Nature* **468** 545
[6] Marelic J and Nyman R A 2015 *Phys. Rev.* A **91** 033813
[7] Greveling S, Perrier K L and van Oosten D 2017 Density distribution of a Bose–Einstein condensate of photons in a dye-filled microcavity arXiv:1712.07888
[8] Klärs J, Vewinger F and Weitz M 2010 *Nat. Phys.* **6** 512
[9] Zinn-Justin J 2002 *Quantum Field Theory and Critical Phenomena* 4th edn (Oxford: Oxford University Press)
[10] Kleinert H and Schulte-Frohlinde V 2001 *Critical Properties of Φ^4-Theories* (Singapore: World Scientific)
[11] Zinn-Justin J 2007 *Phase Transitions and Renormalization Group* (Oxford: Oxford University Press)
[12] Gullans M, Stehlik J, Liu Y-Y, Eichler C, Petta J and Taylor J 2016 *Phys. Rev. Lett.* **117** 056801
[13] Hafezi M, Adhikari P and Taylor J M 2015 *Phys. Rev.* B **92** 174305
[14] de Leeuw A-W, van der Wurff E C I, Duine R A, van Oosten D and Stoof H T C 2016 *Phys. Rev.* A **94** 013615
[15] Pethick C J and Smith H 2008 *Bose–Einstein Condensation in Dilute Gases* 2nd edn (Cambridge: Cambridge University Press)
[16] Pitaevskii L P and Stringari S 2016 *Bose–Einstein Condensation* 2nd edn (Oxford: Oxford University Press)
[17] Schmitt J, Damm T, Dung D, Vewinger F, Klärs J and Weitz M 2015 *Phys. Rev.* A **92** 011602
[18] Bajoni D, Senellart P, Lemaître A and Bloch J 2007 *Phys. Rev.* B **76** 201305
[19] Fischer B and Bekker A 2013 *Opt. Photonics News* **24** 40

[20] Chiocchetta A, Gambassi A and Carusotto I 2017 Laser operation and Bose–Einstein condensation: analogies and differences *Universal Themes of Bose–Einstein Condensation* ed N P Proukakis, D W Snoke and P B Littlewood (Cambridge: Cambridge University Press)
[21] Leymann H A M *et al* 2017 *Phys. Rev.* X **7** 021045
[22] Nyman R A and Walker B T 2018 *J. Mod. Opt.* **65** 754
[23] Walker B T, Flatten L C, Hesten H J, Mintert F, Hunger D, Smith J M and Nyman R A 2017 Driven-dissipative Bose–Einstein condensation of just a few photons arXiv:1711.11087
[24] Demokritov S O, Demidov V E, Dzyapko O, Melkov G A, Serga A A, Hillebrands B and Slavin A N 2006 *Nature* **443** 430
[25] Demokritov S O, Demidov V E, Dzyapko O, Melkov G A and Slavin A N 2008 *New J. Phys.* **10** 045029
[26] Chumak A V, Melkov G A, Demidov V E, Dzyapko O, Safonov V L and Demokritov S O 2009 *Phys. Rev. Lett.* **102** 187205
[27] Bozhko D A, Clausen P, Chumak A V, Kobljanskyj Y V, Hillebrands B and Serga A A 2015 *Low Temp. Phys.* **41** 801
[28] Bozhko D A, Serga A A, Clausen P, Vasyuchka V I, Heussner F, Melkov G A, Pomyalov A, L'vov V S and Hillebrands B 2016 *Nat. Phys.* **12** 1057
[29] Kasprzak J *et al* 2006 *Nature* **443** 409
[30] Malpuech G, Rubo Y G, Laussy F P, Bigenwald P and Kavokin A V 2003 *Semicond. Sci. Technol.* **18** S395
[31] Butov L V 2007 *Nature* **447** 540
[32] Kasprzak J, Solnyshkov D D, André R, Dang L S and Malpuech G 2008 *Phys. Rev. Lett.* **101** 146404
[33] Byrnes T, Kim N Y and Yamamoto Y 2014 *Nat. Phys.* **10** 803
[34] Schneider C, Winkler K, Fraser M, Kamp M, Yamamoto Y, Ostrovskaya E and Hofling S 2017 *Rep. Prog. Phys.* **80** 1
[35] Plumhof J D, Stöferle T, Mai L, Scherf U and Mahrt R F 2014 *Nat. Mater.* **13** 3
[36] Stöferle T, Plumhof J D, Mai L, Scherf U and Mahrt R F 2015 *Proc. SPIE* **9370** 93702T
[37] Richard M, Kasprzak J, Romestain R, André R and Dang L S 2005 *Phys. Rev. Lett.* **94** 187401
[38] Kirton P and Keeling J 2013 *Phys. Rev. Lett.* **111** 100404
[39] Kirton P and Keeling J 2015 *Phys. Rev.* A **91** 033826
[40] Keeling J and Kirton P 2016 *Phys. Rev.* A **93** 013829
[41] Moodie R I, Kirton P and Keeling J 2017 *Phys. Rev.* A **96** 043844
[42] Weidlich W and Haake F 1965 *Z. Phys.* **185** 30
[43] Lindblad G 1976 *Commun. Math. Phys.* **48** 119
[44] Kopylov W, Radonjić M, Brandes T, Balaž A and Pelster A 2015 *Phys. Rev.* A **92** 063832
[45] Hesten H J, Nyman R A and Mintert F 2018 *Phys. Rev. Lett.* **120** 040601
[46] de Leeuw A-W, Stoof H T C and Duine R A 2013 *Phys. Rev.* A **88** 033829
[47] de Leeuw A-W, Stoof H T C and Duine R A 2014 *Phys. Rev.* A **89** 053627
[48] de Leeuw A-W, van der Wurff E C I, Duine R A and Stoof H T C 2014 *Phys. Rev.* A **90** 043627
[49] Chiocchetta A and Carusotto I 2014 *Phys. Rev.* A **90** 023633
[50] Lebreuilly J, Chiocchetta A and Carusotto I 2018 *Phys. Rev.* A **97** 033603
[51] Nyman R A and Szymańska M H 2014 *Phys. Rev.* A **89** 033844
[52] Vorberg D, Ketzmerick R and Eckardt A 2018 A unified theory for excited-state, fragmented, and equilibrium-like Bose condensation in pumped photonic many-body systems arXiv:1803.08866
[53] Wouters M and Carusotto I 2007 *Phys. Rev. Lett.* **99** 140402
[54] Lagoudakis K G, Wouters M, Richard M, Baas A, Carusotto I, André R, Dang L S and Deveaud-Plédran B 2008 *Nat. Phys.* **4** 706
[55] Bobrovska N, Ostrovskaya E A and Matuszewski M 2014 *Phys. Rev.* B **90** 205304
[56] Gross E P 1961 *Il Nuovo Cimento* **20** 454
[57] Pitaevskii L 1961 *Sov. Phys. –JETP* **13** 451
[58] Diver M, Robb G R M and Oppo G-L 2014 *Phys. Rev.* A **89** 033602
[59] Chiocchetta A and Carusotto I 2013 *Europhys. Lett.* **102** 67007
[60] Klärs J, Schmitt J, Damm T, Vewinger F and Weitz M 2011 *Appl. Phys.* B **105** 17
[61] Bloch I, Dalibard J and Zwerger W 2008 *Rev. Mod. Phys.* **80** 885
[62] Marelic J, Walker B T and Nyman R A 2016 *Phys. Rev.* A **94** 063812
[63] van der Wurff E C I, de Leeuw A-W, Duine R A and Stoof H T C 2014 *Phys. Rev. Lett.* **113** 135301
[64] Schmitt J, Damm T, Dung D, Vewinger F, Klärs J and Weitz M 2014 *Phys. Rev. Lett.* **112** 030401
[65] Greveling S, van der Laan F, Perrier K L and van Oosten D 2017 The effective interaction strength in a Bose–Einstein condensate of photons in a dye-filled microcavity arXiv:1712.07922
[66] Strasberg P, Schaller G, Lambert N and Brandes T 2016 *New J. Phys.* **18** 073008
[67] Suaréz A and Silbey R 1991 *J. Chem. Phys.* **94** 4809
[68] Wilson-Rae I and Imamoğlu A 2002 *Phys. Rev.* B **65** 235311
[69] Keeling J and Kirton P 2018 private communication
[70] Gardiner C and Zoller P 2004 *Quantum Noise: A Handbook of Markovian and Non-Markovian Quantum Stochastic Methods with Applications to Quantum Optics* 3rd edn (Berlin: Springer)
[71] Marthaler M, Utsumi Y, Golubev D S, Shnirman A and Schön G 2011 *Phys. Rev. Lett.* **107** 093901
[72] Kubo R 1962 *J. Phys. Soc. Jpn.* **17** 1100
[73] Henschel K, Majer J, Schmiedmayer J and Ritsch H 2010 *Phys. Rev.* A **82** 033810
[74] Leymann H A M, Foerster A and Wiersig J 2014 *Phys. Rev.* B **89** 085308
[75] Foerster A, Leymann H A M and Wiersig J 2017 *Comput. Phys. Commun.* **212** 210
[76] Weiss U 2012 *Quantum Dissipative Systems* 4th edn (Singapore: World Scientific)
[77] Lee C K, Moix J and Cao J 2012 *J. Chem. Phys.* **136** 204120
[78] Kennard E H 1918 *Phys. Rev.* **11** 29
[79] Kennard E H 1926 *Phys. Rev.* **28** 672
[80] Stepanov B I 1957 *Dokl. Akad. Nauk SSSR* **112** 839 [*Sov. Phys. Dokl.* **2** 81]
[81] Schmitt J 2017 private communication
[82] Schäfer F P 1990 *Dye Lasers* 3rd edn (Berlin: Springer)
[83] Greveling S, van der Laan F, Jagers H C and van Oosten D 2017 Polarization of a Bose–Einstein condensate of photons in a dye-filled Microcavity arXiv:1712.08426
[84] Masujima M 2005 *Applied Mathematical Methods in Theoretical Physics* (Weinheim: Wiley)

Macroscopic Superpositions as Quantum Ground States

Borivoje Dakić[1,2] and Milan Radonjić[2,3]
[1]Institute for Quantum Optics and Quantum Information (IQOQI), Austrian Academy of Sciences, Boltzmanngasse 3, A-1090 Vienna, Austria
[2]Faculty of Physics, University of Vienna, Boltzmanngasse 5, A-1090 Vienna, Austria
[3]Institute of Physics Belgrade, University of Belgrade, Pregrevica 118, 11080 Belgrade, Serbia
(Received 24 June 2016; revised manuscript received 20 June 2017; published 1 September 2017)

We study the question of what kind of a macroscopic superposition can(not) naturally exist as a ground state of some gapped local many-body Hamiltonian. We derive an upper bound on the energy gap of an arbitrary physical Hamiltonian provided that its ground state is a superposition of two well-distinguishable macroscopic "semiclassical" states. For a large class of macroscopic superposition states we show that the gap vanishes in the macroscopic limit. This in turn shows that preparation of such states by simple cooling to the ground state is not experimentally feasible and requires a different strategy. Our approach is very general and can be used to rule out a variety of quantum states, some of which do not even exhibit macroscopic quantum properties. Moreover, our methods and results can be used for addressing quantum marginal related problems.

DOI: 10.1103/PhysRevLett.119.090401

Introduction.—Ever since Schrödinger's cat gedanken experiment [1] the question of whether a macroscopic system can be found in a quantum superposition state remains unanswered. Various attempts were made to address our inability to detect macroscopic quantum superpositions. Decoherence-type arguments are commonly employed in which one advocates that the quantumness of a macroscopic system is lost due to interactions with a noisy environment [2]. Alternatively, it was indicated that classical behavior can emerge because our measurements suffer from limited resolution or limited sensitivity [3–5]. Moreover, various spontaneous collapse models introduce a stochastic nonlinear modification of the Schrödinger equation that causes macroscopic superpositions to quickly appear as classical, while giving the same experimental predictions as quantum theory in the microscopic regime [6].

Naturally, the boundary between the quantum and classical realms should be explored by experiments [7–9]. In recent decades, typical quantum features have been demonstrated in large molecules [10,11], hundreds of photons [12,13], superconducting circuits [14,15], micromechanical oscillators [16,17], and fragmented Bose condensates [18,19]. Nonetheless, quantum superpositions of truly macroscopic objects remain an uncharted territory that will hopefully be revealed by future experiments.

Recently, different measures have been proposed to quantify macroscopicity of quantum states [20–30]. The literature about this topic is diverse and various measures are mutually compared in Refs. [20,21] and summarized in Ref. [22]. Generally speaking, a macroscopic quantum state (MQS) is a state capable of displaying macroscopic quantum effects that can be utilized to validate quantum mechanics (against classical theories) on a macroscopic scale. An important task is the identification of a characteristic parameter that measures the "size" or "macroscopicity" of a certain quantum state [7], such as the characteristic energy, mass, number of elementary constituents, etc. Here we focus on the case of macroscopically large number of particles N that interact via a local Hamiltonian.

An important subclass of MQS are macroscopic superpositions (MS): states of the type $|\psi\rangle = |\psi_1\rangle + |\psi_2\rangle$, where $|\psi_{1,2}\rangle$ are macroscopically well-distinguishable states. However, such a definition is not operational as there are infinitely many decompositions of the kind $|\psi_1\rangle + |\psi_2\rangle$ and it might not be clear how to unambiguously identify the "semiclassical" components of the MS. Therefore, we define MS with respect to a measurement of an additive (collective) observable [20,21,23,28,29]. A pure state $|\psi\rangle$ is MS if a measurement of some additive observable $\hat{S}$ can sharply distinguish the semiclassical states that constitute MS; e.g., the distribution of eigenvalues of $\hat{S}$ exhibits two well-resolvable regions (see Fig. 1). Our main focus here is on (i) the possibility of the natural appearance of such states as unique ground states of macroscopic quantum systems and, consequently, (ii) the feasibility of preparing MS by simply cooling down such systems. The latter might be achievable provided that the system has a unique MS ground state; i.e., there is a finite energy gap in the thermodynamic limit. In this respect, it was proven that no MS of "locally distinguishable" states can be the unique ground state of N spins described by a local Hamiltonian whose energy gap is at least $O(1/\mathrm{poly}(N))$ [31]. Conversely, numerical evidence was given in Ref. [32] that the energy gap of a certain N-qubit Hamiltonian decays exponentially fast in the macroscopic limit when its ground state actually is MS. Moreover, relation between the

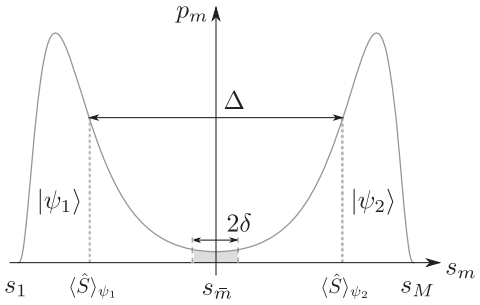

FIG. 1. The distribution p_m of eigenvalues s_m of an additive observable $\hat{S}$ for a MS state $|\psi_1\rangle + |\psi_2\rangle$. A continuous curve is used for aesthetic purposes. The distribution has two well-resolved regions (left and right from the separation point $s_{\bar{m}}$) each corresponding to the superimposed semiclassical states $|\psi_1\rangle$ and $|\psi_2\rangle$, respectively. The distance between the regions is $\Delta := |\langle\hat{S}\rangle_{\psi_2} - \langle\hat{S}\rangle_{\psi_1}|$. The separation probability related to the finite-sized shaded segment $|s - s_{\bar{m}}| \leq \delta = O(N^0)$ should be vanishing in the macroscopic limit $N \to \infty$.

spectral gap and ground state properties of spin lattice systems was studied in Refs. [33,34].

We provide a simple sufficient criterion enforcing the energy gap to vanish in the thermodynamic limit for a very general class of ground states of local many-body Hamiltonians. The most important feature of our approach is an operational method to identify semiclassical states that constitute the macroscopic superposition. We show that in many cases local Hamiltonians are not capable of linking such states, so that the corresponding MS can only represent a degenerate ground state in the macroscopic limit. Our main theorem provides an interesting relation between the energy gap and the order of interaction (i.e., the number K in the case of a K-body interaction). Therefore, one may derive the lowest order of interaction for which a given MS might be a unique ground state. We discuss our results in the context of different physical systems and various proposals for preparation of MS. Furthermore, we show that a certain class of states that are not even considered to be macroscopically quantum (e.g., W states) cannot naturally exist as ground states of gapped local Hamiltonians. Finally, we demonstrate that the methods and results derived here are relevant for quantum marginal related problems.

Preliminaries.—Let us consider a system of N interacting particles described by a K-local Hamiltonian $\hat{H} = \sum_{(i_1,i_2,\ldots,i_K)\in\mathcal{I}_N^{(K)}} \hat{H}_{i_1 i_2 \ldots i_K}$, where $\hat{H}_{i_1 i_2 \ldots i_K}$ is the contribution due to interaction between particles $i_1, i_2, \ldots, i_K$ and $\mathcal{I}_N^{(K)}$ is the set of all K-tuples of N interacting particles. We call K the order of interaction. For instance, usual physical interactions are pairwise with the order $K = 2$.

We begin with the following general lemma:

Lemma.—Let a Hamiltonian $\hat{H}$ have a unique ground state of the form $|\psi\rangle = a_1|\psi_1\rangle + a_2|\psi_2\rangle$, where $|\psi_{1,2}\rangle$ are normalized, $\langle\psi_2|\psi_1\rangle = \lambda$ and $a_1, a_2 > 0$. Then the energy gap ΔE satisfies the inequality

$$\Delta E \leq \frac{|\langle\psi_2|\hat{H}|\psi_1\rangle - \lambda E_0|}{a_1 a_2 (1 - |\lambda|^2)}, \tag{1}$$

where E_0 denotes the ground state energy (see Supplemental Material [35] for the proof).

Without loss of generality we set $E_0 = 0$ hereafter. We start our analysis with the simple observation that the energy gap is essentially upper bounded by a magnitude of the matrix element $\langle\psi_2|\hat{H}|\psi_1\rangle = H_{21}$ [assuming that the overlap λ is vanishingly small and $a_{1,2} = O(N^0)$ when $N \to \infty$]. Therefore, the system cannot have a finite gap in the macroscopic limit if H_{21} is vanishing when $N \to \infty$.

An archetypal example of MS is a so-called GHZ state [44], closely related to an original Schrödinger's proposal as it is a superposition of two macroscopically distinct states of N particles, i.e., $|\psi\rangle \propto |\varphi_1\rangle^{\otimes N} + |\varphi_2\rangle^{\otimes N}$. The states $|\varphi_{1,2}\rangle$ are normalized with the fixed nonzero overlap $\omega = |\langle\varphi_1|\varphi_2\rangle| < 1$. Here, one can naturally identify the two constituents $|\psi_{1,2}\rangle = |\varphi_{1,2}\rangle^{\otimes N}$ with exponentially small overlap $|\lambda| = \omega^N$ and $a_{1,2} \overset{N\to\infty}{\to} 1/\sqrt{2}$. Denote by $H_{21}^{[K]}$ the maximal magnitude of all matrix elements $\langle\varphi_2|^{\otimes K}\hat{H}_{i_1,i_2,\ldots,i_K}|\varphi_1\rangle^{\otimes K}$. The value of $H_{21}^{[K]}$ does not scale with N and solely depends on the nature of the interaction. It is not difficult to see that

$$|H_{21}| \leq |\mathcal{I}_N^{(K)}|\omega^{N-K}H_{21}^{[K]} \leq \binom{N}{K}\omega^{N-K}H_{21}^{[K]}, \tag{2}$$

since for K fixed the total number of interaction terms grows at most polynomially with N, i.e., $|\mathcal{I}_N^{(K)}| \leq \binom{N}{K} = O(N^K)$. Therefore, we conclude that the energy gap vanishes exponentially fast when $N \to \infty$, as long as the order of interaction is fixed. In other words, all the states $|\psi(\alpha)\rangle \propto |\varphi_1\rangle^{\otimes N} + e^{i\alpha}|\varphi_2\rangle^{\otimes N}$ give the same energy in the thermodynamic limit and the ground state becomes at least doubly degenerate. Consequently, cooling down the system towards zero temperature will result in a classical mixture $\frac{1}{2}|\psi(0)\rangle\langle\psi(0)| + \frac{1}{2}|\psi(\pi)\rangle\langle\psi(\pi)|$. In order to make the energy gap finite in the thermodynamic limit, it is necessary that the order of interaction K grows with the number of particles N, which is usually considered nonphysical. This reasoning can be trivially extended to a finite sum $|\varphi_1\rangle^{\otimes N} + \cdots + |\varphi_n\rangle^{\otimes N}$ of macroscopically distinguishable states, i.e., $\langle\varphi_i|\varphi_j\rangle = O(N^0)$ when $i \neq j$. In the Supplemental Material [35] we show that the same result holds for a more general class of states, i.e., the superpositions of locally distinguishable states that have been considered in literature as a natural generalization of the GHZ-like states [20,24].

Whereas the previous examples are fairly easy to grasp, as the superimposed states are identifiable by definition, such a clean prescription is not *a priori* available for arbitrary MQS. Therefore, we continue our analysis by invoking a measurement of some collective observable $\hat{S}$ that should serve as a reference point to identify $|\psi_{1,2}\rangle$.

Consider a system of N particles in a total Hilbert space $\mathcal{H}^N = \otimes_{i=1}^N \mathcal{H}_i$, with $\dim(\mathcal{H}_i) = d$. Let $\hat{S} = \sum_{i=1}^N \hat{S}_i$ be an additive observable. The single-particle operators satisfy $\hat{S}_i|\sigma_i, \mu_i\rangle_i = \sigma_i|\sigma_i, \mu_i\rangle_i$, where $\sigma_i \in \{\varsigma_1 < \varsigma_2 < \ldots < \varsigma_\ell\}$ and $2 \leq \ell \leq d$, while $\mu_i = 1, \ldots, \mu(\sigma_i)$ enumerate the degeneracies obeying $\sum_{l=1}^{\ell} \mu(\varsigma_l) = d$. We denote the different eigenvalues of $\hat{S}$ by $s_1 < s_2 < \ldots < s_M$, where $s_m = \sum_{l=1}^{\ell} n_{m,l}\varsigma_l$, $n_{m,l} \in \mathbb{N}_0$ and $\sum_{l=1}^{\ell} n_{m,l} = N$. Clearly, $s_1 = N\varsigma_1$ and $s_M = N\varsigma_\ell$. The states $|\boldsymbol{\sigma}, \boldsymbol{\mu}\rangle = \otimes_{i=1}^N |\sigma_i, \mu_i\rangle_i$ constitute a complete basis in $\mathcal{H}^N$, i.e., $\sum_{\boldsymbol{\sigma}} \sum_{\boldsymbol{\mu}} |\boldsymbol{\sigma}, \boldsymbol{\mu}\rangle\langle\boldsymbol{\sigma}, \boldsymbol{\mu}| = \mathbb{1}$, where $\boldsymbol{\sigma} = (\sigma_1, \sigma_2, \ldots, \sigma_N)$ and $\boldsymbol{\mu} = (\mu_1, \mu_2, \ldots, \mu_N)$. This yields a decomposition

$$|\psi\rangle = \sum_{\boldsymbol{\sigma}} \sum_{\boldsymbol{\mu}} |\boldsymbol{\sigma}, \boldsymbol{\mu}\rangle\langle\boldsymbol{\sigma}, \boldsymbol{\mu}|\psi\rangle = \sum_{m=1}^{M} \sqrt{p_m}\, |s_m\rangle, \quad (3)$$

where $\hat{S}|s_m\rangle = s_m|s_m\rangle$, and $|s_m\rangle$ contains all the terms from the multisums such that $\sum_{i=1}^N \sigma_i = s_m$. The numbers $p_m \geq 0$ correspond to the probabilities of obtaining the value s_m when measuring the observable $\hat{S}$ in the state $|\psi\rangle$, hence, $\sum_{m=1}^M p_m = 1$.

Now, if the state $|\psi\rangle$ is MS of two states $|\psi_1\rangle$ and $|\psi_2\rangle$, then we expect that the probability distribution $\mathcal{P}_\psi = \{p_m\}_{m=1}^M$ has two distinguishable regions with corresponding probabilities of the order $O(N^0)$ and with vanishingly small probability within the finite-sized bordering segment around some eigenvalue $s_{\bar{m}}$ of $\hat{S}$ (see Fig. 1). Those regions should precisely be related to the semiclassical constituents of the state $|\psi\rangle$. The distance between the regions $\Delta := |\langle\hat{S}\rangle_{\psi_2} - \langle\hat{S}\rangle_{\psi_1}|$ is closely related to the fluctuation of the observable $\hat{S}$ in the state $|\psi\rangle$ and it is commonly assumed that MS displays $\Delta = O(N)$ [20,29,30]. However, we will address quantum states from another aspect, which will render our main result independent of Δ. Namely, the prime quantity in our analysis is the separation probability $P_\psi(|s - s_{\bar{m}}| \leq \delta)$, i.e., the probability of finding the result s, when measuring $\hat{S}$, within a tiny segment of size $2\delta = O(N^0)$ centered at the separation point $s_{\bar{m}}$. We will provide an upper bound on the energy gap, which essentially depends on the separation probability and the order of interaction. Thus, the interplay between the two will have a crucial role in vanishing of the gap.

Next, we will make use of $s_{\bar{m}}$ to express the ground state in the form of a superposition

$$|\psi\rangle = a_1|\psi_1\rangle + a_2|\psi_2\rangle, \quad (4)$$

with

$$a_1|\psi_1\rangle = \sum_{m=1}^{\bar{m}-1} \sqrt{p_m}|s_m\rangle, \quad a_2|\psi_2\rangle = \sum_{m=\bar{m}}^{M} \sqrt{p_m}|s_m\rangle, \quad (5)$$

where $a_1 = (p_1 + \cdots + p_{\bar{m}-1})^{1/2}$, $a_2 = (p_{\bar{m}} + \cdots + p_M)^{1/2}$, and, presumably, $a_{1,2} = O(N^0)$. By construction, one has $\langle\psi_2|\psi_1\rangle = 0$. We will employ the introduced separation to derive an upper estimate of the energy gap.

Let us suppose that the Hamiltonian of the physical system is 2-local, i.e., $\hat{H} = \sum_{(i,j)\in\mathcal{I}_N^{(2)}} \hat{H}_{ij}$, where $\hat{H}_{ij}$ represents pairwise interaction between particles i and j and $\mathcal{I}_N^{(2)}$ is the set of pairs of interacting particles. Obviously, the number of interaction terms in the Hamiltonian satisfies $|\mathcal{I}_N^{(2)}| \leq N(N-1)/2 = O(N^2)$. The magnitude of the matrix element in the inequality (1) can be estimated in order to obtain the following central result:

Theorem.—Under the assumptions given in the text, the energy gap of the system is bounded as

$$\Delta E \leq \frac{|\mathcal{I}_N^{(2)}|}{2a_1^2 a_2^2} \max_{(i,j)\in\mathcal{I}_N^{(2)}} \|\hat{H}_{ij}\| \cdot P_\psi(|s - s_{\bar{m}}| \leq 2\delta_\varsigma), \quad (6)$$

where $\max_{(i,j)\in\mathcal{I}_N^{(2)}} \|\hat{H}_{ij}\|$ sets the characteristic energy scale (independent of N) and $\delta_\varsigma = \varsigma_\ell - \varsigma_1$. Here, $\|\cdot\|$ denotes the operator spectral norm. The complete proof is given in the Supplemental Material [35].

The bound (6) is valid for any $s_{\bar{m}}$, which has been arbitrary up to now. Clearly, one should select $\hat{S}$ and the corresponding $s_{\bar{m}}$ so that $P_\psi(|s - s_{\bar{m}}| \leq 2\delta_\varsigma)$ vanishes as fast as possible for $N \to \infty$. In the previously discussed GHZ-like case, the separation probability scales as $\exp[-O(N)]$ and the energy gap vanishes exponentially fast with N. Furthermore, it is clear that for any state exhibiting $P_\psi = o(1/N^2)$ the gap will vanish in the thermodynamic limit and the state can only represent a degenerate ground state. In general, such a state does not necessarily display anomalous fluctuation of $\hat{S}$. One can even find examples where $\Delta = O(N^0)$ [such as $|\psi\rangle = (|s_{m_1}\rangle + |s_{m_2}\rangle)/\sqrt{2}$, where $s_{m_1} = s_{\bar{m}} - 2\delta$ and $s_{m_2} = s_{\bar{m}} + 2\delta$, with $\delta > \delta_\varsigma$]. Conversely, when the system features a finite energy gap, the relation (6) puts a lower bound $P_\psi(|s - s_{\bar{m}}| \leq 2\delta_\varsigma) \geq O(1/N^2)$ for any gapped 2-local Hamiltonian and arbitrary observable $\hat{S}$.

The appearance of probabilities corresponding to the interval of size $4\delta_\varsigma$ centered at $s_{\bar{m}}$ is a direct consequence of the 2-local nature of the Hamiltonian. We note that the Theorem could easily be generalized for arbitrary K-local Hamiltonians. In that case, one would consider the set $\mathcal{I}_N^{(K)}$ of K-tuples of interacting particles, for which $|\mathcal{I}_N^{(K)}| \leq \binom{N}{K} = O(N^K)$, and the corresponding estimate of the gap would involve the probability $P_\psi(|s - s_{\bar{m}}| \leq 2K\delta_\varsigma)$. Thus, for a gapped K-local Hamiltonian we conclude that the best possible separation probability one can achieve for a ground state is asymptotically lower bounded by $O(1/N^K)$. Consequently, all the states exhibiting the scaling $P_\psi = o(1/N^K)$ are excluded as possible unique ground states.

Various examples.—Our general result nicely complies with the investigation of ground states of various physical systems. For example, a twofold fragmented condensate of interacting bosons trapped in a single well [18] features a

doubly degenerate ground state, in the thermodynamic limit. It was shown in Ref. [19] that in the appropriate Fock space basis the corresponding ground states are identical to the photon cat states. In accordance with our findings, the proposed preparation of these states requires other means than simple cooling, i.e., the rapid sweep of interaction couplings [45]. Another example is a one-dimensional array of circuit quantum electrodynamic (cQED) systems in the ultrastrong cavity-qubit coupling regime [46]. The authors showed that the photon hopping between cavities can be mapped to the Ising interaction between the lowest two levels of individual cQED of the chain. Based on the mapping, they found two nearly degenerate GHZ-type ground states with energy splitting exponentially small in the system size. Again, this is in perfect agreement with our results. Moreover, we mention the study of a bosonic Josephson junction made of N ultracold and dilute atoms confined by a quasi-one-dimensional double-well potential within the two-site Bose-Hubbard model framework [47]. Detailed treatment showed that the ground state of the system evolves towards NOON state when increasing attractive interatomic interaction. The estimated gap between two lowest energy states vanishes exponentially with N, in full compliance with our considerations. Our work also nicely agrees with Ref. [48] where the possibility of creating many-particle catlike states was examined for a Bose-Einstein condensate trapped in a double-well potential. It was discussed in detail that creating cat states via adiabatic manipulation of the many-body ground state is experimentally unfeasible due to the fact that the end state is nearly degenerate with the first-excited state; hence, such a process would require an exponentially long time. This difficulty was surpassed by proposing to exploit dynamic evolution following a sudden flipping of the sign of the atomic interaction, accomplished via Feshbach resonance technique [49]. Finally, we mention that our treatment assumes a close correspondence between the macroscopicity of the system and the number of its constituents. However, the macroscopicity might be related to other quantities and only weakly depend on the system size. SQUID systems, which were proposed as good candidates to host the "genuine" MS [7], are a paramount example of that. Although our results are not directly applicable to such a case, in the Supplemental Material [35] we provide a discussion of SQUIDs showing some similarities with our findings.

Our generic analysis demonstrates that more sophisticated experimental techniques are needed for the preparation of a variety of macroscopic superpositions in the thermodynamic limit. This may require some form of dynamical driving of a system, as in the mentioned examples, advanced matter-wave interferometric approaches [50] or use of demanding postselection techniques [51].

Furthermore, we present an example to demonstrate that our results can be used to address the states that are more general than MQS (see Supplemental Material [35]). Consider a lattice model of N spin-1/2 particles interacting with the fixed number of neighbors. Thus, one has $d = 2$, $\ell = 2$, $\delta_\varsigma = 1$, and $|\mathcal{I}_N^{(2)}| = O(N)$. In order to prove that the model becomes gapless in the limit $N \to \infty$, one has to find an appropriate additive observable $\hat{S}$ for which the ground-state-related separation probability vanishes as $o(1/N)$. Collective states that naturally appear in spin systems are the Dicke states [52] $|j, m\rangle$ $(m = -j, \ldots, j)$, where $j = N/2$. They are permutation invariant and satisfy $\hat{J}^2|j, m\rangle = j(j+1)|j, m\rangle$ and $\hat{J}_z|j, m\rangle = m|j, m\rangle$. All Dicke states are unique ground states of some fully 2-local, gapped Hamiltonian for which $|\mathcal{I}_N^{(2)}| = N(N-1)/2$ (all the particles mutually interact pair wisely, such as indistinguishable particles) [31]. However, such Hamiltonians do not correspond to the present case. Therefore, we will show that, for example, an N-qubit W state $|j, j-1\rangle$, which represents the case of symmetrically distributed one-spin excitations, cannot be a unique ground state of any considered spin-lattice model. First, we find the appropriate collective observable to be $\hat{J}_x$. Let $|j, m\rangle_x$ $(m = -j, \ldots, j)$ be the common eigenbasis of $\hat{J}^2$ and $\hat{J}_x$. The related probability distribution is $p_m = |\langle j, j-1|j, m\rangle_x|^2$ (see Fig. 1 in the Supplemental Material [35]), $s_m = m$, and we choose $s_{\bar{m}} = 0$ for j integer or $s_{\bar{m}} = 1/2$ for j half-integer. As presented in the Supplemental Material [35], we find

$$p_m = \frac{2m^2}{2^{2j} j} \binom{2j}{j+m} \sim \frac{2m^2}{\sqrt{\pi} j^{3/2}}, \tag{7}$$

where the last asymptotic behavior holds for fixed m and $j \to \infty$. We conclude that the separation probability $P_\psi(|s - s_{\bar{m}}| \leq 2)$ scales as $O(1/j^{3/2})$, i.e., $O(1/N^{3/2})$. Thus, the W state can only be a degenerate ground state of the arbitrary spin-lattice model considered here. Moreover, the distance between the two peaks has sublinear asymptotic scaling $\sim\sqrt{2N}$. Hence, the W state is an example of a state that is not even a MQS according to the anomalous fluctuation criterion, but is nevertheless amenable to our present analysis.

Finally, our results can be naturally related to quantum marginal problem [53,54]. There, the main task is to check whether or not a given set of marginal states $\hat{\boldsymbol{\rho}} = (\hat{\rho}_{s_1}, \hat{\rho}_{s_2}, \ldots)$ can be extended to some N-particle quantum state $\hat{\varrho}^{[N]}$, i.e., $\hat{\rho}_{s_k} = \mathrm{Tr}_{\bar{s}_k} \hat{\varrho}^{[N]}$, where s_k denotes a subset of N particles. The set of all representable marginals $\hat{\boldsymbol{\rho}}$ is convex and completely characterized by its extremal points (for finite-dimensional systems); therefore, their identification is of great importance. On the other hand, the set of extremal points is in unique correspondence to the set of N-particle nondegenerate ground states of the local Hamiltonians [54]. Namely, for a given Hamiltonian $\hat{H} = \sum_k \hat{H}_{s_k}$, where $\hat{H}_{s_k}$ denotes local Hamiltonian acting on the subset of particles s_k, we have $E = \mathrm{Tr}(\hat{\varrho}^{[N]}\hat{H}) = \sum_k \mathrm{Tr}_{s_k}(\hat{\rho}_{s_k}\hat{H}_{s_k}) = \mathrm{Tr}(\hat{\boldsymbol{\rho}}\hat{\boldsymbol{H}})$, where $\hat{\boldsymbol{H}} = (\hat{H}_{s_1}, \hat{H}_{s_2}, \ldots)$.

Thus, the energy E is a linear functional on the set of all representable marginals $\hat{\boldsymbol{\rho}}$ and it reaches its extreme values on the set of nondegenerate ground states. Our criterion (6) implies that a large class of degenerate ground states (in the thermodynamic limit) has the set of marginals that cannot be extremal.

Summary and outlook.—In this Letter we provided a powerful generic method to analyze the possibility for ground states of gapped many-body quantum systems to be superpositions of macroscopically distinct quantum states. We have ruled out a large class of quantum states that cannot be prepared by simply cooling macroscopic quantum systems that exhibit interactions involving some finite number of their constituents. For such a state, we require that the separation probability, related to the small segment around the separation point between its two semiclassical components, vanishes sufficiently fast in the thermodynamic limit. We expect our results to be valuable for future experiments aiming at preparing quantum states that exhibit macroscopic quantum properties. Furthermore, we have shown that our study is relevant for quantum marginal problem.

We thank Časlav Brukner, Nikola Paunković, and Jacques Pienaar for helpful comments and gratefully acknowledge financial support from the European Commission through the projects RAQUEL (No. 323970) and QUCHIP (No. 641039).

[1] E. Schrödinger, Die gegenwärtige Situation in der Quantenmechanik, Naturwissenschaften **23**, 807 (1935).
[2] W. H. Zurek, Decoherence, einselection, and the quantum origins of the classical, Rev. Mod. Phys. **75**, 715 (2003).
[3] J. Kofler and Č. Brukner, Classical World Arising out of Quantum Physics under the Restriction of Coarse-Grained Measurements, Phys. Rev. Lett. **99**, 180403 (2007).
[4] S. Raeisi, P. Sekatski, and C. Simon, Coarse Graining Makes It Hard to See Micro-Macro Entanglement, Phys. Rev. Lett. **107**, 250401 (2011).
[5] P. Sekatski, N. Gisin, and N. Sangouard, How Difficult Is It to Prove the Quantumness of Macroscropic States?, Phys. Rev. Lett. **113**, 090403 (2014).
[6] A. Bassi, K. Lochan, S. Satin, T. P. Singh, and H. Ulbricht, Models of wave-function collapse, underlying theories, and experimental tests, Rev. Mod. Phys. **85**, 471 (2013).
[7] A. J. Leggett, Testing the limits of quantum mechanics: motivation, state of play, prospects, J. Phys. Condens. Matter **14**, R415 (2002).
[8] M. Arndt and K. Hornberger, Testing the limits of quantum mechanical superpositions, Nat. Phys. **10**, 271 (2014).
[9] T. Farrow and V. Vedral, Classification of macroscopic quantum effects, Opt. Commun. **337**, 22 (2015).
[10] O. Nairz, M. Arndt, and A. Zeilinger, Quantum interference experiments with large molecules, Am. J. Phys. **71**, 319 (2003).
[11] S. Eibenberger, S. Gerlich, M. Arndt, M. Mayor, and J. Tüxen, Matter-wave interference of particles selected from a molecular library with masses exceeding 10000 amu, Phys. Chem. Chem. Phys. **15**, 14696 (2013).
[12] N. Bruno, A. Martin, P. Sekatski, N. Sangouard, R. T. Thew, and N. Gisin, Displacement of entanglement back and forth between the micro and macro domains, Nat. Phys. **9**, 545 (2013).
[13] A. I. Lvovsky, R. Ghobadi, A. Chandra, A. S. Prasad, and C. Simon, Observation of micro-macro entanglement of light, Nat. Phys. **9**, 541 (2013).
[14] C. H. van der Wal *et al.*, Quantum Superposition of Macroscopic Persistent-Current States, Science **290**, 773 (2000).
[15] J. R. Friedman, V. Patel, W. Chen, S. K. Tolpygo, and J. E. Lukens, Quantum superposition of distinct macroscopic states, Nature (London) **406**, 43 (2000).
[16] A. D. O'Connell *et al.*, Quantum ground state and single-phonon control of a mechanical resonator, Nature (London) **464**, 697 (2010).
[17] N. Kiesel, F. Blaser, U. Delić, D. Grass, R. Kaltenbaek, and M. Aspelmeyer, Cavity cooling of an optically levitated submicron particle, Proc. Natl. Acad. Sci. U.S.A. **110**, 14180 (2013).
[18] P. Bader and U. R. Fischer, Fragmented Many-Body Ground States for Scalar Bosons in a Single Trap, Phys. Rev. Lett. **103**, 060402 (2009).
[19] U. R. Fischer and M.-K. Kang, "Photonic" Cat States from Strongly Interacting Matter Waves, Phys. Rev. Lett. **115**, 260404 (2015).
[20] F. Fröwis and W. Dür, Measures of macroscopicity for quantum spin systems, New J. Phys. **14**, 093039 (2012).
[21] F. Fröwis, N. Sangouard, and N. Gisin, Linking measures for macroscopic quantum states via photon-spin mapping, Opt. Commun. **337**, 2 (2015).
[22] H. Jeong, M. Kang, and H. Kwon, Characterizations and quantifications of macroscopic quantumness and its implementations using optical fields, Opt. Commun. **337**, 12 (2015).
[23] G. Björk and P. G. L. Mana, A size criterion for macroscopic superposition states, J. Opt. B **6**, 429 (2004).
[24] J. I. Korsbakken, K. B. Whaley, J. Dubois, and J. I. Cirac, Measurement-based measure of the size of macroscopic quantum superpositions, Phys. Rev. A **75**, 042106 (2007).
[25] F. Marquardt, B. Abel, and J. von Delft, Measuring the size of a quantum superposition of many-body states, Phys. Rev. A **78**, 012109 (2008).
[26] S. Nimmrichter and K. Hornberger, Macroscopicity of Mechanical Quantum Superposition States, Phys. Rev. Lett. **110**, 160403 (2013).
[27] P. Sekatski, N. Sangouard, and N. Gisin, Size of quantum superpositions as measured with classical detectors, Phys. Rev. A **89**, 012116 (2014).
[28] A. Shimizu and T. Miyadera, Stability of Quantum States of Finite Macroscopic Systems against Classical Noises, Perturbations from Environments, and Local Measurements, Phys. Rev. Lett. **89**, 270403 (2002).
[29] A. Shimizu and T. Morimae, Detection of Macroscopic Entanglement by Correlation of Local Observables, Phys. Rev. Lett. **95**, 090401 (2005).
[30] C.-W. Lee and H. Jeong, Quantification of Macroscopic Quantum Superpositions within Phase Space, Phys. Rev. Lett. **106**, 220401 (2011).

[31] F. Fröwis, M. van den Nest, and W. Dür, Certifiability criterion for large-scale quantum systems, New J. Phys. **15**, 113011 (2013).
[32] T. Morimae, Low-temperature coherence properties of Z_2 quantum memory, Phys. Rev. A **81**, 022304 (2010).
[33] T. Kuwahara, I. Arad, L. Amico, and V. Vedral, Local reversibility and entanglement structure of many-body ground states, Quantum Sci. Technol. **2**, 015005 (2017).
[34] T. Kuwahara, Asymptotic behavior of macroscopic observables in generic spin systems, J. Stat. Mech. (2016) 053103.
[35] See Supplemental Material at http://link.aps.org/supplemental/10.1103/PhysRevLett.119.090401 for the proofs, further examples and discussion. Additional Refs. [36–43] are also included therein.
[36] J. Watrous, *Theory of Quantum Information* (University of Waterloo, Waterloo, 2016).
[37] L. C. Biedenharn and J. D. Louck, *Angular Momentum in Quantum Physics: Theory and Application* (Addison-Wesley, Reading, MA, 1981).
[38] C. L. Frenzen and R. Wong, A uniform asymptotic expansion of the Jacobi polynomials with error bounds, Can. J. Math. **37**, 979 (1985).
[39] R. Wong and Y.-Q. Zhao, Uniform asymptotic expansion of the Jacobi polynomials in a complex domain, Proc. R. Soc. A **460**, 2569 (2004).
[40] X.-X. Bai and Y.-Q. Zhao, A uniform asymptotic expansion for Jacobi polynomials via uniform treatment of Darboux's method, J. Approx. Theory **148**, 1 (2007).
[41] U. Eckern, G. Schön, and V. Ambegaokar, Quantum dynamics of a superconducting tunnel junction, Phys. Rev. B **30**, 6419 (1984).
[42] M. Robnik, L. Salasnich, and M. Vranicar, WKB Corrections to the Energy Splitting in Double Well Potentials, Nonlin. Phenom. Complex Syst. (Minsk) **2**, 49 (1999).
[43] A. L. DiRienzo, Ph.D. thesis, The University of Arizona, 1982.
[44] D. M. Greenberger, M. A. Horne, and A. Zeilinger, in *Bell's Theorem, Quantum Theory, and Conceptions of the Universe*, edited by M. Kafatos (Kluwer, Dordrecht, 1989), p. 69.
[45] U. R. Fischer, K.-S. Lee, and B. Xiong, Emergence of a new pair-coherent phase in many-body quenches of repulsive bosons, Phys. Rev. A **84**, 011604(R) (2011).
[46] M.-J. Hwang and M.-S. Choi, Large-scale maximal entanglement and Majorana bound states in coupled circuit quantum electrodynamic systems, Phys. Rev. B **87**, 125404 (2013).
[47] G. Mazzarella, L. Salasnich, A. Parola, and F. Toigo, Coherence and entanglement in the ground state of a bosonic Josephson junction: From macroscopic Schrödinger cat states to separable Fock states, Phys. Rev. A **83**, 053607 (2011).
[48] Y. P. Huang and M. G. Moore, Creation, detection, and decoherence of macroscopic quantum superposition states in double-well Bose-Einstein condensates, Phys. Rev. A **73**, 023606 (2006).
[49] H. Feshbach, *Theoretical Nuclear Physics* (Wiley, New York, 1992).
[50] N. Dörre, J. Rodewald, P. Geyer, B. von Issendorff, P. Haslinger, and M. Arndt, Photofragmentation Beam Splitters for Matter-Wave Interferometry, Phys. Rev. Lett. **113**, 233001 (2014).
[51] X.-L. Wang *et al.*, Experimental Ten-Photon Entanglement, Phys. Rev. Lett. **117**, 210502 (2016).
[52] R. Dicke, Coherence in spontaneous radiation processes, Phys. Rev. **93**, 99 (1954).
[53] A. A. Klyachko, Quantum marginal problem and N-representability, J. Phys. Conf. Ser. **36**, 72 (2006).
[54] A. J. Coleman, Structure of fermion density matrices, Rev. Mod. Phys. **35**, 668 (1963).

Supplemental Material: Macroscopic superpositions as quantum ground states

Borivoje Dakić[1,2] and Milan Radonjić[2,3]

[1] *Institute for Quantum Optics and Quantum Information (IQOQI), Austrian Academy of Sciences, Boltzmanngasse 3, A-1090 Vienna, Austria*
[2] *Faculty of Physics, University of Vienna, Boltzmanngasse 5, A-1090 Vienna, Austria*
[3] *Institute of Physics Belgrade, University of Belgrade, Pregrevica 118, 11080 Belgrade, Serbia*

(Dated: August 17, 2017)

In this Supplemental Material we provide the proofs of the statements from the main text. Furthermore, we study an example of certain superpositions of Dicke states as possible ground states of local Hamiltonians of spin-lattice models. At the end, we provide the discussion about quantum superpositions in superconducting quantum interference devices (SQUIDs).

Proof of the Lemma

To ease the notation, we introduce the operator $\hat{h} = \hat{H} - E_0$. The ground state energy of $\hat{h}$ is zero, whereas the energy of the first excited state is equal to the energy gap ΔE of $\hat{H}$. The ground state $|\psi\rangle = a_1|\psi_1\rangle + a_2|\psi_2\rangle$ satisfies the condition $\hat{h}|\psi\rangle = 0$. Therefore, we get the following set of equations

$$a_1 h_{11} + a_2 h_{12} = 0, \tag{1a}$$
$$a_1 h_{21} + a_2 h_{22} = 0, \tag{1b}$$

with $h_{ij} = \langle\psi_i|\hat{h}|\psi_j\rangle$. The linear system above has non-trivial solutions if its determinant is zero. Hence, $h_{11}h_{22} = h_{12}h_{21} \equiv |h_{21}|^2$. Obviously, $h_{11}, h_{22} \geq 0$ as the ground state energy of $\hat{h}$ is zero. Consider now the expansion $|\psi_1\rangle = c_1|\psi\rangle + \sqrt{1-|c_1|^2}|\psi^\perp\rangle$, where $|\psi^\perp\rangle$ is the linear combination of $|\psi_1\rangle$ and $|\psi_2\rangle$ such that $\langle\psi|\psi^\perp\rangle = 0$. We get the following inequality

$$\langle\psi_1|\hat{h}|\psi_1\rangle = (1-|c_1|^2)\langle\psi^\perp|\hat{h}|\psi^\perp\rangle \geq (1-|c_1|^2)\Delta E. \tag{2}$$

The last inequality follows from the fact that the lowest energy of $\hat{h}$ in the subspace orthogonal to $|\psi\rangle$ is ΔE. It is easy to obtain $1-|c_1|^2 = |a_2|^2(1-|\lambda|^2)$, so that

$$\Delta E \leq \frac{\langle\psi_1|\hat{h}|\psi_1\rangle}{1-|c_1|^2} = \frac{h_{11}}{|a_2|^2(1-|\lambda|^2)}. \tag{3}$$

From the equations (1) we find $h_{11}/|a_2|^2 = |h_{12}|/|a_1 a_2| = |h_{21}|/|a_1 a_2| = h_{22}/|a_1|^2$. Consequently, we get

$$\Delta E \leq \frac{|h_{21}|}{|a_1 a_2|(1-|\lambda|^2)}. \tag{4}$$

Recalling the assumptions $a_1, a_2 > 0$ from the main text, the previous result proves the Lemma.

Macroscopic superpositions of "locally distinguishable" states

Let us assume that the unique ground state $|\psi\rangle$ is a macroscopic superposition of two states $|\psi_1\rangle$ and $|\psi_2\rangle$. We will rely on the measurement-based measure of the size of macroscopic quantum superpositions in terms of "local distinguishability", introduced in Ref. [1] and elaborated in Ref. [2]. In this context, it was shown in Ref. [3] that if the energy gap scales as $O(1/\mathrm{poly}(N))$, then no MS of locally distinguishable states can be the unique ground state of N spins described by a local Hamiltonian. Our goal here is to prove the opposite − if such a state is a ground state of local Hamiltonian, then the energy gap vanishes exponentially fast in the macroscopic limit. Following [1, 2], we divide N particles into a maximal number $\tilde{N}$ of distinct groups of particles such that $|\psi_1\rangle$ can be distinguished from $|\psi_2\rangle$ with probability $P > 1/2$ by performing a measurement on any single group. The superposition state $|\psi\rangle$ is called macroscopic if $\tilde{N} = O(N)$. To avoid cumbersome notation, we assume that the size of every group is $N/\tilde{N}$ and introduce the abbreviation $[N] = \{1, 2, \ldots, N\}$. In the sequel, we will derive an exponential bound for the magnitude of the matrix element of a 2-local Hamiltonian

$$\begin{aligned}\langle\psi_2|\hat{H}|\psi_1\rangle &= \sum_{(i,j)\in\mathcal{I}_N^{(2)}} \langle\psi_2|\hat{H}_{ij}|\psi_1\rangle \\ &= \sum_{(i,j)\in\mathcal{I}_N^{(2)}} \mathrm{Tr}_{i,j}\Big(\hat{H}_{ij}\mathrm{Tr}_{[N]\setminus\{i,j\}}\big(|\psi_1\rangle\langle\psi_2|\big)\Big).\end{aligned} \tag{5}$$

Our approach is based on the one given in the Appendix C of Ref. [3]. Denote by $\hat{A}^{(k)}$ the measurement operator on group k that optimally distinguishes the states $|\psi_1\rangle$ and $|\psi_2\rangle$. One can always choose it so that its spectrum is $\{-1, +1\}$. In such a case, the success probability to distinguish the two states is given by $P = 1/2 + 1/4\,|\langle\hat{A}^{(k)}\rangle_{\psi_1} - \langle\hat{A}^{(k)}\rangle_{\psi_2}|$. Since $P > 1/2$, we can assume that $-1 \leq \langle\hat{A}^{(k)}\rangle_{\psi_2} < \langle\hat{A}^{(k)}\rangle_{\psi_1} \leq 1$ for all k. For the kth group, the projection operator on outcome α is denoted by $\hat{\Pi}_\alpha^{(k)}$. The measurement probabilities are then $\|\hat{\Pi}_{\pm1}^{(k)}|\psi_i\rangle\|^2 = (1 \pm \langle\hat{A}^{(k)}\rangle_{\psi_i})/2 \equiv p_{i,\pm}$ for $i = 1, 2$. One additional comment is in order. Namely, in the generic case $\tilde{N}$ can depend on the success probability P. As discussed in Ref. [2], the additional assumption,

that the measurements on any group do not influence the measurement outcomes on other groups, resolves this issue. It basically means that only correlations within the groups exist and not among different groups. Thus, we formally require that $\langle \hat{A}^{(k)}\hat{A}^{(k')}\rangle_{\psi_i} = \langle \hat{A}^{(k)}\rangle_{\psi_i}\langle \hat{A}^{(k')}\rangle_{\psi_i}$, for $i = 1, 2$ and for all groups $k \neq k'$. This in turn implies the factorization $\|\hat{\Pi}^{(k)}_{\alpha}\hat{\Pi}^{(k')}_{\alpha'}|\psi_i\rangle\|^2 = p_{i,\alpha}\, p_{i,\alpha'}$ for $i = 1, 2$. Similar factorization is found for the joint probabilities of the results of measurements on more than two distinct groups.

Denote by $\mathbf{\Gamma} = \{\Gamma^{(k)}\}_{k=1}^{\tilde{N}}$ the set of the considered distinct groups of particles. Let us examine the partial trace of $|\psi_1\rangle\langle\psi_2|$ over n groups $\{\Gamma^{(k_1)}, \ldots, \Gamma^{(k_n)}\} \equiv \mathbf{\Gamma}^{(\boldsymbol{k})}_n$

$$
\begin{aligned}
\mathrm{Tr}_{\mathbf{\Gamma}^{(\boldsymbol{k})}_n}\big(|\psi_1\rangle\langle\psi_2|\big) &= \mathrm{Tr}_{\mathbf{\Gamma}^{(\boldsymbol{k})}_n}\Big(\overset{n}{\underset{i=1}{\otimes}}(\hat{\Pi}^{(k_i)}_{+1} + \hat{\Pi}^{(k_i)}_{-1})\,|\psi_1\rangle\langle\psi_2|\,\overset{n}{\underset{j=1}{\otimes}}(\hat{\Pi}^{(k_j)}_{+1} + \hat{\Pi}^{(k_j)}_{-1})\Big)\\
&= \mathrm{Tr}_{\mathbf{\Gamma}^{(\boldsymbol{k})}_n}\Big(\sum_{\alpha_1,\ldots,\alpha_n=\pm1}\;\sum_{\alpha'_1,\ldots,\alpha'_n=\pm1}\hat{\Pi}^{(k_1)}_{\alpha_1}\ldots\hat{\Pi}^{(k_n)}_{\alpha_n}\,|\psi_1\rangle\langle\psi_2|\,\hat{\Pi}^{(k_1)}_{\alpha'_1}\ldots\hat{\Pi}^{(k_n)}_{\alpha'_n}\Big)\\
&= \mathrm{Tr}_{\mathbf{\Gamma}^{(\boldsymbol{k})}_n}\Big(\sum_{\alpha_1,\ldots,\alpha_n=\pm1}\hat{\Pi}^{(k_1)}_{\alpha_1}\ldots\hat{\Pi}^{(k_n)}_{\alpha_n}\,|\psi_1\rangle\langle\psi_2|\,\hat{\Pi}^{(k_1)}_{\alpha_1}\ldots\hat{\Pi}^{(k_n)}_{\alpha_n}\Big)\\
&= \mathrm{Tr}_{\mathbf{\Gamma}^{(\boldsymbol{k})}_n}\Big(\sum_{\boldsymbol{\alpha}\in\{-1,1\}^n}\hat{\Pi}^{(\boldsymbol{k})}_{\boldsymbol{\alpha}}\,|\psi_1\rangle\langle\psi_2|\,\hat{\Pi}^{(\boldsymbol{k})}_{\boldsymbol{\alpha}}\Big),
\end{aligned}
\tag{6}
$$

where $\hat{\Pi}^{(\boldsymbol{k})}_{\boldsymbol{\alpha}} = \hat{\Pi}^{(k_1)}_{\alpha_1}\ldots\hat{\Pi}^{(k_n)}_{\alpha_n}$. We used the orthogonality $\hat{\Pi}^{(k)}_{\alpha}\hat{\Pi}^{(k)}_{\alpha'} = \delta_{\alpha\alpha'}\hat{\Pi}^{(k)}_{\alpha}$ and the completeness relation $\hat{\Pi}^{(k)}_{+1} + \hat{\Pi}^{(k)}_{-1} = \mathbb{I}^{(k)}$. In evaluating (5) we will encounter two types of terms, the ones where both particles i and j belong to two different groups, say $\Gamma^{(k_i)}$ and $\Gamma^{(k_j)}$, and the ones where they belong to the same group, say $\Gamma^{(k_{ij})}$. In both cases we have to perform partial traces over at least $\tilde{N} - 2$ groups of particles. To make the derivation more compact, we will treat the two cases on the same footing. Namely, we shall introduce $\mathbf{\Gamma}_{ij} = \{\Gamma^{(k_i)}, \Gamma^{(k_j)}\}$ in the former case. In the latter case, we define $\mathbf{\Gamma}_{ij} = \{\Gamma^{(k_{ij})}, \Gamma^{(k^*_{ij})}\}$, where to each group k we assign its "partner" group $k^* \neq k$. For instance, one may set $1^* = 2$, $2^* = 3, \ldots$, $(N-1)^* = N$ and $N^* = 1$. We then have

$$
\mathrm{Tr}_{[N]\setminus\{i,j\}}\big(|\psi_1\rangle\langle\psi_2|\big) = \mathrm{Tr}_{\mathbf{\Gamma}_{ij}\setminus\{i,j\}}\mathrm{Tr}_{\mathbf{\Gamma}\setminus\mathbf{\Gamma}_{ij}}\big(|\psi_1\rangle\langle\psi_2|\big),
\tag{7}
$$

where the last partial trace is always over $\tilde{N} - 2$ groups. Let $\boldsymbol{k}_{i,j}$ label those groups. Combining the previous, we get

$$
\begin{aligned}
|\langle\psi_2|\hat{H}|\psi_1\rangle| &= \Big|\sum_{(i,j)\in\mathcal{I}_N^{(2)}}\mathrm{Tr}_{i,j}\Big(\hat{H}_{ij}\mathrm{Tr}_{\mathbf{\Gamma}_{ij}\setminus\{i,j\}}\mathrm{Tr}_{\mathbf{\Gamma}\setminus\mathbf{\Gamma}_{ij}}\big(|\psi_1\rangle\langle\psi_2|\big)\Big)\Big|\\
&= \Big|\sum_{(i,j)\in\mathcal{I}_N^{(2)}}\mathrm{Tr}_{i,j}\Big(\hat{H}_{ij}\mathrm{Tr}_{\mathbf{\Gamma}_{ij}\setminus\{i,j\}}\mathrm{Tr}_{\mathbf{\Gamma}\setminus\mathbf{\Gamma}_{ij}}\big(\sum_{\boldsymbol{\alpha}\in\{-1,1\}^{\tilde{N}-2}}\hat{\Pi}^{(\boldsymbol{k}_{i,j})}_{\boldsymbol{\alpha}}\,|\psi_1\rangle\langle\psi_2|\,\hat{\Pi}^{(\boldsymbol{k}_{i,j})}_{\boldsymbol{\alpha}}\big)\Big)\Big|\\
&= \Big|\sum_{(i,j)\in\mathcal{I}_N^{(2)}}\;\sum_{\boldsymbol{\alpha}\in\{-1,1\}^{\tilde{N}-2}}\mathrm{Tr}_{i,j}\Big(\hat{H}_{ij}\mathrm{Tr}_{[N]\setminus\{i,j\}}\big(\hat{\Pi}^{(\boldsymbol{k}_{i,j})}_{\boldsymbol{\alpha}}\,|\psi_1\rangle\langle\psi_2|\,\hat{\Pi}^{(\boldsymbol{k}_{i,j})}_{\boldsymbol{\alpha}}\big)\Big)\Big|\\
&\leq \sum_{(i,j)\in\mathcal{I}_N^{(2)}}\;\sum_{\boldsymbol{\alpha}\in\{-1,1\}^{\tilde{N}-2}}\Big|\mathrm{Tr}_{i,j}\Big(\hat{H}_{ij}\mathrm{Tr}_{[N]\setminus\{i,j\}}\big(\hat{\Pi}^{(\boldsymbol{k}_{i,j})}_{\boldsymbol{\alpha}}|\psi_1\rangle\langle\psi_2|\,\hat{\Pi}^{(\boldsymbol{k}_{i,j})}_{\boldsymbol{\alpha}}\big)\Big)\Big|\\
&\leq \sum_{(i,j)\in\mathcal{I}_N^{(2)}}\;\sum_{\boldsymbol{\alpha}\in\{-1,1\}^{\tilde{N}-2}}\|\hat{H}_{ij}\|\cdot\big\|\mathrm{Tr}_{[N]\setminus\{i,j\}}\big(\hat{\Pi}^{(\boldsymbol{k}_{i,j})}_{\boldsymbol{\alpha}}|\psi_1\rangle\langle\psi_2|\,\hat{\Pi}^{(\boldsymbol{k}_{i,j})}_{\boldsymbol{\alpha}}\big)\big\|_1\\
&\leq \max_{(i,j)\in\mathcal{I}_N^{(2)}}\|\hat{H}_{ij}\|\sum_{(i,j)\in\mathcal{I}_N^{(2)}}\;\sum_{\boldsymbol{\alpha}\in\{-1,1\}^{\tilde{N}-2}}\big\|\mathrm{Tr}_{[N]\setminus\{i,j\}}\big(\hat{\Pi}^{(\boldsymbol{k}_{i,j})}_{\boldsymbol{\alpha}}|\psi_1\rangle\langle\psi_2|\,\hat{\Pi}^{(\boldsymbol{k}_{i,j})}_{\boldsymbol{\alpha}}\big)\big\|_1\\
&\leq \max_{(i,j)\in\mathcal{I}_N^{(2)}}\|\hat{H}_{ij}\|\sum_{(i,j)\in\mathcal{I}_N^{(2)}}\;\sum_{\boldsymbol{\alpha}\in\{-1,1\}^{\tilde{N}-2}}\big\|\hat{\Pi}^{(\boldsymbol{k}_{i,j})}_{\boldsymbol{\alpha}}|\psi_1\rangle\langle\psi_2|\,\hat{\Pi}^{(\boldsymbol{k}_{i,j})}_{\boldsymbol{\alpha}}\big\|_1\\
&= \max_{(i,j)\in\mathcal{I}_N^{(2)}}\|\hat{H}_{ij}\|\sum_{(i,j)\in\mathcal{I}_N^{(2)}}\;\sum_{\boldsymbol{\alpha}\in\{-1,1\}^{\tilde{N}-2}}\big\|\hat{\Pi}^{(\boldsymbol{k}_{i,j})}_{\boldsymbol{\alpha}}|\psi_1\rangle\big\|\cdot\big\|\hat{\Pi}^{(\boldsymbol{k}_{i,j})}_{\boldsymbol{\alpha}}|\psi_2\rangle\big\|.
\end{aligned}
\tag{8}
$$

In the second inequality we used Hölder's inequality for the operator spectral and 1-norm $\left|\mathrm{Tr}\left(\hat{X}\hat{Y}\right)\right| \leq \|\hat{X}\| \cdot \|\hat{Y}\|_1$. In the third inequality we utilized the property $\|\mathrm{Tr}_1\left(\hat{X}_{12}\right)\|_1 \leq \|\hat{X}_{12}\|_1$ for $\hat{X}_{12} \in \mathcal{L}(\mathcal{H}_1 \otimes \mathcal{H}_2)$ [4], and finally in the last one we used $\left\||u\rangle\langle v|\right\|_1 = \||u\rangle\| \cdot \||v\rangle\|$. Now, from the factorization of joint probabilities we get

$$\begin{aligned}\left\|\hat{\Pi}_{\boldsymbol{\alpha}}^{(\boldsymbol{k}_{i,j})}|\psi_l\rangle\right\| &= \left\|\hat{\Pi}_{\alpha_1}^{(k_1)}\hat{\Pi}_{\alpha_2}^{(k_2)}\ldots\hat{\Pi}_{\alpha_{\tilde{N}-2}}^{(k_{\tilde{N}-2})}|\psi_l\rangle\right\| \\ &= \left(p_{l,\alpha_1}\, p_{l,\alpha_2}\cdots p_{l,\alpha_{\tilde{N}-2}}\right)^{1/2} = \left(p_{l,+}\right)^{\frac{m}{2}}\left(p_{l,-}\right)^{\frac{\tilde{N}-2-m}{2}},\end{aligned} \tag{9}$$

where m is the number of positive eigenvalues among $\alpha_1, \alpha_2, \ldots, \alpha_{\tilde{N}-2}$. Hence, we find

$$\begin{aligned}|\langle\psi_2|\hat{H}|\psi_1\rangle| &\leq \max_{(i,j)\in\mathcal{I}_N^{(2)}}\|\hat{H}_{ij}\| \sum_{(i,j)\in\mathcal{I}_N^{(2)}}\sum_{\boldsymbol{\alpha}\in\{-1,1\}^{\tilde{N}-2}}\left(p_{1,+}\, p_{2,+}\right)^{\frac{m}{2}}\left(p_{1,-}\, p_{2,-}\right)^{\frac{\tilde{N}-2-m}{2}} \\ &\leq |\mathcal{I}_N^{(2)}| \max_{(i,j)\in\mathcal{I}_N^{(2)}}\|\hat{H}_{ij}\| \sum_{\boldsymbol{\alpha}\in\{-1,1\}^{\tilde{N}-2}}\left(p_{1,+}\, p_{2,+}\right)^{\frac{m}{2}}\left(p_{1,-}\, p_{2,-}\right)^{\frac{\tilde{N}-2-m}{2}} \\ &= |\mathcal{I}_N^{(2)}| \max_{(i,j)\in\mathcal{I}_N^{(2)}}\|\hat{H}_{ij}\| \sum_{m=0}^{\tilde{N}-2}\binom{\tilde{N}-2}{m}\left(p_{1,+}\, p_{2,+}\right)^{\frac{m}{2}}\left(p_{1,-}\, p_{2,-}\right)^{\frac{\tilde{N}-2-m}{2}} \\ &= |\mathcal{I}_N^{(2)}| \max_{(i,j)\in\mathcal{I}_N^{(2)}}\|\hat{H}_{ij}\|\, q^{\tilde{N}-2},\end{aligned} \tag{10}$$

where $q = \sqrt{p_{1,+}\, p_{2,+}} + \sqrt{p_{1,-}\, p_{2,-}}$. Since by assumption $\langle\hat{A}^{(k)}\rangle_{\psi_2} < \langle\hat{A}^{(k)}\rangle_{\psi_1}$, we have $p_{1,\pm} \neq p_{2,\pm}$. Using the inequality $\sqrt{xy} < (x+y)/2$ for distinct positive numbers, we obtain

$$q < \frac{p_{1,+}+p_{2,+}}{2} + \frac{p_{1,-}+p_{2,-}}{2} = 1. \tag{11}$$

In addition, due to $\tilde{N} = O(N)$ for a macroscopic superposition state, we find the estimate $|\langle\psi_2|\hat{H}|\psi_1\rangle| \leq \exp[-O(N)]$. Thus, we have derived an exponential bound with respect to N. In the general case of K-local Hamiltonian one could analogously derive the bound

$$|\langle\psi_2|\hat{H}|\psi_1\rangle| \leq |\mathcal{I}_N^{(K)}| \max_{(i_1,\ldots,i_K)\in\mathcal{I}_N^{(K)}}\|\hat{H}_{i_1\ldots i_K}\|\, q^{\tilde{N}-K}. \tag{12}$$

Based on this result, the Lemma implies that the energy gap as well vanishes exponentially fast in the macroscopic limit $N \to \infty$.

Proof of the Theorem

Our task is to estimate the magnitude of the matrix element $\langle\psi_2|\hat{H}|\psi_1\rangle$ of a 2-local Hamiltonian, under the assumptions from the main text. Recall that an additive observable $\hat{S} = \sum_{i=1}^N \hat{S}_i$ introduces the decomposition of a given state $|\psi\rangle = \sum_{m=1}^M \sqrt{p_m}|s_m\rangle$, where $\hat{S}|s_m\rangle = s_m|s_m\rangle$, $\sqrt{p_m}|s_m\rangle = \sum_{|\boldsymbol{\sigma}|=s_m}\sum_{\boldsymbol{\mu}}|\boldsymbol{\sigma},\boldsymbol{\mu}\rangle\langle\boldsymbol{\sigma},\boldsymbol{\mu}|\psi\rangle$ and $|\boldsymbol{\sigma}| \equiv \sum_{i=1}^N \sigma_i$. Furthermore, we used the separating eigenvalue $s_{\bar{m}}$ to express the ground state in the form of superposition $|\psi\rangle = a_1|\psi_1\rangle + a_2|\psi_2\rangle$, with $a_1|\psi_1\rangle = \sum_{m=1}^{\bar{m}-1}\sqrt{p_m}|s_m\rangle$ and $a_2|\psi_2\rangle = \sum_{m=\bar{m}}^M \sqrt{p_m}|s_m\rangle$. Then, we find the following

$$\langle\psi_2|\hat{H}|\psi_1\rangle = \sum_{(i,j)\in\mathcal{I}_N^{(2)}}\langle\psi_2|\hat{H}_{ij}|\psi_1\rangle = \frac{1}{a_1 a_2}\sum_{(i,j)\in\mathcal{I}_N^{(2)}}\sum_{m=1}^{\bar{m}-1}\sum_{m'=\bar{m}}^{M}\sqrt{p_{m'}}\langle s_{m'}|\hat{H}_{ij}|s_m\rangle\sqrt{p_m}. \tag{13}$$

Evaluation of $\langle s_{m'}|\hat{H}_{ij}|s_m\rangle$ boils down to considering $\langle\boldsymbol{\sigma}',\boldsymbol{\mu}'|\hat{H}_{ij}|\boldsymbol{\sigma},\boldsymbol{\mu}\rangle = \mathrm{Tr}_{i,j}\left(\hat{H}_{ij}\mathrm{Tr}_{[N]\setminus\{i,j\}}\left(|\boldsymbol{\sigma},\boldsymbol{\mu}\rangle\langle\boldsymbol{\sigma}',\boldsymbol{\mu}'|\right)\right)$, where $|\boldsymbol{\sigma}'| = s_{m'}$ and $|\boldsymbol{\sigma}| = s_m$. One finds that

$$\mathrm{Tr}_{[N]\setminus\{i,j\}}\left(|\boldsymbol{\sigma},\boldsymbol{\mu}\rangle\langle\boldsymbol{\sigma}',\boldsymbol{\mu}'|\right) = |\sigma_i,\mu_i\rangle_i|\sigma_j,\mu_j\rangle_j\langle\sigma_i',\mu_i'|_i\langle\sigma_j',\mu_j'|_j\prod_{k\in[N]\setminus\{i,j\}}\delta_{\sigma_k',\sigma_k}\delta_{\mu_k',\mu_k}. \tag{14}$$

A necessary condition for the last product to be nonzero is $\sum_{k\in[N]\setminus\{i,j\}}(\sigma'_k-\sigma_k)=0$, i.e., $s_{m'}-s_m=\sigma'_i+\sigma'_j-(\sigma_i+\sigma_j)$. Since $-2\delta_\varsigma\leq\sigma'_i+\sigma'_j-(\sigma_i+\sigma_j)\leq 2\delta_\varsigma$, all the nonvanishing terms from (13) must obey $-2\delta_\varsigma\leq s_{m'}-s_m\leq 2\delta_\varsigma$, while by construction we have $s_{m'}\geq s_{\bar{m}}$ and $s_m<s_{\bar{m}}$. Hence, the only nonzero terms are those related to the triangular region $\mathcal{T}_{\bar{m}}$ in the (m,m')-plane that is determined by the previous inequalities. Let $m_>$ be the largest m such that $s_m<s_{\bar{m}}+2\delta_\varsigma$. Similarly, let $m_<$ be the smallest m such that $s_m\geq s_{\bar{m}}-2\delta_\varsigma$. We obtain the following

$$
\begin{aligned}
|\langle\psi_2|\hat{H}|\psi_1\rangle| &= \frac{1}{a_1a_2}\Big|\sum_{(i,j)\in\mathcal{I}_N^{(2)}}\sum_{(m,m')\in\mathcal{T}_{\bar{m}}}\sqrt{p_{m'}}\langle s_{m'}|\hat{H}_{ij}|s_m\rangle\sqrt{p_m}\Big| \\
&= \frac{1}{a_1a_2}\Big|\sum_{(i,j)\in\mathcal{I}_N^{(2)}}\sum_{m=m_<}^{\bar{m}-1}\sum_{m'=\bar{m}}^{m_>}\sqrt{p_{m'}}\langle s_{m'}|\hat{H}_{ij}|s_m\rangle\sqrt{p_m}\Big| && \text{(15a)} \\
&= \frac{1}{a_1a_2}\Big|\sum_{(i,j)\in\mathcal{I}_N^{(2)}}\sum_{m=m_<}^{\bar{m}-1}\sum_{m'=\bar{m}}^{m_>}\mathrm{Tr}_{i,j}\Big(\hat{H}_{ij}\mathrm{Tr}_{[N]\setminus\{i,j\}}\big(\sqrt{p_m}|s_m\rangle\langle s_{m'}|\sqrt{p_{m'}}\big)\Big)\Big| \\
&= \frac{1}{a_1a_2}\Big|\sum_{(i,j)\in\mathcal{I}_N^{(2)}}\mathrm{Tr}_{i,j}\Big(\hat{H}_{ij}\mathrm{Tr}_{[N]\setminus\{i,j\}}\big(\sum_{m=m_<}^{\bar{m}-1}\sqrt{p_m}|s_m\rangle\sum_{m'=\bar{m}}^{m_>}\sqrt{p_{m'}}\langle s_{m'}|\big)\Big)\Big| \\
&\leq \frac{1}{a_1a_2}\sum_{(i,j)\in\mathcal{I}_N^{(2)}}\Big|\mathrm{Tr}_{i,j}\Big(\hat{H}_{ij}\mathrm{Tr}_{[N]\setminus\{i,j\}}\big(\sum_{m=m_<}^{\bar{m}-1}\sqrt{p_m}|s_m\rangle\sum_{m'=\bar{m}}^{m_>}\sqrt{p_{m'}}\langle s_{m'}|\big)\Big)\Big| \\
&\leq \frac{1}{a_1a_2}\sum_{(i,j)\in\mathcal{I}_N^{(2)}}\|\hat{H}_{ij}\|\cdot\Big\|\mathrm{Tr}_{[N]\setminus\{i,j\}}\big(\sum_{m=m_<}^{\bar{m}-1}\sqrt{p_m}|s_m\rangle\sum_{m'=\bar{m}}^{m_>}\sqrt{p_{m'}}\langle s_{m'}|\big)\Big\|_1 && \text{(15b)} \\
&\leq \frac{1}{a_1a_2}\sum_{(i,j)\in\mathcal{I}_N^{(2)}}\|\hat{H}_{ij}\|\cdot\Big\|\sum_{m=m_<}^{\bar{m}-1}\sqrt{p_m}|s_m\rangle\sum_{m'=\bar{m}}^{m_>}\sqrt{p_{m'}}\langle s_{m'}|\Big\|_1 && \text{(15c)} \\
&\leq \frac{|\mathcal{I}_N^{(2)}|}{a_1a_2}\max_{(i,j)\in\mathcal{I}_N^{(2)}}\|\hat{H}_{ij}\|\cdot\Big\|\sum_{m=m_<}^{\bar{m}-1}\sqrt{p_m}|s_m\rangle\sum_{m'=\bar{m}}^{m_>}\sqrt{p_{m'}}\langle s_{m'}|\Big\|_1 \\
&= \frac{|\mathcal{I}_N^{(2)}|}{a_1a_2}\max_{(i,j)\in\mathcal{I}_N^{(2)}}\|\hat{H}_{ij}\|\cdot\Big\|\sum_{m=m_<}^{\bar{m}-1}\sqrt{p_m}|s_m\rangle\Big\|\cdot\Big\|\sum_{m'=\bar{m}}^{m_>}\sqrt{p_{m'}}\langle s_{m'}|\Big\| && \text{(15d)} \\
&= \frac{|\mathcal{I}_N^{(2)}|}{a_1a_2}\max_{(i,j)\in\mathcal{I}_N^{(2)}}\|\hat{H}_{ij}\|\cdot\Big(\sum_{m=m_<}^{\bar{m}-1}p_m\Big)^{1/2}\cdot\Big(\sum_{m'=\bar{m}}^{m_>}p_{m'}\Big)^{1/2} \\
&\leq \frac{|\mathcal{I}_N^{(2)}|}{2a_1a_2}\max_{(i,j)\in\mathcal{I}_N^{(2)}}\|\hat{H}_{ij}\|\cdot\Big(\sum_{m=m_<}^{\bar{m}-1}p_m+\sum_{m'=\bar{m}}^{m_>}p_{m'}\Big) && \text{(15e)} \\
&\leq \frac{|\mathcal{I}_N^{(2)}|}{2a_1a_2}\max_{(i,j)\in\mathcal{I}_N^{(2)}}\|\hat{H}_{ij}\|\cdot P_\psi(|s-s_{\bar{m}}|\leq 2\delta_\varsigma). && \text{(15f)}
\end{aligned}
$$

In the line (15a) we found convenient to extend the summation over $\mathcal{T}_{\bar{m}}$ to the summation over the encompassing rectangular region. Note that all the added terms are actually zero-terms. Thereafter, m and m' index the eigenvalues of $\hat{S}$ within the interval $[s_{\bar{m}}-2\delta_\varsigma, s_{\bar{m}})$ and $[s_{\bar{m}}, s_{\bar{m}}+2\delta_\varsigma)$, respectively. The line (15b) is a consequence of Hölder's inequality for operator spectral and 1-norm $\big|\mathrm{Tr}\big(\hat{X}\hat{Y}\big)\big|\leq\|\hat{X}\|\cdot\|\hat{Y}\|_1$, whereas the line (15c) follows from $\|\mathrm{Tr}_1\big(\hat{X}_{12}\big)\|_1\leq\|\hat{X}_{12}\|_1$ for $\hat{X}_{12}\in\mathcal{L}(\mathcal{H}_1\otimes\mathcal{H}_2)$ [4] and we used $\||u\rangle\langle v|\|_1=\||u\rangle\|\cdot\||v\rangle\|$ in the line (15d). Finally, in the line (15e) we invoked the inequality $\sqrt{xy}\leq(x+y)/2$ for nonnegative reals. Recalling the Lemma from the main text, the fact $\langle\psi_2|\psi_1\rangle=0$ and the choice $E_0=0$, we find

$$\Delta E \leq \frac{|\mathcal{I}_N^{(2)}|}{2a_1^2 a_2^2} \max_{(i,j)\in\mathcal{I}_N^{(2)}} \|\hat{H}_{ij}\| \cdot P_\psi(|s - s_{\bar{m}}| \leq 2\delta_\varsigma). \tag{16}$$

The proof of the Theorem is now completed.

Example of W state $|j, j-1\rangle$

Here, we give the derivation of the probability distribution $p_m = |\langle j, j-1|j, m\rangle_x|^2$ for $j \to \infty$ and small m, where $|j, m\rangle_x = e^{-i\frac{\pi}{2}\hat{J}_y}|j, m\rangle$. Particular example of such distribution is given in Fig. 1. First, we will evaluate the overlap

$$\begin{aligned}\langle j, j-1|j, m\rangle_x &= \frac{1}{\sqrt{2j}}\langle j, j|\hat{J}^+|j, m\rangle_x \\ &= \frac{1}{\sqrt{2j}}\langle j, j|(\hat{J}_x + i\hat{J}_y)e^{-i\frac{\pi}{2}\hat{J}_y}|j, m\rangle \\ &= \frac{1}{\sqrt{2j}}\langle j, j|e^{-i\frac{\pi}{2}\hat{J}_y}(\hat{J}_z + i\hat{J}_y)|j, m\rangle, \end{aligned} \tag{17}$$

where we used properties and definition of the angular momentum ladder operator $\hat{J}^+$, as well as the relation $e^{i\frac{\pi}{2}\hat{J}_y}\hat{J}_x e^{-i\frac{\pi}{2}\hat{J}_y} = \hat{J}_z$. Next, we employ

$$\begin{aligned} 0 &= \langle j, j|\hat{J}^- e^{-i\frac{\pi}{2}\hat{J}_y} \\ &= \langle j, j|(\hat{J}_x - i\hat{J}_y)e^{-i\frac{\pi}{2}\hat{J}_y} \\ &= \langle j, j|e^{-i\frac{\pi}{2}\hat{J}_y}(\hat{J}_z - i\hat{J}_y), \end{aligned} \tag{18}$$

so that

$$\langle j, j|e^{-i\frac{\pi}{2}\hat{J}_y}\hat{J}_z = \langle j, j|e^{-i\frac{\pi}{2}\hat{J}_y} i\hat{J}_y, \tag{19}$$

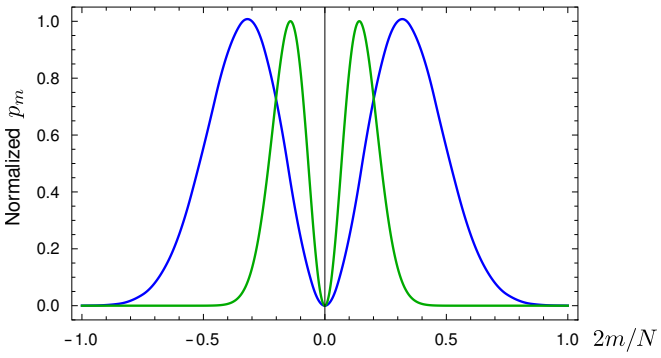

FIG. 1. Normalized probability distributions p_m for W state for $N = 40$ (blue line) and $N = 200$ (green line). Normalization is such that the maximal value is unity. Continuous curves are used for aesthetic purposes.

and we conclude

$$\begin{aligned}\langle j, j-1|j, m\rangle_x &= \frac{1}{\sqrt{2j}}\langle j, j|e^{-i\frac{\pi}{2}\hat{J}_y} 2\hat{J}_z|j, m\rangle \\ &= m\sqrt{\frac{2}{j}}\langle j, j|e^{-i\frac{\pi}{2}\hat{J}_y}|j, m\rangle \equiv m\sqrt{\frac{2}{j}}\, c_m. \end{aligned} \tag{20}$$

In order to calculate the matrix element, denoted by c_m, we proceed as follows. First, from (19) and the relation $2i\hat{J}_y = \hat{J}^+ - \hat{J}^-$, we get

$$\begin{aligned} 2mc_m &= \sqrt{(j-m)(j+m+1)}\, c_{m+1} \\ &\quad - \sqrt{(j+m)(j-m+1)}\, c_{m-1}. \end{aligned} \tag{21}$$

Second, using $e^{i\frac{\pi}{2}\hat{J}_y}\hat{J}_z e^{-i\frac{\pi}{2}\hat{J}_y} = -\hat{J}_x$ together with $\hat{J}_x = (\hat{J}^+ + \hat{J}^-)/2$, we find

$$\begin{aligned}\langle j, j|\hat{J}_z e^{-i\frac{\pi}{2}\hat{J}_y} &= -\langle j, j|e^{-i\frac{\pi}{2}\hat{J}_y}\hat{J}_x \\ &= -\frac{1}{2}\langle j, j|e^{-i\frac{\pi}{2}\hat{J}_y}(\hat{J}^+ + \hat{J}^-), \end{aligned} \tag{22}$$

which allows us to obtain

$$\begin{aligned} 2jc_m &= -\sqrt{(j-m)(j+m+1)}\, c_{m+1} \\ &\quad - \sqrt{(j+m)(j-m+1)}\, c_{m-1}. \end{aligned} \tag{23}$$

From the two relations (21) and (23), we derive the recurrence relation $c_m = -\sqrt{\frac{j+m+1}{j-m}}\, c_{m+1}$, which leads to $c_m = (-1)^{j-m}\sqrt{\binom{2j}{j+m}}\, c_j$. Using the normalization condition $\sum_{m=-j}^{j} |c_m|^2 = 1$, we get $|c_j| = \frac{1}{2^j}$ and $|c_m| = \frac{1}{2^j}\sqrt{\binom{2j}{j+m}}$. Finally, from (20) we obtain

$$p_m = \frac{2m^2}{2^{2j}\, j}\binom{2j}{j+m}, \tag{24}$$

as stated in the main text. The asymptotic behavior for fixed m and $j \to \infty$ can be easily obtained using Stirling's asymptotic series.

Example of superpositions of Dicke states

Additionally, we will demonstrate that certain superpositions of Dicke states cannot be unique ground states of 2-local Hamiltonians. We consider $N = 2j$ spin-1/2 particles, with j integer (for the notational simplicity). Thus, $d = 2$, $\ell = 2$, and $\delta_\varsigma = 1$. Assume that the unique

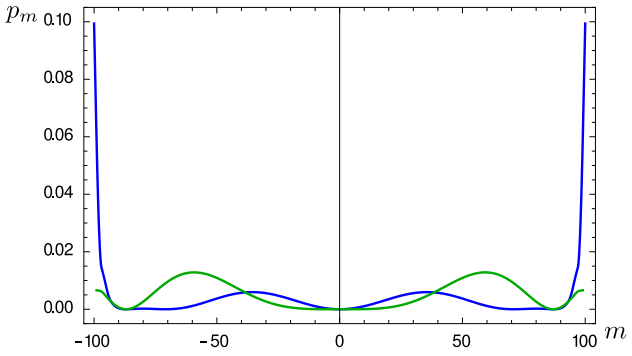

FIG. 2. The probability distribution p_m for the superposition $(|j,-1\rangle+|j,5\rangle)/\sqrt{2}$ of two Dicke states for $j=100$. The blue (green) line labels p_m for m even (odd). Continuous curves are used for aesthetic purposes.

ground state of some 2-local Hamiltonian of the spins has the following form

$$|\psi_n^{\pm}\rangle=\sum_{k=0}^{n}(\pm)^k c_k|j,-n+2k\rangle,\quad n=O(N^0)\in\mathbb{N},\quad (25)$$

where the coefficients $c_k\in\mathbb{C}$ satisfy $\sum_{k=0}^{n}|c_k|^2=1$ and $\sum_{k=0}^{n}c_k=0$. Some particular instances of such states are $(|j,-1\rangle\mp|j,1\rangle)/\sqrt{2}$, $(|j,-2\rangle\mp|j,4\rangle)/\sqrt{2}$, $(|j,-3\rangle-2|j,1\rangle+|j,5\rangle)/\sqrt{6}$, etc. It can be verified that the proper additive observable for $|\psi_n^{+}\rangle$ states is $\hat{J}_y$, while for $|\psi_n^{-}\rangle$ states it is $\hat{J}_x$. All the states (25) are in fact general macroscopic quantum states since the variance of the additive observable scales as $O(N^2)$.

We first concentrate on $|\psi_n^{-}\rangle$ states. The required probability distribution is given by $p_m=|\langle\psi_n^{-}|j,m\rangle_x|^2$, $s_m=m$, and we again select $s_{\bar{m}}=0$ (see Fig. 2 for an example). We are going to analyze the behavior of the probabilities p_m for $j\to\infty$ and small m, i.e., we want to examine the overlap $\langle j,m'|j,m\rangle_x=\langle j,m'|e^{-i\frac{\pi}{2}\hat{J}_y}|j,m\rangle=d^j_{m'm}(\pi/2)$ for j large. In the last equality we recognized the Wigner (small) d function that can be related to Jacobi polynomials $P_n^{(a,b)}(z)$ in the following manner [5]

$$d^j_{m'm}(\theta)=\left[\frac{(j+m)!(j-m)!}{(j+m')!(j-m')!}\right]^{\frac{1}{2}}P_{j-m}^{(m-m',m+m')}(\cos\theta)\times\left(\sin\frac{\theta}{2}\right)^{m-m'}\left(\cos\frac{\theta}{2}\right)^{m+m'}.\quad (26)$$

Thus, we find

$$d^j_{m'm}\left(\frac{\pi}{2}\right)=\frac{1}{2^m}\left[\frac{(j+m)!(j-m)!}{(j+m')!(j-m')!}\right]^{\frac{1}{2}}P_{j-m}^{(m-m',m+m')}(0).\quad (27)$$

Using Stirling's asymptotic series and asymptotic expansion of Jacobi polynomials [6–8] in the limit $j\to\infty$ and m,m' finite, we obtain

$$\langle j,m'|j,m\rangle_x\sim\sqrt{\frac{2}{\pi j}}\cos\frac{(j-m+m')\pi}{2}+O\big(j^{-3/2}\big).\quad (28)$$

so that

$$\begin{aligned}\langle\psi_n^{-}|j,m\rangle_x&=\sum_{k=0}^{n}(-1)^k c_k^*\langle j,-n+2k|j,m\rangle_x\\&\sim\sqrt{\frac{2}{\pi j}}\sum_{k=0}^{n}(-1)^k c_k^*\cos\left[\frac{(j-m-n)\pi}{2}+k\pi\right]+O\big(j^{-3/2}\big)\\&=\sqrt{\frac{2}{\pi j}}\cos\frac{(j-m-n)\pi}{2}\sum_{k=0}^{n}c_k^*+O\big(j^{-3/2}\big)\\&=O\big(j^{-3/2}\big),\end{aligned}\quad (29)$$

since by construction we have $\sum_{k=0}^{n}c_k=0$. Thus, we establish the asymptotic relation $p_m=|\langle\psi_n^{-}|j,m\rangle_x|^2=O(j^{-3})$. The choice $s_{\bar{m}}=0$ guaranties that $a_k\to 1/\sqrt{2}$ $(k=1,2)$ as $j\to\infty$, so that the separation probability $P_\psi(|s-s_{\bar{m}}|\leq 2)$ vanishes at least as $O(j^{-3})$, i.e., $O(N^{-3})$. Essentially the same approach can also be applied to $|\psi_n^{+}\rangle$ states. Finally, we conclude that none of the states (25) can be reached by cooling the system of N spin-1/2 particles described by an arbitrary 2-local Hamiltonian.

This example can also be put into the context of double-well (or twofold fragmented single-well) Bose-Einstein condensates of N particles via the Schwinger representation of angular momentum operators in terms of two bosonic modes. Hence, for arbitrary pairwise particle interactions and potential trap designs the considered superpositions of Dicke states cannot in principle arise as a result of the simple condensation process and necessitate other means of preparation. Contrarily, we conclude from our previous analysis that one would need genuine 3-particle interactions in order for it to be possible to prepare such states by the process of cooling.

Quantum superpositions in SQUIDs

Here we provide the discussion of superpositions of magnetic-flux states in SQUIDs and show the relation to our analysis. We will consider the simplest form of Josephson device which displays all the features relevant for the present discussion, namely a single rf SQUID [9]. In the thermodynamic limit (the number of Cooper pairs N tends to infinity), the full many-body description reduces to a simple model with one macroscopic quantum variable, i.e., the total flux Φ trapped through the SQUID ring, and the dynamics follows an effective single-particle 1D Schrödinger equation, where the effective Hamiltonian $\hat{H}_{\rm eff}(\Phi)$ has a usual kinetic $\propto-\partial^2/\partial\Phi^2$ and a potential term $U(\Phi)$ [10]. The system exhibits a finite energy

gap ΔE independent of N. For an appropriate choice of external magnetic field, the problem boils down to the analysis of a 1D quantum particle in a double-well potential $U(\Phi)$ [9]. The ground state wave function $\psi_0(\Phi)$ has two peaks to which we can associate the states $\psi_-(\Phi)$ and $\psi_+(\Phi)$. They correspond to the states of supercurrent flowing in one or in the other direction around the ring. Since the magnitude of the total magnetic moment in each of the cases can be $10^6\mu_B$ [11], or even $10^{10}\mu_B$ [12], these states are asserted to be macroscopically distinct.

For simplicity reasons, let us assume the symmetric potential $U(-\Phi) = U(\Phi)$ with two degenerate wells separated by a classically impenetrable barrier [9]. For the case of an even potential, the well-known textbook result states that the ground state wave function is even, i.e. $\psi_0(-\Phi) = \psi_0(\Phi)$, whereas the first excited state wave function is odd $\psi_1(-\Phi) = -\psi_1(\Phi)$. Here $\hat{H}_{\text{eff}}(\Phi)\psi_i(\Phi) = E_i\psi_i(\Phi)$ and $\Delta E = E_1 - E_0$. Since $\psi_0'(0) = 0$, the probability density $|\psi_0(\Phi)|^2$ attains a minimum at the center of the barrier $\Phi = 0$. Precisely this is the natural choice for the separation point that divides the ground state wave function into the two components $\psi_\pm(\Phi)$.

Following Ref. [13], simple algebraic manipulation of eigenequations $\hat{H}_{\text{eff}}(\Phi)\psi_i(\Phi) = E_i\psi_i(\Phi)$ yields the relation

$$\Delta E = \text{const} \times \frac{\psi_0(0)\psi_1'(0)}{\int_0^\infty \psi_0(\Phi)\psi_1(\Phi)d\Phi}, \tag{30}$$

meaning that the energy gap is directly proportional to the ground state probability amplitude $\psi_0(0)$ at the center of the barrier. Since ΔE is nonzero, $\psi_0(0)$ must be nonvanishing as well. Therefore, as long as the energy gap is finite, there is a nonvanishing macroscopic probability density $|\psi_0(0)|^2$ of Cooper pairs at the center of the barrier (the separation point). Thus, one concludes that the states $\psi_\pm(\Phi)$ cannot be arbitrarily well separated whenever the energy gap is finite. In addition, the same general conclusion as above holds for arbitrary confining potential. Namely, it is a well-known fact that a nondegenerate ground state wave function has no nodes, i.e., it exhibits the nonzero probability density everywhere.

Finally, we point out that instead of an effective description and an analysis of the flux variable, one might consider the full 2-local many-body Hamiltonian and invoke the analysis of some additive observable, such as the pseudo-angular-momentum [14]. In such a case, the dependence on the number of Cooper pairs N would explicitly be taken into account. Our main theorem would then directly yield the conclusion that for any considered additive observable there is a lower bound on the separation probability $P_\psi \geq O(1/N^2)$. In other words, this is the best separation of the two wave function components one can expect to have.

[1] J. I. Korsbakken, K. B. Whaley, J. Dubois, and J. I. Cirac, Phys. Rev. A **75**, 042106 (2007).
[2] F. Fröwis, W. Dür, New J. Phys. **14**, 093039 (2012).
[3] F. Fröwis, M. van den Nest, and W. Dür, New J. Phys. **15**, 113011 (2013).
[4] J. Watrous, *Theory of Quantum Information* (University of Waterloo, Waterloo, 2016).
[5] L. C. Biedenharn and J. D. Louck, *Angular Momentum in Quantum Physics: Theory and Application* (Addison-Wesley, Reading, MA, 1981).
[6] C. L. Frenzen and R. Wong, Can. J. Math. **37**, 979 (1985).
[7] R. Wong and Y.-Q. Zhao, Proc. R. Soc. Lond. A **460**, 2569 (2004).
[8] X.-X. Bai, Y.-Q. Zhao, J. Approx. Theory **148**, 1 (2007).
[9] A. J. Leggett, J. Phys.: Condens. Matter **14**, R415 (2002).
[10] U. Eckern, G. Schön, and V. Ambegaokar, Phys. Rev. B **30**, 6419 (1984).
[11] C. H. van der Wal *et al.*, Science **290**, 773 (2000).
[12] J. R. Friedman *et al.*, Nature **406**, 43 (2000).
[13] M. Robnik, L. Salasnich, M. Vranicar, Nonlin. Phenom. Complex Syst. (Minsk) **2**(2), 49 (1999).
[14] A. L. DiRienzo, *A coupled angular momentum model for the Josephson junction*, Ph.D. thesis, The University of Arizona, 1982.

Dark-polariton bound pairs in the modified Jaynes-Cummings-Hubbard model

A. Maggitti,* M. Radonjić,† and B. M. Jelenković
Institute of Physics Belgrade, University of Belgrade, Pregrevica 118, 11080 Belgrade, Serbia
(Received 29 July 2015; published 19 January 2016)

We investigate a one-dimensional modified Jaynes-Cummings-Hubbard chain of N identical QED cavities with nearest-neighbor photon tunneling and periodic boundary conditions. Each cavity contains an embedded three-level atom which is coupled to a cavity mode and an external classical control field. In the case of two excitations and common large detuning of two Raman-resonant fields, we show the emergence of two different species of dark-polariton bound pairs (DPBPs) that are mutually localized in their relative spatial coordinates. Due to the high degree of controllability, we show the appearance of either one or two DPBPs, having the energies within the energy gaps between three bands of mutually delocalized eigenstates. Interestingly, in a different parameter regime with negatively detuned Raman fields, we find that the ground state of the system is a DPBP which can be utilized for the photon storage, retrieval, and controllable state preparation. Moreover, we propose an experimental realization of our model system.

DOI: 10.1103/PhysRevA.93.013835

I. INTRODUCTION

The interaction between light and matter is one of the most fundamental and basic processes in nature, and it represents a milestone in our understanding of a broad range of physical phenomena. The recent experimental success in engineering strong interactions between photons and atoms in high-quality microcavities opens up the possibility to use light-matter systems as quantum simulators for many-body physics [1]. Key examples as first-principles proposals are quantum phase transitions of light in coupled cavities [2–4], quantum fluids of light (see [5]) and the Mott-insulator-to-superfluid phase transition of polaritons in an array of coupled QED cavities [6–11]. Coupled cavities are realized in a variety of physical systems, among them microcavities and nanocavities in photonic crystals [12]. These have paved the way to study strongly correlated phenomena in a controlled way by using such systems. Richness in these systems emerges from the interplay of two main effects. At one side, light-matter interaction inside the cavity leads to a strong effective Kerr nonlinearity between photons. By controlling the atomic level spacings as well as the cavity-mode frequency, it is possible to achieve a photon-blockade regime [13–16] where photon fluctuations are suppressed in each cavity. On the other side, photon hopping between neighboring cavities supports delocalization and competes with the photon blockade.

At the end of the past century, Fleischhauer and Lukin introduced the theoretical concept of dark-state polaritons (DSPs), form-stable coupled excitations of light and matter associated with the propagation of quantum fields in electromagnetically induced transparency (EIT), and showed their potential usage as quantum memories for photons [17,18]. Since then, DSPs have been in the focus of intense theoretical and experimental investigations [19–33]. The first proposal for realization of strong interactions among DSPs and Mott-insulator-to-superfluid phase transition thereof was given by Hartmann *et al.* [9]. They demonstrated the possibility to generate attractive onsite potentials for polaritons yielding highly entangled states and a phase with particles much more delocalized than in superfluids. Moreover, two-polariton bound states, composite excitations of two polaritons that may be spatially confined together, were predicted by Wong and Law [34]. Very recently, two-polariton bound states have been related to spin-orbit interactions by Li *et al.* [35]. Both are features of the systems described by the one-dimensional Jaynes-Cummings-Hubbard model (JCH) and represent an important connection between condensed matter physics and quantum optics. In such systems, it is possible to realize various many-body effects where the particles of interest are photons rather than electrons.

In this paper, we present a scheme based on a modified Jaynes-Cummings-Hubbard model (MJCH) that enables the formation of two different species of spatially, mutually localized dark-polariton bound pairs (DPBPs). Our scheme is based on N identical coupled QED cavities with periodic boundary conditions. Each cavity embeds a single three-level atom. A cavity mode and an external control field, which are in two-photon Raman resonance, drive the transitions from the two atomic ground states to the excited state. We assume that a common single-photon detuning of the fields is large compared to the coupling strengths. Under such conditions, the description of the three-level atoms is effectively reduced to ground-state two-level systems with tunable coupling strength between the ground levels and controllable level Stark shifts. Hence, our model circumvents the drawbacks of the excited-state spontaneous emission and provides a tunable extension of two-polariton bound states of the classical Jaynes-Cummings-Hubbard model [34]. Furthermore, we find that when the common detuning of the coupling fields is negative, the lowest-energy eigenstate of the system becomes a mutually localized DPBP of a new type that may be used as a quantum memory of light. This may find potential use in quantum information processing and controllable state preparation.

This paper is organized as follows. In Sec. II, we recapitulate the standard Jaynes-Cummings model and focus on its spectrum and eigenstates. In Sec. III, we discuss the modified Jaynes-Cummings model where we derive the modified

*mangelo@ff.bg.ac.rs
†Present address: Faculty of Physics, University of Vienna, Boltzmanngasse 5, 1090 Vienna, Austria.

Jaynes-Cummings Hamiltonian from a bare model. Further, we analyze the eigenstates and highlight the differences to the standard Jaynes-Cummings model. In Sec. IV, we present the considered model system and extend the modified Jaynes-Cummings model to a modified Jaynes-Cummings-Hubbard model, highlighting that it features the formation of bound states of two dark-polaritons. In Sec. V, we present a detailed discussion of the two-excitation subspace and explain the formation of dark-polariton bound pairs (DPBPs), accentuating their tunability through the control field Stark shift. In Sec. VI, we demonstrate an application of a ground-state DPBP as a quantum memory on which storage and retrieval of a single photon can be performed, while the second photon remains not influenced by the storage and retrieval process. Even though two photons are bound, exactly one photon can be addressed. The state composition of the ground-state DPBP can be tuned by the relative importance of the intercavity photon hopping, e.g., increasing the common single-photon detuning $|\Delta|$. In Sec. VII, we propose an experimental realization of our model system, where we state not only promising candidates to the creation of one-dimensional chains of N-coupled QED cavities, but also name single Λ atoms which can be considered. In addition, we point out that for Cs the measured strong-coupling constant g_m fits very well with our theoretical prediction, where the formation of DPBPs as well as the storage and retrieval process can be seen. Finally, In Sec. VIII we draw our conclusions.

II. STANDARD JAYNES-CUMMINGS MODEL

Within this section, we recapitulate the standard Jaynes-Cummings model (JC). Especially, we focus on its spectrum and eigenstates. In this model, a two-level atom with ground level $|g\rangle$ and excited level $|e\rangle$ having energies ω_g and ω_e interacts with a single mode of an electromagnetic field of frequency ω_0 that couples the transition $|g\rangle \rightarrow |e\rangle$ with the strength g_0. In the (rotating-wave) approximation (RWA), JC Hamiltonian has the form ($\hbar = 1$) [36,37]

$$\hat{H}^{(\mathrm{JC})} = \omega_0 \hat{n} + \delta \hat{\sigma}^+ \hat{\sigma}^- - g_0(\hat{a}\hat{\sigma}^+ + \hat{a}^\dagger \hat{\sigma}^-), \tag{1}$$

where $\hat{c}^\dagger$ ($\hat{c}$) is the photonic creation (annihilation) operator and $\hat{\sigma}^+ = |e\rangle\langle g|$ ($\hat{\sigma}^- = |g\rangle\langle e|$) is the atomic raising (lowering) operator. $\hat{n} = \hat{c}^\dagger \hat{c} + \hat{\sigma}^+ \hat{\sigma}^-$ is the number operator of the combined photonic and atomic excitations (polaritons) which is a conserved quantity, i.e., $[\hat{H}^{(\mathrm{JC})}, \hat{n}] = 0$. $\delta = \omega_e - \omega_0$ is the detuning. Due to the conservation of $\hat{n}$, $\hat{H}^{(\mathrm{JC})}$ in the subspace $\{|g,n\rangle, |e,n-1\rangle\}$ is represented with the block matrix h_n:

$$h_n = \begin{pmatrix} \omega_0 n & -g_0\sqrt{n} \\ -g_0\sqrt{n} & \omega_0 n + \delta \end{pmatrix}, \tag{2}$$

with $n = 1,2,3,\ldots$ being the total number of excitations. The matrix in (2) is a 2×2 matrix and can be analytically diagonalized. The eigenenergies are given as

$$E_n = \begin{cases} E_{n\pm} = \omega_0 n + \frac{1}{2}[\delta \pm \chi_n(\delta)], & n \geqslant 1 \\ E_0 = 0, & n = 0 \end{cases} \tag{3}$$

with $\chi_n(\delta) = \sqrt{\delta^2 + 4g_0^2 n}$ being the generalized Rabi frequency and $+$ stands for the higher and $-$ for the lower eigenenergy, while the eigenstates are

$$|n,+\rangle := \sin(\theta_n)|g,n\rangle + \cos(\theta_n)|e,n-1\rangle, \tag{4a}$$

$$|n,-\rangle := \cos(\theta_n)|g,n\rangle - \sin(\theta_n)|e,n-1\rangle. \tag{4b}$$

$n = 0$ corresponds to the state of zero polaritons. It takes on the form

$$|0,\pm\rangle \equiv |0,g\rangle = |0\rangle, \tag{5}$$

whereas the occurring mixing angle θ_n is defined as

$$\theta_n = \frac{1}{2}\arctan\left(\frac{2g_0\sqrt{n}}{\delta}\right). \tag{6}$$

The eigenstates (4) are called polaritons. Polaritons are low-energy quasiparticles which are composed of photonic and atomic excitations in superposition. As we change the mixing angle θ_n by a rotation from 0 to $\frac{\pi}{2}$, which basically corresponds to a change of the detuning δ, we tune the polaritons to either pure photonic or pure atomic excitations in a reversible manner. Due to the contribution of the excited atomic state $|e,n-1\rangle$, these polaritons in a more precise way can be called bright polaritons similar to [17–19,33].

III. MODIFIED JAYNES-CUMMINGS MODEL

For the subsequent discussion, we need to derive the modified Jaynes-Cummings (mJC) Hamiltonian which describes an effective interaction of a Λ system with a highly detuned mode of an electromagnetic and classical field. We show that due to the large, common single-photon detuning Δ, i.e., $|\Delta| \gg |g_m|, |\Omega|$, it is possible to circumvent the drawback of the excited-state spontaneous emission that would plague realizations of the JC model by using atoms and optical cavities [37]. Moreover, we focus on the discussion of the eigenstates and eigenspectrum in two specific cases which naturally arise in our case.

A. Derivation of the modified Jaynes-Cummings model Hamiltonian

We consider a single photon in a single-mode QED cavity in which a Λ three-level atom is embedded. The ground levels are $|g\rangle$ and $|f\rangle$ with their level energies ω_g and ω_f, whereas the excited level $|e\rangle$ with level energy ω_e is detuned by a large, common single-photon detuning Δ with respect to two coupling fields. The cavity field with frequency ω_m couples the transition $|g\rangle \rightarrow |e\rangle$ with strength g_m. Further, a classical control field with frequency ω_c and Rabi frequency Ω couples the transition $|f\rangle \rightarrow |e\rangle$. Our bare model Hamiltonian ($\hbar = 1$) has the form

$$\hat{H}_{\mathrm{bare}}(t) = \hat{H}_c + \hat{H}_a + \hat{H}_{\mathrm{int}}(t), \tag{7a}$$

$$\hat{H}_c = \omega_m \hat{c}^\dagger \hat{c}, \tag{7b}$$

$$\hat{H}_a = \omega_g \hat{\sigma}_{gg} + \omega_f \hat{\sigma}_{ff} + \omega_e \hat{\sigma}_{ee}, \tag{7c}$$

$$\hat{H}_{\mathrm{int}}(t) = -(g_m \hat{c}\hat{\sigma}_{eg} + g_m^* \hat{c}^\dagger \hat{\sigma}_{ge} + \Omega e^{-i\omega_c t}\hat{\sigma}_{ef} + \Omega^* e^{i\omega_c t}\hat{\sigma}_{fe}), \tag{7d}$$

where $\hat{H}_c$ denotes the free-field Hamiltonian of the QED cavity, $\hat{H}_a$ stands for the free-atomic Hamiltonian, and $\hat{H}_{\rm int}(t)$ describes the interaction of the fields with the atom. $\hat{c}^\dagger$ ($\hat{c}$) is the photonic creation (annihilation) operator and $\hat{\sigma}_{\alpha\beta} = |\alpha\rangle\langle\beta|$ ($\alpha,\beta \in \{g,f\}$) are the atomic operators. $\hat{H}_{\rm bare}(t)$ in (7) satisfies the time-dependent Schrödinger equation

$$i\,\partial_t|\Psi(t)\rangle = \hat{H}'(t)|\Psi(t)\rangle. \tag{8}$$

We move to a rotating frame in which (7) is time independent. The corresponding gauge transformation [19,33] has the form ($\hbar = 1$)

$$\hat{H}^T = \hat{U}(t)\hat{H}_{\rm bare}(t)\hat{U}^\dagger(t) + i\,\partial_t[\hat{U}(t)]\hat{U}^\dagger(t), \tag{9}$$

where $\hat{U}(t)$ is a unitary transformation. Under the gauge (9), $\hat{H}_{\rm bare}(t)$ reads as

$$\hat{H}^T_{\rm bare} = \hat{H}_c + \hat{H}_a + \hat{H}_{\rm int}, \tag{10a}$$

$$\hat{H}_c = \omega_m\hat{c}^\dagger\hat{c}, \tag{10b}$$

$$\hat{H}_a = \omega_g\hat{\sigma}_{gg} + (\omega_f + \omega_c)\hat{\sigma}_{ff} + \omega_e\hat{\sigma}_{ee}, \tag{10c}$$

$$\hat{H}_{\rm int} = -(g_m\hat{c}\hat{\sigma}_{eg} + g_m^*\hat{c}^\dagger\hat{\sigma}_{ge} + \Omega\hat{\sigma}_{ef} + \Omega^*\hat{\sigma}_{fe}). \tag{10d}$$

$\hat{U}(t) = e^{-i\omega_c t\hat{\sigma}_{ff}}$ has been chosen as the unitary transformation in deriving (10). Assume that the Λ three-level atom is initially prepared in the state $|g,n\rangle = |g\rangle \otimes |n\rangle$. n represents the arbitrary but fixed number of excitations with $n = 1,2,3\ldots$ and $|n\rangle$ the corresponding number state. Under the action of $\hat{H}^T_{\rm bare}$ onto the state $|g,n\rangle = |g\rangle \otimes |n\rangle$, we get the relations

$$\hat{H}^T_{\rm bare}|g,n\rangle = (\omega_m n + \omega_g)|g,n\rangle - g_m\sqrt{n}|e,n-1\rangle, \tag{11a}$$

$$\hat{H}^T_{\rm bare}|e,n-1\rangle = [\omega_m(n-1) + \omega_e]|e,n-1\rangle - g_m^*\sqrt{n}|g,n\rangle - \Omega^*|f,n-1\rangle, \tag{11b}$$

$$\hat{H}^T_{\rm bare}|f,n-1\rangle = [\omega_m(n-1) + \omega_f + \omega_c]|f,n-1\rangle - \Omega|e,n-1\rangle. \tag{11c}$$

In the subspace $\{|g,n\rangle, |e,n-1\rangle, |f,n-1\rangle\}$, $\hat{H}^T_{\rm bare}$ has the matrix representation

$$h_{\rm bare} = \begin{pmatrix} (\omega_m n + \omega_g) & -g_m\sqrt{n} & 0 \\ -g_m^*\sqrt{n} & \omega_m(n-1) + \omega_e & -\Omega^* \\ 0 & -\Omega & (\omega_m(n-1) + \omega_f + \omega_c) \end{pmatrix}. \tag{12}$$

Under Raman resonance condition $\omega_m n + \omega_g = \omega_f + \omega_c = \omega_e - \Delta$, we get

$$h_{\rm bare} = \begin{pmatrix} (\omega_m n + \omega_g) & -g_m\sqrt{n} & 0 \\ -g_m^*\sqrt{n} & (\omega_m(n-1) + \omega_e) & -\Omega^* \\ 0 & -\Omega & (\omega_m(n-1) + \omega_f + \omega_c) \end{pmatrix}. \tag{13}$$

Under a rotating-wave approximation, (13) is reduced to

$$h^{\rm Raman}_{\rm bare} = \begin{pmatrix} 0 & -g_m\sqrt{n} & 0 \\ -g_m^*\sqrt{n} & \Delta & -\Omega^* \\ 0 & -\Omega & 0 \end{pmatrix}. \tag{14}$$

In addition, as we have a far detuned excited state $|e,n-1\rangle$, i.e., $|\Delta| \gg |g_m|, |\Omega|$ [36,38] we can adiabatically eliminate the contribution of the excited state $|e,n-1\rangle$ directly on the level of (14). This yields to

$$h^{(\rm mJC)} = \begin{pmatrix} -\frac{|g_m|^2 n}{\Delta} & -\frac{g_m^*\Omega\sqrt{n}}{\Delta} \\ -\frac{g_m\Omega^*\sqrt{n}}{\Delta} & -\frac{|\Omega|^2}{\Delta} \end{pmatrix}. \tag{15}$$

Equation (15) represents the matrix form of the modified Jaynes-Cummings Hamiltonian (mJC) in the subspace $\{|g,n\rangle, |f,n-1\rangle\}$. The operator form of the modified Jaynes-Cummings Hamiltonian (mJC) reads as

$$\hat{H}^{(\rm mJC)} = \hat{H}_S + \hat{H}_{\rm int}, \tag{16a}$$

$$\hat{H}_S = -\left(\frac{|g_m|^2}{\Delta}\hat{c}^\dagger\hat{c}\hat{\sigma}_{gg} + \frac{|\Omega|^2}{\Delta}\hat{\sigma}_{ff}\right), \tag{16b}$$

$$\hat{H}_{\rm int} = -\left(\frac{g_m^*\Omega}{\Delta}\hat{c}^\dagger\hat{\sigma}_{gf} + \frac{g_m\Omega^*}{\Delta}\hat{c}\hat{\sigma}_{\rm fg}\right). \tag{16c}$$

The term $\hat{H}_S$ incorporates the influence of Stark shifts of the detuned fields, while $\hat{H}_{\rm int}$ represents the interaction of the cavity field and the atom, where $G = g_m^*\Omega/\Delta$ is the effective atom-photon coupling constant. Hamiltonians $\hat{H}_S$ and $\hat{H}_{\rm int}$ constitute the modified Jaynes-Cummings Hamiltonian. In the sequel, we are going to discuss the eigenstates of $\hat{H}^{(\rm mJC)}$ and look at the effect of the control field Stark shift.

B. Eigenstates of the modified Jaynes-Cummings model Hamiltonian

In the following, we calculate the eigenenergies and eigenstates of $\hat{H}^{(\rm mJC)}$. We show that dependent on whether one compensates the control field Stark shift by using external fields or not, the eigenenergies, composition of the eigenstates, and the mixing angle θ_n differ significantly. First, we consider the case of noncompensated control field Stark shift. $\hat{H}^{(\rm mJC)}$ of (16) reduces in the subspace $\{|g,n\rangle, |f,n-1\rangle\}$ as

$$h^{(m)}_n = \begin{pmatrix} -\frac{|g_m|^2 n}{\Delta} & -G\sqrt{n} \\ -G^*\sqrt{n} & -\frac{|\Omega|^2}{\Delta} \end{pmatrix}, \tag{17}$$

with $n = 1,2,3,\ldots$ the total number of excitations and corresponding number state $|n\rangle$. The eigenenergies are given as

$$E^{(m)}_{+,n} = 0, \tag{18}$$

$$E^{(m)}_{-,n} = -\left(\frac{|g_m|^2 n}{\Delta} + \frac{|\Omega|^2}{\Delta}\right). \tag{19}$$

The eigenstates to the eigenenergies $E^{(m)}_{+,n}$ and $E^{(m)}_{-,n}$ read as

$$|n,{\rm DP}^{(+)}\rangle := \sin(\theta_n)|f,n-1\rangle - \cos(\theta_n)|g,n\rangle, \tag{20a}$$

$$|n,{\rm DP}^{(-)}\rangle := \cos(\theta_n)|f,n-1\rangle + \sin(\theta_n)|g,n\rangle \tag{20b}$$

with the occurring mixing angle θ_n which is defined as

$$\theta_n = \frac{1}{2}\arctan\left(\frac{2|g_m|\sqrt{n}}{|\Omega|}\right). \tag{21}$$

However, $|n,{\rm DP}^{(\pm)}\rangle$ are called dark-polaritons. A dark-polariton is a quasiparticle which is a superposition of photonic and atomic excitations, where the atomic excitations have

only contributions of ground levels $|g\rangle$ and $|f\rangle$ and not the excited level $|e\rangle$. Such dark-polaritons are very similar to the known dark-state polaritons [17,18], but with one major difference. Dark-state polaritons are defined at Raman resonance of two coupling fields and formed independently of the single-photon detuning. Instead, dark-polaritons, which are also defined at Raman resonance, are formed for a large single, common photon detuning Δ of the two coupling fields, i.e., $|\Delta| \gg |g_m|,|\Omega|$. The dependence on Δ enables to tune the eigenstate $|n,\mathrm{DP}^{(\pm)}\rangle$ from an excited to a ground eigenstate. This follows from the eigenenergy $E^{(m)}_{-,n}$ of the dark-polariton $|n,\mathrm{DP}^{(-)}\rangle$. If $\Delta > 0$ ($\Delta < 0$), $|n,\mathrm{DP}^{(+)}\rangle$ is an excited (a ground) eigenstate and $|n,\mathrm{DP}^{(-)}\rangle$ a ground (an excited) eigenstate. Note that $|n,\mathrm{DP}^{(+)}\rangle$ is a degenerate eigenstate because the corresponding eigenenergy $E^{(m)}_{+,n}$ does not depend on the dark-polariton number n. $|n,\mathrm{DP}^{(-)}\rangle$ is a degenerate eigenstate as well for $n \geqslant 2$. Thus, the spectrum is discrete and degenerate in dependence of the dark-polariton number n. Now, we switch to the case of compensated control field Stark shift. Compensation is achieved by using an additional field, which couples the ground state $|f\rangle$ with some far-off-resonant excited state [39]. Within (17) we set the control field Stark shift $\frac{|\Omega|^2}{\Delta}$ to zero. Hence, the new block-matrix representation $h^{(m,\mathrm{comp})}_n$ in the subspace $\{|g,n\rangle,|f,n-1\rangle\}$ reads as

$$h^{(m,\mathrm{comp})}_n = \begin{pmatrix} -\frac{|g_m|^2 n}{\Delta} & -G\sqrt{n} \\ -G^*\sqrt{n} & 0 \end{pmatrix}, \tag{22}$$

with $n = 1,2,3,\ldots$ the total number of excitations and corresponding number state $|n\rangle$. The block-matrix (22) is a 2×2 matrix and can be analytically diagonalized. The eigenenergies are given as

$$\begin{aligned} E^{(\mathrm{comp},m)}_{-,n} &= -\frac{|g_m|^2 n + |g_m|\sqrt{n}\sqrt{|g_m|^2 n + 4|\Omega|^2}}{2\Delta}, \\ E^{(\mathrm{comp},m)}_{+,n} &= \frac{-|g_m|^2 n + |g_m|\sqrt{n}\sqrt{|g_m|^2 n + 4|\Omega|^2}}{2\Delta}. \end{aligned} \tag{23}$$

The respective eigenstates to the eigenenergies $E^{(\mathrm{comp},m)}_{+,n}$ and $E^{(\mathrm{comp},m)}_{-,n}$ are

$$|n,\mathrm{DP}^{(+)}_{\mathrm{comp}}\rangle := \sin(\theta_n)|f,n-1\rangle + \cos(\theta_n)|g,n\rangle, \tag{24a}$$

$$|n,\mathrm{DP}^{(-)}_{\mathrm{comp}}\rangle := \cos(\theta_n)|f,n-1\rangle - \sin(\theta_n)|g,n\rangle, \tag{24b}$$

with the occurring mixing angles θ_n which are defined as

$$\theta_n = \frac{1}{2}\arctan\left[\frac{A(\Omega,n)}{B(g_m,\Omega,n)}\right], \tag{25a}$$

$$A(\Omega,n) = 2\sqrt{2}\times|\Omega|\sqrt{n}, \tag{25b}$$

$$B(g_m,\Omega,n) = \sqrt{C(g_m,\Omega,n)}, \tag{25c}$$

$$C(g_m,\Omega,n) = |g_m|n^2 + 4|\Omega|^2 n + D(g_m,\Omega,n), \tag{25d}$$

$$D(g_m,\Omega,n) = |g_m|n\sqrt{n}\sqrt{|g_m|^2 n + 4|\Omega|^2}. \tag{25e}$$

$|n,\mathrm{DP}^{(\pm)}_{\mathrm{comp}}\rangle$ are dark-polaritons, but of a different type compared to the case of noncompensated control field Stark shift. First of all, the eigenenergies $E^{(\mathrm{comp},m)}_{s,n}$ with $s = +,-$ depend on the generalized Rabi frequency $\xi(n) = \sqrt{|g_m|^2 n + 4|\Omega|^2}$. Second, $|n,\mathrm{DP}^{(\pm)}_{\mathrm{comp}}\rangle$ have a common mixing angle θ_n that depends on the generalized Rabi frequency $\xi(n)$ as well. In addition, the two dark-polariton branches, represented through $|n,\mathrm{DP}^{(\pm)}_{\mathrm{comp}}\rangle$, are separated by the energy amount

$$E^{(\mathrm{comp},m)}_{-,n} - E^{(\mathrm{comp},m)}_{+,n} = \frac{|g_m|\sqrt{n}\sqrt{|g_m|^2 n + 4|\Omega|^2}}{\Delta}. \tag{26}$$

The separation energy is directly dependent on the generalized Rabi frequency $\xi(n)$ and the common single-photon detuning Δ as well. This separation is related to the photon-photon repulsion. It is a consequence of the onsite repulsion $U(n)$ which is a measure of the Kerr nonlinearity [40].

C. Comparison to standard Jaynes-Cummings model

On the level of the individual Hamiltonians, major differences are that at first, in $\hat{H}^{(\mathrm{mJC})}$ the number operator depends on the projection operator $\hat{\sigma}_{gg}$ of the ground level $|g\rangle$ which is not the case in $\hat{H}^{(\mathrm{JC})}$. Second, in $\hat{H}^{(\mathrm{mJC})}$ the atom-cavity field coupling strength $G = g_m\Omega/\Delta$ is rescaled by the common single-photon detuning Δ and the Rabi frequency Ω, where G is chosen to be real. Regarding the eigenstates, a key difference between $\hat{H}^{(\mathrm{mJC})}$ and $\hat{H}^{(\mathrm{JC})}$ is that in the modified Jaynes-Cummings model we have eigenstate dependence on the control field Stark shift. In addition, within the modified Jaynes-Cummings model, we only have a dependence on ground levels, whereas in the standard Jaynes-Cummings model there exists a dependence on the excited level. Hence, these dependencies affect the coherences. Namely, the bright polaritons in the standard Jaynes-Cummings model only consist of optical coherences $\hat{\sigma}_{eg}$ and are explored to spontaneous emission, while in the modified Jaynes-Cummings model, dark-polaritons only consist of spin coherences $\hat{\sigma}_{\mathrm{fg}}$ and no exploration to spontaneous emission is present. This enables the usage of dark-polaritons as a quantum memory for photons over their spin coherences likewise the dark-state polaritons [17–33]. Changing the mixing angles in (21) and (25) over rotations from $0 \to \frac{\pi}{2}$, which corresponds to an adiabatical change of the Rabi frequency Ω, photons are transferred to and stored in the spin coherences in a reversible manner. Optical coherences have shorter coherence times compared to the spin coherences which have longer coherence times. Coherence times of spin coherences are in the range of μs to ms in dark-state polaritons [17,18]. Similar is the case for dark-polaritons. In the sequel, we focus on our model system and state the effective model Hamiltonian which is based on our derivation of the modified Jaynes-Cummings model.

IV. MODEL SYSTEM AND EFFECTIVE MODEL HAMILTONIAN

In the previous sections, we have investigated the standard and modified Jaynes-Cummings model on the level of a single QED cavity. In the subsequent step, we extend the modified Jaynes-Cummings model to a one-dimensional array of coupled QED cavities. This will lead us to the modified Jaynes-Cummings Hubbard model as our effective model Hamiltonian. It includes the hopping between adjacent

cavities. First, we state the model system and, second, present the effective model Hamiltonian.

A. Model system

The system we consider consists of a one-dimensional array of N-coupled QED cavities. We assume periodic boundary conditions, i.e., the cavity labeled by $n = N + 1$ corresponds to the cavity $n = 1$. Each cavity embeds a three-level atom with two ground levels $|g\rangle$ and $|f\rangle$, and an excited level $|e\rangle$. The level energies are ω_g, ω_f, and ω_e, respectively, and the excited level $|e\rangle$ is detuned by the common single-photon detuning Δ. In reality, the levels can be either fine or hyperfine levels of alkali-metal atoms. Their D_1 or D_2 line transitions are nowadays easily accessible via available lasers and optical modes of QED cavities. One mode of a tunable cavity [41,42] of frequency ω_m couples the transition $|g\rangle \rightarrow |e\rangle$ with the strength g_m, and the classical control field of frequency ω_c and Rabi-frequency Ω couple the transition $|f\rangle \rightarrow |e\rangle$. This configuration is known to feature vacuum induced transparency, as first experimentally demonstrated by the group of Vuletić [43]. Both g_m and Ω are typically in MHz range for alkali-metal atoms, which are strongly coupled to QED cavities, and for moderate laser powers.

B. Effective model Hamiltonian

As we consider a one-dimensional chain of N identical coupled QED cavities, the derived modified Jaynes-Cummings model for a single QED cavity is valid for all QED cavities in the one-dimensional chain. Therefore, our effective model Hamiltonian (modified Jaynes-Cummings Hubbard model) ($\hbar = 1$) has the form

$$\hat{H}^{(\mathrm{mJCH})} = \hat{H}^{(\mathrm{mJC})} + \hat{H}_{\mathrm{hop}}, \tag{27a}$$

$$\hat{H}^{(\mathrm{mJC})} = \hat{H}_S + \hat{H}_{\mathrm{int}}, \tag{27b}$$

$$\hat{H}_S = -\sum_{\mu=1}^{N}\left(\frac{g_m^2}{\Delta}\hat{c}_\mu^\dagger\hat{c}_\mu\hat{\sigma}_{gg}^{(\mu)} + \frac{\Omega^2}{\Delta}\hat{\sigma}_{ff}^{(\mu)}\right), \tag{27c}$$

$$\hat{H}_{\mathrm{int}} = -G\sum_{\mu=1}^{N}\left(\hat{c}_\mu^\dagger\hat{\sigma}_{gf}^{(\mu)} + \hat{c}_\mu\hat{\sigma}_{\mathrm{fg}}^{(\mu)}\right), \tag{27d}$$

$$\hat{H}_{\mathrm{hop}} = -J\sum_{\mu=1}^{N}(\hat{c}_{\mu+1}^\dagger\hat{c}_\mu + \hat{c}_\mu^\dagger\hat{c}_{\mu+1}), \tag{27e}$$

where $\hat{c}_\mu^\dagger$ ($\hat{c}_\mu$) is the photonic creation (annihilation) operator and $\hat{\sigma}_{\alpha\beta}^{(\mu)} = |\alpha\rangle_\mu\langle\beta|$ ($\alpha,\beta \in \{g,f\}$) are the atomic operators for the site number μ. The term $\hat{H}_S$ incorporates the influence of Stark shifts of the detuned fields, while $\hat{H}_{\mathrm{int}}$ represents the interaction of the cavity field and the atom, where $G = g_m\Omega/\Delta$ is the effective atom-photon coupling constant which is set to be real. Hamiltonians $\hat{H}_S$ and $\hat{H}_{\mathrm{int}}$ constitute the modified Jaynes-Cummings Hamiltonian. As will be shown in the sequel, the Stark shifts have profound influence on the energy eigenspectrum. $\hat{H}_{\mathrm{hop}}$ describes the photon hopping between adjacent cavities, based on evanescent field coupling, with J as the intercavity photon hopping strength. Similar effective Hamiltonian has been previously used to describe a network of fiber coupled cavities, embedded with three-level atoms [39]. However, while that scheme requires the compensation of the level Stark shifts, here we utilize the individual Stark shifts to achieve tunability. Our effective model Hamiltonian (27) supports the formation of dark-polariton bound pairs. We will see that the different dark-polaritons, which have been discussed in Sec. III, are actually involved in the formation of the energy bands and the bound states. Moreover, we show and discuss that the bound states are formed due to the presence of a force called Kerr nonlinearity which is determined by the onsite repulsion.

V. FORMATION OF DARK-POLARITON BOUND PAIRS

In the following, we discuss the formation of dark-polariton bound pairs in our system. In order to exploit the invariance of the system under cyclic permutations of the sites, we introduce the following operators via discrete Fourier transforms:

$$\hat{b}_k = \frac{1}{\sqrt{N}}\sum_{\mu=1}^{N} e^{-\frac{2\pi i}{N}\mu k}\,\hat{c}_\mu, \tag{28a}$$

$$\hat{s}_{gf}^{(k)} = \frac{1}{\sqrt{N}}\sum_{\mu=1}^{N} e^{-\frac{2\pi i}{N}\mu k}\,\hat{\sigma}_{gf}^{(\mu)}, \tag{28b}$$

where $k = 0,1,\ldots,N-1$ is related to the (discrete) quasimomentum of the excitation. Similarly to [34], we work in the two-excitation subspace that is spanned by the states $|kj\rangle_F \equiv \hat{b}_k^\dagger\hat{b}_j^\dagger|\Phi_0\rangle$, $|k\rangle_F|j\rangle_A \equiv \hat{b}_k^\dagger\hat{s}_{gf}^{(j)\dagger}|\Phi_0\rangle$, and $|kj\rangle_A \equiv \hat{s}_{gf}^{(k)\dagger}\hat{s}_{gf}^{(j)\dagger}|\Phi_0\rangle$. The subscripts F and A stand for the photonic and atomic excitations, respectively. The state $|\Phi_0\rangle = \otimes_{\mu=1}^{N}|g\rangle_\mu|0\rangle_\mu$ is the ground state of the system, where $|0\rangle_\mu$ denotes the vacuum state of the cavity number μ. We note that the excitations (polaritons) are in our case dark in a sense that they do not have the contribution of the excited levels $|e\rangle$ and are not subjected to spontaneous emission. The atomic excitations $|kj\rangle_A$ are in general not orthogonal to each other because of ${}_A\langle k'j'|kj\rangle_A = \delta_{k,k'}\delta_{j,j'} + \delta_{k,j'}\delta_{j,k'} - \frac{2}{N}\delta_{k+j,k'+j'}$. $\hat{b}_k$ and $\hat{b}_j^\dagger$ fulfill the bosonic commutation relation $[\hat{b}_k,\hat{b}_j^\dagger] = \delta_{kj}$, while the atomic operators fulfill the commutation relation $[\hat{s}_{gf}^{(k)},\hat{s}_{gf}^{(j)\dagger}] = -\frac{1}{N}\sum_{\mu=1}^{N} e^{\frac{2\pi i}{N}\mu(j-k)}\hat{\sigma}_z^{(\mu)}$ with $\hat{\sigma}_z^{(\mu)}$ as the Pauli z matrix for the atom in the μth cavity. Under the action of $\hat{H}$ on the states which form the two-excitation subspace, we get the relations

$$\hat{H}|kj\rangle_F = (\omega_k + \omega_j - 2a)|kj\rangle_F - G(|k\rangle_A|j\rangle_F + |j\rangle_A|k\rangle_F), \tag{29a}$$

$$\hat{H}|k\rangle_A|j\rangle_F = (\omega_j - a - b)|k\rangle_A|j\rangle_F - G(|kj\rangle_A + |kj\rangle_F) + \frac{a}{N}\sum_{(k',j')\in S_P}(|k'\rangle_A|j'\rangle_F + |j'\rangle_A|k'\rangle_F) + \frac{2G}{N}\sum_{(k',j')\in S_P}|k'j'\rangle_A, \tag{29b}$$

$$\hat{H}|j\rangle_A|k\rangle_F = (\omega_k - a - b)|j\rangle_A|k\rangle_F - G(|kj\rangle_A + |kj\rangle_F) + \frac{a}{N}\sum_{(k',j')\in S_P}(|k'\rangle_A|j'\rangle_F + |j'\rangle_A|k'\rangle_F) + \frac{2G}{N}\sum_{(k',j')\in S_P}|k'j'\rangle_A, \tag{29c}$$

$$\hat{H}|kj\rangle_A = -G(|k\rangle_A|j\rangle_F + |j\rangle_A|k\rangle_F) - 2b|kj\rangle_A, \tag{29d}$$

where $\omega_l = -2J\cos(\frac{2\pi l}{N})$ for $l \in \{k, j\}$, $a = g_m^2/\Delta$, and $b = \Omega^2/\Delta$. Within Eqs. (29b) and (29c), we have a sum over the set $S_P = \{(k,j) \mid 0 \leqslant k < j \leqslant N-1, k+j \equiv P \,(\mathrm{mod}\, N)\}$ that is determined by the quasimomentum P. From Eqs. (29a)–(29d) we can deduce that the quasimomentum P is a conserved quantity and hence a good quantum number. Apart from the quasimomentum, the total number of excitations (dark-polaritons) $\hat{N} = \sum_{\mu=1}^{N}(\hat{c}_\mu^\dagger\hat{c}_\mu + \hat{\sigma}_{ff}^{(\mu)})$ is a conserved quantity.

We can construct the complete set of eigenvectors by solving the eigenproblem within each of the subspaces $P = 0,1,\ldots,N-1$. Following [34], we restrict the discussion to the case of even N and odd P. A general dark two-polariton eigenvector $|\Psi_P^{(D)}\rangle$ has the form

$$|\Psi_P^{(D)}\rangle = \sum_{(k,j)\in S_P}(\alpha_{kj}|kj\rangle_F + \beta_{kj}|k\rangle_A|j\rangle_F + \beta'_{kj}|j\rangle_A|k\rangle_F + \gamma_{kj}|kj\rangle_A). \tag{30}$$

$|\Psi_P^{(D)}\rangle$ satisfies the time-independent Schrödinger equation $\hat{H}|\Psi_P^{(D)}\rangle = \lambda|\Psi_P^{(D)}\rangle$ which yields within each of the subspaces $P = 1,3,\ldots,N-1$ an eigenproblem that is given by the subsequent set of linear equations

$$\lambda\alpha_{kj} = (\omega_k + \omega_j - 2a)\alpha_{kj} - G(\beta_{kj} + \beta'_{kj}), \tag{31a}$$

$$\lambda\beta_{kj} = -G\alpha_{kj} + (\omega_j - a - b)\beta_{kj} - G\gamma_{kj} + \frac{a}{N}\sum_{(k',j')\in S_P}(\beta_{k'j'} + \beta'_{k'j'}) + \frac{2G}{N}\sum_{(k',j')\in S_P}\gamma_{k'j'} \tag{31b}$$

$$\lambda\beta'_{kj} = -G\alpha_{kj} + (\omega_k - a - b)\beta_{kj} - G\gamma_{kj} + \frac{a}{N}\sum_{(k',j')\in S_P}(\beta_{k'j'} + \beta'_{k'j'}) + \frac{2G}{N}\sum_{(k',j')\in S_P}\gamma_{k'j'}, \tag{31c}$$

$$\lambda\gamma_{kj} = -G(\beta_{kj} + \beta'_{kj}) - 2b\gamma_{kj}, \tag{31d}$$

where λ is the corresponding eigenvalue. As it was demonstrated in [34], for various values of the quasimomentum P the majority of eigenvalues are at most distributed among three bands. When all three bands are well resolved, it was shown that each of the two band gaps contains an eigenenergy of the single two-polariton bound state. For sufficiently large intercavity photon hopping strength J comparing to the strength of the atom-photon interaction, the bands start to overlap.

However, since we are not dealing with the standard JCH model, but rather with a modified one, we find some important differences and new features. Namely, as opposed to [34] there is only one mutually localized DPBP within one of the existing band gaps, while the other one joins the adjacent outer band. The other DPBP can reappear provided that the Stark shift of the control field is compensated. In both cases, when $\Delta < 0$, $g_m \gg \Omega$ and $g_m^2/|\Delta| \gtrsim 1.5\,J$, the ground state of the system is DPBP of a different type than the aforementioned ones. In the sequel, we report on the state composition of the different DPBP types.

The Kerr nonlinearity is a known force in light-atom interactions which depends on the atomic level structure as well as on the coupling strength of light-atom interactions. In our case, the strength of light-atom interaction is described by the effective coupling strength $G = g_m\Omega/\Delta$. Tuning g_m and/or Ω directly affects the Kerr nonlinearity. Compared to [34], we can not only tune and control the Kerr nonlinearity by the cavity-mode coupling strength g_m, but also by the Rabi frequency Ω. This force can be attractive or repulsive [1,13–16]. This force generates the bound state of two dark-polaritons in our case. A measure of the Kerr nonlinearity is the onsite repulsion $U(n)$ which is in general defined as

$$U(n) := (E_+ - E_-)(n+1) - (E_+ - E_-)(n) \tag{32}$$

with $E_\pm$ the eigenenergies of the considered eigenstates. In case of the standard Jaynes-Cummings model, the onsite repulsion $U(n) = \chi(n+1) - \chi(n)$ is determined by the generalized Rabi frequency $\chi(n)$ [3]. This will be different in our case as we will see in the following. In our DPBPs we have bound photons and bound atoms. In [44], they have experimentally shown bound states of atoms in coupled QED cavities, when atoms occupy the same site.

A. Dark-polariton bound pairs in the regime of noncompensated control field Stark shift

We focus on the single DPBP solution of Eqs. (31) which is given in red color within Fig. 1(a) representing the energy eigenspectrum of the model Hamiltonian $\hat{H}$ in dependence of odd values of quasimomentum P. Three energy bands are visible for the used parameter values. We define the gap between the two upper energy bands as the high-energy band gap and in accordance the gap between the two lower-energy bands as the low-energy band gap. The dark-polaritons, which are involved in the formation of energy bands and the single DPBP in Fig. 1(a), are given in (20). This can be seen by solving Eqs. (31) for intercavity hopping $J = 0$. Note that the bands are a consequence of repulsively interacting dark-polaritons of different types with respect to the eigenenergies $E_{\pm,n}^{(m)}$. By different types here, we mean that the dark-polariton with eigenenergy $E_{+,n}^{(m)}$ interacts with the dark-polariton of eigenenergy $E_{-,n}^{(m)}$ in a repulsive way at the same site μ. This is a consequence of the onsite repulsion $U(n)$. On different sites, dark-polaritons with eigenenergies $E_{+,n}^{(m)}$ and $E_{-,n}^{(m)}$ are noninteracting. Instead, the mentioned Kerr nonlinearity, expressed through the onsite repulsion $U(n) = \frac{g_m^2}{\Delta}$, enables the single DPBP state formation by the two dark-polaritons with eigenenergies $E_{-,n}^{(m)}$ which is placed at the same site μ in case of $\Delta > 0$. There is an additional DPBP, formed by the two dark-polaritons with eigenenergies $E_{+,n}^{(m)}$ in case of $\Delta > 0$, but is not visible in the spectrum as it is attached to the central

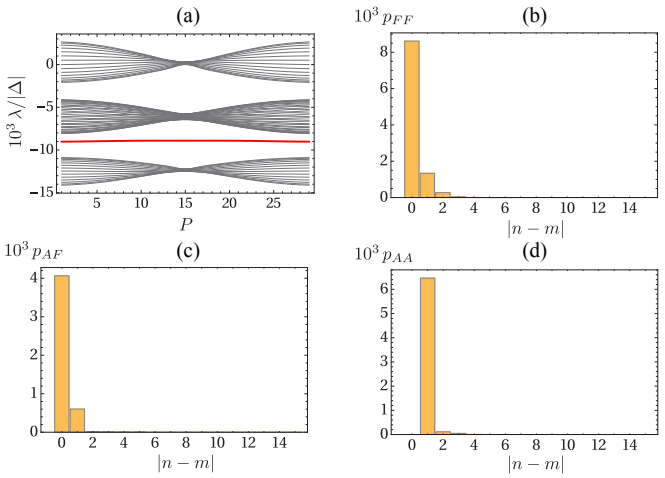

FIG. 1. (a) Normalized eigenvalues dependence on the quasimomentum P for $N = 30$ cavities. Dark-polariton bound pair state (red curve) appears in the low-energy band gap. The eigenvalues are joined by lines for ease of visualization. (b)–(d) Joint probabilities for different types of double excitations associated to DPBP state for $P = 1$. Used parameters: $\Delta > 0$, $g_m = 0.05\,|\Delta|$, $\Omega = 0.06\,|\Delta|$, and $J = 0.001\,|\Delta|$.

band. On the contrary, formation of single DPBP interchanges for $\Delta < 0$. Our determined $U(n)$ from [3] is mainly affected by the cavity field coupling strength g_m. By increasing g_m we increase the onsite repulsion $U(n)$ which directly enhances the interaction between the two dark-polaritons with eigenenergies $E^{(m)}_{-,n}$ at the same site μ with $\Delta > 0$. Thus, single DPBP is strengthened. Due to the interaction, the single DPBP lies inside the energy band gaps. Depending on the sign of the common single-photon detuning Δ, DPBP lies either in the high- or low-energy band gap. In the case $\Delta > 0$, DPBP lies in the low-energy band gap, whereas in the opposite case it resides within the high-energy band gap. In order to get some information on the inherent state composition of the single DPBP, we calculate, in line with [34], the joint probabilities

$$p_{FF} = \left| \langle \Psi_P^{(D)} | \frac{\hat{c}_n^\dagger \hat{c}_m^\dagger}{\sqrt{1+\delta_{nm}}} | \Phi_0 \rangle \right|^2, \tag{33a}$$

$$p_{AF} = \left| \langle \Psi_P^{(D)} | \hat{c}_n^\dagger \hat{\sigma}_{gf}^{(m)\dagger} | \Phi_0 \rangle \right|^2, \tag{33b}$$

$$p_{AA} = \left| \langle \Psi_P^{(D)} | \hat{\sigma}_{gf}^{(n)\dagger} \hat{\sigma}_{gf}^{(m)\dagger} | \Phi_0 \rangle \right|^2 \tag{33c}$$

of finding pure photonic, photon-atom, and pure atomic excitations, respectively, in cavities at positions n and m. These excitations (pure photonic, pure atomic, and photon-atom) reflect the unique property of dark-polaritons in which the superposition of photonic and collective atomic excitations can be tuned by changing Ω in first place. In our case, we can not only change Ω, but also g_m as we use tunable cavities [41,42]. For a given value of quasimomentum P, all three joint probabilities only depend on the relative distance $|n - m|$ within the cavities.

In Figs. 1(b)–1(d) we present the joint probabilities for the single DPBP state of Fig. 1(a). We have chosen the number of coupled QED cavities to be $N = 30$, single-photon detuning $\Delta > 0$, cavity-mode coupling strength $g_m = 0.05\,\Delta$, the control field Rabi frequency $\Omega = 0.06\,\Delta$, intercavity photon hopping strength $J = 0.001\,\Delta$, and subspace $P = 1$. One can see that the DPBP excitations are well confined together, and all three possible excitation types coexist with roughly equal contributions. The state composition gradually changes by decreasing the contribution of double atomic excitations when P approaches the midrange values. This regime is roughly characterized by $g_m \approx \Omega$ and $(g_m^2 + \Omega^2)/|\Delta| > 5J$. The energy band gaps close when decreasing the ratio of $(g_m^2 + \Omega^2)/|\Delta|$ and J. At the same time, DPBP becomes relatively delocalized, similarly as in [34].

B. Dark-polariton bound pairs in the regime of compensated control field Stark shift

The tunability of our model enables not only the control of the shape of the energy bands, but also the emergence of an additional DPBP state. Namely, if the control field Stark shift is compensated by using an additional field, which couples the ground state $|f\rangle$ with some far-off-resonant excited state [39], another DPBP state appears in the formerly empty energy band gap. Such an add reflects in the removal of the parameter b from Eqs. (31). The energy bands in Fig. 2(a), shown for discrete and distinct quasimomenta P, are formed by the dark-polaritons in (24). This can be seen by solving Eqs. (31) for the intercavity hopping strength $J = 0$ and set the parameter b equal to zero. The onsite repulsion $U(n)$, which ensures the formation of the two DPBPs, is given as $U(n) = \frac{g_m\sqrt{n+1}\sqrt{g_m^2(n+1)+4\Omega^2} - g_m\sqrt{n}\sqrt{g_m^2 n+4\Omega^2}}{\Delta}$ for positive and negative common single-photon detuning Δ. Thus, the onsite repulsion $U(n)$ is invariant under the sign change of Δ. Distinctly to the DPBP formation under noncompensated control field Stark shift, the onsite repulsion $U(n)$ apart from the cavity field coupling strength g_m directly depends on the Rabi frequency Ω. This gives the opportunity to effectively control and enhance the interaction through g_m and Ω. Further, in Fig. 2(a) one can observe that each of the two energy band gaps now contains a single DPBP state (blue and red curves). We used the same parameter values as in Fig. 1, but with compensated control field Stark shift. In Figs. 2(b)–2(d) and Figs. 2(e)–2(g) we characterize the state composition of lower- and higher-energy DPBP states, respectively, by considering the joint probabilities as in the previous subsection. The DPBP in the lower-energy band gap is dominantly composed of two-photon excitation, while in the other DPBP state atom-photon excitation prevails. Moreover, higher-energy DPBP state is further apart from the outer energy band and it is relatively more localized than the lower-energy DPBP state. We checked that the same behavior persists for other values of quasimomentum P. Note that the described situation is for $\Delta > 0$, while it interchanges for $\Delta < 0$.

VI. QUANTUM MEMORY OF LIGHT IN A DARK-POLARITON BOUND PAIR

In the parameter regime where the common single-photon detuning Δ is negative and the cavity-atom coupling strength g_m is significantly larger than the control field Rabi frequency Ω, we have a single DPBP state which is the ground state

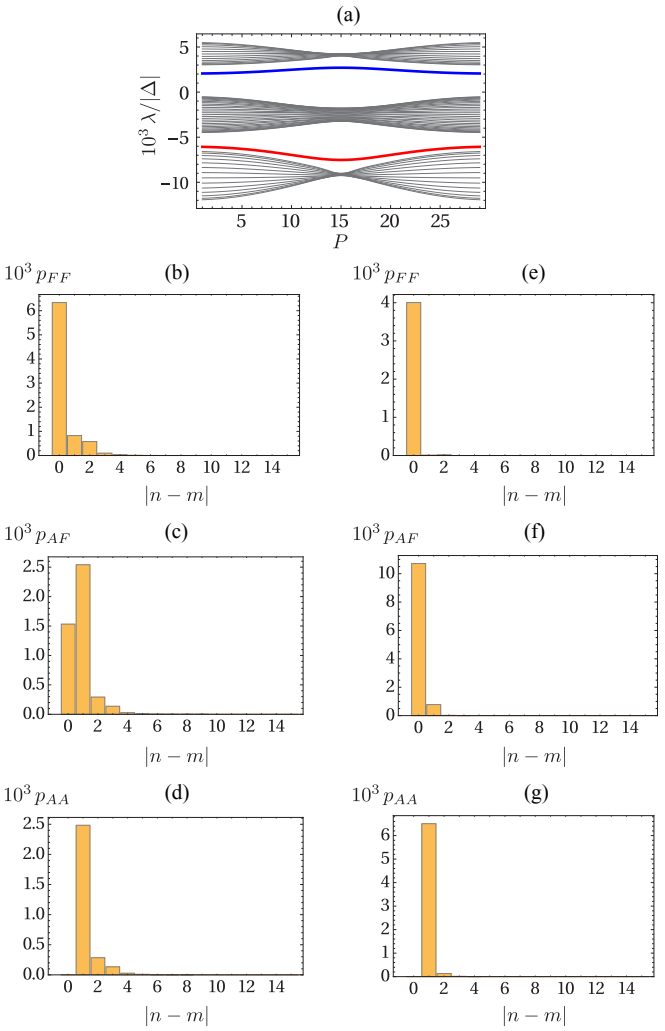

FIG. 2. (a) Normalized eigenvalues dependence on the quasimomentum P for $N = 30$ cavities. Two dark-polariton bound pair states (blue and red curves) appear in both energy band gaps. The eigenvalues are joined by lines for ease of visualization. (b)–(d) Joint probabilities for different types of double excitations associated to lower-energy DPBP state. (e)–(g) Joint probabilities for different types of double excitations associated to higher-energy DPBP state for $P = 1$. Used parameters: $\Delta > 0$, $g_m = 0.05\,|\Delta|$, $\Omega = 0.06\,|\Delta|$, and $J = 0.001\,|\Delta|$.

of the system. It is well separated from the rest of the energy spectrum when $g_m^2/|\Delta| \gtrsim 1.5\,J$. This is presented in Fig. 3(a). DPBP state composition, given in Figs. 3(b)–3(d) by the corresponding joint probabilities, reveals that the state is dominantly composed of combined atomic and photonic excitations which are localized in their relative spatial coordinates. Note that this DPBP state is of a completely different type than the ones found in the previous section.

It is important that this state also enables the storage of a single photon in the form of a collective atomic spin coherence excitation to which the other photon is closely bound. Namely, when $\Omega \to 0$ adiabatically, a DPBP becomes a pure combination of an atomic and photonic excitation. From this we can deduce that one photon remains attached

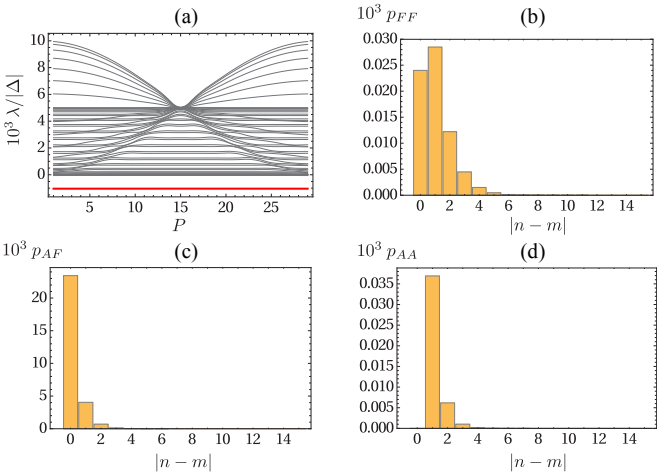

FIG. 3. (a) Normalized eigenvalues dependence on the quasimomentum P for $N = 30$ cavities. Dark-polariton bound pair state (red curve) appears as the ground state. The eigenvalues are joined by lines for ease of visualization. (b)–(d) Joint probabilities for different types of double excitations associated to DPBP state for $P = 1$. Used parameters: $\Delta < 0$, $g_m = 0.05\,|\Delta|$, $\Omega = 0.001\,|\Delta|$, and $J = 0.00125\,|\Delta|$.

to the atomic spin coherence wave. This is reminiscent of the atom-photon molecule [36].

The state composition can be tuned by increasing the relative importance of the intercavity photon hopping, e.g., by increasing $|\Delta|$. This is achieved gradually for distinct values of quasimomentum, starting from the values $P = 1$, $N - 1$ and proceeding towards the midrange values of P. Figure 4(a) shows the energy spectrum in such a case. For $P \in \{1, 3, N-3, N-1\}$ the DPBP state is predominantly composed of two-photon excitations which become delocalized in their relative

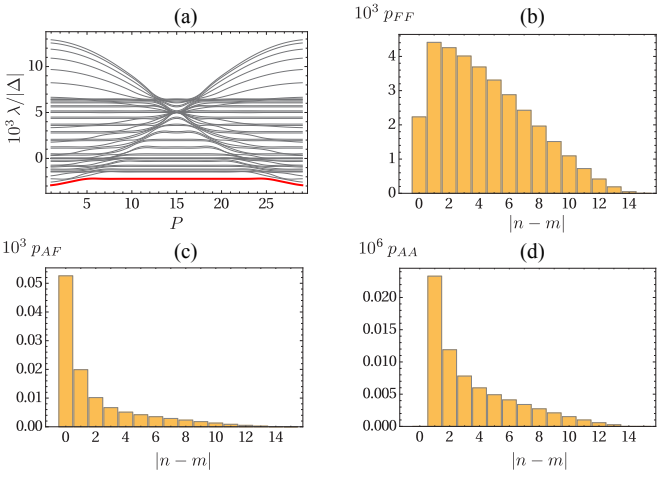

FIG. 4. (a) Normalized eigenvalues dependence on the quasimomentum P for $N = 30$ cavities. Dark-polariton bound pair state (red curve) appears as the ground state. The eigenvalues are joined by lines for ease of visualization. (b)–(d) Joint probabilities for different types of double excitations associated to DPBP state for $P = 1$. Used parameters: $\Delta < 0$, $g_m = 0.05\,|\Delta|$, $\Omega = 0.001\,|\Delta|$, and $J = 0.002\,|\Delta|$.

spatial positions, as can be seen in Figs. 4(b)–4(d). The reason for such behavior can be traced back to the emergence of the avoided crossings of the ground state and the first excited state near the edges of the quasimomentum zone. The crossings shift towards the P-zone center as the influence of the photon hopping is being increased. For the quasimomentum values between the crossings, the DPBP state remains dominantly of the atom-photon type. In the case when the control field strength adiabatically reduces to zero, the DPBP state becomes of a pure two-photon type. Therefore, this corresponds to the retrieval procedure of the previously stored photon excitation.

VII. EXPERIMENTAL REALIZATION

Our model system is a large, one-dimensional mJCH chain of N-coupled QED cavities. In order to realize it, we need a structure, in which large arrays of coupled QED cavities can be realized. Promising candidates are photonic band-gap cavities [12,45]. It is manageable to produce and position them with high precision and in large numbers. A tempting alternative are photonic crystals as they offer the possibility of fabricating large arrays of QED cavities in one- or two-dimensional lattices as well as networks [46–48]. A third possibility would be the use of toroidal micro-QED cavities that are coupled via tapered optical fibers [49]. Single atoms, embedded in each QED cavity, are three-level atoms where the excited level is far detuned by the common single-photon detuning with respect to the two coupling fields. In real experiments, Cs and ultracold ^{87}Rb atoms have shown to be very suitable [44,50,51]. For Cs in a toroidal micro-QED cavity it has be shown that g_m in the strong-coupling regime reaches the value of ~ 50 MHz [50]. This fits pretty well with our theoretically chosen value for the formation of individual DPBP inside the energy band gaps, but also for the ground DPBP at $\Delta < 0$ with its potential use as a quantum memory for a single photon.

VIII. CONCLUSION

To summarize, we have derived a modified Jaynes-Cummings model from the bare model under two conditions: (i) two-photon Raman resonance of the cavity mode and classical control field, (ii) common single-photon detuning $|\Delta| \gg g_m, \Omega$. We have shown that the eigenstates on one hand depend on the common single-photon detuning and, on the other hand, their composition differs with respect to the control field Stark shift. Moreover, we have extended the modified Jaynes-Cummings model to a modified Jaynes-Cummings-Hubbard model where an array of N-coupled QED cavities, each having an embedded single three-level atom, is considered. The modified Jaynes-Cummings-Hubbard model supports DPBPs. The formation of two different species of spatially localized dark-polariton bound pairs (DPBPs) has been elaborated when there are exactly two excitations in the system. It was shown that the onsite repulsion $U(n)$ as a consequence of the Kerr nonlinearity represents the attractive force between interacting dark-polaritons and enables the existence of DPBP states. Furthermore, it is demonstrated that our model system offers a high degree of tunability that can affect both quantitative and qualitative behavior. In particular, the number of DPBP states can be controlled by (not) compensating the Stark shift due to the control field. Further, in the regime when cavity-atom coupling overwhelms the influence of the control field, and the common single-photon detuning of the fields is negative, we obtained a ground DPBP eigenstate on which the storage and readout of a single photon can be effectively performed. An experimental realization is proposed for our model system. Cs atom has been mentioned as a promising candidate as its value of the cavity-mode coupling strength g_m fits very well with our theoretically chosen and determined one. We expect that future investigations of this kind of system under different settings, i.e., with distinct and alternating hopping strengths between the cavities, in the presence of disorder, or in two-dimensional lattice configurations, may lead to various effects and rich physics.

ACKNOWLEDGMENT

This work was supported by the Ministry of Education, Science, and Technological Development of the Republic of Serbia, under Grants No. III45016 and No. OI171038 and also by Scopes JRP Grant No. IZ73Z0_152511.

[1] M. J. Hartmann, F. G. S. L. Brandão, and M. B. Plenio, Laser Photon Rev. **2**, 527 (2008).
[2] A. D. Greentree, C. Tahan, J. H. Cole, and L. C. L. Hollenberg, Nat. Phys. **2**, 856 (2006).
[3] M. I. Makin, J. H. Cole, C. Tahan, L. C. L. Hollenberg, and A. D. Greentree, Phys. Rev. A **77**, 053819 (2008).
[4] M. Schiró, M. Bordyuh, B. Öztop, and H. E. Türeci, Phys. Rev. Lett. **109**, 053601 (2012).
[5] I. Carusotto and C. Ciuti, Rev. Mod. Phys. **85**, 299 (2013).
[6] R. A. Street and N. F. Mott, Phys. Rev. Lett. **35**, 1293 (1975).
[7] D. G. Angelakis, M. F. Santos, and S. Bose, Phys. Rev. A **76**, 031805 (2007).
[8] J. Quach, M. I. Makin, C. H. Su, A. D. Greentree, and L. C. L. Hollenberg, Phys. Rev. A **80**, 063838 (2009).
[9] M. J. Hartmann, F. G. S. L. Brandão, and M. B. Plenio, Nat. Phys. **2**, 849 (2006).
[10] J. Koch and K. Le Hur, Phys. Rev. A **80**, 023811 (2009).
[11] K. Kamide, M. Yamaguchi, T. Kimura, and T. Ogawa, Phys. Rev. A **87**, 053842 (2013).
[12] Y. Akahane, T. Asano, B.-S. Song, and S. Noda, Nature (London) **425**, 944 (2003).
[13] A. Imamoglu, H. Schmidt, G. Woods, and M. Deutsch, Phys. Rev. Lett. **79**, 1467 (1997).
[14] S. Rebić, S. M. Tan, A. S. Parkins, and D. F. Walls, J. Opt. B **1**, 490 (1999).

[15] J. Kim, O. Benson, H. Kan, and Y. Yamamoto, Nature (London) **397**, 500 (1999).
[16] K. M. Birnbaum, A. Boca, R. Miller, A. D. Boozer, T. E. Northup, and H. J. Kimble, Nature (London) **436**, 87 (2005).
[17] M. Fleischhauer and M. D. Lukin, Phys. Rev. Lett. **84**, 5094 (2000).
[18] M. Fleischhauer and M. D. Lukin, Phys. Rev. A **65**, 022314 (2002).
[19] Y. D. Chong and M. Soljačić, Phys. Rev. A **77**, 013823 (2008).
[20] X. J. Liu, H. Jing, X. T. Zhou, and M. L. Ge, Phys. Rev. A **70**, 015603 (2004).
[21] Z. J. Liu, W. B. Yan, and L. Zhou, Eur. Phys. J. D **57**, 111 (2010).
[22] F. E. Zimmer, J. Otterbach, R. G. Unanyan, B. W. Shore, and M. Fleischhauer, Phys. Rev. A **77**, 063823 (2008).
[23] A. Joshi and M. Xiao, Phys. Rev. A **71**, 041801 (2005).
[24] Y. Li, P. Zhang, P. Zanardi, and C. P. Sun, Phys. Rev. A **70**, 032330 (2004).
[25] J. Ruseckas, A. Mekys, and G. Juzeliunas, Phys. Rev. A **83**, 023812 (2011).
[26] P. Li, Y. Gu, K. Wang, and Q. Gong, Phys. Rev. A **73**, 032343 (2006).
[27] Y. Li, L. Zheng, Y. X. Liu, and C. P. Sun, Phys. Rev. A **73**, 043805 (2006).
[28] J. Appel, K. P. Marzlin, and A. I. Lvovsky, Phys. Rev. A **73**, 013804 (2006).
[29] X. J. Liu, X. Liu, Z. X. Liu, L. C. Kwek, and C. H. Oh, Phys. Rev. A **75**, 023809 (2007).
[30] S. D. Jenkins, D. N. Matsukevich, T. Chaneliere, A. Kuzmich, and T. A. B. Kennedy, Phys. Rev. A **73**, 021803 (2006).
[31] L. Karpa, F. Vewinger, and M. Weitz, Phys. Rev. Lett. **101**, 170406 (2008).
[32] L. R. Wang, Y. T. Zhao, J. Ma, J. M. Zhao, L. T. Xiao, and S. T. Jia, Chin. Phys. **15**, 365 (2006).
[33] A. Maggitti, M. Radonjić, and B. M. Jelenković, Laser Phys. **23**, 105202 (2013).
[34] M. T. C. Wong and C. K. Law, Phys. Rev. A **83**, 055802 (2011).
[35] C. Li *et al.*, Sci. Rep. **5**, 11945 (2015).
[36] D. A. Steck, Quantum and Atom Optics, Sec. 10.3.2, http://steck.us/teaching.
[37] E. T. Jaynes and F. W. Cummings, Proc. IEEE **51**, 89 (1963).
[38] O. Gamel and D. F. V. James, Phys. Rev. A **82**, 052106 (2010).
[39] S. Kumar and D. Kumar, Phys. Rev. A **85**, 052317 (2012).
[40] S. Rebić, A. S. Parkins, and S. M. Tan, Phys. Rev. A **65**, 063804 (2002).
[41] M. Sandberg, F. Persson, I. C. Hoi, C. M. Wilson, and P. Delsing, Phys. Scr. **T137**, 014018 (2009).
[42] J. R. Johansson, G. Johansson, C. M. Wilson, and F. Nori, Phys. Rev. Lett. **103**, 147003 (2009).
[43] H. Tanji-Suzuki, W. Chen, R. Landig, J. Simon, and V. Vuletić, Science **333**, 1266 (2011).
[44] K. Winkler *et al.*, Nature (London) **441**, 853 (2006).
[45] B. S. Song, S. Noda, T. Asano, and Y. Akahane, Nat. Mater. **4**, 207 (2005).
[46] A. Yarif, Y. Xu, R. K. Lee, and A. Scherer, Opt. Lett. **24**, 711 (1999).
[47] A. Badolato *et al.*, Science **308**, 1158 (2005).
[48] B. Lev, K. Srinivasan, P. Barclay, O. Painter, and H. Mabuchi, Nanotechnology **15**, S556 (2004).
[49] D. K. Armani, T. J. Kippenberg, S. M. Spillane, and K. J. Vahala, Nature (London) **421**, 925 (2003).
[50] T. Aoki *et al.*, Nature (London) **443**, 671 (2006).
[51] K. M. Birnbaum, A. S. Parkins, and H. J. Kimble, Phys. Rev. A **74**, 063802 (2006).

IOP Publishing | Astro Ltd
Laser Physics Letters
Laser Phys. Lett. 13 (2016) 015205 (5pp)
doi:10.1088/1612-2011/13/1/015205

Efficient parametric non-degenerate four-wave mixing in hot potassium vapor

B Zlatković[1], A J Krmpot[1], N Šibalić[1,2], M Radonjić[1] and B M Jelenković[1]

[1] Insitute of Physics Belgrade, University of Belgrade, Pregrevica 118, 11080 Belgrade, Serbia
[2] Faculty of Physics, University of Belgrade, POB 368, 11001 Belgrade, Serbia

E-mail: krmpot@ipb.ac.rs

Received 20 August 2015, revised 5 November 2015
Accepted for publication 9 November 2015
Published 30 November 2015

Abstract

We have observed high gains of the probe and the conjugate beams in non-degenerate four-wave mixing in hot potassium vapor, using a double-Λ configuration at the D1 line of the ^{39}K isotope. Gains of up to 82 for the conjugate beam and 63 for the probe beam have been achieved. Higher gains were obtained than with other alkali atoms under comparable experimental conditions due to lower ground state hyperfine splitting in the potassium atom. Experimental parameters for maximal gain have been determined. Notable gains are achieved at low pump intensities (~10 W cm^{-2}) that are attainable even by conventional laser diodes. Due to their high gains, the probe and the conjugate beams may be suitable for utilization in quantum correlation and relative intensity squeezing experiments.

Keywords: four-wave mixing, potassium, squeezed states, nonlinear optics

(Some figures may appear in colour only in the online journal)

Four-wave mixing (FWM) is a nonlinear interaction of light and a medium accompanied by a characteristic transfer of energy between four modes of the electric field while these modes interact with the medium [1]. FWM in atomic vapors is a valuable tool for the generation of non-classical states of light. Signal and idler beams (here referred to as the probe and the conjugate beams, respectively) generated by this process display intensity correlations and entanglement [2]. These features make them applicable in high-precision spectroscopy [3], sub-shot-noise measurements [4, 5], quantum imaging [6–8], quantum communications and quantum information processing [9, 10].

The first experimental demonstration of squeezed light was made using FWM in an atomic beam of Na [11]. Since such FWM processes generate squeezed light near atomic resonance, the amount of squeezing is limited by other resonant processes such as one-photon absorption and spontaneous emission. Renewed interest in FWM came after predictions [12, 13] that non-degenerate FWM in atomic systems with a double-Λ scheme could overcome these limitations. Experiments that followed confirmed that it was indeed possible to obtain squeezing near atomic resonance [14–16].

Higher gains of the probe and the conjugate beams (also called 'twin' beams) in a non-degenerate FWM process leads to higher relative intensity squeezing and deeper noise reduction [17]. The gains of the probe and the conjugate are defined as $G_p = P_p/P_{in}$ and $G_c = P_c/P_{in}$, respectively, where P_p and P_c are the measured powers of the probe and the conjugate beams, respectively, and P_{in} is initial power of the probe seed inside the amplifying medium. The ability of different mediums to yield large gains of the twin beams was tested with different interaction schemes. So far, all alkali atoms except Fr and Li have been used as the gain medium for FWM [11, 14–26]. In the majority of studies the counter-propagating geometry of two pump beams and one probe beam was used and the degenerate case of FWM process was observed.

However, new beams generated in the aforementioned arrangements are not suitable for applications that require spatially separated beams. The most suitable interaction scheme and experimental arrangement for employing twin beams in relative intensity squeezing experiments was realized by McCormick *et al* [15]. The coupling of hyperfine levels of an alkali atom by a double-Λ scheme is depicted in figure 1. The first Λ scheme consists of a strong pump that couples the lower hyperfine sublevel $|1\rangle$ of the ground state to

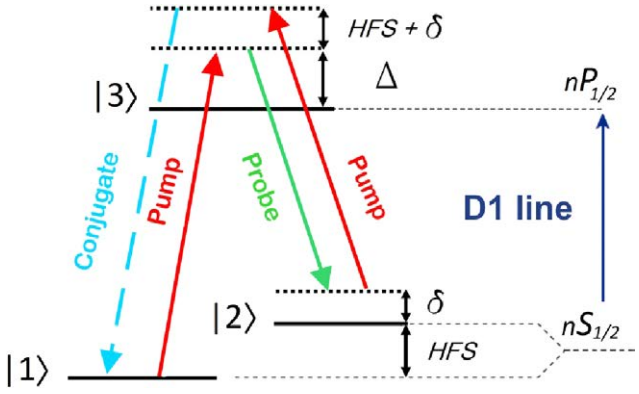

Figure 1. Double-Λ scheme at the D1 line of an alkali atom. HFS—hyperfine splitting, Δ—one photon detuning, δ—two photon detuning. HFS of the $nP_{1/2}$ (i.e. $|3\rangle$) level is negligible in comparison with the ground state HFS.

the excited level $|3\rangle$ with one-photon detuning Δ of typically several hundred MHz. The other 'leg' of the first Λ scheme is the weak probe that stimulates the Stokes scattering from $|3\rangle$ to the higher hyperfine sublevel $|2\rangle$ of the ground state, having two-photon detuning δ. The pump is sufficiently strong to drive the off-resonant transition starting from $|2\rangle$. The newly created conjugate closes the second Λ scheme by stimulating anti-Stokes scattering to the lower hyperfine sublevel.

Such an arrangement, yielding non-degenerate FWM and spatially separated twin beams, was employed with achieved gains ≈20 [16, 24] or even 30 [25] in rubidium, ≈32 in sodium [26] and recently ≈ 2 in cesium [27]. The theoretical explanations for this arrangement were also provided [24, 28, 29]. Apart from relative intensity squeezing experiments, this scheme is used in other applications such as slow light [25, 30–32], storage of light [33, 34], and heralded state density matrix reconstruction [35], and is also proposed for all-optical quantum networks [36–39].

In this paper we report FWM in a double-Λ scheme in hot potassium vapor. There are very few works on FWM in potassium vapor [19, 20] and all of them are done with counter-propagating pumps. Ground state hyperfine splitting (HFS) in ^{39}K (461 MHz [40]) is lower than in any other alkali atom, both for lighter atoms such as ^{7}Li (803 MHz [41, 42]) or ^{23}Na (1772 MHz [42, 43]) and heavier atoms, like ^{85}Rb (3036 MHz [42–44]) or ^{133}Cs (9193 MHz [43, 45]). In addition, all the transitions of the D1 line of ^{39}K completely overlap due to Doppler broadening. This affects the dynamics of pumping and repopulating ground state hyperfine sublevels in a different way than in other alkali atoms. All of the aforementioned properties of ^{39}K make it interesting as a medium for FWM and other applications.

The influence of ground state HFS on the efficiency of FWM can be estimated from the theoretical model given by Turnbull *et al* [24]. In the model, the following equations describe the change of the probe E_p and the conjugate E_c electric field along the z axis (the propagation direction of the pump beam):

$$\frac{\partial}{\partial z}E_\mathrm{p} = \frac{\mathrm{i}k_\mathrm{p}}{2}\chi_\mathrm{pp}(\omega_\mathrm{p})E_\mathrm{p} + \frac{\mathrm{i}k_\mathrm{p}}{2}\chi_\mathrm{pc}(\omega_\mathrm{p})\mathrm{e}^{\mathrm{i}\Delta k_z z}E_\mathrm{c}^{*} \qquad (1)$$

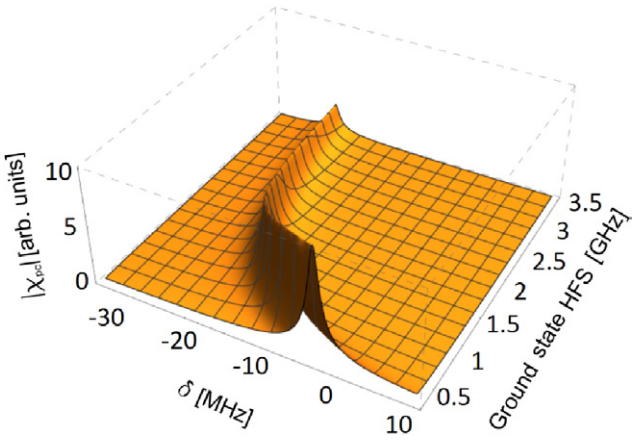

Figure 2. Dependence of $|\chi_\mathrm{pc}|$ on ground state HFS and two-photon detuning δ. The one-photon detuning ($\Delta = 700$ MHz) and dipole matrix elements of the double-Λ scheme transitions were kept constant.

$$\frac{\partial}{\partial z}E_\mathrm{c} = \frac{\mathrm{i}k_\mathrm{c}}{2}\chi_\mathrm{cc}(\omega_\mathrm{c})E_\mathrm{c} + \frac{\mathrm{i}k_\mathrm{c}}{2}\chi_\mathrm{cp}(\omega_\mathrm{c})\mathrm{e}^{\mathrm{i}\Delta k_z z}E_\mathrm{p}^{*} \qquad (2)$$

where, k_p and k_c are the magnitudes of the probe and the conjugate wave vectors, Δk_z is the projection of the phase mismatch $\Delta\boldsymbol{k}$ on the z axis, χ_pp and χ_cc are the effective linear susceptibilities for the probe and the conjugate and χ_pc and χ_cp are cross-susceptibilities that give rise to FWM process. The phase mismatch is defined as $\Delta\boldsymbol{k} = 2\boldsymbol{k}_0 - \boldsymbol{k}_\mathrm{p} - \boldsymbol{k}_\mathrm{c}$ where $\boldsymbol{k}_0$ is the pump wave vector.

Atomic susceptibilities govern the FWM process and affect the gains. The dependence of $|\chi_\mathrm{pc}|$ on HFS and two-photon detuning is shown in figure 2 and is calculated according to equations A12–A20 given in the appendix of [24].The equations enable the calculation of the stationary values of $|\chi_\mathrm{pc}|$ as a function of the relevant experimental parameters: one-photon detuning, two-photon detuning, ground state HFS, pump laser Rabi frequencies, and the concentration of the atoms, i.e. the temperature. The equations are given under the assumption that Rabi frequencies for both pump transitions in figure 1 are equal. The probe and conjugate fields are assumed to be weak and their contribution is kept only to the first order. Since we want to estimate the influence of ground state HFS of alkali atoms on the efficiency of FWM we kept all other quantities constant, except the two-photon detuning. The results show that the maximum of $|\chi_\mathrm{pc}|$ increases as HFS decreases. The model also predicts that the two-photon detuning δ, corresponding to the maximum $|\chi_\mathrm{pc}|$, also decreases, thus both Λ schemes are closer to Raman resonance.

Motivated by the above analysis, the present work investigates the properties of FWM in hot potassium vapor using the non-degenerate scheme of figure 1 and a co-propagating geometry of the pump and probe beams. To the best of our knowledge there are no previous investigations of this kind in potassium. Exceptionally high gains could make potassium vapor the preferred medium for relative intensity squeezing experiments [16] and other applications utilizing highly efficient FWM [3–10]

We have performed the double-Λ scheme on the D1 line of ^{39}K. Level $|3\rangle$ from figure 1 is $4P_{1/2}$ while two lower levels

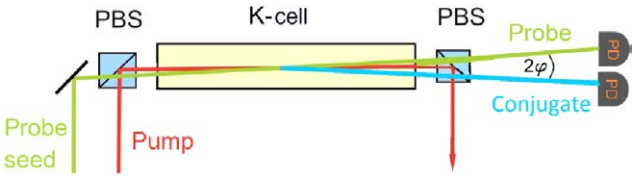

Figure 3. Experimental setup. Pump (red) and probe seed (green) beams are combined at a polarization beam splitter (PBS). They intersect at a small angle φ inside the potassium vapor cell (K-cell) yielding the conjugate beam (blue) and amplified probe beam (green) via the FWM process. The probe and the conjugate beams are detected by two photodiodes (PD). Note that angle between the conjugate and the probe beams is 2φ.

$|1\rangle$ and $|2\rangle$ are $4S_{1/2}$, $F = 1$ and $4S_{1/2}$, $F = 2$ respectively. The simplified scheme of the experimental setup is presented in figure 3. A single-mode frequency stabilized Ti:Saphire laser was used in the experiment. It delivers 600 mW at the 770 nm D1 line of ^{39}K and it is used for both the pump and probe seed beams. The probe seed (≈200 μW) is obtained by picking up a small fraction of the pump at the 90:10 beam splitter and sending it through the two acousto–optic modulators (AOMs). The first AOM produces a tunable frequency shift (170–200 MHz) and it operates in a double-pass configuration. The second AOM has a fixed frequency shift (80 MHz), making the overall frequency offset between the pump and probe seed close to the HFS of the ^{39}K ground state. Two-photon detuning δ is scanned by changing the RF frequency fed to the first AOM.

The pump and the probe seed have mutually orthogonal linear polarizations. The beams are combined at a polarization beam splitter and sent through the heated, 50 mm long, natural-abundance vacuum potassium vapor cell, where they intersect at a small angle that we change in the range of 2–10 mrad. Both beams, the pump and the probe seed, are focused at the intersection and their waists are 1.05 mm and 0.8 mm, respectively. The windows of the cell are Brewster angled and the cell is rotated to provide the maximal pump transmission (≈95% per window). Since the probe seed is polarized perpendicularly to the pump, its transmission is lower (≈70% per window).

After passing through the vapor cell, the pump beam is rejected by the second polarizing beam splitter. The conjugate beam (which has the same polarization as the probe seed) and the amplified probe beam are detected by two photodiodes.

We have investigated the dependence of the probe and the conjugate gains on two-photon detuning δ with one-photon detuning Δ as a parameter. The δ step was 2 MHz. The results for various values of Δ are shown in figure 4.

The maximal conjugate gain ($G_c = 82$; peak value in figure 4(b)) was obtained at $\Delta = 700$ MHz and $\delta = -6$ MHz. The probe gain for the same parameters was $G_p = 58$. The reason for the maximum gains occurring at a particular Δ is the competition of two effects: amplification and absorption [16, 24]. When Δ increases, the amplification of the probe and the conjugate beams decreases, but so does one-photon absorption. The trade-off is in our case for $\Delta = 700$ MHz (figure 4(c)). Since the frequency offset between the probe and the conjugate beams is ≈920 MHz (approximately double the HFS) and the probe beam is tuned closer to the resonance, one-photon absorption is stronger for the probe beam. This is the reason why we observe different G_p and G_c for smaller Δ (figures 4(a) and (b)). At larger Δ , one-photon absorption becomes smaller, thus G_p and G_c get closer (figure 4(d)), but are rather small due to detuning far from resonance.

According to our expectations, qualitatively supported by results in figure 2, we have obtained higher gains than in other alkali atoms under comparable experimental conditions. For more detailed theoretical study and quantitative comparison between experimental and theoretical results one might consider adjusting the theoretical model from [24] for particular properties of potassium. Unlike rubidium, all the transitions forming the double-Λ scheme in potassium are overlapped due to large Doppler broadening at specified temperatures. Moreover, one might also consider the geometry and intensity profiles of overlapping laser beams and their spectral properties.

The dependence of G_p and G_c on the temperature for various values of Δ is shown in figure 5. For each Δ on the graph, we set δ to maximize the gains of the probe and the conjugate beams. As the concentration of potassium atoms increases, the cross-susceptibilities (χ_{cp} and χ_{pc}) also increase [24]. On the other hand, large susceptibilities lead to large values of the refractive index and its transverse gradient that cause beam focusing and beam filamentation [1, 24]. Stars in figure 5 indicate the highest temperatures for particular values of Δ, above which these effects prevent the proper measurement of the intensities of the probe and the conjugate beams. At high vapor temperatures and/or pump intensities self-focusing of the probe and conjugate beams appears gradually, ending up with beam break-up. As the pump intensity and/or vapor temperature increases the probe and the conjugate beams become more divergent due to self-focusing. This makes the beams partially overlapped and hinders proper measurement of the powers independently.

Varying the temperature and Δ we have determined that the values of $T = 140$ °C and $\Delta = 1500$ MHz provide the highest probe gain, $G_p = 63$ (we found $G_c = 69$ for the same set of parameters).

The dependence of G_p and G_c on the mutual angle between the pump and the probe beam is presented in figure 6(a). While in rubidium [24] the dependence on this angle has a maximum at 5 mrad, in potassium it monotonically decreases. This is in accordance with Glassner *et al* [19] where, in their configuration of counter-propagating pumps and degenerate FWM, the probe reflectivity can be considered as an analogue to the probe gain, since both are affected by atomic susceptibility.

The dependence of the probe and the conjugate gains on the pump power is shown in figure 6(b). We found that the lowest pump intensity, at which we were able to detect the conjugate beam, is about 10 W cm^{-2} corresponding to laser power of ≈100 mW. This, relatively low, laser power can easily be attained with conventional lasers diodes. We were able to measure even higher gains (96 for the conjugate, 73 for the probe) at a pump intensity of 51 W cm^{-2} but the laser becomes unstable at high powers.

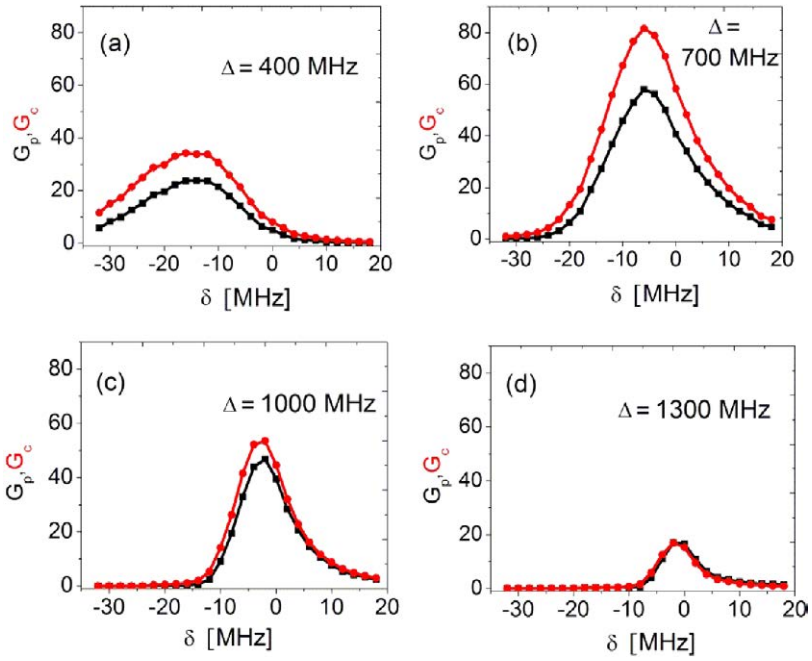

Figure 4. The probe (black squares) and the conjugate (red circles) gain curves versus two-photon detuning δ in the vicinity of Raman resonance ($\delta = 0$) at Δ equal to (a) 400 MHz, (b) 700 MHz, (c) 1000 MHz and (d) 1300 MHz. The pump power was $P_0 = 400$ mW and the probe seed power was $P_{\text{in}} = 200$ μW. Vapor temperature was kept constant at 120 °C ($\approx 3 \times 10^{12}$ atoms cm^3), and angle between the pump and the probe was $\varphi = 3$ mrad. The lines are to guide the eye.

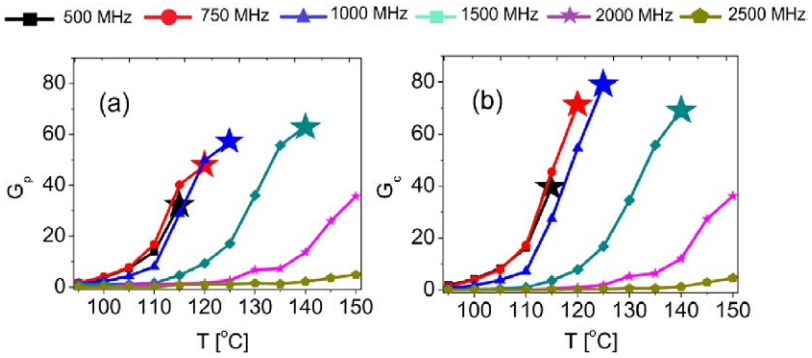

Figure 5. Temperature dependence of (a) the probe gain G_{p} and (b) the conjugate gain G_{c}. Different colors correspond to the different values of Δ (given in the legend). For the given range of the temperature of potassium vapor the number density of the atoms, calculated according to Ticke [40], is between 3.7×10^{11} atoms cm^{-3} (at 90 °C) and 1.7×10^{13} atoms cm^{-3} (at 150 °C). Stars denote the temperatures at which filamentation and self-focusing of the probe and the conjugate beams occur. Parameters are $P_0 = 400$ mW, $P_{\text{in}} = 200$ μW, $\varphi = 2$ mrad.

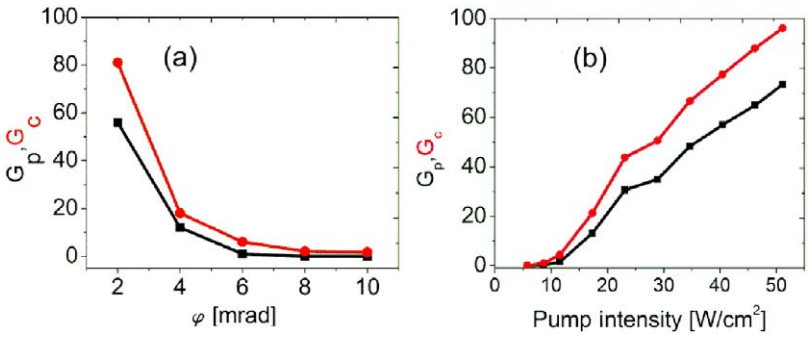

Figure 6. Dependence of the probe (black squares) and the conjugate (red circles) gain on (a) the angle φ between the pump and the probe for $P_0 = 400$ mW and (b) the pump intensity for $\varphi = 2$ mrad. Parameters for both cases are $P_{\text{in}} = 200$ μW, $T = 120$ °C, $\Delta = 700$ MHz.

In conclusion, we have observed non-degenerate FWM in hot potassium vapor at the D1 line using co-propagating pump and probe beams and a double-Λ coupling scheme. In accordance with simple qualitative theoretical considerations, the obtained gains are among the highest in alkali atoms. This is due to the high atomic susceptibilities caused by the lowest ground state HFS in potassium. We expect that the obtained high gains might find useful application in experiments for relative intensity squeezing, sub-shot-noise measurements and other applications requiring efficient FWM.

Acknowledgments

The study was financially supported by the Serbian Ministry of Education, Science, and Technological Development (Projects Nos. ON171038, III45016). We thank Ennio Arimondo for providing us with the vapor cell and useful discussions. We also thank R C Pooser for helpful comments on our manuscript.

References

[1] Boyd R W 2003 *Nonlinear Optics* (NewYork: Academic)
[2] Reid M D and Drummond P D 1988 *Phys. Rev. Lett.* **60** 2731
[3] Souto Ribeiro P H, Schwob C, Maître A and Fabre C 1997 *Opt. Lett.* **22** 1893
[4] Gao J, Cui F, Xue C, Xie C and Peng K 1998 *Opt. Lett.* **23** 870
[5] Pooser R C and Lawrie B 2015 *Optica* **2** 393–9
[6] Boyer V, Marino A M, Pooser R C and Lett P D 2008 *Science* **321** 544
[7] Clark J B, Zhou Z, Glorieux Q, Marino A M and Lett P D 2012 *Opt. Express* **20** 17050–8
[8] Lawrie B J and Pooser R C 2013 *Opt. Express* **21** 7549–59
[9] Braunstein S L and van Loock P 2005 *Rev. Mod. Phys.* **77** 513
[10] Duan L-M, Lukin M D, Cirac J I and Zoller P 2001 *Nature* **414** 413–8
[11] Slusher R E, Hollberg L W, Yurke B, Mertz J C, Valley J F 1985 *Phys. Rev. Lett.* **55** 2409
[12] Lukin M D, Hemmer P R, Löffler M and Scully M O 1998 *Phys. Rev. Lett.* **81** 2675
[13] Lukin M D, Hemmer P R and Scully M O 2000 *Advances in Atomic Molecular, and Optical Physics* vol 42 ed B Bederson and H Walther (San Diego: Elsevier Academic) pp 347–86
[14] van der Wal C H *et al* 2003 *Science* **301** 196
[15] McCormick C F, Boyer V, Arimondo E and Lett P D 2007 *Opt. Lett.* **32** 178
[16] McCormick C F, Marino V, Boyer A M and Lett P D 2008 *Phys. Rev.* A **78** 043816
[17] Hemmer P R *et al* 1995 *Opt. Lett.* **20** 982–4
[18] Grove T T *et al* 1997 *Opt. Lett.* **22** 769–71
[19] Glassner D S and Knize R J 1995 *Appl. Phys. Lett.* **66** 1593–5
[20] Lanzerotti M Y, Schirmer R W and Gaeta A L 1996 *Appl. Phys. Lett.* **69** 1199
[21] Davis W V *et al* 1995 *Phys. Rev.* A **51** 4152
[22] Ai B, Glassner D S, Knize R J and Partanen J P 1994 *Appl. Phys. Lett.* **64** 951
[23] Katharakis M *et al* 2002 *J. Phys. B: At. Mol. Opt. Phys.* **35** 4969
[24] Turnbull M T *et al* 2013 *Phys. Rev.* A **88** 033845
[25] Boyer V, McCormick C F, Arimondo E and Lett P D 2007 *Phys. Rev. Lett.* **99** 143601
[26] Harada K, Mori K, Okuma J, Hayashi N and Mitsunaga M 2008 *Phys. Rev.* A **78** 013809
[27] Guo M *et al* 2014 *Phys. Rev.* A **89** 033813
[28] Glorieux Q *et al* 2010 *Phys. Rev.* A **82** 033819
[29] Jasperse M, Turner L D and Scholten R E 2011 *Opt. Express* **19** 3765
[30] Wu Y and Yang X 2004 *Phys. Rev.* A **70** 053818
[31] Okuma J, Hayashi N, Fujisawa A and Mitsunaga M 2009 *Opt. Lett.* **34** 1654–6
[32] Marino A M *et al* 2009 *Nature* **457** 859–62
[33] Camacho R M, Vudyasetu P K and Howell J C 2009 *Nat. Photonics* **3** 103–6
[34] Eilam A, Wilson-Gordon A D and Friedmann H 2008 *Opt. Lett.* **33** 1605–7
[35] MacRae A, Brannan T, Achal R and Lvovsky A I 2012 *Phys. Rev. Lett.* **109** 033601
[36] Jing J *et al* 2003 *Phys. Rev. Lett.* **90** 167903
[37] Qin Z *et al* 2014 *Phys. Rev. Lett.* **113** 023602
[38] Cai Y *et al* 2015 *Phys. Rev* A **91** 013843
[39] Pooser R C and Jing J 2014 *Phys. Rev.* A **90** 043841
[40] 2011 www.tobiastiecke.nl/archive/PotassiumProperties.pdf; accessed 10 August 2015
[41] 2003 www.physics.ncsu.edu/jet/techdocs/pdf/PropertiesOfLi.pdf; accessed 10 August 2015
[42] Arimondo E, Inguscio M and Violino P 1977 *Rev. Mod. Phys.* **49** 31–75
[43] 2010 http://steck.us/alkalidata; accessed 10 August 2015
[44] Bize S *et al* 1999 *Europhys. Lett.* **45** 558
[45] 1967/1968 www.bipm.org/en/publications/si-brochure/second.html; accessed 10 August 2015

Dissipative two-mode Tavis-Cummings model with time-delayed feedback control

Wassilij Kopylov,[1] Milan Radonjić,[2,*] Tobias Brandes,[1] Antun Balaž,[3] and Axel Pelster[4]
[1]*Institut für Theoretische Physik, Technische Universität Berlin, D-10623 Berlin, Germany*
[2]*Photonics Center, Institute of Physics Belgrade, University of Belgrade, Pregrevica 118, 11080 Belgrade, Serbia*
[3]*Scientific Computing Laboratory, Institute of Physics Belgrade, University of Belgrade, Pregrevica 118, 11080 Belgrade, Serbia*
[4]*Physics Department and Research Center OPTIMAS, Technische Universität Kaiserslautern, Germany*
(Received 18 August 2015; published 21 December 2015)

We investigate the dynamics of a two-mode laser system by extending the two-mode Tavis-Cummings model with dissipative channels and incoherent pumping and by applying the mean-field approximation in the thermodynamic limit. To this end we analytically calculate up to four possible nonequilibrium steady states (fixed points) and determine the corresponding complex phase diagram. Various possible phases are distinguished by the actual number of fixed points and their stability. In addition, we apply three time-delayed Pyragas feedback control schemes. Depending on the time delay and the strength of the control term, this can lead to the stabilization of unstable fixed points or to the selection of a particular cavity mode that is macroscopically occupied.

DOI: 10.1103/PhysRevA.92.063832 PACS number(s): 42.50.Pq, 37.30.+i, 42.60.By, 05.70.Ln

I. INTRODUCTION

Lasers build one of the key technologies in the current world as their rich dynamical behavior and high degree of control establish a solid basis for a wide range of applications [1]. Specifically, time-delayed feedback control [2] can effectively manipulate short and long time behavior of a laser system [3]. Typical examples are the control of laser bistability [4], chaos, and noise [5], as well as the manipulation of the laser emission [6,7].

A common description of the controlled laser dynamics, particularly in the case of a quantum dot laser, is based on the semiclassical rate equations known as the Lang-Kobayashi model [8]. It provides good agreement with the experiments if the photon output power is high enough [9]. However, there exists a more general microscopic quantum treatment [10,11] which describes successfully the photon statistics of laser light. It turned out that this microscopic laser theory also represents an essential ingredient for describing the Bose-Einstein condensation of photons [12], which has been realized in dye-filled microcavities in a seminal experiment in Bonn [13] and recently also in London [14]. Both lasing transition and Bose-Einstein condensation of light may appear in such systems under appropriate conditions, although the former reveals nonequilibrium physics, whereas the latter represents an equilibrium phenomenon. For low cavity losses and above the external pumping threshold, the modes of the cavity become thermally populated according to a Bose-Einstein distribution with the macroscopically occupied lowest mode [15]. However, for higher cavity losses the system behavior switches to be laserlike, where one of the excited cavity modes becomes macroscopically occupied and all thermal properties are lost [16].

Here we work out a two-mode laser model which allows us to study under which conditions one of the two cavity modes becomes macroscopically occupied. To this end we extend the Tavis-Cummings model and consider N noninteracting two-level atoms in a two-mode optical cavity with incoherent pumping and decay channels. Starting from a quantum master equation for the density operator, we apply a mean-field approximation and determine the equations of motion for the statistical averages of the respective system operators in the thermodynamic limit. We find an analytical solution for the steady states and obtain the resulting complex phase diagram. Under proper conditions, either the lower or the excited cavity mode can become macroscopically occupied. Hence, our model can be seen as a minimalistic precursor of the detailed model of photon condensation [12,16]. In this sense, the former case could be referred to as condensatelike and the latter case as a laserlike state of light, although a direct analogy is not applicable due to the absence of the temperature scale in our simplified approach. The richness of possible phases even within this reduced model indicates that the inclusion of realistic processes, like the thermalization via phonon dressing of the absorption and emission of the emitters, can potentially lead to an even larger variety of states.

Additionally, we design different feedback control schemes to stabilize or to select one of the two radiating modes. The two-mode laser, also known as two-color laser, with feedback was already studied both experimentally [17,18] and theoretically [19]. However, these studies within the Lang-Koboyashi model were focused on switching between the two modes using a non-Pyragas feedback type. In contrast to that, we apply here the Pyragas type of feedback that was originally designed to prevent chaos by stabilizing an unstable periodic orbit [20]. It is generally known as a powerful tool to change the stability of stationary states without modifying them. This is due to the fact that the feedback control term vanishes in the stationary state since it is proportional to the difference of the system observable at two times, $t - \tau$ and t [21,22].

The paper is structured as follows. In Sec. II we introduce the underlying model and apply a mean-field approximation in the thermodynamic limit. In Sec. III we calculate the fixed points, investigate their stability, and discuss the resulting phase diagram. In Sec. IV we suggest several Pyragas feedback control schemes to stabilize the unstable mode or to select the mode of interest. Section V contains the summary of the obtained results with a short outlook.

*Present address: Faculty of Physics, University of Vienna, Boltzmanngasse 5, A-1090 Vienna, Austria.

II. MODEL

We consider N noninteracting two-level atoms inside a two-mode cavity. The light-atom interaction is assumed to be of the Jaynes-Cummings type [23]. Thus, the total Hamiltonian of the system is

$$\hat{H} = \sum_{i=1}^{2} \omega_i \hat{a}_i^\dagger \hat{a}_i + \Delta \hat{J}_z + \frac{g}{\sqrt{N}} \sum_{i=1}^{2} (\hat{a}_i \hat{J}^+ + \hat{a}_i^\dagger \hat{J}^-) \quad (1)$$

and represents an extension of the Tavis-Cummings (TC) model [24,25] from one to two modes. Here, we put $\hbar = 1$, and $\hat{a}_i^{(\dagger)}$ ($i \in \{1,2\}$) is a ladder algebra of the first or second cavity mode with frequency $\omega_{1,2}$, where we assume $\omega_1 < \omega_2$ without loss of generality. The collective angular momentum operators are given by the sums $\hat{J}_z = \frac{1}{2}\sum_{k=1}^{N} \sigma_k^z$ and $\hat{J}^\pm = \sum_{k=1}^{N} \sigma_k^\pm$ over all Pauli matrices of each two-level atom with energy-level splitting Δ. The population inversion of the atomic ensemble is directly related to $\hat{J}_z$, while its dipole moment can be expressed in terms of $\hat{J}^\pm$. The coupling between the atoms and the optical mode assumes a rotating wave approximation (RWA) and has the strength $g/\sqrt{N}$ that is taken to be the same for both modes. In spite of RWA, the TC model for large values of g has its own physical relevance since it can be experimentally realized in an ingenious setup using Raman transitions [26,27].

To generate a lasing behavior and the interesting dynamics we add decay channels and incoherent pumping to the system. We note in passing that two-mode Jaynes-Cummings models were studied in the past either with mode degeneracy [28,29] or without dissipative effects [30], or without pumping of the atomic system but in the presence of additional driving of the cavity mode [31,32]. Following Ref. [33], we couple our system to three different baths. Both cavity fields are damped by coupling them to a zero-temperature bath of harmonic modes with the characteristic decay rate κ, while the atomic system radiates into the noncavity modes with a rate $\gamma_\downarrow$. Additionally, the atomic system is incoherently pumped with a rate $\gamma_\uparrow$. Pumping can be formally described as coupling the atomic system to a bath of inverted harmonic oscillators [34]. All these effects are captured by the following Markovian master equation of Lindblad type for the density operator $\hat{\rho}$:

$$\frac{d\hat{\rho}(t)}{dt} = -i[\hat{H},\hat{\rho}] - \kappa \boldsymbol{L}[\hat{a}_1]\hat{\rho} - \kappa \boldsymbol{L}[\hat{a}_2]\hat{\rho} - \frac{\gamma_\uparrow}{2}\sum_{k=1}^{N} \boldsymbol{L}[\hat{\sigma}_k^+]\hat{\rho} - \frac{\gamma_\downarrow}{2}\sum_{k=1}^{N} \boldsymbol{L}[\hat{\sigma}_k^-]\hat{\rho}, \quad (2)$$

with the Lindblad operator $\boldsymbol{L}[\hat{x}]\hat{\rho} = \hat{x}^\dagger \hat{x}\hat{\rho} + \hat{\rho}\hat{x}^\dagger \hat{x} - 2\hat{x}\hat{\rho}\hat{x}^\dagger$. Pumping effectively occurs provided that $\gamma_\uparrow > \gamma_\downarrow$.

The dynamics of the statistical average $\langle \hat{A} \rangle = \mathrm{Tr}(\hat{A}\hat{\rho})$ of an arbitrary system operator $\hat{A}$ is described by $d\langle \hat{A} \rangle/dt = \mathrm{Tr}(\hat{A}\dot{\hat{\rho}})$. To obtain a closed set of semiclassical equations, we perform the thermodynamic limit where the number N of two-level atoms tends to infinity [35–39]. Therefore, we factorize the averages of an atomic operator $\hat{A}$ and a light operator $\hat{L}$ according to $\langle \hat{A}\hat{L} \rangle \approx \langle \hat{A} \rangle \langle \hat{L} \rangle$ and rescale them with the atom number N, denoting the rescaled operator averages by corresponding symbols without the hat symbol, i.e., $J^\pm \equiv \langle \hat{J}^\pm \rangle/N$, $J_z \equiv \langle \hat{J}_z \rangle/N$, and $a_{1,2}^{(*)} \equiv \langle \hat{a}_{1,2}^{(\dagger)} \rangle/\sqrt{N}$, where the asterisk denotes complex conjugation. The resulting mean-field equations of the two-mode laser model are then

$$\dot{a}_1 = (-\kappa - i\omega_1)a_1 - igJ^-, \quad (3a)$$

$$\dot{a}_1^* = (-\kappa + i\omega_1)a_1^* + igJ^+, \quad (3b)$$

$$\dot{a}_2 = (-\kappa - i\omega_2)a_2 - igJ^-, \quad (3c)$$

$$\dot{a}_2^* = (-\kappa + i\omega_2)a_2^* + igJ^+, \quad (3d)$$

$$\dot{J}^- = (-\Gamma_D - i\Delta)J^- + 2ig(a_1 + a_2)J_z, \quad (3e)$$

$$\dot{J}^+ = (-\Gamma_D + i\Delta)J^+ - 2ig(a_1^* + a_2^*)J_z, \quad (3f)$$

$$\dot{J}_z = \Gamma_T(z_0 - J_z) + ig(a_1^* + a_2^*)J^- - ig(a_1 + a_2)J^+, \quad (3g)$$

where we have introduced the abbreviations $\Gamma_T = 2\Gamma_D = \gamma_\downarrow + \gamma_\uparrow$ and $z_0 = \frac{\gamma_\uparrow - \gamma_\downarrow}{2(\gamma_\uparrow + \gamma_\downarrow)}$. Note that $J^- = (J^+)^*$ and J_z is a real quantity, and by definition, one has $-1/2 \leqslant z_0 \leqslant 1/2$.

In the one-mode limit, the corresponding equations similar to Eqs. (3) represent a common example of a laser model. For the critical value of $g_c = \{\frac{\kappa\Gamma_D}{2z_0}[1 + \frac{(\omega_1 - \Delta)^2}{(\kappa + \Gamma_D)^2}]\}^{1/2}$, the optical mode becomes macroscopically occupied, i.e., a phase transition occurs from a nonlasing to a lasing state. In the limit of vanishing pumping and losses, i.e., $\Gamma_T \to 0, \kappa \to 0$, Eqs. (3) describe the quantum phase transition in the Dicke model with RWA from a normal to a superradiant phase [37,40–43]. Thus, the presence of the two modes and the pumping term allows the generation of a much more complicated dynamics, as either of the two modes can be macroscopically occupied. Moreover, we can influence the dynamical evolution of the system by applying different Pyragas time delay schemes, which allows us to stabilize or destabilize the modes and to select the transition type.

III. DYNAMICS WITHOUT FEEDBACK

Equations (3) describe the dynamical evolution of the two-mode system depending on decay rates and pumping strength. A steady state of these equations can be either a stable fixed point or an oscillating state, i.e., a limit cycle. In the following we provide an analytical description of the possible steady states.

A. Steady states

The system (3) has a trivial fixed point $a_1^0 = a_2^0 = (a_1^*)^0 = (a_2^*)^0 = 0$, $(J^+)^0 = (J^-)^0 = 0$, and $J_z^0 = z_0$, where no cavity mode is occupied and the atomic ensemble has a stationary population inversion with zero dipole moment. Due to the $U(1)$ symmetry of Eqs. (3), there also exist nontrivial solutions that can oscillate in time with some characteristic frequency, so that the observables, like the mode occupation $a_1^* a_1$, reach a fixed value. To find such steady-state solutions, we have to determine the frame where also $a_{1,2}^{(*)}$ and $J^\pm$ reach a fixed value. Therefore, we switch into a frame rotating with frequency ω, which has to be determined, i.e., we put $a_i \to a_i e^{-i\omega t}$, $a_i^* \to a_i^* e^{i\omega t}$, $J^\pm \to J^\pm e^{\pm i\omega t}$. Note that this transformation shifts the natural frequencies of both the cavity modes and the atoms by ω, i.e.,

$$\omega_i \to \omega_i - \omega \equiv \omega_{i,s}, \quad \Delta \to \Delta - \omega \equiv \Delta_s, \quad (4)$$

but does not change the observables like $a_1^* a_1$. Setting $\dot{a}_{1,2}^{(*)}$ in the transformed equations (3a)–(3d) to zero, we can express these cavity quantities in terms of $J^{\pm}$. Next, setting $\dot{J}^{\pm}$ to zero in the transformed equations (3e)–(3f) with the cavity quantities being eliminated, we find the requirement

$$0 \stackrel{!}{=} J^{\pm}\{\pm 2g^2 J_z[\mp 2\kappa + i(\omega_{1,s} + \omega_{2,s})] + (\Gamma_D \mp i\Delta_s)(\kappa \mp i\omega_{1,s})(\kappa \mp i\omega_{2,s})\}. \quad (5)$$

For $J^{\pm} \stackrel{!}{\neq} 0$ the previous equation determines the value of the stationary atomic inversion:

$$J_z^0 = \frac{(\Gamma_D - i\Delta_s)(\kappa - i\omega_{1,s})(\kappa - i\omega_{2,s})}{2g^2(2\kappa - i\omega_{1,s} - i\omega_{2,s})}. \quad (6)$$

However, since J_z^0 has to be real on physical grounds, its imaginary part has to be zero. This condition enforces the characteristic frequency ω to solve the equation

$$\Gamma_D(\omega_{1,s} + \omega_{2,s})(\kappa^2 + \omega_{1,s}\omega_{2,s}) + \kappa\Delta_s\left(2\kappa^2 + \omega_{1,s}^2 + \omega_{2,s}^2\right) = 0. \quad (7)$$

Note that, due to Eq. (4), Eq. (7) is a cubic equation in ω and has up to three real solutions. For each real solution ω, the real part of the expression for J_z^0 in (6) gives the steady-state expectation value

$$J_z^0 = \frac{\kappa\left(\Gamma_D^2 + \Delta_s^2\right)\left(2\kappa^2 + \omega_{1,s}^2 + \omega_{2,s}^2\right)}{2g^2\Gamma_D[4\kappa^2 + (\omega_{1,s} + \omega_{2,s})^2]}. \quad (8)$$

The remaining transformed equation (3g) can be solved for J^+J^- in the steady state, yielding

$$(J^+J^-)^0 = \frac{\Gamma_T\left(z_0 - J_z^0\right)\left(\kappa^2 + \omega_{1,s}^2\right)\left(\kappa^2 + \omega_{2,s}^2\right)}{2g^2\kappa\left(2\kappa^2 + \omega_{1,s}^2 + \omega_{2,s}^2\right)}. \quad (9)$$

Since J^+J^- has to be positive, the obtained steady-state values are physical iff $J_z^0 \leqslant z_0$. If that is the case, the previous equation fixes $J^{\pm}$ up to the phase factor. Therefore, we may choose $(J^+)^0 = (J^-)^0 = \sqrt{(J^+J^-)^0}$ as a steady-state expectation. Finally, the corresponding expressions for a_i^0 and $(a_i^*)^0$ $(i \in \{1,2\})$ in terms of $(J^{\pm})^0$ follow from their transformed equations

$$a_i^0 = -\frac{ig(J^-)^0}{\kappa + i\omega_{i,s}}, \quad (a_i^*)^0 = \frac{ig(J^+)^0}{\kappa - i\omega_{i,s}}. \quad (10)$$

With this we have found a complete set of steady-state solutions for our two-mode model. Each physical solution for a characteristic frequency ω corresponds to a different nontrivial fixed point. Thus, together with the trivial fixed point, the laser model possesses up to four different steady-state configurations, whose stability properties we are going to study in more detail in the next section.

B. Stability of steady states

First, we investigate the stability of the fixed points. This is checked as usual by linearizing the mean-field equations (3) in the rotated frame around the fixed point and by determining the eigenvalues of the linearized system. An eigenvalue with a positive (negative) real part would support the solution divergence (convergence) from (to) the fixed point, which is then unstable (stable). If not mentioned otherwise, we choose the following parameter values: $\omega_1 = 2\Delta$, $\omega_2 = 4\Delta$, $\gamma_\downarrow = 0.1\Delta$, $\gamma_\uparrow = 0.2\Delta$.

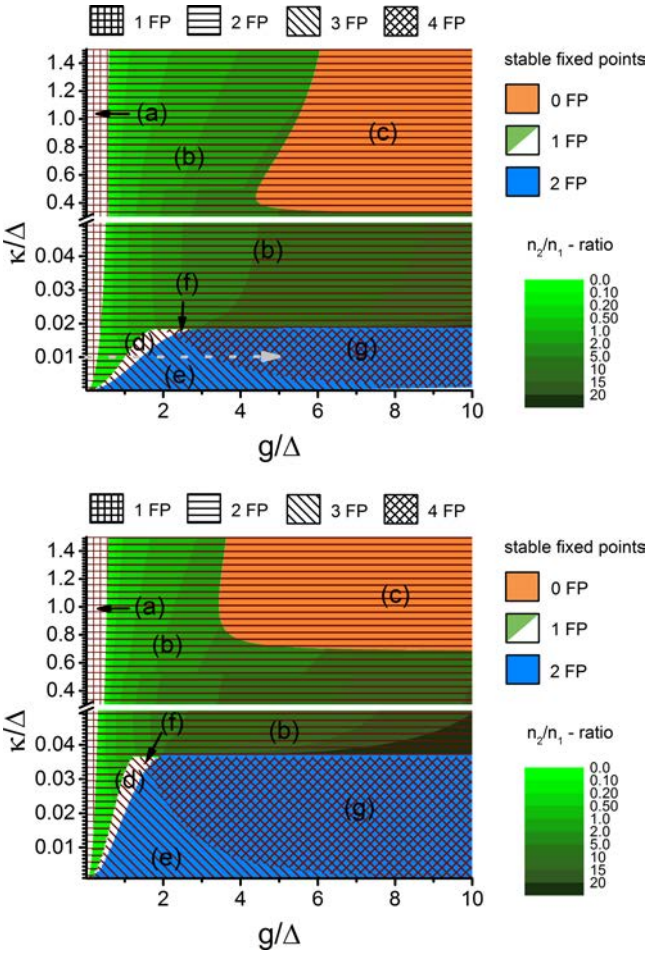

FIG. 1. (Color online) The phase diagram shows the total number of fixed points and the number of stable fixed points in the g-κ plane. For small κ, there exist up to four physical fixed points, two of which are stable. In region (c) all fixed points are unstable. Table I sums up the main properties of regions (a)–(g). The green color gradient encodes the mode population ratio n_1/n_2, where $n_i = a_i^* a_i$. The lower part shows the effect of increased pumping. Parameters: $\omega_1 = 2\Delta, \omega_2 = 4\Delta, \gamma_\downarrow = 0.1\Delta, \gamma_\uparrow = 0.2\Delta$ (upper), $\gamma_\uparrow = 0.5\Delta$ (lower).

Figure 1 shows the main result in the form of a complex phase diagram in the $g-\kappa$ plane for two different pumping rates $\gamma_\uparrow = 0.2\Delta, 0.5\Delta$, encoding the total number and the number of stable fixed points. We see that, if the atom-field coupling is too small, only one trivial solution exists which corresponds to region (a). By overcoming some critical value for g, at least one nontrivial solution appears; thus the ω_1 and ω_2 modes become macroscopically occupied. For smaller κ rates, we see a rich structure in the phase diagram. One can have different combinations of possible and stable fixed points, which are represented by a combination of color and dashing in Fig. 1. For example, the region (d) has two nontrivial physical solutions, but only one is stable. Table I provides the corresponding overview. For larger κ and g values, the phase diagram contains region (c) without any stable fixed

TABLE I. Overview of the total number of fixed points #(FP) and the number of stable fixed points #(SFP) within different regions of the phase diagram in Fig. 1.

Area	(a)	(b)	(c)	(d)	(e)	(f)	(g)
#(FP)	1	2	2	3	3	4	4
#(SFP)	1	1	0	1	2	1	2

points. Here the system observables, like the mode occupation, oscillate with fixed frequency and amplitude; thus a limit cycle represents the only stable solution in this area. Note that we have found no stable limit cycles except in region (c). The coloring in the (b) region shows the ratio n_1/n_2 of occupation of both modes, where $n_i = a_i^* a_i$. We observe that the occupation ratio and thus the dominating mode changes with the dissipation rate κ and the coupling strength g. Note that in the regions (e) and (g), where we have two stable fixed points, both ratios $n_1/n_2 \gtrless 1$ for fixed κ and g values exist. Especially in this region one of the modes is much more occupied and vice versa; thus the emitted radiation comes here mainly from one mode.

The lower part of Fig. 1 shows the effect of increased pumping. We see that the region with more than two fixed points (d)–(g) becomes larger, while the limit cycle region (c) is shifted to higher κ values.

Figure 2 shows the occupation of both modes as a function of coupling strength g for a fixed value of $\kappa = 0.01\Delta$, along the horizontal gray arrow in the phase diagram of Fig. 1. We plot all possible stationary solutions including the unstable ones. The unstable fixed points are dashed, while the occupations, which belong to the same fixed point, have the same color and the same thickness. The curves of the second mode are additionally marked with crosses. We see different types of bifurcations while increasing g. First, at $g = 0.3\Delta$ a pitchfork bifurcation occurs, where the trivial solution becomes unstable and a new

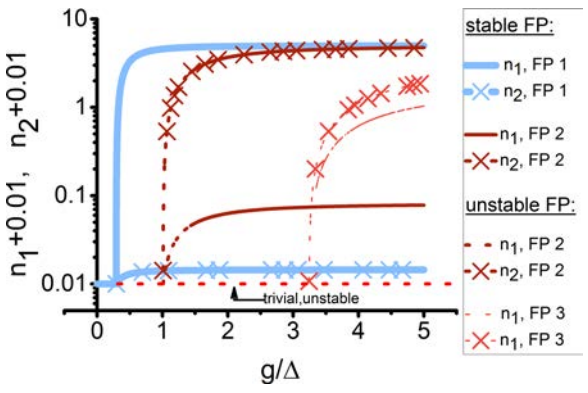

FIG. 2. (Color online) All stationary solutions of the mean-field Eq. (3) for the occupation of both modes (n_1,n_2) are plotted as a function of g for fixed κ value along the horizontal dashed arrow in Fig. 1 (upper). The unstable solutions are dashed, the solution set is marked by the same color and the same thickness. The trivial solution with zero-mode occupation is always present but unstable beyond a critical g. Note that all occupations in the plot are shifted by 10^{-2} due to the log scaling. Parameters: $\kappa = 0.01\Delta, \omega_1 = 2\Delta, \omega_2 = 4\Delta, \gamma_\downarrow = 0.1\Delta, \gamma_\uparrow = 0.2\Delta$.

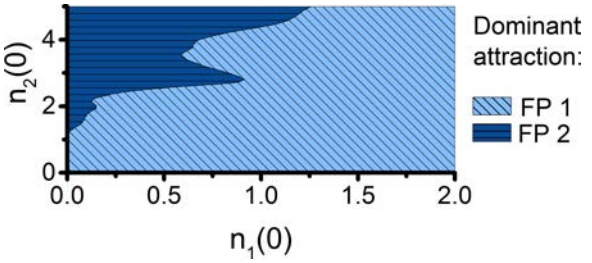

FIG. 3. (Color online) Attraction region of two stable fixed points from Fig. 2 depending on the initial population of the cavity modes $n_1(0)$ and $n_2(0)$. Used parameters: $J^+(0) = J^-(0) = 0.185$, $J_z(0) = 0.076$, $g = 2\Delta$, $\kappa = 0.01\Delta$, $\omega_1 = 2\Delta$, $\omega_2 = 4\Delta$, $\gamma_\downarrow = 0.1\Delta$, $\gamma_\uparrow = 0.2\Delta$.

stable solution occurs. Afterwards, an additional bifurcation takes place at $g = \Delta$, where an unstable solution splits up from the trivial one and becomes stable at $g = 1.5\Delta$. Later, at $g = 3.2\Delta$, a third bifurcation with an unstable solution splits up. For the used parameter values Eq. (7) has three real roots; nevertheless at least one of the observables in Eqs. (8) and (9) is unphysical, for instance, a negative mode population n_i or an imaginary J^+J^- value. Thus we have only two nontrivial solutions for $g > 1.5\Delta$. The two solutions allow the lower or the upper mode to have a high occupation, respectively. Note that the solution depends crucially on the chosen initial condition. Figure 3 shows an example of this behavior where we vary the initial state of the cavity modes $n_1(0)$,$n_2(0)$ for a given initial state of the atomic system. In the light blue area (diagonal lines) the system converges to the fixed point FP 1, in the dark blue area (vertical lines), to the fixed point FP 2 from Fig. 2.

In the next section we present different Pyragas feedback schemes. They allow us to switch between a macroscopic occupation of the two cavity modes irrespective of the chosen initial condition and also to change further dynamical properties like the fixed point attraction region of the considered model.

IV. DYNAMICS WITH FEEDBACK

We now demonstrate the impact of time-delayed feedback control on the system. As a feedback signal we always use one of the system properties and restrict ourselves only to Pyragas-type feedback [20]. Therefore, we insert into the mean-field equations, Eqs. (3), an additional control term, which is conditioned on the difference of a system property at two different times $t - \tau$ and t, where τ represents a time delay between the signal determination and the feedback into the system. Due to the rich phase diagram, even without feedback in Fig. 1, it seems impossible to engineer one feedback scheme which works in every part of the phase diagram. Hence, we have to find for each part of the phase diagram a scheme which produces the desired results, such as mode selection or stabilization. However, the chosen feedback may not work in other parts of the phase diagram or will have other influences onto the system dynamics. In the following, we present three feedback schemes for different purposes and parts of the phase diagram, give a possible implementation picture for each

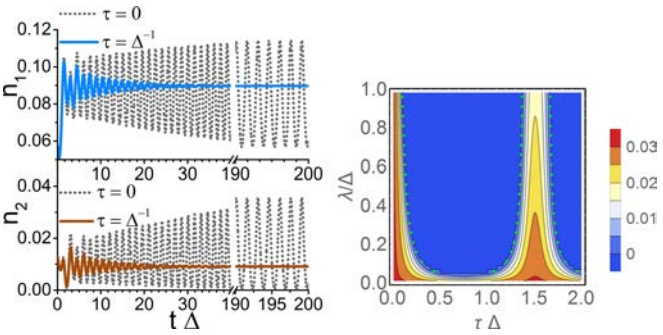

FIG. 4. (Color online) (left) Pyragas feedback control of J_z (11) stabilizes the nontrivial fixed point in region (c) of phase diagram Fig. 1. Without feedback the stationary solution is a limit cycle (gray dotted curves). With feedback the solution converges to a fixed point (solid curves). Parameters: $\tau = \Delta^{-1}$, $\lambda = 0.4\Delta$. (right) Control diagram in τ-λ plane. Vertical scale bar gives the largest real part of the eigenvalues of the linearized equations. In the blue region the fixed point becomes stable. Green dots show the boundaries from an analytical expression [see Eq. (A7)]. Parameters: $\kappa = 0.5\Delta$, $g = 5\Delta$, $\omega_1 = 2\Delta$, $\omega_2 = 4\Delta$, $\gamma_\downarrow = 0.1\Delta$, $\gamma_\uparrow = 0.2\Delta$.

scheme, and demonstrate exemplarily their influence onto the system evolution.

A. Stabilization of fixed points

The phase diagram in Fig. 1 has regions with nontrivial unstable steady states, which do not attract the solution. If no stable point exists, the solution oscillates periodically. This occurs only in the region (c); see gray dotted curve in Fig. 4 (left) obtained using the parameters $\kappa = 0.5\Delta$, $g = 5\Delta$. To stabilize the unstable nontrivial fixed point, we suggest the following feedback scheme of Pyragas type [20]:

$$\dot{J}_z \to \dot{J}_z - \lambda[J_z(t-\tau) - J_z(t)]. \tag{11}$$

Thus we modify the population inversion by a difference of the J_z spin component at two different times $t - \tau$ and t, where τ denotes the time delay parameter. Additionally, this difference is scaled by λ. The feedback term in Eq. (11) can be realized, for instance, by extra pumping of the atomic system or by opening additional decay channels, depending on the value of the feedback signal $\lambda[J_z(t-\tau) - J_z(t)]$.

The solid lines in Fig. 4 (left) show feedback actions for a point in the region (c). We see that for $t \gg 1/\Delta$, the mode occupations become constant; thus the fixed point is stabilized and the feedback signal vanishes. In contrast, without feedback the oscillations with finite amplitude are always present (gray dotted line). The right part of Fig. 4 shows the control diagram [44] in the $\tau - \lambda$ plane. The color encodes the largest real part of all existing eigenvalues, obtained from the linearized equation of motion [21] (see Appendix A 1). The fixed point is stable if this value is negative, which is the case in the blue area (Fig. 4, right). For the boundaries (green dots in Fig. 4, right) an analytical expression can be derived (see Appendix A 1).

B. Selection of the dominantly occupied mode

We now focus on region (e), which features two stable nontrivial fixed points. The main interest in this region is the occupation of the respective cavity modes. In each of both solutions one mode has a high occupation, whereas the other one has a low occupation (see Fig. 2). In that way, the light leaking out from a cavity is generated by mostly one of the two modes. Without feedback the dominating mode is selected by the initial condition (see Fig. 3), which is usually hard to control. Interestingly, we found a feedback scheme which allows one to select the mode of interest, i.e., to select the frequency of the radiated light, which was also achieved for a quantum dot laser in Ref. [19] with a non-Pyragas feedback type. We argue that our feedback type can switch the system behavior between a macroscopic occupation of the higher or the lower cavity mode.

To select the lower mode ω_1 we modify its frequency in Eqs. (3) as

$$\omega_1 \to \omega_1 + \lambda[n_2(t-\tau) - n_2(t)], \tag{12}$$

where $n_2 = a_2^* a_2$ represents the occupation of the second mode. This feedback type is also measurement based, as the mean photon flux is proportional to the mean occupation of the photonic modes [45,46]. Thus, the frequency of the first mode has to be changed according to the difference of mean photon fluxes of the second mode at times $t - \tau$ and t.

However, the previous (or similar) feedback scheme does not work well for selecting the upper mode ω_2. For that purpose we modify the feedback scheme according to [47]

$$\dot{a}_1 \to \dot{a}_1 - \lambda[a_1(t-\tau) - a_1(t)], \tag{13}$$

which is now a coherent type of feedback, as one can interpret it as a direct control without measurement [47]. One possible realization is the back coupling of emitted photons by a mirror, where the mirror distance fixes the time delay τ [48]. This scheme works for a properly chosen τ parameter [21] as, for instance, $\tau = 2\pi/\omega$ (or multiples of it), where ω denotes the characteristic frequency of the rotated frame determined by Eq. (7). This choice guarantees that the feedback term in Eq. (13) vanishes for $t \gg 1/\Delta$.

The action of both feedback types is shown in Fig. 5 for the system parameters $\kappa = 0.005\Delta, g = 2\Delta$ and the feedback parameters $\lambda = 0.01\Delta, \tau = \Delta^{-1}$ (upper) or $\lambda = \Delta, \tau = 2\pi/\omega$ (lower), where ω denotes the rotating frame frequency determined from Eq. (7). Solid marked curves show the cavity mode occupations with feedback, dashed curves without feedback. Both feedback schemes destabilize only one fixed point in region (e) of Fig. 1; thus the system converges to the other one. In the top figure we see the action of feedback Eq. (12). Without the feedback, the excited mode ω_2 has a dominant population (dashed violet line), whereas with control its occupation becomes low (violet line with markers) and instead the ground mode ω_1 (red line with markers) is macroscopically occupied. The bottom figure shows the opposite behavior. Instead of the lower mode (red, dashed), the higher mode is macroscopically occupied (violet line with markers). Note that both stable steady states exist without feedback in region (e) of Fig. 1. However, their attraction regions depend on the initial condition, as is shown without feedback in Fig. 3. We emphasize that with feedback the selection of modes works independently of the chosen initial condition for the tested parameter values.

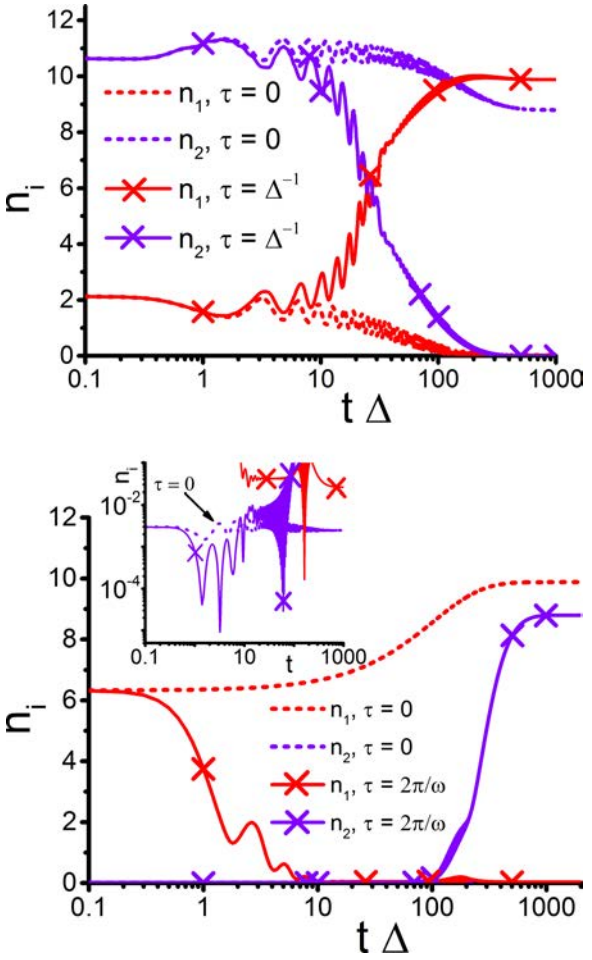

FIG. 5. (Color online) Usage of feedback schemes in region (e) of Fig. 1 for driving the system toward a macroscopic occupation of the lower (top) or higher cavity mode (bottom). (Top) Feedback scheme Eq. (12) selects highly populated ground mode (red line with markers), whereas (bottom) control type Eq. (13) selects highly populated excited mode (violet line with markers). The inset (bottom) shows the zoom for small photon numbers. Without feedback the other modes have a macroscopic population (dashed violet and red lines in both figures). Parameters: $\lambda = 0.01\Delta$ (top), $\lambda = \Delta$ (bottom), $\kappa = 0.005\Delta$, $g = 2\Delta$, $\omega_1 = 2\Delta$, $\omega_2 = 4\Delta$, $\gamma_\downarrow = 0.1\Delta$, $\gamma_\uparrow = 0.2\Delta$.

Figure 6 shows the control diagram in the τ-λ space with $\kappa = 0.005\Delta$, $g = 2\Delta$ for the feedback type Eq. (12) obtained from a linear stability analysis. We see that there are parameter regions where only one of the fixed points becomes unstable and also where both fixed points become unstable. In the blue-dotted area the fixed point with $n_2 \gg n_1$ becomes unstable, whereas in the green-dashed region another fixed point with $n_1 \gg n_2$ is destabilized. The boundaries are calculated analytically (see Appendix A 2). In order to reach the fixed point with a macroscopic occupation of the lower cavity mode, we have to choose the parameters in the region having only blue dots. Fixing the feedback parameter in the region having only green dashes (arrow in the diagram) should select the fixed point with a macroscopic population of the higher cavity mode. However, there are some exceptions. The fixed point with $n_2 \gg n_1$ attracts the solution if the initial condition is rather close to it; otherwise the solution converges

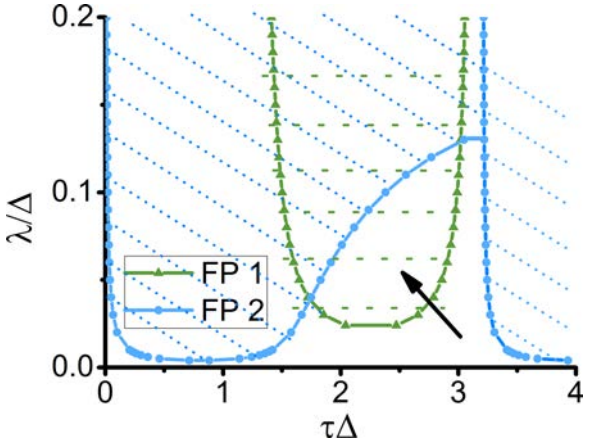

FIG. 6. (Color online) Stability diagram for Pyragas feedback type Eq. (12). In the dashed (dotted) region the first (second) fixed point (FP), related to a macroscopic population of the lower (higher) cavity mode as in Fig. 2, becomes unstable. Parameters: $\kappa = 0.005\Delta$, $g = 2\Delta$, $\omega_1 = 2\Delta$, $\omega_2 = 4\Delta$, $\gamma_\downarrow = 0.1\Delta$, $\gamma_\uparrow = 0.2\Delta$.

to a limit cycle, which appears in this case in the presence of Pyragas control [22]. Limit cycle solutions are also present in the parameter area where both fixed points become unstable due to the time-delayed feedback control.

V. SUMMARY AND OUTLOOK

In this paper we have investigated the mean-field dynamics of a two-mode laser model based on an extended Tavis-Cummings model in the thermodynamic limit without and with time-delayed feedback. The corresponding mean-field equations can be solved analytically in the steady state. Even without feedback control this model exhibits a complex phase diagram with multiple stable fixed points. Our Pyragas feedback schemes allow us to drive the system to different phases by selecting or stabilizing one preferred stationary solution.

We studied also other feedback schemes of the Pyragas type, but they led to similar results as already shown. However, especially in phases with a combination of unstable and stable nontrivial fixed points, it is difficult to design a feedback scheme which stabilizes or selects one stable configuration for a wide range of initial conditions. The reason for this is that the Pyragas control type affects the stability of all fixed points. For example, the stabilization succeeds only close to the corresponding fixed point in the sense of the linear stability analysis. Farther away from the fixed point, we have often observed the appearance of limit cycles with large attraction regions or even chaotic solutions, which is a known feature in laser systems with feedback [49] and also occurs for other nonlinear dynamical systems with time delay [50–53].

Since our calculations were done at a semiclassical level by restricting ourselves to first-order cumulants, we expect that the results should hold in the thermodynamic limit, where the number N of two-level atoms tends to infinity. On the one hand, the fluctuations scale like $1/\sqrt{N}$ with the number of atoms N [34]. On the other hand, the laser dynamics or a condensation is usually studied at this level. Furthermore, the semiclassical regime of the quantum-optical models like Dicke [54] or Lipkin-Meshkov-Glick [55] predicts

correctly their main properties, like observable averages or the occurrence of a quantum phase transition [37,39,56]. However, going beyond the factorization assumption could be performed by including higher-order cumulants, e.g., by using the Gaussian approximation, which involves first- and second-order cumulants [36,38,57].

It would be certainly interesting to analyze the impact of control on the quantum fluctuations. This could be investigated with other approaches to feedback [58,59], which usually requires a high numerical effort. In this respect a promising feedback scheme was introduced in Refs. [60] and [61], which allows one to control the entanglement and light bunching by structured environment and converges to a Pyragas control type in the one excitation limit. However, the general quantum version of Pyragas control type remains an unsolved question. A new, conceptually significant approach has been recently introduced in Ref. [62], although it appears to be numerically demanding.

Finally, we note that it would be worthwhile to extend our two-mode laser model with the thermalization mechanism along the lines of Refs. [12] and [16]. This would yield a minimal model to study the transition between a condensatelike and a laserlike state, which originate from a macroscopic occupation of the lower and higher cavity mode, respectively. Adding Pyragas feedback control terms as suggested here should thus allow one to switch the system behavior between condensatelike and laserlike.

ACKNOWLEDGMENTS

The authors gratefully acknowledge financial support from the Deutscher Akademischer Austauschdienst (DAAD) through Grants NAI-DBEC and IBEC; Deutsche Forschungsgemeinschaft (DFG) Grants No. BR 1528/7-1, No. 1528/8-2, No. 1528/9-1, No. SFB 910, No. GRK 1558, and No. SFB/TR49; and the Ministry of Education, Science, and Technological Development of the Republic of Serbia, Grants No. ON171017, No. ON171038, No. III45016, NAI-DBEC, and IBEC.

APPENDIX

In the following we show how to determine the boundary condition in the stability diagrams Fig. 4 (right) and of Fig. 6 in the presence of time-delayed Pyragas feedback control terms Eq. (11) and Eq. (12), respectively.

1. Stabilization of fixed points

Linearizing the equation of motion (3) together with the feedback condition Eq. (11) we obtain the equation

$$\delta\dot{\mathbf{v}}(t) = \boldsymbol{A}\,\delta\mathbf{v}(t) + \boldsymbol{B}\,\delta\mathbf{v}(t-\tau), \tag{A1}$$

where $\mathbf{v} = (a_1, a_1^*, a_2, a_2^*, J^+, J^-, J_z)$, $\delta\mathbf{v}$ gives a deviation from the fixed point $\mathbf{v}^0$ determined via the procedure given in Sec. III A, and we have introduced the matrices

$$\boldsymbol{A} = \begin{pmatrix}
-i\omega_{1,s}-\kappa & 0 & 0 & 0 & 0 & -ig & 0 \\
0 & i\omega_{1,s}-\kappa & 0 & 0 & ig & 0 & 0 \\
0 & 0 & -i\omega_{2,s}-\kappa & 0 & 0 & -ig & 0 \\
0 & 0 & 0 & i\omega_{2,s}-\kappa & ig & 0 & 0 \\
0 & -2igJ_z^0 & 0 & -2igJ_z^0 & i\Delta_s-\Gamma_D & 0 & -2ig((a_1^*)^0+(a_2^*)^0) \\
2igJ_z^0 & 0 & 2igJ_z^0 & 0 & 0 & -i\Delta_s-\Gamma_D & 2ig\left(a_1^0+a_2^0\right) \\
-ig(J^+)^0 & ig(J^-)^0 & -ig(J^+)^0 & ig(J^-)^0 & -ig\left(a_1^0+a_2^0\right) & ig((a_1^*)^0+(a_2^*)^0) & -\Gamma_T
\end{pmatrix},$$

$$\boldsymbol{B} = \lambda\cdot(0,0,0,0,0,0,1)^T \otimes (0,0,0,0,0,0,1).$$

The stability condition is then [21]

$$0 = \det\left[(\boldsymbol{A}-\boldsymbol{B}) - \boldsymbol{B}\cdot e^{-\Lambda\tau} - \Lambda\mathbf{1}\right]. \tag{A2}$$

The fixed point is stable if all possible solutions for Λ have a negative real part. From Eq. (A2) the equation for phase boundaries can be obtained as follows. At the phase boundaries, Λ has a vanishing real part. Thus, by replacing $\Lambda \to i\Omega$ ($\Omega \in \mathbb{R}$) in Eq. (A2) and calculating the determinant, we obtain

$$0 = e^{-i\Omega\tau}\sum_{j=0}^{6} c_j A_j \Omega^j + \sum_{j=0}^{7} c_j B_j \Omega^j, \tag{A3}$$

$$c_j = \begin{cases} 1, & j \text{ even}, \\ i, & j \text{ odd}, \end{cases} \tag{A4}$$

where A_i, B_i, $i \in \{1,2,\ldots.7\}$ are real coefficients which depend on the system parameters both explicitly and implicitly via the fixed point solution, and on the feedback strength λ. However, the corresponding expressions are too long for showing them here.

Splitting the equation into real and imaginary parts, we obtain the following two equations:

$$\begin{aligned} 0 &= C_1 + C_2\cos(\Omega\tau) + C_3\sin(\Omega\tau), \\ 0 &= C_4 + C_3\cos(\Omega\tau) - C_2\sin(\Omega\tau), \end{aligned} \tag{A5}$$

where

$$\begin{aligned} C_1 &= B_0 + B_2\Omega^2 + B_4\Omega^4 + B_6\Omega^6, \\ C_2 &= A_0 + A_2\Omega^2 + A_4\Omega^4 + A_6\Omega^6, \\ C_3 &= A_1\Omega + A_3\Omega^3 + A_5\Omega^5, \\ C_4 &= B_1\Omega + B_3\Omega^3 + B_5\Omega^5 + B_7\Omega^7. \end{aligned} \tag{A6}$$

Squaring and summing Eqs. (A5), we can eliminate the τ dependence and obtain a 14th-order polynomial equation in Ω. This provides up to 14 solutions for Ω, but only two of them turn out to be real. Next, we sum both of the Eqs. (A5)

together in a suitable way in order to eliminate the sin term. The resulting equation can then be solved for τ as

$$\tau = \frac{1}{\Omega}\arccos\left(-\frac{C_3C_4 + C_1C_2}{C_2^2 + C_3^2}\right) + \frac{2\pi}{\Omega}z,\ z \in \mathbb{Z}. \quad \text{(A7)}$$

This yields the boundaries in Fig. 4 (right), which perfectly agree with the corresponding numerical calculations. Two valid solutions for Ω build the $\bigcup$-shaped structure in the diagram, whereas z is responsible for its periodic structure.

2. Selecting the fixed point

The procedure is similar to Appendix A 1, but the feedback condition is given now by Eq. (12). The matrix $\boldsymbol{B}$ is then redefined as

$$\boldsymbol{B} = -i\lambda\begin{pmatrix} 0 & 0 & (a_2^*)^0 a_1{}^0 & (a_2^*)^0 a_1{}^0 & 0 & 0 & 0 \\ 0 & 0 & -a_2{}^0(a_1^*)^0 & -a_2{}^0(a_1^*)^0 & 0 & 0 & 0 \\ 0 & 0 & 0 & 0 & 0 & 0 & 0 \\ 0 & 0 & 0 & 0 & 0 & 0 & 0 \\ 0 & 0 & 0 & 0 & 0 & 0 & 0 \\ 0 & 0 & 0 & 0 & 0 & 0 & 0 \\ 0 & 0 & 0 & 0 & 0 & 0 & 0 \end{pmatrix}.$$

The further procedure is the same. First we calculate the determinant Eq. (A2) and write it in a similar form as Eq. (A3):

$$0 = e^{-i\Omega\tau}\sum_{j=0}^{4} c_j \tilde{A}_j \Omega^j + \sum_{j=0}^{7} c_j \tilde{B}_j \Omega^j, \quad \text{(A8)}$$

$$c_j = \begin{cases} 1, & j \text{ even}, \\ i, & j \text{ odd}. \end{cases} \quad \text{(A9)}$$

As the parameters $\tilde{A}_j, \tilde{B}_j$ are real, Eq. (A8) can be split into real and imaginary parts, which yields

$$\begin{aligned} 0 &= \tilde{C}_1 + \tilde{C}_2\cos(\Omega\tau) + \tilde{C}_3\sin(\Omega\tau), \\ 0 &= \tilde{C}_4 + \tilde{C}_3\cos(\Omega\tau) - \tilde{C}_2\sin(\Omega\tau), \end{aligned} \quad \text{(A10)}$$

where

$$\begin{aligned} \tilde{C}_1 &= \tilde{B}_0 + \tilde{B}_2\Omega^2 + \tilde{B}_4\Omega^4 + \tilde{B}_6\Omega^6, \\ \tilde{C}_2 &= \tilde{A}_0 + \tilde{A}_2\Omega^2 + \tilde{A}_4\Omega^4, \\ \tilde{C}_3 &= \tilde{A}_1\Omega + \tilde{A}_3\Omega^3, \\ \tilde{C}_4 &= \tilde{B}_1\Omega + \tilde{B}_3\Omega^3 + \tilde{B}_5\Omega^5 + \tilde{B}_7\Omega^7. \end{aligned} \quad \text{(A11)}$$

From the upper equations one can then eliminate the τ dependence to determine possible Ω values. With this τ can be calculated as in Eq. (A7), but C_i is then replaced by $\tilde{C}_i$. The resulting (Ω, τ) combinations are the boundaries in Fig. 6.

[1] A. E. Siegman, *Lasers* (University Science Books, Mill Valley, CA, 1986).
[2] W. Just, A. Pelster, M. Schanz, and E. Schöll, Philos. Trans. R. Soc., A **368**, 303 (2009).
[3] H. G. Schuster and K. Lüdge, *Nonlinear Laser Dynamics: From Quantum Dots to Cryptography* (John Wiley & Sons, Weinheim, 2012).
[4] C. Masoller, T. Sorrentino, M. Chevrollier, and M. Oria, IEEE J. Quantum Electron. **43**, 261 (2007).
[5] N. Kikuchi, Y. Liu, and J. Ohtsubo, IEEE J. Quantum Electron. **33**, 56 (1997).
[6] C. Hopfmann, F. Albert, C. Schneider, S. Höfling, M. Kamp, A. Forchel, I. Kanter, and S. Reitzenstein, New J. Phys. **15**, 025030 (2013).
[7] F. Schulze, B. Lingnau, S. M. Hein, A. Carmele, E. Schöll, K. Lüdge, and A. Knorr, Phys. Rev. A **89**, 041801 (2014).
[8] R. Lang and K. Kobayashi, IEEE J. Quantum Electron. **16**, 347 (1980).
[9] M. C. Soriano, J. García-Ojalvo, C. R. Mirasso, and I. Fischer, Rev. Mod. Phys. **85**, 421 (2013).
[10] M. Sargent, M. Scully, and W. Lamb, *Laser Physics*, Advanced book program (Perseus Books Group, New York, NY, 1978).
[11] H. Haken, *Laser Theory*, Encyclopedia of Physics Vol. XXV/2C (Berlin, 1970); reprint (Springer, 1984).
[12] P. Kirton and J. Keeling, Phys. Rev. Lett. **111**, 100404 (2013).
[13] J. Klaers, J. Schmitt, F. Vewinger, and M. Weitz, Nature (London) **468**, 545 (2010).
[14] J. Marelic and R. A. Nyman, Phys. Rev. A **91**, 033813 (2015).
[15] J. Klaers, J. Schmitt, T. Damm, F. Vewinger, and M. Weitz, Phys. Rev. Lett. **108**, 160403 (2012).
[16] P. Kirton and J. Keeling, Phys. Rev. A **91**, 033826 (2015).
[17] N. A. Naderi, F. Grillot, K. Yang, J. B. Wright, A. Gin, and L. F. Lester, Opt. Express **18**, 27028 (2010).
[18] M. Virte, S. Breuer, M. Sciamanna, and K. Panajotov, Appl. Phys. Lett. **105**, 121109 (2014).
[19] M. Virte, K. Panajotov, and M. Sciamanna, IEEE J. Quantum Electron. **49**, 578 (2013).
[20] K. Pyragas, Phys. Lett. A **170**, 421 (1992).
[21] P. Hövel and E. Schöll, Phys. Rev. E **72**, 046203 (2005).
[22] W. Kopylov, C. Emary, E. Schöll, and T. Brandes, New J. Phys. **17**, 013040 (2015).
[23] M. O. Scully, *Quantum Optics* (Cambridge University Press, Cambridge, UK, 1997).
[24] M. Tavis and F. W. Cummings, Phys. Rev. **170**, 379 (1968).
[25] L. M. Narducci, M. Orszag, and R. A. Tuft, Phys. Rev. A **8**, 1892 (1973).
[26] M. P. Baden, K. J. Arnold, A. L. Grimsmo, S. Parkins, and M. D. Barrett, Phys. Rev. Lett. **113**, 020408 (2014).
[27] F. Dimer, B. Estienne, A. S. Parkins, and H. J. Carmichael, Phys. Rev. A **75**, 013804 (2007).
[28] P. P. Munhoz and F. L. Semião, Eur. Phys. J. D **59**, 509 (2010).
[29] J. Fan, Z. Yang, Y. Zhang, J. Ma, G. Chen, and S. Jia, Phys. Rev. A **89**, 023812 (2014).
[30] F. O. Prado, F. S. Luiz, J. M. Villas-Bôas, A. M. Alcalde, E. I. Duzzioni, and L. Sanz, Phys. Rev. A **84**, 053839 (2011).
[31] A. Wickenbrock, M. Hemmerling, G. R. M. Robb, C. Emary, and F. Renzoni, Phys. Rev. A **87**, 043817 (2013).
[32] C. Emary, J. Phys. B **46**, 224008 (2013).
[33] A. Chiocchetta and I. Carusotto, Phys. Rev. A **90**, 023633 (2014).

[34] C. Gardiner and P. Zoller, *Quantum Noise: A Handbook of Markovian and non-Markovian Quantum Stochastic Methods with Applications to Quantum Optics* (Springer, Berlin, 2004).
[35] P. Ribeiro, J. Vidal, and R. Mosseri, Phys. Rev. Lett. **99**, 050402 (2007).
[36] K. Henschel, J. Majer, J. Schmiedmayer, and H. Ritsch, Phys. Rev. A **82**, 033810 (2010).
[37] M. J. Bhaseen, J. Mayoh, B. D. Simons, and J. Keeling, Phys. Rev. A **85**, 013817 (2012).
[38] H. A. M. Leymann, A. Foerster, and J. Wiersig, Phys. Rev. B **89**, 085308 (2014).
[39] G. Engelhardt, V. M. Bastidas, W. Kopylov, and T. Brandes, Phys. Rev. A **91**, 013631 (2015).
[40] C. Emary and T. Brandes, Phys. Rev. E **67**, 066203 (2003).
[41] M. Hayn, C. Emary, and T. Brandes, Phys. Rev. A **84**, 053856 (2011).
[42] P. Pérez-Fernández, A. Relaño, J. M. Arias, P. Cejnar, J. Dukelsky, and J. E. García-Ramos, Phys. Rev. E **83**, 046208 (2011).
[43] M. A. Bastarrachea-Magnani, S. Lerma-Hernández, and J. G. Hirsch, Phys. Rev. A **89**, 032102 (2014).
[44] E. Schöll and H. G. Schuster, *Handbook of Chaos Control*, 2nd ed. (John Wiley & Sons, Weinheim, 2008).
[45] B. Öztop, M. Bordyuh, Ö. E. Müstecaplıoğlu, and H. E. Türeci, New J. Phys. **14**, 085011 (2012).
[46] W. Kopylov, C. Emary, and T. Brandes, Phys. Rev. A **87**, 043840 (2013).
[47] A. Grimsmo, A. Parkins, and B. Skagerstam, New J. Phys. **16**, 065004 (2014).
[48] J. Kabuss, D. O. Krimer, S. Rotter, K. Stannigel, A. Knorr, and A. Carmele, Phys. Rev. A **92**, 053801 (2015).
[49] C. Otto, K. Lüdge, and E. Schöll, Phys. Status Solidi B-Basic Solid State Phys. **247**, 829 (2010).
[50] W. Wischert, A. Wunderlin, A. Pelster, M. Olivier, and J. Groslambert, Phys. Rev. E **49**, 203 (1994).
[51] E. Grigorieva, H. Haken, S. Kashchenko, and A. Pelster, Physica D **125**, 123 (1999).
[52] M. Schanz and A. Pelster, SIAM J. Appl. Dyn. Syst **2**, 277 (2003).
[53] M. Schanz and A. Pelster, Phys. Rev. E **67**, 056205 (2003).
[54] R. H. Dicke, Phys. Rev. **93**, 99 (1954).
[55] H. J. Lipkin, N. Meshkov, and A. Glick, Nucl. Phys. **62**, 188 (1965).
[56] P. Ribeiro, J. Vidal, and R. Mosseri, Phys. Rev. E **78**, 021106 (2008).
[57] R. Kubo, J. Phys. Soc. Jpn. **17**, 1100 (1962).
[58] H. M. Wiseman and G. J. Milburn, *Quantum Measurement and Control* (Cambridge University Press, Cambridge, UK, 2009).
[59] C. Emary, Philos. Trans. R. Soc., A **371**, 20120468 (2013).
[60] N. L. Naumann, S. M. Hein, A. Knorr, and J. Kabuss, Phys. Rev. A **90**, 043835 (2014).
[61] S. M. Hein, F. Schulze, A. Carmele, and A. Knorr, Phys. Rev. A **91**, 052321 (2015).
[62] A. L. Grimsmo, Phys. Rev. Lett. **115**, 060402 (2015).

Positive-operator-valued measures in the Hamiltonian formulation of quantum mechanics

D. Arsenović, N. Burić,* D. B. Popović, M. Radonjić, and S. Prvanović
Institute of Physics, University of Belgrade, Pregrevica 118, 11080 Belgrade, Serbia
(Received 16 January 2015; published 12 June 2015)

In the Hilbert space formulation of quantum mechanics, ideal measurements of physical variables are discussed using the spectral theory of Hermitian operators and the corresponding projector-valued measures (PVMs). However, more general types of measurements require the treatment in terms of positive-operator-valued measures (POVMs). In the Hamiltonian formulation of quantum mechanics, canonical coordinates are related to PVM. In this paper the results of an analysis of various aspects of applications of POVMs in the Hamiltonian formulation are reported. Several properties of state parameters and quantum observables given by POVMs or represented in an overcomplete basis, including the general Hamiltonian treatment of the Neumark extension, are presented. An analysis of the phase operator, given by the corresponding POVMs, in the Hilbert space and the Hamiltonian frameworks is also given.

DOI: 10.1103/PhysRevA.91.062114 PACS number(s): 03.65.Fd, 03.65.Sq

I. INTRODUCTION

The Hamiltonian formulation of quantum mechanics (HQM) [1–4] provides an alternative mathematical formulation that is equivalent to the more standard one based on Hilbert spaces and has proven to be useful in discussing such issues as nonlinear constraints [5,6] the geometry of entanglement [2], the classical limit [7,8], hybrid quantum-classical systems [9–11], and nonlinear and stochastic generalizations of quantum mechanics (QM) [1,2,12]. In the Hamiltonian formulation quantum pure states are represented by points of an appropriate smooth manifold $\mathcal{M}$ and the quantum dynamics is represented by a Hamiltonian flow on $\mathcal{M}$. In order to formulate probabilistic aspects of QM and in particular describe ideal measurements in the sense of von Neumann, the manifold $\mathcal{M}$ is equipped with a Riemannian metric. Standard postulates of QM about states, observables, and dynamics are formulated in terms of notions associated directly with a Hamiltonian dynamical system on $\mathcal{M}$, without any reference to the Hilbert space formulation.

An ideal measurement of a quantum observable, represented in the von Neumann scheme by a Hermitian operator and its spectral projector-valued measure (PVM), is in the Hamiltonian framework formulated using quadratic functions of canonical coordinates on $\mathcal{M}$, their critical values and critical points, and the Riemannian metric on $\mathcal{M}$. However, there are legitimate questions that can be asked about the preparation of a quantum system that cannot be cast into the von Neumann ideal measurement conception [13–15]. Data about the system can be collected that cannot be obtained as eigenvalues of an appropriate self-adjoined operator. On the other hand, such sets of data do satisfy certain conditions, such as covariance with respect to some natural transformations [13,14], which justify association of such data with certain physical quantities. Important examples of such data sets, like those related to polarization or the phase of quantum motion, are conveniently described by positive-operator-valued measures (POVMs) instead of PVMs. Another instance where the use of POVMs appears most naturally is in the context of approximate or indirect measurements or joined measurements of canonically related observables. It is our goal to formulate and analyze important properties of POVMs in the framework of the Hamiltonian formulation and thus prepare the way for the Hamiltonian formulation of the generalized measurement.

The paper is organized as follows. In the next section we provide a brief presentation of the Hamiltonian formulation of QM, insisting on its independence from the Hilbert space formulation. Section III is devoted to an abstract treatment in the framework of the Hamiltonian formulation of various questions related to the use of the POVM, with all considerations restricted to a finite-dimensional state space. In particular, we discuss in detail the kinematical and the dynamical aspects of the Hamiltonian analog of the Neumark extension for a POVM. In Sec. IV we treat in detail the example of a POVM corresponding to the phase of quantum motion. The Neumark extension of the phase POVM in the Hilbert space formulation is derived and the corresponding Hamiltonian formulation is presented. Section V provides a brief summary.

II. BASICS OF THE HAMILTONIAN FORMULATION

The Hamiltonian formulation of quantum mechanics is formally rather similar to the standard theory of Hamiltonian dynamical systems as it is used in classical mechanics [16]. The additional features are related to the statistical properties of quantum systems. Pure states of a quantum system are in the HQM mathematically represented by points of a smooth manifold with Kahler structure $(\mathcal{M},G,\Omega,J)$, where $\mathcal{M}$ is a smooth manifold admitting a Riemannian G and symplectic Ω structures and J is a map on the tangent space $T\mathcal{M}$ satisfying $G(X,Y)=\Omega(X,JY)$. One refers to $(\mathcal{M},G,\Omega,J)$ as the quantum phase space. In fact, in the case of systems with a finite N-dimensional Hilbert space $\mathcal{H}^N$, the Hamiltonian formulation is given using $\mathcal{M}=\mathbf{R}^{2N}$ with the standard Riemannian, symplectic, and complex structures. On the other hand, phase spaces for systems with infinite-dimensional Hilbert spaces can be considered as direct sums of an even number of real infinite-dimensional vector

*buric@ipb.ac.rs

spaces. In this and the next section we restrict our attention to the finite-dimensional cases. In any case, a pure quantum state is represented by an equivalence class of points in $\mathcal{M}$. Nevertheless, we almost always refer to the points of $\mathcal{M}$ as the quantum states neglecting the fact that many points correspond to physically the same quantum pure state.

The symplectic two-form Ω associates a Hamiltonian vector field X_f with a sufficiently smooth function f on $\mathcal{M}$ by the formula

$$\Omega(X, X_f) = df(X), \tag{1}$$

where X is a vector field on $\mathcal{M}$. Thus, any smooth function generates a symplectic transformation. The symplectic structure also defines a Poisson bracket between smooth functions f and g on $\mathcal{M}$,

$$\{f,g\} = \Omega(X_f, X_g), \tag{2}$$

where X_f, X_g are Hamiltonian vector fields corresponding to f,g.

The Euclidian space $\mathbf{R}^{2N}$ admits global canonical coordinates $(q,p) \equiv \{q_i, p_j; i,j = 1,2,\ldots,N\}$, which satisfy $\{q_i, p_j\} = \delta_{ij}$ and $\{q_i, q_j\} = \{p_i, p_j\} = 0$. In the classical mechanical application of Hamiltonian dynamics any real smooth function of (q,p) represents a physical variable. Quantum mechanics is characterized also by the metric structure and therefore the set of physical variables of a quantum system, defined as generators of transformations that preserve the typical structures Ω and G, is different: Only real quadratic functions of the form

$$f(q,p) = \sum_{ij}^{N} f^1_{ij}(q_i q_j + p_i p_j) + f^2_{ij} q_i p_j, \tag{3}$$

where f^1_{ij} are real symmetric and f^2_{ij} are real antisymmetric, are assumed to be related to quantum physical observables. The most important property of such quadratic functions is that the corresponding Hamiltonian vector fields generate symplectic maps that preserve the Riemannian structure. Thus, the physical variables generate transformations that preserve the two constituting structures of the quantum phase space $(\mathcal{M}, G, \Omega, J)$. It is important to stress that, contrary to the case of classical mechanics, not all values of a function (3) representing a physical variable can be obtained as a result of quantum measurements of this physical variable. Possible results of measurements in the Hamiltonian formulation will be discusses shortly.

It is convenient to introduce the set of complex coefficients π_{lm} such that

$$\begin{aligned} f(q,p) &= \sum_{ij}^{N} f^1_{ij}\left(q_i^2 + p_i^2\right) + f^2_{ij} q_i p_j \\ &= \sum_{lm}^{N} \pi_{lm}(q_l - i p_l)(q_m + i p_m). \end{aligned} \tag{4}$$

Obviously, one has

$$\mathrm{Re}\pi_{ij} = f^1_{ij}, \quad \mathrm{Im}\pi_{ij} = -f^2_{ij}/2. \tag{5}$$

In fact, π_{lm} form an $N \times N$ Hermitian matrix, so there is a Hermitian operator $\hat{F}$ on a Hilbert space $\mathcal{H}^N$ and a proper basis $|e_l\rangle$, $l = 1,2,\ldots,N$, such that

$$\pi_{lm} = \langle e_l | \hat{F} | e_m \rangle. \tag{6}$$

Here the Hermitian scalar product between two vectors $\langle \psi_1 | \psi_2 \rangle$ is related to the metric and symplectic structures on $\mathcal{M}$ by $\langle \psi_1 | \psi_2 \rangle = G(\psi_1, \psi_2)/2 + i\Omega(\psi_1, \psi_2)/2$, where on the right-hand side we identified $\mathbf{R}^{2N}$ with its tangent space.

Using the proper basis $|e_l\rangle$, one associates a Hilbert space vector $|\psi_{qp}\rangle \in \mathcal{H}^N$ with the point $m \in \mathbf{R}^{2N}$ parametrized by the canonical coordinates values $\{q_l = m_l, p_l = m_{l+N}; l = 1,2,\ldots,N\}$. The relation is

$$|\psi\rangle = \sum_{l}^{N} (q_l + i p_l)|e_l\rangle. \tag{7}$$

The operator $\hat{F}$ in (6) is given in terms of this proper basis by

$$\hat{F} = \sum_{ij}^{N} \pi_{ij} |e_i\rangle\langle e_j| \tag{8}$$

and the quadratic function

$$F(q,p) = \langle \psi_{qp} | \hat{F} | \psi_{qp} \rangle \tag{9}$$

is to be interpreted as the quantum expectation of the quantum observable $\hat{F}$ in the state $|\psi_{qp}\rangle$. The Poisson bracket between two quadratic functions F_1 and F_2 is related to the quadratic function corresponding to the commutator between the corresponding operators $\hat{F}_1$ and $\hat{F}_2$:

$$\frac{1}{i}\langle \psi | [\hat{F}_1, \hat{F}_2] | \psi \rangle = \{F_1, F_2\}, \tag{10}$$

where, as before, $F_i(\psi) = \langle \psi | \hat{F}_i | \psi \rangle$.

The kinematic part of the Hamiltonian formulation of QM will be referred to as the quantum phase-space formulation. The dynamics of a quantum system is in the HQM given by the abstract Hamiltonian equations

$$\dot{m} = X_H(m), \tag{11}$$

where $m \in \mathcal{M}$ and X_H is the Hamiltonian vector field corresponding to the function $H(m) = \langle \psi_m | \hat{H} | \psi_m \rangle$, where $\hat{H}$ is the Hamiltonian of the system. In the complex space the corresponding equation is the Schrödinger equation

$$i\hbar |\dot{\psi}(t)\rangle = \hat{H} |\psi(t)\rangle. \tag{12}$$

In canonical coordinates Eq. (11) is

$$\begin{aligned} \dot{q}_i &= \{H(q,p), q_i\} = \frac{\partial H(q,p)}{\partial p_i}, \\ \dot{p}_i &= \{H(q,p), p_i\} = -\frac{\partial H(q,p)}{\partial q_i}, \quad i = 1,2,\ldots,N. \end{aligned} \tag{13}$$

Information about the state of a quantum system is obtained by performing operations with the considered systems and possibly additional systems. A quite restricted class of such operations is the ideal measurements in the sense of von Neumann. In the Hilbert space formulation, the data collected by such a measurement involve spectral decomposition of an appropriate Hermitian operator, i.e., involve an appropriate PVM. In the Hamiltonian formulation of quantum mechanics, the data collected by such measurements involve only the

functions of the form (9) and the Riemannian structure G. A full description of the von Neumann measurement of an observable with a possibly degenerate and continuous spectrum in the Hamiltonian framework is discussed in [1]. As an illustration, we recapitulate the case of an observable with a discrete nondegenerate spectrum. Possible results of a measurement from this class are exhausted by the critical values of a function of the form (9). We denote these critical values and the corresponding critical points from $\mathbf{R}^{2N}$ by $F_{0,i}$, $i = 1,2,\ldots,N$, and $X_{F,i}$, respectively. For the system in a state $m_{in} \equiv (q_{in}, p_{in})$ the probability of the measurement result $F_{0,i}$ is given by $G(m_{in}, X_{F,i})$, where $X_{F,i}$ is the ith critical point of F. In terms of the quadratic function (9), the possible results of an F measurement are obtained by diagonalization of the Hermitian matrix π^f_{ij}. Spectral decomposition of the operator $\hat{F}$ corresponds to the harmonic-oscillator representation of the quadratic function $f(q',p') = \sum_l \pi^f_l (q'^2_l + p'^2_l)$, where the sum goes over distinct eigenvalues π^f_l of the matrix π^f_{ij} and $\{q'_l, p'_l\}$ denote here the real and imaginary parts of the eigenvalues of $\hat{F}$. The transformation from (q,p) to (q',p') coordinates is of course canonical and isometric.

However, the most general class of quantum operations that can be used to obtain information about a quantum state is in the Hilbert space formulation described by POVMs [14,15]. A description of such a generalized measurement process in terms of a POVM involves two important mathematical properties of POVMs. (i) For all purposes related to quantum information processing, a POVM can always be given in terms of an overcomplete basis (Davis theorem [15,17]). (ii) A POVM can be obtained by projecting a PVM acting in a larger Hilbert space (Neumark theorem [15,18]). The Hamiltonian formulation of these properties of POVMs is the topic of this paper.

III. POSITIVE-OPERATOR-VALUED MEASURES AND FUNCTIONS REPRESENTING PHYSICAL VARIABLES

Consider an overcomplete set of vectors $\{|b_i\rangle, i \in I\}$ where the index i can be discrete $i = 1,2,\ldots,M > N$ or continuous. It is sometimes convenient to use a multidimensional or complex index set I, for example, in the case of ordinary coherent states. The one-dimensional (1D) projectors $|b_i\rangle\langle b_i|$ are not mutually orthogonal. Such an overcomplete set provides a POVM $\{\hat{B}_i = |b_i\rangle\langle b_i|, i \in I\}$. Such a POVM can be used, instead of a PVM, to define a Hermitian operator or to represent a Hermitian operator as a function of the corresponding $2M$ noncanonical variables. Furthermore, there is a Hilbert space $\bar{\mathcal{H}}$, a PVM $\{\hat{P}_i\}$, and a projector $\hat{\Pi}, \mathcal{H} \to \bar{\mathcal{H}}$, such that a POVM $\{\hat{B}_i\}$ is given by $\hat{B}_i = \hat{\Pi}\hat{P}_i\hat{\Pi}$. We analyze the formulation and consequences of these facts in the Hamiltonian framework of QM. In the abstract treatment of this section we restrict our attention to the case when the index i, enumerating the vectors of the overcomplete basis, is discrete and finite. The case when the index enumerating the overcomplete basis is real and continuous but bounded will be treated in detail in the next section using the example of a POVM associated with the quantum phase. Another common example of an overcomplete basis and the corresponding POVM with an interesting Hamiltonian formulation, which, however, will not be treated here, is provided by the coherent states of a single linear harmonic oscillator on $L_2(\mathbf{R})$. The index set here is the complex plane $\mathbf{C}$. The Neumark extension of this POVM is the PVM given by the multiplication operator on the Hilbert space $L_2(\mathbf{R}^2)$. The Hamiltonian formulations of the original and the extended system with constraints both involve infinite-dimensional Hamiltonian systems.

A. Positive-operator-valued measures as a set of dependent coordinates

A set of canonical coordinates (q,p) is uniquely related to a basis of mutually orthogonal vectors, i.e., with a PVM. On the other hand, an overcomplete basis $\{|b_j\rangle\}$ with the index j continuous or discrete with $\max j = M > N$ can be used to associate with each vector in the $2N$-dimensional space a set of $2M > 2N$ real numbers. Thus, the overcomplete basis provides $2M$ parameters to characterize the points from $\mathbf{R}^{2N}$. Obviously, the values of these parameters on $\mathbf{R}^{2N}$ cannot be linearly independent.

Consider a set of vectors $\mathcal{B} = \{|b_j\rangle\}_{j=1}^M$ $(M \geqslant N)$ generating a resolution of unity in $\mathcal{H}^N$,

$$\sum_{j=1}^{M} |b_j\rangle\langle b_j| = \mathbb{I}_N. \tag{14}$$

The set $\mathcal{B}$ could be a proper basis $(M = N)$ where the vectors are necessarily mutually orthogonal, but could also be an overcomplete basis $(M > N)$, when at least two of the vectors are not orthogonal. In any case, a (normalized) state $|\psi\rangle$ from the Hilbert space $\mathcal{H}^N$ can be expanded, using (14), as

$$|\psi\rangle = \sum_{j=1}^{M} c_j |b_j\rangle = \sum_{j=1}^{M} (q_j + ip_j)/\sqrt{2\hbar}\,|b_j\rangle, \tag{15}$$

with real q_j and p_j. Coefficients (q_j, p_j) are uniquely defined if and only if the vectors $|b_j\rangle$ form a proper basis. On the other hand, if the resolution of unity (14) is overcomplete, i.e., if some of the $|b_j\rangle$ are not mutually orthogonal, the coefficients (q_j, p_j) satisfying (15) are not unique, but any such set of $2M$ coefficients satisfies the relations

$$\begin{aligned} q_i &= \sum_j q_j \mathrm{Re}\langle b_i|b_j\rangle - p_j \mathrm{Im}\langle b_i|b_j\rangle, \\ p_i &= \sum_j p_j \mathrm{Re}\langle b_i|b_j\rangle + q_j \mathrm{Im}\langle b_i|b_j\rangle. \end{aligned} \tag{16}$$

Obviously, if the basis $\mathcal{B}$ is proper then Eq. (16) are reduced to trivial identities and the explicit expressions for the coefficients are

$$q_j = \mathrm{Re}\langle b_j|\psi\rangle, \quad p_j = \mathrm{Im}\langle b_j|\psi\rangle. \tag{17}$$

However, if the basis is overcomplete the relations are nontrivial and express the nonuniqueness of the expansion (15). The general explicit form of the coefficients in this case is given later in (22).

The coordinate form of the abstract Schrödinger equation (12) or equivalently of the abstract Hamilton equations (11), corresponding to the general set $\mathcal{B}$ satisfying (14), is equivalent

to the set of equations

$$\boldsymbol{G}_{\mathcal{B}}\begin{bmatrix}\dot{\boldsymbol{q}}\\ \dot{\boldsymbol{p}}\end{bmatrix}=\begin{bmatrix}\partial H/\partial \boldsymbol{p}\\ -\partial H/\partial \boldsymbol{q}\end{bmatrix}, \tag{18}$$

where the vectors of coordinates are given by $\boldsymbol{q}=[q_1,\ldots,q_M]^T$ and $\boldsymbol{p}=[p_1,\ldots,p_M]^T$, while $H(\boldsymbol{q},\boldsymbol{p})=\langle\psi_{q,p}|\hat{H}|\psi_{q,p}\rangle$. The Gram matrix of the set $\mathcal{B}$ can be cast into the real form

$$\boldsymbol{G}_{\mathcal{B}}=\begin{bmatrix}\boldsymbol{g} & -\boldsymbol{\pi}\\ \boldsymbol{\pi} & \boldsymbol{g}\end{bmatrix}, \tag{19}$$

where matrices $\boldsymbol{g}$ and $\boldsymbol{\pi}$ have the elements $g_{jk}=\mathrm{Re}\langle b_j|b_k\rangle$ and $\pi_{jk}=\mathrm{Im}\langle b_j|b_k\rangle$, respectively. If $\mathcal{B}$ is a proper basis ($M=N$), then $\boldsymbol{G}_{\mathcal{B}}$ becomes an identity matrix of dimension $2N$ and Eq. (18) assumes the form of the Hamilton equations in a canonical basis

$$\begin{bmatrix}\dot{\boldsymbol{q}}\\ \dot{\boldsymbol{p}}\end{bmatrix}=\begin{bmatrix}\partial H/\partial \boldsymbol{p}\\ -\partial H/\partial \boldsymbol{q}\end{bmatrix}. \tag{20}$$

Consider now the case when the set $\mathcal{B}$ is overcomplete ($M>N$). Due to the overcompleteness of the basis $\mathcal{B}$, there are $M-N$ nontrivial zero-valued complex linear combinations of basis vectors or equivalently $2(M-N)$ real linear combinations

$$\boldsymbol{G}_{\mathcal{B}}\begin{bmatrix}\boldsymbol{x}^{(k)}\\ \boldsymbol{y}^{(k)}\end{bmatrix}=0,\quad \boldsymbol{G}_{\mathcal{B}}\begin{bmatrix}-\boldsymbol{y}^{(k)}\\ \boldsymbol{x}^{(k)}\end{bmatrix}=0,\quad k=1,\ldots,M-N, \tag{21}$$

where $\boldsymbol{x}^{(k)}=[x_1^{(k)},\ldots,x_M^{(k)}]^T$ and $\boldsymbol{y}^{(k)}=[y_1^{(k)},\ldots,y_M^{(k)}]^T$ are $M-N$ independent solutions of (21). Thus, the general form of the (q_j,p_j) coefficients satisfying (15) is

$$\begin{bmatrix}\boldsymbol{q}\\ \boldsymbol{p}\end{bmatrix}=\begin{bmatrix}\mathrm{Re}\langle\boldsymbol{b}|\psi\rangle\\ \mathrm{Im}\langle\boldsymbol{b}|\psi\rangle\end{bmatrix}+\sum_{k=1}^{M-N}\left(a_k\begin{bmatrix}\boldsymbol{x}^{(k)}\\ \boldsymbol{y}^{(k)}\end{bmatrix}+b_k\begin{bmatrix}-\boldsymbol{y}^{(k)}\\ \boldsymbol{x}^{(k)}\end{bmatrix}\right). \tag{22}$$

The matrix $\boldsymbol{G}_{\mathcal{B}}$ is singular and Eq. (18) cannot be cast into the canonical form of Hamiltonian equations. The parameters $\{q_j,p_j\}$ do not form a set of canonical coordinates on $\mathbf{R}^{2N}$. In fact, (18) has the equivalent form

$$\begin{bmatrix}\dot{\boldsymbol{q}}\\ \dot{\boldsymbol{p}}\end{bmatrix}=\boldsymbol{G}_{\mathcal{B}}^{(-1)}\begin{bmatrix}\partial H/\partial \boldsymbol{p}\\ -\partial H/\partial \boldsymbol{q}\end{bmatrix}+\sum_{k=1}^{M-N}\left(\lambda_k\begin{bmatrix}\boldsymbol{x}^{(k)}\\ \boldsymbol{y}^{(k)}\end{bmatrix}+\mu_k\begin{bmatrix}-\boldsymbol{y}^{(k)}\\ \boldsymbol{x}^{(k)}\end{bmatrix}\right), \tag{23}$$

where λ_k and μ_k are arbitrary real numbers and $\boldsymbol{G}_{\mathcal{B}}^{(-1)}$ is the Moore-Penrose pseudoinverse. The terms in (23) under the sum do not influence the evolution of the state $|\psi\rangle$. In anticipation of the Hamiltonian treatment, in the next section the numbers λ_k and μ_k can be considered as corresponding to the gauge degrees of freedom. Fixing their values would give additional $2(M-N)$ constraints and yield one possible solution. For example, the natural gauge could be $\lambda_k=0$ and $\mu_k=0$ for $k=1,\ldots,M-N$.

B. Hamiltonian formulation of the Neumark extension

We shall first briefly recapitulate the Hilbert space formulation of the Neumark extension, introducing the appropriate notation at the same time. It will then be demonstrated that the Hamiltonian description of the relation between the Neumark extension and the original system is in fact given in terms of a reduction of the Hamiltonian systems with primary constraints. i.e., with gauge degrees of freedom.

Let $\{|e_k\rangle\}_{k=1}^N$ be a proper orthonormal basis of $\mathcal{H}^N$. Then one has

$$|b_j\rangle=\sum_{k=1}^{N}\beta_{kj}|e_k\rangle,\quad j=1,\ldots,M, \tag{24}$$

with $\beta_{kj}=\langle e_k|b_j\rangle$. Using (14) we get the relations

$$\sum_{j=1}^{M}\beta_{kj}\beta_{k'j}^{*}=\sum_{j=1}^{M}\langle e_k|b_j\rangle\langle b_j|e_{k'}\rangle=\langle e_k|e_{k'}\rangle=\delta_{k'k}. \tag{25}$$

The relation means that we have a set $\{\boldsymbol{b}_k=[\beta_{k1},\ldots,\beta_{kM}]^T\}_{k=1}^N$ of N orthonormal vectors from $\mathbb{C}^M$. We can choose $M-N$ auxiliary vectors $\{\boldsymbol{b}_{N+1},\ldots,\boldsymbol{b}_M\}$ such that $\{\boldsymbol{b}_k\}_{k=1}^M$ is an orthonormal basis of $\mathbb{C}^M$. Now let us consider an enlarged Hilbert space

$$\mathcal{H}^M=\mathcal{H}^N\oplus\mathcal{H}^{\perp}, \tag{26}$$

where $\mathcal{H}^{\perp}=\mathcal{S}(\{|e_k\rangle\}_{k=N+1}^M)$ with orthonormal auxiliary basis states $\{|e_k\rangle\}_{k=N+1}^M$ and $\mathcal{S}$ denoting the span. The states $\{|B_j\rangle=\sum_{k=1}^M\beta_{kj}|e_k\rangle\}_{j=1}^M$ are also orthonormal. Hence, an arbitrary normalized state $|\Psi\rangle\in\mathcal{H}^M$ has the unique expansion

$$|\Psi\rangle=\sum_{j=1}^{M}(Q_j+iP_j)/\sqrt{2\hbar}\,|B_j\rangle, \tag{27}$$

with real Q_j and P_j that can be regarded as a pair of canonical coordinates on the extended phase space $\mathbf{R}^{2M}$. Define the projector operator by

$$\hat{\Pi}|e_k\rangle=|e_k\rangle,\quad k=1,\ldots,N \tag{28a}$$

$$\hat{\Pi}|e_k\rangle=0,\quad k=N+1,\ldots,M. \tag{28b}$$

This leads to

$$\hat{\Pi}|B_j\rangle=|b_j\rangle \tag{29}$$

and

$$\hat{\Pi}|\Psi\rangle=\sum_{j=1}^{M}(Q_j+iP_j)/\sqrt{2\hbar}\,|b_j\rangle, \tag{30}$$

which is of the same form as (15). In other words, the PVM given by the proper basis $\{|B_j\rangle\}$ in $\mathcal{H}^M$ is the Neumark extension of the POVM given on $\mathcal{H}^N$ by $\{|b_j\rangle\}$).

Strictly speaking, the Neumark theorem is not concerned with the dynamics, i.e., Hamiltonians, on $\mathcal{H}^N$ versus that on $\mathcal{H}^M$. Nevertheless, it is natural to require that $\hat{H}$ on $\mathcal{H}^N$ and the corresponding $\hat{H}_{ex}$ on $\mathcal{H}^M$ satisfy the following condition: All states from $\mathcal{H}^M$ that are projected onto the same state $|\psi(t_0)\rangle$ in $\mathcal{H}^N$ evolve during $t-t_0$ into the states that are all projected onto the same state $|\psi(t)\rangle$. This is the case if

$$\hat{H}_{ex}=\hat{\Pi}^{-1}\hat{H}\hat{\Pi}. \tag{31}$$

In anticipation of the Hamiltonian formulation, expectation values of $\hat{H}_{ex}$ in $|\Psi\rangle$ and $\hat{H}$ in $|\psi\rangle=\hat{\Pi}|\Psi\rangle$ are related

by

$$\begin{aligned} H_{ex}(Q,P) &= \langle \Psi_{Q,P}|\hat{H}_{ex}|\Psi_{Q,P}\rangle \\ &= \sum_{j,j'}(Q_j - iP_j)(Q_{j'} + iP_{j'})\langle B_j|\hat{\Pi}^{-1}\hat{H}\hat{\Pi}|B_{j'}\rangle \\ &= \sum_{j,j'}(Q_j - iP_j)(Q_{j'} + iP_{j'})\langle b_j|\hat{H}|b_{j'}\rangle \\ &= H(Q_j,P_j), \end{aligned} \tag{32}$$

where (Q,P) in $H_{ex}(Q,P)$ and in $H(Q,P)$ are the same numbers but are treated as values of independent coordinates on $\mathbf{R}^{2M}$ or dependent parameters on $\mathbf{R}^{2N}$, respectively.

We now present the phase-space formulation of the Neumark extension. Consider the space $\mathbf{R}^{2M}$ as a symplectic manifold of a Hamiltonian system with the canonical coordinates denoted by $\{(Q_j,P_j); j = 1,2,\ldots,M\}$. The natural conditions $\langle e_k|\Psi(t)\rangle = 0$ for $k = N+1,\ldots,M$ are implemented as constraints on the phase space $\mathbf{R}^{2M}$. Explicitly, the $2(M-N)$ constraints are

$$\phi_k(\boldsymbol{Q},\boldsymbol{P}) \equiv \sum_{j=1}^{M}\left(\beta^R_{kj}Q_j - \beta^I_{kj}P_j\right) = 0, \tag{33a}$$

$$\pi_k(\boldsymbol{Q},\boldsymbol{P}) \equiv \sum_{j=1}^{M}\left(\beta^I_{kj}Q_j + \beta^R_{kj}P_j\right) = 0, \tag{33b}$$

where $\beta^R_{kj} = \mathrm{Re}\beta_{kj}$ and $\beta^I_{kj} = \mathrm{Im}\beta_{kj}$. The constraints satisfy the Poisson brackets

$$\{\phi_k,\pi_{k'}\}_{Q,P} = \mathrm{Re}\sum_{j=1}^{M}\beta^*_{k'j}\beta_{kj} = \delta_{k'k}, \tag{34a}$$

$$\{\phi_k,\phi_{k'}\}_{Q,P} = \{\pi_k,\pi_{k'}\}_{Q,P} = \mathrm{Im}\sum_{j=1}^{M}\beta^*_{k'j}\beta_{kj} = 0. \tag{34b}$$

In the general case of arbitrary constraints, the constrained manifold need not be symplectic and need not support a Hamiltonian system. However, in our case (33), the matrix of Poisson brackets between the constraints (34) is nonsingular, i.e., the constraints are primary, and therefore the manifold determined by the constraints is also symplectic. The symplectic structure on the constrained manifold is given by the Dirac-Poisson bracket on $\mathbf{R}^{2N}$ [19,20],

$$\begin{aligned} \{f_1,f_2\}_{\mathbf{R}^{2N}} = \{f_1,f_2\}_{\mathbf{R}^{2M}} + c\sum_{m,n}^{2(M-N)}\{F_n,f_1\}_{\mathbf{R}^{2M}} \\ \times\{F_m,F_n\}^{-1}_{\mathbf{R}^{2M}}\{F_m,f_2\}_{\mathbf{R}^{2M}}, \end{aligned} \tag{35}$$

where f_1,f_2 are functions on the constrained manifold, the symbols $F_n,F_m,m,n = 1,2,\ldots,2(M-N)$ denote the constraints (33), and the Poisson brackets on the right-hand side are the canonical brackets on $\mathbf{R}^{2M}$. The general formula (35) in the notation (33) assumes the explicit form

$$\{f_1,f_2\}_{\mathbf{R}^{2N}} = \{f_1,f_2\}_{Q,P} - \sum_{k=N+1}^{M}\left(\frac{\partial f_1}{\partial\phi_k}\frac{\partial f_2}{\partial\pi_k} - \frac{\partial f_2}{\partial\phi_k}\frac{\partial f_1}{\partial\pi_k}\right). \tag{36}$$

Consider now the relation between the Hamiltonian function $H(Q,P)$ as a function of the dependent parameters on $\mathbf{R}^{2N}$, i.e., as the Hamiltonian of the system given on $\mathbf{R}^{2N}$, and the Hamiltonian system on $\mathbf{R}^{2M}$ with the Hamiltonian $H(Q,P)$ [where (Q,P) are now independent and canonical on $\mathbf{R}^{2M}$] with imposed constraints (33). In the case of general constraints they can be incorporated into the dynamics using the standard Dirac approach [19,20]. Namely, the total Hamilton function has the form

$$\begin{aligned} H_T &= H + \sum_{k=N+1}^{M}(\phi_k\lambda_k - \pi_k\mu_k), \\ H_T &= H + \sum_{k=N+1}^{M}(\phi_k\{\pi_k,H\}_{Q,P} - \pi_k\{\phi_k,H\}_{Q,P}), \end{aligned} \tag{37}$$

where the appropriate Lagrange multipliers λ_k,μ_k have been determined from the compatibility conditions and using (34). However, if the constraints are such that the constrained manifold is symplectic, as they are in our case, then the general procedure of constructing the Hamiltonian on the constrained manifold can be bypassed. In fact, in this case the Hamiltonian of the system on the constrained manifold is simply obtained as a restriction of the Hamiltonian on $\mathbf{R}^{2M}$ on the constrained manifold $\mathbf{R}^{2N}$. This is precisely the relation between the expectation values of the Hamiltonian operators (32) introduced within the treatment of the Neumark extension.

What has been demonstrated is that the $2M$ real state parameters $\{Q_j,P_j; j = 1,2,\ldots,M\}$ given by the POVM, i.e., by the overcomplete set $\{|b_j\rangle\langle b_j|; j = 1,2,\ldots,2M\}$ in $\mathcal{H}^N$, can be considered as parameters on $\mathbf{R}^{2N}$ or equivalently as canonical coordinates of an extended Hamiltonian system on $\mathbf{R}^{2M}$ with imposed primary constraints. We see that the overcomplete description given by a POVM involves in the Hamiltonian formulation the existence of constraints, i.e., the gauge degrees of freedom, and the corresponding reduction of an extended Hamiltonian system. This is yet another example of the insights into the quantum-mechanical formalism provided by the Hamiltonian formulation.

C. Functions associated with POVMs

In this section we derive several simple but useful formulas.

1. *Functions corresponding to PVMs or POVMs*

As before, $\mathcal{B} = \{|b_k\rangle; k = 1,2,\ldots,M \geqslant N\}$ denotes an arbitrary set of vectors, with the corresponding set of 1D projectors $\{\hat{P}_k = |b_k\rangle\langle b_k|\}$. Using another set $\mathcal{B}' = \{|b'_l\rangle; l = 1,2,\ldots,M' \geqslant N\}$, with the corresponding set $\{\hat{P}_l = |b'_l\rangle\langle b'_l|\}$ that satisfies (14), each of the projectors $|b_k\rangle\langle b_k|$ is associated with a quadratic function of the parameters (q'_l,p'_l) provided by $\mathcal{B}'$. Thus, corresponding to the set $\{\hat{P}_k\}$ is the set of quadratic functions

$$P_k(q',p') = \sum_{lm}^{M'}\pi^k_{lm}(q'_l - ip'_l)(q'_m + ip'_m), \tag{38a}$$

where

$$\pi^k_{lm} = \langle b'_l|\hat{P}_k|b'_m\rangle, \quad k = 1,2,\ldots,M. \tag{38b}$$

It is our goal to obtain explicit conditions that distinguish the sets of coefficients π_{lm}^k in (38), given by $\mathcal{B}$ and $\mathcal{B}'$ representing a PVM and/or a POVM. In this setup, N is the dimension of the Hilbert space, $M \geqslant N$ is the number of vectors in the set $\mathcal{B}$ whose properties such as the resolution of unity and orthogonality are to be studied, and $M' \geqslant N$ is the number of vectors in the complete (or overcomplete) set $\mathcal{B}'$ that is used to associate functions with projectors from the set $\mathcal{B}$.

If the set of functions (38) corresponds to either a PVM or a POVM, an analog of the condition (14) must be satisfied by the coefficients π_{lm}^k. Furthermore, if the set corresponds to a PVM, then the condition of mutual orthogonality of the involved projectors has its analog in terms of the coefficients π_{lm}^k.

2. *Resolution of unity in terms of π_{lm}^k coefficients*

Consider the scalar product $\langle b_l'|b_m'\rangle$ between arbitrary two-vectors from $\mathcal{B}'$. The condition (14) on $\mathcal{B}$ would imply

$$\langle b_l'|b_m'\rangle = \langle b_l'|\sum_k^M \hat{P}_k|b_m'\rangle = \sum_k^M \langle b_l'|\hat{P}_k|b_m'\rangle = \sum_k^M \pi_{lm}^k, \quad l,m = 1,2,\ldots,M'. \tag{39}$$

Thus, if $\mathcal{B}$ is complete, then

$$\sum_k^M \pi_{lm}^k = \langle b_l'|b_m'\rangle, \quad l,m = 1,2,\ldots,M'. \tag{40}$$

Obviously, if the coordinates (q_l', p_l') in the set of functions (38) are associated with an orthogonal (and complete) basis, then

$$\sum_k^M \pi_{lm}^k = \delta_{lm}. \tag{41}$$

It is equally simple to show that if (40) is true, then the set $\mathcal{B}$ satisfies (14). This follows from the equalities in the reverse order of (39) and from the fact that if an operator has all matrix elements between vectors from a complete (or overcomplete) set equal to zero, then it is the zero operator, i.e., it annihilates each vector from the Hilbert space. Thus, the set of functions given by (38) satisfies (40) if and only if the set of projectors $\{\hat{P}_k = |b_k\rangle\langle b_k|; k = 1,2,\ldots,M \geqslant N\}$ generates a resolution of unity (14).

3. *Orthogonality of two projectors in terms of π_{lm}^k coefficients*

The orthogonality of projectors $\hat{P}_k$ and $\hat{P}_{k'}$ is equivalent to

$$\hat{P}_k\hat{P}_{k'} = \delta_{kk'}\hat{P}_{k'}. \tag{42}$$

Using arbitrary set $\mathcal{B}'$ satisfying (14), the condition (42) implies the following conditions on all pairs of coefficients $\pi_{lm}^k, \pi_{lm}^{k'}$:

$$\sum_l^{M'} \pi_{l'l}^k \pi_{ll''}^{k'} = \delta_{kk'}\pi_{ll''}^k, \quad l,l' = 1,2,\ldots,M; \quad k,k' = 1,2,\ldots,M. \tag{43}$$

Observe that the two conditions (43) and (40) are based only on the assumption that $|\psi\rangle = \sum_l^{M'}(q_l' + ip_l')|b_l'\rangle$, which is true since $\mathcal{B}'$ satisfies (14).

The two criteria (43) and (40) taken together imply that the set of functions $\mathcal{P}^k = \sum_{l,m}^{M'} \pi_{lm}^k (q_l' - ip_l')(q_m' + ip_m')$, $k = 1,2,\ldots,M$, represents a PVM if all pairs $\pi_{lm}^{k_1}, \pi_{lm}^{k_2}$ $(k_1,k_2 = 1,2,\ldots,M)$ correspond to orthogonal projectors, i.e., satisfy (43), and if the condition (40) is satisfied. If only the condition (40) is satisfied but there is a pair of π^{k_1}, π^{k_2} violating (43), then the set of functions corresponds to a POVM. Furthermore, the parameters appearing as the arguments in the considered functions are canonical, i.e., the basis is proper orthonormal if (41) is satisfied.

Let us also briefly discuss the notion of orthogonality of the quadratic functions representing observables in a proper basis. Consider two operators $\hat{A}_1$ and $\hat{A}_2$. The operators are orthogonal if

$$\mathrm{Tr}[\hat{A}_1\hat{A}_2] = 0. \tag{44}$$

In terms of the coefficients π_{ij}^k in the quadratic functions corresponding to $\hat{A}_1, \hat{A}_2$ the previous condition is written as

$$\mathrm{Tr}[\hat{A}_1\hat{A}_2] = \sum_i^N \langle a_i|\hat{A}_1\hat{A}_2|a_i\rangle = \sum_{ii'}^N \langle a_i|\hat{A}_1|a_i'\rangle\langle a_i'|\hat{A}_2|a_i\rangle = \sum_{i,i'}^N \pi_{ii'}^1\pi_{i'i}^2 = 0. \tag{45}$$

Thus, it makes sense to call two quadratic functions of the form (9) orthogonal if

$$\sum_{ij}^N \pi_{ij}^1\pi_{ji}^2 = 0. \tag{46}$$

The condition (46) supplies us with the notion of orthogonality between two quadratic functions solely in terms of these functions, with no reference to the analogous Hilbert space formulation.

An alternative criterion for orthogonality of two 1D projectors in terms of the associated quadratic function, i.e., in terms of π_{ij}^1, π_{ij}^2, is obtained from the fact that orthogonal 1D projectors commute and the relation (10). In fact,

$$\begin{aligned}\langle[\hat{P}_\mu,\hat{P}_\nu]\rangle &= \delta_{\mu,\nu} = i\{P_\mu,P_\nu\} \\ &= i\sum_{ij}\langle a_k|e_\mu\rangle\langle e_\mu|a_l\rangle\langle a_k|e_\nu\rangle\langle e_\nu|a_l\rangle \\ &\quad\times[-i\{p_i,q_j\} - i\{q_i,p_j\}] \\ &= 2\sum_k \pi_{ii}^\mu\pi_{ii}^\nu.\end{aligned} \tag{47}$$

If the two 1D projectors are orthogonal, the sum of the products of the diagonal coefficients in the corresponding quadratic functions is zero.

4. Relations between functions representing an operator given by PVMs or by POVMs

A Hermitian operator can be defined using a proper basis $|e_i\rangle$, $i = 1,2,\ldots,N$, or an overcomplete basis $|b_l\rangle$, $l = 1,2,\ldots,M$. Similarly, the operator can be represented as a quadratic function of $2N$ canonical variables (q,p) using the proper basis or as a quadratic function of the $2M$ noncanonical parameters (Q,P). Relations between different representations are given by the simple formula

$$\pi_{lm} = \sum_{ij} a_{ij}\langle b_l|e_i\rangle\langle e_j|b_m\rangle, \tag{48}$$

where π_{lm} $(l,m = 1,2,\ldots,M)$ and a_{ij} $(i,j = 1,2,\ldots,N)$ are the coefficients in representations given by the overcomplete and the proper orthogonal basis, respectively.

The inverse relation expressing a_{ij} $(i,j = 1,2,\ldots,N)$ in terms of π_{lm} $(l,m = 1,2,\ldots,M)$ reads

$$a_{ij} = \sum_{lm} \pi_{lm}\langle e_i|b_l\rangle\langle b_m|e_j\rangle. \tag{49}$$

In formulas (48) and (49) the Hermitian scalar product could be replaced by the combination of the Riemannian scalar product and the symplectic skew product, expressing the relations entirely in terms of objects appearing in the Hamiltonian formulation. However, the corresponding transformations are not canonical.

IV. RELEVANT EXAMPLE: THE PHASE

The phase of quantum motion is an observable physical quantity that is naturally expressed using an appropriate POVM (see [21] and references therein). For our purpose it is enough to discuss the phase POVM in the case of the simplest quantum systems with finite Hilbert spaces and with a nondegenerate energy spectrum. In this section we first illustrate the construction of the relevant nonorthogonal basis and the POVM in the Hilbert space formulation. We then present the corresponding Neumark extension. The Hilbert space analysis will be followed by the corresponding Hamiltonian treatment.

A. Phase POVMs and the Neumark extension

Consider an N_1-dimensional Hilbert space $\mathcal{H}_1$ with an arbitrary proper basis denoted by $|n\rangle_1$, $n = 1,2,\ldots,N_1$. With this basis one associates an infinite set of vectors parametrized by an angle $\varphi \in [0,2\pi)$ defined as

$$|\varphi\rangle_1 = \frac{1}{\sqrt{2\pi}}\sum_{n=1}^{N} e^{ik_n\varphi}|n\rangle_1, \quad \varphi \in [0,2\pi), \tag{50}$$

where $k_n \in \mathbf{Z}$ are integers. In the general construction presented here these integers are arbitrary. However, if the constructed POVM is to correspond to the phase, then the integers are to be precisely the nondegenerate and discrete energy eigenvalues of the considered system.

A collection of operators defined as

$$\hat{\Theta}_1(\varphi_1,\varphi_2) = \int_{\varphi_1}^{\varphi_2} \hat{\mathcal{P}}_1(\varphi)d\varphi \tag{51}$$

and

$$\hat{\mathcal{P}}_1(\varphi) \equiv |\varphi\rangle_{11}\langle\varphi| = \frac{1}{2\pi}\sum_{n=1}^{N}\sum_{m=1}^{N} e^{i(k_n-k_m)\varphi}|n\rangle_{11}\langle m| \tag{52}$$

forms a resolution of unity, i.e.,

$$\hat{\Theta}_1(0,2\pi) = \hat{I}, \tag{53}$$

but the operators associated with disjoined subsets of $\varphi \in [0,2\pi)$ are not orthogonal. Thus the collection (52) forms a POVM. As pointed out, if the integers k_n coincide with the energy eigenvalues, the collection of operators (51) satisfies the so-called covariance condition

$$\exp -ia\hat{H}\,\hat{\Theta}_1(\varphi_1,\varphi_2)\exp ia\hat{H} = \hat{\Theta}_1((\varphi_1+a)\mathrm{mod}2\pi,(\varphi_2+a)\mathrm{mod}2\pi). \tag{54}$$

This fact justifies the association of the POVM (52) with the data corresponding to the phase of the quantum motion.

In order to formulate the Neumark extension of the phase POVM one needs an appropriate Hilbert space $\mathcal{H}_2$ with dimension $N_2 > N_1$ and a projector-valued measure $\mathcal{P}_2(\varphi)$ with projectors onto orthogonal subspaces of $\mathcal{H}_2$ associated with disjoined intervals. Then the theorem claims that there is a projector $P_{2\to1}$ from $\mathcal{H}_1$ onto $\mathcal{H}_2$ such that $P_{2\to1}\hat{\Theta}_2 P_{2\to1}$ is isomorphic to $\hat{\Theta}_1$.

For the case of the POVM given by (52) the Hilbert space $\mathcal{H}_2$, the PVM $\hat{\mathcal{P}}_2$, and the projector $P_{2\to1}$ are given as follows. The Hilbert space $\mathcal{H}_2$ is in fact the complex vector space of square integrable functions on the interval $(0,2\pi)$. The coordinate representation is determined by generalized vectors $|\varphi\rangle_2$ and ${}_2\langle\varphi|\varphi'\rangle_2 = \delta(\varphi-\varphi')$ and a proper basis $|k\rangle_2$ is given by

$${}_2\langle\varphi|k\rangle_2 \equiv \psi_k(\varphi) = \frac{1}{\sqrt{2\pi}}e^{-ik\varphi}, \quad k \in \mathbf{Z}. \tag{55}$$

The proper basis with orthogonal generalized vectors

$$|\varphi\rangle_2 = \frac{1}{\sqrt{2\pi}}\sum_{k=-\infty}^{+\infty} e^{ik\varphi}|k\rangle_2 \tag{56}$$

is used to define the PVMs

$$\hat{\Theta}_2(a,b) = \int_b^b \hat{\mathcal{P}}_2 d\varphi, \tag{57}$$

$$\hat{\mathcal{P}}_2(\varphi) = |\varphi\rangle_{22}\langle\varphi| = \frac{1}{2\pi}\sum_{k=-\infty}^{+\infty}\sum_{k'=-\infty}^{+\infty} e^{i(k-k')\varphi}|k\rangle_{22}\langle k'|. \tag{58}$$

The relevant projector $P_{2\to1}$ is defined as

$$\hat{P}_{2\to1} = |q_1\rangle_{22}\langle q_1| + |q_2\rangle_{22}\langle q_2| + \cdots + |q_N\rangle_{22}\langle q_N|, \tag{59}$$

where $|q_i\rangle_2$ are vectors (56) with $k = |q_i\rangle$. It follows that

$$\hat{P}_{2\to1}\hat{\mathcal{P}}_2(\varphi)\hat{P}_{2\to1} = \hat{P}_{2\to1}|\varphi\rangle_{22}\langle\varphi|\hat{P}_{2\to1} = \frac{1}{2\pi}\sum_{i=1}^{N}\sum_{i'=1}^{N} e^{i(q_i-q_{i'})\varphi}|q_i\rangle_{22}\langle q_{i'}|, \tag{60}$$

which is isomorphic to the measure $\hat{\mathcal{P}}_1(\varphi)$. This is the Neumark theorem for the POVM given by (52).

B. The phase in the Hamiltonian formulation

The Hamiltonian formulation of the original quantum system on the finite-dimensional Hilbert space $\mathcal{H}_1$ is given on the finite even-dimensional phase space $\mathcal{M}_1$. The Neumark extension involves a Hamiltonian system on an infinite-dimensional symplectic manifold $\mathcal{M}_2$, which is a direct sum of two real vector spaces of square integrable functions on $[0,2\pi)$.

The phase POVM involves an overcomplete set of vectors $\{|\varphi\rangle\}$ indexed by the continuous index $\varphi \in [0,2\pi)$. Consequently, the expansion of an arbitrary $|\psi\rangle \in \mathbf{C}^N$,

$$|\psi\rangle = \int d\varphi[q(\psi;\varphi) + ip(\psi;\varphi)]|\varphi\rangle, \tag{61}$$

generates functional parameters $[q(\psi;\varphi), p(\psi;\varphi)]$ of points $\psi \in \mathbf{C}^N$. On the other hand, the proper energy basis $\{|n\rangle_1\}$ (with eigenvalues $k_n \neq k_{n'}, n \neq n'$) generates, via

$$|\psi\rangle = \sum_n^N [q_n(\psi) + ip_n(\psi)]|n\rangle_1, \tag{62}$$

$2N$ canonical coordinates $\{q_n(\psi), p_n(\psi)\}$ of a point ψ indexed by discrete and finite n. All relevant formulas from Sec. III involve either of the expressions

$$\langle\varphi_1|\varphi_2\rangle = \frac{1}{2\pi}\sum_n^N \exp ik_n(\varphi_2 - \varphi_1) \tag{63}$$

or

$$\langle n|\varphi\rangle = \frac{1}{\sqrt{2\pi}}\exp ik_n\varphi \tag{64}$$

and the real and the imaginary parts thereof. For example, the arbitrary vector $|\Psi\rangle_2$ from $\mathcal{H}_2$ is expended as

$$|\Psi\rangle_2 = \int_0^{2\pi} d\varphi[Q(\varphi) + iP(\varphi)]|\varphi\rangle_2, \tag{65}$$

where the conditions $\langle e_l|\Psi\rangle_2 = 0$, $l \neq k_n$, and $n = 1,\ldots,N$ obtain the explicit form

$$\int_0^{2\pi} d\varphi[Q(\varphi) + iP(\varphi)]\langle e_l|\varphi\rangle_2 = \int_0^{2\pi} d\varphi[Q(\varphi) + iP(\varphi)]\frac{1}{\sqrt{2\pi}}e^{il\varphi} = 0. \tag{66}$$

The functions $Q(\varphi), P(\varphi)$ are the canonical coordinates on $\mathcal{M}_2$. The constraints (33) are explicitly given by

$$\begin{aligned}\phi_l(Q(\varphi),P(\varphi)) &= \frac{1}{\sqrt{2\pi}}\int_0^{2\pi} d\varphi[\cos(l\varphi)Q(\varphi) - \sin(l\varphi)P(\varphi)] = 0,\\ \pi_l(Q(\varphi),P(\varphi)) &= \frac{1}{\sqrt{2\pi}}\int_0^{2\pi} d\varphi[\sin(l\varphi)Q(\varphi) + \cos(l\varphi)P(\varphi)] = 0.\end{aligned} \tag{67}$$

Variational derivatives of the constraints read

$$\begin{aligned}\frac{\delta\phi_l}{\delta Q} &= \frac{1}{\sqrt{2\pi}}\cos(l\varphi), \quad \frac{\delta\phi_l}{\delta P} = -\frac{1}{\sqrt{2\pi}}\sin(l\varphi),\\ \frac{\delta\pi_l}{\delta Q} &= \frac{1}{\sqrt{2\pi}}\sin(l\varphi), \quad \frac{\delta\pi_l}{\delta P} = \frac{1}{\sqrt{2\pi}}\cos(l\varphi).\end{aligned} \tag{68}$$

Poisson brackets between the constraints are, as in the general case (34),

$$\begin{aligned}\{\phi_l,\pi_{l'}\}_{Q,P} &= \int_0^{2\pi} d\varphi\left(\frac{\delta\phi_l}{\delta Q}\frac{\delta\pi_{l'}}{\delta P} - \frac{\delta\phi_l}{\delta P}\frac{\delta\pi_{l'}}{\delta Q}\right)\\ &= \frac{1}{2\pi}\int_0^{2\pi} d\varphi[\cos(l\varphi)\cos(l'\varphi)\\ &\quad + \sin(l\varphi)\sin(l'\varphi)] = \delta_{ll'},\\ \{\phi_l,\phi_{l'}\}_{Q,P} &= \frac{1}{2\pi}\int_0^{2\pi} d\varphi[-\cos(l\varphi)\sin(l'\varphi)\\ &\quad + \sin(l\varphi)\cos(l'\varphi)] = 0,\\ \{\pi_l,\pi_{l'}\}_{Q,P} &= \frac{1}{2\pi}\int_0^{2\pi} d\varphi[\sin(l\varphi)\cos(l'\varphi)\\ &\quad - \cos(l\varphi)\sin(l'\varphi)] = 0.\end{aligned} \tag{69}$$

The functions $\Theta_2^{(a,b)}(Q,P)$ of the canonical (Q,P) corresponding to the PVM $\hat{\Theta}_2(a,b)$ is given, after some computation, by the simple expression

$$\begin{aligned}\Theta_2^{(a,b)}(Q,P) &= {}_2\langle\Psi|\int_a^b d\varphi|\varphi\rangle_{22}\langle\varphi|\Psi\rangle_2\\ &= \int_a^b d\varphi[Q^2(\varphi) + P^2(\varphi)],\end{aligned} \tag{70}$$

which is as expected for the coordinates corresponding to the eigenbases of $\hat{\Theta}_2$. The functions corresponding to the POVM $\hat{\Theta}_1(a,b)$ in the original space are by definition

$$P_1^{(a,b)}(Q,P) = {}_1\langle\Psi|\int_a^b d\varphi|\varphi\rangle_{11}\langle\varphi|\Psi\rangle_1. \tag{71}$$

Due to nonorthogonality of the vectors $|\varphi\rangle_1$, this expression cannot be significantly simplified. The explicit expression reads

$$P_1^{(a,b)}(Q,P) = \int_0^{2\pi} d\varphi\int_0^{2\pi} d\varphi''[Q(\varphi) - iP(\varphi)] \times [Q(\varphi'') + iP(\varphi'')]\int_a^b d\varphi'\,{}_1\langle\varphi|\varphi'\rangle_{11}\langle\varphi'|\varphi''\rangle_1,$$

where

$${}_1\langle\varphi|\varphi'\rangle_{11}\langle\varphi'|\varphi''\rangle_1 = \frac{1}{2\pi}\sum_{n=1}^N e^{ik_n(\varphi'-\varphi)}\frac{1}{2\pi}\sum_{m=1}^N e^{ik_m(\varphi''-\varphi')}.$$

This expression results also from explicit substitution of the constraints (67) satisfied by (Q,P) into the expression (70).

V. SUMMARY

We have studied several questions related to the description and interpretation of POVMs in the Hamiltonian formulation

of quantum mechanics. The topic is important from the point of view that considers the Hamiltonian formulation as independent and equivalent to the Hilbert space formulation, because the POVMs appear as a description of important quantum mechanical concepts, originally represented mathematically within the Hilbert space formulation. In particular, the POVMs appear in the treatment of approximate and indirect measurements and in the description of joint measurement of conjugate variables. Furthermore, a physically justified definition of certain observables requires the corresponding POVMs instead of standard representation via PVMs. As pointed out, if the Hamiltonian formulation is to be considered as a viable alternative approach to the mathematical formulation of quantum mechanics, it is important to analyze properties of representatives of the POVMs within the Hamiltonian approach.

In particular we have studied the properties of the sets of state coordinates corresponding in the Hamiltonian formulation to an overcomplete basis in the Hilbert space formulation. Coordinates in such a set are dependent and the relations can be treated as constraints on the Hamiltonian formulation in a larger phase space. We have demonstrated that the Hamiltonian treatment of systems with linear primary constraints corresponds to the Neumark extension and reduction. We have also provided the criteria that distinguish between objects representing POVMs from those of PVMs entirely within the Hamiltonian formulation. Finally, these abstract considerations have been illustrated using the example of a POVM corresponding to the phase of quantum motion. The Hilbert space formulation of the phase POVM and the corresponding Neumark extension was described first and then the corresponding Hamiltonian description was provided.

ACKNOWLEDGMENTS

This work was supported in part by the Ministry of Education and Science of the Republic of Serbia under Contracts No. 171006, No. 171017, No. 171020, No. 171038, and No. 45016 and by COST (Action No. MP1006).

[1] A. Aschtekar and T. A. Schilling, in *On Einstein's Path*, edited by A. Harvey (Springer, Berlin, 1998).
[2] D. C. Brody and L. P. Hughston, J. Geom. Phys. **38**, 19 (2001).
[3] E. Ercolessi, G. Marmo, and G. Morandi, Riv. Nuovo Cimento **33**, 401 (2010).
[4] P. Bona, Acta Phys. Slovaca **50**, 1 (2000).
[5] N. Burić, Ann. Phys. (N.Y.) **323**, 17 (2008).
[6] D. C. Brody, A. C. T. Gustavsson, and L. Hughston, J. Phys. A **41**, 475301 (2008).
[7] M. Radonjić, S. Prvanović, and N. Burić, Phys. Rev. A **84**, 022103 (2011).
[8] M. Radonjić, S. Prvanović, and N. Burić, Phys. Rev. A **85**, 022117 (2012).
[9] H.-T. Elze, Phys. Rev. A **85**, 052109 (2012).
[10] N. Burić, D. B. Popović, M. Radonjić, and S. Prvanović, Found. Phys. **43**, 1459 (2013).
[11] N. Burić, I. Mendaš, D. B. Popović, M. Radonjić, and S. Prvanović, Phys. Rev. A **86**, 034104 (2012).
[12] N. Burić, D. B. Popović, M. Radonjić, and S. Prvanović, Ann. Phys. (N.Y.) **343**, 1 (2014).
[13] A. S. Holevo, *Probabilistic and Statistical Aspects of Quantum Theory* (North-Holland, Amsterdam, 1982).
[14] P. Busch, M. Grabowski, and P. J. Lahti, *Operational Quantum Physics*, 2nd ed. (Springer, Berlin, 1997).
[15] A. Peres, *Quantum Theory: Concepts and Methods* (Kluwer, New York, 1993).
[16] V. I. Arnold, *Mathematical Methods of Classical Mechanics* (Springer, New York, 1978).
[17] E. B. Davies, IEEE Trans. Inform. Theory **24**, 596 (1978).
[18] M. A. Neumark, Izv. Akad. Nauk SSSR **53**, 277 (1940); C. R. Dokl. Acad. Sci. URSS **41**, 359 (1943).
[19] P. A. M. Dirac, Can. J. Math. **2**, 129 (1950).
[20] V. I. Arnold, V. V. Kozlov, and A. I. Neisthadt, *Dynamical Systems III* (Springer, Berlin, 1988).
[21] D. Arsenović, N. Burić, D. Davidović, and S. Prvanović, Phys. Rev. A **88**, 022117 (2013).

Raman–Ramsey electromagnetically induced transparency in the configuration of counterpropagating pump and probe in vacuum Rb cell

Ivan S. Radojičić,* Milan Radonjić, Marina M. Lekić, Zoran D. Grujić, Dragan Lukić, and Branislav Jelenković

Institute of Physics, University of Belgrade, Pregrevica 118, 11080 Belgrade, Serbia
**Corresponding author: ivan.radojicic@ipb.ac.rs*

Received November 19, 2014; revised January 22, 2015; accepted January 22, 2015;
posted January 22, 2015 (Doc. ID 226841); published February 13, 2015

Counterpropagating, spatially separated hollow pump and coaxial probe laser beams generate narrow Zeeman electromagnetically induced transparency (EIT) resonances in the vacuum Rb cell. The lasers are locked to D_2 line transition $F_g = 2 \rightarrow F_e = 1$ of ^{87}Rb. For the probe laser beam intensity between 0.1 and 3.0 mW/cm^2 this Ramsey-type configuration yields dual-structured resonances having a narrow peak on top of a broader pedestal. Linewidths of the narrow peak are nearly independent of the probe laser beam intensity and of the probe diameter (for diameters 0.8 and 2.7 mm), provided that the dark region between the pump and the probe beams is fixed. At the probe laser beam intensities below 0.1 mW/cm^2 Zeeman EIT is a single narrow resonance. With this geometry of laser beams, and at low probe intensity, the presence of the pump enables the probe EIT, i.e., the probe transmission becomes enhanced in a narrow spectral window. Accompanying theoretical model showed good quantitative agreement with the measurements.

OCIS codes: (270.1670) Coherent optical effects; (300.3700) Linewidth.
http://dx.doi.org/10.1364/JOSAB.32.000426

1. INTRODUCTION

Electromagnetically induced transparency (EIT) is a laser(s) transmission peak due to coherences between atomic levels induced by the same laser(s) whose transmission is monitored [1]. EIT as a quantum phenomenon has its classical analog [2]. In a typical interaction scheme, two lasers couple two hyperfine levels (hyperfine coherence) or Zeeman sublelevels (Zeeman coherence) with the common excited-state hyperfine level. Hyperfine (Zeeman) level (sublevels) are long lived and degeneracy of the ground-state angular momentum is larger or equal to that of the excited state. Alkali atoms with two long-lived hyperfine levels in the ground state, and optical transitions to excited-state hyperfine level in a suitable wavelength region are most often used in EIT experiments. Quantum EIT, the subject of this investigation, is a manifestation of the coherent superposition of Zeeman sublevels of the ground hyperfine level due to interactions with the laser field. Superposition called dark state [3–5] is decoupled from the interaction and presents foundation of EIT. EIT has gained considerable interest because of nonlinear response and steep dispersion around the atomic resonance at reduced absorption.

A method analog to the Ramsey method of separated oscillatory fields [6] can be utilized for narrowing dark resonances in alkali atoms using thermal atomic beam [7–9] or atoms contained in vacuum glass cells, by spatially separating pump and probe beams [10,11]. Ramsey-like mechanisms yield very narrow EIT resonances in alkali-metal vapor cells with buffer gas (or with antirelaxation wall coating), even with a single laser beam [12,13].

In experiments with vacuum gas cells it is necessary to apply a particular geometry of a hollow pump and a narrow coaxial probe in order to see narrow fringes on the probe EIT [14], or to implement a multizone spectroscopy like in [15]. Instead of spatially separating continuous wave pump and probe, pulses of the pump and probe were used in a Ramsey-like method for narrowing EIT by switching the laser beams on and off. Hyperfine EIT produced in the double Λ scheme with the pump and the weak probe pulse have produced high contrast, very narrow fringes ($\approx$100 Hz) in the probe EIT in Cs buffer gas cell [16,17].

In this work we use counterpropagating pump and probe beams to study Ramsey effect on linewidths and amplitudes of the probe Zeeman EIT in Rb vacuum cell. Zeeman coherences are generated in the $F_g = 2$ hyperfine level of the ground state of ^{87}Rb by the pump beam, made in the form of a hollow cylinder. The atomic coherence is carried by the atomic thermal motion to a small-diameter probe beam that passes through the center of the hollow pump laser. There is dark region between the pump and probe beam, which we keep constant in the study. This counterpropagating geometry allows EIT with much weaker probe intensity as opposed to the copropagating pump and probe [14] due to reduced multiple scattering of pump light into the direction of the probe and toward the photodetector. Therefore in this work we cover much lower probe laser beam intensities than in [14]. Also, differently than in [14], here we investigate EIT line shapes for D_2 line of ^{87}Rb. We examine how different probe diameters, for the same dark region, change the shape

of the dual-structured probe EIT resonances having a narrower central peak (due to atomic coherence coming from the pump) and a wider pedestal (due to probe beam influence). The dependence of narrow resonances as a function of the probe laser beam intensity and diameter is studied. Experimental results are compared with the detailed theoretical model based on time-dependent optical Bloch equations (OBEs). We determine the range of the probe intensity when Zeeman EIT has only narrow structure, i.e., the transmission of the probe beam becomes enhanced when the pump is turned on. EIT resonances in vacuum cells, even with the Ramsey method, are wider than EIT in buffer gas cells. However, there is an interest for narrow EIT in vacuum cells at room temperature because atomic collisions, and temperature fluctuations are reduced, which is important for EIT applications.

2. EXPERIMENTAL SETUP

The schematic of the experiment, given in Fig. 1, describes the geometry of laser beams we have used to investigate effects of spatially separating the probe and pump beam on the EIT line shapes. A large-diameter hollow pump beam and narrow coaxial probe beam counterpropagate through the Rb cell. The two beams are generated from the same external cavity diode laser (ECDL). Employing counterpropagating probe and pump beams requires precise laser frequency tuning to the optical transition; otherwise the probe and pump will not be able to interact with the same atoms (atomic velocity is not expected to change in the region between the pump and probe). The laser is locked using the Doppler free dichroic atomic laser lock (DDAVLL) technique [18] on D_2 line transition $F_g = 2 \rightarrow F_e = 1$ of ^{87}Rb, and is linearly polarized. The vacuum Rb cell, 85 mm long and of 25 mm in diameter, is kept at room temperature. The Rb cell is inside cylindrical solenoid that provides longitudinal magnetic field. The triple layers of μ-metal, around the cell, minimize effects of stray magnetic fields. In the experiment we measure the probe transmission as a function of the external magnetic field. Pump intensity is 11.5 mW/cm^2 and the probe intensity varies from 0.1 to 3.0 mW/cm^2.

We have measured Zeeman EIT by sweeping the magnetic field for two probe $1/e^2$ diameters, 2.7 and 0.8 mm. The pump beam inner diameter is changed from 5 to 7 mm when the probe diameter is changed from 0.8 to 2.7 mm, respectively.

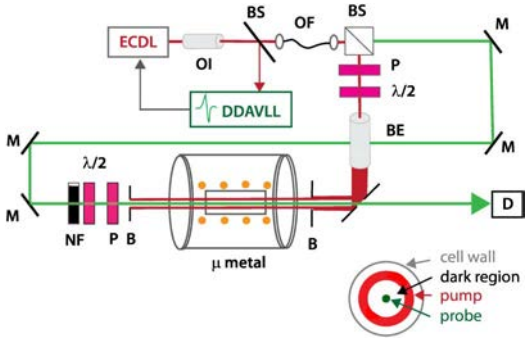

Fig. 1. Experimental setup: ECDL, external cavity diode laser; OI, optical isolator; DDAVLL, Doppler free dichroic atomic laser lock; BS, beam splitter; OF, optical fiber; M, mirrors; P, polarizer; NF, variable neutral density filter; BE, beam expander; $\lambda/2$, retardation plate; B, blade iris diaphragm; D, photodetector.

Thus, the distance between pump and the probe, or "dark region," is the same and equals 2.1 mm.

3. THEORY

The model is similar to one described in more detail in [19]. The difference stems from the fact that in this case the pump and probe are counterpropagating. The evolution of Rb atoms interacting with spatially separated pump and probe laser beams is described using time-dependent OBEs for the atomic density matrix

$$\frac{d\hat{\rho}}{dt} = -\frac{i}{\hbar}[\hat{H}_{\text{atom}}(B) + \hat{H}_{\text{int}}(t), \hat{\rho}] + \left(\frac{d\hat{\rho}}{dt}\right)_{\text{SE}} + \left(\frac{d\hat{\rho}}{dt}\right)_{\text{relax}}, \quad (1)$$

where

$$\hat{H}_{\text{atom}}(B) = \sum_j \hbar\omega_j(B)|g_j\rangle\langle g_j| + \sum_k \hbar\omega_k(B)|e_k\rangle\langle e_k| \quad (2)$$

is the Hamiltonian of an atom in the external magnetic field **B**, aligned with the laser beam propagation direction. Zeeman-shifted energies $\hbar\omega_j(B)$ ($\hbar\omega_k(B)$) correspond to ground (excited) states $|g_j\rangle$ ($|e_k\rangle$). The interaction of an atom with laser is treated in dipole approximation

$$\hat{H}_{\text{int}}(t) = -\sum_{j,k} \mathbf{E}(t)\cdot\mathbf{d}_{jk}(|g_j\rangle\langle e_k| + |e_k\rangle\langle g_j|), \quad (3)$$

where $\mathbf{E}(t)$ is the laser electric field (in the atomic reference frame) and $\mathbf{d}_{jk}$ is the atomic electric dipole moment for the transition between states $|g_j\rangle$ and $|e_k\rangle$. Spontaneous emission is given by

$$\left(\frac{d\hat{\rho}}{dt}\right)_{\text{SE}} = \sum_m 2\hat{\Gamma}_m\hat{\rho}\hat{\Gamma}_m^\dagger - \hat{\Gamma}_m^\dagger\hat{\Gamma}_m\hat{\rho} - \hat{\rho}\hat{\Gamma}_m^\dagger\hat{\Gamma}_m, \quad (4)$$

where $\hat{\Gamma}_m$ are Lindblad operators related to dipole transitions from the excited- to ground-state manifold. In order to obtain good agreement with experimental line shapes, and in addition to [19], we include relaxation of ground-state populations toward the equilibrium

$$\left(\frac{d\hat{\rho}}{dt}\right)_{\text{relax}} = -\gamma\sum_j\left(\rho_{g_j,g_j} - \frac{1-\pi_e}{8}\right)|g_j\rangle\langle g_j|, \quad (5)$$

where π_e is the total excited-state population. When considering D_2 line transition $F_g = 2 \rightarrow F_e = 1$, the excited hyperfine levels $F_e = 2$ and $F_e = 3$ are also populated due to the Doppler broadening and therefore have to be taken into account. Equations for $F_g = 1$ ground-level density matrix elements are disregarded since that level is not laser-coupled. OBEs are numerically integrated for a collection of atoms passing through the laser beams at different trajectories with velocities sampling Maxwell–Boltzmann distribution. The cylindrical symmetric atomic ensemble density matrix is obtained after averaging over velocities and suitable angular integration. This enables the calculation of atomic vapor polarization, the laser electric field after propagation through the Rb cell and, eventually, Zeeman EIT resonances. Additional details can be found in [20,21].

Pump and probe laser beams have linear polarization and the same frequency. Their propagation directions are

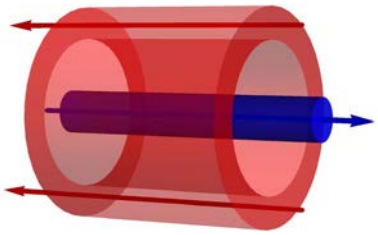

Fig. 2. Radial profiles of counterpropagating hollow pump and coaxial probe laser beams used in the theoretical model.

opposite. As schematically presented in Fig. 2, the probe laser beam passes coaxially through the center of the hollow pump beam. The probe beam profile along radial distance r at the Rb cell entrance is modeled by a Gaussian,

$$I_{\text{probe}}(r) = 2\bar{I}_{\text{probe}} \exp(-2r^2/r_0^2), \tag{6}$$

where r_0 is $1/e^2$ the radius of the probe beam and $\bar{I}_{\text{probe}}$ is the probe beam intensity (total probe power divided by $r_0^2\pi$). The pump beam radial intensity profile is taken to be the same along the cell length and ring-shaped:

$$I_{\text{pump}}(r) = \bar{I}_{\text{pump}} a(\text{erf}(p(r - r_1)) - \text{erf}(p(r - r_2))), \tag{7}$$

where $\bar{I}_{\text{pump}}$ is the pump beam intensity and a is the normalization constant. Parameter p controls the steepness of the profile near the beam inner and outer edge that are determined by the parameters r_1 and r_2, respectively.

4. RESULTS AND DISCUSSION

We show results of interactions of the probe beam with atoms prepared in the dark state by the spatially separated pump beam. Both the pump and probe have linear and mutually parallel polarizations. Sweep of the magnetic field provides detuning of two circular components from the two photon resonance among Zeeman sublevels for which $\Delta m_F = 2$. In the following we present EIT line shapes, amplitudes, and linewidths obtained by measuring the probe transmission at different magnetic fields. In this work we are not concerned with absolute values of the probe transmission. Therefore, we present EIT line shapes normalized such that maximal transmission is set to unity.

Figure 3(a) shows measured and Fig. 3(b) calculated Zeeman EIT resonances for two probe laser beam intensities, 0.2 mW/cm^2 (upper rows) and 1.4 mW/cm^2 (lower rows), and two probe laser beam diameters, 0.8 mm (left column) and 2.7 mm (right column). EIT line shapes for both laser beam intensities have dual structure, a narrow peak with fringes appearing on top of a broader pedestal. A broader pedestal is generated by the probe itself, while narrow peak and fringes result from Ramsey interference. Ramsey fringes are well pronounced for the narrower probe beam because of the shorter interaction time of Rb atoms with the probe light, i.e., smaller probe influence. When the probe laser beam intensity is increased, or its diameter is increased, the Ramsey fringes lose their visibility. Theoretical results in Fig. 3(b) are in quite good agreement with the experiment.

EIT widths and amplitudes of the narrow and wide structures are obtained after resolving the two structures in EIT line shapes. Figure 4 presents widths of the narrow structure

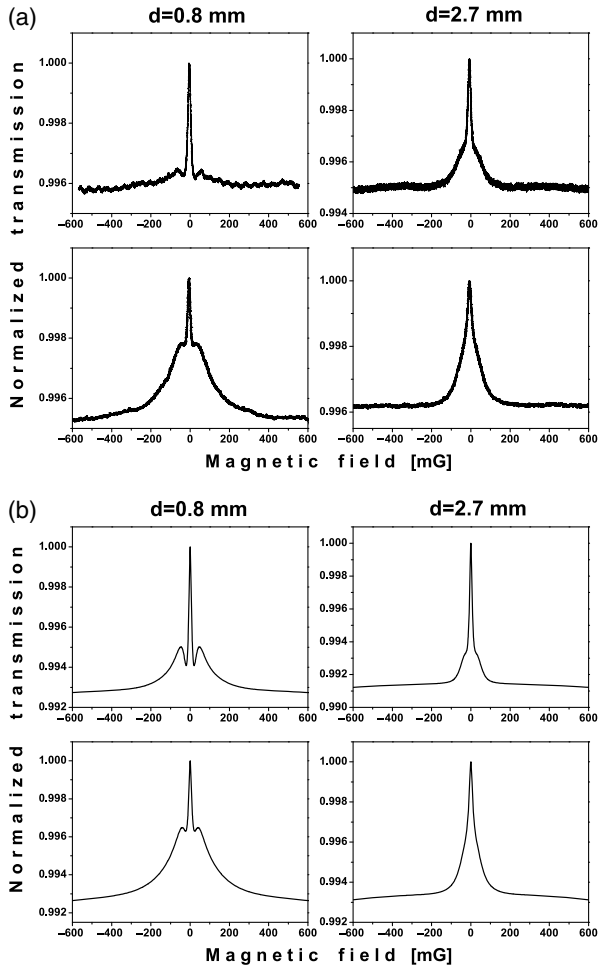

Fig. 3. (a) Experimental and (b) theoretical Zeeman EIT at D_2 line, for two probe laser beam intensities, 0.2 mW/cm^2 (upper rows) and 1.4 mW/cm^2 (lower rows), and two probe laser beam diameters, 0.8 mm (left column) and 2.7 mm (right column).

of EIT resonances, for two probe laser beam diameters. Experimental results are in Fig. 4(a), and theoretical in Fig. 4(b). The linewidth of the narrow structure in our experiment is ≈15 mG or ≈18 kHz. This is similar to the narrowest EIT obtained in vacuum alkali gas cells with multizone Ramsey technique [15]. As seen from Fig. 4, the narrow structure EIT linewidth is narrower and also more robust against probe intensity for the narrower probe beam. The behavior of the pedestal width is as expected for a single beam EIT [22]: it is narrower for the wider probe, and it changes much more rapidly with the probe laser beam intensity. Calculated linewidths follow the same trend and the narrower probe beam also gives narrower linewidth.

In the experiment with a single laser beam and coated cell [13], EIT has also dual structure. Similar to our result, narrow structure of EIT in [13] is narrower for the smaller laser beam diameter. Moreover, intensity dependence of the linewidths of the narrower peak is similar as in our setup: EIT linewidth obtained with the narrower beam is less dependent on the laser intensity. Such intensity dependence given in [13] is due to the geometry of the cell and the Ramsey effect of a multiple interaction of atoms with the same laser beam—narrowing the laser increases the dark region, i.e., time that the atom spends in the dark. The similar behavior of the

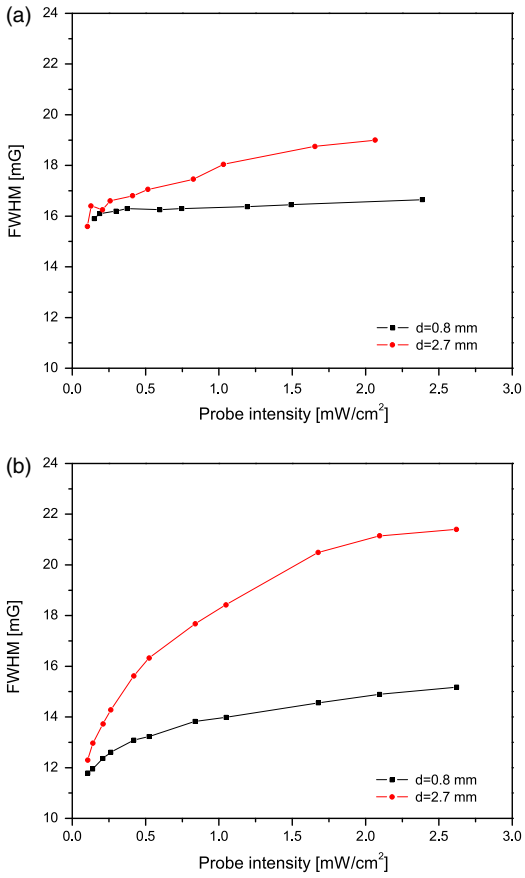

Fig. 4. (a) Experimental and (b) theoretical full width at half-maximum of the narrow structure of EIT as a function of the probe laser beam intensity, for two probe laser beam diameters, 0.8 and 2.7 mm.

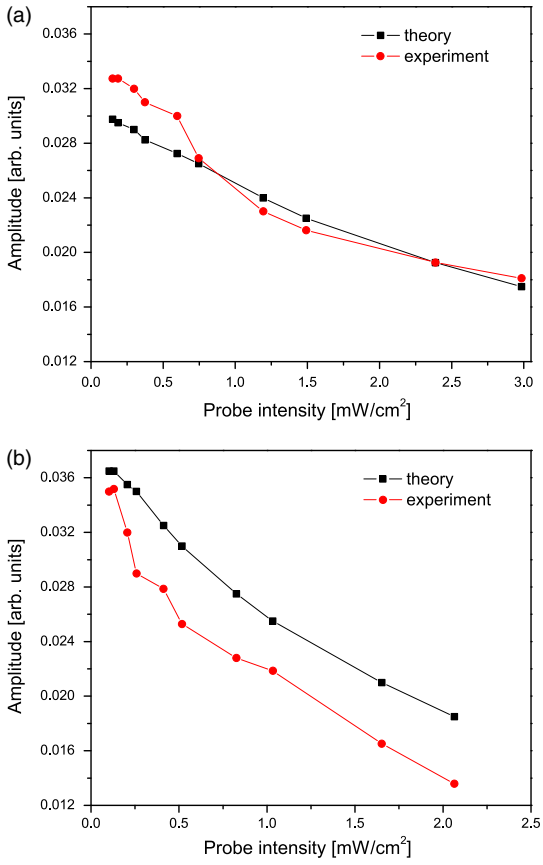

Fig. 5. Experimental and theoretical results for the amplitudes of the narrow structure of EIT resonances for two probe laser beam diameters: (a) 0.8 mm and (b) 2.7 mm.

narrow peak of the EIT in our work has a different explanation. The probe laser beam, apart from probing the atoms coherently prepared in the pump beam, influences the atomic evolution, which affects the narrow structure linewidth. During atomic passage through the laser beams the atomic state changes due to competitive effects of the laser electric field and the external magnetic field. The laser field continuously prepares the atoms into the dark state. The external magnetic field causes oscillations of the atomic ground-state coherences at the corresponding Larmor frequency and alters the atoms from the dark state. When the external magnetic field is zero the atoms reach the dark state inside the strong pump beam, which consequently leads to a maximum in the probe transmission. At nonzero magnetic field the state of the atoms passing through the probe beam differs from the dark state, so that the probe transmission decreases. However, this decrease in probe transmission due to the influence of the magnetic field is partially compensated by preparation of the atoms into the dark state within the probe beam. Hence, the actual probe transmission at some magnetic field is somewhat larger than the one expected without the probe influence. This causes broadening of the narrow structure in Zeeman EIT resonances that becomes more pronounced as the probe intensity and/or diameter increases.

Figure 5 shows measured and calculated amplitudes of the narrow structure of EIT resonances, for probe laser beam diameters 0.8 mm [Fig. 5(a)] and 2.6 mm [Fig. 5(b)]. As both experiment and theory show, amplitudes of narrow peaks of the probe EIT are nearly independent on probe beam diameter. Their dependence on the probe intensity and diameter is different than the amplitude of the wide structure EIT.

Amplitudes of the narrow peak of the probe EIT (obtained when the pump laser beam is turned on) have different dependence on the probe laser beam intensity than a single beam EIT, tuned to the same Raman resonance and with the same diameter. This is demonstrated in Fig. 6 where we plot amplitudes of both narrow and wide structure as a

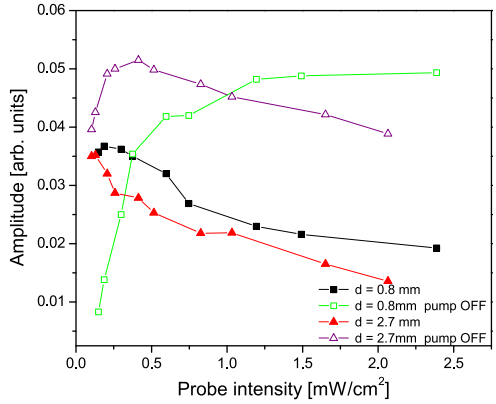

Fig. 6. Amplitudes of the probe EIT with and without pump laser beam, for two probe laser beam diameters: 0.8 and 2.7 mm. Amplitudes of wide (narrow) structures are shown for the pump laser beam turned off (on).

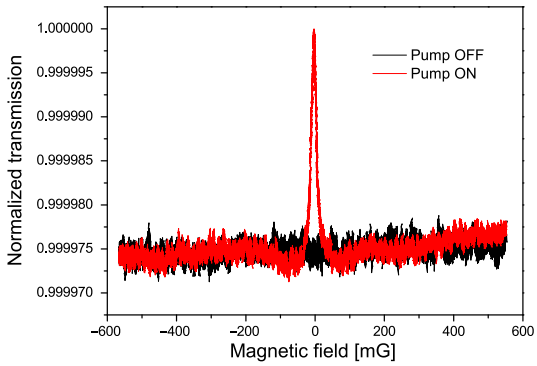

Fig. 7. Probe beam Zeeman EIT at D_2 line, with and without the pump beam. Intensities of the probe and pump beams are 0.1 mW/cm^2 and 11.5 mW/cm^2, respectively.

function of probe intensity, for two probe diameters. The maximum of the narrow structure of the probe EIT in the Raman–Ramsey configuration is at very low laser intensities, below values that we can detect in the experiment.

At very low probe laser beam intensities, below 0.1 mW/cm^2, the probe EIT has only narrow structure. The transmission of the weak probe can be controlled in a narrow spectral range around zero magnetic field by switching the pump beam on/off. For small magnetic fields and when the pump laser beam is present, the atoms coming into the probe beam are already coherently prepared into the dark state. This leads to the increase of the probe transmission, as presented in Fig. 7, where we show probe EIT for 0.8 mm probe beam diameter and for probe beam intensity of 0.1 mW/cm^2, without or with pump beam of intensity 11.5 mW/cm^2. Enhancement of the probe transmission is better for larger pump beam intensities.

5. CONCLUSION

We presented effects of the counterpropagating spatially separated pump and probe laser beam configuration on the probe Zeeman EIT. Both pump and probe beams are tuned to the D_2 line of ^{87}Rb. For the geometry of the experiment, with the probe coaxial with the surrounding hollow pump and small dark region between the pump and probe, we showed that in the vacuum cell, like in cells with antirelaxation coating, resonances can be narrower when the probe diameter is smaller. For the probe of 0.8 mm in diameter we observed and calculated narrower linewidths, almost independent of the probe laser beam intensity. Also, for this small probe diameter, when its intensity is below 0.1 mW/cm^2, dual structure of Zeeman EIT turns in to a single narrow EIT. Probe transmission is enhanced in a narrow range of small magnetic fields when the pump laser beam is present, which is akin to optical switch behavior.

ACKNOWLEDGMENTS

This work was supported by the Ministry of Education and Science of Serbia, under grants III45016 and OI171038, and also by SCOPES JRP IZ73Z0_127942.

REFERENCES

1. S. E. Harris, "Electromagnetically induced transparency," Phys. Today **50**(7), 36–42 (1997).
2. C. L. Garrido Alzar, M. A. G. Martinez, and P. Nussenzveig, "Classical analog of electromagnetically induced transparency," Am. J. Phys. **70**, 37–42 (2002).
3. G. Alzetta, A. Gozzini, L. Moi, and G. Orriols, "An experimental method for the observation of r.f. transitions and laser beat resonances in oriented Na vapour," Nuovo Cimento B **36**, 5–20 (1976).
4. E. Arimondo and G. Orriols, "Nonabsorbing atomic coherences by coherent two-photon transitions in a three-level optical pumping," Lett. Nuovo Cimento Soc. Ital. Fis. **17**, 333–338 (1976).
5. F. Renzoni, W. Maichen, L. Windholz, and E. Arimondo, "Coherent population trapping with losses observed on the Hanle effect of the D_1 sodium line," Phys. Rev. A **55**, 3710–3718 (1997).
6. N. F. Ramsey, *Molecular Beams* (Oxford University, 1956).
7. B. Schuh, S. I. Kanorsky, A. Weis, and T. W. Hänsch, "Observation of Ramsey fringes in nonlinear Faraday rotation," Opt. Commun. **100**, 451–455 (1993).
8. J. E. Thomas, P. R. Hemmer, S. Ezekiel, C. C. Leiby, Jr., R. H. Picard, and C. R. Willis, "Observation of Ramsey fringes using a stimulated, resonance Raman transition in a sodium atomic beam," Phys. Rev. Lett. **48**, 867–870 (1982).
9. G. Theobald, V. Giordano, N. Dimatcq, and P. Cerez, "Observation of narrow Ramsey-type resonances in a caesium beam due to Zeeman coherences," J. Phys. B **24**, 2957–2966 (1991).
10. S. Nakayama, G. W. Series, and W. Gawlik, "Larmor precession in polarization spectroscopy with spatially separated beams," Opt. Commun. **34**, 389–392 (1980).
11. A. S. Zibrov and A. B. Matsko, "Optical Ramsey fringes induced by Zeeman coherence," Phys. Rev. A **65**, 013814 (2001).
12. Y. Xiao, I. Novikova, D. F. Phillips, and R. L. Walsworth, "Diffusion-induced Ramsey narrowing," Phys. Rev. Lett. **96**, 043601 (2006).
13. M. Klein, M. Hohensee, D. F. Phillips, and R. L. Walsworth, "Electromagnetically induced transparency in paraffin-coated vapor cells," Phys. Rev. A **83**, 013826 (2011).
14. Z. D. Grujić, M. Mijailović, D. Arsenović, A. Kovačević, M. Nikolić, and B. M. Jelenković, "Dark Raman resonances due to Ramsey interference in vacuum vapor cells," Phys. Rev. A **78**, 063816 (2008).
15. H. Failache, L. Lenci, and A. Lezama, "Raman-Ramsey multizone spectroscopy in a pure rubidium vapor cell," Phys. Rev. A **81**, 023801 (2010).
16. T. Zanon, S. Guerandel, E. de Clercq, D. Holleville, N. Dimarcq, and A. Clairon, "High contrast Ramsey fringes with coherent-population-trapping pulses in a double lambda atomic system," Phys. Rev. Lett. **94**, 193002 (2005).
17. X. Liu, J.-M. Mérolla, S. Guérandel, E. de Clercq, and R. Boudot, "Ramsey spectroscopy of high-contrast CPT resonances with push-pull optical pumping in Cs vapor," Opt. Express **21**, 12451 (2013).
18. K. L. Corwin, Z. Lu, C. F. Hand, R. J. Epstein, and C. E. Wieman, "Frequency-stabilized diode laser with the Zeeman shift in an atomic vapor," Appl. Opt. **37**, 3295–3298 (1998).
19. Z. D. Grujić, M. Lekić, M. Radonjić, D. Arsenović, and B. M. Jelenković, "Ramsey effects in coherent resonances at closed transition $F_g = 2 \rightarrow F_e = 3$ of ^{87}Rb," J. Phys. B **45**, 245502 (2012).
20. M. Radonjić, D. Arsenović, Z. Grujić, and B. M. Jelenković, "Coherent population trapping linewidths for open transitions: cases of different transverse laser intensity distribution," Phys. Rev. A **79**, 023805 (2009).
21. A. J. Krmpot, M. Radonjić, S. M. Ćuk, S. N. Nikolić, Z. D. Grujić, and B. M. Jelenković, "Evolution of dark state of an open atomic system in constant intensity laser field," Phys. Rev. A **84**, 043844 (2011).
22. E. Figueroa, F. Vewinger, J. Appel, and A. I. Lvovsky, "Decoherence of electromagnetically induced transparency in atomic vapor," Opt. Lett. **31**, 2625–2627 (2006).

IOP Publishing Journal of Physics B: Atomic, Molecular and Optical Physics
J. Phys. B: At. Mol. Opt. Phys. **48** (2015) 045501 (11pp) doi:10.1088/0953-4075/48/4/045501

Transient development of Zeeman electromagnetically induced transparency during propagation of Raman–Ramsey pulses through Rb buffer gas cell

S N Nikolić, M Radonjić, N M Lučić, A J Krmpot and B M Jelenković

Institute of Physics, University of Belgrade, Pregrevica 118, 11080 Belgrade, Serbia

E-mail: stankon@ipb.ac.rs

Received 7 November 2014
Accepted for publication 18 December 2014
Published 30 January 2015

Abstract

We investigate, experimentally and theoretically, time development of Zeeman electromagnetically induced transparency (EIT) during propagation of two time separated polarization laser pulses, preparatory and probe, through Rb vapour. The pulses were produced by modifying laser intensity and degree of elliptical polarization. The frequency of the single laser beam is locked to the hyperfine $F_g = 2 \rightarrow F_e = 1$ transition of the D_1 line in ^{87}Rb. Transients in the intensity of σ^- component of the transmitted light are measured or calculated at different values of the external magnetic field, during both preparatory and probe pulse. Zeeman EIT resonances at particular time instants of the pulse propagation are reconstructed by appropriate sampling of the transients. We observe how laser intensity, Ramsey sequence and the Rb cell temperature affect the time dependence of EIT line shapes, amplitudes and linewidths. We show that at early times of the probe pulse propagation, several Ramsey fringes are present in EIT resonances, while at later moments a single narrow peak prevails. Time development of EIT amplitudes are determined by the transmitted intensity of the σ^- component during the pulse propagation.

Keywords: electromagnetically induced transparency, Ramsey effect, rubidium

(Some figures may appear in colour only in the online journal)

1. Introduction

Electromagnetically induced transparency (EIT) [1–3] is a quantum interference phenomenon which is manifestated as a narrow spectral resonance observed in transmitted laser light through otherwise opaque vapour of, typically, alkali metals. EIT is attained when two light fields couple two atomic ground levels to a common excited level (so-called Λ-scheme). Within the spectral bandwidth of the EIT there is a strong dispersion of the index of refraction, resulting in a slow light and storage of light phenomena in EIT medium [4, 5]. EIT is demonstrated as a coherent technique for controlling the propagation of classical light pulses and other nonlinear optics applications [4]. A review of EIT in various atomic schemes is given in [6].

Studies of pulse propagation through EIT medium is a mature field. Measurements of transient fluorescence [7], of transient gains of the probe pulse [8], and of non-resonant (for both preparation and probe beams) transients [9] were done. Also, transient effects in adiabatic [10] and non-adiabatic [11] regimes, depending if the rise time of the pulse is slow or fast compared to the Rabi period and relaxation times, were analyzed. Transients of transmission of the probe pulse were studied for cases when the pump beam is turned off [9] or on [11], when the probe itself is turned on, and when pump and probe fields are suddenly detuned from the resonance [8, 12]. Detailed theoretical investigation of EIT and features of the space-time dependent probe field in Λ-, V-, and cascade-type schemes are presented in [13]. The same authors performed a time-dependent analysis of the four-wave mixing process

(FWM) in a double-Λ system, showing that generated FWM field can acquire ultraslow group velocity [14].

It was shown that the pulse strength of the laser, the pulse switching rate, and the magnetic field determine the rate at which transmitted pulse reaches a new steady state. These parameters also determine transient behavior of the probe transmission with or without free induction decay [15]. Stepwise Raman detuning of circularly polarized pump and probe beams resulted in the oscillatory behavior of the transient signal, with the period of oscillations depending on the Raman detuning [16]. Dependence of decay rates of the amplitudes of the signal oscillations on the cell temperature and laser power was studied in [12]. Behavior of transmission of lasers inducing Zeeman EIT, when magnetic field is suddenly turned off and on, was studied both experimentally and theoretically [17]. Transients in coherent population trapping (CPT) can be also induced by ac magnetic field as calculated in [18, 19]. Transient response of an EIT media to a phase-modulated pump was examined in [20].

Propagation of a probe pulse through EIT medium is closely related to temporal evolution of EIT resonance. However, the transient development of EIT was much less studied than transmission of the laser pulse. In [21], the build up of EIT was observed after sudden two-photon detuning from EIT. It was found that the Zeeman EIT width decreases inversely with the interaction time and approaches an asymptotic value determined by the preparatory laser intensity [21].

Various models of transient effects were developed to predict, or to explain, the propagation of the laser pulse through EIT medium. Typically, analytical solutions of equations for density matrix describing a three-state model is used [15]. In [22] the authors compared transients for the dressed-atom and bare-atom pictures. The calculations of temporal evolution of EIT were also studied [23]. The transient response of atomic system was calculated when the laser is suddenly turned on in the presence of external magnetic field [24].

The Ramsey method of separated oscillatory fields [25] was applied to alkali atoms contained in the glass cell in order to narrow resonance linewidth. Application of two or more successive laser pulses leads to the appearance of high contrast and narrow (~100 Hz) CPT and EIT fringes [26–30]. Calculations have also shown that quantum interference, driven by two identical pulses, results in Ramsey-like fringes [31]. Two-photon free-induction decay in a three-level Λ system used to obtain EIT was reported in [32]. Ramsey interference effect appears after pulsed excitation, with fringes observed as time-domain oscillations in the transmission amplitude of a long attenuated query pulse [33]. Transient of Raman–Ramsey fringes (RRF) and EIT have been measured in sodium vapour in the hyperfine Λ system [34]. Ramsey fringes induced by Zeeman coherence in various Rb cells for both spatially and temporally separated laser fields were reported in [35]. Ramsey-like measurements of Zeeman decoherence that determine the dumping rate of such oscillations are presented in [36]. One application of Ramsey interference is frequency selective magnetometer based on light-pulse atom interferometry, as described in [37]. Implementation of a compact atomic clock based on Ramsey–CPT interference is proposed in [38].

This work extends previous studies of laser pulse propagation through EIT medium by observing transient development of Zeeman EIT during the pulse propagation. Experimentally and theoretically, we monitor intensity of the σ^- component during propagation of two time separated elliptically polarized laser pulses. The laser is locked to the D_1 line of ^{87}Rb. Zeeman EIT curves are reconstructed from transients of σ^- intensity at different external magnetic fields. We investigate transient behavior of the EIT line shapes, amplitudes and linewidths from the moments when laser pulses enter the Rb buffer gas cell. In particular, we investigated the case when pulses are highly elliptical (maximum relative optical power of σ^- component is only 15%), since several slow and stored light experiments typically use this level of ellipticity [4, 39]. We explore the effects of Ramsey sequences by comparing the behavior of EIT during the preparatory and the probe pulse by varying the length of the dark time between them. The Zeeman EIT resonances are then expected to exhibit the oscillation of transmission in magnetic field caused by Larmor precession during the dark time. The motivation of this work was in part to investigate the properties of the foreseen Ramsey oscillation with respect to pulse intensities and Rb density. Experimentally observed developments of the Zeeman EIT are compared with corresponding theoretical results. Our theoretical model based on time dependent Maxwell–Bloch equations qualitatively reproduces experimental observations. We are not aware of previous publications that show the time evolution of Zeeman EIT and Ramsey effect on this evolution when fast developing pulse propagates through Rb cell with buffer gas.

The detection of Raman–Ramsey oscillations on EIT line shapes presented in this work can find application in high precision magnetic field measurements and in determining the atomic decoherence rates.

2. Theory

2.1. Description of the model

The evolution of Rb atoms contained in a buffer-gas cell is calculated using time dependent optical Bloch equations for Rb density matrix $\hat{\rho}$

$$\frac{\partial\hat{\rho}}{\partial t} = D\nabla^2\hat{\rho} - \frac{\mathrm{i}}{\hbar}\Big[\hat{H}_{\mathrm{atom}}(B) + \hat{V}_{\mathrm{int}}(r,t),\hat{\rho}\Big] + \left(\frac{\partial\hat{\rho}}{\partial t}\right)_{\mathrm{SE}} + \left(\frac{\partial\hat{\rho}}{\partial t}\right)_{\mathrm{coll}}, \quad (1)$$

where $\hat{H}_{\mathrm{atom}}(B)$ is the atomic Hamiltonian in the external longitudinal magnetic field, $\hat{V}_{\mathrm{int}}(r,t)$ describes laser-atom interaction and the term with subscript SE corresponds to spontaneous emission. The hyperfine levels either coupled to the laser light or populated due to spontaneous emission are shown in the energy level diagram in figure 1.

Collisions with the buffer-gas affect the atomic evolution in several ways. First, Rb atoms acquire diffusive motion within the cell, as described by the first term at the right-hand

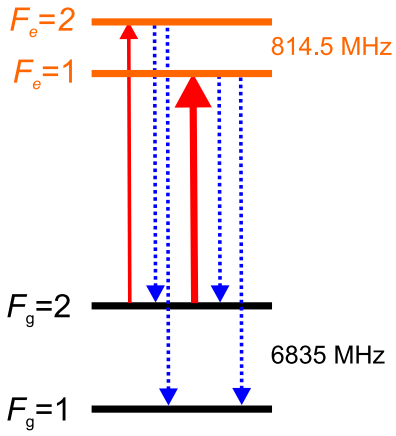

Figure 1. Energy level diagram for D_1 line transitions considered in the theoretical model. Solid lines represent transitions induced by the laser, while dotted lines correspond to possible spontaneous emission channels from excited levels. Frequency differences between adjacent hyperfine levels are shown.

side of (1) with D as the diffusion coefficient. Second, within each excited state manifold the populations of Zeeman sublevels are equalized, while the coherences are destroyed due to total collisional depolarization of the excited state [40, 41]. The collisions with the buffer gas also broaden the optical transition and together with the Rb–Rb collisions lead to the relaxation of the ground state populations and coherences. These effects correspond to the last term at the right-hand side of (1). For the buffer gas pressure of 30 Torr the collisional broadening of ≈300–400 MHz is comparable with the Doppler width, so that we use the approximation of the motionless atoms in the direction of the laser beam propagation. Detailed exposition of the theoretical model is given in [42]. The present experimental configuration requires some additions concerning time dependent features. Contrary to the steady state calculations in [42], here we are solving (1) in cylindrical coordinates (r, z) and *in time*. The effects of propagation of slowly varying envelopes (SVEs) of the laser electric field $\mathcal{E}$ and the polarization $\mathcal{P}$ of the Rb vapour are also incorporated via

$$\frac{1}{c}\frac{\partial \boldsymbol{\mathcal{E}}(r, z, t; B)}{\partial t} + \frac{\partial \boldsymbol{\mathcal{E}}(r, z, t; B)}{\partial z} = \frac{\mathrm{i}\omega}{2\epsilon_0 c}\boldsymbol{\mathcal{P}}(r, z, t; B), \quad (2)$$

where ϵ_0 is the vacuum dielectric constant, c is vacuum speed of light and ω is the laser frequency. The time dependence of these SVEs originates from the time dependent boundary condition for the electric field at the entrance to the Rb cell $\mathcal{E}(r, z = 0, t; B) = \mathcal{E}_{\mathrm{in}}(r, t)$. In the frequency domain the propagation equation is

$$\mathrm{i}\frac{\nu}{c}\boldsymbol{\mathcal{E}}(r, z, \nu; B) + \frac{\partial \mathcal{E}(r, z, \nu; B)}{\partial z} = \frac{\mathrm{i}\omega}{2\epsilon_0 c}\boldsymbol{\mathcal{P}}(r, z, \nu; B). \quad (3)$$

The frequencies for which $\mathcal{E}_{\mathrm{in}}(r, \nu)$ is significant satisfy

$$\left|\frac{\nu}{c}\boldsymbol{\mathcal{E}}(r, z, \nu; B)\right| \ll \left|\frac{\partial \boldsymbol{\mathcal{E}}(r, z, \nu; B)}{\partial z}\right| \sim \left|\frac{\mathcal{E}_{\mathrm{in}}(r, \nu)}{L}\right|, \quad (4)$$

where L is the cell length, so that we can safely drop the first term from (2). This leads to

$$\frac{\partial \boldsymbol{\mathcal{E}}(r, z, t; B)}{\partial z} = \frac{\mathrm{i}\omega}{2\epsilon_0 c}\boldsymbol{\mathcal{P}}(r, z, t; B), \quad (5)$$

which is used, in conjunction with (1), for calculation of the transmitted electric field at $z = L$ and Zeeman EIT resonances at particular time instants. The normalized σ^- transmission corresponds to the ratio $I_{\mathrm{tr}}^-/I_{\mathrm{in}}^-$, where I_{tr}^- and I_{in}^- denote intensities of the σ^- component of a laser beam, after propagation through and before entering into the Rb cell, respectively. Numerical calculations are performed using the DOLFIN finite element library [43] (part of the FEniCS project [44]) and CBC.PDESys package [45].

2.2. Theoretical results

The EIT resonances were determined from calculated σ^- transmissions at a given time instant after the σ^- pulse is launched into the Rb cell, at various magnetic fields. The cell temperature is 67 °C. The period between the two pulses, when the laser beam was turned off, was set to 60 μs. Overall laser intensities during the first (preparatory) and the second (probe) pulse were 4.9 and 0.9 mW cm^{-2}, respectively. Both pulses were elliptically polarized with 15% of photons carrying the σ^- polarization. Calculated EIT curves at t = 6, 16, 100, and 328 μs from the beginning of the probe pulse are shown in figures 2(a)–(d), respectively.

From the calculated transmission signals, the amplitudes and the linewidths of Zeeman EIT resonances evolving in time were extracted and shown in figures 3(a) and (b), respectively. These results show that the central peak has higher amplitude and wider line shape soon after the start of the probe pulse.

3. Experiment

3.1. Description of the experiment

Propagation of the polarization laser pulses and temporal evolution of Zeeman EIT resonances are experimentally realized in the Hanle configuration. A schematic of the experiment is given in figure 4(a).

The external cavity diode laser is frequency locked to the hyperfine $F_g = 2 \rightarrow F_e = 1$ transition of the D_1 line in ^{87}Rb using the Doppler-free dichroic atomic vapour laser lock method [46, 47]. Gaussian profile for the laser beam is obtained by the short single mode optical fiber. In order to apply the Ramsey method of repeated interactions of a laser light with Rb atoms, the power of the first order diffracted beam from the AOM is modulated and transmitted through the cell. The linear polarization of the laser light is assured by the high quality polarizer. The Pockels cell and the $\lambda/4$ plate are used to generate laser pulses with elliptical polarization: pure σ^+ circular polarization is obtained when no voltage is applied to the cell, while 15% of the σ^- light is produced

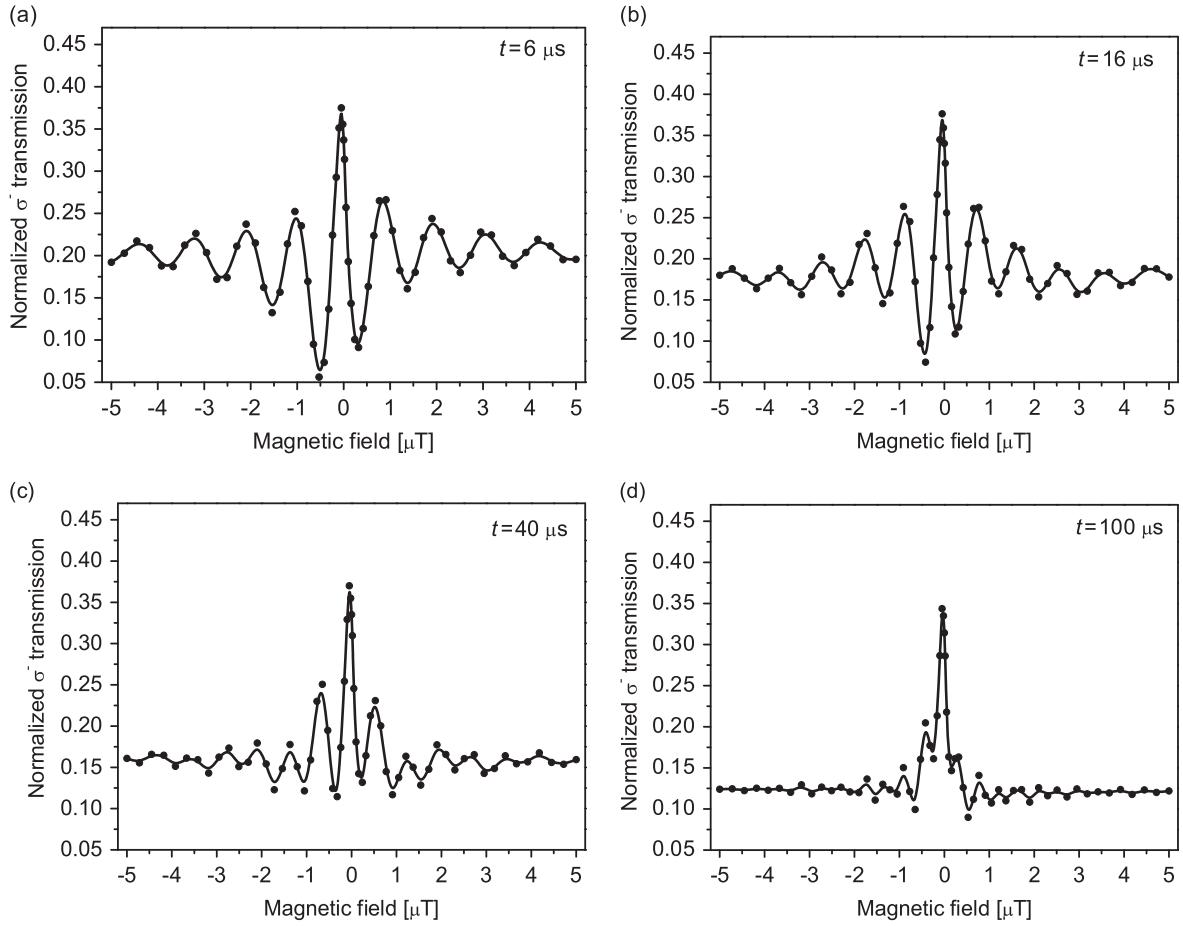

Figure 2. Time evolution of calculated Zeeman EIT resonances during the probe pulse with overall laser beam intensity of $I_2 = 0.9$ mW cm^{-2}. The overall laser beam intensity during the preparatory pulse is $I_1 = 4.9$ mW cm^{-2}. The dark period is $T_D = 60\,\mu$s. The resonances are reconstructed and normalized from σ^- transmission signals at four different times: (a) $t = 6\,\mu$s, (b) $t = 16\,\mu$s, (c) $t = 40\,\mu$s, and (d) $t = 100\,\mu$s. The cell temperature is 67 °C.

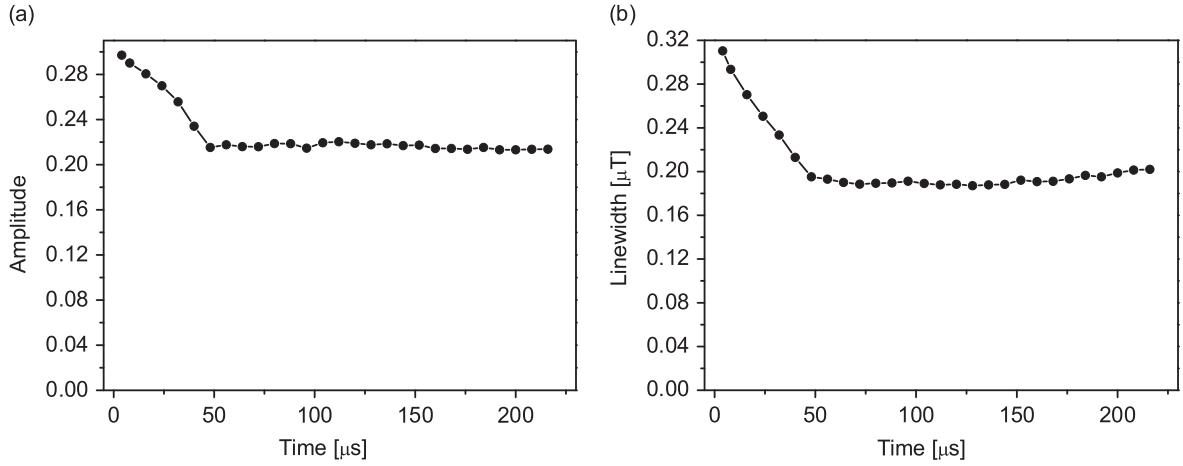

Figure 3. Theoretically obtained time evolution of Zeeman EIT (a) amplitudes and (b) linewidths of the central fringe during the probe pulse, for overall laser beam intensity of $I_2 = 0.9$ mW cm^{-2}. The overall laser beam intensity during the preparatory pulse is $I_1 = 4.9$ mW cm^{-2}. The dark period is $T_D = 60\,\mu$s. The cell temperature is 67 °C.

otherwise. The Rb cell containing 30 Torr of Ne buffer gas is 8 cm long and has 2.5 cm in diameter. The Rb cell was heated by using hot air circulating around the cell. Measurements were done at 67 °C and 85 °C. The Rb cell is shielded from stray magnetic fields by the triple μ-metal layers which reduce stray magnetic fields below 10 nT. In order to obey two-photon detuning, long solenoid placed around the Rb cell produces controllable longitudinal magnetic field in the range

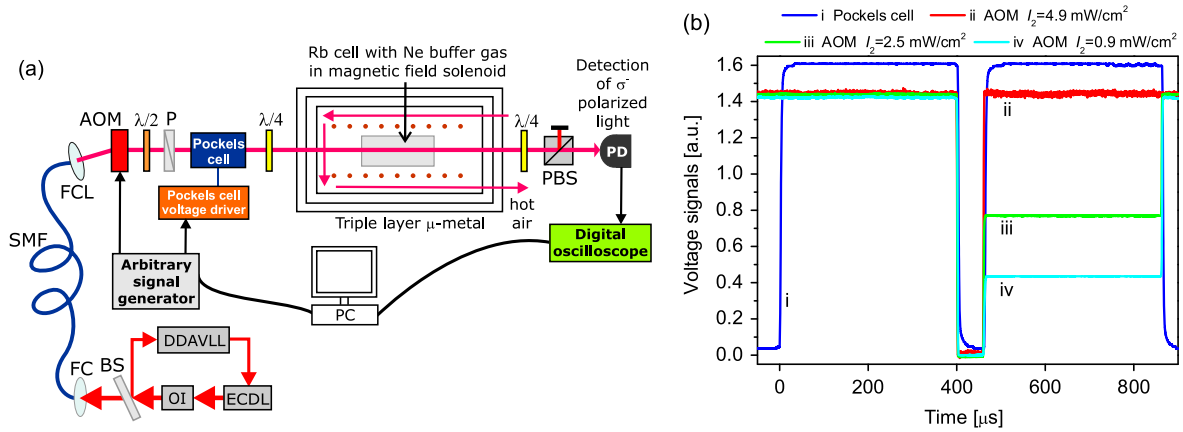

Figure 4. (a) Experimental setup: ECDL—external cavity diode laser; OI—optical insulator; DDAVLL—Doppler-free dichroic atomic vapour laser lock; BS—beam splitter; FC—fiber coupler; SMF—single-mode fiber; FCL—fiber collimator; AOM—acousto-optic modulator; P—polarizer; PBS—polarizing beam splitter; PD—photodetector. Hot air is used for heating the cell. (b) Pockels cell and AOM signals used in the experiment.

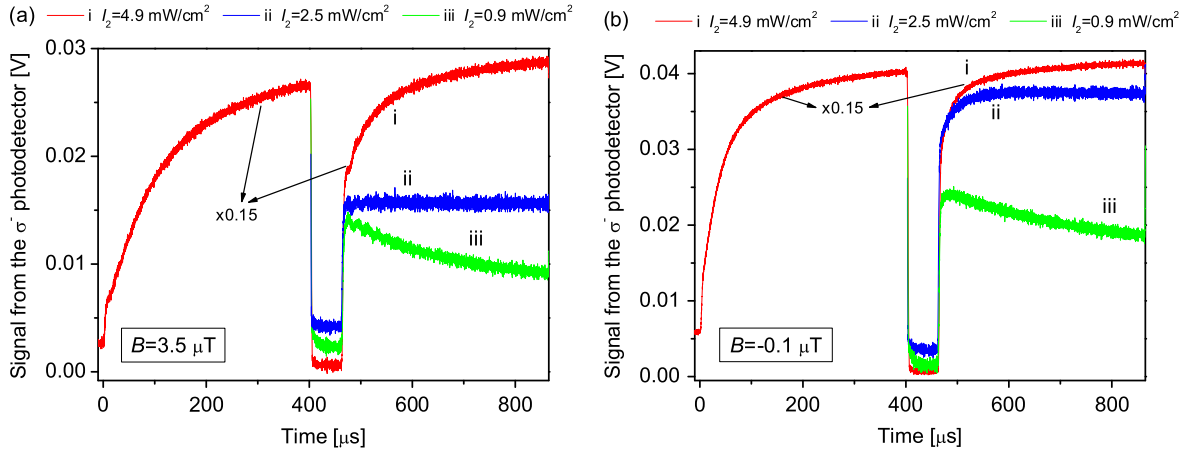

Figure 5. Measured σ^- transmission signals during preparatory and probe polarization laser pulse for magnetic field (a) 3.5 μT and (b) −0.1 μT. The curves in both figures correspond to the probe pulse overall intensity of (i) $I_2 = 4.9$ mW cm^{-2}, (ii) $I_2 = 2.5$ mW cm^{-2}, and (iii) $I_2 = 0.9$ mW cm^{-2}. The overall laser beam intensity during the preparatory pulse is $I_1 = 4.9$ mW cm^{-2}. The cell temperature is 67 °C.

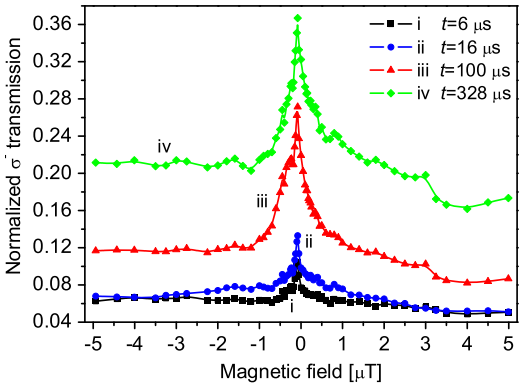

Figure 6. Time evolution of Zeeman EIT resonances during the preparatory pulse with overall laser beam intensity of $I_1 = 4.9$ mW cm^{-2}. The resonances are reconstructed and normalized from the σ^- transmission signals at four different times: $t = 6\,\mu$s (curve i), $t = 16\,\mu$s (curve ii), (c) $t = 100\,\mu$s (curve iii), and (d) $t = 328\,\mu$s (curve iv). The cell temperature is 67 °C.

of ±10 μT. The σ^- light is extracted from the transmitted laser beam with the $\lambda/4$ plate and the PBS. Transmitted σ^- laser intensity over time, for a given magnetic field, is measured by the photodetector and recorded by the digital storage oscilloscope.

Laser pulses are produced after applying voltage pulses to the AOM and the Pockels cell as shown in figure 4(b). Note that the laser pulse here refers to the temporal change of a laser beam polarization. That is, polarization changes from σ^+ before the pulse, to elliptical polarization with 15% of σ^- relative optical power during the pulse. The first voltage pulse to the Pockels cell (signal (i)) is preparatory pulse that prepares Rb atoms into the dark state. Then, the voltages on the Pockels cell and the AOM are synchronously turned off for a certain period of dark time. During the dark time, Zeeman coherence makes a Larmor precession if the external magnetic field is not zero. After the dark time, the voltage pulses are again applied to AOM and Pockels cell and the second (probe) pulse, with the same polarization but intensity that can

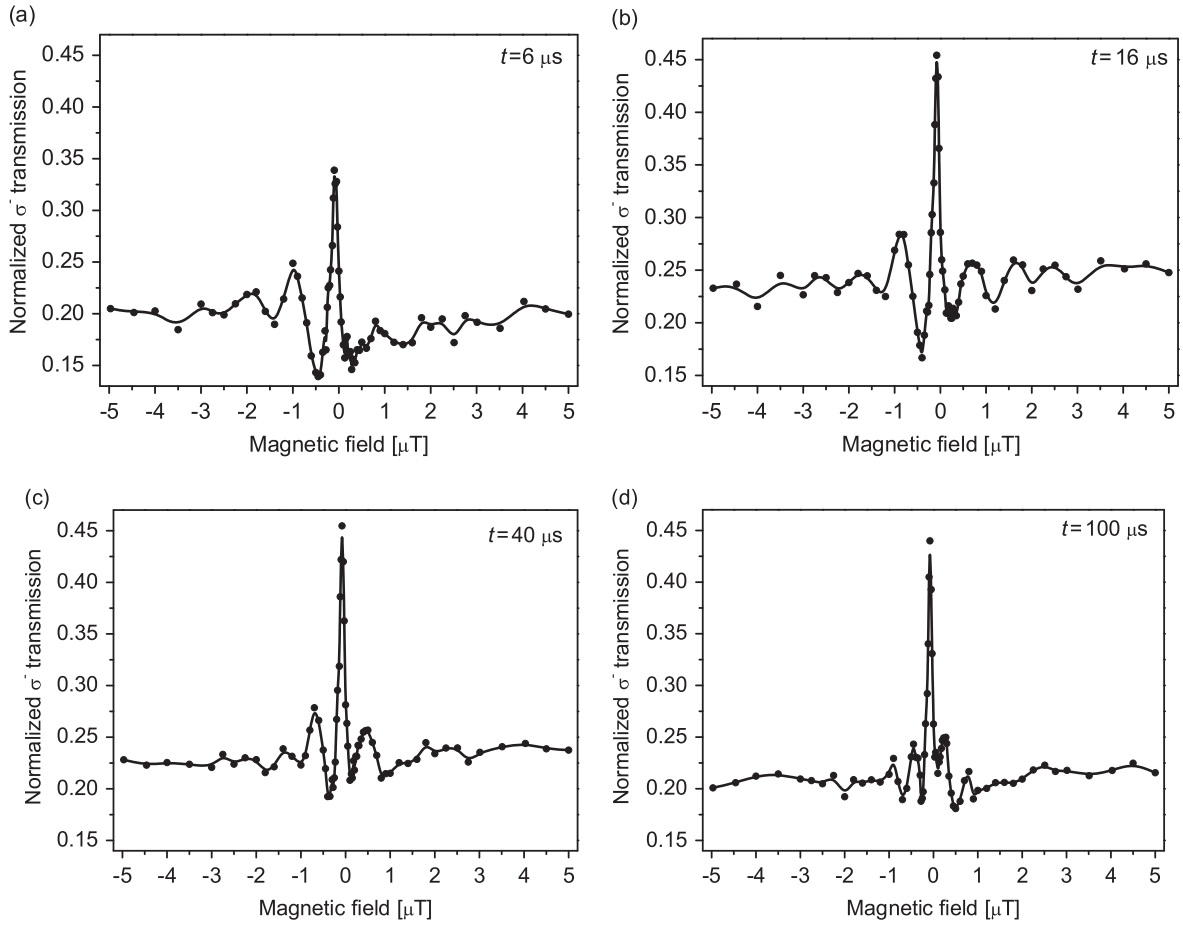

Figure 7. Time evolution of Zeeman EIT resonances during the probe pulse with overall laser beam intensity of $I_2 = 0.9$ mW cm^{-2}. The overall laser intensity during the preparatory pulse is $I_1 = 4.9$ mW cm^{-2}. The dark period is $T_D = 60\,\mu$s. The resonances are reconstructed and normalized from the σ^- transmission signals at four different times (from top to bottom): $t = 6\,\mu$s, $t = 16\,\mu$s, $t = 40\,\mu$s, and $t = 100\,\mu$s. The cell temperature is 67 °C.

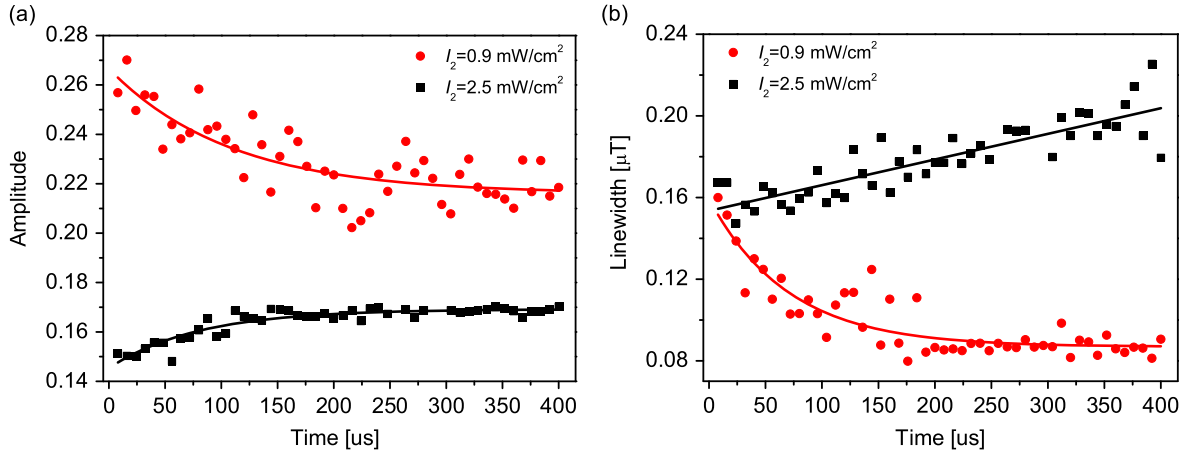

Figure 8. Experimentally obtained time evolution of Zeeman EIT (a) amplitude and (b) linewidth during the probe pulse. The overall intensities of the probe pulse are $I_2 = 0.9$ mW cm^{-2} or $I_2 = 2.5$ mW cm^{-2}. The overall laser intensity during the preparatory pulse is $I_1 = 4.9$ mW cm^{-2}. The dark period is $T_D = 60\,\mu$s. The cell temperature is 67 °C. Solid lines are to guide the eye.

be different than the preparatory pulse, is created to probe the atomic coherences. At the end of the probe pulse, we return to a strong σ^+ polarization for several ms to repump atoms back to the Zeeman sublevels of the ground state before the next Ramsey sequence of pulses. Note that all the time we measure only the σ^- component of the elliptically polarized laser beam. We denote by I_1 and I_2 overall intensities of a laser beam during the preparatory (duration T_1) and probe pulse (duration T_2), respectively. Two synchronous voltage signals, controlling the AOM and the Pockels cell with fully

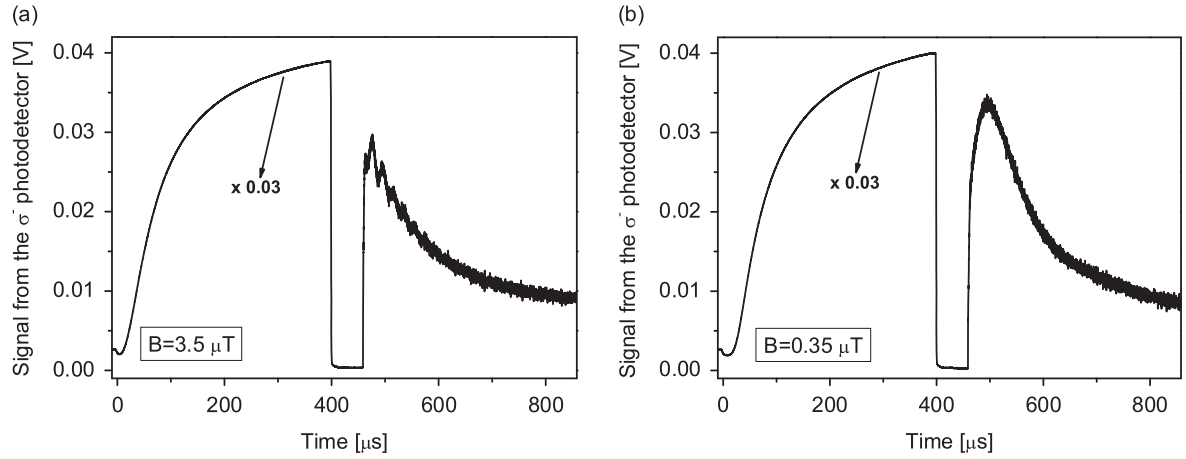

Figure 9. Measured σ^- transmission signals during preparatory and probe polarization laser pulse for magnetic field (a) 3.5 μT and (b) 0.35 μT. The curves in both figures correspond to the probe pulse overall intensity of $I_2 = 4.8\ \mathrm{mW\ cm^{-2}}$. The overall laser beam intensity during the preparatory pulse is $I_1 = 49\ \mathrm{mW\ cm^{-2}}$. The cell temperature is 85 °C.

adjustable amplitudes and durations, were generated by field-programmable gate array based signal generator and oscilloscope, as described in [48].

Development of Zeeman EIT for cell temperature of 67 °C, corresponding to Rb density of $5\times10^{11}\ \mathrm{cm^{-3}}$ [49], was measured with the following sequence of pulses: $I_1 = 4.9\ \mathrm{mW\ cm^{-2}}$, $T_1 = 400\ \mu$s; $T_D = 60\ \mu$s and $T_D = 160\ \mu$s; $T_2 = 400\ \mu$s. We varied the overall laser intensity during the probe pulse: $I_2 = 4.9\ \mathrm{mW\ cm^{-2}}$ (AOM signal (ii)), $I_2 = 2.5\ \mathrm{mW\ cm^{-2}}$ (AOM signal (iii)), and $I_2 = 0.9\ \mathrm{mW\ cm^{-2}}$ (AOM signal (iv)) in order to measure the intensity dependencies of the: (1) σ^- transmission and (2) Zeeman EIT temporal development. The same Ramsey sequence was used for the cell temperature of 85 °C (Rb density of $1.4\times10^{12}\ \mathrm{cm^{-3}}$ [49]), except the higher laser intensity was required during the two pulses due to increased residual absorption: $I_1 = 49\ \mathrm{mW\ cm^{-2}}$ and $I_2 = 4.8\ \mathrm{mW\ cm^{-2}}$.

3.2. Experimental results

In this section we show effects of the probe pulse intensity, the Ramsey sequences of successive excitation pulses, the external magnetic field and the cell temperature on propagation of pulses and development of EIT.

Measured transmissions of the σ^- component of a laser beam, during the preparatory and the probe pulse are shown in figure 5. The Rb cell temperature is 67 °C. Presented results are obtained for three values of the overall laser intensities during the probe pulse, and for the two values of magnetic field. The intensity and duration of the preparatory pulse are always $I = 4.9\ \mathrm{mW\ cm^{-2}}$ and $T_1 = 400\ \mu$s, so that during this pulse ^{87}Rb atoms are efficiently prepared into the dark state.

Transient behavior of the probe pulse depends on the laser intensity, duration of the dark time, and magnetic field. We show in figure 5 propagation of preparatory and probe pulse for two values of magnetic field, 3.5 and −0.1 μT, for three values of the probe pulse intensity, and for dark time of 60 μs. For the preparatory pulse intensity of $4.9\ \mathrm{mW\ cm^{-2}}$, transmission of the probe pulse can be quite different depending on its intensity. At high intensity of the probe pulse ($4.9\ \mathrm{mW\ cm^{-2}}$), probe transmission increases with time due to optical pumping. When probe intensity is decreased to $2.5\ \mathrm{mW\ cm^{-2}}$, transmission is constant in time. For the lowest probe intensity of $0.9\ \mathrm{mW\ cm^{-2}}$, the probe pulse probes the coherences without significantly contributing to atomic evolution and optical pumping. The signal then decays due to decoherence and relaxation. At low magnetic field, the transmission of the probe is higher compared to transmission at higher magnetic fields (compare figures 5(a) and (b)), because more atoms are coherently prepared into the dark state by the preparatory pulse.

Due to Larmor precession of atomic polarization during the dark time, oscillations in the measured intensity of the probe pulse can be seen in figure 5(a), when intensity is low and magnetic field is different from zero. Frequency of observed fringes depends on the magnetic field, while their amplitudes depend on the amount of coherence between Zeeman sublevels. These results are in agreement with [35, 36]. The fringes on the transmission signal disappear when the σ^+ polarized laser beam is kept on between the preparatory and probe pulse (not shown), providing the evidence that observed fringes are indeed due to interference between coherently prepared atoms and the probe light.

From the transient curves of the σ^- transmission, like those in figure 5, taken at 70 different values of the longitudinal magnetic field, we have reconstructed Zeeman EIT resonances at different times during the development of preparatory and probe pulse. We first show Zeeman EIT resonances developing during the preparatory pulse (see curves (i)–(iv) in figure 6). As time progresses, EIT resonances keep the similar shape and only have higher amplitude since more atoms undergo dark state preparation.

Development of EIT during the probe pulse, when dark time is $T_D = 60\ \mu$s is shown in figure 7. The overall laser beam intensities during the preparatory and the probe pulses were $I_1 = 4.9\ \mathrm{mW\ cm^{-2}}$ and $I_2 = 0.9\ \mathrm{mW\ cm^{-2}}$. Characteristically, EIT resonance has central peak and fringes due to interference between atomic coherence precessing in the

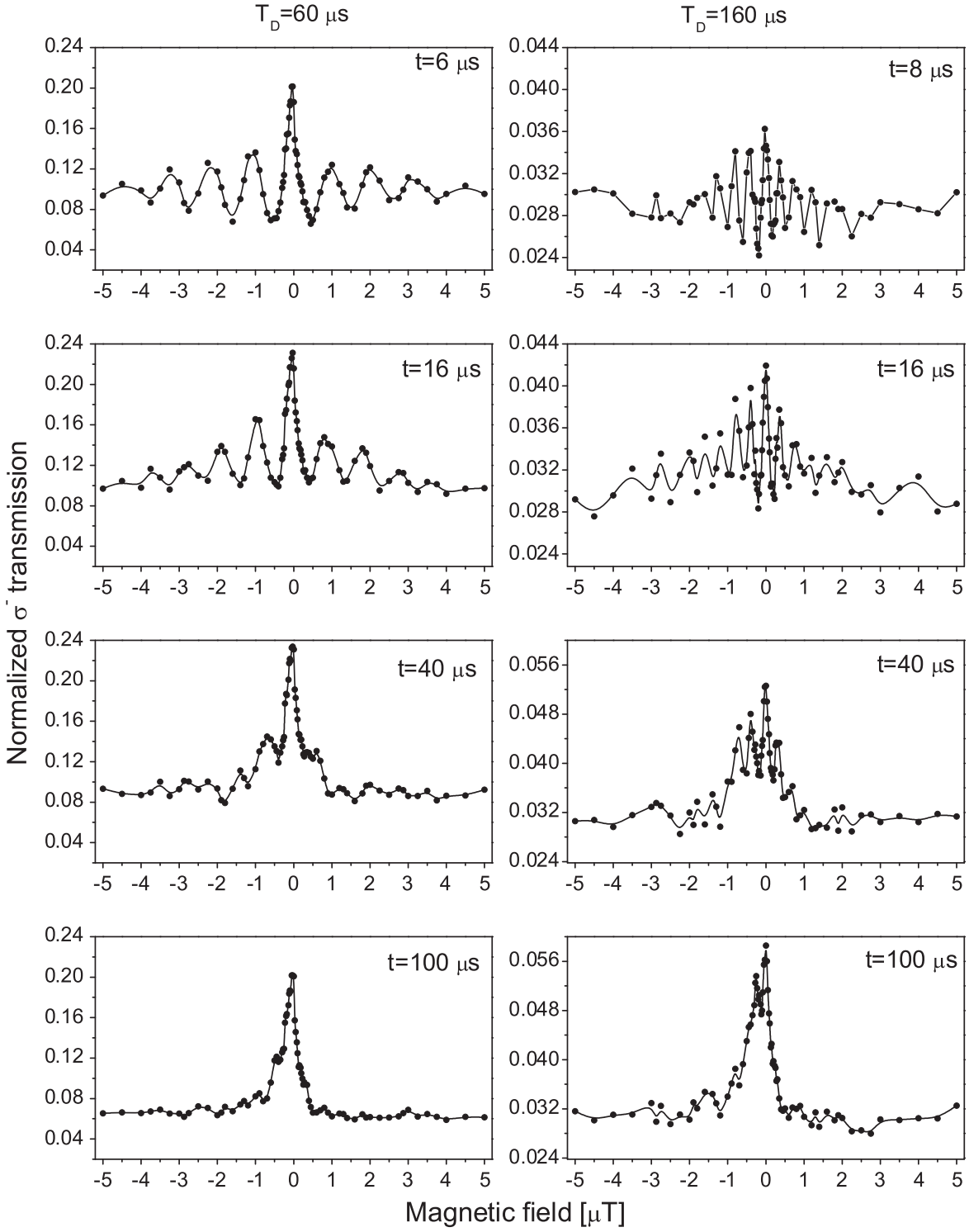

Figure 10. Time evolution of Zeeman EIT resonances during the probe pulse with overall laser beam intensity of $I_2 = 4.8\ \mathrm{mW\ cm^{-2}}$. The overall laser intensity during the preparatory pulse is $I_1 = 49\ \mathrm{mW\ cm^{-2}}$. The dark period is $T_D = 60\ \mu\mathrm{s}$ (left column) and $T_D = 160\ \mu\mathrm{s}$ (right column). The resonances are reconstructed and normalized from σ^- transmission signals at four different times (from top to bottom): $t = 6$ or 8 μs, $t = 16\ \mu$s, $t = 40\ \mu$s, and $t = 100\ \mu$s. The cell temperature is 85 °C.

magnetic field and probe electric field (at $t = 6\,\mu$s and $t = 16\,\mu$s). The frequency width of the fringes decreases with time of precession. At about 40 μs since the beginning of the probe pulse only first order fringes are visible. At longer time they start merging with the central peak ($t = 100\,\mu$s), and at even longer time only central peak remains. Experimental waveforms of EIT are in qualitative agreement with theoretical curves shown in figure 2, which are calculated under the same experimental conditions. We also found similar transition from EIT with fringes to EIT with only central peak at higher pulse intensity, except this transition is during shorter time.

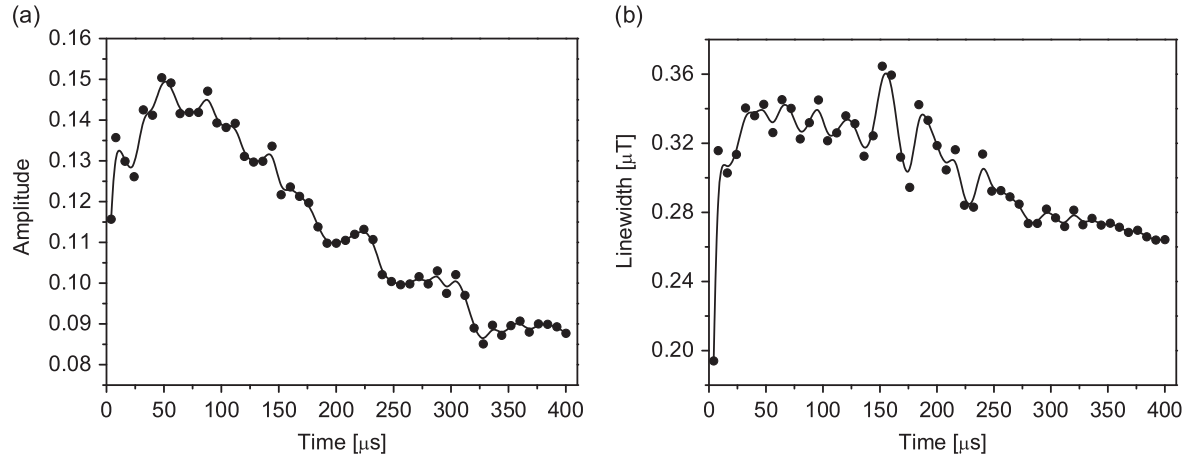

Figure 11. Experimentally obtained time evolution of Zeeman EIT (a) amplitude and (b) linewidth during the probe pulse. The overall intensities of the laser beam during preparatory and probe pulse are $I_1 = 49$ mW cm^{-2} and $I_2 = 4.8$ mW cm^{-2}, respectively. The dark period is $T_D = 60\,\mu$s. The cell temperature is 85 °C.

Time dependencies of Zeeman EIT amplitudes and linewidths are shown in figures 8(a) and (b), respectively, for dark time of 60 μs and two values of probe intensity, 0.9 and 2.5 mW cm^{-2}. One can see that more contrasted and narrower resonances are obtained when the probe pulse intensity is lower. Amplitudes of EIT behave differently at different pulse intensities. Similar to time dependence of transmitted probe intensity in figure 5, amplitudes of EIT resonances increase (decrease) with time for high (lower) probe intensity. When the pulse intensity is higher there is prevalent influence of power broadening. High intensity of the probe pulse also affects time evolution of Zeeman EIT. At high intensities (black squares at figure 8(b)) the strong electric field slows the precession, causing merging of the fringes with the central peak and broadening of the peak. However, at the beginning of the pulse, the EIT width is independent on the pulse intensity. It remains the same even when two pulses have very different intensities, as seen in figure 8. The significance of this finding is that EIT width will not vary with variations of intensities of the probe pulse as long as the pulse is shorter then a few μs. The width of the central peak is not sensitive to the intensity/power but to the absorbed energy of the laser light. The measured amplitudes agree well with calculated data shown in figure 3(a). However, the calculated linewidths (figure 3(b)) are somewhat larger than experimental ones.

In the investigation of the development of EIT when Raman detuning is achieved by modulating laser frequency at constant magnetic field, Yoshida *et al* have distinguished between the Raman–Ramsey and the hyperfine EIT spectra depending on the time gating within excitation pulse [34]. RRF were obtained at the pulse beginning while the EIT spectrum was obtained at its end. Due to variable magnetic field in our experiment, reconstructed σ^- transmission curve at each time instant consists of both Raman–Ramsey and EIT spectra.

Dependence of the transient development of Zeeman EIT resonances on Rb density and on the length of the dark time is studied by measuring signal pulse waveforms for Rb cell temperature of 85 °C and for two dark times: 60 μs and 160 μs. Similarly, σ^- transmission signal was measured at different magnetic fields during the preparatory and the probe pulse.

For investigations of transient behavior of EIT resonances, the intensities of preparatory and probe pulse were 49 and 4.8 mW cm^{-2}, respectively. At higher Rb density we needed to increase incident intensities in order to obtain signal from the transmitted σ^- component, that is high enough for good visibility of reconstructed EIT fringes. Measured transmissions of the σ^- component of the laser beam, during the preparatory and the probe pulse, are shown in figure 9 for two values of external magnetic field. As seen from figure 9(b), transmission of the σ^- component at very low magnetic field increases once the probe pulse has been established, and reaches the maximal value at some instant. After that moment, transmission starts to decay. This could be explained in terms that the probe pulse has enough optical power to further pump the atoms into the dark state, but at later times decoherence prevails and transmission drops. In the case of higher magnetic field, transmission drops right after the pulse is generated because of the higher value of two-photon detuning.

The reconstructed EIT curves for two dark times of 60 and 160 μs, are shown in figure 10.

RRF are observed at 6 and 8 μs after the beginning of the probe pulse. The fringes get narrower and weaker with precession time due to Zeeman decoherence, leading to a single EIT peak at later time instants. In classical Ramsey effect, the frequency width of the central Ramsey fringe is $1/(2 \cdot T_D)$. We have found that for dark times of 60 and 160 μs, the ratio of widths of the first order Ramsey fringes is in agreement with $1/(2 \cdot T_D)$ dependence. At these density and laser intensities fringes decay faster comparing to lower intensities (case with 67 °C cell temperature) because precession of the dark state is affected by electric field. The central peak is at each time instant also narrower when the dark time is 160 μs. Its narrowing could be explained by the work from [36]

where authors have shown the increase of Zeeman decoherence rate because of the Rb–Rb spin-exchange collisions.

Measured time dependencies of EIT amplitudes and linewidths during the probe pulse when dark time is 60 μs and temperature is 85 °C are shown in figures 11(a) and (b), respectively. The amplitudes increase at the beginning of the probe pulse and decay later. This is in qualitative agreement with the σ^- transmission time dependence as presented in figure 9(b). The linewidths of EIT resonances are wider at higher density (85 °C versus 67 °C) due to the power broadening caused by higher laser beam intensity. At high pulse intensities needed for this Rb vapour density, the precession of the Zeeman coherences is slowed in the laser electric field and fringes start to merge with the central peak, thus broadening the resonance at earlier times.

4. Conclusion

We presented experimental and theoretical study of the transient response of EIT medium to propagation of laser polarization pulses resonant to EIT transition. Through observed time development of the σ^- pulse transmission at different magnetic fields, we reconstructed Zeeman EIT resonances corresponding to various time instants during pulse propagation. The EIT resonances during the probe pulse have characteristic Ramsey fringes at early times and a narrow central peak at later moments. Ramsey fringes or oscillations of probe transmission during pulse propagation in magnetic field are caused by Larmor precession during the dark time. The disappearance of fringes is faster for larger probe pulse intensities due to incoherent pumping and effects of electric field on precession of atomic coherences. The behavior of amplitudes and linewidths of the EIT central peak depends on the probe intensity and Rb density. At very low probe intensity they both monotonically decay if Rb density is low, while at higher density amplitudes and widths they first increase and then decay.

We have studied transients of the polarization laser pulses for the system that is often used in slow light and storage of light experiments. Thus, better knowledge of polarization pulse transmission and time development of EIT resonances is valuable.

Acknowledgments

We thank J Dimitrijević and Z D Grujić for fruitful and useful discussions. Authors acknowledge funding from Grants No. III45016 and OI171038 of the Ministry of Education, Science and Technological Development of the Republic of Serbia and Scopes JRP IZ7370_127942.

References

[1] Boller K J, Imamoğlu A and Harris S E 1991 *Phys. Rev. Lett.* **66** 2593
[2] Field J E, Hahn K H and Harris S E 1991 *Phys. Rev. Lett.* **67** 3062
[3] Arimondo E 1996 *Prog. Opt.* **35** 257
[4] Phillips D F, Fleischhauer A, Mair A, Walsworth D F and Lukin M D 2001 *Phys. Rev. Lett.* **86** 783
[5] Klein M J 2009 Slow and stored light in atomic vapor cells *PhD Thesis* Harvard University
[6] Fleischhauer M, Imamoğlu A and Marangos J P 2005 *Rev. Mod. Phys.* **77** 633
[7] Bai Y S, Mossberg T W, Lu N and Berman P R 1986 *Phys. Rev. Lett.* **57** 1692
[8] Fry E S, Li X, Nikonov D, Padmabandu G G, Scully M O, Smith A V, Tittel F K, Wang C, Wilkinson S R and Zhu S Y 1993 *Phys. Rev. Lett.* **70** 3235
[9] Greentree A D, Smith T B, Echaniz S R, Durrant A V, Marangos J P, Segal D M and Vaccaro J A 2002 *Phys. Rev. A* **65** 053802
[10] Harris S E and Luo Z-F 1995 *Phys. Rev.* A **52** R928
[11] Chen H X, Durrant A V, Marangos J P and Vaccaro J A 1998 *Phys. Rev.* A **58** 1545
[12] Park S J, Cho H, Kwon T Y and Lee H S 2004 *Phys. Rev. A* **69** 023806
[13] Wu Y and Yang X 2005 *Phys. Rev.* A **71** 053806
[14] Wu Y and Yang X 2004 *Phys. Rev.* A **70** 053818
[15] Meinert F, Basler C, Lambrecht A, Welte S and Helm H 2012 *Phys. Rev.* A **85** 013820
[16] Vanier J, Godone A and Levi F 1998 *Phys. Rev.* A **58** 2345
[17] Valente P, Failache H and Lezama A 2002 *Phys. Rev.* A **65** 023814
[18] Margalit L, Rosenbluh M and Wilson-Gordon A D 2012 *Phys. Rev.* A **85** 063809
[19] Margalit L, Rosenbluh M and Wilson-Gordon A D 2013 *Phys. Rev.* A **88** 023827
[20] Shwa D and Katz N 2014 *Phys. Rev.* A **90** 023858
[21] Valente P, Failache H and Lezama A 2003 *Phys. Rev.* A **67** 013806
[22] Berman P R and Salomaa R 1982 *Phys. Rev.* A **25** 2667
[23] Li Y Q and Xiao M 1995 *Opt. Lett.* **20** 1489
[24] Dimitrijević J, Arsenović D and Jelenković B M 2011 *New J. Phys.* **13** 033010
[25] Ramsey N F 1956 *Molecular Beams* (New York: Oxord University Press)
[26] Zanon T, Guérandel S, Clercq de E, Holleville D, Dimarcq N and Clairon A 2005 *Phys. Rev. Lett.* **94** 193002
[27] Zanon T, Trémine S, Guérandel S, Clercq de E, Holleville D, Dimarcq N and Clairon A 2005 *IEEE Trans. Instrum. Meas.* **54** 776
[28] Liu X, Mérolla J-M, Guérandel S, Clercq de E and Boudot R 2013 *Opt. Express* **21** 12451
[29] Chen X, Yang G-Q, Wang J and Zhan M-S 2010 *Chin. Phys. Lett.* **27** 113201
[30] Yisheng M, Jianliao D, Zhengfeng H, Huijuan H and Yuzhu W 2013 *Chin. Opt. Lett.* **11** 032701
[31] Supplee J M 2010 *J. Opt. Soc. Am.* B **27** 1543
[32] Chen J F, Lu W, Wang S, Loy M M T, Wong G K L and Du S 2010 *Opt. Lett.* **35** 1923
[33] Pati G S, Fatemi F K and Shahriar M S 2011 *Opt. Express* **19** 22388
[34] Yoshida I, Hayashi N, Fujita K, Taniguchi S, Hoshina Y and Mitsunaga M 2013 *Phys. Rev.* A **87** 023836
[35] Zibrov A S and Matsko A B 2001 *Phys. Rev.* A **65** 013814
[36] Shuker M, Firstenberg O, Sagi Y, Ben-kish A, Davidson N and Ron A 2008 *Phys. Rev.* A **78** 063818
[37] Braje D A, DeSavage S A, Adler C L, Davis J P and Narducci F A 2014 *J. Mod. Opt.* **61** 61
[38] Yang J, Tian Y, Tan B, Yun P and Gu S 2014 *J. Appl. Phys.* **115** 093109
[39] Mair A, Hager J, Phillips D F, Walsworth R L and Lukin M D 2002 *Phys. Rev.* A **65** 031802(R)

[40] Taichenachev A V, Yudin V I, Wynands R, Stahler M, Kitching J and Hollberg L 2003 *Phys. Rev.* A **67** 033810
[41] Failache H, Valente P, Ban G, Lorent V and Lezama A 2003 *Phys. Rev.* A **67** 043810
[42] Nikolić S N, Radonjić M, Krmpot A J, Lučić N M, Zlatković B V and Jelenković B M 2013 *J. Phys. B: At. Mol. Opt. Phys.* **46** 075501
[43] Anders L and Garth W 2010 *ACM Trans. Math. Softw.* **37** 20:1–20:28
[44] Logg A, Mardal K-A and Wells G N 2012 *Automated Solution of Differential equations by the Finite Element Method* (*Lecture Notes in Computational Science and Engineering* vol 84) (Berlin: Springer)
[45] Mortensen M, Langtangen H P and Wells G N 2011 *Adv. Water Resour.* **34** 1082
[46] Wasik G, Gawlik W, Zachorowski J and Zawadzki W 2002 *Appl. Phys.* B **75** 613
[47] Petelski T, Fattori M, Lamporesi G, Stuhler J and Tino G M 2003 *Eur. Phys. J.* D **22** 279
[48] Nikolić S N, Batić V, Panić B and Jelenković B M 2013 *Rev. Sci. Instrum.* **84** 063108
[49] Steck D A 2008 *Rubidium 87 D Line Data* (http://steck.us/alkalidata)

Parametric non-degenerate four wave mixing in hot potassium vapor

Bojan Zlatković*[a], Aleksandar J. Krmpot[a],Nikola Šibalić[b],Milan Radonjić[a], Branislav M. Jelenković[a]
[a]Institute of Physics, University of Belgrade, Pregrevica 118, 11080 Belgrade, Serbia; [b]Faculty of Physics, University of Belgrade, Studentski trg 16, 11000 Belgrade, Serbia

ABSTRACT

In this study we show the results for parametric non-degenerate four wave mixing (FWM) obtained using double lambda scheme at D1 line in hot potassium vapor. We have investigated the influence of one-photon detuning and two-photon detuning on the FWM gain. The laser frequency is locked at approximately 1GHz from the resonance $4S_{1/2}$ $F_g=1$ -> $4P_{1/2}$, using external reference cavity. The probe beam passes through acoustooptic modulator that enables controllable detuning around 460 MHz (ground state hyperfine splitting) in respect to the pump beam. The vacuum glass cell containing the potassium vapor was heated by hot air in order to achieve necessary concentration of atoms. The efficiency of FWM process is studied by measuring the gains of the conjugate beam the probe beam, simultaneously. The maximal gain was achieved for nonzero two photon detuning.

Keywords: four wave mixing, potassium, copropagating beams

1. INTRODUCTION

Four wave mixing in atomic vapors is a non-linear interaction between atoms and light that allows exchange of energy between four different modes of light in a nonlinear medium. It has been investigated in inhomogeneously broadened hot atomic vapor[1], and in cold atomic samples[2], using different atomic level schemes. FWM in alkali atoms have shown success in generating high gain of twin beams, probe and conjugate photons, and efficient amount of relative intensity squeezing[3, 4]. Although there is a number of studies exploring FWM in Rb and Cs[5] to our knowledge this is the first investigation of FWM in double-Λ schemes in K.

We study FWM in ^{39}K, using double-Λ scheme, driven by far detuned (compared to Doppler width), and nearly co-propagating pump and probe laser beams. The pump and the probe are in near two-photon resonance between ground state hyperfine levels. Such FWM relies on coherence among two hyperfine levels[6] in the ground state of K, and elimination of resonant absorption due to electromagnetically induced transparency[3].The goal is to investigate ability of this scheme in K for efficient FWM and large gains of both pump and conjugate beam. Potassium hyperfine splitting in the ground state is 460 MHz[7], narrower that the Doppler broadened width. Therefore, detuning of the probe photons from the exited state hyperfine levels, in the outer Λ branch, is much smaller than in other alkalis and this could lead to very efficient FWM process and high gains. Besides atomic scheme, laser intensity and a single photon detuning, i.e., saturation intensity, together with atomic density and two-photon detuning play major roles in efficiency of FWM. In this work we investigate gains of the probe and the conjugate beams as a function of two-photon detuning, for various values of a single photon detuning. The pump laser power, atomic density, angle between the pump and the probe beams and diameters of the pump and the probe are kept fixed.
FWM in the atomic scheme of this experiment is suggested to efficiently generate non-classical beams and relative intensity squeezed light[8]. Our aim in this work is to maximize the gain of the FWM process since the degree of relative intensity squeezing depends on this gain. Interactions like FWM offer many promising applications due to unique properties of the conjugate beam and high entanglement between probe and conjugate[9].

*bojan@ipb.ac.rs; +381 64 2366555; www.photonics.ipb.ac.rs

18th International School on Quantum Electronics: Laser Physics and Applications, edited by Tanja Dreischuh, Sanka Gateva, Alexandros Serafetinides, Proc. of SPIE Vol. 9447, 944706 · © 2015 SPIE
CCC code: 0277-786X/15/$18 · doi: 10.1117/12.2177885

2. EXPERIMENTAL SETUP

We have used the D_1 line of potassium for the realization of the double-Λ system. The lower levels of the Λ scheme are two hyperfine sublevels of K ground level $^2S_{1/2,}$ F=1 and $^2S_{1/2,}$ F=2 (figure 1). For the upper level we neglect the hyperfine splitting since it is small compared to detuning. The hyperfine splitting between two lower levels is 461.7 MHz[7].

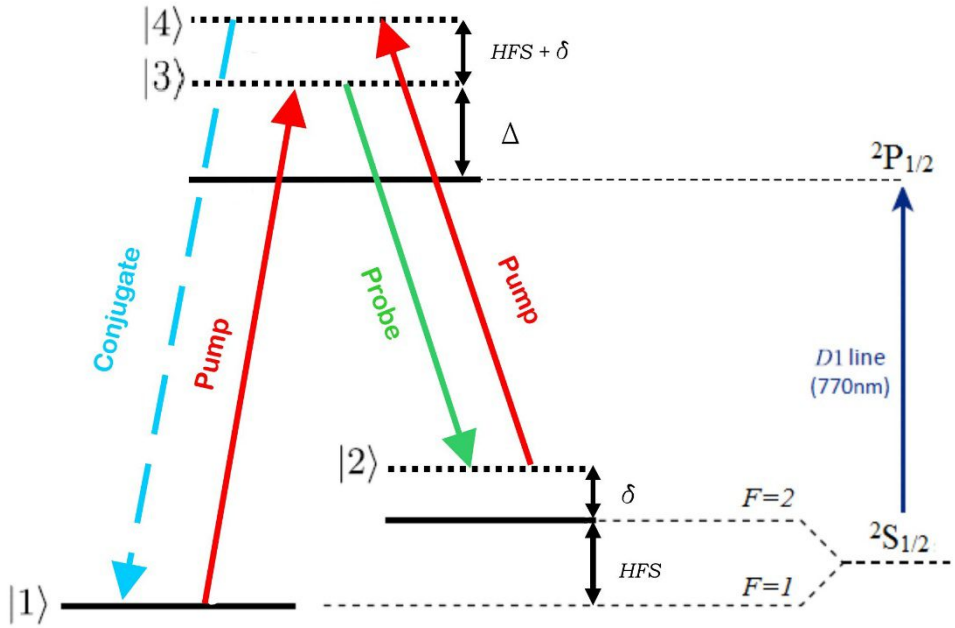

Figure 1. Double-Λ scheme on the D_1 line of ^{39}K. *HFS* – hyperfine splitting of the ground state, Δ- one photon detuning, δ- two photon detuning.

The experimental scheme is presented in Figure 2. Ti:Sapphire ring laser (MBR 110, Coherent Inc) is used as a light source. The pump and the probe beams are obtained by dividing the same laser beam with an asymmetric (90:10) beam splitter. Main part of the laser power is used as a pump beam, driving the D_1 line of ^{39}K at 770 nm and it is detuned for approximately 1GHz. The probe beam passes an acousto optic (AOM) modulator which operates on 230 MHz in double-pass configuration. The pump and the probe beams are focused with two pairs of lenses in order to achieve 1mm and 0.8 mm diameters respectively. They are perpendicularly polarized and combined on polarization beam splitter at the small angle of 1.5 mrad. Two beams intersect in the center of a 50 mm long natural-abundance potassium vapor cell. The temperature of the cell is kept at 100°C. Concentration of potassium atoms on this temperature is $7.6*10^{17}$ atoms/m^3. In order to heat up the cell we have put it in an aluminum cylinder with drilled holes along its axis through which the hot air was blown. The windows of the cell are Brewster's angled and the position of the cell is optimized for maximal pump transmission (∼90%). Since the probe is polarized perpendicularly to the pump transmission of the probe is much lower (∼50%). Optical powers of the pump and the probe inside the cell are estimated to 400 mW and 0.2 mW respectively upon direct measurements in front of the cell and windows transmissivity. The four wave mixing process occurs in the intersection volume creating probe and conjugate photons. The amplified probe and the conjugate beams leave the cell and hit two photodiodes while the pump beam is reflected away by another polarizing beam splitter after the cell.

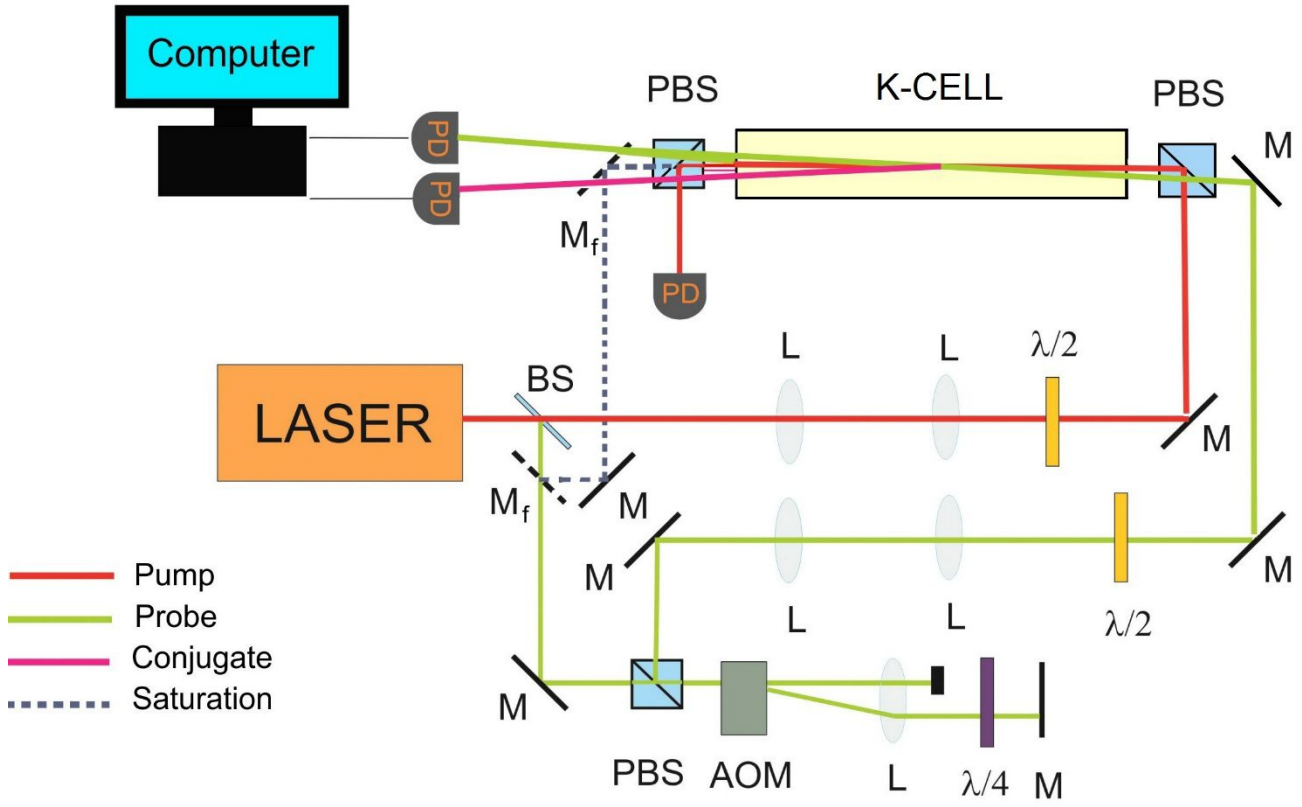

Figure 2. Experimental setup. BS - beam splitter, M - mirrors, M_f - flip mirrors, PBS - polarizing beam splitter, AOM - acousto optic modulator, L - lenses, λ/4 - lambda-quarter wave plate, λ/2 - lambda-half wave plates, PD - photodiodes.

The probe beam frequency i.e. the two photon detuning δ is scanned by changing the AOM frequency. The double-pass configuration of the AOM allows us to scan this frequency without the change of the probe beam direction. The frequency of the laser was locked by the internal locking system of the laser. Internal locking system of the laser has two stages. Firstly the single mode oscillation is achieved with an intracavity etalon and secondly the frequency was locked to the external reference cavity using Pound-Hall-Drever method. In order to determine the long term frequency stability of the laser and to measure one photon detuning we have incorporated the saturation spectroscopy (SS) setup into our experiment. To this end we have added two flip mirrors which divert the probe beam before the AOM making it the saturation beam in SS configuration which counter propagates the pump in the vapor cell. Initial pump is highly attenuated and used like probe beam in SS configuration. Spectrum with hyperfine resolved features are given in Figure 3.The temperature of the vapor was 67°C.This spectra is obtained by subtracting Doppler profile from the SS signal. We can distinguish three groups of lines corresponding to different sublevels of ground state. Within these three groups there are three peaks (except for $F_g=2$ group) which correspond to different hyperfine transitions. We have used the $F_g=1$ -> CO transitions as our reference for one-photon detuning.

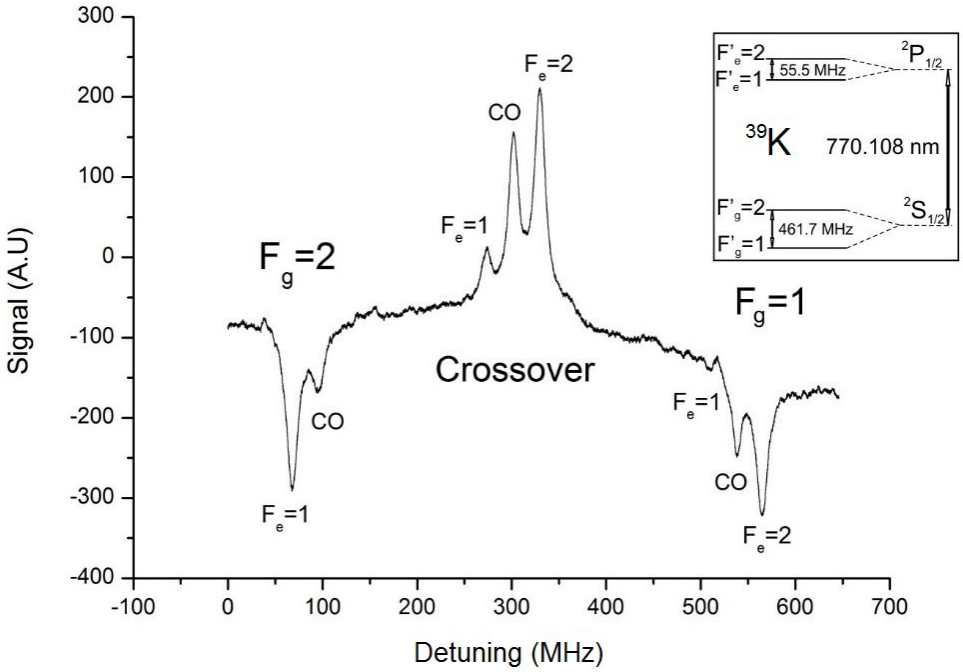

Figure 3. Measured saturation spectra of the D_1 line of ^{39}K (Scheme of levels is given in the inset[1]).

3. EXPERIMENTAL RESULTS

In our experiment we have measured the gain of the probe and conjugate as a function of two-photon detuning for three different values of one-photon detuning. The gain of the pump and the conjugate is defined as $G_p=P_p/P_{in}$ and $G_c=P_c/P_{in}$ respectively where P_p and P_c are measured powers of the probe and the conjugate respectively and P_{in} is initial power of the probe inside the vapor cell. The losses of the probe and the conjugate due to the output window of the vapor cell ($\sim$30%) are not taken in count. Two-photon detuning (δ) is swept over 60 MHz around the two-photon resonance in 4 MHz steps. The values of one-photon detuning (Δ) in the experiment are chosen to be 700 MHz, 1000 MHz and 1300 MHz. The results are given in figure 4a, b, and c respectively. For Δ=700 MHz maximal gains of the conjugate and the probe beam are 2 and 0.55 respectively. They are located at $\delta\approx$-20 MHz. For this particular set of the parameters maximal gain for the conjugate is rather small while the probe amplification is negligible. The gain region spans about MHz of two-photon detuning determined as full width at half maximum (FWHM)

For Δ=1000 MHz maximal gains of the conjugate and the probe beam are significantly higher, and reach 8.2 and 2.2 respectively. These maximal gains occur at $\delta\approx$- 9 MHz. The gain region is a bit narrower and spans around 16 MHz, also measured as FWHM.

For Δ= 1300 MHz maximal gain of the conjugate and the probe is 5.9 and 1.7 respectively which is lower than for the Δ=1000 MHz case. They are placed around $\delta\approx$-5 MHz. Gain region is even narrower and spans about 12 MHz.

Regarding to the measurements, the highest gains are achieved for Δ=1000 MHz. Possible reason for that is the competition between the resonant absorption and the FWM process. The probe and the conjugate photons which are created in the FWM process are subjected to the resonant absorption on the D_1 line. Increasing the detuning of the pump and with it the detuning of the probe and the conjugate decreases the probability for resonant absorption, but decreases the probability for FWM process as well. The optimum is found at the wing of the Doppler profile (the width of the Doppler profile for ^{39}K vapor at t=100^oC is 860 MHz[10]) which is in our case about 1000 MHz. The conjugate is detuned about 920 MHz (two hyperfine splitting of ground states plus δ) more from the D_1 line than the probe which may explain its larger gain.

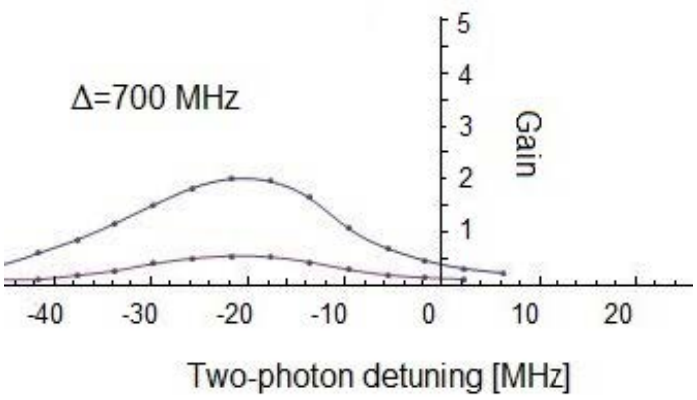

a)

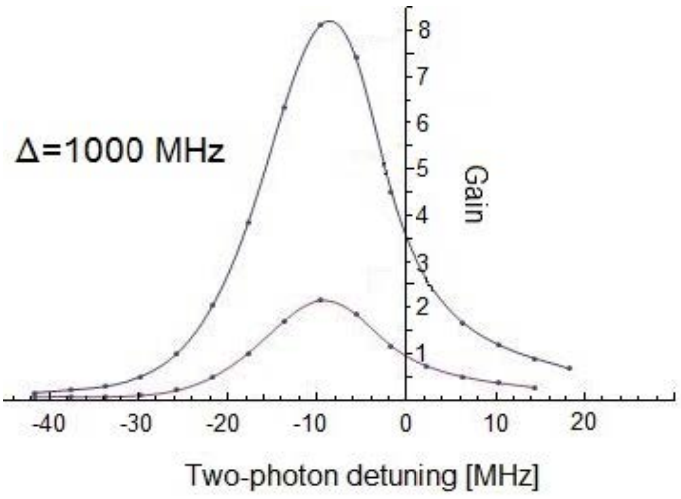

b)

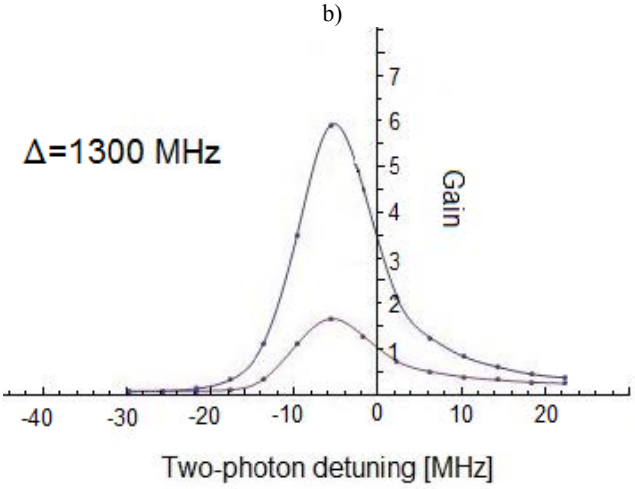

c)

Figure 4. Gain of the conjugate (blue) and probe (purple) versus two-photon detuning for a) Δ=700 MHz, b) Δ=1000 MHz, c) Δ=1300 MHz

4. CONCLUSION

We have demonstrated non-degenerate four wave mixing in hot potassium vapor based on coherent population trapping. The experiments of this type and generated twin beams are mostly used further for relative intensity squeezing and sub shot noise measurements. Unlike of ours, most of the experiments with similar problematic are performed in rubidium or cesium vapor. FWM process in potassium vapor is predicted to yield lager gain due to smaller ground state hyperfine splitting and thus smaller mutual detuning of the two lambda schemes.

The achieved effect is examined for maximum gain regarding to two most important parameters, one and two photon detuning. Counter intuitively we found out that maximum gain is achieved for non zero two photon detuning. This finding is in accordance with results of Turnbull *et al*[1]. Also, one photon detuning for the maximum gain is determined. Other parameters, such as vapor temperature, mutual pump-probe angle and intensities were fixed in the experiment, and the dependence of the FWM process on those parameters is not examined in details in this study.

These parameters will be investigated in the future studies, aiming to characterize relative intensity squeezing, and achieve noise below standard quantum limit.

REFERENCES

[1] Turnbull, M. T., Petrov, P. G., Embrey, C. S., Marino, A. M., Boyer, V., "Role of the phase-matching condition in nondegenerate four-wave mixing in hot vapors for the generation of squeezed states of light," Phys. Rev. A 88, 033845 (2013)

[2] Braje, D. A., Balic, V., Goda, S., Yin, G.Y., Harris, S. E., "Frequency Mixing Using Electromagnetically Induced Transparency in Cold Atoms," Phys. Rev. Lett. 93, 183601 (2004)

[3] McCormick, C. F.,Boyer, V., Arimondo, E., Lett, P. D., "Strong relative intensity squeezing by four-wave mixing in rubidium vapor." Optics Letters, Vol. 32, Issue 2, pp. 178-180 (2007)

[4] Glorieux, Q., Guidoni,Guibal, L. S., Likforman, J.-P., Coudreau, T., "Quantum correlations by four-wave mixing in an atomic vapor in a nonamplifying regime:Quantum beam splitter for photons," Phys. Rev. A 84, 053826 (2011)

[5] Guo, M., Zhou, H., Wang, D., Gao, J., Zhang, J., Zhu, S., "Experimental investigation of high-frequency-difference twin beams in hot cesium atoms," Phys. Rev. A 89, 033813 (2014)

[6] Hemmer, P. R., Katz, D. P., Donoghue, J., Cronin-Golomb, M., Shahriar, M. S., Kumar, P., "Efficient low-intensity optical phase conjugation based on coherent population trapping in sodium," Opt. Lett. 20, 9, 982-984 (1995)

[7] Tiecke, T. G., "Properties of potassium," http://www.tobiastiecke.nl/archive/PotassiumProperties.pdf (2011)

[8] Pooser, R. C., Marino, A. M., Boyer, V., Jones, K. M., Lett, P. D., "Quantum correlated light beams from nondegenerate four-wave mixing in an atomic vapor: the D1 and D2 lines of ^{85}Rb and ^{87}Rb," Opt. Express, Vol. 17, No. 19, 16722 (2009)

[9] Boyer, V., Marino, A. M., Pooser, R. C., Lett, P. D., "Entangled Images from Four-Wave Mixing," Science, Vol. 321 no. 5888, pp. 544-547 (2008)

[10] Demtroder, W., "Laser Spectroscopy Vol. 1," Springer-Verlag, Berlin, Heidelberg, 70-73 (2008)

IOP Publishing | Royal Swedish Academy of Sciences Physica Scripta

Phys. Scr. **T163** (2014) 014003 (4pp) doi:10.1088/0031-8949/2014/T163/014003

A quantum-classical theory with nonlinear and stochastic dynamics

N Burić, D B Popović, M Radonjić and S Prvanović

Institute of Physics, University of Belgrade, Pregrevica 118, 11080 Belgrade, Serbia

E-mail: buric@ipb.ac.rs

Received 13 February 2014
Accepted for publication 2 April 2014
Published 19 December 2014

Abstract

The method of constrained dynamical systems on the quantum-classical phase space is utilized to develop a theory of quantum-classical hybrid systems. Effects of the classical degrees of freedom on the quantum part are modeled using an appropriate constraint, and the interaction also includes the effects of neglected degrees of freedom. Dynamical law of the theory is given in terms of nonlinear stochastic differential equations with Hamiltonian and gradient terms. The theory provides a successful dynamical description of the collapse during quantum measurement.

Keywords: quantum-classical systems, degrees of freedom, hybrid theory

1. Introduction

The general motivation for hybrid theories of quantum-classical systems are given in the contribution by Prof. H-T Elze [1]. Hybrid theories can be divided into two groups according to the conceptual status and aims. In the theories of the first group one considers all systems in nature as described at the fundamental level by quantum theory and therefore the hybrid system is an approximation of two interacting quantum systems, where one of the systems is treated in the corresponding classical limit [2–4]. In the other approach, one assumes from the beginning that the classical and quantum mechanics are both correct theories with different domains of validity (illustrative examples of this approach are given in [5, 6]). The only restriction on the descriptions of the quantum-classical (QC) interaction is then given by the experiments involving micro-macro objects and the phenomenological collapse postulate. Of course, it is clear that a macro-object has many degrees of freedom which are not described by the macroscopic model of the classical theory. The effects of those degrees of freedom have to be somehow included into the manner a hybrid theory treats the QC interaction. The hybrid theory constructed in the present paper presents a particular way of doing this.

2. Construction of the hybrid theory

The mathematical framework of the hybrid theory to be developed is that of an abstract dynamical system $\left(\mathcal{M}, \Omega, G, H\right)$ on a differentiable manifold $\mathcal{M}$ with symplectic and Riemannian structures Ω and G respectively, with some preferred function, the Hamiltonian H. Let us stress right at the beginning that the dynamical law of the hybrid theory need not be of the Hamiltonian form, but will involve differential equations on $\mathcal{M}$ given in terms of Ω and G. The manifold is also assumed to possess a complex structure $J^2 = -I$, where I stands for identity, such that $G\left(x, y\right) = \Omega\left(x, Jy\right)$.

Formulation of the classical mechanics of isolated conservative systems using $\left(\mathcal{M}, \Omega, H\right)$ is standard [7]. The formulation of quantum mechanics in terms of $\left(\mathcal{M}, \Omega, G, H\right)$ is perhaps less well known, but shall not be presented here in any detail since there exist excellent reviews [8] and brief accounts [9–11] which are sufficient for our purposes. The generic point from $\mathcal{M}$ is usually denoted by (x, y), X or X^a, where $a = 1, 2, \ldots 2N$ is an abstract index. In what follows the symplectic and Riemannian structures on the quantum phase space are denoted by ω^{ab} and g^{ab}. The Hamilton's function $H(X)$ is given by the quantum expectation of the Hamiltonian $\hat{H}$ in the state $\left|\psi_X\right\rangle$ corresponding to a point X: $H\left(X\right) = \left\langle \psi_X|\hat{H}|\psi_X\right\rangle \Big/ \left\langle \psi_X\Big|\psi_X\right\rangle$. In fact, all observables are represented by quadratic functions $A(X)$ on $\mathcal{M}$, and are the quantum mechanical expectations of the corresponding quantum observables $A\left(X\right) = \left\langle \psi_X|\hat{A}|\psi_X\right\rangle \Big/ \left\langle \psi_X\Big|\psi_X\right\rangle$. The

Schrödinger dynamical law is that of Hamiltonian mechanics

$$\dot{X}^a = \omega^{ab}\nabla_b H. \tag{1}$$

2.1. Elements of the hybrid model

In the hybrid theory to be constructed, the hybrid phase space $\mathcal{M}$ is assumed to be given by the Cartesian product $\mathcal{M} = \mathcal{M}_{qp} \times \mathcal{M}_{QP} \times \mathcal{M}_{xy}$. Local canonical coordinates are separated into three groups: (q, p), (Q, P) and (x, y). The first two groups $(q, p) \in \mathcal{M}_{qp}$ and $(Q, P) \in \mathcal{M}_{QP}$ correspond to the degrees of freedom of the macroscopic system, and the third $(x, y) \in \mathcal{M}_{xy}$ to the degrees of freedom of the microscopic quantum system, called quantum degrees of freedom (QDF). The coordinates (q, p) represent (usually a small number of) distinguished macroscopic degrees of freedom of the macroscopic object. They are supposed to be well described by classical mechanics and are called classical degrees of freedom (CDF). If in a particular physical situation there are no degrees of freedom that are well described by classical mechanics then the whole idea of hybrid description is meaningless.

The degrees of freedom denoted by (Q, P) describe the physical quantities that are not used in the characterization of the CDF of the macroscopic object nor of the QDF of the micro-system. Apart from the fact that there are many of these degrees of freedom, nothing else about their character is assumed in the hybrid theory. One could argue that the acroscopic system is composed of quantum microscopic components which interact and entangle with the micro-system. Therefore, the hybrid theory, with no possibility of explicit entanglement between CDF and QDF, must take the fact of entanglement due to micro-system and micro-components of the macro-system into account in some manner. The influence of (Q, P) degrees of freedom on the CDF-QDF system might be interpreted partly as due to the entanglement between the micro and macro-system, and partly due to the physical interaction of the micro degrees of freedom of the macro-system with QDF and with CDF. Alternatively, one could just conceive (Q, P) degrees of freedom as a sufficiently general type of environment of the CDF-QDF degrees of freedom.

Interactions between various types of degrees of freedom might be of a different nature. We shall assume that the interactions between (q, p) and (x, y) are conservative and described by the corresponding Hamiltonian. On the other hand, interactions between the unspecified degrees of freedom (Q, P) and the QDF (x, y) might be more general, and are described by a complex Hamiltonian of the form $H_{int}\left(x, y, Q, P\right) = F\left(Q, P\right)A\left(x, y\right)$ where $A\left(x, y\right)$ is a quadratic function of (x, y) corresponding to the operator $\hat{A}$ of the micro-system and $F\left(Q, P\right) = F_R\left(Q, P\right) + \mathrm{i}F_I\left(Q, P\right)$ in terms of real functions $F_R\left(Q, P\right)$ and $F_I\left(Q, P\right)$. Of course, the equations of motion for the real coordinates (q, p, x, y) must be expressed only in terms of real quantities. The dynamics of the total system is thus determined by the complex Hamiltonian of the following form

$$\begin{aligned} H = {} & H_{cl}\left(q, p\right) + H_q\left(x, y\right) + H_{QP}\left(Q, P\right) \\ & + f\left(q, p\right)A\left(x, y\right) + F\left(Q, P\right)A\left(x, y\right), \end{aligned} \tag{2}$$

where the notation is obvious. We have neglected the influence of (Q, P) on CDF (q, p) but this can be easily added.

2.2. Dynamics of QDF

The main requirement on the hybrid theory of QDF evolution, based on the collapse model, is that if the state of the quantum system is a superposition of $\hat{A}$ eigenstates then, because of the interaction with the macro-system, the state must evolve towards one of the $\hat{A}$ eigenstates. However, such behavior is not obtained starting from the Hamiltonian dynamics with the Hamiltonian (2) of the hybrid. One is therefore forced to adopt different approaches in modeling the collapse requirements. One approach, adopted here, is to consider the collapse requirements as appropriate constraints onto the otherwise Hamiltonian dynamics and to derive the dynamical law as the constrained dynamics.

The eigenstates of any observable $\hat{A}$ are characterized by the property that the dispersion $\Delta A = \left\langle \hat{A}^2 \right\rangle - \left\langle \hat{A} \right\rangle^2$ is equal to zero. In the case when all observables $\left\{\hat{A}_n\right\}$ interacting with the macro-system commute, the relevant constraint might be given in the form

$$\Gamma_A\left(x, y\right) = \sum_n \Delta A_n\left(x, y\right) = 0, \tag{3}$$

which corresponds to a common eigenstate of all the observables $\left\{\hat{A}_n\right\}$. Generalization to several non-commuting observables mediating the QC interaction is not trivial and is indicated in [12].

Besides the appropriate constraint we shall also suppose that the complicated functions of time $Q\left(t\right)$, $P\left(t\right)$ are well approximated by white noise. The full derivation of the resulting dynamical equations is given in [12]. The result is the dynamical equation of QDF in interaction with the macro-system, given by the following stochastic differential equation of a non-autonomous diffusion process,

$$\begin{aligned} dX^a = {} & \omega^{ab}\nabla_b\left(H_q + f\left(q, p\right)A\left(x, y\right)\right)\mathrm{d}t \\ & - k\frac{\left\{\Gamma_A, H_q\right\}}{\left\|\nabla\Gamma_A\right\|^2}g^{ab}\nabla_b\Gamma_A\mathrm{d}t + \omega^{ab}\nabla_b A\ \mathrm{d}W_R \\ & + g^{ab}\nabla_b A\ \mathrm{d}W_I. \end{aligned} \tag{4}$$

The equation (4) is the main dynamical equation of the QDF interacting with the macro-system of the hybrid theory developed here. The free parameter $k \in \left[0, 1\right]$ takes the value $k = 1$ if the dynamics of isolated (q, p) degrees of freedom is well described by classical mechanics. This corresponds to the proper hybrid theory. At the other extreme are the systems where isolated (q, p) degrees of freedom are

described also by quantum mechanics. In this case $k = 0$. The first part of the drift in (4) describes Hamiltonian evolution with the Hamiltonian $H_q(x, y) + f(q, p)A(x, y)$. The second term of the drift represents a gradient flow with the tendency to decrease the total dispersion $\Delta A = \sum_n \Delta A_n$. The joint effect of the Hamiltonian and the gradient drift terms is to preserve constant the total dispersion (when $k = 1$). If there is only one observable $A(x, y)$, or a set of commuting observables, then the role of the gradient terms is to force the evolution towards the common eigenstates of $\{\hat{A}_n\}$. If the observables $\{\hat{A}_n\}$ do not commute, then there is a competition of tendencies due to the corresponding gradient terms. If these observables generate a representation of a semi-simple Lie algebra, then the gradient terms drive the system towards the invariant manifold of the coherent states of the algebra.

The stochastic terms are divided into two quite different groups. The Hamiltonian terms, which can be included as stochastic perturbations of the Hamiltonian, describe the Hamiltonian influence of the (Q, P) degrees of freedom on the motion of the quantum system. The gradient stochastic terms, on the other hand, describe the influence of (Q, P) degrees of freedom which is not Hamiltonian. However, as opposed to the Hamiltonian stochastic terms, the gradient stochastic terms induce localization onto the constraint manifold.

2.3. Dynamics of CDF

Classical degrees of freedom (q, p) satisfy the Hamiltonian evolution equations given by the Hamiltonian (2). The equations in terms of (q, p) are

$$\dot{q} = \frac{\partial H_{cl}(q, p)}{\partial p} + A(x, y)\frac{\partial f(q, p)}{\partial p}$$
$$\dot{p} = -\frac{\partial H_{cl}(q, p)}{\partial q} - A(x, y)\frac{\partial f(q, p)}{\partial q}. \quad (5)$$

The evolution of CDF is also stochastic because the quantum observables $A(x(t), y(t))$ evolve stochastically. We have neglected possible direct stochastic perturbation of (q, p) dynamics by $Q(t)$, $P(t)$. This could be included easily, but does not play any fundamental role.

Remark. Most of the well known dynamical collapse models are given as nonlinear and stochastic modifications of the Schrödinger equation, and contain the Schrödinger term, the nonlinear gradient term and the stochastic term [13, 14]. One such equation, with minimal appropriate generalization, can be postulated for the QDF dynamics of the hybrid and coupled with the Hamiltonian equations for the CDF. An example of such approach is studied in [14]. The result is a set of stochastic differential equations of the form similar to (4). However, there are technical and conceptual differences [12].

2.4. Quantum measurement process

Additional assumptions can be used in order to simplify the evolution equations (4) and (5) in the case of a quantum measurement process. One such approximation is based on the assumption that the dynamics of QDF is much faster than that of CDF. Consequently, one can replace in (4) the functions $(q(t), p(t))$ with their initial values (q_0, p_0). The equation for QDF becomes autonomous.This is useful for an analytic treatment of the asymptotic states using methods of stochastic stability analysis. The situation when QDF and CDF are coupled via only one observable $\hat{A}$ with the interaction term given by $H_{int} = pA(x, y)$, and when the gradient terms dominate the QDF dynamics, corresponds to the process of measurement of $\hat{A}$. Numerical computations [12] show that the state $\hat{A}$, and the probability of the asymptotic eigenstate (x_α, y_α) depends on its distance from the initial state $(x, y)_{init} \equiv |\psi\rangle_{init}$, i.e. on $\| \langle \psi_{init} | \alpha \rangle \|^2$. At the same time, the dynamics of the apparatus is dominated by the asymptotic eigenvalue. Thus, the approximate equations describe well the dynamics and the results of the measurement process.

3. Summary

Our goal was to derive a theory that provides a dynamical description of the Schrödinger evolution supplemented with the collapse postulate. It is assumed that such a theory would suggest a unified dynamical description of system with quantum and classical degrees of freedom. The basic requirement imposed on the theory is to obtain dynamical equations of the hybrid systems such that the sum of dispersions of the quantum observables that figure in the quantum-classical interaction are constrained to be minimal during the evolution. The crucial assumption that was used to simplify the constrained equations is that the dynamics of the unobserved degrees of freedom is to be replaced by white noise. Furthermore, it was assumed that part of the interaction with the unobserved degrees of freedom is described by a complex Hamiltonian, but the equations for the real canonical coordinates (q, p, x, y) are real. The resulting evolution of the hybrid system is nonlinear and stochastic. If the hybrid system is intended as a model of the measurement process of one observable, then the constraint gives the dynamics with eigenstates as attractors, and the stochastic term describes the stochastic nature of the process with the correct probabilities for different asymptotic eigenstates.

Acknowledgments

We acknowledge support of the Ministry of Science and Education of the Republic of Serbia, contracts No. 171006, 171017, 171020, 171038 and 45016 and COST (Action MP1006).

References

[1] Fratino L, Lampo A and Elze H-T 2014 *Phys. Scr.* **T163** 014005
[2] Diósi L, Gisin N and Strunz W T 2000 *Phys. Rev.* A **61** 022108

[3] Radonjić M, Prvanović S and Burić N 2012 *Phys. Rev.* A **85** 064101
[4] Burić N, Popović D B, Radonjić M and Prvanović S 2013 *Phys. Rev.* A **87** 054101
[5] Barcelo C, Carballo-Rubio R, Garay L J and Gmez-Escalante R 2012 *Phys. Rev.* A **86** 042120
[6] Elze H-T 2012 *Phys. Rev.* A **85** 052109
[7] Arnold V I 1978 *Mathematical Methods of Classical Mechanics* (New York: Springer)
[8] Aschtekar A and Schilling T A 1998 *On Einsteins Path* ed A Harvey (Berlin: Springer)
Brody D C and Hughston L P 2011 *J. Geom. Phys.* **38** 19
[9] Burić N 2008 *Ann. Phys. (NY)* **233** 17
[10] Radonjić M, Prvanović S and Burić N 2011 *Phys. Rev. A: Math. Theor.* **84** 022103
[11] Brody D C, Gustavsson A C T and Hughston L 2008 *J. Phys. A: Math. Theor.* **41** 475301
[12] Burić N, Popović D B, Radonjić M and Prvanović S 2014 *Ann. Phys. (NY)* **343** 1
[13] Bassi A, Lochan K, Satin S, Singh T P and Ulbricht H 2013 *Rev. Mod. Phys.* **85** 471
[14] Diósi L and Halliwell J J 1998 *Phys. Rev. Lett.* **81** 2846

Cloning in nonlinear Hamiltonian quantum and hybrid mechanics

D. Arsenović, N. Burić,* D. B. Popović, M. Radonjić, and S. Prvanović
Institute of Physics, University of Belgrade, Pregrevica 118, 11080 Belgrade, Serbia
(Received 20 May 2014; published 21 October 2014)

The possibility of state cloning is analyzed in two types of generalizations of quantum mechanics with nonlinear evolution. It is first shown that nonlinear Hamiltonian quantum mechanics does not admit cloning without the cloning machine. It is then demonstrated that the addition of the cloning machine, treated as a quantum or as a classical system, makes cloning possible by nonlinear Hamiltonian evolution. However, a special type of quantum-classical theory, known as the mean-field Hamiltonian hybrid mechanics, does not admit cloning by natural evolution. The latter represents an example of a theory where it appears to be possible to communicate between two quantum systems at superluminal speed, but at the same time it is impossible to clone quantum pure states.

DOI: 10.1103/PhysRevA.90.042115 PACS number(s): 03.65.Fd, 03.65.Sq

I. INTRODUCTION

The impossibility of cloning unknown quantum states is a fundamental property of quantum systems [1,2]. It has been used as a basis for information theoretic axiomatization of quantum mechanics (QM) [3] and is crucial in several quantum-information-processing tasks [4]. Roughly speaking, state cloning is a process which involves at least two systems: an object system whose state is to be cloned and a target system whose state is transformed into the state which is equal to the state of the object system. Often, and in order to allow for the most general type of process, one includes also an ancilla system, which in the context of cloning is called the cloning machine. Standard simple proofs of no cloning involve properties of quantum processes, such as (a) linearity or (b) preservation of a nontrivial distance between quantum states, and also use (c) the direct product structure of composite quantum systems. The properties (a), (b), and (c) are not independent in QM, but each of them implies crucial differences between QM and classical mechanics (CM). Modifying any of the three properties leads to generalization of QM, which is also different from CM. Some of generalizations are mathematically inconsistent or in conflict with other fundamental physical theories like special relativity or thermodynamics [5,6]. Depending on the modification, cloning of states in the modified theory might, but need not, be possible. The possibility of cloning in a modified theory need not be related to superluminal signaling, like it is in standard QM. It is the purpose of this paper to discuss possibility of cloning in two types of modifications of QM. Both types of modified theories are formulated in the framework of Hamiltonian dynamical systems (HDSs). Standard QM can be formulated as a linear HDS on an appropriate phase space [7,8]. Mathematically consistent generalizations of QM can be obtained by modifying some of the standard QM properties but remaining within the framework of HDS. It is known that cloning is possible in classical mechanics with Hamiltonian dynamics [9]. Thus, it is interesting to investigate the possibility of cloning within different Hamiltonian generalizations of QM. The first class of modified theories that we study retains all the kinematical properties of QM in HDS formulation but allows evolution given by general nonlinear Hamiltonian equations. Weinberg [10] and Bialynicki–Birula and Mycielski [11] nonlinear Schrödinger equations are actually of this type. We abbreviate this type of theories as NHQM, which stands for nonlinear Hamiltonian QM. The second type of modified theory assumes that some of the degrees of freedom (DFs) of the HDS corresponding to a bipartite system are constrained to behave as classical DF [12,13]. We call this type Hamiltonian hybrid mechanics (HHM). The constraint implies nonlinear evolution of both classical-like DF (CDF) and of quantum DF (QDF) [12,14], but also changes the way in which the phase spaces of QDF and CDF are composed to form the phase space of the total hybrid system. Thus, in these types of theories the evolution is nonlinear and the tensor product rule is not valid for all DF. Our main results are (a) self-replication, i.e., a type of cloning in the restricted sense without the cloning machine, is impossible in NHQM; (b) inclusion of a *quantum* cloning machine makes the cloning in NHQM possible, and (c) cloning with the object and the target quantum systems and a *classical* cloning machine is also possible with nonlinear hybrid evolution. Thus, these two types of nonlinear generalizations of quantum mechanics, in which the evolution of the total system is Hamiltonian, allow the cloning of quantum states by natural evolution. However, cloning is impossible in a type of HHM with the Hamiltonian of a special mean-field form. These results are to be contrasted with the known result that the cloning is impossible within bipartite classical Hamiltonian systems (object and target), but becomes possible within three-partite systems [9] (object, target, and cloning machine). In the latter case the cloning can be achieved by a linear symplectic map [9]. Thus, it seems that if the object and the target are quantum (tensor product) and the evolution of the total system that includes the machine is Hamiltonian, then the cloning map is necessarily nonlinear, irrespective of the quantum or classical nature of the cloning machine. However, if all three systems are classical (Cartesian product), then the cloning is possible by linear transformations which are symplectic on the total phase space.

The structure of the paper is as follows: The next section serves to recapitulate, very briefly, the Hamiltonian formulation of QM and of the HHM, and then to formulate the definitions of the the cloning and self-replication processes in NHQM and in HHM. In Sec. III we prove our main results concerning the cloning (and self-replication) in NHQM and in

*buric@ipb.ac.rs

HHM. Section IV contains several remarks which provide a discussion of our results. A summary is given in Sec. V.

II. FORMULATION OF CLONING IN HAMILTONIAN QUANTUM AND HYBRID THEORIES

A. Hamiltonian formulation of quantum mechanics and of hybrid mechanics

1. *Hamiltonian quantum mechanics and nonlinear generalizations*

Quantum and classical mechanics can be formulated by using the same mathematical framework of Hamiltonian dynamical systems $(\mathcal{M},\omega,H)$, where $\mathcal{M}$ is a symplectic manifold, ω is the corresponding symplectic structure, and H is the Hamilton's function. Formulation of the classical mechanics of isolated conservative systems using $(\mathcal{M},\omega,H)$ is standard [15]. The formulation of quantum mechanics in terms of $(\mathcal{M},\omega,g,H)$, where g is an appropriate Riemann structure, is perhaps less well known but shall not be presented here in any detail since there exist excellent reviews [7,8]. Very briefly, the basic observation beyond the Hamiltonian formulation of quantum mechanics is that the evolution of a pure quantum state in a Hilbert space $\mathcal{H}^N$, given by the Schrödinger equation, can be equivalently described by a HDS on an Euclidean manifold $\mathcal{M}=\mathbb{R}^{2N}$. Here N is the complex dimension of the relevant Hilbert space. The manifold $\mathcal{M}$ is just the Hilbert space considered as a real manifold, with the symplectic and Riemann structures given by the real and the imaginary parts of the Hilbert scalar product. The manifold also possesses an almost complex structure $J^2=-I$ such that $g(x,y)=\omega(x,Jy)$. Normalization and global phase invariance of quantum states can be incorporated into the formulation of the phase space of quantum states which is the projective space $P\mathcal{H}^{N-1}\sim S^{2N-1}/S^1$, with the corresponding symplectic, Riemann, and almost complex structures. However, in our computation we shall use the Hamiltonian formulation based on $\mathbb{R}^{2N}$, so that, when treating the problem of cloning, we shall have to take care of the global phase invariance explicitly. Representing a normalized vector $|\psi\rangle\in\mathcal{H}^N$ in an arbitrary basis $\{|e_j\rangle\}_{j=1}^N$ as $|\psi\rangle=\sum_{j=1}^N c_j|e_j\rangle$, one can introduce the real canonical coordinates $x_j=(\bar{c}_j+c_j)/\sqrt{2\hbar}$, $y_j=i(\bar{c}_j-c_j)/\sqrt{2\hbar}$, $j=1,2,\ldots,N$, where bar indicates complex conjugation. Change of the basis by a unitary map involves a linear symplectic transformation of the canonical coordinates. A generic point from $\mathcal{M}$ will also be denoted by X or X^a, where $a=1,2,\ldots,2N$ is an abstract index, such that $X^a=x_a$, $a=1,2,\ldots,N$ and $X^a=y_a$, $a=N+1,\ldots,2N$. If we want to stress that the point X corresponds to the vector $|\psi\rangle\in\mathcal{H}^N$ we write X_ψ, and vice versa $|\psi_X\rangle$ for the vector corresponding to the point X. It should be stressed, perhaps, that the canonical coordinates (x_j,y_j) have nothing to do with the canonical coordinates of the classical system that after quantization gives the considered quantum system with the Hilbert space $\mathcal{H}^N$. The Hamilton's function $H(X)$ is given by the quantum expectation of the Hamiltonian $\hat{H}$ in the state $|\psi_X\rangle$: $H(X)=\langle\psi_X|\hat{H}|\psi_X\rangle$. The Schrödinger dynamical law is that of Hamiltonian mechanics:

$$\dot{X}^a=\omega^{ab}\nabla_b H, \tag{1}$$

where ω^{ab} is the standard unit symplectic matrix

$$\omega=\begin{pmatrix}\mathbf{0} & \mathbf{1}\\ -\mathbf{1} & \mathbf{0}\end{pmatrix}, \tag{2}$$

where $\mathbf{0}$ and $\mathbf{1}$ are zero and unit matrices of dimension N.

In the Hilbert space QM and in Hamiltonian CM the dynamical variables can be introduced formally as generators of the isomorphisms of the respective relevant structures. In QM these are self-adjoined operators generating unitary transformations that preserve the Hilbert scalar product. In the Hamiltonian formulation of QM the Hilbert scalar product generates both the symplectic and the metric Riemann structures. The symplectic structure is preserved by Hamiltonian vector fields of arbitrary smooth functions, but the metric is preserved only by the Killing vector fields, i.e., by the Hamiltonian vector fields generated by quadratic functions of the canonical variables. In particular, the unitarity of the QM evolution implies that the Hamilton equations (1) are linear. All observables are represented by quadratic functions $A(X)$ on $\mathcal{M}$ and are the quantum-mechanical expectations of the corresponding quantum observables $A(X)=\langle\psi_X|\hat{A}|\psi_X\rangle$. On the other hand, the canonical coordinates of the quantum phase space do not have physical interpretation. It is important to observe that the Poisson bracket between two quadratic functions is also a quadratic function and satisfies

$$\{A_1(X),A_2(X)\}=\frac{1}{i\hbar}\langle\psi_X|[\hat{A}_1,\hat{A}_2]|\psi_X\rangle. \tag{3}$$

In what follows we shall need to consider a bipartite quantum system composed of two systems with Hilbert spaces $\mathcal{H}_1^{N_1}$ and $\mathcal{H}_2^{N_2}$. The phase space of the total system is the manifold $\mathcal{M}_{12}=\mathbb{R}^{2N_1N_2}\sim\mathcal{H}_1^{N_1}\otimes\mathcal{H}_2^{N_2}$. Of course, the space $\mathcal{M}_{12}$ is much larger than the Cartesian product $\mathcal{M}_1\times\mathcal{M}_2$, which is relevant for the formation of classical compound systems. If $|e_j^1\rangle$ and $|e_k^2\rangle$ are basis vectors in $\mathcal{H}_1^{N_1}$ and $\mathcal{H}_2^{N_2}$ respectively, with the corresponding canonical coordinates (x_j^1,y_j^1) and (x_k^2,y_k^2), then the canonical coordinates (x_l^{12},y_l^{12}) corresponding to the basis $|e_j^1\rangle\otimes|e_k^2\rangle$ in $\mathcal{H}_1^{N_1}\otimes\mathcal{H}_2^{N_2}$ are given by rather complicated formulas in general. Fortunately, we shall need only the formulas in the most simple cases, further simplified by a special choice of the target system state before the cloning transformation. In what follows we denote the composition of phase spaces of two systems with phase spaces $\mathcal{M}_1$ and $\mathcal{M}_2$ by $\mathcal{M}_1\odot\mathcal{M}_2$, which means $\mathcal{M}_{12}$ in the quantum and $\mathcal{M}_1\times\mathcal{M}_2$ in the classical case.

The Hamiltonian formulation of QM suggests natural formal generalizations [7]. Several such generalizations could be seen as special cases of the theory called extended quantum mechanics which was introduced and extensively studied in Ref. [16]. The most obvious one is to consider a theory where the evolution can be generated by functions which are not quadratic [7,10,17] but to retain the assumption that only the quadratic functions correspond to physical observables, and to retain the composition rule for compound systems. This would correspond to a nonlinear Schrödinger evolution equation. Such a theory, which we abbreviate by NHQM, is still a HDS with the same set of states and observables as in QM, but the Hamiltonian evolution equations are nonlinear and the metric is not evolution invariant. Since the proofs

of the no-cloning property in QM are based on linearity or unitarity of the QM evolution, it is interesting to investigate if the cloning is possible in NHQM.

2. *Hamiltonian hybrid theory*

There is no unique generally accepted theory of interaction between micro and macro degrees of freedom, where the former are described by quantum and the latter by classical theory. The reason is primarily because each of the suggested theories has some unexpected or controversial features (see Ref. [13] for an informative review). Partial selection of hybrid theories can be found in Refs. [18–23]. Some of the suggested hybrid theories are mathematically inconsistent, and "no-go" type theorems have been formulated [24], suggesting that no consistent hybrid theory can be formulated. Nevertheless, mathematically consistent but inequivalent hybrid theories exist [13,22,23]. The Hamiltonian hybrid theory, as formulated and discussed, for example, in Refs. [12,13], has many of the properties commonly expected of a good hybrid theory. In fact, the dynamical formulas of the Hamiltonian theory are equivalent to the well-known mean-field approximation, the main novelty being that the theory is formulated entirely in the framework of the theory of Hamiltonian dynamical systems, which enables useful insights and methods of analysis [25–27]. Analysis of cloning in the Hamiltonian hybrid system is one such application. In fact, we analyze the possibility of cloning in general HHM where the Hamiltonian is not necessarily of mean-field form and contrast the results with the HHM of the restricted type where the Hamiltonian is of mean-field form.

The phase space in the Hamiltonian theory of a hybrid classical-quantum system, denoted by $\mathcal{M}$, is considered as a Cartesian product $\mathcal{M} = \mathcal{M}_c \times \mathcal{M}_q$ of the classical subsystem phase space $\mathcal{M}_c$ with $\dim \mathcal{M}_c = 2N_c$ and of the quantum subsystem phase space $\mathcal{M}_q$ with $\dim \mathcal{M}_q = 2N_q$. Local coordinates on the product are denoted (q,p,x,y), where $(q,p) \in \mathcal{M}_c$ are called the classical degrees of freedom (CDF) and $(x,y) \in \mathcal{M}_q$ are called the quantum degrees of freedom (QDF). Notice that the classical and the quantum parts are composed as if both were classical, i.e., there is no possibility of entanglement between CDF and QDF. Generalized Hamiltonian hybrid theory is given by a Hamiltonian dynamical system on the phase space $\mathcal{M} = \mathcal{M}_c \times \mathcal{M}_q$. In the general case, nothing is supposed about the total Hamiltonian, and it is only the structure of the phase space that justifies the terminology of hybrid quantum-classical systems. The Poisson bracket on $\mathcal{M}$ of arbitrary functions of the local coordinates (q,p,x,y) is defined as

$$\{f_1,f_2\}_{\mathcal{M}} = \sum_{i=1}^{N_c}\left(\frac{\partial f_1}{\partial q_i}\frac{\partial f_2}{\partial p_i} - \frac{\partial f_2}{\partial q_i}\frac{\partial f_1}{\partial p_i}\right) + \frac{1}{\hbar}\sum_{j=1}^{N_q}\left(\frac{\partial f_1}{\partial x_j}\frac{\partial f_2}{\partial y_j} - \frac{\partial f_2}{\partial x_j}\frac{\partial f_1}{\partial y_j}\right). \quad (4)$$

Thus, the Hamiltonian form of the hybrid dynamics on $\mathcal{M}$ as the phase space reads

$$\dot{q} = \{q,H\}_{\mathcal{M}}, \quad \dot{p} = \{p,H\}_{\mathcal{M}}, \quad \dot{x} = \{x,H\}_{\mathcal{M}}, \quad \dot{y} = \{y,H\}_{\mathcal{M}}, \quad (5)$$

where H is an arbitrary smooth function on the total phase space $\mathcal{M}$.

A particular case of HHM, treated, for example, in Refs. [12,13] and equivalent to the mean-field approach, is obtained by further assumptions about the form of the Hamiltonian. The evolution equations of the hybrid system are in this type of HHM given by the Hamiltonian of the following form:

$$H_t(q,p,x,y) = \langle\psi_{x,y}|\hat{H}_q + \hat{V}_{\rm int}(q,p)|\psi_{x,y}\rangle + H_c(q,p) = H_c(q,p) + H_q(x,y) + V_{\rm int}(q,p,x,y), \quad (6)$$

where H_c is the Hamilton's function of the classical subsystem, $H_q(x,y) = \langle\psi_{x,y}|\hat{H}_q|\psi_{x,y}\rangle$ is the Hamilton's function of the quantum subsystem, and $V_{\rm int}(q,p,x,y) = \langle\psi_{x,y}|\hat{V}_{\rm int}(q,p)|\psi_{x,y}\rangle$, where $\hat{V}_{\rm int}(q,p)$ is a Hermitian operator in the Hilbert space of the quantum subsystem which depends on the classical coordinates (q,p) and describes the interaction between the subsystems. Despite the fact that the Hamiltonian is a quadratic function of QDF (and arbitrary function of CDF) the evolution of the QDF is nonlinear because of the coupling between QDF and CDF.

It is important to mention the evolution of statistical ensembles of hybrid systems in this type of HHM. Such an ensemble is described by a probability distribution $\rho(q,p,x,y)$, which evolves by the Liouville equation with the Hamiltonian (6). The following expression:

$$\hat{\rho}(t) = \int_{\mathcal{M}} \rho(q,p,x,y;t)\hat{\Pi}(x,y)dxdydqdp = \int_{\mathcal{M}} \rho_q(x,y;t)\hat{\Pi}(x,y)dxdy = \int_{\mathcal{M}} \hat{\rho}_{cl}(q,p;t)dqdp, \quad (7)$$

where $\hat{\Pi}(x,y)$ is a normalized projector onto the vector $|\psi_{x,y}\rangle$, is a well-defined density matrix representing a state of the QDF at each t. There are many $\rho_q(x,y;t)$ giving the same density matrix $\hat{\rho}(t)$. From the evolution equation satisfied by Eq. (7), or from Eq. (5), it is seen that a pure state $|\psi(t)\rangle\langle\psi(t)|$ obtained from an initial ensemble $\rho(q,p,x,y) = \delta(q-q_0)\delta(p-p_0)\delta(x-x_0)\delta(y-y_0)$ with CDF (and QDF) in pure states is always a pure state of QDF. The evolution equation satisfied by this pure state is in the form of a (linear) Schrödinger equation with the Hamiltonian which is a Hermitian operator that depends explicitly on $(q(t),p(t))$. On the other hand, if the CDF are initially in a mixed state, a pure state of the QDF will evolve into a mixed state. Furthermore, it was shown in Ref. [26] that the evolution of a general $\rho(t)$ will involve explicitly the convex expansion (7), and not only $\rho(t)$. Therefore, it seems that this type of HHM can be used for superluminal communication between distant subparts of the quantum DF.

Discussion of cloning within the restricted type of HHM with the classical part playing the role of the cloning machine requires special treatment as compared with the general HHM.

B. Definitions of cloning and self-replication

Cloning is a process involving three systems: the object system S_o with the state space $\mathcal{S}_o$, a target system S_t with the state space $\mathcal{S}_t$ the same as that of S_o, and an auxiliary system,

the cloning machine S_m, with the state space of dimension M that is not specified in advance. It is said that cloning of some arbitrary object state $X_o \in \mathcal{S}_o$ is possible if there is a state of the target $X_{t,in} \in \mathcal{S}_t$ and a state of the machine $X_{m,in} \in \mathcal{S}_m$ such that

$$X_o \odot X_{t,in} \odot X_{m,in} \to X_o \odot \{X_t = X_o\} \odot X_m(X_o). \quad (8)$$

The arbitrary state of the object system is conserved by cloning; one fixed state of the target and another fixed state of the machine are chosen as initial, independently of the object state. The fixed initial target state is mapped into the initial state of the object. The final state of the machine might depend on the object state X_o. It is not assumed that the final machine state is uniquely related to X_o. Observe that the possibility of cloning does not imply that the cloning is achieved with any initial target and machine states, but only with a specific choice of these states. The domain and the range of the cloning map (8) are proper subsets of the sets of possible states of the object + target + machine system.

The system $S_o \bigcup S_t \bigcup S_m$ is characterized by its natural evolution, and the question is if the cloning map belongs to that class. In our case the natural evolution is given by a Hamiltonian flow on $\mathcal{S}_o \odot \mathcal{S}_t \odot \mathcal{S}_m$ and thus preserves the symplectic structure on $\mathcal{S}_o \odot \mathcal{S}_t \odot \mathcal{S}_m$. In NHQM all three systems are quantum and, as was stated in the previous section, $\odot$ is the tensor product. In HHM we shall consider the case when the object system and the target are quantum and the machine is classical. Thus, in this case, $\odot$ between the machine and object + target is the Cartesian product. Alternatively, which we shall not do, one could analyze cloning with all three systems of the hybrid nature. The only fixed property of the cloning problems within the Hamiltonian framework is the canonical Hamiltonian evolution and the fact that pure states are represented by points in the corresponding phase spaces. If X_o and X_t represent phase space points in the Hamiltonian formulation corresponding to the vectors $|\psi_o\rangle$ and $|\psi_t\rangle$, respectively, then it is natural to assume that the cloning is successful if at the output $|\psi_t\rangle \exp(i\theta) = |\psi_o\rangle$, i.e.,

$$\begin{aligned} x_t^i \cos\theta - y_t^i \sin\theta &= x_o^i, \\ y_t^i \cos\theta + x_t^i \sin\theta &= y_o^i, \\ i &= 1,2,\ldots,N. \end{aligned} \quad (9)$$

The role of the machine DF can be justified from two different points of view. One is the operational point of view, where the appearance of the cloning machine is natural. The other role of the cloning machine is to actually enable the object + target subsystem to evolve in a non-Hamiltonian way. Quite analogously to the role of the machine in the standard QM formulation of cloning, here the presence of the cloning machine enables the total object + target + machine system to evolve canonically while enabling a more general type of evolution of the subsystem object + target. In this respect a related more restrictive problem with no cloning machine is sometimes considered. Such a process has been termed self-replication and consists of mapping a fixed state of the target system into an arbitrary state of the object system, the latter remaining unchanged, but without any influence of the third system. In the self-replication process the object + target system is considered as isolated. Together with the problem of proper cloning within NHQM (with the cloning machine) we shall also analyze the possibility of self-replication in such theories.

III. MAIN RESULTS

Our strategy to analyze the possibility of self-replication and cloning will be the same in NHQM and HHM. Let us denote by $\mathcal{M}_{otm}$ the total phase space of the object + target + machine system. By $\mathcal{M}_{in} \subset \mathcal{M}_{otm}$ we denote the submanifold of the total phase space of the form $\mathcal{M}_o \odot X_{t,in} \odot X_{m,in}$, where $X_{t,in}$ and $X_{m,in}$ are specific initial vectors representing states of the target and the machine, respectively. We shall all the time deal with vectors of unit norm. Similarly, we denote by $\mathcal{M}_f \subset \mathcal{M}_{otm}$ the submanifold which is the image of $\mathcal{M}_{in}$ by the cloning map. Points in $\mathcal{M}_f$ are of the form $X_o \odot X_o \odot X_{m,f}(X_o)$, $X_o \in \mathcal{M}_o$, and thus $\dim \mathcal{M}_f = \dim \mathcal{M}_{in} = \dim \mathcal{M}_o$. We then choose an arbitrary point $X \in \mathcal{M}_{in}$ and two arbitrary normalized tangent vectors $g_X, h_X \in T_X(\mathcal{M}_{in}) \subset T_X(\mathcal{M}_{otm})$. The value of the symplectic area $\omega_X(g_X, h_X)$ is then computed. Cloning (or self-replication) is represented by the mapping $\phi : \mathcal{M}_{in} \to \mathcal{M}_f$ with the tangent map $\phi_\star : T_X(\mathcal{M}_{in}) \to T_{\phi(X)}(\mathcal{M}_f)$. Symplectic area between the images of the two vectors $\omega_{\phi(X)}(\phi_\star g_X, \phi_\star h_X)$ is then computed. If ϕ is a symplectic map, i.e., can be generated by a piecewise smooth Hamiltonian flow, then

$$\omega_{\phi(X)}(\phi_\star g_X, \phi_\star h_X) = \omega_X(g_X, h_X). \quad (10)$$

If Eq. (10) is not satisfied, for any choice of $X_{t,in}, X_{m,in}$, and $X_{m,f}$, then the cloning (self-replication) map ϕ cannot be realized by a Hamiltonian flow. To apply the procedure, we shall write explicitly the cloning map ϕ and its tangent map $\phi_\star$, corresponding to the phase spaces $\mathcal{M}_{in}$ and $\mathcal{M}_f$ with a specific choice of the initial target and machine states in the NHQM and HHM. The only difference will be in the way the machine phase space $\mathcal{M}_m$ is added to the phase space of the object + target.

In our discussion, we consider the simplest possible systems as object, target, and machine. The object and the target are each taken to be a single qubit. An arbitrary state of the object qubit is a normalized $\mathbb{C}^2$ vector with complex coefficients (α, β) corresponding to some basis of $\mathcal{S}_o$. Furthermore, the initial state of the target qubit will be represented by vector $(1,0)$ in a basis of $\mathcal{S}_t$ chosen in the same way as the basis in $\mathcal{S}_o$. This does not seem to be a restriction with crucial consequences, but grossly simplifies explicit formulas for the self-replication (and later cloning) map.

In the case of NHQM the machine is also a quantum system and the coupling of it with the object + target is via tensor product. In order to demonstrate that, in NHQM, cloning by a symplectic (nonlinear) transformation is possible, it is enough to assume that the cloning machine is also a qubit, set initially in the state $(\alpha_m, \beta_m) = (1,0)$, represented in some basis of $\mathcal{S}_m$. Cloning is also possible by a symplectic map in the case of general HHM, when the machine is a classical system with two degrees of freedom and is coupled to the object + target via the Cartesian product. However, an additional argument is used to show that in the specific HHM with the Hamiltonian of the form (6), i.e., quadratic in the QDF, cloning of the quantum

state is impossible by symplectic transformation generated by the Hamilton functions of the stated form.

A. Impossibility of self-replication in NHQM

Let us first illustrate the computations for the case of self-replication in NHQM. The real dimension of $\mathcal{M}_{in}$ with normalized object states is three. In the complex notation the initial point in $\mathcal{M}_{in}$ representing the state of object + target before self-replication is

$$X_{in} = (\alpha,0,\beta,0), \quad |\alpha|^2 + |\beta|^2 = 1. \tag{11}$$

Two normalized tangent vectors g and h in $T(\mathcal{M}_{in})$ at X_{in} are given as

$$g_{re} = (-g_1\alpha_{im} + g_3\beta_{re},0, -g_3\alpha_{re} - g_2\beta_{im},0), \tag{12a}$$

$$g_{im} = (g_1\alpha_{re} + g_3\beta_{im},0, -g_3\alpha_{im} + g_2\beta_{re},0), \tag{12b}$$

with arbitrary real numbers g_1, g_2, and g_3 chosen to respect the unity norm. Analogous formulas apply to h_{re} and h_{im}. Subscripts re and im stand for real and imaginary parts. The skew product of the two tangent vectors is

$$\omega(g,h) = [g_3(h_1 - h_2) + (g_2 - g_1)h_3](\alpha_{re}\beta_{re} + \alpha_{im}\beta_{im}). \tag{13}$$

In formulas (12) and (13) we have, for the sake of brevity, skipped the subscript indicating the related point X_{in}.

Image by the self-replication map ϕ of X_{in}, again in the complex coordinates, is given by

$$X_f = (\alpha^2,\alpha\beta,\beta\alpha,\beta^2)\exp[i\theta(\alpha,\beta)]. \tag{14}$$

Notice the arbitrary phase factor added to the result of the self-replication operation. Images of g and h by the tangent map $\phi_\star$ are given by rather long formulas which we do not reproduce here. However, the skew product of $\phi_\star g$ and $\phi_\star h$ at the point X_f is given by

$$\omega(\phi_\star g,\phi_\star h) = 2[g_3(h_1 - h_2) + (g_2 - g_1)h_3] \times (\alpha_{re}\beta_{re} + \alpha_{im}\beta_{im})(|\alpha|^2 + |\beta|^2). \tag{15}$$

Notice that the previous result is independent of arbitrary phase factor. The ratio of the symplectic areas after and before the application of the self-replication map is

$$\frac{\omega(\phi_\star g,\phi_\star h)}{\omega(g,h)} = 2(|\alpha|^2 + |\beta|^2) = 2. \tag{16}$$

Thus, the self-replication map does not preserve the skew product and therefore cannot be realized by any symplectic map between $\mathcal{M}_{in}$ and $\mathcal{M}_f$.

B. Possibility of cloning in NHQM

Consider now the proper cloning map in NHQM with the quantum machine included. Since we shall see that the cloning map is symplectic with the cloning machine given by a qubit, it is enough to assume this simplest realization of the machine. The final state of the machine (α_{mf},β_{mf}) is free to chose, and the choice can be done such that the factor of two appearing in the result of self-replication (16) can be canceled.

Formulas for the initial point and its image by the cloning map for the indicated choice of initial states of the target and the machine in the complex notation are given by:

$$X_{in} = (\alpha,0,0,0,\beta,0,0,0), \tag{17}$$

$$X_f = (\alpha^2\alpha_{mf},\alpha^2\beta_{mf},\alpha\beta\alpha_{mf},\alpha\beta\beta_{mf}, \times \alpha\beta\alpha_{mf},\alpha\beta\beta_{mf},\beta^2\alpha_{mf},\beta^2\beta_{mf}), \tag{18}$$

where (α_{mf},β_{mf}) denote the final state of the machine. The tangent vector g is given by

$$g_{re} = (-g_1\alpha_{im} + g_3\beta_{re},0,0,0, -g_3\alpha_{re} - g_2\beta_{im},0,0,0), \tag{19a}$$

$$g_{im} = (g_1\alpha_{re} + g_3\beta_{im},0,0,0, -g_3\alpha_{im} + g_2\beta_{re},0,0,0), \tag{19b}$$

and analogously for h. The skew product between g and h is

$$\omega(g,h) = [g_3(h_1 - h_2) + h_3(g_2 - g_1)](\alpha_{re}\beta_{re} + \alpha_{im}\beta_{im}). \tag{20}$$

The images of g and h by the tangent map, their skew product, and the ratio $\omega(\phi_\star g,\phi_\star h)/\omega(g,h)$ are given by rather long formulas, which depend on the final machine state. However, we have found that the choice of final machine state as $(\alpha_{mf},\beta_{mf}) = (\bar{\alpha},\bar{\beta})$, where the bar indicates complex conjugation, renders the ratio equal to unity for the normalized state (α,β) of the object. Therefore, the cloning map can be realized by a symplectic transformation. From the standard QM it follows that the symplectic cloning transformation in NHQM must be nonlinear.

C. Possibility of cloning in general HHM

We chose the object and the target to be the same systems and to be in the same states as in the case of NHQM. The machine is chosen to be a convenient classical system with two DF and coordinates $(q_{1m},q_{2m},p_{1m},p_{2m})$ or in complex notation $(q_{1m} + ip_{1m},q_{2m} + ip_{2m}) = (\alpha_m,\beta_m)$. Formulas for the initial point for the indicated special choice of initial target and machine states are given in the complex coordinates by

$$X_{in} = (\alpha,0,\beta,0,1,0). \tag{21}$$

The machine final state is free to choose. With the choice $(\alpha_{mf} = \alpha_{im} + i\alpha_{re},\beta_{mf} = \beta_{im} + i\beta_{re})$ the state after cloning operation is

$$X_f = (\alpha^2,\alpha\beta,\beta\alpha,\beta^2,\alpha_{im} + i\alpha_{re},\beta_{im} + i\beta_{re}). \tag{22}$$

Tangent normalized vector g is given by

$$g_{re} = (-g_1\alpha_{im} + g_3\beta_{re},0, -g_3\alpha_{re} - g_2\beta_{im},0,0,0), \tag{23a}$$

$$g_{im} = (g_1\alpha_{re} + g_3\beta_{im},0, -g_3\alpha_{im} + g_2\beta_{re},0,0,0), \tag{23b}$$

and similarly for tangent vector h. The skew product between g and h is given by

$$\omega(g,h) = [g_3(h_1 - h_2) + h_3(g_2 - g_1)](\alpha_{re}\beta_{re} + \alpha_{im}\beta_{im}). \tag{24}$$

The images of the normalized tangent vectors and their skew product are again given by rather long formulas. However, the

above choice of the machine final state renders the ratio

$$\frac{\omega(\phi_\star g, \phi_\star h)}{\omega(g,h)} = 1, \tag{25}$$

for normalized initial object states. Again, the cloning map can be realized by a symplectic transformation.

D. Impossibility of cloning in the HHM with the specific form of the Hamiltonian

Special form of the hybrid Hamiltonian (6) implies special status of the cloning operation in this type of HHM, as compared with the general case. In fact, due to the properties of the evolution of pure hybrid states, summarized in Sec. II, pure states of QDF remain pure if the initial state of CDF is also pure. Furthermore, the scalar product between two QDF pure states is preserved. Therefore, the standard no-cloning argument from linear QM applies. Thus, cloning of quantum states is impossible within the specific HHM with Hamiltonian (6), and with classical DF assuming the role of the cloning machine. Here we have an example of a theory that does not admit cloning of pure quantum states, but whose natural extension that includes ensembles admits superluminal communication.

IV. DISCUSSION

Remark 1: Physical interpretation and consequences. Cloning is commonly considered as an information-processing task. From this point of view, the problem formulated in Sec. II and discussed in Sec. III is rather formal and is concerned with an idealized system that could never occur in information-processing protocols with real systems. Pure states of isolated systems and their idealized evolution are only probabilistically related to information and its processing. Therefore, the relation between the system's states and information must be probabilistic, and the processing of such information necessary involves stochastic perturbations. This has been analyzed in the standard QM [28]. The question of cloning in real, experimentally available systems was not studied in the present publication but is important in analyzing the fundamental and practical consequences. In order to do that, one needs to use probability ensembles, represented by distributions on the relevant phase spaces and stochastic evolution equations. We believe that only with such an analysis could one attempt to draw conclusions as to the physical consistency of the nonlinear HQM and HHM.

Remark 2: Cloning vs superluminal signaling. It is well known that, if cloning would be possible in the standard QM then, also in the framework of this theory, it would also be possible to communicate information at superluminal speed. It has also been claimed that the condition of no superluminal signaling puts an upper bound on the fidelity of cloning, in effect excluding the perfect cloning in QM [29]. The condition of no superluminal signaling is in Ref. [29] expressed in terms of convex expansions of mixed states. In the opposite direction, it has been argued [2,17] that a nonlinear evolution of pure quantum states would enable signaling at superluminal speed. This is consistent with our results which show the possibility of cloning in NHQM. However, the argument does not exclude theories in which pure quantum states cannot be perfectly cloned, but the superluminal signaling is possible. Mean-field HHM with the special form of the Hamiltonian (6) is an example of such a theory.

Remark 3: Cloning in classical mechanics. It is commonly understood that perfect cloning of classical information contained in a classical pure state is possible. Of course, in order to discuss the possibility of cloning, one needs a precise definition of the state space and the type of dynamics characterizing the classical system. One formulation of the problem, particularly relevant in fundamental physics and for comparison with our results, is for the classical system modeled by using the framework of classical Hamiltonian dynamical systems. States of the system, the target, and the machine are described by the corresponding symplectic manifolds, their union is given by the Cartesian product and the symplectic structure on the total space is such that the symplectic structures on the components are obtained by the corresponding projections. It is known that the self-replication is not, but the cloning is possible by symplectic mappings on the total phase space, provided that the machine space has enough dimensions [9]. The proof of no self-replication is similar to the case in nonlinear quantum mechanics, presented in Sec. III. The possibility of cloning in Hamiltonian CM is established and discussed by concrete examples of symplectic cloning maps. It should be stressed that cloning is performed by linear symplectic mapping. On the other hand, cloning in NHQM and general HHM can be achieved by a symplectic map which must be nonlinear. This seems to be the crucial difference between the theories involving tensor or Cartesian products between the target and the object systems.

Remark 4: Cloning in classical statistical mechanics. Evolution of a probability distribution generated by a measure preserving mapping of a phase space is by definition linear and preserves the relative entropy between two distributions. These two properties, i.e., preservation of a nontrivial (quasi) distance between states and linearity are features of the Schrödinger evolution of pure quantum states. Also, the space of statistical states of a compound system, for example, $L^1(\mathcal{M}_1 \times \mathcal{M}_2)$ can be considered as the tensor product of $L^1(\mathcal{M}_1)$ and $L^1(\mathcal{M}_2)$. Thus, all three ingredients that are used in the standard proofs of no cloning in QM are also properties of classical statistical mechanics. Therefore, one expects, and it has been proved to be true [30], that cloning in classical statistical mechanics is impossible. Due to the creation of correlations between the subsystems, it is also possible to formulate the question of cloning in a more general way, more akin to the notion of broadcasting in QM. The answer to the question of possibility of broadcasting in Hamiltonian CM is also negative [30].

V. SUMMARY

We have analyzed the possibility of exact cloning of unknown quantum states in two types of nonlinear generalizations of quantum mechanics. Both types of generalizations were formulated as Hamiltonian dynamical systems on appropriate phase spaces. In the first type, which we called nonlinear Hamiltonian quantum mechanics (NHQM), the object, the target and the machine are treated as quantum systems, and it is shown that cloning can be realized by a nonlinear symplectic

mapping. On the other hand, the process of self-replication, involving only the system and the target, cannot be realized by any symplectic transformation in NHQM. The other type of nonlinear generalizations of QM which we treated describes hybrid quantum-classical systems, again using the framework of Hamiltonian dynamical systems. Here, the object and the target are quantum, but the machine is a classical system. We show that there exists a nonlinear symplectic transformation which realizes the cloning operation. However, the cloning transformation cannot be realized in the Hamiltonian hybrid theory of the mean-field type, in which case the Hamiltonian must be a quadratic function of the quantum degrees of freedom and an arbitrary one of the classical degrees of freedom. It would be interesting to try to extend these results to the problem of broadcasting of mixed states in the nonlinear generalizations. This would require analysis of the Liouville evolution of densities and might result in possibility of broadcasting also in the mean-field Hamiltonian hybrid theory.

ACKNOWLEDGMENTS

We acknowledge support of the Ministry of education, science and technological development of the Republic of Serbia, under Contracts No. 171006, No. 171017, No. 171020, No. 171038, and No. 45016 and COST (Action MP1006).

[1] W. K. Wootters and W. H. Zurek, Nature (London) **299**, 802 (1982).
[2] V. Scarani, S. Iblisdir, N. Gisin, and A. Acín, Rev. Mod. Phys. **77**, 1225 (2005).
[3] R. Clifton, H. Halvorson, and J. Bub, Found. Phys. **33**, 1561 (2003).
[4] M. A. Nielsen and I. L. Chuang, *Quantum Computation and Quantum Information* (Cambridge University Press, Cambridge, 2001).
[5] N. Gisin, Phys. Lett. A **143**, 1 (1990).
[6] A. Peres, Phys. Rev. Lett. **63**, 1114 (1989).
[7] A. Aschtekar and T. A. Schilling, in *On Einstein's Path*, edited by A. Harvey (Springer-Verlag, Berlin, 1998).
[8] D. C. Brody and L. P. Hughston, J. Geom. Phys. **38**, 19 (2001).
[9] N. J. Teh, Stud. Hist. Phil. Sci. B **43**, 47 (2012).
[10] S. Weinberg, Ann. Phys. (NY) **194**, 336 (1989).
[11] I. Bialynicki-Birula and J. Mycielski, Ann. Phys. (NY) **100**, 62 (1976).
[12] M. Radonjić, S. Prvanović, and N. Burić, Phys. Rev. A **85**, 064101 (2012).
[13] H-T. Elze, Phys. Rev. A **85**, 052109 (2012).
[14] N. Burić, Ann. Phys. (NY) **323**, 17 (2008).
[15] V. I. Arnold, *Mathematical Methods of Classical Mechanics* (Springer, New York, 1978).
[16] P. Bona, Acta Physica Slovaca **50**, 1 (2000).
[17] B. Mielnik, Phys. Lett. A **289**, 1 (2001).
[18] T. N. Sherry and E. C. G. Sudarshan, Phys. Rev. D **18**, 4580 (1978).
[19] W. Boucher and J. Traschen, Phys. Rev. D **37**, 3522 (1988).
[20] I. V. Aleksandrov, Z. Naturf. **36A**, 902 (1981).
[21] A. Peres and D. R. Terno, Phys. Rev. A **63**, 022101 (2001).
[22] L. Diósi, N. Gisin, and W. T. Strunz, Phys. Rev. A **61**, 022108 (2000).
[23] M. J. W. Hall and M. Reginatto, Phys. Rev. A **72**, 062109 (2005).
[24] L. L. Salcedo, Phys. Rev. A **85**, 022127 (2012).
[25] H.-T. Elze, Int. J. Quantum Inform. **10**, 1241012 (2012).
[26] N. Burić, I. Mendaš, D. B. Popović, M. Radonjić, and S. Prvanović, Phys. Rev. A **86**, 034104 (2012).
[27] N. Burić, D. B. Popović, M. Radonjić, and S. Prvanović, Found. Phys. **43**, 1459 (2013).
[28] H. Barnum, C. M. Caves, C. A. Fuchs, R. Jozsa, and B. Schumacher, Phys. Rev. Lett. **76**, 2818 (1996).
[29] N. Gisin, Phys. Lett. A **242**, 1 (1998).
[30] A. Daffertshofer, A. R. Plastino, and A. Plastino, Phys. Rev. Lett. **88**, 210601 (2002).

IOP Publishing | Royal Swedish Academy of Sciences Physica Scripta
Phys. Scr. **T162** (2014) 014038 (4pp) doi:10.1088/0031-8949/2014/T162/014038

Optical Ramsey fringes observed during temporal evolution of Zeeman coherences in Rb buffer gas cell

S N Nikolić, M Radonjić, N M Lučić, A J Krmpot and B M Jelenković

Institute of Physics, University of Belgrade, Pregrevica 118, 11080 Belgrade, Serbia

E-mail: stankon@ipb.ac.rs

Received 13 August 2013
Accepted for publication 16 March 2014
Published 19 September 2014

Abstract

We experimentally studied the temporal evolution of Zeeman electromagnetically induced transparency (EIT) resonances induced by the laser resonant to hyperfine transition $F_g = 2 \rightarrow F_e = 1$ of ^{87}Rb in a rubidium buffer gas cell. We simultaneously modulated the laser beam intensity and polarization to achieve the repeated interaction of the laser beam with coherently prepared atoms. Our cell was placed in a homogenous magnetic field to obtain the Larmor precession of the phase of coherences. The weak laser beam was used to probe the atoms at the end of the Ramsey sequence. We measured the transparency of the probe pulse at different magnetic fields for a given excitation pulse and the period of free evolution of Zeeman coherences in the dark. From these data, we reconstructed the temporal evolution of EIT resonances. The Ramsey fringes that appeared on the EIT curves at the beginning of the second probing pulse disappeared at later moments due to various decay processes.

Keywords: electromagnetically induced transparency (EIT), Zeeman coherences, slow light, storage of light, Ramsey fringes

(Some figures may appear in colour only in the online journal)

1. Introduction

Electromagnetically induced transparency (EIT) is a phenomenon characterized by a narrow transparency resonance of a laser field through coherent media, such as alkali atomic vapor [1]. This effect is of special interest because it allows for fine control of pulse propagation. EIT-based slow and stored light observations [2] may benefit telecommunications and quantum memories.

EIT resonance in Hanle configuration is based on Zeeman coherences between magnetic sublevels of a given hyperfine state of an alkali atom electronic ground state. When such an atom is exposed to the external magnetic field, its magnetic dipole moment rotates around the field direction with a Larmor frequency. This allows the possibility for a Ramsey method of separated oscillatory fields [3]. For instance, in the interaction of an atom with a first light field, coherence between atomic levels is created. Under the influence of the magnetic field, the phase of the rotation of the magnetic dipole moment defines the coherence phase. The second light field, which can be either spatially or temporally separated from the first field, probes the coherence [4]. The result is an interferometric picture with Ramsey fringes in the probe transparency signal, due to the phase differences between the coherence and the probe field.

Ramsey-like measurements of Zeeman decoherence that determine the dumping rate of the oscillations are presented in [5]. The effects of Ramsey narrowing of EIT resonances due to atomic diffusion in and out from the interaction region were discussed in [6, 7]. High contrast Ramsey fringes in a double Λ atomic scheme were obtained in [8]. Raman–Ramsey fringes are also shown in vacuum Rb cells using time-delayed optical pulses [9] and a probe beam that was spatially enclosed by the pump beam [10].

In this work, we present the experimental study of the temporal evolution of the Zeeman EIT resonances based on repeated interaction of coherently prepared atoms with the laser beam. The obtained transparency of the σ^- probe at

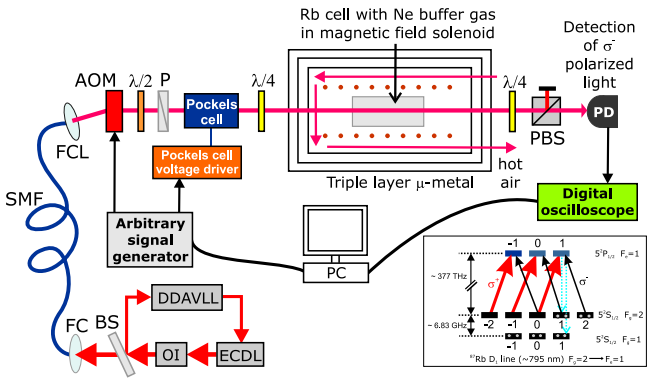

Figure 1. Experimental setup and atomic transition [15] used in the experiment. ECDL—external cavity diode laser; OI—optical insulator; DDAVLL—Doppler-free dichroic atomic vapor laser lock; BS—beam splitter; FC—fiber coupler; SMF—single-mode fiber; FCL—fiber collimator; AOM—acousto-optic modulator; P—polarizer; PBS—polarizing beam splitter; PD—photodetector. Hot air is used to heat the cell.

different magnetic fields was used to reconstruct the EIT resonances at different moments from the beginning of the probe pulse. The studies of dark states temporal behavior [11] and transient effects of EIT phenomenon [12–14] have been previously shown. In our work, the evolutions of (i) damped Ramsey fringes on the probe transparency and (ii) reconstructed EIT resonances during the probe propagation allowed for unique observation of the development and decay of Zeeman coherences.

2. Experimental setup

The experimental setup is shown in figure 1. The external cavity diode laser is frequency locked to the hyperfine $F_g = 2 \rightarrow F_e = 1$ transition of the D_1 line in ^{87}Rb in vacuum cell using the Doppler-free dichroic atomic vapor laser lock (DDAVLL) method [16, 17]. Gaussian distribution of radial laser intensity is obtained using the single-mode optical fiber. To achieve the repeated interaction of the laser light with Rb atoms, the power of the acousto-optical modulator (AOM) first-order diffracted beam is modulated and transmitted through the cell. The linear polarization of the laser light is assured by the high-quality linear polarizer. The Pockels cell and the $\lambda/4$ plate are used to modulate the polarization of the laser beam, so that pure σ^+ circular polarization is obtained when no voltage is applied to the cell and some percent of the σ^- light is produced otherwise. The arbitrary signal generator is programmed by the computer, whereas its two synchronized outputs control the AOM and the Pockels cell. The Rb cell containing 30 Torr of Ne buffer gas is 8 cm long and 25 mm in diameter. The difference between the $F_g = 2 \rightarrow F_e = 1$ transition frequencies in a vacuum and our buffer gas cell is approximately −20 MHz [18], which in total gives one photon detuning of −90 MHz in the experiment, due to −110 MHz AOM frequency shift in the first diffraction maximum. The Rb cell was heated using hot air circulating around the cell. The Rb vapor is shielded from external magnetic fields by the triple μ-metal layers, which reduce stray magnetic fields below 10 nT. To obey two-photon detuning, a long solenoid placed around the Rb cell produces a controllable longitudinal magnetic field in the range of ± 40 μT. The estimated magnetic field error is on the order of 10 nT. The transmitted σ^- laser light is extracted with $\lambda/4$ plate and polarizing beam splitter (PBS). The σ^- laser intensity as a function of applied magnetic field is measured by the photodetector and recorded by the storage oscilloscope. The intensities of polarization pulses were 4.9 and 0.95 mW cm^{-2} and the cell temperature was set to 67 ° C.

The signals applied to the AOM and the Pockels cell are shown in figure 2(a). We first generate a 400 μs pulse, in which 15% of the optical power is carried by σ^- polarized photons. Two coherent light fields (strong σ^+ and weak σ^-) pump the Rb atoms into the nonabsorbing dark state. After completion, the voltage on the Pockels cell is set back to zero and the AOM is synchronously turned off for 60 μs. During this dark interval, Zeeman coherence makes a Larmor precession in the external magnetic field. After this dark interval, the Pockels cell again generates the same elliptically polarized pulse and the AOM is turned back on to produce five times weaker light. This second pulse, with 400 μs duration, probes the previously created Zeeman coherences. Finally, we return the full beam power and set circular σ^+ polarization during 5 ms to reset atoms back in the ground state before the next pulse train. In this way, we produced Ramsey-like measurements with two temporally separated polarization pulses.

3. Results and discussions

The σ^- transparency signals measured for three different values of the external magnetic field are shown in figure 2(b). As expected, in the case of zero magnetic field, we see no Ramsey fringes in the transparency curve. We measured the linear dependence of fringes' frequency on the applied magnetic field with a slope close to magnetic sublevels energy splitting factor of ^{87}Rb hyperfine state $5^2S_{1/2}$ $F_g = 2$ (not shown). Due to decoherence processes, the oscillations are dumped.

The noise in figure 2(b) comes from the low transparency of the σ^- signal and the photo detector's electronic noise. The measured value of signal to noise ratio is 12 dB in the 21 MHz bandwidth of the entire data acquisition system. From these data, we were able to reconstruct the EIT resonances at different times during the probe pulse propagation. First, we set $t = 0$ at the beginning of the second polarization pulse. Next, we take the values of the σ^- transparency at a particular time instant t for all magnetic field values and plot this data set using the B-spline routine. EIT resonances obtained this way, as shown in figure 3(a), show clean oscillations because the reconstruction process takes one transparency value at a time and therefore eliminates the noise itself. However, because of measurement uncertainty, these oscillations are not perfect, i.e., fringes of the same order have slightly different amplitudes. The reconstructed EIT resonances are shown in figure 3 for the Rb density of $\sim 4.5 \cdot 10^{11}$

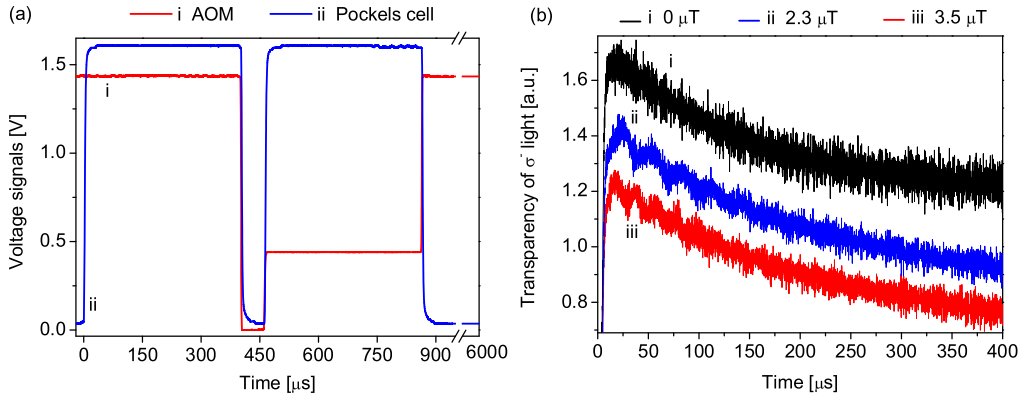

Figure 2. (a) The signals used in the experiment: AOM (i) and Pockels cell (ii). (b) Transparency of the σ^- light measured during the second probing pulse for various magnetic fields: 0 μT (i), 2.3 μT (ii), and 3.5 μT (iii).

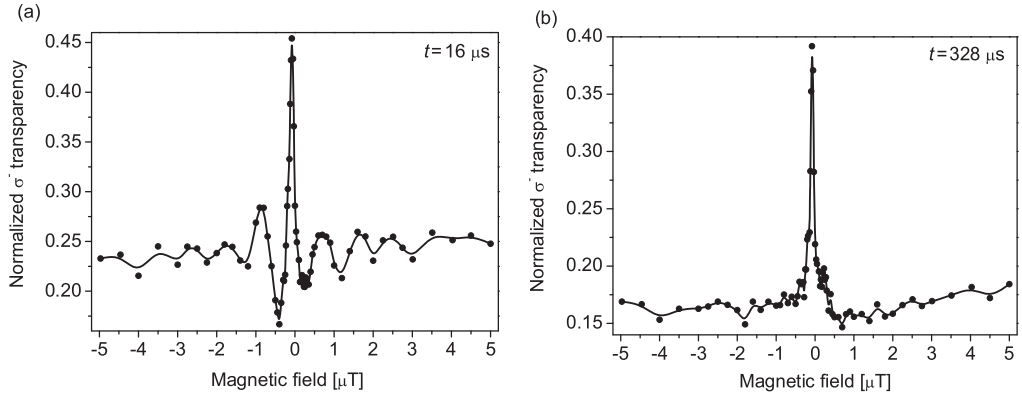

Figure 3. Reconstructed Zeeman EIT resonances from the σ^- transparency signal at different time moments t from the beginning of the second polarization pulse: (a) t = 16 μs and (b) t = 328 μs.

cm^{-3} and the laser beam diameter of 1.3 mm. Ramsey fringes were observed at EIT resonances for $t \lesssim 196$ μs and vanish at later moments due to the finite lifetime of Zeeman coherence. The decay rate of Zeeman coherences γ_2 was obtained by fitting the σ^- transparency signal (ii) from figure 2(b) to function $y = A_1 e^{-\gamma_1 t} + A_2 e^{-\gamma_2 t} \sin(\omega t + \varphi_0)$ (not shown). The measured γ_2 value is on the order of $\sim$9000 s^{-1}. In figure 3(a), an EIT resonance with oscillation pattern at $t = 16$ μs is shown. In figure 3(b), an EIT curve at $t = 328$ μs with no fringes is presented.

4. Conclusion

We experimentally studied the Zeeman coherence using Ramsey fringes obtained at the transparency signal of the probe σ^- laser field in the presence of the external magnetic field. Temporal evolution of Zeeman EIT resonances in Rb buffer gas cell were also presented. The first polarization pulse containing weak σ^- and strong σ^+ fields was used to create Zeeman coherences in Rb atoms. The subsequent weaker probe pulse with the same polarization state was produced to probe these coherences. The laser beam was completely turned off between the pulses to enable free evolution of the dark state in the magnetic field. The oscillatory pattern on the reconstructed EIT curves obtained soon after the second pulse generation disappeared at later times because of the various decoherence processes.

Acknowledgments

We thank Jelena Dimitrijević for fruitful discussions. Authors acknowledge funding from Grants nos. 45016 and 171038 of the Ministry of Education, Science and Technical Development of the Republic of Serbia and Scopes JRP IZ7370_127942.

References

[1] Fleischhauer M, Imamoglu A and Marangos J P 2005 Electromagnetically induced transparency: optics in coherent media *Rev. Mod. Phys.* **77** 633–73
[2] Phillips D F, Fleischhauer A, Mair A, Walsworth R L and Lukin M D 2001 Storage of light in atomic vapor *Phys. Rev. Lett.* **86** 783–6
[3] Ramsey N F 1956 *Molecular Beams* (Oxford: Oxford University Press)
[4] Zibrov A S and Matsko A B 2001 Optical Ramsey fringes induced by Zeeman coherence *Phys. Rev.* A **65** 013814

[5] Shuker M, Firstenberg O, Sagi Y, Ben-kish A, Davidson N and Ron A 2008 Ramsey-like measurement of the decoherence rate between Zeeman sublevels *Phys. Rev.* A **78** 063818
[6] Xiao Y, Novikova I, Phillips D F and Walsworth R L 2006 Diffusion-induced Ramsey narrowing *Phys. Rev. Lett.* **96** 043601
[7] Xiao Y, Novikova I, Phillips D F and Walsworth R L 2008 Repeated interaction model for diffusion-induced Ramsey narrowing *Opt. Express* **16** 14128
[8] Zanon T, Guerandel S, Clercq de E, Holleville D, Dimarcq N and Clairon A 2005 High contrast Ramsey fringes with coherent-population-trapping pulses in a double lambda atomic system *Phys. Rev. Lett.* **94** 193002
[9] Pati G S, Salit K, Tripathi R and Shahriar M S 2008 Demonstration of Raman Ramsey fringes using time delayed optical pulses in rubidium vapor *Opt. Comm.* **281** 4676–80
[10] Grujić Z D, Mijailović M, Arsenović D, Kovačević A, Nikolić M and Jelenković B M 2008 Dark Raman resonances due to Ramsey interference in vacuum vapor cells *Phys. Rev.* A **78** 063816
[11] Valente P, Failache H and Lezama A 2003 Temporal buildup of electromagnetically induced transparency and absorption resonances in degenerate two-level transitions *Phys. Rev.* A **67** 013806
[12] Meinert F, Basler C, Lambrecht A, Welte S and Helm H 2012 Quantitative analysis of the transient response of the refractive index to conditions of electromagnetically induced transparency *Phys. Rev.* A **85** 013820
[13] Park S J, Cho H, Kwon T Y and Lee H S 2004 Transient coherence oscillation induced by a detuned Raman field in a rubidium Λ system *Phys. Rev.* A **69** 023806
[14] Greentree A D, Smith T B, Echaniz de S R, Durrant A V, Marangos J P, Segal D M and Vaccaro J A 2002 Resonant and off-resonant transients in electromagnetically induced transparency: Turn-on and turn-off dynamics *Phys. Rev.* A **65** 053802
[15] Steck D A 2008 *Rubidium 87 D Line Data* (http://steck.us/alkalidata/rubidium87numbers.pdf)
[16] Wasik G, Gawlik W, Zachorowski J and Zawadzki W 2002 Laser frequency stabilization by Doppler-free magnetic dichroism *Appl. Phys.* B **75** 613–9
[17] Petelski T, Fattori M, Lamporesi G, Stuhler J and Tino G M 2003 Doppler-free spectroscopy using magnetically induced dichroism of atomic vapor: a new scheme for laser frequency locking *Eur. Phys. J.* D **22** 279–83
[18] Demtröder W 2002 Laser spectroscopy *Basic Concept and Instrumentation* (Werlag Berlin Heidelberg New York: Springer)

Geometric Phase for Analytically Solvable Driven Time-Dependent Two-Level Quantum Systems

I. Mendaš*, N. Burić, D.B. Popović, S. Prvanović and M. Radonjić
Institute of Physics, University of Belgrade, Pregrevica 118, 11080 Belgrade, Serbia

(Received May 11, 2013; revised version April 16, 2014; in final form May 23, 2014)

Geometric phase for novel analytical solutions (Barnes and Das Sarma) of time-dependent two-level quantum systems is discussed, specifically for a general single-axis driving term, which is represented by a function $J(t)$ in the Hamiltonian, and its corresponding evolution operator. It is demonstrated how general results for corresponding phases (total, dynamic and geometric) can be obtained. Using a specific case, it was found that over time in which the driving field is appreciably different from zero, the corresponding geometric phase changes (in the specific example by $\Delta\beta \approx 0.8$ radians) thus enabling detection. The results are relevant to qubit control and to quantum computing applications.

DOI: 10.12693/APhysPolA.126.670
PACS: 03.65.Aa, 03.65.Vf, 07.05.Dz

1. Introduction

Driven two-level systems are ubiquitous in quantum mechanics. Examples of exactly soluble two-level problems include Landau–Zener [1, 2], and Rabi [3] problems, Jaynes–Cummings [4] model, and others [6–11]. A new theoretical approach to the driven two-state system was recently introduced by Barnes and Das Sarma [12]. This uses a single-axis control field along the z axis, which is represented by a driving field $J(t)$ in the Hamiltonian (the time varying energy splitting between states):

$$H(t) = \frac{1}{2}\begin{bmatrix} J(t) & h \\ h & -J(t) \end{bmatrix}. \tag{1}$$

Here h represents a constant (an energy splitting between the two levels). The evolution operator, from an initial time $t = 0$, to a later t, and corresponding to H is represented by the 2×2 unitary matrix

$$U(t) = \begin{bmatrix} U_{11} & -U_{21}^* \\ U_{21} & U_{11}^* \end{bmatrix}, \tag{2}$$

with $|U_{11}(t)|^2 + |U_{21}(t)|^2 = 1$.

One then uses an innovative approach [12] to solve the corresponding time-dependent Schrödinger equation for the evolution operator and obtains the forms for the matrix elements of the evolution operator, Eqs. (12)–(16) in [12].

It turns out that the driving field, $J(t)$, appearing in the Hamiltonian (1) is related to a function $q(t)$, with corresponding initial conditions given by Eq. (17) in [12], via

$$J(t) = \frac{\ddot{q} + h^2 q}{\sqrt{h^2(1-q^2) - \dot{q}^2}}. \tag{3}$$

Such a simple prescription enables one to generate a number of novel, analytically solvable two-state problems together with their explicit solutions.

*corresponding author; e-mail: mendas@ipb.ac.rs

With such solutions one is able (at least in principle) to determine corresponding total, dynamic and geometric phases [13–19], in order to study and monitor the time development of the state vectors evolving under the Hamiltonian given by Eq. (1). This is of interest in the context of qubit control and quantum computing. The phases, for a pure state, are as follows. The total phase, $\varphi(0,t)$, of the state vector $|\Psi,t\rangle = U(t)|\Psi,0\rangle$, accumulated during the evolution from an initial time 0 to a final t, is determined by the argument of the inner product

$$\langle\Psi,0|\Psi,t\rangle \equiv r(0,t)\exp\left(\mathrm{i}\varphi(0,t)\right),$$
$$\varphi(0,t) = \arg\left[\langle\Psi,0|\Psi,t\rangle\right]. \tag{4}$$

Here we restrict ourselves to $r(0,t) > 0$, so that the two states in question are not orthogonal, and the relative phases can be determined. By convention the result of the argument of the complex number z, $\arg(z)$, is always between $-\pi$ and $+\pi$. Thus the total phase is in radians and ranges across this interval. A part of the total phase is the dynamic phase, which is given by the time integral of the expectation value of the Hamiltonian (we use units $\hbar = 1$)

$$\delta(0,t) \equiv -\int_0^t \langle\Psi,\tau|H(\tau)|\Psi,\tau\rangle\,\mathrm{d}\tau. \tag{5}$$

The geometric phase is then simply the surplus in the total phase over $\delta(0,t)$:

$$\beta(0,t) \equiv \varphi(0,t) - \delta(0,t). \tag{6}$$

Thus, in order to determine the geometric phase, the road is in principle simple. If one can solve the time-dependent Schrödinger equation (and this is precisely the case treated in [12]), the total phase is determined by the argument of the inner product $\langle\Psi,0|\Psi,t\rangle$, Eq. (4). Subsequently, the corresponding dynamic phase follows from the time integral of the expectation value of the Hamiltonian, Eq. (5). Finally, the difference between the two, Eq. (6), yields the geometric phase. There are numerous papers related to the geometric phase e.g. [20–22].

Here, in Sect. 2, we first present in some detail the theory on which the results of the calculations reported here

are based, while in the subsequent Sect. 3 we describe the calculation of the phases. Finally a brief summary is presented.

2. Spin polarization vector

It is convenient to parametrize the time dependent Hamiltonian operator of a two-level system as

$$H(t) = H_0(t)1_2 + \boldsymbol{H}(t)\cdot\boldsymbol{\sigma}, \tag{7}$$

where $\boldsymbol{\sigma}$ denotes the vector of three Pauli 2×2 matrices $(\sigma_1,\sigma_2,\sigma_3)$, and 1_2 denotes the 2×2 unit matrix. In the case of the Hamiltonian (1) one has $H_0(t)=0$, $H_1(t)=\frac{1}{2}h$, $H_2(t)=0$ and $H_3(t)=\frac{1}{2}J(t)$.

Similarly one parametrizes the 2×2 unitary matrix Eq. (2) as

$$U(t) = U_0(t)1_2 + \mathrm{i}\boldsymbol{U}(t)\cdot\boldsymbol{\sigma}, \tag{8}$$

with additional condition which stems from the unitarity condition of the evolution operator $\boldsymbol{U}(t)$: $\boldsymbol{U}(t)\cdot\boldsymbol{U}(t)+U_0^2=1$. In the case of (2) one has $U_0(t)=\Re\{U_{11}(t)\}$, $U_1(t)=\Im\{U_{21}(t)\}$, $U_2(t)=-\Re\{U_{21}(t)\}$, and $U_3(t)=\Im\{U_{11}(t)\}$, where $\Re$ and $\Im$ denote the corresponding real and imaginary parts, respectively. Finally, the corresponding 2×2 density matrix is of the form

$$\rho(t) = |\,\Psi,t\rangle\langle\Psi,t\,| = \frac{1}{2}\big(1_2 + \boldsymbol{P}(t)\cdot\boldsymbol{\sigma}\big). \tag{9}$$

Here $\boldsymbol{P}(t)$ denotes the time dependent average spin polarization vector. Using this notation one has, from Eqs. (5) and (6)

$$\varphi(0,t) = \arg\big(\mathrm{Tr}\,(U(t)\rho(0))\big) = \arctan\left(\frac{\boldsymbol{U}(t)\cdot\boldsymbol{P}(0)}{U_0(t)}\right) \equiv \arctan\alpha, \tag{10}$$

with $\alpha=\alpha(t)\equiv\big(\Im\{U_{21}\}(t)P_1(0)-\Re\{U_{21}(t)\}P_2(0)+\Im\{U_{11}(t)\}P_3(0)\big)/\Re\{U_{11}(t)\}$, and

$$\begin{aligned}\delta(0,t) &= -\int_0^t \mathrm{Tr}\,(H(\tau)\rho(\tau))\,\mathrm{d}\tau\\ &= -\int_0^t \Big(H_0(\tau)+\boldsymbol{H}(\tau)\cdot\boldsymbol{P}(\tau)\Big)\mathrm{d}\tau\\ &= -\frac{1}{2}h\int_0^t P_1(\tau)\,\mathrm{d}\tau - \frac{1}{2}\int_0^t J(\tau)P_3(\tau)\,\mathrm{d}\tau.\end{aligned} \tag{11}$$

With the known evolution operator, given by Eqs. (2), (3) and (8), the average spin polarization vector is obtained readily from the formal solution of the quantum Liouville equation

$$\boldsymbol{P}(t)\cdot\boldsymbol{\sigma} = U(t)\big(\boldsymbol{P}(0)\cdot\boldsymbol{\sigma}\big)U^\dagger(t) = U(t)A(t), \tag{12}$$

where part of the rhs is an auxiliary 2×2 matrix $A(t)\equiv\big(\boldsymbol{P}(0)\cdot\boldsymbol{\sigma}\big)U^\dagger(t)$. For a general case of the initial spin polarization vector $\boldsymbol{P}(0)=(P_1(0),P_2(0),P_3(0))$, one finds the matrix elements

$$\begin{aligned}A_{11}(t) &= P_3(0)U_{11}^* + [P_1(0)-\mathrm{i}P_2(0)](-U_{21}),\\ A_{12}(t) &= P_3(0)U_{21}^* + [P_1(0)-\mathrm{i}P_2(0)]U_{11},\\ A_{21}(t) &= [P_1(0)+\mathrm{i}P_2(0)]U_{11}^* - P_3(0)(-U_{21}),\\ A_{22}(t) &= [P_1(0)+\mathrm{i}P_2(0)]U_{21}^* - P_3(0)U_{11}.\end{aligned}$$

Since in Eq. (12) the rhs is a known 2×2 matrix, and because the lhs is the 2×2 matrix

$$\boldsymbol{P}(t)\cdot\boldsymbol{\sigma} = \begin{bmatrix} P_3(t) & P_1(t)-\mathrm{i}P_2(t)\\ P_1(t)+\mathrm{i}P_2(t) & -P_3(t)\end{bmatrix}, \tag{13}$$

by equating the corresponding elements of the two matrices one determines the components of the spin polarization vector at a time t. One finds

$$\begin{aligned}P_1(t) &= \Re\{U_{11}(t)A_{12}(t) - U_{21}^*A_{22}(t)\},\\ P_2(t) &= \Im\{U_{11}(t)A_{12}(t) - U_{21}^*A_{22}(t)\},\\ P_3(t) &= \Re\{U_{11}(t)A_{11}(t) - U_{21}^*A_{21}(t)\}.\end{aligned} \tag{14}$$

Let us note that the magnitude of $\boldsymbol{P}(t)$ is a constant throughout the evolution and is, in fact, equal to one for a pure state.

3. Calculation of phases

Despite the existence of a number of analytical solutions to the time-dependent Schrödinger equation for relatively simple examples describing a driven two-level system provided in [12], these are mainly not translated to the corresponding *analytical* expressions for the phases and one has to turn to numerical analysis. This nevertheless enables an efficient analysis in a number of cases. We illustrate the typical results for the total, dynamic and geometric phases, obtained from Eqs. (10), (11) and (6). For a typical case considered in [12], namely the choice (Eq. (19) in [12])

$$q(t) = \exp\left((-2/a)\sinh^2(\sqrt{a}ht/2)\right), \tag{15}$$

with a real constant $a\le 2$, and the corresponding driving field is from Eq. (3)

$$\frac{J(t)}{h} = \frac{\frac{1}{a}\sinh^2(\sqrt{a}ht) - 2\sinh^2(\sqrt{a}ht/2)}{\sqrt{\mathrm{e}^{\frac{4}{a}\sinh^2(\sqrt{a}ht/2)} - \frac{1}{a}\sinh^2(\sqrt{a}ht) - 1}}. \tag{16}$$

For such a driving field, the total, dynamic and geometric phases, as functions of time t are plotted in Figs. 1 and 2 for $h=1$ and $a=\frac{2}{3}$.

It is seen that from an initial time $t=0$ to a final $t=10$, during which the driving field $J(t)$ is appreciably different from zero, the corresponding geometric phase changes (by $\Delta\beta\approx 0.8$ radians) thus enabling detection. Analogous results are also obtained for other driving fields considered in [12].

4. Conclusions

Phase is a fundamental notion in quantum mechanics, and in particular the study of geometric phases is an attempt to understand quantum mechanics better. It is known that the total phase and visibility are directly observable in an interference experiment [23]. Geometric phases have some implications in quantum information theory. These phases can form the basis of any quantum computation [24, 25], resilient to certain types of errors. It offers the potential of a fault-tolerant way of performing geometric quantum computation. Two references concerning the robustness of the geometric phase for non-Abelian gates and Berry phase are [26, 27].

Here we determine the geometric phase corresponding to a new type of driven two-state system [12] which is thus of relevance to qubit control. The main result of

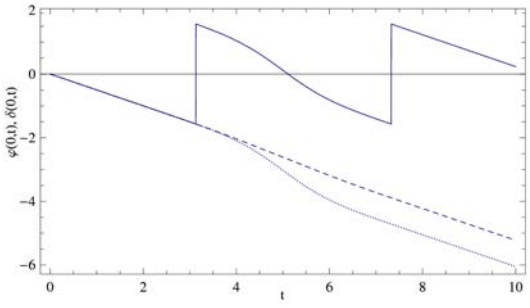

Fig. 1. Total phase $\varphi(0,t)$ (solid curve) and dynamic phase $\delta(0,t)$ (dashed curve), in radians, for driven time-dependent two-level quantum system, with the Hamiltonian (1), and in the case of the driving field Eq. (16). The initial spin polarization vector is $\boldsymbol{P}(0) = (1,0,0)$, completely along the x-axis, while the two other constants are $h = 1$ and $a = \frac{2}{3}$. It is seen that the dynamic phase is a smooth, monotonically decreasing function of the elapsed time t. The two jumps by $+\pi$ radians in the total phase, stem from the multiple-valued arctan function appearing in Eq. (10) for the total phase, represent the change of sign in the probability amplitude, and are experimentally observable. By using the principal value of the function arctan, one removes the jumps and obtains for the total phase the dotted curve.

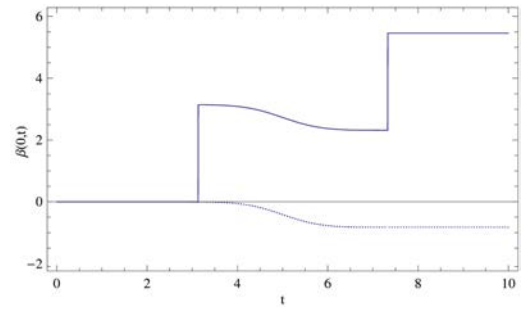

Fig. 2. Geometric phase $\beta(0,t)$, in radians (solid curve), for driven time-dependent two-level quantum system, with the Hamiltonian (1), and in the case of the driving field Eq. (16). It is seen that there is a considerable change in the geometric phase of ≈ 5.5 radians (solid curve). By removing the jumps in the total phase (there are two jumps of $+\pi$), one finds a slight net decrease in geometric phase of ≈ 0.8 rad (dotted curve). The initial spin polarization vector is $\boldsymbol{P}(0) = (1,0,0)$, while the two other constants are $h = 1$ and $a = \frac{2}{3}$. The resulting geometric phase reflects the behavior of the total and dynamic phases presented in Fig. 1.

our work is contained in Eqs. (11) and (14), which give explicit expressions for computing geometric phase for a given evolution.

Acknowledgments

This work was supported by the Ministry of Science and Education of the Republic of Serbia, contracts No. 171006, No. 171017, No. 171020, No. 171028, and No. 171038, and by COST (Action MP1006).

References

[1] L. Landau, *Phys. Z. Sov.* **2**, 46 (1932).
[2] C. Zener, *Proc. R. Soc. A* **137**, 696 (1932).
[3] I. Rabi, *Phys. Rev.* **51**, 652 (1937).
[4] E.T. Jaynes, F.W. Cummings, *Proc. IEEE* **51**, 89 (1963).
[5] S.L. McCall, E.L. Hahn, *Phys. Rev.* **183**, 457 (1969).
[6] S.E. Economou, L.J. Sham, Y. Wu, D.G. Steel, *Phys. Rev. B* **74**, 205415 (2006).
[7] A. Greilich, S.E. Economou, S. Spatzek, D.R. Yakovlev, D. Reuter, A.D. Wieck, T.L. Reinecke, M. Bayer, *Nature Phys.* **5**, 262 (2009).
[8] E. Poem, O. Kenneth, Y. Kodriano, Y. Benny, S. Khatsevich, J.E. Avron, D. Gershoni, *Phys. Rev. Lett.* **107**, 087401 (2011).
[9] P.K. Jha, Y.V. Rostovtsev, *Phys. Rev. A* **81**, 033827 (2010).
[10] A. Gangopadhyay, M. Dzero, V. Galitski, *Phys. Rev. B* **82**, 024303 (2010).
[11] Q. Xie, W. Hai, *Phys. Rev. A* **82**, 032117 (2010).
[12] E. Barnes, S. Das Sarma, *Phys. Rev. Lett.* **109**, 060401 (2012).
[13] M.V. Berry, *Proc. R. Soc. Lond. A* **392**, 45 (1984).
[14] M.V. Berry, *J. Phys. A, Math. Gen.* **18**, 15 (1985).
[15] Y. Aharonov, J. Anandan, *Phys. Rev. Lett.* **58**, 1593 (1987).
[16] J. Samuel, R. Bhandari, *Phys. Rev. Lett.* **60**, 2339 (1988).
[17] S. Pancharatnam, *Proc. Indian Acad. Sci. A* **44**, 247 (1956).
[18] *Collected Works of S. Pancharatnam*, Oxford University Press, London 1975.
[19] D.M. Tong, J.L. Chen, J.F. Du, *Chin. Phys. Lett.* **20**, 793 (2003).
[20] I. Mendaš, *Phys. Rev. A* **55**, 1514 (1997).
[21] I. Mendaš, *Phys. Rev. A* **67**, 044101 (2003).
[22] M.A. Bouchene, M. Abdel-Aty, *Phys. Rev. A* **79**, 055402 (2009).
[23] E. Sjöqvist, A.K. Pati, A. Ekert, J.S. Anandan, M. Ericsson, D.K.L. Oi, V. Vedral, *Phys. Rev. Lett.* **85**, 2845 (2000).
[24] A. Ekert, M. Ericsson, P. Hayden, H. Inamori, J.A. Jones, D.K.L. Oi, V. Vedral, *J. Mod. Opt.* **47**, 2501 (2000).
[25] J.A. Jones, V. Vedral, A. Ekert, G. Castagnoli, *Nature* **403**, 869 (2000).
[26] M. Johansson, E. Sjöqvist, I. Mauritz Andersson, M. Ericsson, B. Hessmo, K. Singh, D.M. Tong, *Phys. Rev. A* **86**, 062322 (2012).
[27] S. Filipp, J. Klepp, Y. Hasegawa, C. Plonka-Spehr, U. Schmidt, P. Geltenbort, H. Rauch, *Phys. Rev. Lett.* **102**, 030404 (2009).

Annals of Physics 343 (2014) 16–26

Contents lists available at ScienceDirect

Annals of Physics

journal homepage: www.elsevier.com/locate/aop

Phase space theory of quantum–classical systems with nonlinear and stochastic dynamics

Nikola Burić *, Duška B. Popović, Milan Radonjić, Slobodan Prvanović

Institute of Physics, University of Belgrade, Pregrevica 118, 11080 Belgrade, Serbia

HIGHLIGHTS

- A novel theory of quantum–classical systems is developed.
- Framework of quantum constrained dynamical systems is used.
- A dynamical description of the measurement induced collapse is obtained.

ARTICLE INFO

Article history:
Received 24 September 2013
Accepted 12 January 2014
Available online 18 January 2014

Keywords:
Hybrid system
Dynamical reduction

ABSTRACT

A novel theory of hybrid quantum–classical systems is developed, utilizing the mathematical framework of constrained dynamical systems on the quantum–classical phase space. Both, the quantum and classical descriptions of the respective parts of the hybrid system are treated as fundamental. Therefore, the description of the quantum–classical interaction has to be postulated, and includes the effects of neglected degrees of freedom. Dynamical law of the theory is given in terms of nonlinear stochastic differential equations with Hamiltonian and gradient terms. The theory provides a successful dynamical description of the collapse during quantum measurement.

1. Introduction

Interaction of a quantum system with a classical one is in the standard formulation of quantum mechanics described by the collapse postulate, introduced by von Neumann [1]. However, a dynamical description of the postulate requires a consistent theory of systems which cannot be described by either quantum or classical mechanics alone. Such a description of interacting quantum–classical

* Corresponding author.
E-mail address: buric@ipb.ac.rs (N. Burić).

0003-4916/$ – see front matter
http://dx.doi.org/10.1016/j.aop.2014.01.007

systems is commonly called a hybrid theory. The Schrödinger evolution of an isolated quantum system is linear and deterministic, and the evolution of classical systems is also deterministic, but is typically nonlinear. The collapse postulate requires the evolution of a quantum system interacting with the classical apparatus to be nonlinear and stochastic. The hybrid theory, developed in the present paper, incorporates both types of evolution into a single dynamical process.

Hybrid systems are interesting independently of their fundamental aspects (for a recent review see [2]). Despite "no go" theorems [3], several nonequivalent mathematically consistent hybrid theories have been constructed [4–8]. Formulation of the classical dynamics in terms of unitary transformations in an appropriate Hilbert space exists since long time ago [9]. Likewise, there is a formulation of quantum mechanics in terms of Hamiltonian dynamical systems with the appropriate symplectic phase space and the corresponding Hamiltonian dynamics [10,11]. However, the crucial difference between the two theories is not in the mathematical framework, but in the treatment of the interactions between subsystems.

Hybrid theories can be divided into two groups according to the conceptual status and aims. In the theories of the first group one considers all systems in Nature as described at the fundamental level by quantum theory and therefore the hybrid system is an approximation of two interacting quantum systems, where one of the systems is treated in the corresponding classical limit [4,8]. In the other approach, one assumes from the beginning that the classical and quantum mechanics are both fundamental theories with different domains of validity. The only restriction on the descriptions of the quantum–classical (QC) interaction is then given by the experiments involving micro–macro objects and the phenomenological collapse postulate. Of course, it is clear that a macro-object has many degrees of freedom which are not described by the macroscopic model of the classical theory. The effects of those degrees of freedom have to be somehow included into the manner a hybrid theory treats the QC interaction. The hybrid theory constructed in the present paper, and denoted by FHT (for "Fundamental Hybrid Theory" [12]), presents a particular way of doing this.

2. Mathematical framework

Mathematical framework of the hybrid theory to be developed is that of an abstract dynamical system $(\mathcal{M}, \Omega, G, H)$ on a differentiable manifold $\mathcal{M}$ with symplectic and Riemannian structures Ω and G respectively, with some preferred function, the Hamiltonian H. Let us stress right at the beginning that the dynamical law of the hybrid theory need not be of the Hamiltonian form, but will involve differential equations on $\mathcal{M}$ given in terms of Ω and G. The manifold is also assumed to possess a complex structure $J^2 = -I$, where I stands for identity, such that $G(x, y) = \Omega(x, Jy)$. Furthermore, the evolution law of the hybrid theory might be given in terms of a stochastic process, in which case the points from $\mathcal{M}$ are values of random variables on some probability space. The latter will not be explicitly referred.

Formulation of the classical mechanics of isolated conservative systems using $(\mathcal{M}, \Omega, H)$ is standard [13]. The formulation of quantum mechanics in terms of $(\mathcal{M}, \Omega, G, H)$ is perhaps less well known, but shall not be presented here in any detail since there exist excellent reviews [10,11,14] and brief accounts [15–19] which are sufficient for our purposes. Very briefly, the basic observation beyond the Hamiltonian formulation of quantum mechanics is that the evolution of a quantum pure state in a Hilbert space $\mathcal{H}$, as given by the Schrödinger equation, can be equivalently described by a Hamiltonian dynamical system on an Euclidean manifold $\mathcal{M}$. The manifold is just the Hilbert space considered as a real manifold, with the symplectic and Riemannian structures given by the real and imaginary parts of the Hilbert space scalar product. Representing a vector $|\psi\rangle \in \mathcal{H}$ in a basis $\{|k\rangle \mid k = 1, 2, \ldots, N\}$, where N is the dimension of the complex Hilbert space, by coefficients $\{c_k \mid k = 1, 2, \ldots, N\}$, one can introduce the canonical coordinates $x^k = (c_k^* + c_k)/\sqrt{2}$ and $y^k = i(c_k^* - c_k)/\sqrt{2}$, $k = 1, 2, \ldots, N$. Generic point from $\mathcal{M}$ is usually denoted by (x, y), X or X^a, where $a = 1, 2, \ldots, 2N$ is an abstract index. In what follows the symplectic and Riemannian structures on the quantum phase space are denoted by ω^{ab} and g^{ab}. The Hamilton's function $H(X)$ is given by the quantum expectation of the Hamiltonian $\hat{H}$ in the state $|\psi_X\rangle$ corresponding to a point X: $H(X) = \langle\psi_X|\hat{H}|\psi_X\rangle/\langle\psi_X|\psi_X\rangle$. In fact, all observables are represented by quadratic functions $A(X)$ on $\mathcal{M}$, and are the quantum mechanical ex-

pectations of the corresponding quantum observables $A(X) = \langle\psi_X|\hat{A}|\psi_X\rangle/\langle\psi_X|\psi_X\rangle$. The Schrödinger dynamical law is that of Hamiltonian mechanics

$$\dot{X}^a = \omega^{ab}\nabla_b H. \tag{1}$$

The Hamiltonian formulation is also crucial in the formulation and applications of nonlinear constraints within quantum mechanics [15,18,19,16,17,8].

3. Construction of the hybrid theory

The total system is conceived as composed of a microscopic quantum system and a macro-system. It is the central assumption of the present hybrid theory that the macro-system has a distinguished set of degrees of freedom, described by classical mechanics. Usually, it is not claimed that macro-systems are composed of something other than microscopic parts well described by quantum theory. However, it is assumed that the dynamics of at least some of the observable degrees of freedom of a macroscopic system is correctly described by classical mechanics, and that the classical mechanical description need not be reduced or derived from quantum description of all the microscopic components.

3.1. Elements of the hybrid model

In the FHT the hybrid phase space $\mathcal{M}$ is assumed to be given by the Cartesian product $\mathcal{M} = \mathcal{M}_{qp} \times \mathcal{M}_{QP} \times \mathcal{M}_{xy}$. Local canonical coordinates are separated into three groups: (q, p), (Q, P) and (x, y). The first two groups $(q, p) \in \mathcal{M}_{qp}$ and $(Q, P) \in \mathcal{M}_{QP}$ correspond to the degrees of freedom of the macroscopic system, and the third $(x, y) \in \mathcal{M}_{xy}$ to the degrees of freedom of the microscopic quantum system, called quantum degrees of freedom (QDF). The coordinates (q, p) represent (usually a small number of) distinguished macroscopic degrees of freedom of the macroscopic object. They are supposed to be well described by classical mechanics and are called classical degrees of freedom (CDF).

The degrees of freedom denoted by (Q, P) describe the physical quantities that are not used in the characterization of the CDF of the macroscopic object nor of the QDF of the micro-system. Apart from the fact that there are many of these degrees of freedom, nothing else about their character is assumed in the hybrid theory. In other words, the FHT does not assume that (Q, P) are either classical or quantum. In the hybrid theory, it is assumed that the state of the system is completely described by the values of CDF and QDF, and the dynamical equations of the theory will be formulated in terms of (q, p, x, y) only, with no explicit reference to (Q, P). Particular physical interpretation of the (Q, P) degrees of freedom is not strictly a part of FHT. However, one could think of several different physical interpretations depending on the conceptual background and on the particular system. On the conceptual side, one could argue that the macroscopic system is composed of quantum microscopic components which interact and entangle with the micro-system. Therefore, the hybrid theory, with no possibility of explicit entanglement between CDF and QDF, must take the fact of entanglement due to the micro-system and micro-components of the macro-system into account in some manner. The influence of (Q, P) degrees of freedom on the CDF–QDF system might be interpreted partly as due to the entanglement between the micro and macro-systems, and partly due to the influence of the microscopic degrees of freedom of the macro-system on the CDF. This argument is expressed more formally as follows. The phase space of a bipartite quantum system, corresponding to the micro–macro system, is the real manifold $\mathcal{M}_{12}$ associated with the Hilbert space $\mathcal{H}_{12} = \mathcal{H}_1 \otimes \mathcal{H}_2$, where $\mathcal{H}_1$ and $\mathcal{H}_2$ are the Hilbert spaces of the micro and macro-systems, respectively. The phase space corresponding to the macro-system is denoted by $\mathcal{M}_2$. A submanifold, denoted by $\Gamma \subset \mathcal{M}_2$ corresponds to CDF of the macro-system. Local coordinates (x, y) of $\mathcal{M}_1$ correspond to QDF. The degrees of freedom (Q, P) are then the local coordinates of the complement of $\mathcal{M}_1 \times \Gamma$ in $\mathcal{M}_{12}$. Alternatively, one could just conceive (Q, P) degrees of freedom as a sufficiently general type of environment of the CDF–QDF degrees of freedom. Furthermore, the physical interpretation of (Q, P) degrees of freedom will depend on the physical picture of the particular macro-system. For example, the macro-system might be a large magnet, conceived as a large collection of spins, interacting via

the Heisenberg interaction. It is the main assumption of the hybrid theory that the interaction of such a magnet with a micro quantum system can be described by the selected degrees of freedom of the magnet, i.e. the macroscopic magnetization, which are well described by classical physics, provided that the effects of the unobserved degrees of freedom are somehow included in the hybrid theory.

Interactions between various types of degrees of freedom might be of different nature. We shall assume that the interactions between (q, p) and (x, y) are conservative and described by the corresponding Hamiltonian. On the other hand, interactions between the unspecified degrees of freedom (Q, P) and the QDF (x, y) might be more general, and are described by a complex Hamiltonian of the form $H_{int}(x, y, Q, P) = F(Q, P)A(x, y)$ where $A(x, y)$ is a quadratic function of (x, y) corresponding to the operator $\hat{A}$ of the micro-system and $F(Q, P) = F_R(Q, P) + iF_I(Q, P)$ in terms of real functions $F_R(Q, P)$ and $F_I(Q, P)$. Of course, the equations of motion for the real coordinates (q, p, x, y) must be expressed only in terms of real quantities. We shall also suppose that the influence of the (Q, P) degrees of freedom on the macroscopic classical variables (q, p) is negligible. The dynamics of the total system is thus determined by the complex Hamiltonian of the following form

$$H = H_{cl}(q, p) + H_q(x, y) + H_{QP}(Q, P) + f(q, p)A(x, y) + F(Q, P)A(x, y). \tag{2}$$

The meaning of the first three terms is obvious, and the rest describes the interaction between the macroscopic system and the quantum system. In order to shorten the notation we have denoted the collection of all observables $\{A_n\}$, appearing in the interaction terms, by a single letter A. In the simplified version, presented here, all degrees of freedom of the macro-system are assumed to interact with the same quantum observables $A(x, y)$ which might, but need not, form canonical pairs. As pointed out the functions $F(Q, P)$ are complex. However, they do not enter into the part of the Hamiltonian that depends only on the (q, p, x, y) degrees of freedom

$$H_{phys}(q, p, x, y) = H_{cl}(q, p) + H_q(x, y) + f(q, p)A(x, y). \tag{3}$$

The equations of motion for the real quantities as functions of (q, p, x, y) must be real, but need not be Hamiltonian.

The main requirement on the hybrid theory of QDF evolution, based on the collapse model, is that if the state of the quantum system is a superposition of $\hat{A}$ eigenstates then, because of the interaction with the macro-system, the state must evolve towards one of the $\hat{A}$ eigenstates. However, such behavior is not obtained starting from the Hamiltonian dynamics with the Hamiltonian (2) of the hybrid. One is therefore forced to adopt different approaches in modeling the collapse requirements. One approach, adopted here, is to consider the collapse requirements as appropriate constraints onto the otherwise Hamiltonian dynamics and to derive the dynamical law as the constrained dynamics. The phase space formulation of quantum mechanics is specially suitable for the formulation and treatment of nonlinear constraints [15,18,19,16,17,8].

3.2. Constrained dynamics approach

The eigenstates of any observable $\hat{A}$ are characterized by the property that the dispersion $\Delta A = \langle \hat{A}^2 \rangle - \langle \hat{A} \rangle^2$ is equal to zero. In the case when all observables $\{\hat{A}_n\}$ interacting with the macro-system commute, the relevant constraint might be given in the form

$$\Gamma_A(x, y) = \sum_n \Delta A_n(x, y) = 0, \tag{4}$$

which corresponds to the common eigenstate of all the observables $\{\hat{A}_n\}$. However, if there are several non-commuting observables, then the relevant constraint assumes the form

$$\Gamma_A(x, y) = \sum_n \Delta A_n(x, y) - \Delta_{\min} = 0, \tag{5}$$

where $\Delta_{\min}$ is the minimal possible value of the sum of the relevant dispersions. If these observables generate a representation of a semi-simple Lie algebra, then the constraint submanifold given by (5) is in fact the manifold of coherent states of the algebra [20].

In order to satisfy the constraint, the component of the Hamiltonian vector field orthogonal to the constraint submanifold $\Gamma_A(x, y) = 0$ has to be removed, so that the QDF $X \equiv (x, y)$ evolve according to

$$\dot{X}^a = \omega^{ab}\nabla_b H - \lambda g^{ab}\nabla_b \Gamma_A, \tag{6}$$

where λ is a single Lagrange multiplier to be determined. Substitution of (6) in $\dot{\Gamma}_A(X(t))$ results in

$$\omega^{ab}\nabla_a \Gamma_A \nabla_b H = \lambda g^{ab}\nabla_a \Gamma_A \nabla_b \Gamma_A. \tag{7}$$

Substituting λ from (7) into (6) results in the constrained dynamical equations

$$\dot{X}^a = \omega^{ab}\nabla_b H - \frac{\{\Gamma_A, H\}}{\|\nabla \Gamma_A\|^2} g^{ab}\nabla_b \Gamma_A, \tag{8}$$

where $\{F_1, F_2\} = \omega^{ab}\nabla_a F_1 \nabla_b F_2$. The first term can be written more explicitly as

$$\begin{aligned} \omega^{ab}\nabla_b H &= \omega^{ab}\nabla_b H_{phys} + (F_R\omega^{ab} + F_I(J\omega)^{ab})\nabla_b A \\ &= \omega^{ab}\nabla_b H_{phys} + F_R\omega^{ab}\nabla_b A + F_I g^{ab}\nabla_b A. \end{aligned} \tag{9}$$

The last two terms contain a large number of complicated functions of time $Q(t)$, $P(t)$. We shall suppose that these processes are well approximated by white noise. Consequently, functions $F_R(Q(t), P(t))$ and $F_I(Q(t), P(t))$ are also stochastic processes. The corresponding increments, denoted by dW_R and dW_I and understood in the Itô sense, are assumed to satisfy

$$\begin{aligned} &E[dW_{nR}] = 0, \qquad E[dW_{nI}] = 0, \\ &dW_{nR}dW_{mR} = dW_{nI}dW_{mI} = \delta_{nm}dt, \\ &dW_{nR}dW_{mI} = 0, \\ &dW_{nR}dt = dW_{nI}dt = 0, \end{aligned} \tag{10}$$

where $E[\,\cdot\,]$ denotes the expectation with respect to the stochastic process and n, m count up to the number of observables $\{\hat{A}_n\}$. This implies, among other things, that all $F_R(t)$, $F_I(t)$ satisfy the Markovian property. Finally, the dynamical equation of QDF in interaction with the macro-system is given by the stochastic differential equation of a non-autonomous diffusion process,

$$dX^a = \omega^{ab}\nabla_b H_{phys}dt - \frac{\{\Gamma_A, H_q\}}{\|\nabla \Gamma_A\|^2} g^{ab}\nabla_b \Gamma_A dt + \omega^{ab}\nabla_b A\, dW_R + g^{ab}\nabla_b A\, dW_I. \tag{11}$$

Equation (11) is the main dynamical equation of the QDF interacting with the macro-system of the FHT developed here. If all degrees of freedom of the system are described by quantum mechanics, then unitary quantum evolution applies and there is only the first term with $H_{phys} = H_q$. If there is an interaction of QDF and the macro-system, i.e. some of the degrees of freedom are a priori described by classical mechanics, then the full equation (11) applies. Notice that no unobservable degrees of freedom (Q, P) appear in the equation. The first part of the drift in (11) describes Hamiltonian evolution with the Hamiltonian $H_q(x, y) + f(q, p)A(x, y)$. The second term of the drift represents a gradient flow with the tendency to decrease the total dispersion $\Delta A = \sum_n \Delta A_n$. The joint effect of the Hamiltonian and gradient drift terms is to preserve constant the total dispersion. If there is only one observable $A(x, y)$, or a set of commuting observables, then the role of the gradient terms is to force the evolution towards the common eigenstates of $\{\hat{A}_n\}$. If the observables $\{\hat{A}_n\}$ do not commute, then there is a competition of tendencies due to the corresponding gradient terms. If these observables generate a representation of a semi-simple Lie algebra, then the gradient terms drive the system towards the invariant manifold of the coherent states of the algebra.

The stochastic terms are divided into two quite different groups. The Hamiltonian terms, which can be included as stochastic perturbations of the Hamiltonian H_{phys}, describe the Hamiltonian influence of the (Q, P) degrees of freedom on the motion of the quantum system. For example, this is like the influence of an external stochastic electromagnetic field. However, these terms do not contribute to the localization onto the constraint manifold. The gradient stochastic terms, on the other hand,

describe the influence of (Q, P) degrees of freedom which is not Hamiltonian. However, as opposed to the Hamiltonian stochastic terms, the gradient stochastic terms induce localization onto the constraint manifold. If all $\{\hat{A}_n\}$ are commuting, then the stochastic terms of both types are zero if $\nabla A_n(x, y) = 0$ for all observables. This means that the point (x, y) is a fixed point of the Hamiltonian evolution with each A_n as the Hamiltonian. Such a point corresponds to a common eigenstate of the nonlinear operators $\hat{A}_n - \langle\hat{A}_n\rangle$ with all eigenvalues being zero. The common eigenstates of these operators coincide with the common eigenstates of $\hat{A}_n$. Thus, the stochastic terms in Eq. (11) are equal to zero if only commuting quantum observables appear, and (x, y) corresponds to a common eigenstate of $\{\hat{A}_n\}$.

Dynamics of CDF

Classical degrees of freedom (q, p) satisfy the Hamiltonian evolution equations given by the Hamiltonian (3). The equations in terms of (q, p) are

$$\dot{q} = \frac{\partial H_{cl}(q,p)}{\partial p} + A(x,y)\frac{\partial f(q,p)}{\partial p}$$
$$\dot{p} = -\frac{\partial H_{cl}(q,p)}{\partial q} - A(x,y)\frac{\partial f(q,p)}{\partial q}. \tag{12}$$

The evolution of CDF is also stochastic because the quantum observables $A(x(t), y(t))$ evolve stochastically.

3.3. Quantum measurement process

Additional assumptions can be used in order to simplify the evolution equations (11) and (12) in the case of a quantum measurement process. One such approximation is based on the assumption that the dynamics of QDF is much faster than that of CDF. Consequently, one can replace in (11) the functions $(q(t), p(t))$ with their initial values (q_0, p_0). The equation for QDF becomes autonomous. The situation when QDF and CDF are coupled via only one observable $\hat{A}$ with the interaction term given by $H_{int} = pA(x, y)$, and when the gradient terms dominate the QDF dynamics, corresponds to the process of measurement of $\hat{A}$. QDF dynamics is approximately given by

$$dX^a = \omega^{ab}\nabla_b(H_q + p_0A(x,y))dt - \frac{\{\Gamma_A, H_q\}}{\|\nabla\Gamma_A\|^2}g^{ab}\nabla_b\Gamma_A dt$$
$$+ \omega^{ab}\nabla_b A(x,y)dW_R + g^{ab}\nabla_b A(x,y)dW_I. \tag{13}$$

Due to the gradient terms, the state approaches one of the eigenstates of $\hat{A}$, denoted by $(x_\alpha, y_\alpha) \equiv |\alpha\rangle$, with the eigenvalue $A(x_\alpha, y_\alpha) = \alpha$. The stochastic term introduces fluctuations, and the probability of the asymptotic eigenstate (x_α, y_α) depends on its distance from the initial state $(x, y)_{init} \equiv |\psi\rangle_{init}$, i.e. on $\|\langle\psi_{init}|\alpha\rangle\|^2$. These facts can be demonstrated numerically as we shall do shortly. The asymptotic dynamics of (13), or of (11) and (12), can also be analyzed using methods of stochastic stability analysis [21], in particular the stochastic generalization of the first Lyapunov method with the constraint Γ_A playing the role of the Lyapunov function, as will be illustrated elsewhere. Using the same assumption about different time scales and assuming that H_{cl} is negligible, the CDF dynamics of the coordinate of the apparatus pointer is approximated by

$$\dot{q} = \alpha \tag{14}$$

and reads the eigenvalue of $\hat{A}$. Thus, the approximate equations describe well the dynamics and the results of the measurement process.

3.4. Numerical example

We shall illustrate the hybrid dynamics modeling the measurement as given by (11) and (12) using the simplest example where the quantum system is a single 1/2-spin and the classical system is an

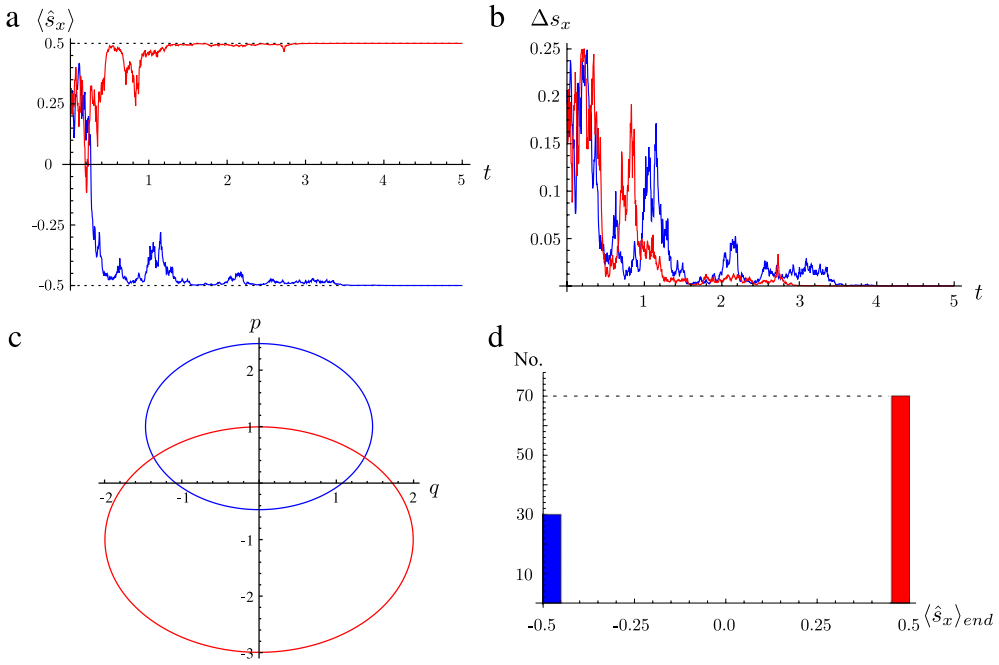

Fig. 1. (Color online) (a) $\langle \hat{s}_x \rangle(t)$ and (b) $\Delta s_x(t)$ for two typical stochastic paths. (c) Classical orbits corresponding to the stochastic paths in parts (a) and (b). (d) Histogram of the number of paths converged to $+1/2$ or $-1/2$ eigenstate of $\hat{s}_x$.

oscillator. The phase space of the quantum part corresponding to the Hilbert space $\mathbb{C}^2$ is $\mathbb{R}^4$, with the canonical coordinates (x_1, x_2, y_1, y_2). The relations between the real canonical coordinates and the complex expansion coefficients, (c_1, c_2) in the computational basis, of a normalized vector from $\mathbb{C}^2$ are given by the following formulas

$$c_k = \frac{x_k + iy_k}{\sqrt{2}}, \qquad c_k^* = \frac{x_k - iy_k}{\sqrt{2}}, \quad k = 1, 2. \tag{15}$$

The quantum Hamiltonian of a single spin is $\hat{H}_q = \omega \hat{s}_z$, the classical Hamiltonian of the oscillator is $H_{cl} = p^2/2m + m\Omega^2 q^2/2$ and the interaction $\hat{H}_{int} = \mu p \hat{s}_x$ corresponds to the measurement of $\hat{s}_x$. The functions on the QC phase space corresponding to $\hat{H}_q$ and $\hat{H}_{int}$ are

$$H_q(x, y) = \frac{\omega}{2} \frac{x_1^2 + y_1^2 - x_2^2 - y_2^2}{x_1^2 + y_1^2 + x_2^2 + y_2^2} \tag{16}$$

$$H_{int}(q, p, x, y) = \mu p \frac{x_1 x_2 + y_1 y_2}{x_1^2 + y_1^2 + x_2^2 + y_2^2}. \tag{17}$$

The constraint Γ_{s_x}, corresponding to the measurement of $\hat{s}_x$, is $\Delta s_x = \langle \hat{s}_x^2 \rangle - \langle \hat{s}_x \rangle^2 = 0$, and is given in terms of the canonical coordinates (x, y) by a slightly more complicated expression

$$\Gamma_{s_x} = \frac{((x_1 - x_2)^2 + (y_1 - y_2)^2)((x_1 + x_2)^2 + (y_1 + y_2)^2)}{(x_1^2 + y_1^2 + x_2^2 + y_2^2)^2}. \tag{18}$$

The Poisson bracket $\{\Gamma_{s_x}(x, y), H_q(x, y)\}_{x,y}$, the gradients $\nabla \Gamma_{s_x}(x, y)$ and $\nabla s_x(x, y)$ are easily computed and shall not be presented. These expressions are used to write down the dynamical equations (11) and (12), which are solved using the appropriate code for numerical solutions of SDE. Results are illustrated in Fig. 1(a)–(d). Each of 100 sample stochastic paths after some time converges to either

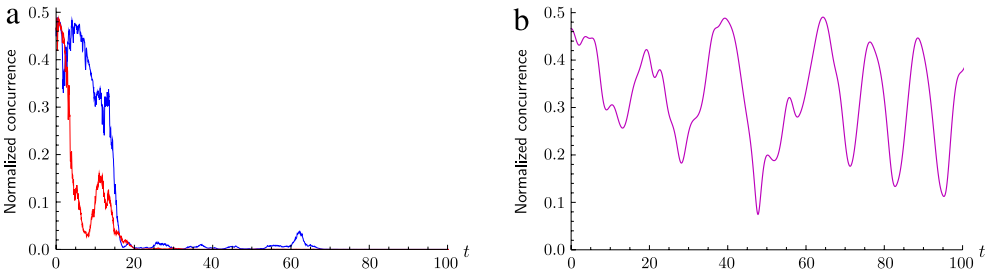

Fig. 2. (Color online) Normalized concurrence for two typical sample paths of FHT evolution (a) and for purely Hamiltonian evolution (b) starting from the same initial state (see text for details).

$-1/2$ or $1/2$ eigenstate of $\hat{s}_x$, denoted by $|1/2, -1/2\rangle$ and $|1/2, 1/2\rangle$, respectively. Fig. 1(a) and (b) show $\langle\hat{s}_x\rangle(t)$ and $\Delta s_x(t)$ for two typical realizations of the stochastic process starting from the same initial state and converging to the state $|1/2, 1/2\rangle$ (red curves) and the state $|1/2, -1/2\rangle$ (blue curves), respectively. The initial state is determined by $|\psi\rangle_{init} \equiv (x_1, x_2, y_1, y_2)_{init} = \sqrt{2}(2, 4, -2, 1)/5$ and $(q, p) = (1, 1)$, which yield $|\langle 1/2, -1/2|\psi_{init}\rangle|^2 = 0.26$ and $|\langle 1/2, 1/2|\psi_{init}\rangle|^2 = 0.74$. Fig. 1(c) illustrates the evolution of CDF (q, p) for the two stochastic sample trajectories related to Fig. 1(a) and (b). The two classical orbits are obviously different. The percentage of stochastic paths converging to either of the eigenstates is illustrated in Fig. 1(d) and is proportional to the distance of the initial state form the eigenstates. Qualitatively the same results are obtained for all different initial states that we have tested.

Let us point out that in the described numerical example the full system of equations (11) and (12) was used, and the sufficiently fast convergence of the QDF and the inertial properties of the CDF are obtained by the appropriate choice of the parameter values.

4. Remarks

(1) *Dynamics of entanglement* in a quantum system coupled to a classical one, as described in FHT, can be studied using, for example, a pair of qubits interacting with a classical oscillator. The relevant part of the Hamiltonian is given by

$$\begin{aligned} \hat{H}_q &= \omega\hat{s}_z^1 + \omega\hat{s}_z^2 + c\hat{s}_x^1\hat{s}_x^2, \\ H_{cl} &= \frac{p^2}{2m} + \frac{m\Omega^2 q^2}{2}, \\ \hat{H}_{int}(q, p) &= \mu p\hat{s}_z^1. \end{aligned} \tag{19}$$

The complex coefficients of an arbitrary two spin state $|\psi\rangle \in \mathbb{C}^4$ in the computational basis are denoted by c_1, c_2, c_3, c_4 and their real and imaginary parts are the canonical coordinates given by $(x_k, y_k) = \sqrt{2}(\mathrm{Re}(c_k), \mathrm{Im}(c_k))$, $k = 1, 2, 3, 4$. The total Hamilton's function is $H(x, y, q, p) = H_q(x, y) + H_{int}(x, y, q, p) + H_{cl}(q, p)$ where $H_q(x, y) = \langle\psi|\hat{H}_q|\psi\rangle/\langle\psi|\psi\rangle$ and $H_{int}(x, y) = \langle\psi|\hat{H}_{int}|\psi\rangle/\langle\psi|\psi\rangle$. The constraint corresponding to $\hat{H}_{int}$ in (19) is $\Delta s_z^1 = 0$.

It can be shown, by numerical computations, that the entanglement of an initial entangled state of the qubits evolves to zero for sufficiently large ratio μ/c. The entanglement dynamics is most easily studied by monitoring the normalized concurrence of the pure state of QDF given by $C = |c_1c_4 - c_2c_3|/(|c_1|^2 + |c_2|^2 + |c_3|^2 + |c_4|^2)$. A pure state of the qubit pair is separable iff the concurrence is zero. The asymptotic QDF state of the evolution for μ/c sufficiently large has zero concurrence. This fact is illustrated by the time series $C(t)$ with full FHT equations in Fig. 2(a) and with the purely Hamiltonian dynamics discussed in the remark (2) in Fig. 2(b) starting from the same initial state. The asymptotic state of QDF is a product state of the form $|1/2, \pm 1/2\rangle_1 \otimes |\psi\rangle_2$, where $|1/2, \pm 1/2\rangle_1$ are the eigenstates of $\hat{s}_z^1$ and $|\psi\rangle_2$ is a state of the second qubit. Two sample paths in Fig. 2(a) correspond to the concurrence in these two cases.

(2) The constraint (5) was introduced so as to obtain a hybrid system such that the selected observables of the quantum part behave as almost classical. This is admittedly an *ad hoc* assumption. Alternatively one might study the Hamiltonian system (2) *with no additional constraints*, and analyze it as a purely Hamiltonian system with possibly complicated interactions. This is the approach adopted for example in [2], where it was supposed that there are no (Q, P) degrees of freedom so that the evolution is given by the Hamiltonian system on $\mathcal{M}_{qp} \times \mathcal{M}_{xy}$ with $H = H_q(x, y) + H_{cl}(q, p) + H_{int}(q, p, x, y)$. The result is mathematically consistent purely Hamiltonian theory of a hybrid system. However, application of the theory to the measurement situation shows that classical pointer variable is in general coupled to the expectation $\langle \hat{A} \rangle$ of the measured observable $\hat{A}$ and not to its eigenvalues [22,23]. Furthermore, the theory in its exact form predicts some features of QDF which might imply possibility of superluminal communication [24]. The evolution of QDF can be presented in the form of the Schrödinger equation with the Hamiltonian that depends on the total system state. Also, different initial convex representations of a mixed state $\hat{\rho}$ might evolve into different $\hat{\rho}(t)$. Furthermore, investigations of entanglement dynamics, like in the remark (1), show that the entanglement between qubits oscillates with large amplitudes forever and for any values of the parameters. It is well known that the possibility of entanglement and nonlinear evolution, or the dependence of a density matrix evolution on its initial convex representation, might be used for superluminal communication [25,26]. In the FHT this nonphysical effect might be prevented by the stochastic terms in the evolution.

In short, the purely Hamiltonian theory predicts properties of QDF, interacting with CDF, that are not displayed by physical systems. The way to remedy the theory might be to include the influence of the internal degrees of freedom $(Q(t), P(t))$, perhaps in the form of stochastic perturbations. This has not been done in full generality. Some results [2], where the CDF are treated as an environment and are supposed to introduce stochastic perturbations, indicate that such an approach might be successful. In conclusion, purely Hamiltonian theory with the Hamiltonian (2) must be supplemented by an analysis of complicated classical systems with complex CDF dynamics, and only after physically plausible approximations might explain the observed behavior.

(3) Instead of imposing the main effects of the collapse process as the general requirements on the dynamical equation for QDF, and realizing those requirements as a minimal but adequate constraint, one can postulate that the dynamical equations of QDF are given by some of the existing *dynamical collapse models*, reviewed recently in [27] or open quantum system dynamics [28,29] or models of continuous measurements [30]. Such equations usually assume some properties, and specific form, that are not necessary for the most general description of the hybrid dynamics. The most well known dynamical collapse models are given as nonlinear and stochastic modifications of the Schrödinger equation, and contain the Schrödinger term, the nonlinear gradient term and the stochastic term. Similarly, the master equation for the density operator $\hat{\rho}(t)$ of an open quantum system under the Markovian assumption is of the Lindblad form, and can be written as a stochastic diffusion equation for the individual quantum systems in pure states [29,28], with terms of the similar form and the same effect on the evolution as in the explicit collapse models. One such equation, with minimal appropriate generalization, can be postulated for the QDF dynamics of the hybrid and coupled with the Hamiltonian equations (11) for the CDF. An example of such approach is studied in [30]. The result is a set of stochastic differential equations of the form similar to those of *FHT*. Nevertheless, conceptual differences should be stressed. The theories of explicit collapse do not make an a priori distinction between quantum and classical systems. Instead, unique nonlinear and stochastic dynamics for micro and macro systems is postulated, the only difference being in the values of the relevant parameters. If there is a micro-system coupled to a macro-system, then the micro-system dynamics is indistinguishable from the linear Schrödinger evolution, and the collapse occurs in the macroscopic part of the system. This collapse is a consequence of the macroscopic size of the macro-system. In *FHT*, classical behavior of CDF of the macro-systems is assumed from the beginning, and in this respect the theory is conceptually similar to the hybrid theory in [30]. The collapse occurs directly in the quantum part and is a consequence of the interaction between the quantum system and the macro-system, where the latter is conceived as a system with some degrees of freedom described by classical mechanics.

We shall illustrate a possible hybrid theory based on an explicit collapse model, given basically by Hughston [31], since it has been formulated using the quantum phase space. We present the equations in the case when there is only one observable $\hat{A}$, and in terms of evolution on $\mathcal{M}$. A hybrid theory with

typical collapse equation for the QDF would then be of the form

$$dX^a = 2\omega^{ab}\nabla H(X, q, p)dt - \frac{\mu^2}{4}g^{ab}\nabla_b(\Delta A(X))dt + \mu\nabla A(X)dW \tag{20}$$

where $X \equiv (x, y)$ and dW are the stochastic increments of the Wiener process. Eq. (20) for QDF should be supplemented by Eq. (12) for the CDF. Other models of continuous collapse or individual open system dynamics might be written in forms quite similar to (20) with real or complex noise. In Hughston [31] and QMUPL [27] equations dW are real, while in the QSD equation [29] dW are increments of a complex Wiener process. The Hamiltonian $H = \langle\hat{H}\rangle$ is modified to include the interaction with CDF given by $\mu f(p, q)A(x, y)$. Together with the corresponding equations (12) for the CDF dynamics the system represents a model of an individual hybrid system evolution, which has not been investigated in the literature (to the best of our knowledge). Eq. (20) is similar with (11) in that it has a deterministic gradient term, given by the gradient of the relevant dispersion, and the gradient stochastic term given by the gradient of the relevant observable. However, the dynamics of a single quantum open system, for example in QSD [29], is equivalent to the Lindblad equation which is physically justified using weak coupling approximation, and no such approximation is assumed in (11). The major technical difference between (20) and (11) is that the latter has a pre-factor multiplying the deterministic gradient term. A further and deeper comparison of the hybrid theories with Eq. (11) or (20) for the QDF part will certainly be of some interest.

5. Summary

In summary, we have constructed a novel theory of hybrid quantum–classical systems of the type where the quantum and the classical mechanics are both treated as fundamental theories. We have started from the observation that if all degrees of freedom of the system are considered as quantum then the evolution is given by the Schrödinger law, while if there are some degrees of freedom which behave as described by classical mechanics then the collapse postulate should be added to the Schrödinger evolution of the quantum degrees of freedom. Our goal was to derive a theory that provides a dynamical description of the Schrödinger evolution supplemented with the collapse postulate. It is assumed that such a theory would provide a unified dynamical description of the system with quantum and classical degrees of freedom. The basic requirement imposed on the theory is to obtain dynamical equations of the hybrid systems such that the sum of dispersions of the quantum observables that figure in the quantum–classical interaction are constrained to be minimal during the evolution. The crucial assumption that was used to simplify the constrained equations is that the dynamics of the unobserved degrees of freedom is to be replaced by white noise. Furthermore, it was assumed that part of the interaction with the unobserved degrees of freedom is described by complex Hamiltonian, but the equations for the real canonical coordinates (q, p, x, y) are real. The resulting evolution of the hybrid system is nonlinear and stochastic. Some of the stochastic terms are multiplied by the gradients of expectations of the chosen quantum observables, and together with the deterministic gradient terms lead to localization onto the constraint manifold. If the hybrid system is intended as a model of the measurement process of one observable, then the constraint gives the dynamics with eigenstates as attractors, and the stochastic term describes the stochastic nature of the process with the correct probabilities for different asymptotic eigenstates. At the same time, interaction establishes the necessary correlations between the states of the quantum and classical parts.

The hybrid theory derived here has been considered at an abstract level, with the primary goal of demonstrating that consistent hybrid theories, formulated within the specific mathematical framework, are possible. Validity of the theory was tested only with reference to the simplified description of the measurement process as summarized by quantum mechanics with the collapse postulate. There are several immediate questions that are interesting and should be analyzed. On the theoretical side, one should analyze if the hybrid dynamics given by FHT can be used for superluminal communication between entangled quantum systems in interaction with the corresponding macroscopic objects. To this end, one should analyze the FHT dynamics of ensembles of hybrid systems with the corresponding

master equation for the QDF. Because of the stochastic terms, and perhaps under physically justified assumptions, one expects that the evolution of the suitably defined density matrix pertaining to QDF can be expressed with no reference to particular convex representations of the density matrix. However, the Fokker–Planck equation for general hybrid densities implied by the stochastic FHT dynamics (11) of pure states is rather complicated, and we are not presently able to obtain from it a closed form equation for the mixed states of the quantum system. This question will certainly be thoroughly analyzed. Such analysis will also help to clarify the relation of FHT with the hybrid theories based on models of explicit collapse, as discussed in the remark (3). Another theoretical task is to analyze in detail, using suitable examples, the form of the theory where the quantum and macroscopic systems interact via several non-commuting observables. This would pave the way to apply the theory onto realistic physical systems, other than the rudimentary measurement setting, which are expected to be in the domains of hybrid theories.

Acknowledgments

We acknowledge support of the Ministry of Science and Education of the Republic of Serbia, contract Nos. 171006, 171017, 171020, 171038 and 45016 and COST (Action MP1006).

References

[1] J. von Neumann, Mathematische Grundlagen der Quantenmechanik, Springer, Berlin, 1932.
[2] H-T. Elze, Phys. Rev. A 85 (2012) 052109.
[3] L.L. Salcedo, Phys. Rev. A 85 (2012) 022127.
[4] L. Diósi, N. Gisin, W.T. Strunz, Phys. Rev. A 61 (2000) 022108.
[5] M.J.W. Hall, Phys. Rev. A 78 (2008) 042104;
M.J.W. Hall, M. Reginatto, Phys. Rev. A 72 (2005) 062109.
[6] C. Barceló, R. Carballo-Rubio, L.J. Garay, R. Gómez-Escalante, Phys. Rev. A 86 (2012) 042120.
[7] B. Wu, J. Liu, Q. Niu, Phys. Rev. Lett. 94 (2005) 140402.
[8] M. Radonjić, S. Prvanović, N. Burić, Phys. Rev. A 85 (2012) 064101.
[9] B.O. Koopman, Proc. Natl. Acad. Sci. 17 (1931) 315.
[10] A. Heslot, Phys. Rev. D 31 (1985) 1341.
[11] A. Aschtekar, T.A. Schilling, in: A. Harvey (Ed.), On Einsteins Path, Springer-Verlag, Berlin, 1998.
[12] "Fundamental" is not meant to imply that the theory is considered more fundamental than alternative hybrid theories.
[13] V.I. Arnold, Mathematical Methods of Classical Mechanics, Springer, New York, 1978.
[14] D.C. Brody, L.P. Hughston, J. Geom. Phys. 38 (2001) 19.
[15] N. Burić, Ann. Phys. (N.Y.) 233 (2008) 17.
[16] M. Radonjić, S. Prvanović, N. Burić, Phys. Rev. A 84 (2011) 022103.
[17] M. Radonjić, S. Prvanović, N. Burić, Phys. Rev. A 85 (2012) 022117.
[18] D.C. Brody, A.C.T. Gustavsson, L. Hughston, J. Phys. A 41 (2008) 475301.
[19] D.C. Brody, A.C.T. Gustavsson, L. Hughston, J. Phys. A 42 (2009) 295303.
[20] S. Boixo, L. Viola, G. Ortiz, Europhys. Lett. 79 (2007) 40003.
[21] L. Arnold, Stochastic Differential Equations, Theory and Applications, Krieger, Malabar Florida, 1974.
[22] H-T. Elze, Int. J. Quant. Inf. 10 (2012) 1241012.
[23] N. Burić, D.B. Popović, M. Radonjić, S. Prvanović, Phys. Rev. A 87 (2013) 054101.
[24] N. Burić, I. Mendaš, D.B. Popović, M. Radonjić, S. Prvanović, Phys. Rev. A 86 (2012) 034104.
[25] N. Gisin, Phys. Lett. A 143 (1990) 1.
[26] B. Mielnik, Phys. Lett. A 289 (2001) 1.
[27] A. Bassi, K. Lochan, S. Satin, T.P. Singh, H. Ulbricht, Rev. Modern Phys. 85 (2013) 471.
[28] H.-P. Breuer, F. Petruccione, The Theory of Open Quantum Systems, Oxford Uni. Press, Oxford, 2001.
[29] I.C. Percival, Quantum State Difussion, Cambridge Uni. Press, Cambridge UK, 1999.
[30] L. Diósi, J.J. Halliwell, Phys. Rev. Lett. 81 (1998) 2846.
[31] L.P. Hughston, Proc. R. Soc. Lond. Ser. A 452 (1996) 953.

Physics Letters A 378 (2014) 1081–1084

Contents lists available at ScienceDirect

Physics Letters A

www.elsevier.com/locate/pla

Orbits of hybrid systems as qualitative indicators of quantum dynamics

N. Burić *, D.B. Popović, M. Radonjić, S. Prvanović

Institute of Physics, University of Belgrade, Pregrevica 118, 11080 Belgrade, Serbia

ARTICLE INFO

Article history:
Received 2 December 2013
Accepted 26 February 2014
Available online 4 March 2014
Communicated by A.P. Fordy

ABSTRACT

Hamiltonian theory of hybrid quantum–classical systems is used to study dynamics of the classical subsystem coupled to different types of quantum systems. It is shown that the qualitative properties of orbits of the classical subsystem clearly indicate if the quantum subsystem does or does not have additional conserved observables.

1. Introduction

Linear Schrödinger equation of any quantum mechanical system is equivalent to an integrable Hamiltonian dynamical system [1–6]. As such, the linear Schrödinger equation of a bounded system has only periodic or quasi-periodic orbits. However, integrable systems are exceptional [7]. Typical Hamiltonian system has also plenty of irregular, i.e. chaotic orbits [7], but these do not appear in standard quantum mechanics. Integrability, or the lack of it, of Hamiltonian dynamical systems is related to the symmetries of the model and to the existence of a sufficient number of integrals of motion. The difference between integrable and non-integrable systems is clearly manifested in the qualitative properties of orbits. The former have only regular, periodic or quasi-periodic orbits, and in the latter the chaotic orbits dominate. Classification of quantum system into regular or irregular such as ergodic or chaotic, is possible using different plausible and variously motivated criteria without reference to the orbital properties. Usually, the criteria are formulated in terms of the properties of the energy spectrum, and the connection with the classical, well developed, notions of regular or chaotic dynamics, formulated in terms of orbital properties, is obscured.

The purpose of our work was to investigate qualitative properties of orbits of a hybrid quantum–classical system, where the classical part is integrable when isolated and the quantum part is characterized as symmetric or non-symmetric by the existence of constant observables. In particular, we want to see if the symmetry, or the lack of it, might be displayed in the qualitative properties of orbits of the classical part. To this end we utilized recently developed Hamiltonian hybrid theory of quantum–classical (QC) systems [8–12]. Our main result is that indeed quantum systems, characterized as non-symmetric imply chaotic orbits of the classical degrees of freedom (CDF) coupled to the quantum system. On the other hand, CDF show regular dynamics if coupled to a symmetric quantum system, i.e. a quantum system with sufficient number of constant observables.

One of the first to introduce some sort of dynamical distinction between quantum systems was von Neumann [13] with his definition of quantum ergodicity based on the properties of the Hamiltonian eigenspectrum. Further developments and different approaches to the problems of quantum irregular dynamics can be divided into three groups. The literature on the topic is enormous, and we shall give only a few examples or a relevant review for each of the approaches. The most popular was the type of studies analyzing the spectral properties of quantum systems obtained by quantization of chaotic classical systems (see the reviews collected in [14]). Still in the framework of systems whose classical analog is chaotic, there were studies of semi-classical dynamics [14] and phase space distributions [14]. The second group of studies consists of those works where an intrinsic definition of quantum chaoticity is attempted [15]. Neither the works in the first nor those in the second group rely on the topological properties of pure state orbits of quantum systems. The third group originates from the studies of open quantum systems, and here the properties of orbits of an open quantum system are important. Classical property of chaoticity defined in terms of orbital properties was analyzed in quantum systems interacting with different types of environments [16–18]. It was observed that orbits of such open quantum systems in the macro-limit might be chaotic.

In the next section we shall briefly recapitulate the Hamiltonian theory of hybrid systems. In Section 3 we present the hybrid models consisting of qualitatively different pairs of qubits as the quantum part and the linear oscillator as the classical part. Section 4 will describe numerical computations of hybrid dynamics and our main results. Brief summary will be given in Section 5.

* Corresponding author.
E-mail address: buric@ipb.ac.rs (N. Burić).

http://dx.doi.org/10.1016/j.physleta.2014.02.037
0375-9601/

2. Hamiltonian hybrid theory

There is no unique generally accepted theory of interaction between micro and macro degrees of freedom, where the former are described by quantum and the latter by classical theory (see [8] for an informative review). Some of the suggested hybrid theories are mathematically inconsistent, and "no go" type theorems have been formulated [19], suggesting that no consistent hybrid theory can be formulated. Nevertheless, mathematically consistent but inequivalent hybrid theories exist [8,20–23].

The Hamiltonian hybrid theory, as formulated and discussed for example in [8,11,12], has many of the properties commonly expected of a good hybrid theory, but has also some controversial features. Its physical content is equivalent to the standard mean field approximation, but it is formulated entirely in terms of the Hamiltonian framework, which provides useful insights such as the one presented in this communication. The theory is based on the equivalence of the Schrödinger equation on $\mathcal{H}^N$ and the corresponding Hamiltonian system on $\mathbb{R}^{2N}$. The Riemannian g and the symplectic ω structures on the phase space $\mathcal{M}_q = \mathbb{R}^{2N}$ are given by the real and imaginary parts of the Hermitian scalar product on $\mathcal{H}^N$: $\langle\psi|\phi\rangle = g(\psi,\phi) + i\omega(\psi,\phi)$. Schrödinger equation in an abstract basis $\{|n\rangle\}$ of $\mathcal{H}^N$

$$i\hbar\frac{\partial c_n}{\partial t} = \sum_m H_{nm}c_m \tag{1}$$

where $|\psi\rangle = \sum_n c_n|n\rangle$ and $H_{nm} = \langle n|\hat{H}|m\rangle$ is equivalent to Hamiltonian equations

$$\dot{x}_n = \frac{\partial H(x,y)}{\partial y_n}, \qquad \dot{y}_n = -\frac{\partial H(x,y)}{\partial x_n} \tag{2}$$

where $c_n = (x_n + iy_n)/\sqrt{2\hbar}$ and

$$H(x,y) = \langle\psi_{xy}|\hat{H}|\psi_{xy}\rangle, \tag{3}$$

where (x,y) stands for $(x_1, x_2 \ldots x_N, y_1, y_2 \ldots y_N)$. Only quadratic functions $A(x,y)$ of the form $A(x,y) = \langle\psi_{xy}|\hat{A}|\psi_{xy}\rangle$ are related to the physical observables $\hat{A}$. In particular, the canonical coordinates (x,y) of quantum degrees of freedom (QDF) do not have such interpretation.

Hamiltonian hybrid theory uses the Hamiltonian formulations of quantum and classical dynamics, and couples the classical and quantum systems as they would be coupled in the theory of Hamiltonian systems. The phase space of QC system is given by the Cartesian product

$$\mathcal{M}_{qc} = \mathcal{M}_q \times \mathcal{M}_c, \tag{4}$$

and the total Hamiltonian is of the form

$$H_{qc}(x,y,q,p) = H_q(x,y) + H_{cl}(q,p) + H_{int}(x,y,q,p). \tag{5}$$

The dynamical equations of the hybrid theory are just the Hamiltonian equations with the Hamiltonian (5).

Observe two fundamental properties of the Hamiltonian hybrid theory: (a) There is no entanglement between QDF and CDF and (b) the canonical coordinates of CDF have the interpretation of conjugate physical variables and have sharp values in any pure state (x,y,q,p) of the hybrid. Hamiltonian theory of hybrid systems can be developed starting from the Hamiltonian formulation of a composite quantum system and imposing a constraint that one of the components is behaving as a classical system [11].

3. Qualitatively different quantum systems coupled to the classical harmonic oscillator

We shall consider the following three examples of quantum system with different symmetry properties. All three examples involve a pair of interacting qubits, where $\sigma^{1,2}_{x,y,z}$ denote x, y or z Pauli matrix of the qubit 1 or the qubit 2, and ω, μ and β are parameters. The simplest is given by

$$\hat{H}_s = \hbar\omega\sigma_z^1 + \hbar\omega\sigma_z^2 + \hbar\mu\sigma_z^1\sigma_z^2. \tag{6}$$

The system has two additional independent constant observables σ_z^1 and σ_z^2 corresponding to the $SO(2)\times SO(2)$ symmetry of the model. Next two models are examples of non-symmetric systems. The system

$$\hat{H}_{ns1} = \hat{H}_s + \hbar\beta\sigma_y^1 \tag{7}$$

has only σ_z^2 as the additional constant observable, and in the system

$$\hat{H}_{ns2} = \hbar\omega\sigma_z^1 + \hbar\omega\sigma_z^2 + \hbar\mu\sigma_x^1\sigma_x^2, \tag{8}$$

there are no additional dynamical constant observables. Let us stress that the Hamiltonian systems with the Hamiltonian functions given by $\langle\psi|\hat{H}|\psi\rangle$ are integrable with only the regular (non-chaotic) orbits irrespective of their symmetry properties.

The Hamilton functions corresponding to the three quantum systems (6), (7) and (8) are given by the general rule (3). In the computational basis $|1\rangle = |1,1\rangle$, $|2\rangle = |1,-1\rangle$, $|3\rangle = |-1,1\rangle$, $|4\rangle = |-1,-1\rangle$, where for example $|1,1\rangle = |1\rangle\otimes|1\rangle$ and $|\pm1\rangle$ are the eigenvectors of σ_z, the Hamilton functions are

$$H_s(x,y) = \omega\big(x_1^2 + y_1^2 - x_4^2 - y_4^2\big) + \frac{\mu}{2}\big(x_1^2 - x_2^2 - x_3^2 + x_4^2 + y_1^2 - y_2^2 - y_3^2 + y_4^2\big), \tag{9}$$

$$H_{ns1}(x,y) = \omega\big(x_1^2 + y_1^2 - x_4^2 - y_4^2\big) + \frac{\mu}{2}\big(x_1^2 - x_2^2 - x_3^2 + x_4^2 + y_1^2 - y_2^2 - y_3^2 + y_4^2\big) + \beta(y_3x_1 + y_4x_2 - y_1x_3 - y_2x_4) \tag{10}$$

and

$$H_{ns2}(x,y) = \omega\big(x_1^2 + y_1^2 - x_4^2 - y_4^2\big) + \mu(x_2x_3 + x_1x_4 + y_2y_3 + y_1y_4). \tag{11}$$

Observe that, due to the $1/\sqrt{2\hbar}$ scaling of the canonical coordinates (x,y), $\hbar$ does not appear in the Hamilton functions (9), (10) and (11) nor in the corresponding Hamilton equations and their solutions $x(t)\ldots$. Of course, $\hbar$ reappears in the functions $\langle\sigma_x^1\rangle\ldots$.

The classical system that we want to couple with quantum systems (9), (10) or (11) is one-dimensional linear oscillator with the Hamiltonian

$$H_{cl}(q,p) = \frac{p^2}{2m} + kq^2, \tag{12}$$

which of course has only regular periodic orbits.

The *QC* interaction term is taken to be such that it does not interfere with the existence of operators commuting with the Hamiltonian of the quantum part. In other words, the operator $\hat{H}_q + \hat{H}_{int}$ has the same additional constant observables as the quantum part $\hat{H}_q$. Furthermore, $\hat{H}_{int}$ must depend on observables of the qubit 1 and of the qubit 2. For example $\hat{H}_{int} = q(c_1\hbar\sigma_z^1 + c_2\hbar\sigma_z^2)$ implying $H_{int}(x,y,q,p) = q(c_1\hbar\langle\sigma_z^1\rangle + c_2\hbar\langle\sigma_z^2\rangle)$ or explicitly

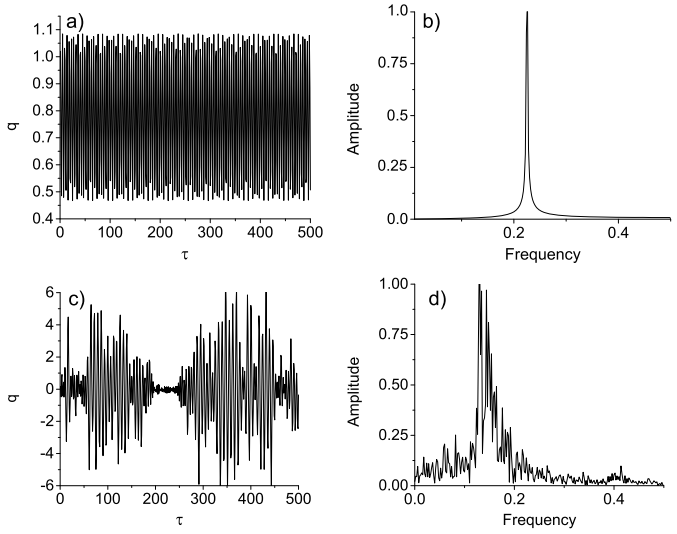

Fig. 1. Figures illustrate the time series $q(\tau)$ (a, c) and the corresponding amplitudes of the Fourier spectra (b, d), of the classical oscillator subpart of the hybrid system with the quantum subpart given by symmetric (9) (a, b) and non-symmetric (11) (c, d) systems. The values of the parameters are $\omega = 1$, $\mu = 5$, $m = k = 1$, $c_1 = 15$, $c_2 = 1$.

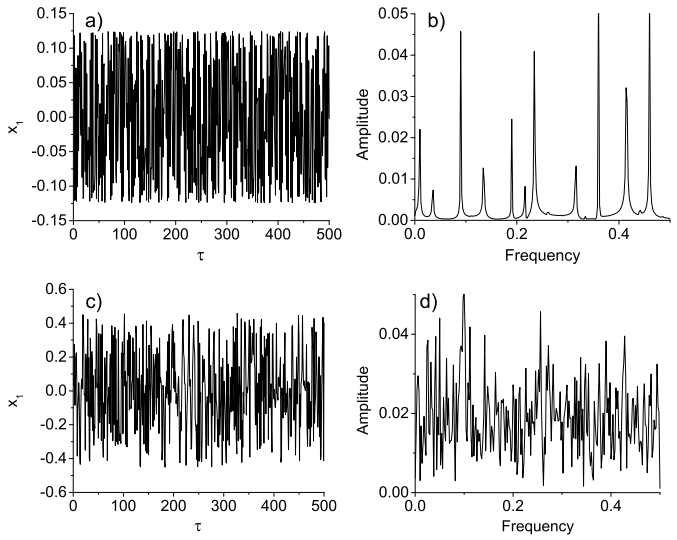

Fig. 2. Figures illustrate the time series (a, c) and the corresponding amplitudes of the Fourier spectra (b, d), of the x_1 canonical coordinate of the quantum subpart of the hybrid system given by symmetric H_s(9) (a, b) and non-symmetric H_{ns2}(11) (c, d) systems. The values of the parameters are the same as in Fig. 1.

$$H_{int} = \frac{c_1 q}{2}\left(x_1^2 + x_2^2 - x_3^2 - x_4^2 + y_1^2 + y_2^2 - y_3^2 - y_4^2\right) + \frac{c_2 q}{2}\left(x_1^2 - x_2^2 + x_3^2 - x_4^2 + y_1^2 - y_2^2 + y_3^2 - y_4^2\right). \quad (13)$$

The total Hamiltonian is given by the sum of (12), (13) and one of (9), (10) or (11). Observe that the functions $\langle\sigma_z^1\rangle$ and $\langle\sigma_z^2\rangle$ are constants of motion for the hybrid $H_s + H_{int} + H_{cl}$, as is the function $\langle\sigma_z^2\rangle$ constant for the hybrid $H_{ns1} + H_{int} + H_{cl}$. Thus, H_{int} given by (13) satisfies the general condition that we impose on the QC interaction.

4. Numerical computations and the results

Hamiltonian equations are solved numerically and the dynamics of CDF, illustrated in Fig. 1 and Figs. 3a, b and of QDF illustrated in Fig. 2 and Figs. 3c, d, is observed in the cases corresponding to the symmetric or non-symmetric quantum parts for different values of the parameters μ and c. Let us first stress again that if there is no classical system then all orbits are regular for either of the quantum systems. On the other hand the hybrid system displays different behavior. Consider first the time series generated by the CDF. Figs. 1a, b, c, d and Figs. 3a, b show the time series $q(\tau)$ (Figs. 1a, c and Fig. 3a), where $\tau = \omega t$ is the dimensionless time, and the corresponding Fourier amplitude spectra (Figs. 1b, d and Fig. 3b). Figs. 1a, b are obtained with the quantum symmetric system (9), Figs. 1c, d with quantum non-symmetric system (11) and Fig. 3 with quantum non-symmetric system (10). Obviously, the orbits of the CDF are periodic, with single frequency, in the symmetric case, and chaotic with a broad-band spectrum in the non-symmetric cases. We can conclude that the qualitative properties of orbits of a classical system coupled with a quantum system are excellent indicators of the symmetries of the quantum system.

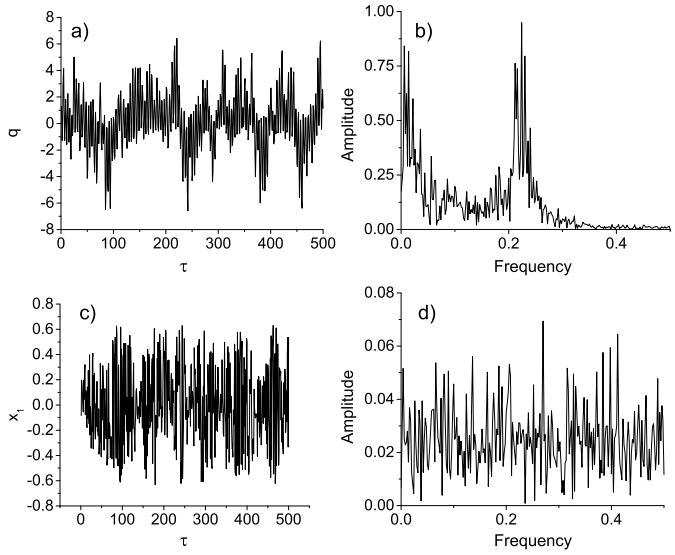

Fig. 3. Figures illustrate the time series $q(\tau)$ (a) and $x_1(\tau)$ and the corresponding amplitudes of the Fourier spectra (b, d). The Hamiltonian is non-symmetric H_{ns1} (10). The values of the parameters are the same as in Fig. 1.

Consider now the dynamics of QDF illustrated in Figs. 2a, b, c, d and Figs. 3c, d by plotting the time series generated by $x_1(t)$ and the corresponding Fourier amplitudes spectra. Qualitatively the same properties are displayed by dynamics of other canonical coordinates $x_2, x_3, x_4, y_1, y_2, y_3, y_4$ or, for example, by the dynamics of expectation values $\langle\sigma_x^1(t)\rangle, \ldots$. Again, the time series are regular if the quantum systems are symmetric and are chaotic in the quantum non-symmetric case. The same conclusion is obtained with H_{ns2} replaced by H_{ns1}. We can conclude that the orbits of the hybrid system, are regular or chaotic, in the sense of Hamiltonian dynamics, depending on the quantum subpart being symmetric or non-symmetric. Thus, the relation between symmetry and existence of independent constants of motion on one hand and the qualitative properties of orbits on the other, which is the characteristic feature of classical mechanics and is not a feature of isolated quantum systems, is restored by appropriate coupling of the quantum and a classical integrable system.

Observe that such behavior cannot be obtained by coupling two quantum systems (instead of quantum–classical coupling). In this case, and even for the simplest quantum system in place of the classical one, the phase space of the quantum composite system is much larger than $\mathcal{M}_{qc}$ because of the degrees of freedom corresponding to the possibility of entanglement, and the total system is always linear. All degrees of freedom of a quantum–quantum system in the Hamiltonian formulation display only regular dynamics, independently of the symmetries of the quantum Hamiltonian. On the other hand, the hybrid systems are nonlinear, due to the QC

coupling and the phase space of the form (4), and the relation between the symmetries and the qualitative properties of orbits is like in the general Hamiltonian theory.

Explanation of the observed properties relies on the fact that the five degrees of freedom hybrid Hamiltonian system with quantum symmetric subpart has enough independent constants of motion in involution. These are given by $H(x, y, q, p)$, $H_s(x, y)$, $\langle\sigma_z^1\rangle$, $\langle\sigma_z^2\rangle$ and the norm of the state of the quantum subpart. On the other hand $H_{ns1} + H_{int} + H_{cl}$, or $H_{ns2} + H_{int} + H_{cl}$ do not have enough such constants of motion since the quantum part $\hat{H}_{ns2}$ does not commute with σ_z^1 and σ_z^2 and $\hat{H}_{ns1}$ with σ_z^1. Only $H_s + H_{int} + H_{cl}$ is integrable while those obtained with non-symmetric quantum subparts are not and thus have some chaotic orbits.

5. Summary

In summary, we have shown that the orbits of an integrable classical system when coupled to a quantum system in an appropriate way remain regular or become chaotic depending on the presence or lack of symmetries in the quantum part. To this end we used the Hamiltonian theory of quantum–classical systems and examples of qubit systems. The first fact is an important restriction on our work. On the second point, the nature of our results is qualitative and is therefore expected to be valid generically, and not only for the considered examples. Considering the choice of Hamiltonian theory to describe QC interaction, we were motivated by the mathematical consistency of the theory and the fact that the theory describes orbits of pure states of a deterministic Hamiltonian system. There are other consistent hybrid theories, but they are either formulated in terms of probability densities [21,22] or in terms of stochastic pure state evolution [20,23]. Of course, the significance of our result could be properly judged only after the status of Hamiltonian hybrid theory is sufficiently understood.

Acknowledgements

We acknowledge support of the Ministry of Education and Science of the Republic of Serbia, contracts Nos. 171006, 171017, 171020, 171038 and 45016 and COST (Action MP1006).

References

[1] V.I. Arnold, Mathematical Methods of Classical Mechanics, Springer, New York, 1978.
[2] A. Heslot, Phys. Rev. D 31 (1985) 1341.
[3] A. Aschtekar, T.A. Schilling, in: A. Harvey (Ed.), On Einstein's Path, Springer-Verlag, Berlin, 1998.
[4] D.C. Brody, L.P. Hughston, J. Geom. Phys. 38 (2001) 19.
[5] N. Burić, Ann. Phys. (NY) 233 (2008) 17.
[6] M. Radonjić, S. Prvanović, N. Burić, Phys. Rev. A 84 (2011) 022103.
[7] R.S. MacKay, J.D. Meiss (Eds.), Hamiltonian Dynamical Systems, Adam Hilger, Bristol, 1987.
[8] H.-T. Elze, Phys. Rev. A 85 (2012) 052109.
[9] H.-T. Elze, Int. J. Quantum Inf. 10 (2012) 1241012.
[10] B. Wu, J. Liu, Q. Niu, Phys. Rev. Lett. 94 (2005) 140402.
[11] M. Radonjić, S. Prvanović, N. Burić, Phys. Rev. A 85 (2012) 064101.
[12] N. Burić, I. Mendaš, D.B. Popović, M. Radonjić, S. Prvanović, Phys. Rev. A 86 (2012) 034104.
[13] J. von Neumann, Z. Phys. 57 (1929) 30.
[14] M.-J. Giannoni, A. Voros, J. Zinn-Justin, Chaos and Quantum Physics, North-Holland, Amsterdam, 1991.
[15] J. Bolte, R. Glasser, Nonlinearity 13 (2000) 1987.
[16] I.C. Percival, Quantum State Diffusion, Cambridge Univ. Press, Cambridge, UK, 1999.
[17] M.J. Everitt, Phys. Rev. E 75 (2007) 036217.
[18] N. Buric, Phys. Lett. A 374 (2010) 4090.
[19] L.L. Salcedo, Phys. Rev. A 85 (2012) 022127.
[20] L. Diósi, J.J. Halliwell, Phys. Rev. Lett. 81 (1998) 2846.
[21] L. Diósi, N. Gisin, W.T. Strunz, Phys. Rev. A 61 (2000) 022108.
[22] M.J.W. Hall, Phys. Rev. A 78 (2008) 042104;
M.J.W. Hall, M. Reginatto, Phys. Rev. A 72 (2005) 062109.
[23] N. Burić, D.B. Popović, M. Radonjić, S. Prvanović, arXiv:1307.8424, 2013.

Ehrenfest principle and unitary dynamics of quantum-classical systems with general potential interaction

M. Radonjić, D. B. Popović, S. Prvanović, and N. Burić*
Institute of Physics, University of Belgrade, Pregrevica 118, 11080 Belgrade, Serbia
(Received 4 January 2014; published 28 February 2014)

Representation of classical dynamics by unitary transformations has been used to develop a unified description of hybrid classical-quantum systems with a particular type of interaction, and to formulate abstract systems interpolating between classical and quantum ones. We solved the problem of a unitary description of two interpolating systems with general potential interaction. The general solution is used to show that with arbitrary potential interaction between the two interpolating systems the evolution of the so-called unobservable variables is decoupled from that of the observable ones if and only if the interpolation parameters in the two interpolating systems are equal.

DOI: 10.1103/PhysRevA.89.024104 PACS number(s): 03.65.Fd, 03.65.Sq

I. INTRODUCTION

Koopman–von Neumann (KvN) [1] unitary description of the Liouville equation of classical Hamiltonian dynamical systems was utilized for modeling hybrid quantum-classical systems by Sherry and Sudarshan [2]. They analyzed particular types of interaction between the classical and the quantum parts, and ad hoc prescriptions for definitions of the corresponding Hilbert space operators. It was shown that the premeasurement process can be modeled as an interaction between a classical apparatus and a quantum system within the unitary framework. Sherry and Sudarshan also analyzed the so-called integrity conditions which ought to be satisfied in order that classical variables remain classical during the hybrid unitary evolution in the Heisenberg form. Peres and Terno [3] analyzed consistency of the Koopman–von Neumann–Sudarshan (KNS) hybrid dynamics with the quantum-quantum and the classical-classical limits for the case of linear interaction between harmonic oscillators. Some aspects of the KNS formalism for a hybrid system with specific interaction have also been studied in [4]. The authors investigated the role of unphysical variables which are called unobservables because they do not influence the evolution of the physical observables of the quantum or the classical part if there is no quantum-classical interaction. It was observed, using particular examples of quantum-classical interaction and specific forms of its Hilbert space description, that the evolution of the unobservable and observable variables become coupled.

More recently, KvN formalism and Ehrenfest principle were used to propose a family of abstract unitary systems interpolating between classical system and its quantized counterpart [5]. The problem of hybrid dynamics was not analyzed using the interpolating systems. Our goal is to study the same type of questions, but for the most general potential interaction between the classical and the quantum systems. In fact, we shall obtain unitary dynamical equations for two interpolating abstract systems (IAS) with general potential interaction, and use this to show that generally the evolution of the unphysical variables is decoupled from that of the physical ones if and only if the interpolation parameters in the two IAS are equal. In particular, unitary dynamics of hybrid systems with potential interaction in general couples the dynamics of the two types of variables. However, there is one special case in the family of general solutions such that the corresponding quantum-classical potential interaction does not couple the physical and the unphysical variables, and implies other properties consistent with this fact.

II. INTERPOLATING ABSTRACT SYSTEMS AND HYBRID MODELS

Dynamical equations for averages of the basic observables of a classical system and that of its quantized counterpart can be mathematically interpolated by an abstract system that depends on a suitable parameter. The first step to achieve this is to rewrite the dynamics of classical and quantum averages using the same mathematical framework. This can be done by rewriting the classical dynamics as a unitary evolution on a suitable Hilbert space, or by rewriting the unitary Schrödinger equation as a (linear) Hamiltonian system on a symplectic manifold. We shall treat here the unitary approach with general potential interaction.

Consider an abstract dynamical system with the basic variables x_j, p_j, χ_j, π_j (hereafter $j = 1,2$). Properties of the system, expressed through appropriate algebraic relations between the basic variables, are supposed to depend on parameters a_j. The basic variables satisfy commutation relations

$$[x_j, p_j] = i\hbar a_j, \quad [x_j, \pi_j] = [\chi_j, p_j] = i\hbar, \tag{1}$$

with all other commutators being zero. Let us suppose that the algebra (1) is represented by operators acting on a Hilbert space $\mathcal{H}$. Assume that the dynamical variables x_j, p_j are measurable and that their averages in a state $|\psi\rangle \in \mathcal{H}$ are computed as

$$\langle x_j\rangle_\psi = \langle\psi|\hat{x}_j|\psi\rangle, \quad \langle p_j\rangle_\psi = \langle\psi|\hat{p}_j|\psi\rangle. \tag{2}$$

*buric@ipb.ac.rs

Suppose that the dynamics of these averages is given by the Ehrenfest principle

$$\frac{d}{dt}\langle\psi(t)|\hat{x}_j|\psi(t)\rangle = \langle\psi(t)|\frac{\hat{p}_j}{m_j}|\psi(t)\rangle, \tag{3a}$$

$$\frac{d}{dt}\langle\psi(t)|\hat{p}_j|\psi(t)\rangle = \langle\psi(t)|-V_j'(\hat{x}_j)|\psi(t)\rangle, \tag{3b}$$

and that the state evolution is unitary $i\hbar|\dot{\psi}\rangle = \hat{H}_{\rm IAS}|\psi\rangle$. The corresponding evolution equations for the dynamical variables in the Heisenberg form are $i\hbar\, d\hat{x}_j/dt = [\hat{x}_j, \hat{H}_{\rm IAS}]$ and analogously for $\hat{p}_j, \hat{\chi}_j, \hat{\pi}_j$. The operator $\hat{H}_{\rm IAS}$ is the evolution generator and might depend on all dynamical variables $\hat{H}_{\rm IAS} = H_{\rm IAS}(\hat{x}_j, \hat{p}_j, \hat{\chi}_j, \hat{\pi}_j)$. It is not necessarily interpreted as the physical energy. It should be remarked that the relations (2) and (3) are treated as axioms in the general abstract formulation [5], expressing the conservative nature of the dynamics. Following the approach of [5], one can obtain the class of evolution generators yielding (3),

$$\hat{H}_{\rm IAS} = \sum_{j=1,2}\frac{1}{a_j}\left(\frac{\hat{p}_j^2}{2m_j}+V_j(\hat{x}_j)\right)+F_j(\hat{x}_j - a_j\hat{\chi}_j, \hat{p}_j - a_j\hat{\pi}_j), \tag{4}$$

where F_j are arbitrary functions of the indicated arguments. Observe that, consistent with (3), there are no terms coupling observables with different subscripts, so that the abstract system (4) can be interpreted as a compound system with two noninteracting components.

Explicit representation of the operator $\hat{H}_{\rm IAS}$ depends on the representation space $\mathcal{H}$, and is not important in our analysis. Nevertheless, it should be remarked that the Hilbert space $\mathcal{H}$ is determined as a space of an irreducible representation of the algebra (1), and is the same space for any value of the parameters a_j. In particular, it is seen that in the case we want to represent two quantum systems, the Hilbert space needed to accommodate (1) with $a_1 = a_2 = 1$ is larger than the space $L_2(x_1)\otimes L_2(x_2) \equiv L_2(x_1, x_2)$, which is relevant in the standard quantum mechanics without the additional variables χ_j, π_j. It can be shown that one irreducible representation of the algebra is provided with the Hilbert space of operators on $L_2(x_1, x_2)$ [6]. Thus, the vectors from $\mathcal{H}$ can be considered as density matrices or mixed states of the quantum-quantum system [5]. Similarly, if the abstract systems represent two classical systems, i.e., when $a_1 = a_2 = 0$ so that $\hat{x}_j, \hat{p}_j$ all commute, the interpretation of the state $|\psi\rangle$ is that of the amplitude of a probability density $\rho(x_1, x_2, p_1, p_2) = |\langle x_1, x_2, p_1, p_2|\psi\rangle|^2$ on the corresponding phase space $\mathcal{M}(x_1, x_2, p_1, p_2)$ [5]. The scalar product in (2) coincides with the ensemble average $\int_{\mathcal{M}}\rho\, x_j\, dM$ or $\int_{\mathcal{M}}\rho\, p_j\, dM$. Observe that the classical Hilbert space can be partitioned into equivalence classes $|\psi\rangle \sim e^{i\phi}|\psi\rangle$, where each class corresponds to a single density ρ. The evolution equations preserve the equivalence classes because there is no interaction [4].

Convenient choices of the arbitrary functions F_j can reproduce the evolution equations for noninteracting classical-classical (C-C) ($a_1 = a_2 = 0$), quantum-quantum (Q-Q) ($a_1 = a_2 = 1$), and classical-quantum systems (C-Q) ($a_1 = 0$, $a_2 = 1$). The relevant choice of functions F_j and the corresponding equations can be obtained as the special case from the general equations, that will be given later, with interaction set to zero.

For arbitrary $a_1, a_2 \neq 0, 1$ the dynamical equations describe the evolution of an abstract system interpolating between the quantum and the classical systems (hence the notation $\hat{H}_{\rm IAS}$). Because there is no interaction between the two systems, the evolution of $\hat{x}_j, \hat{p}_j$ is also independent of $\hat{\chi}_j, \hat{\pi}_j$. The system has $2+2$ degrees of freedom, and each of the degrees of freedom evolves independently of the others. If the abstract system (4) is meant to represent two quantum or two classical systems, the variables $\hat{x}_j, \hat{p}_j$ are interpreted as physical observables of coordinates and momenta. The variables $\hat{\chi}_j, \hat{\pi}_j$, similarly as $\hat{H}_{\rm IAS}$, do not represent physical observables. They are dynamically separated from the physical observables and appear because the family of systems (4) must interpolate between the classical and the quantum dynamics [5].

III. IAS WITH GENERAL POTENTIAL INTERACTION

Potential interaction between two quantum systems or between two classical systems appears in the equations of motion in the form of gradients of the corresponding scalar potential. In the extended Hilbert space formalism, which is required for the formulation of the IAS, such potential Q-Q or C-C interaction can be represented by an operator expression in terms of all variables with the role of coordinates $\hat{W} = W(\hat{x}_1, \hat{x}_2, \hat{\chi}_1, \hat{\chi}_2)$. We assume that in the dynamical equations for the corresponding momenta $\hat{W}$ should appear as a gradient with respect to the corresponding coordinate.

We shall now consider dynamics of two abstract systems with arbitrary values of a_1, a_2 and with an arbitrary potential interaction between them. Like in the Q-Q and C-C cases, we demand that the following relations hold:

$$\frac{d}{dt}\langle\Psi(t)|\hat{x}_j|\Psi(t)\rangle = \langle\Psi(t)|\frac{\hat{p}_j}{m_j}|\Psi(t)\rangle, \tag{5a}$$

$$\frac{d}{dt}\langle\Psi(t)|\hat{p}_j|\Psi(t)\rangle = \langle\Psi(t)|-V_j'(\hat{x}_j) - \frac{\partial\hat{W}}{\partial\hat{x}_j}|\Psi(t)\rangle. \tag{5b}$$

Notice that the potential interaction can be completely general. Particular examples of interaction which do not necessarily satisfy (5) have been assumed in a somewhat ad hoc manner and studied in [2–4]. Our goal is to determine the unitary evolution generator $\hat{H}_{\rm IAS} = H_{\rm IAS}(\hat{x}_1, \hat{p}_1, \hat{x}_2, \hat{p}_2, \hat{\chi}_1, \hat{\pi}_1, \hat{\chi}_2, \hat{\pi}_2)$ such that $i\hbar|d\Psi(t)/dt\rangle = \hat{H}_{\rm IAS}|\Psi(t)\rangle$ holds. The unitary evolution and (5) give the following relations:

$$\frac{1}{i\hbar}[\hat{x}_j, \hat{H}_{\rm IAS}] = \frac{\hat{p}_j}{m_j}, \quad -\frac{1}{i\hbar}[\hat{p}_j, \hat{H}_{\rm IAS}] = V_j'(\hat{x}_j) + \frac{\partial\hat{W}}{\partial\hat{x}_j}, \tag{6}$$

and the related system of partial differential equations (PDEs) for the function $H_{\rm IAS}$,

$$a_j\frac{\partial H_{\rm IAS}}{\partial p_j} + \frac{\partial H_{\rm IAS}}{\partial\pi_j} = \frac{p_j}{m_j}, \tag{7a}$$

$$a_j\frac{\partial H_{\rm IAS}}{\partial x_j} + \frac{\partial H_{\rm IAS}}{\partial\chi_j} = V_j'(x_j) + \frac{\partial W}{\partial x_j}. \tag{7b}$$

The commutation relations (6), i.e., the PDEs (7), are not consistent for an arbitrary choice of the interaction potential $\hat{W}$. Jacobi identity $[\hat{H}_{\rm IAS},[\hat{p}_1,\hat{p}_2]]+[\hat{p}_1,[\hat{p}_2,\hat{H}_{\rm IAS}]]+[\hat{p}_2,[\hat{H}_{\rm IAS},\hat{p}_1]]=0$ and the commutation relation $[\hat{p}_1,\hat{p}_2]=0$ imply that $[\hat{p}_1,[\hat{p}_2,\hat{H}_{\rm IAS}]]=[\hat{p}_2,[\hat{p}_1,\hat{H}_{\rm IAS}]]$, so that

$$\left[a_1\frac{\partial}{\partial x_1}+\frac{\partial}{\partial\chi_1},a_2\frac{\partial}{\partial x_2}+\frac{\partial}{\partial\chi_2}\right]H_{\rm IAS}=0 \tag{8}$$

must be satisfied. Invoking the second relation of (7), we get the consistency requirement

$$\left(a_1\frac{\partial}{\partial x_1}+\frac{\partial}{\partial\chi_1}\right)\frac{\partial W}{\partial x_2}-\left(a_2\frac{\partial}{\partial x_2}+\frac{\partial}{\partial\chi_2}\right)\frac{\partial W}{\partial x_1}=0. \tag{9}$$

The general solution of (9) is

$$W=\int_{-\infty}^{\infty}\mathcal{W}(x_1+(\alpha-a_1)\chi_1,x_2+(\alpha-a_2)\chi_2,\alpha)\,d\alpha, \tag{10}$$

where $\mathcal{W}$ is an arbitrary function such that the previous integral is defined. Note that when $a_1\neq a_2$, i.e., when the systems are of different type, the interaction potential $\hat{W}$ will depend on at least one of the unobservables $\hat{\chi}_1,\hat{\chi}_2$. This conclusion remains valid in the particular case of a hybrid classical-quantum system, where $a_1=0$ corresponds to the classical part and $a_2=1$ is related to the quantum part. Let us stress that this fact is proved here for quite general potential interaction and not just observed for some special choices of the interaction [3,4].

Consider a particular choice of $\mathcal{W}\propto\delta(\alpha-a)$ yielding the interaction potential $\hat{W}=W(\hat{x}_1+(a-a_1)\hat{\chi}_1,\hat{x}_2+(a-a_2)\hat{\chi}_2)$. The related solution of the PDEs (7) gives

$$\begin{aligned}\hat{H}_{\rm IAS}=&\sum_{j=1,2}\frac{1}{a_j}\left(\frac{\hat{p}_j^2}{2m_j}+V_j(\hat{x}_j)\right)\\&+\frac{1}{a}W(\hat{x}_1+(a-a_1)\hat{\chi}_1,\hat{x}_2+(a-a_2)\hat{\chi}_2)\\&+F(\hat{x}_1-a_1\hat{\chi}_1,\hat{p}_1-a_1\hat{\pi}_1,\hat{x}_2-a_2\hat{\chi}_2,\hat{p}_2-a_2\hat{\pi}_2),\end{aligned} \tag{11}$$

where F is arbitrary real-valued smooth function that commutes with the observables $O(\hat{x}_1,\hat{p}_1,\hat{x}_2,\hat{p}_2)$. Let us observe that when the two systems are of the same type, the unobservables do not influence the evolution of the physical observables for the choice $a_1=a_2=a$. The result (11) can be extended, although with some care, to the limit $a\to0$, which will turn out to be interesting for the hybrid Q-C system. Namely, one can take a part of the function F to be of the suitable form $-\frac{1}{a}W(\hat{x}_1-a_1\hat{\chi}_1,\hat{x}_2-a_2\hat{\chi}_2)$ that yields in the $a\to0$ limit,

$$\begin{aligned}\hat{H}_{\rm IAS}=&\sum_{j=1,2}\frac{1}{a_j}\left(\frac{\hat{p}_j^2}{2m_j}+V_j(\hat{x}_j)\right)\\&+\partial_1W(\hat{x}_1-a_1\hat{\chi}_1,\hat{x}_2-a_2\hat{\chi}_2)\,\hat{\chi}_1\\&+\partial_2W(\hat{x}_1-a_1\hat{\chi}_1,\hat{x}_2-a_2\hat{\chi}_2)\,\hat{\chi}_2\\&+F(\hat{x}_1-a_1\hat{\chi}_1,\hat{p}_1-a_1\hat{\pi}_1,\hat{x}_2-a_2\hat{\chi}_2,\hat{p}_2-a_2\hat{\pi}_2),\end{aligned} \tag{12}$$

where ∂_jW denotes partial derivative of the potential with respect to the jth argument.

The limit of (11) when $a_j\to0$ can also be obtained by choosing a part of the function F in the form $-\frac{1}{a_j}[\frac{(\hat{p}_j-a_j\hat{\pi}_j)^2}{2m_j}+V_j(\hat{x}_j-a_j\hat{\chi}_j)]$, as in [5]. In particular, this yields the Hamiltonian, as the dynamics generator, of a hybrid classical-quantum system ($a_1\to0$, $a_2=1$)

$$\begin{aligned}\hat{H}_{\rm hyb}=&\frac{\hat{p}_1}{m_1}\hat{\pi}_1+V_1'(\hat{x}_1)\,\hat{\chi}_1+\frac{\hat{p}_2^2}{2m_2}+V_2(\hat{x}_2)\\&+\frac{1}{a}W(\hat{x}_1+a\hat{\chi}_1,\hat{x}_2+(a-1)\hat{\chi}_2)\\&+F(\hat{x}_1,\hat{p}_1,\hat{x}_2-\hat{\chi}_2,\hat{p}_2-\hat{\pi}_2),\end{aligned} \tag{13}$$

where the first four terms describe a noninteracting hybrid system. As already mentioned, the interaction potential depends on at least one of the unobservables $\hat{\chi}_1,\hat{\chi}_2$. The appearance of the unphysical variables in the Hamiltonian is not a problem *per se*, because the Hamiltonian is anyway interpreted as the dynamics generator and not as the physical energy. Additionally, in the purely C-C case ($a_1=a_2=a\to0$) one gets

$$\begin{aligned}\hat{H}_{\rm C\text{-}C}=&\frac{\hat{p}_1}{m_1}\hat{\pi}_1+V_1'(\hat{x}_1)\,\hat{\chi}_1+\frac{\hat{p}_2}{m_2}\hat{\pi}_2+V_2'(\hat{x}_2)\,\hat{\chi}_2\\&+\partial_1W(\hat{x}_1,\hat{x}_2)\,\hat{\chi}_1+\partial_2W(\hat{x}_1,\hat{x}_2)\,\hat{\chi}_2,\end{aligned} \tag{14}$$

with the unobservables being present, but not within the arguments of the interaction potential. However, in the C-C case the unphysical variables do not appear in the evolution equations of the physical observables. We may remark in passing that $\hat{W}$ is not interpreted as the potential energy of the hybrid, but as a term in the generator of dynamics corresponding to the potential interaction. However, the crucial property of hybrid Q-C systems is that the equations of motion for the physical and unphysical variables become coupled. Those equations are easily obtained from the generator (13). Thus, we have shown that the dynamical equations couple physical and unphysical variables in the case of a potential Q-C interaction in general, that is with the Hamiltonian of the general hybrid form (13).

A very special case of (13) is obtained in the limit $a\to0$ with the appropriate choice of the function F yielding the Hamiltonian

$$\begin{aligned}\hat{H}_{\rm hyb}=&\frac{\hat{p}_1}{m_1}\hat{\pi}_1+V_1'(\hat{x}_1)\,\hat{\chi}_1+\frac{\hat{p}_2^2}{2m_2}+V_2(\hat{x}_2)\\&+\partial_1W(\hat{x}_1,\hat{x}_2-\hat{\chi}_2)\,\hat{\chi}_1+\partial_2W(\hat{x}_1,\hat{x}_2-\hat{\chi}_2)\,\hat{\chi}_2,\end{aligned} \tag{15}$$

with the corresponding equations of motion of the variables

$$\frac{d\hat{x}_j}{dt}=\frac{\hat{p}_j}{m_j}, \tag{16a}$$

$$\frac{d\hat{p}_j}{dt}=-V_j'(\hat{x}_j)-\partial_jW(\hat{x}_1,\hat{x}_2-\hat{\chi}_2), \tag{16b}$$

$$\frac{d}{dt}(\hat{x}_2-\hat{\chi}_2)=0. \tag{16c}$$

This solution describes the situation when the evolution of the classical system depends on the quantum system only through a constant of motion $\hat{x}_2 - \hat{\chi}_2$. In this very special case of the general hybrid solution, the classical variables see only a quite coarse-grained effect of the quantum evolution. On the other hand, the dynamics of the quantum sector is influenced by the details of the dynamics of the classical physical variables $\hat{x}_1, \hat{p}_1$. In addition, this is the only case of the potential Q-C interaction which satisfies the integrity principle of Sudarshan [2]. Namely, the terms $\partial_j W(\hat{x}_1, \hat{x}_2 - \hat{\chi}_2)$ in this form of the Hamiltonian commute with the momenta $\hat{p}_1, \hat{p}_2$, which assures commutation of the classical variables at different times.

IV. SUMMARY

We have studied the type of theory of hybrid quantum-classical systems where the evolution is described by unitary transformations on an appropriate Hilbert space. The fact that both classical and quantum mechanics can be formulated on the same Hilbert space makes it possible to introduce a parameter dependent family of abstract systems interpolating between a classical system and its quantized counterpart [5]. The variables involved in the formulation of the abstract interpolating model can be divided into two groups, one with the standard physical interpretation and one with no physical interpretation. In the limits of the classical or the quantum system the two groups of variables are dynamically separated. We have studied two such abstract interpolating systems with quite arbitrary potential interaction between them. General solution for the problem of constructing dynamical equations for such a pair of systems is provided. It is shown that, with the most general type of potential interaction, the dynamics of the two groups of variables is separated if and only if the two abstract interpolating systems have the same value of the interpolation parameter. On the other hand, if the interpolation parameters of the two system are different, the two groups of variables dynamically influence each other. The variables which can be considered as unphysical and cannot be observed in the purely quantum or in the purely classical case, do have an observable effect in the hybrid quantum-classical system. Our results demonstrate this fact for arbitrary potential interaction, in line with the previous special cases [3,4]. Analogous conclusions are obtained in the symplectic approach to the conservative hybrid dynamics [7,8], and the analogy is worth further investigation. We have also analyzed the particular case of the general solution corresponding to the situation when the classical part is influenced by the quantum part only through a particular combination of the variables from the quantum system that remains constant during the evolution. This, rather special case, is the only possible dynamics of the hybrid system within the framework of unitary dynamics with potential interaction, when the physical and the unphysical variables can be considered as decoupled, and also when the Sudarshan integrity condition of the classical system is satisfied.

ACKNOWLEDGMENTS

We acknowledge support of the Ministry of Education and Science of the Republic of Serbia, Contracts No. 171006, No. 171017, No. 171020, No. 171038, and No. 45016 and COST (Action MP1006).

[1] B. O. Koopman, Proc. Natl. Acad. Sci. USA **17**, 315 (1931); J. von Neumann, Ann. Math. **33**, 587 (1932); **33**, 789 (1932).

[2] T. N. Sherry and E. C. G. Sudarshan, Phys. Rev. D **18**, 4580 (1978); **20**, 857 (1979); S. R. Gautam, T. N. Sherry, and E. C. G. Sudarshan, *ibid.* **20**, 3081 (1979).

[3] A. Peres and D. R. Terno, Phys. Rev. A **63**, 022101 (2001).

[4] C. Barceló, R. Carballo-Rubio, L. J. Garay, and R. Gómez-Escalante, Phys. Rev. A **86**, 042120 (2012).

[5] D. I. Bondar, R. Cabrera, R. R. Lompay, M. Y. Ivanov, and H. A. Rabitz, Phys. Rev. Lett. **109**, 190403 (2012); D. I. Bondar, R. Cabrera, D. V. Zhdanov, and H. A. Rabitz, Phys. Rev. A **88**, 052108 (2013).

[6] N. Mukunda, Pramana **11**, 1 (1978).

[7] H-T. Elze, Phys. Rev. A **85**, 052109 (2012).

[8] M. Radonjić, S. Prvanović, and N. Burić, Phys. Rev. A **85**, 064101 (2012); N. Burić, I. Mendaš, D. B. Popović, M. Radonjić, and S. Prvanović, *ibid.* **86**, 034104 (2012).

Int J Theor Phys (2014) 53:1046–1055
DOI 10.1007/s10773-013-1898-3

Unified Treatment of Geometric Phases for Statistical Ensembles of Classical, Quantum and Hybrid Systems

N. Burić · D.B. Popović · M. Radonjić · S. Prvanović

Received: 17 July 2013 / Accepted: 29 October 2013 / Published online: 13 November 2013

Abstract Geometric phases for evolution of statistical ensembles of Hamiltonian dynamical systems are introduced utilizing the fact that the Liouville equation is itself an infinite integrable Hamiltonian system. This general framework provides unified treatment of geometric phases for pure or mixed states of classical, quantum or hybrid quantum-classical systems.

Keywords Geometric phases · Statistical ensembles

1 Introduction

Geometric phases have been introduced in order to describe non-holonomic effects in the evolution of pure quantum states (the most relevant references are listed and commented in [1]). Originally defined for adiabatic and cyclic evolution, the notion of the geometric phases has been extended to arbitrary curves in the space of pure states. It has been realized that objects with analogous meaning exist in the dynamics of pure states of an integrable classical mechanical system [2, 3]. However, most states in applications and experiments are mixed rather than pure. The problem of an appropriate definition of geometric phases for mixed states has been approached from different perspectives, and the different approaches resulted in nonequivalent definitions [4–9]. Geometric ideas analogous to those applied in the case of pure states have been explored also in the context of mixed states [10]. It is fair to say that the proper definition of geometric phases for mixed states is still an unsettled issue. In this communication we present a unified treatment of a special type of geometric phases for statistical ensembles of Hamiltonian dynamical systems with different details and physical interpretation. The type of geometric phase treated here is a generalization of Hannay angles introduced for adiabatic time-periodic Hamiltonian evolution of integrable classical systems in pure states. Our approach is based on: (a) the fact that quantum systems

N. Burić (✉) · D.B. Popović · M. Radonjić · S. Prvanović
Institute of Physics, University of Belgrade, P.O. Box 68, 11000 Belgrade, Serbia
e-mail: buric@ipb.ac.rs

(with finite state spaces) and classical mechanical systems are examples of Hamiltonian dynamical systems with finite number of degrees of freedom [11–13]; and (b) the fact that the Liouville evolution of statistical ensembles of such Hamiltonian systems is an integrable (functional) Hamiltonian system. The approach applies also on the Hamiltonian description of so-called hybrid systems, i.e. systems composed of interacting classical and quantum units [14–17]. In what follows we shall first present the general theory leading to the notion of Hannay angles for statistical ensembles of Hamiltonian systems (with arbitrary physical interpretation). The general definition provides the corresponding definitions for the Hannay angles of classical, quantum and of hybrid systems in mixed and in pure states. Our presentation is conceptual rather than mathematically rigorous. Presentation containing all necessary details would require much larger space, but is possible, using the methods and results presented for example in [18, 19].

2 Hamiltonian Framework for Pure States

Evolution of conservative systems, either of classical mechanical or of quantum variety or of hybrid type, can be described using the mathematical framework of Hamiltonian dynamical systems. Formulation of classical mechanics as a Hamiltonian dynamical system is well known [18]. In the case of a quantum system with an N dimensional Hilbert space $\mathcal{H}^N$ the corresponding phase space is given as $\mathcal{M} = R^{2N}$, or using normalization and global phase invariance by $\mathcal{M} = CP^{N-1} \equiv S^{2N-1}/S^1$. The symplectic structure on $\mathcal{M}$ is given by the imaginary part of the Hilbert space scalar product, and the system also has real Riemannian structure given by the real part of the scalar product. A point from $\mathcal{M}$ associated with the state $|\psi\rangle$ (or the corresponding ray) is denoted as x_ψ. Generic point from $\mathcal{M}$ will also be denoted by x or x^a, where $a = 1, 2, \ldots, 2N$ is an abstract index. The dimension of the quantum phase space is $2N$ where N is the complex dimension of the system's Hilbert space. It should be stressed, perhaps, that the canonical coordinates have nothing to do with the canonical coordinates of the classical system that after quantization gives the considered quantum system with the Hilbert space $\mathcal{H}$. The Hamilton's function $H(x)$ is given by the quantum expectation of the Hamiltonian $\hat{H}$ in the state $|\psi_x\rangle \leftrightarrow x$: $H(x) = \langle\psi_x|\hat{H}|\psi_x\rangle$. The Schrödinger dynamical law is that of Hamiltonian mechanics

$$\dot{x}^a = \omega^{ab}\nabla_b H. \tag{1}$$

In the Hamiltonian formulation of QM, only the quadratic functions generate the automorphisms, and only such functions are related to dynamical variables or observables. In fact, all dynamical variables are represented by quadratic functions $A(x)$ on $\mathcal{M}$ and are the quantum mechanical expectations of the corresponding quantum observables $A(x) = \langle\psi_x|\hat{A}|\psi_x\rangle$. In particular, the canonical coordinates of the quantum phase space do not have this physical interpretation. It is important to observe that the Poisson bracket between two quadratic functions is also a quadratic function and satisfies

$$\{A_1(x), A_2(x)\} = \frac{1}{i\hbar}\langle\psi_X|[\hat{A}_1, \hat{A}_2]|\psi_X\rangle. \tag{2}$$

An arbitrary density on $\mathcal{M}$ generates a statistical operator

$$\hat{\rho} = \int_{\mathcal{M}} \rho(x)\hat{\Pi}(x)dx \tag{3}$$

where $\hat{\Pi}(x)$ is the projector on the state $|\psi_x\rangle$ and dx is the appropriate volume element. Expectation of an observable $h(x)$ in an ensemble $\rho(x)$ is given by

$$\langle \rho | h \rangle = \int_{\mathcal{M}} h(x)\rho(x)dx = \mathrm{Tr}[\hat{\rho}\hat{h}]. \tag{4}$$

All densities $\rho(x)$ with the same second moments give the same expectation of the observable $h(x)$, and the same $\hat{\rho}$ via (3), and are therefore equivalent. The Liouville equation maps equivalent densities into equivalent densities, and generates the von Neumann equation of $\hat{\rho}(t) = \int_{\mathcal{M}} \rho(x;t)\hat{\Pi}(x)dx$.

Hamiltonian formulations of a quantum system and of a classical system are combined to give the Hamiltonian formulation of a hybrid system as in [14–17]. Ensembles of such hybrid systems are represented as for any Hamiltonian system by the phase space densities, but the corresponding Liouville equation generates evolution of the quantum degrees of freedom with peculiar properties. This will be further discussed later in the context of the appropriate geometric phases.

3 Liouville Equation as a Hamiltonian System

In general, the triple $(\mathcal{M}, \omega, h)$ consisting of the $2N$ dimensional symplectic manifold $\mathcal{M}$, some symplectic structure ω and the Hamiltonian function $h(x)$ on $\mathcal{M}$ completely specifies the Hamiltonian system, which could correspond to a classical, quantum or hybrid system. Points from $\mathcal{M}$ represent the pure states of the considered system. If the system with the Hamiltonian h is integrable, then there is a preferred choice of the canonical coordinates, the action and the angle coordinates (j_i, θ_i), $i = 1, 2, \ldots, N$, and there exist N geometric phases (called Hannay angles) [2, 3] associated with the evolution of the pure states. If the Hamiltonian system is of the quantum origin, then it is linear and therefore integrable, and the Hannay angles reproduce standard geometric phases associated with an adiabatic unitary evolution of a pure quantum state [15, 16].

A statistical ensemble of Hamiltonian systems is described by a probability density $\rho(x)$ on $\mathcal{M}$. The set of densities has the structure of an infinite-dimensional manifold and is denoted by $\tilde{\mathcal{M}}$. Physically, $\rho \in \tilde{\mathcal{M}}$ may correspond to an ensemble of classical mechanical systems, to a mixed quantum state $\hat{\rho} = \int_{\mathcal{M}} \rho(x)\hat{\Pi}(x)$ or to an ensemble of hybrid systems. From the interpretation of $\rho(x)$ as a probability density follows the evolution equation for $\rho(x;t)$, which is just the linear Liouville equation

$$\partial\rho/\partial t = -\{\rho, h\}_{\mathcal{M}}. \tag{5}$$

The central point of our approach to the general construction of Hannay angles is the fact that the Liouville equation for $\rho(x;t)$ on a finite-dimensional $\mathcal{M}$ can be presented in the form of an appropriate functional Hamiltonian dynamical system [18–20]. The infinite manifold $\tilde{\mathcal{M}}$ admits Poisson structure which, however, is degenerate. Degeneracies correspond to gauge degrees of freedom and the Liouville equation needs to be restricted onto an invariant submanifold of $\tilde{\mathcal{M}}$ which admits a nondegenerate i.e. symplectic structure. The relevant submanifold is determined by the automorphism group of the original system $(\mathcal{M}, \omega, h)$. In the general case this is the group of canonical transformations on $\mathcal{M}$, denoted by $\mathcal{G}$. The Lie algebra g of the infinite Lie group $\mathcal{G}$ consists of the Hamiltonian vector fields on $\mathcal{M}$ and

is isomorphic to the Lie algebra of smooth functions $C^\infty(\mathcal{M})$. The dual of $C^\infty(\mathcal{M})$ is the coadjoint algebra g^* isomorphic with the space of densities $\rho \in \tilde{\mathcal{M}}$. The paring is given by:

$$\langle \rho | h \rangle = \int_{\mathcal{M}} \rho(x) h(x) dx. \tag{6}$$

In order to present the Liouville equation $\dot{\rho} = -\{\rho, H\}_{\mathcal{M}}$ as a Hamiltonian dynamical system, one follows the standard construction of the symplectic structure on a coadjoint orbit $O_\rho = \mathcal{G}/\mathcal{G}_\rho$ of the Lie group $\mathcal{G}$, where $\mathcal{G}_\rho$ is the invariance subgroup of ρ. First, a Poisson structure is defined on $\tilde{\mathcal{M}}$ [20, 21] as

$$\begin{aligned} \big\{H_1(\rho), H_2(\rho)\big\}_{\tilde{\mathcal{M}}} &= \int_{\mathcal{M}} \rho \left\{ \frac{\delta H_1}{\delta \rho}, \frac{\delta H_2}{\delta \rho} \right\}_{\mathcal{M}} dx \\ &= \int_{\mathcal{M}} \rho \{h_1, h_2\}_{\mathcal{M}} dx, \end{aligned} \tag{7}$$

where $H_i(\rho) = \int_{\mathcal{M}} \rho h_i dx$. The Poisson structure (7) on $\tilde{\mathcal{M}}$ is degenerate but its restriction on an orbit of $\mathcal{G}$ in S

$$O_\rho = \{\rho \circ \lambda \,|\, \lambda \in \mathcal{G}\} \tag{8}$$

gives the desired symplectic structure on O_ρ denoted by $\omega(\rho)$. It follows, from an appropriate formulation of Darboux theorem, that O_ρ admits canonically conjugate variables $\rho(x) \to (Q(x), P(x))$ [18]. The manifold $\tilde{\mathcal{M}}$ is a union of disjoint symplectic submanifolds O_ρ.

Remark The order of introducing the Poissonian structure on $\tilde{\mathcal{M}}$ and the symplectic structure on the coadjoint orbit O_ρ can be reversed. In fact, a tangent vector to O_ρ at $\rho \in O_\rho$ has the following form $\{\rho, h\}_{\mathcal{M}}$ for some $h \in g$. The Kirillov, Kostant and Souriau symplectic form [19, 20] on O_ρ is given at ρ by

$$\omega\big(\{\rho, h\}_{\mathcal{M}}, \{\rho, k\}_{\mathcal{M}}\big) = \big\langle \rho | \{h, k\}_{\mathcal{M}} \big\rangle. \tag{9}$$

The Hamiltonian vector fields X_F on O_ρ are given by functionals $F : g^* \to \mathbf{R}$ by the formula

$$X_F(\rho) = \left\{ \rho, \frac{\delta F}{\delta \rho} \right\}_{\mathcal{M}} \tag{10}$$

In this order of definitions, the Poisson bracket on $\tilde{\mathcal{M}}$ is given by

$$\big\{H_1(\rho), H_2(\rho)\big\}_{\tilde{\mathcal{M}}} = \omega(X_{H_1}, X_{H_2}) \tag{11}$$

which, by (9) and (10), coincides with the definition via (7).

The Liouville equation (5) appears as a Hamiltonian system on $\tilde{\mathcal{M}}$ with the corresponding Hamiltonian $H(\rho) = \int_{\mathcal{M}} \rho h dx$ and the Hamiltonian equations

$$\dot{\rho} = \{\rho, H\}_{\tilde{\mathcal{M}}} = \{h, \rho\}_{\mathcal{M}}. \tag{12}$$

In fact, as pointed out, a coadjoint orbit is invariant under such an evolution so that the Liouville equation can be regarded as an integrable Hamiltonian system (O_ρ, ω, H) on each

coadjoint orbit. The Hamiltonian system on the coadjoint orbit $(O_\rho, \omega, H(\rho))$ has no gauge degrees of freedom and all invariant quantities are due to symmetries. The Hamilton equations (12) are linear and therefore integrable.

Remark In what follows we shall have to deal with a Hamiltonian that depends on time-dependent parameters $R(t)$. Furthermore, it will be assumed that the time dependence is periodic $R(t+T) = R(t)$ and adiabatic. The major observation is that any solution $\rho(t)$ of the Hamiltonian system (12), corresponding to the Liouville equation with such periodic time-dependent Hamiltonian, belongs to a single coadjoint orbit.

The functional Hamiltonian dynamical system $(\tilde{\mathcal{M}}, \Omega, H)$, or its restriction on an orbit O_ρ, will be refereed to as the ensemble Hamiltonian system. This Hamiltonian formulation of the Liouville equation on the phase space $\mathcal{M}$ is different from the Hamiltonian formulation for ensembles on a configuration space utilized in [22, 23]. Notice that in the Hamiltonian formulation of the Liouville equation presented here, the abstract Hamiltonian system and the Liouville equation, and also the ensemble Hamiltonian, are of the same form irrespective of the physical origin of the Hamiltonian system $(\mathcal{M}, \Omega, H)$. In the "ensemble on configuration space" approach of [22, 23], the ensemble Hamiltonian corresponding to a classical system differs in form from the one corresponding to a quantum system. Furthermore, only pure quantum states are treated in [22, 23].

4 Hannay Angles for Densities

The Hamiltonian evolution equation (12) for $\rho(x;t)$ is linear. Therefore, the ensemble Hamiltonian system is an integrable Hamiltonian system with an infinite number of degrees of freedom. As an integrable Hamiltonian system the ensemble evolution has the appropriate geometric (Hannay) angles. The geometric angles are introduced via generalization of the standard procedure for the Hannay angles of an integrable system with finite number of degrees of freedom.

The action-angle variables of the integrable system $(O_\rho, \omega, H(\rho))$ are denoted as $(J, \Theta) \equiv \{(J_k(Q,P), \Theta_k(Q,P)),\ k = 1, 2 \dots\}$. The evolution of $\rho(x;t)$ is restricted onto a single one of the infinite number of infinite dimensional invariant Lagrangian submanifolds. If the Hamiltonian h depends on a time-depended multi-parameter $R(t)$ the ensemble Hamiltonian $H(\rho; R(t))$ also depends on $R(t)$. As in the standard definition of the Hannay angles, we shall assume that the time dependence is periodic $R(t+T) = R(t)$ and adiabatic. The generating functional of the time-dependent canonical transformation $S(R(t)) : (Q,P) \to (J,\Theta)$ such that H does not depend on Θ is analogous to the standard treatment of the Hannay angles in the finite mechanical case. The new Hamiltonian is

$$H'(\Theta, J; t) = H\big(Q(\Theta, J; t), P(\Theta, J; t)\big) + \frac{\partial S(Q, J; t)}{\partial t} \tag{13}$$

where $S'(\Theta, J; t) = S(Q, J; t)$ satisfies the chain rule

$$\frac{\partial S'}{\partial t} = \frac{\partial S}{\partial t} + \frac{\delta S}{\delta Q}\frac{\partial Q}{\partial t} = \frac{\partial S}{\partial t} + P\frac{\partial Q}{\partial t}. \tag{14}$$

Integration of the Hamilton's equation $\frac{d\Theta}{dt} = \frac{\delta H'}{\delta J}$ followed by Θ integration over each one of the infinite-dimensional Lagrangian submanifolds parameterized by values of J gives

$$\Delta\Theta_k(\tau) = \frac{\delta}{\delta J_k}\int_0^\tau dt \int D\Theta H\big(Q(\Theta, J), P(\Theta, J); t\big) - \frac{\delta}{\delta J_k}\int_0^\tau dt \int D\Theta P(\Theta, J; t)\frac{\partial}{\partial t}Q(\Theta, J; t) \tag{15}$$

where $D\Theta$ is the normalized measure in the functional angle space. For each k the first term is the dynamical phase $\Delta\Theta_{d,k}$ and the second term is the geometric phase $\Delta\Theta_{g,k}$, acquired by the evolution of ρ. There is an infinite number of geometric phases $\Delta\Theta_{g,k}$. These phases are by construction gauge invariant.

5 Special Cases

5.1 Hannay Angles in the Case of a Pure State

If ρ is a pure state represented by a delta function on $\mathcal{M}$, then O_ρ coincides with $\mathcal{M}$. In this case and for an integrable Hamiltonian system on $\mathcal{M}$, as in the quantum case, the above general procedure gives standard Hannay angles. As is well known [15, 16] these are equivalent to the geometric phases of the corresponding quantum system in a pure state.

5.2 Hannay Angles for a Quantum Mixed State

Consider now the above formalism appropriate for quantum systems, where the preservation of the Riemannian structure of $\mathcal{M}$ introduces the corresponding restrictions on $\mathcal{G}$, g and g^*. The structure isomorphism group $\mathcal{G}_q$ in the quantum case is the finite subgroup of canonical transformations generated by quadratic functions on $\mathcal{M}$. This is isomorphic to the unitary group $U(N)$. The group Lie algebra g_q is the Lie algebra of real quadratic functions identical to the Hermitian operators on $\mathcal{H}^N$. It is a peculiarity of quantum mechanics to consider as representatives of mixed states of a system only those elements of the dual algebra which are given by density matrices $\hat{\rho}$, or equivalently by equivalence classes of densities. The pairing between the algebras is given by $\int_{\mathcal{M}} \rho(x)h(x)dx = \mathrm{Tr}[\hat{\rho}\hat{h}]$ where ρ is any element of the equivalence class $\rho_{\hat{\rho}}$ and $h(x)$ is the quadratic function representing $\hat{h}$. The coadjoint orbit through $\hat{\rho}$ is isomorphic to

$$U(N)/U(k_1)\ldots U(k_m),\ k_1 + k_2 + \cdots + k_m = N, \tag{16}$$

where $k_1, k_2 \ldots k_m$ are dimensions of the eigenspaces of $\hat{\rho}$. The symplectic structure on $O_{\hat{\rho}}$, introduced in Eq. (9), turns $O_{\hat{\rho}}$ into a finite-dimensional symplectic manifold. The dimension of $O_{\hat{\rho}}$ depends on the spectrum of $\hat{\rho}$. The algebra of density matrices is a union of disjoint symplectic manifolds $O_{\hat{\rho}}$. The von Neumann equation for $\hat{\rho}$ restricted onto the symplectic manifold $O_{\hat{\rho}}$ is seen as an integrable Hamilton system with finite number of degrees of freedom. An equivalent construction directly in terms of finite Hilbert spaces and unitary evolution was treated in detail for special types of density matrices in [10]. The orbit $O_{\hat{\rho}}$ is invariant under the evolution with periodic and adiabatic time dependence of the Hamiltonian. The finite number of Hannay angles for this Hamiltonian system on $O_{\hat{\rho}}$ provide an example of geometric phases for the mixed state $\hat{\rho}(t)$. The orbit $O_{\hat{\rho}}$ and the definition of the Hannay angles depend only on $\hat{\rho}$ and not on particular convex mixture representation of $\hat{\rho}$. As in the general case, the geometric phases are gauge invariant by construction.

5.3 Hannay Angles for a Hybrid System

There is no unique generally accepted theory of interaction between micro and macro degrees of freedom, where the former are described by quantum and the later by classical theory. The reason is primarily because each of the suggested theories has some unexpected or controversial features (see [14] for an informative review). Partial selection of hybrid theories can be found in [22, 24–28]. Some of the suggested hybrid theories are mathematically inconsistent, and "no go" type theorems have been formulated [29], suggesting that no consistent hybrid theory can be formulated. Nevertheless, mathematically consistent but inequivalent hybrid theories exist [14, 22, 28]. The Hamiltonian hybrid theory, as formulated and discussed for example in [14–17], has many of the properties commonly expected of a good hybrid theory. In fact, the dynamical formulas of the Hamiltonian theory are equivalent to the well known mean field approximation, the main novelty being that the theory is formulated entirely in the framework of the theory of Hamiltonian dynamical systems.

General procedure for construction of Hannay angles requires construction of the symplectic manifold O_ρ using the group of automorphisms of the relevant structure. Therefore, we need to determine the automorphism group of a hybrid system in the Hamiltonian formulation. To this end we first present a brief recapitulation of the Hamiltonian formulation of hybrid systems dynamics as described in [14, 17].

The phase space of the hybrid system $\mathcal{M}$ is considered as a Cartesian product $\mathcal{M} = \mathcal{M}_c \times \mathcal{M}_q$ of the classical subsystem phase space $\mathcal{M}_c$ with $\dim \mathcal{M}_c = 2N_c$ and of the quantum subsystem phase space $\mathcal{M}_q$ with $\dim \mathcal{M}_q = 2N_q$. Local coordinates on the product are denoted $\{p, q, x, y\}$, where $(p, q) \in \mathcal{M}_c$ are called the classical degrees of freedom (CDF) and $(x, y) \in \mathcal{M}_q$ are called the quantum degrees of freedom (QDF). The evolution equations of the hybrid system are of the Hamiltonian form with the Hamilton's function comprised of three terms

$$H_t(p, q, x, y) = H_c(p, q) + H_q(x, y) + V_{int}(p, q, x, y), \tag{17}$$

where H_c is the Hamilton's function of the classical subsystem, $H_q(x, y)$ is the Hamilton's function of the quantum subsystem and $V_{int}(p, q, x, y) = \langle \psi_{x,y} | \hat{V}_{int}(p, q) | \psi_{x,y} \rangle$, where $\hat{V}_{int}(p, q)$ is an operator in the Hilbert space of the quantum subsystem which depends on the classical coordinates (p, q) and describes the interaction between the subsystems. The Poisson bracket on $\mathcal{M}$ of arbitrary functions of the local coordinates (p, q, x, y) is defined as

$$\{f_1, f_2\}_{\mathcal{M}} = \sum_{i=1}^{k} \left(\frac{\partial f_1}{\partial q_i} \frac{\partial f_2}{\partial p_i} - \frac{\partial f_2}{\partial q_i} \frac{\partial f_1}{\partial p_i} \right) + \frac{1}{\hbar} \sum_j \left(\frac{\partial f_1}{\partial x_j} \frac{\partial f_2}{\partial y_j} - \frac{\partial f_2}{\partial x_j} \frac{\partial f_1}{\partial y_j} \right). \tag{18}$$

Thus, the Hamiltonian form of the hybrid dynamics on $\mathcal{M}$ as the phase space reads

$$\dot{q} = \{q, H_t\}_{\mathcal{M}}, \qquad \dot{p} = \{p, H_t\}_{\mathcal{M}}, \tag{19}$$

$$\dot{x} = \{x, H_t\}_{\mathcal{M}}, \qquad \dot{y} = \{y, H_t\}_{\mathcal{M}}, \tag{20}$$

where H_t is given by (17). The evolution of QDF might be nonlinear due to the nonlinear evolution of CDF and the interaction between the QDF and CDF.

The most general ensemble of hybrid systems is represented by some probability density $\rho(p,q,x,y)$. The densities evolve according to the Liouville equation with a solution $\rho(p,q,x,y;t)$. The density $\rho(p,q,x,y;t)$ for any fixed t generates a unique statistical operator:

$$\hat{\rho}(t) = \int_{\mathcal{M}} \rho(p,q,x,y;t)\hat{\Pi}(x,y)dM. \tag{21}$$

Due to the properties of the Liouville evolution of $\rho(p,q,x,y;t)$ the formula (21) defines a continuous one-parameter family of statistical operators on $\mathcal{H}$.

The dynamical equation for $\hat{\rho}(t)$ [30] is

$$\frac{d\hat{\rho}(t)}{dt} = \frac{1}{i\hbar}\big[\hat{H}_q, \hat{\rho}(t)\big] + \frac{1}{i\hbar}\int_{\mathcal{M}_c}\big[\hat{V}_{int}(p,q), \hat{\rho}(p,q;t)\big]dM_c. \tag{22}$$

The first term generates the unitary part of the evolution and the second term does not preserve the norm of $\hat{\rho}$ and is responsible for non-unitary effects. Nevertheless, the evolution of the density of the total system is Hamiltonian and given by the Liouville equation. Notice that the evolution of $\hat{\rho}(t)$ cannot be expressed only in terms of $\hat{\rho}(t)$, but irreducibly involves the full probability density $\rho(p,q,x,y;t)$. Many hybrid ensembles represented by different $\rho(p,q,x,y;t_0)$ have the QDF in the same mixed state $\hat{\rho}(t_0)$. However, different $\rho(p,q,x,y;t_0)$ that give the same $\hat{\rho}(t_0)$, generate different evolution of $\hat{\rho}(t)$ and thus must be considered as physically different [30].

The evolution equation (22) for $\hat{\rho}(t)$ is reduced to (19) and (20) if the initial $\rho(p,q,x,t;t_0)$ is a pure state in $\mathcal{M}$. If however, the initial density is of the form $\delta(x-x_0)\delta(y-y_0)\rho(q,p)$, the pure state $\hat{\rho}(t_0) = |\psi_{xy}(t_0)\rangle\langle\psi_{xy}(t_0)|$ might evolve according to (22) into a non-pure mixture. This in an important observation for the hybrid description of the quantum measurement process.

The evolution of QDF of a hybrid system is fundamentally different from the linear evolution of a quantum subsystem of a quantum system. The characteristic main features of the QDF evolution are expressed by the nonlinearity of the pure state evolution, or by the dynamically induced differences of $\hat{\rho}(t)$ with different convex mixture representations of the initial $\hat{\rho}(t_0)$. Therefore, the automorphism group of a hybrid system is not $G_c(N_c)\otimes U(N_q)$, but must be taken to be the infinite group of all canonical transformations i.e. $G_c(N_c+N_q)$. Therefore, the Hannay angles for a hybrid system in a general mixed state $\rho(x)$ are given by the formula (15) of the general case. Infinite number of Hannay angles for the QDF can be interpreted as dependence of the QDF geometric phases on the convex mixture representation $\hat{\rho} = \int \rho(x)\hat{\Pi}(x)dx$ i.e. on the full details of the density ρ. In the case of the initial state which is pure in both QDF and CDF, and for an integrable classical subsystem, the situation is reduced to the general pure case, and the corresponding $N_q + N_c$ Hannay angles provide the geometric phases and the Hannay angles of the quantum and the classical subsystems respectively.

6 Summary

Our goal in this paper was to indicate the existence of a general framework for unified treatment of geometric phases in classical, quantum and hybrid system in pure or mixed

states. In the general case the Liouville dynamical equation can be presented in the form of a Hamiltonian dynamical system and this fact enables one to introduce the concepts of geometric phases quite generally. In this way the geometric phases in all these cases could be seen as a consequence of the geometry of Hamiltonian dynamics. However, in this paper we have treated only the very special case of geometric phases, that are generalizations of the Hannay angles of a classical integrable system in a pure state undergoing time periodic and adiabatic evolution. The Hamiltonian formulation of the Liouville equation is applied for the treatment of linear time-periodic and adiabatic Hamiltonian dynamics and the derivation of the corresponding generalized Hannay angles. Hannay angles in the particular cases like quantum, integrable hybrid and integrable classical systems in pure or mixed states can be obtained as special instances of the general procedure. Thus, we have used the general framework to explore only a very special issue, and in this way illustrate our main point. To the best of our knowledge, there has been no discussion of Hannay angles for mixed states in either quantum or classical case, and therefore no direct relation with existing constructions of geometric phases for mixed states in the form of Hannay angles is possible. Unified treatment of geometric phases, and geometric issues, in other types of evolution that have been treated, specially in the context of quantum mechanics, have not been discussed. In particular we did not pursue the relation of the symplectic area of the phase space in the general formulation with the possibility to introduce a single geometric phase. Also, we did not analyze the importance of bundle structures and parallel transport conditions of the general state space for the geometric understanding of generalized geometric phases. These issues will have to be treated within the general framework in order to discuss the cases of single geometric phase introduced in quantum cyclic unitary dynamics of mixed states like in [6] and [10]. The generalized Hamiltonian framework presented here is probably not suited for the treatment of very relevant case of the geometric phase of non-unitary evolution of mixed states [7–9].

Acknowledgements This work was supported by the Ministry of Science and Education of the Republic of Serbia, contracts Nos. 171006, 171017, 171020, 171028 and 171038 and by COST (Action MP1006).

References

1. Anandan, J., Christian, J., Wanelik, K.: Resource letter GPP-1: geometric phases in physics (1997). arXiv:quant-ph/9702011
2. Hannay, J.H.: J. Phys. A, Math. Gen. **18**, 221 (1985)
3. Anandan, J.: Phys. Lett. A **129**, 201 (1988)
4. Uhlmann, A.: Lett. Math. Phys. **21**, 229 (1991)
5. Sjöqvist, E., Pati, A.K., Ekert, A., Anandan, J., Ericsson, M., Oi, D.K.L., Vedral, V.: Phys. Rev. Lett. **85**, 2845 (2000)
6. Singh, K., Tong, D.M., Basu, K., Chen, J.L., Du, J.K.: Phys. Rev. A **67**, 032106 (2003)
7. Carollo, A., Fuentes-Guridi, I., Santos, M.F., Vedral, V.: Phys. Rev. Lett. **90**, 160402 (2003)
8. Bassi, A., Ippoliti, E.: Phys. Rev. A **73**, 062104 (2006)
9. Burić, N., Radonjić, M.: Phys. Rev. A **80**, 014101 (2009)
10. Chaturvedi, S., Ercolessi, E., Marmo, G., Morandi, G., Mukunda, N., Simon, R.: Eur. Phys. J. C **35**, 413 (2004)
11. Heslot, A.: Phys. Rev. D **31**, 1341 (1985)
12. Brody, D.C., Hughston, L.P.: J. Geom. Phys. **38**, 19 (2001)
13. Burić, N.: Ann. Phys. (NY) **233**, 17 (2008)
14. Elze, H.-T.: Phys. Rev. A **85**, 052109 (2012)
15. Wu, B., Liu, J., Niu, Q.: Phys. Rev. Lett. **94**, 140402 (2005)
16. Zhang, Q., Wu, B.: Phys. Rev. Lett. **97**, 190401 (2006)
17. Radonjić, M., Prvanović, S., Burić, N.: Phys. Rev. A **85**, 064101 (2012)

18. Marsden, J.E., Ratiu, T.S.: Introduction to Mechanics and Symmetry. Springer, Berlin (1994)
19. Abraham, R., Marsden, J.: Foundations of Mechanics. Benjamin, New York (1978)
20. Arnold, V.I.: Mathematical Methods of Classical Mechanics. Springer, New York (1978)
21. Berezin, F.A.: Funct. Anal. Appl. **1**, 91 (1967)
22. Hall, M.J.W.: Phys. Rev. A **78**, 042104 (2008)
23. Hall, M.J.W., Reginatto, M.: Phys. Rev. A **72**, 062109 (2005)
24. Sherry, T.N., Sudarshan, E.C.G.: Phys. Rev. D **18**, 4580 (1978)
25. Boucher, W., Traschen, J.: Phys. Rev. D **37**, 3522 (1988)
26. Aleksandrov, I.V.: Z. Naturforsch. **36A**, 902 (1981)
27. Peres, A., Terno, D.R.: Phys. Rev. A **63**, 022101 (2001)
28. Diósi, L., Gisin, N., Strunz, W.T.: Phys. Rev. A **61**, 02108 (2000)
29. Salcedo, L.L.: Phys. Rev. A **85**, 022127 (2012)
30. Burić, N., Mendaš, I., Popović, D.B., Radonjić, M., Prvanović, S.: Phys. Rev. A **86**, 034104 (2012)

Found Phys (2013) 43:1459–1477
DOI 10.1007/s10701-013-9755-z

Hamiltonian Formulation of Statistical Ensembles and Mixed States of Quantum and Hybrid Systems

N. Burić · D.B. Popović · M. Radonjić · S. Prvanović

Received: 8 May 2013 / Accepted: 4 October 2013 / Published online: 1 November 2013

Abstract Representation of quantum states by statistical ensembles on the quantum phase space in the Hamiltonian form of quantum mechanics is analyzed. Various mathematical properties and some physical interpretations of the equivalence classes of ensembles representing a mixed quantum state in the Hamiltonian formulation are examined. In particular, non-uniqueness of the quantum phase space probability density associated with the quantum mixed state, Liouville dynamics of the probability densities and the possibility to represent the reduced states of bipartite systems by marginal distributions are discussed in detail. These considerations are used to study ensembles of hybrid quantum-classical systems. In particular, nonlinear evolution of a single hybrid system in a pure state and unequal evolutions of initially equivalent ensembles are discussed in the context of coupled hybrid systems.

Keywords Statistical ensembles · Hybrid systems

1 Introduction

Schrödinger equation of quantum mechanics (QM) on a Hilbert space $\mathcal{H}$ can be written as a Hamiltonian dynamical system on the corresponding phase space [1–5]. This fact enables elegant treatment of quantum dynamical problems, like for example analysis of quantum dynamics with nonlinear constraints [6, 7] and related issues of classical limit [8, 9]. One hopes that full geometrical formulation of QM analogous to that of classical Hamiltonian systems, besides its usefulness in the dynamical issues and its mathematical elegance, will also provide better intuitive understanding of typically quantum phenomena [4, 5]. Furthermore, the Hamiltonian formulation is specially convenient for the treatment of coupling between

N. Burić (✉) · D.B. Popović · M. Radonjić · S. Prvanović
Institute of Physics, University of Belgrade, Pregrevica 118, 11000 Belgrade, Serbia
e-mail: buric@ipb.ac.rs

classical and quantum systems, called hybrid systems, [10–13], because it provides a unified mathematical framework for both theories. However, the formal similarity between the Hamiltonian formulation of QM and that of classical systems is only partial, and there are differences in some crucial aspects. The purpose of this paper is to analyze the relation of quantum mixed states with the corresponding statistical ensembles of quantum systems in the Hamiltonian formulation, and to utilize such considerations for an analysis of ensembles of hybrid systems.

The fundamental difference between the Hamiltonian formulation of QM and of classical mechanics (CM) is in the classes of phase space functions which are considered as representing dynamical variables in the two theories. In the Hamiltonian formulation of QM only the quadratic functions on the phase space are interpreted as observables. Functions of more general types generate nonlinear evolution of the quantum states. However, non-quadratic functions and nonlinear evolution of the quantum degrees of freedom appear naturally in the theory of hybrid systems. This fact has profound physical significance, and is reflected in the interpretation of the results of the hybrid theory. Another, but related, type of striking differences and incomplete analogies between Hamiltonian formulations of QM and CM are introduced when states more general than pure are considered. Such considerations reveal, from a new perspective, some well known deep features of quantum mixtures, represented by density operators $\hat{\rho}$, but also point out to some less known differences between quantum and classical ensembles represented by density functions ρ on the quantum phase space. Consequences of these differences in the Hamiltonian formulation of hybrid systems is the main topic of this paper. Thus, our main motivation for the discussion of differences between quantum mixed states and general statistical ensembles in the Hamiltonian formulation of QM, given in Sect. 3, is to better understand the behavior of ensembles of hybrid systems, presented in Sect. 4. In particular, we analyze, in Sect. 3.1, relations between classes of equivalent discrete convex combinations of pure quantum states on one side, and classes of equivalent statistical ensembles in the Hamiltonian formulation of QM on the other side. The well known result of Hughston, Josza and Wooters [14], about the relation between different finite convex representations of a mixed state is generalized to Hamiltonian ensembles represented by general densities. Typical representatives of the equivalence classes of densities representing the same mixed state, such as Gaussian densities, are discussed. Correct interpretation of the phase space function $\langle\psi|\hat{\rho}|\psi\rangle$, where $\hat{\rho}$ is a density matrix, versus a density ρ corresponding to that density matrix $\hat{\rho}$ is stressed. In Sect. 3.2 we briefly describe the formulation of Liouville equation as a Hamiltonian dynamical system. We then analyze, in Sect. 3.3, the relation between the statistical operator obtained by tracing out a subsystem of a quantum system in a pure state on one side, and the statistical ensembles given by marginal distributions in the Hamiltonian formulation on the other side. These considerations are important for proper interpretation of some recently obtained results in the Hamiltonian formulation of hybrid systems [10, 13], which we discuss in Sect. 4.

2 Hamiltonian Formulation

Quantum and classical mechanics might be formulated using the same mathematical framework. Relevant references for the CM case are [15, 16] and for the QM case are [1–5]. This fact suggests to formulate the hybrid theory using the same mathematical framework of Hamiltonian dynamical systems. All three theories will be considered here as dynamical systems $(\mathcal{M}, \omega, g, H)$ on a differentiable manifold $\mathcal{M}$ with a symplectic and Riemannian structures ω and g respectively, with some preferred function, the Hamiltonian, H. The manifold is also assumed to posses a complex structure $J^2 = -I$ such that: $g(x, y) = \omega(x, Jy)$. All problems that we would like to discuss appear already in quantum systems with finite-dimensional Hilbert space, implying a finite-dimensional manifold $\mathcal{M}$. Therefore we shall assume that $\mathcal{M}$ is finite-dimensional.

Formulation of the classical mechanics of isolated conservative systems using $(\mathcal{M}, \omega, H)$ is standard [15, 16]. The formulation of quantum mechanics in terms of $(\mathcal{M}, \omega, g, H)$ is perhaps less well known, but shall not be presented here in any detail since there exist excellent reviews [4, 5]. Very briefly, the basic observation beyond the Hamiltonian formulation of quantum mechanics is that the evolution of a pure quantum state in a Hilbert space $\mathcal{H}$, as given by the Schrödinger equation, can be equivalently described by a Hamiltonian dynamical system on an Euclidean manifold $\mathcal{M}$. The manifold is just the Hilbert space considered as a real manifold, with the symplectic and Riemannian structures given by the real and the imaginary parts of the Hilbert scalar product. Representing a normalized vector $|\psi\rangle \in \mathcal{H}$ in a basis, one can introduce the canonical coordinates $x_j = (c_j^* + c_j)/\sqrt{2}$, $y_j = i(c_j^* - c_j)/\sqrt{2}$, $j = 1, 2 \ldots N$. Generic point from $\mathcal{M}$ will also be denoted by X or X^a, where $a = 1, 2 \ldots 2N$ is an abstract index. The dimension of the quantum phase space is $2N$ where N is the complex dimension of the system's Hilbert space. It should be stressed, perhaps, that the canonical coordinates x_j, y_j have nothing to do with the canonical coordinates of the classical system that after quantization gives the considered quantum system with the Hilbert space $\mathcal{H}$. The Hamilton's function $H(X)$ is given by the quantum expectation of the Hamiltonian $\hat{H}$ in the state $|\psi_X\rangle \leftrightarrow X$: $H(X) = \langle\psi_X|\hat{H}|\psi_X\rangle$. The Schrödinger dynamical law is that of Hamiltonian mechanics

$$\dot{X}^a = \omega^{ab}\nabla_b H. \tag{1}$$

In the Hilbert space QM and in the Hamiltonian classical mechanics the dynamical variables can be introduced formally as generators of the isomorphisms of the respective relevant structures. In QM these are self-adjoined operators generating unitary transformations that preserve the Hilbert scalar product. In the Hamiltonian formulation of QM the Hilbert scalar product generates the symplectic and Riemannian structure. The symplectic structure is preserved by Hamiltonian vector fields of arbitrary smooth functions, but the metric is preserved only by the Killing vector fields, i.e., by the Hamiltonian vector fields generated by quadratic functions of the canonical variables. In the Hamiltonian formulation of classical systems, the metric of the phase space has no physical relevance and thus all smooth functions generate isomorphic i.e., canonical transformations, and are interpreted as dynamical variables. In the Hamiltonian formulation of QM, only the quadratic functions generate

the automorphisms, and only such functions are related to dynamical variables or observables. In fact, all observables are represented by quadratic functions $A(X)$ on $\mathcal{M}$ and are the quantum mechanical expectations of the corresponding quantum observables $A(X) = \langle\psi_X|\hat{A}|\psi_X\rangle$. In particular, the canonical coordinates of the quantum phase space do not have physical interpretation. It is important to observe that the Poisson bracket between two quadratic functions is also a quadratic function and satisfies

$$\{A_1(X), A_2(X)\} = \frac{1}{i\hbar}\langle\psi_X|[\hat{A}_1, \hat{A}_2]|\psi_X\rangle. \tag{2}$$

If one considers the Hilbert space vectors of arbitrary norm, then two vectors $|\psi_1\rangle$ and $|\psi_2\rangle$ from $\mathcal{H}$ are representing the same physical pure state if there is a complex scalar $a \neq 0$ such that $|\psi_2\rangle = a|\psi_1\rangle$. The set of equivalence classes defines the complex projective space $\mathbb{C}P^{N-1} \equiv (\mathbb{C}^N - \{0\})/\sim$. The pure state space $\mathbb{C}P^{N-1}$ is isomorphic with the real manifold S^{2N-1}/S^1 which has compatible complex, Riemannian and symplectic structures. These structures are used to formulate geometric Hamiltonian framework of QM based on the pure state space $\mathbb{C}P^{N-1}$. Almost all formulas that we shall present for the Hamiltonian formulation based on $\mathcal{H}$ are of the same form in the formulation based on $\mathbb{C}P^{N-1}$, with the corresponding understanding of the symbols representing the phase space $\mathcal{M}$, the symplectic structure ω and the Riemannian metric g, and renormalization of the functions representing observables, i.e., $A(X) = \langle\psi_X|\hat{A}|\psi_X\rangle/\|\psi_X\|^2$. In particular, the transition probability $|\langle\psi_1|\psi_2\rangle|^2/(\|\psi_1\|\|\psi_2\|)^2$ is expressed as $\cos^2\theta(X_1, X_2)$ of the geodesic distance $\theta(X_1, X_2)$ between the points $X_1, X_2 \in \mathbb{C}P^{N-1}$. Also the eigenstates ψ_a of an observable $\hat{A}$ are represented by the critical points of the Hamiltonian vector field generated by $A(X)$. In the discussion that follows we shall not need to distinguish explicitly between the formulations based on $\mathcal{H}$ and the one based on $\mathbb{C}P^{N-1}$. Rare cases when a statement is applicable only in one of the formulations, with the non-trivial transcription, will be clearly stated.

The Hamiltonian formulation of QM suggests natural formal generalizations [4]. The most obvious one is to consider a theory where the evolution can be generated by functions which are not quadratic [4, 17, 18]. This would correspond to a nonlinear Schrödinger evolution equation. We shall see that such generalizations are dictated quite naturally in the Hamiltonian framework for a theory of hybrid systems. It has been argued, using particular generalization of the nonlinear evolution with all other aspects of QM unaltered, that such nonlinear evolution would enable superluminal communication between distant systems [19, 20], or violate the second law of thermodynamics [21]. However, other aspects of QM could be altered appropriately, and conveniently using the Hamiltonian framework, as is required in a consistent theory of hybrid systems [10, 12, 13], so that such objections do not apply. These issues will be analyzed after a discussion of ensembles of quantum systems and composite quantum systems in the Hamiltonian framework.

3 Hamiltonian Ensembles and Quantum Mixtures

3.1 Statistical Ensembles of Quantum Systems

Ensembles of quantum Hamiltonian systems are in general described by probability distributions $\rho(X)$ on the phase space $\mathcal{M}$. Average value of a quantum observable $A(X)$ over an ensemble $\rho(X)$ is given by

$$\bar{A} = \int_{\mathcal{M}} \rho(X) A(X) dM, \tag{3}$$

where dM represents the appropriate volume element on $\mathcal{M}$. This expression can be interpreted as unconditional expectation of the conditional expectation of $\hat{A}$ in pure states $|\psi_X\rangle$, the later being distributed according to the probability distribution $\rho(X)$. For a function $A(X) = \langle\psi_X|\hat{A}|\psi_X\rangle/\|\psi_X\|^2$, representing an observable, one has

$$\int_{\mathcal{M}} \rho(X) A(X) dM = \mathrm{Tr}(\hat{\rho}\hat{A}), \tag{4}$$

where the quantum mixed state $\hat{\rho}$ associated with the probability distribution $\rho(X)$ is given by

$$\hat{\rho} = \int_{\mathcal{M}} \rho(X) \hat{\Pi}(X) dM, \tag{5}$$

with $\hat{\Pi}(X) = |\psi_X\rangle\langle\psi_X|/\|\psi_X\|^2$ being the projector corresponding to the pure state represented by the point X. In general, the state vectors $|\psi_X\rangle$ can have arbitrary norm.

Special cases of the above formula are provided by densities with the support on a finite set of points from $\mathcal{M}$, giving finite convex combinations of atomic measures

$$\hat{\rho} = \sum_{i=1}^{M} \rho(X_i) \hat{\Pi}(X_i), \tag{6}$$

where $M \geq \mathrm{Rank}(\hat{\rho})$. Incidentally, this special case of (5) is the most often discussed in the standard Hilbert space QM.

The densities $\rho(X)$ satisfy Liouville equation on $\mathcal{M}$

$$\frac{\partial}{\partial t}\rho(X;t) = \big\{H(X), \rho(X;t)\big\}_{\mathcal{M}}, \tag{7}$$

which differs in sign from the evolution equation of functions on $\mathcal{M}$ representing observables.

One observes that all probability densities with the same second moments give the same values for the expectations (4) of quadratic functions, i.e., quantum observables. Consequently all such densities generate the same statistical operator $\hat{\rho}$ via (5). Furthermore, Liouville evolution of all the densities $\rho(X;t_0)$, yielding the same $\hat{\rho}(t_0)$, generates the same von Neumann evolution $\hat{\rho}(t)$. Indeed, the evolution equation satisfied by $\hat{\rho}(t)$, related by (5) to a solution $\rho(X;t)$ of the Liouville equation, is the von-Neumann equation $i\hbar\,\partial\hat{\rho}/\partial t = -[\hat{\rho}, \hat{H}]$. This fact is easily obtained

from the definition (5) and Eq. (7) by using partial integration. Therefore, a quantum mechanical (mixed) state, described by $\hat{\rho}$, is identified with the equivalence class $\{\rho\}_{\hat{\rho}}$ of densities with the same second moments and generating the same $\hat{\rho}$ via (5). Equivalence of densities with the same second moments is seen as a generalization of standard quantum mechanical statement about the non-uniqueness of the convex decomposition of a statistical operator $\hat{\rho}$.

The most known physical consequence of the equivalence $\{\rho\}_{\hat{\rho}}$ is no-signaling by distant steering (see for example [19] and the references therein). We shall discuss some related issues later in the context of hybrid quantum-classical systems.

A pure state $\hat{\rho}_0 = |\psi_{X_0}\rangle\langle\psi_{X_0}|$, where $X_0 \in S^{2N-1}/S^1$, is uniquely represented by the corresponding delta function $\delta(X - X_0)$ on S^{2N-1}/S^1. The equivalence class $\{\rho\}_{\hat{\rho}_0}$ indeed contains a single element, i.e., $\delta(X - X_0)$, as can be seen by the following reasoning. Let $\rho_0(X)$ belong to $\{\rho\}_{\hat{\rho}_0}$, i.e.,

$$\hat{\rho}_0 = \int_{\mathcal{M}} \rho_0(X)\hat{\Pi}(X)dM. \tag{8}$$

Choose an arbitrary state $|\psi^{\perp}\rangle$ orthogonal to the state $|\psi_{X_0}\rangle$. Now, one has

$$0 = \langle\psi^{\perp}|\hat{\rho}_0|\psi^{\perp}\rangle = \int_{\mathcal{M}} \rho_0(X)\big|\langle\psi_X \mid \psi^{\perp}\rangle\big|^2 dM. \tag{9}$$

This means that $\rho_0(X)$ is nonzero only when $\langle\psi_X|\psi^{\perp}\rangle = 0$. Because of the arbitrariness of $|\psi^{\perp}\rangle$, the density $\rho_0(X)$ is nonzero only at $X = X_0$ leading to $\rho_0(X) = \delta(X - X_0)$. Thus, a pure state is uniquely represented by single δ-density, i.e., by a single trivial convex combination on S^{2N-1}/S^1.

Each equivalence class $\{\rho\}_{\hat{\rho}}$ of densities over $\mathcal{M} = \mathbb{R}^{2N}$ based on the Hilbert space $\mathcal{H}$, corresponding to a mixed state $\hat{\rho}$, contains a distribution of a unique form and with fixed normalized second moments. Indeed, consider a statistical operator $\hat{\rho}$ which matrix elements in the abstract (arbitrary) basis satisfy

$$\begin{aligned} \mathrm{Re}(\hat{\rho}_{ij}) &= \int_{\mathcal{M}} \rho(X)\frac{x_i x_j + y_i y_j}{\|X\|^2}dM, \\ \mathrm{Im}(\hat{\rho}_{ij}) &= \int_{\mathcal{M}} \rho(X)\frac{y_i x_j - x_i y_j}{\|X\|^2}dM, \end{aligned} \tag{10}$$

where (x_i, y_i) $(i, j = 1, 2 \ldots N)$ i.e., X^a $(a = 1, 2 \ldots 2N)$ are the components of the Hilbert space vector in the same abstract basis, while $\|X\|^2 = 2\|\psi_X\|^2$ holds. All densities from the equivalence class $\{\rho\}_{\hat{\rho}}$ give the same $\hat{\rho}_{ij}$ by definition. The form of $\hat{\rho}_{ij}$ implies that the expectation of any normalized quadratic function $A_{ab}X^aX^b/\|X\|^2$ $(a, b = 1, 2 \ldots 2N)$ on $\mathcal{M} = \mathbb{R}^{2N}$ is computable once one finds the normalized covariance matrix of the density ρ

$$\sigma_{\rho}^{ab} = \int_{\mathcal{M}} \rho(X)\frac{X^aX^b}{\|X\|^2}dM \equiv \sigma_{\hat{\rho}}^{ab}, \tag{11}$$

which is the same for any density from the equivalence class $\{\rho\}_{\hat{\rho}}$, and is thus equivalently denoted by $\sigma_{\hat{\rho}}^{ab}$. Next we observe that the following distribution, fixed by (11),

over $\mathcal{M} = \mathbb{R}^{2N}$

$$\tilde{\rho}(X) = \frac{\|X\|^2}{(2\pi)^N (\det \sigma_{\hat{\rho}})^{1/2}} \exp\left[-\frac{1}{2}\left(\sigma_{\hat{\rho}}^{-1}\right)_{ab} X^a X^b\right], \tag{12}$$

is a member of the equivalence class $\{\rho\}_{\hat{\rho}}$ because it reproduces the matrix elements (10). Therefore, the only distributions on $\mathcal{M} = \mathbb{R}^{2N}$ that are needed to represent all possible mixed quantum states are of the form (12).

Each equivalence class corresponding to a mixed state could also be represented by other types of distributions. In fact, the distribution given by finite discrete convex combination of delta functions

$$\rho(X) = \sum_{i=1}^{N} \rho_i \delta(X - X_i), \tag{13}$$

where ρ_i are the eigenvalues and X_i correspond to the eigenvectors of the density matrix $\hat{\rho}$, also satisfies (5).

Assume now that the state vectors are normalized, as is customary in the Hamiltonian form of QM. One should be careful with the interpretation of distributions $\rho(X)$ satisfying (5), the function $\langle \psi_X | \hat{\rho} | \psi_X \rangle$ and the quantum mechanical expression $|\langle \psi | \psi' \rangle|^2$. A statistical operator $\hat{\rho}$ is Hermitian and therefore can be formally considered as an observable. The later are represented by the general rule as $\langle \psi_X | \hat{\rho} | \psi_X \rangle$, which we shall denote by $\langle \hat{\rho} \rangle(X)$ in order to distinguish it from the function $\rho(X)$ defined as to satisfy (5). The relation between the two functions is given by

$$\langle \hat{\rho} \rangle(X) = \int_{\mathcal{M}} \rho\left(X'\right) |\langle \psi_{X'} | \psi_X \rangle|^2 dM'. \tag{14}$$

In case of the pure state ensemble $|\psi_{X_0}\rangle\langle\psi_{X_0}|$ uniquely represented by the density $\delta(X - X_0)$, the function $\langle \hat{\rho} \rangle(X)$ is everywhere nonzero except at X corresponding to vectors orthogonal to $|\psi_{X_0}\rangle$. Note that the function $\langle \hat{\rho} \rangle(X)$ cannot be considered as a density on $\mathcal{M}$, representing the quantum ensemble $\hat{\rho}$, because when substituted in (5) it does not give the correct result (4), $\mathrm{Tr}(\hat{\rho}\hat{A})$. In the case $\mathcal{M} = \mathbb{C}P^{N-1}$, the substitution gives [22]

$$\int_{\mathcal{M}} \langle \hat{\rho} \rangle(X) A(X) dM = \frac{V_N}{N(N+1)} \left(\mathrm{Tr}(\hat{\rho}\hat{A}) + \mathrm{Tr}(\hat{A})\right), \tag{15}$$

where V_N is the volume of $\mathbb{C}P^{N-1}$. However, modified function $P(X) = (\langle \hat{\rho} \rangle(X) - 1/(N+1))N(N+1)/V_N$, gives the correct averages [22]. Nevertheless, $P(X)$ is not non-negative for all X even though $\langle \hat{\rho} \rangle(X)$ is. Therefore, $P(X)$ can be used to compute the quantum expectation $\mathrm{Tr}(\hat{\rho}\hat{A})$, but it cannot be considered as a probability density on $\mathbb{C}P^{N-1}$.

Fallacy of the interpretation of the function $\langle \hat{\rho} \rangle(X)$ as a probability distribution for given $\hat{\rho}$ is best seen in the case of a pure state $\hat{\rho}$. Let us be permitted to stress the basic postulate of quantum mechanics concerning the interpretation of the expression $|\langle \psi | \psi' \rangle|^2$. This gives a probability that a system prepared in the state $|\psi\rangle$ with certainty, will transform during measurement of an observable with an eigenvector $|\psi'\rangle$

precisely into the state $|\psi'\rangle$. It is a probability distribution over the eigenbasis of the measured observable and is not a probability distribution over the space of all pure states. Therefore a pure state $|\psi_{X_0}\rangle$ is not represented by function $|\langle\psi_X|\psi_{X_0}\rangle|^2$, but by the probability distribution $\delta(X - X_0)$. Similarly the ensemble $\hat{\rho}$ is represented by some $\rho(X)$ satisfying (5) and not by $\langle\hat{\rho}\rangle(X)$ or $P(X)$.

For further comparison with the Hilbert space formulation one should observe that the set of combinations of delta functions centered at discrete set of points is dense in the space of functionals on the space of continuous functions on $\mathcal{M}$. In other words, any density $\rho(X)$ can be arbitrary well approximated by a finite discrete convex combination of δ-functions

$$\rho(X) = \int_{\mathcal{M}} \rho\big(X'\big)\delta\big(X - X'\big)dM' \approxeq \sum_i \rho_{X_i}\,\delta(X - X_i). \tag{16}$$

Approximation of $\rho(X)$ by finite discrete convex combination of delta functions corresponds to a well known ensemble decomposition $\{\rho_{X_i}, |\psi_{X_i}\rangle\}$ of a density matrix in terms of finite convex combination of pure state projectors. We will call such density *discrete*. $\rho(X)$ and $\rho'(X)$ from the same equivalence class $\{\rho\}_{\hat{\rho}}$ correspond to equivalent ensemble decompositions $\{\rho_{X_i}, |\psi_{X_i}\rangle\}$ and $\{\rho'_{X'_i}, |\psi_{X'_i}\rangle\}$ of the density matrix $\hat{\rho}$. They are related by the Hughston-Jozsa-Wooters formula [14]

$$(\rho_{X_i})^{1/2}|\psi_{X_i}\rangle = \sum_j u_{ij}\left(\rho'_{X'_j}\right)^{1/2}|\psi_{X'_j}\rangle, \tag{17}$$

where $[u_{ij}]$ is unitary matrix of appropriate (not necessary equal) dimensions.

The preceding analysis implies the following generalization of (17) to the case of arbitrary equivalent continuous densities $\rho(X)$ and $\rho'(X)$ from the same equivalence class $\{\rho\}_{\hat{\rho}}$

$$\big(\rho(X)\big)^{1/2}|\psi_X\rangle = \int_{\mathcal{M}} u\big(X|X'\big)\left(\rho'\big(X'\big)\right)^{1/2}|\psi_{X'}\rangle dM', \tag{18}$$

where $u(X|X')$ is a complex integral kernel satisfying

$$\int_{\mathcal{M}} u\big(X|X'\big)\,u^*\big(X|X''\big)\,dM = \delta\big(X' - X''\big), \tag{19}$$

and * denotes complex conjugation.

3.2 Hamiltonian Dynamics of Densities

Since this paper is about applications of the theory of Hamiltonian dynamical systems in QM and in hybrid theories, let us mention in passing that von-Neumann and Liouville equations themselves can be presented in the form of appropriate Hamiltonian dynamical systems [16]. Considerations of these issues reveal from another perspective the importance and the consequences of the QM restriction on the class of functions generating the structure isomorphisms.

The Lie algebra g of the infinite Lie group $\mathcal{G}$ of canonical transformations on some finite dimensional symplectic phase space $\mathcal{M}$ consists of the Hamiltonian vector fields on $\mathcal{M}$, and is isomorphic with the Lie algebra of smooth functions $C^\infty(\mathcal{M})$. The dual of $C^\infty(\mathcal{M})$ is the coadjoint algebra g^* isomorphic with the space of densities $\rho \in S(\mathcal{M})$. The paring is given by $\int_{\mathcal{M}} \rho(X)H(X)dM$. In order to present the Liouville equation $\dot{\rho} = -\{\rho, H\}_{\mathcal{M}}$ as a Hamiltonian dynamical system one follows the standard construction of the symplectic structure on a coadjoint orbit O_ρ of the Lie group $\mathcal{G}$ [16]. First, a Poisson structure is defined on S as

$$\{\mathcal{H}_1(\rho), \mathcal{H}_2(\rho)\}_S = \int_{\mathcal{M}} \rho \left\{ \frac{\delta \mathcal{H}_1}{\delta \rho}, \frac{\delta \mathcal{H}_2}{\delta \rho} \right\}_{\mathcal{M}} dM = \int_{\mathcal{M}} \rho \{H_1, H_2\}_{\mathcal{M}} dM, \tag{20}$$

where $\mathcal{H}_i(\rho) = \int_{\mathcal{M}} \rho H_i dM$. Hamiltonian vector fields on S are given by $X_{\mathcal{H}}(\rho) = -\{\rho, \frac{\delta \mathcal{H}}{\delta \rho}\}_S$. The Poisson structure (20) on S is degenerate, but its restriction on an orbit of $\mathcal{G}$ in S

$$O_\rho = \{\rho \circ \lambda \,|\, \lambda \in \mathcal{G}\} \tag{21}$$

gives the desired symplectic structure on O_ρ.

The Liouville equation appears as a Hamiltonian system on O_ρ with the corresponding Hamiltonian $\mathcal{H}(\rho) = \int_{\mathcal{M}} \rho H dM$ and the Hamiltonian equations

$$\dot{\rho} = -\{\rho, \mathcal{H}\}_{O_\rho} = \{H, \rho\}_{\mathcal{M}}. \tag{22}$$

The Hamiltonian system (22) is linear and therefore integrable.

Consider now the above formalism appropriate for QM, where the preservation of the Riemannian structure of $\mathcal{M}$ introduces the corresponding restrictions on $\mathcal{G}$, g and g^*. The structure isomorphism group $\mathcal{G}_q$ is the finite subgroup of canonical transformations generated by quadratic functions on $\mathcal{M}$. This is isomorphic to the unitary group $U(N)$. The group Lie algebra g_q is the Lie algebra of quadratic functions, and the coadjoint algebra g_q^* is formed by the equivalence classes $\rho_{\hat{\rho}}$. The coadjoint orbit through $\hat{\rho}$ is isomorphic with finite-dimensional manifold

$$U(N)/U(k_1) \otimes U(k_2) \otimes \cdots \otimes U(k_m),\ k_1 + k_2 + \cdots + k_m = N, \tag{23}$$

where $k_1, k_2, \ldots, k_m$ are dimensions of the eigenspaces of $\hat{\rho}$. The orbit $O_{\hat{\rho}}$, given by (23), is a finite-dimensional symplectic manifold, whose dimension depends on the spectrum of $\hat{\rho}$. The symplectic structure on $O_{\hat{\rho}}$ may be introduced as in the general case, and the von Neumann equation for $\hat{\rho}$ is seen as the Hamilton dynamical equation (22).

3.3 Mixtures as States of Subsystems

Consider a quantum system composed of two subsystems, with Hilbert spaces $\mathcal{H}_1$ and $\mathcal{H}_2$ of the components and $\mathcal{H}_{12} = \mathcal{H}_1 \otimes \mathcal{H}_2$ of the total system. Partial trace $\mathrm{Tr}_2(\hat{\rho})$ of a pure $\hat{\rho} = |\psi_{12}\rangle\langle\psi_{12}|$ over the space $\mathcal{H}_2$ gives a density operator $\hat{\rho}_1$ on $\mathcal{H}_1$. The operator $\hat{\rho}_1$ is a projector corresponding to a pure state $|\psi_1\rangle \in \mathcal{H}_1$ if an only if the pure state of the total system $\hat{\rho} = |\psi_{12}\rangle\langle\psi_{12}|$ is separable, i.e., of the form $|\psi_1\rangle \otimes |\psi_2\rangle$ for

some $|\psi_1\rangle \in \mathcal{H}_1$ and $|\psi_2\rangle \in \mathcal{H}_2$. In this case $\hat{\rho}_1 = |\psi_1\rangle\langle\psi_1|$ does not depend on the particular $|\psi_2\rangle$ in $|\psi_{12}\rangle\langle\psi_{12}|$. In the case of a more general non-entangled state, i.e., for a convex mixture of separable states of the form $\hat{\rho} = \sum_i p_i \hat{\rho}_1^i \otimes \hat{\rho}_2^i$, the partial trace $\mathrm{Tr}_2(\hat{\rho})$ gives a convex mixture of the first subsystem states $\hat{\rho}_1^i$ with the same coefficients p_i.

We now consider statistical ensembles in the Hamiltonian formulation of composite systems. The phase space $\mathcal{M}_{12}$ of a bipartite quantum system with the Hilbert space $\mathcal{H}_{12}$ is constructed directly from $\mathcal{H}_{12}$ (or $P\mathcal{H}_{12}$) without any reference to the components $\mathcal{H}_1$ and $\mathcal{H}_2$ with the corresponding phase spaces $\mathcal{M}_1$ and $\mathcal{M}_2$. Of course, the dimensionality of $\mathcal{M}_{12}$ is much larger than that of $\mathcal{M}_1 \times \mathcal{M}_2$. In fact, $\mathcal{M}_1 \times \mathcal{M}_2$ is an embedded submanifold of $\mathcal{M}_{12}$. In the case $\mathcal{M}_1 = \mathbb{C}P^{N-1}$, $\mathcal{M}_2 = \mathbb{C}P^{M-1}$ and $\mathcal{M}_{12} = \mathbb{C}P^{MN-1}$ the embedding $\mathbb{C}P^{N-1} \times \mathbb{C}P^{M-1} \to \mathbb{C}P^{MN-1}$ is known as Segre embedding [5, 23]. We shall denoted the coordinates $\{X^a\}$ adapted to the Segre embedding by (X_1, X_2, X_3) where X_1 and X_2 are the sets of coordinates on $\mathcal{M}_1 \times \mathcal{M}_2$. The set of coordinates denoted by X_3 assume zero values iff the state is separable.

A statistical ensemble of bipartite systems is described by a probability density $\rho(X) \in S(\mathcal{M}_{12})$. A density on $\mathcal{M}_{12}$ gives a statistical operator on $\mathcal{H}_{12}$ according to the general prescription:

$$\hat{\rho}_{12} = \int_{\mathcal{M}_{12}} \rho_{12}(X_{12})\, \hat{\Pi}(X_{12})\, dM_{12}. \tag{24}$$

Mixed state $\hat{\rho}_{12}$ is separable if there exists a convex mixture representation (24) of $\hat{\rho}_{12}$ in terms of separable pure states. If each of the equivalent convex representations contains at least one entangled pure state then $\hat{\rho}_{12}$ is entangled. Therefore, it makes sense to call a density ρ_{12} separable if $\rho_{12}(X_1, X_2, X_3)$ is zero when $X_3 \neq 0$, that is when it's support is contained in $\mathcal{M}_1 \times \mathcal{M}_2$. Such densities will be denoted by $\rho(X_1, X_2)$. If any of the densities in the equivalence class $\{\rho_{12}\}_{\hat{\rho}_{12}}$ is separable then $\hat{\rho}_{12}$ is by definition separable. On the other hand, if $\hat{\rho}_{12}$ is entangled then none of the densities in the equivalence class $\{\rho_{12}\}_{\hat{\rho}_{12}}$ is separable, and each must have an entangled state in its support. However, notice that some of the densities from a single equivalence class, corresponding to a separable mixed state $\hat{\rho}_{12}$, might be separable and some might not. In one word, it is misleading to talk about entangled densities, but the notion of a separable density is perfectly consistent with the standard terminology.

Let us demonstrate the standard relations between the state of a compound system and the state of the first subsystem using the representation (24). We perform a partial trace over the second subsystem

$$\hat{\rho}_1 = \mathrm{Tr}_2(\hat{\rho}_{12}) = \int_{\mathcal{M}_{12}} \rho_{12}(X_{12}) \mathrm{Tr}_2\big(\hat{\Pi}(X_{12})\big) dM_{12}. \tag{25}$$

Let $\mathcal{D}_1$ denotes the manifold of the density matrices $\hat{\sigma}_1$ of the first subsystem and let $\delta_\sigma^{(1)}$ and $dM_\sigma^{(1)}$ be delta function and Lebesgue measure on $\mathcal{D}_1$. By inserting the

identity[1]

$$\int_{\mathcal{D}_1} \delta_\sigma^{(1)}\big(\hat{\sigma}_1 - \mathrm{Tr}_2\big(\hat{\Pi}(X_{12})\big)\big) dM_\sigma^{(1)} = 1, \tag{26}$$

into (25) we express $\hat{\rho}_1$ as a convex combination of density matrices of the first subsystem

$$\hat{\rho}_1 = \int_{\mathcal{D}_1} \rho_1(\hat{\sigma}_1)\hat{\sigma}_1 dM_\sigma^{(1)}, \tag{27}$$

where the distribution ρ_1 over $\mathcal{D}_1$ is normalized to unity and obeys

$$\rho_1(\hat{\sigma}_1) = \int_{\mathcal{M}_{12}} \rho_{12}(X_{12})\delta_\sigma^{(1)}\big(\hat{\sigma}_1 - \mathrm{Tr}_2\big(\hat{\Pi}(X_{12})\big)\big) dM_{12}. \tag{28}$$

In the case of a pure state $\hat{\rho}_{12} = \hat{\Pi}(\bar{X}_{12})$ which is represented by the delta density $\rho_{12}(X_{12}) = \delta(X_{12} - \bar{X}_{12})$, one obtains

$$\rho_1(\hat{\sigma}_1) = \delta_\sigma^{(1)}\big(\hat{\sigma}_1 - \mathrm{Tr}_2(\hat{\rho}_{12})\big), \tag{29}$$

which is expected.

The result (28) can be further analyzed. Let $\hat{\Pi}(X_{12}) = |\psi_{X_{12}}\rangle\langle\psi_{X_{12}}|$ in terms of normalized state vectors. Using the Schmidt decomposition $|\psi_{X_{12}}\rangle = \sum_{i=1}^{R_{12}} \sqrt{p_i}\,|\phi_i^{(1)}\rangle \otimes |\chi_i^{(2)}\rangle$, with $p_i > 0$, one obtains mixed state $\mathrm{Tr}_2(\hat{\Pi}(X_{12})) = \sum_{i=1}^{R_{12}} p_i |\phi_i^{(1)}\rangle\langle\phi_i^{(1)}|$, where $R_{12} = \mathrm{Rank}(\mathrm{Tr}_2(\hat{\Pi}(X_{12})))$. Any other state $|\psi_{X_{12}^\lambda}\rangle$ such that $\mathrm{Tr}_2(\hat{\Pi}(X_{12}^\lambda)) = \mathrm{Tr}_2(\hat{\Pi}(X_{12}))$ has the form $|\psi_{X_{12}^\lambda}\rangle = \sum_{i=1}^{R_{12}} \sqrt{p_i}\,|\phi_i^{(1)}\rangle \otimes |\chi_{i,\lambda}^{(2)}\rangle$, and can be obtained as a result of unitary transformation acting non-trivially on the second subsystem $|\psi_{X_{12}^\lambda}\rangle = \hat{U}_\lambda |\psi_{X_{12}}\rangle$. Such transformation induces the corresponding action $X_{12}^\lambda = U_\lambda X_{12}$ on $\mathcal{M}_{12}$ and yields the following equivalent form of (28)

$$\rho_1(\hat{\sigma}_1) = \int_{\Lambda(\hat{\sigma}_1)} \rho_{12}(U_\lambda \widetilde{X}_{12}) d\lambda, \tag{30}$$

where λ parameterizes the space $\Lambda(\hat{\sigma}_1) \cong U(M)/U(M - \mathrm{Rank}(\hat{\sigma}_1))$ and $\widetilde{X}_{12} \in \mathcal{M}_{12}$ is an arbitrary state satisfying $\mathrm{Tr}_2(\hat{\Pi}(\widetilde{X}_{12})) = \hat{\sigma}_1$.

We now want to consider a possible analog of the partial trace formulated entirely in terms of the Hamiltonian densities and marginal distributions. We shall first consider the cases when the total quantum state $\hat{\rho}_{12}$ is separable pure or mixed. General ensembles are represented by densities on $\mathcal{M}_{12}$ denoted by $\rho_{12}(X)$. In the coordinates X_1, X_2, X_3 adapted to the Segre embedding the densities are written as $\rho_{12}(X) = \rho_{12}(X_1, X_2, X_3)$. In order to treat the separable states it is enough to consider probability densities with the support on $\mathcal{M}_1 \times \mathcal{M}_2$ i.e., densities dependent only on X_1, X_2. This is obvious if the state is pure, and if the state is mixed then there

[1] We are grateful to the referee for this observation and its consequences.

is at least one convex representation of it with the density having the stated property. Ensemble of pure states X_0, corresponding to the pure $\hat{\rho}_{12} = \hat{\Pi}(X_0)$, is represented by the delta function centered at X_0. In the coordinates X_1, X_2, X_3 adapted to the Segre embedding, the ensemble of pure separable states X_0 is represented by $\rho_{12}(X_1, X_2) = \delta(X_1 - X_{01})\delta(X_2 - X_{02})$. If the state is mixed separable then it can be represented by a density of the form $\rho(X) = \rho(X_1, X_2)$. Integration over X_2 in the pure separable case gives

$$\int_{\mathcal{M}_2} \delta(X_1 - X_{01})\delta(X_2 - X_{02})dM_2 = \delta(X_1 - X_{01}),$$
$$\text{separable pure } \hat{\rho}_{12} = \hat{\Pi}(X_0). \tag{31}$$

The result is a delta density on $\mathcal{M}_1$ which reproduces, via the general formula (5), the reduced matrix $\mathrm{Tr}_2(\hat{\Pi}(X_0))$. Similarly, in the mixed separable case the integration over X_2 gives a density on $\mathcal{M}_1$

$$\rho_1(X_1) = \int_{\mathcal{M}_2} \rho(X_1, X_2)dM_2, \quad \text{separable mixed } \hat{\rho}_{12}, \tag{32}$$

which reproduces $\mathrm{Tr}_2(\hat{\rho}_{12})$ if $\rho(X_1, X_2)$ reproduces $\hat{\rho}_{12}$. We see that the analog of the partial trace in the case of separable state, pure or mixed, is provided by taking the marginal distribution of the appropriate distribution on the total phase space.

However, the analogy does not work for entangled states. In fact, consider a pure entangled state, represented by the delta density $\rho_{12}(X; X_0) = \delta(X_1 - X_{01})\delta(X_2 - X_{02})\delta(X_3 - X_{03})$. Integration over X_2, X_3 gives, up to a function dependent on X_0, the delta function of $X_1 - X_{01}$

$$\rho_1(X_1; X_0) = \int_{X_2, X_3} \rho_{12}(X_1, X_2, X_3; X_0)dX_2dX_3 = \delta(X_1 - X_{01})g(X_0)$$
$$\text{entangled pure } \hat{\rho}_{12} = \hat{\Pi}(X_0), \tag{33}$$

which is proportional to the density that represents a pure state in $\mathcal{H}_1$, and not the reduced mixed state.

The general conclusion of this analysis is that if the state of the total system is separable then the marginal distribution of a specific probability distribution reproducing the state of the total system, reproduces the reduced density matrix of the subsystem. Evolution of such reduced density will preserve this property if the Hamiltonian does not entangle the two subsystems. In this case, arbitrary transformations or approximations of the second subsystem density do not effect the evolution of the first subsystem. The case of separable bipartite states is specially important for hybrid systems, when one of the parts is treated as a classical system, since in the Hamiltonian hybrid theory, presented in the next Section, there can be no entanglement between the classical and the quantum parts. On the other hand, if the initial total state of a bipartite quantum system is entangled, or becomes entangled due to the evolution, then the states of the subsystems are not given simply in terms of the marginal distributions.

4 Ensembles of Hybrid Systems

There is no unique generally accepted theory of interaction between micro and macro degrees of freedom, where the former are described by quantum and the later by classical theory. The reason is primarily because each of the suggested theories has some unexpected or controversial features (see [10] for an informative review). Partial selection of hybrid theories can be found in [24–29]. Some of the suggested hybrid theories are mathematically inconsistent, and "no go" type theorems have been formulated [30], suggesting that no consistent hybrid theory can be formulated. Nevertheless, mathematically consistent but inequivalent hybrid theories exist [10, 28, 29]. Even the proper conceptual status and putative domains of application of hybrid theories need not be unique and are not generally agreed upon. Hybrid theories that attempt to describe the quantum measurement process or serve as approximate but consistent models in quantum chemistry or model the interaction between classical gravity and quantized matter might be fundamentally different or differ only in some additional details. Usually, it is not claimed that macroscopic systems are composed of something other that microscopic parts well described by quantum theory. However it is legitimate to assume that dynamics of at least some of the observable degrees of freedom of a macroscopic system are correctly described by classical mechanics, and that the classical mechanical description need not be reduced or derived from quantum description of all the microscopic components. Neither quantum nor classical theory is designed to describe the dynamics of systems consisting of micro and macro subparts, as separately described by the quantum and the classical mechanics respectively.

The Hamiltonian hybrid theory, as formulated and discussed for example in [10–13, 31], has many of the properties commonly expected of a good hybrid theory. In fact, the dynamical formulas of the Hamiltonian theory are equivalent to the well known mean field approximation, the main novelty being that the theory is formulated entirely in the framework of the theory of Hamiltonian dynamical systems. In particular, this demonstrates that the theory is mathematically consistent. However, the theory also has some controversial features concerning the class of mathematical objects that should be interpreted as physical variables and the most general type of states of the hybrid system. In what follows we shall first briefly recapitulate the Hamiltonian formulation of the hybrid systems and present the dynamical laws for pure states and for ensembles of hybrid systems. Unlike the purely quantum case, the dynamics of hybrids in pure states is nonlinear and the dynamics of densities involves the most general class of statistical ensembles. Therefore, one needs to discuss the possibility of superluminal communication between hybrid systems.

Hamiltonian theory of hybrid systems can be developed starting from the Hamiltonian formulation of a composite quantum system and imposing a constraint that one of the components is behaving as a classical system [12]. The result, in the macro-limit imposed on the constrained subsystem, turns out to be equivalent to a Cartesian product of two Hamiltonian systems as in [10]. One of these Hamiltonian systems corresponds to the quantum and one to the classical subsystem of the hybrid. However, the interaction between the two subsystems has crucial influence on their properties.

The space of pure states of the hybrid system $\mathcal{M}$ is considered as a Cartesian product $\mathcal{M} = \mathcal{M}_c \times \mathcal{M}_q$ of the classical subsystem phase space $\mathcal{M}_c$ and of the quantum subsystem phase space $\mathcal{M}_q$. Local coordinates on the product are denoted $\{p, q, x, y\}$, where $(p, q) \in \mathcal{M}_c$ will be called the classical degrees of freedom (CDF) and $(x, y) \in \mathcal{M}_q$ will be called the quantum degrees of freedom (QDF). The constraint that CDF behave as a classical system implies that there is no entanglement between QDF and CDF, but no restriction on the entanglement in QDF is imposed. The evolution equations of the hybrid system are of the Hamiltonian form with the Hamilton's function comprised of three terms

$$H_t(p, q, x, y) = H_c(p, q) + H_q(x, y) + V_{int}(p, q, x, y), \tag{34}$$

where H_c is the Hamilton's function of the classical subsystem, $H_q(x, y) = \langle\psi_{x,y}|\hat{H}_q|\psi_{x,y}\rangle$ is the Hamilton's function of the quantum subsystem and $V_{int}(p, q, x, y) = \langle\psi_{x,y}|\hat{V}_{int}(p, q)|\psi_{x,y}\rangle$ describes the interaction between the subsystems, where $\hat{V}_{int}(p, q)$ is an operator in the Hilbert space of the quantum subsystem which depends on the classical coordinates (p, q). The state vectors $|\psi_{x,y}\rangle$ are normalized by assumption. The Poisson bracket on $\mathcal{M}$ of arbitrary functions of the local coordinates (p, q, x, y) is defined as

$$\{F_1, F_2\}_{\mathcal{M}} = \sum_{i=1}^{n_c}\left(\frac{\partial F_1}{\partial q_i}\frac{\partial F_2}{\partial p_i} - \frac{\partial F_2}{\partial q_i}\frac{\partial F_1}{\partial p_i}\right) + \sum_{j=1}^{n_q}\left(\frac{\partial F_1}{\partial x_j}\frac{\partial F_2}{\partial y_j} - \frac{\partial F_2}{\partial x_j}\frac{\partial F_1}{\partial y_j}\right), \tag{35}$$

where n_c and n_q are numbers of CDF and QDF respectively. Of course, if the Hilbert space of the quantum part is of infinite dimension then n_q is infinite. Thus, the Hamiltonian form of the hybrid dynamics on $\mathcal{M}$ as the phase space reads

$$\dot{q} = \{q, H_t\}_{\mathcal{M}}, \qquad \dot{p} = \{p, H_t\}_{\mathcal{M}}, \tag{36}$$

$$\dot{x} = \{x, H_t\}_{\mathcal{M}}, \qquad \dot{y} = \{y, H_t\}_{\mathcal{M}}, \tag{37}$$

where H_t is given by (34).

In particular, the evolution of QDF can be stated in the form of the Schrödinger equation

$$i\hbar\,\partial_t|\psi_{x,y}\rangle = \hat{H}_{qc}(p, q)|\psi_{x,y}\rangle, \tag{38}$$

with the Hamiltonian operator $\hat{H}_{qc}(p, q) = \langle p, q|\hat{H}|p, q\rangle$ acting on the Hilbert space of quantum subsystem and depending parametrically on the CDF (p, q) through the coherent states $|p, q\rangle$. The evolution of the state vectors (38) is norm-preserving, but nonlinear.

It is worth noticing that the state of QDF in a hybrid system might have nonzero entanglement. We tested this using as an example a pair of $1/2$-spins in interaction with a 2D classical oscillator. The interaction between QDF and CDF couples the classical coordinates with the spins components $\sigma^{1,2}_{x,y,z,}$. It turns out that the concurrence of the pure state of the two spins displays nontrivial dynamics and is often nonzero.

Thus, QDF of the hybrid model display some typically quantum properties and evolve nonlinearly in the same time. Furthermore, the Poisson bracket (35) of two functions $F_1(p,q,x,y)$ and $F_2(p,q,x,y)$ which are both quadratic in QDF and depend on CDF, is not a function quadratic in the QDF. However, the proper interpretation of this fact is nontrivial. Let us first reexamine the situation in the purely quantum case with linear evolution and normalized state vectors. There, a quadratic function $A(x,y) = \langle\psi_{x,y}|\hat{A}|\psi_{x,y}\rangle$ was considered as mathematical representative of a dynamical variable, and the set of quadratic functions is invariant under the evolution. Thus, in the purely quantum case, the evolution of a quadratic function can be interpreted as the Heisenberg picture of the evolution of a dynamical variable or as the Schrödinger picture of the expectation of the variable in an evolving state. On the other hand, in the Hamiltonian hybrid theory one can stick to the original interpretation of $A(x,y)$ as the expectation of the observable $\hat{A}$ in the state $|\psi_{x,y}\rangle$. One could then argue that the Heisenberg picture of the hybrid evolution is not defined, and the non-quadratic expression $A(x,y;t) = \langle\psi_{x,y}(t)|\hat{A}|\psi_{x,y}(t)\rangle$ should be interpreted as the expectation value of the standard Schrödinger quantum variable in the state $|\psi_{x,y}(t)\rangle$ at time t. Nevertheless, the nonlinear evolution of the QDF shows that QDF of a hybrid system do not have all the properties of a purely quantum system. Hybrid systems appear to be qualitatively different from a simple union of classical and quantum systems [10, 12, 13, 31]. This is further illustrated by studying the evolution of ensembles of hybrid systems.

The most general ensemble of hybrid systems is represented by some probability density $\rho(p,q,x,y)$. As pointed out in Sect. 3.1, the function ρ should not be considered as an expectation $\langle\hat{\rho}(q,p)\rangle$ of some density operator $\hat{\rho}(q,p)$ parametrically dependent on (q,p). The densities evolve according to the Liouville equation with a solution $\rho(p,q,x,y;t)$. As in Sect. 3.2, this Liouville equation for the hybrid system is itself a Hamiltonian dynamical system. The density $\rho(p,q,x,y;t)$ for any fixed t generates a unique positive operator valued function (POVF):

$$\hat{\rho}(p,q;t) = \int_{\mathcal{M}_q} \rho(p,q,x,y;t)\hat{\Pi}(x,y)dM_q, \tag{39}$$

which can be called the hybrid statistical operator. The unconditional mixed state of the quantum subsystem of the hybrid in the state $\rho(p,q,x,y;t)$ is also uniquely obtained as

$$\hat{\rho}(t) = \int_{\mathcal{M}} \rho(p,q,x,y;t)\hat{\Pi}(x,y)dM \equiv \int_{\mathcal{M}_q} \rho_q(x,y;t)\hat{\Pi}(x,y)dM_q, \tag{40}$$

where the marginal distribution $\rho_q(x,y;t)$

$$\rho_q(x,y;t) = \int_{\mathcal{M}_c} \rho(p,q,x,y;t)dM_c \tag{41}$$

can be considered as the probability density on $\mathcal{M}_q$ associated with the state $\hat{\rho}(t)$ of QDF. Due to the properties of the Liouville evolution of $\rho(p,q,x,y;t)$, the formula (40) defines for all t a continuous one-parameter family of statistical operators on $\mathcal{H}$. Like in the purely quantum case, $\hat{\rho}(t)$ and $\rho(p,q,x,y;t)$ give the same expectation

$\mathrm{Tr}(\hat{\rho}(t)\hat{A}) = \int \rho A(x, y) dM$ of quantum observables $\hat{A}$ represented by $A(x, y)$. All that was said about many-to-one relation between ρ and $\hat{\rho}$ in the quantum case applies also in the hybrid case.

However, contrary to the purely quantum case, different $\rho(p, q, x, y; t_0)$ that give the same $\hat{\rho}(t_0)$ generate different evolution of $\hat{\rho}(p, q; t)$ (or $\hat{\rho}(t)$) and thus must be considered as physically different (for a related analysis please see [30, 31]). Indeed, the evolution equation satisfied by $\hat{\rho}(p, q; t)$ [13] is

$$\frac{\partial \hat{\rho}(p, q; t)}{\partial t} = \frac{1}{i\hbar}\big[\hat{H}_q + \hat{V}_{int}(p, q), \hat{\rho}(p, q; t)\big] + \big\{H_c(p, q), \hat{\rho}(p, q; t)\big\}_{p,q} + \int_{\mathcal{M}_q} \big\{V_{int}(p, q, x, y), \rho(p, q, x, y; t)\big\}_{p,q} \hat{\Pi}(x, y) dM_q. \quad (42)$$

The dynamical equation for $\hat{\rho}(t)$ is

$$\frac{d\hat{\rho}(t)}{dt} = \frac{1}{i\hbar}\big[\hat{H}_q, \hat{\rho}(t)\big] + \frac{1}{i\hbar}\int_{\mathcal{M}_c} \big[\hat{V}_{int}(p, q), \hat{\rho}(p, q; t)\big] dM_c. \quad (43)$$

The first term of (43) generates the unitary part of the evolution and the second term does not preserve the norm of $\hat{\rho}$ and is responsible for non-unitary effects. Notice that the evolution of $\hat{\rho}(p, q; t)$ ($\hat{\rho}(t)$) cannot be expressed only in terms of $\hat{\rho}(p, q; t)$ ($\hat{\rho}(t)$), but irreducibly involves the probability density $\rho(p, q, x, y; t)$. At this point we might remark that the von Neumann entropy of $S_{vN} = \mathrm{Tr}(\hat{\rho} \ln \hat{\rho})$ of (40) can increase and decrease during the evolution (43) starting from a general initial ensemble. However, this is not an instance of the Peres objection [21] against nonlinear evolution of a quantum system since the QDF form an open dynamical system. On the other hand the Gibbs entropy $S(\rho) = \int_{\mathcal{M}} \rho \ln \rho \, dM$ is conserved by the Liouville evolution of the total density.

The evolution equation for $\hat{\rho}(t)$ is reduced to (36) and (37) if the initial $\rho(p, q, x, y; t_0)$ is a pure state in $\mathcal{M}$. This is intuitively clear since there can be no entanglement between QDF and CDF. Formally, pure initial state is represented as a delta function on the total phase space and the Liouville equation is reduced to the Hamilton equations for pure states. If however, the initial density is of the form $\delta(x - x_0)\delta(y - y_0)\rho(q, p)$ the pure state $\hat{\rho}(t_0) = |\psi(t_0)\rangle\langle\psi(t_0)|$ might evolve according to (43) into a non-pure mixture. Quantum-classical interaction with the classical part in the initially mixed state can transform an initially pure state of the quantum part into a mixed state. This is an important observation.

The evolution of QDF of a hybrid system is fundamentally different from the linear evolution of a quantum subsystem of a quantum system. The reason for this qualitative difference is that dynamical influences of many degrees of freedom corresponding to the entangled states and to the non-classical states of the classical subsystem are completely neglected in the derivation of the hybrid dynamics.

The characteristic main features of the QDF evolution in the hybrid case are expressed by the nonlinearity of the pure state evolution, or by the dynamically induced differences of $\hat{\rho}(t)$ with different convex mixture representations. It is well known [19, 20], that the linearity of the Schrödinger equation and the equivalence of different convex mixtures, are both necessary in order to prevent superluminal communication

in ordinary quantum mechanics of bipartite systems. If either of the two properties is violated, without further modification of the quantum formalism, superluminal communication between entangled parts of a bipartite system is possible. The nonlinear pure state evolution and the evolution dependence on the initially equivalent different ensembles appear quite naturally in the Hamiltonian description of hybrid systems, and in the same time the QDF of the hybrid might be in an entangled state. Therefore, superluminal communication can be avoided only by some further modification of the hybrid theory. It has been argued that the direct product might not be the natural type of coupling between systems with nonlinear evolution [19], and that nonlinear evolution might suggest non-standard computation of correlations [32]. Alternatively, one might consider the model of hybrid systems presented here as insufficient to describe fully the true features of coupled real quantum and macroscopic classical systems. One might resort to *ad hoc* modifications of the hybrid evolution by introducing dissipation and stochastic terms [33, 34] or one might explore the possibilities opened up by replacing a simple classical system by truly complex classical systems with many degrees of freedom [10, 34].

Finally, we would like to stress that the presented theory of quantum-classical interaction does not provide a description of the quantum measurement process (for a discussion of this opinion see [35]) if the total system is initially in a pure state. The Hamiltonian system (36) and (37) with, for example $H_q(x, y) = 0$ and $H_c(p, q) = 0$, but with a nonzero interaction, for example $H_{int}(p, q, x, y) = cx^2 p$, where c is a coupling constant, can describe "classical measurement" of a quantity $A(x) = x^2$ by the meter given by the variable conjugate to p, that is by q. In fact $q(t)$ and the initial x_0 get correlated as $q(t) = cx_0^2 t$ and thus reading of $q(t)$ at some t is a measurement of x_0^2. However, the result of such "classical measurement", i.e., $A(x, y)$, is the expectation of the observable $\hat{A}$, and not one of its eigenvalues, as it should be in ideal quantum measurement on a single system. Only if the initial state of the QDF is an eigenstate of $\hat{A}$ with eigenvalue a_1, the quantum-classical interaction can give the eigenvalue a_1. An arbitrary initial state of the QDF, for example a superposition of a_1 and a_2 eigenstates would lead to $q(t)$ corresponding to the average of the eigenvalues. In conclusion, the proper quantum measurement process seems to involve dynamical entanglement between the quantum system and the apparatus, which, once entangled with the system, must be considered in some sense complex and classical. The initial entanglement is impossible in the present model of quantum-classical interaction, which treats the macroscopic apparatus as completely described by the classical theory from the beginning. On the other hand, in order to reproduce the results of ideal quantum measurement by quantum-classical interaction one could contemplate the hybrid systems as effectively dissipative, supplementing the Hamiltonian model with the attractors indicating the eigenvalues of the quantum observable.

5 Summary

We have explored relations between properties of quantum mixed states as represented by statistical operators or by density distributions on the phase space in the Hamiltonian formulation of quantum mechanics and hybrid systems. Some consequences of the fact that in general many density functions correspond to a single

statistical operator are discussed. Liouville and von Neumann evolution equations are seen as Hamiltonian dynamical systems. This perspective additionally illustrates the restriction imposed on a general Hamiltonian system if it is to represent a physical system with quantum mechanical properties. We then explored representation of the partial trace operation in terms of partial integration over the relevant variables in the Hamiltonian formulation. Our main objective was to analyze ensembles of hybrid quantum-classical systems in the Hamiltonian formulation. In this context relation between the evolution of the quantum degrees of freedom in a pure state and in a mixed state is explored. The quantum degrees of freedom of a hybrid in a pure state evolve nonlinearly and if the hybrid is in a mixed state different convex representations must be considered as nonequivalent because they evolve differently.

Linear evolution of QM, and invariance of the evolution of $\hat{\rho}$ on different convex representations, need to be abandoned if the effects of interaction with CDF, like those occurring during measurements, are to be described dynamically. On the other hand, QM treatment of composite systems is adapted to the linear evolution, and if the later is replaced by a nonlinear one, the kinematic properties of the composite QM systems have to be modified as well. The needed modification of the kinematic properties of quantum composite systems is not supplied by the presented Hamiltonian hybrid theory. Furthermore, the theory does not describe the measurement process. It is fair to say that the Hamiltonian hybrid theory, in its presented form, does not describe the quantum-classical interaction successfully. In fact the QC interaction is treated in an oversimplified manner, because the macro-object in interaction with QDF is considered as fully described by a small subset of distinguished degrees of freedom which are described classically. A large number of degrees of freedom of the macroscopic object which also interact with the quantum system are completely neglected. The presented form of the Hamiltonian hybrid theory must be modified in order to incorporate the effects of these degrees of freedom. It is our belief that such modifications will result in a hybrid theory which is consistent and whose predictions are closer to the experimentally observed facts.

Acknowledgements We acknowledge support by the Ministry of Science and Education of the Republic of Serbia, contract Nos. 171006, 171017, 171020, 171038, 45016 and by COST (Action MP1006). We thank the referee for his detailed suggestions.

References

1. Kibble, T.W.B.: Commun. Math. Phys. **64**, 73 (1978)
2. Kibble, T.W.B.: Commun. Math. Phys. **65**, 189 (1979)
3. Heslot, A.: Phys. Rev. D **31**, 1341 (1985)
4. Ashtekar, A., Schilling, T.A.: Geometrical formulation of quantum mechanics. In: Harvey, A. (ed.) On Einstein's Path. Springer, Berlin (1998)
5. Brody, D.C., Hughston, L.P.: J. Geom. Phys. **38**, 19 (2001)
6. Burić, N.: Ann. Phys. (NY) **233**, 17 (2008)
7. Brody, D.C., Gustavsson, A.C.T., Hughston, L.P.: J. Phys. A **41**, 475301 (2008)
8. Radonjić, M., Prvanović, S., Burić, N.: Phys. Rev. A **84**, 022103 (2011)
9. Radonjić, M., Prvanović, S., Burić, N.: Phys. Rev. A **85**, 022117 (2012)
10. Elze, H.-T.: Phys. Rev. A **85**, 052109 (2012)
11. Zhang, Q., Wu, B.: Phys. Rev. Lett. **97**, 190401 (2006)
12. Radonjić, M., Prvanović, S., Burić, N.: Phys. Rev. A **85**, 064101 (2012)

13. Burić, N., Mendaš, I., Popović, D.B., Radonjić, M., Prvanović, S.: Phys. Rev. A **86**, 034104 (2012)
14. Hughston, L.P., Jozsa, R., Wooters, W.K.: Phys. Lett. A **183**, 14 (1993)
15. Arnold, V.I.: Mathematical Methods of Classical Mechanics. Springer, New York (1978)
16. Marsden, J.E., Ratiu, T.S.: Introduction to Mechanics and Symmetry. Springer, Berlin (1994)
17. Mielnik, B.: Commun. Math. Phys. **37**, 221 (1974)
18. Weinberg, S.: Ann. Phys. **194**, 336 (1989)
19. Mielnik, B.: Phys. Lett. A **289**, 1 (2001)
20. Gisin, N.: Phys. Lett. A **143**, 1 (1990)
21. Peres, A.: Phys. Rev. Lett. **63**, 1114 (1989)
22. Gibbons, G.W.: J. Geom. Phys. **8**, 147 (1992)
23. Hassett, B.: Introduction to Algebraic Geometry. Cambridge University Press, Cambridge (2007)
24. Sherry, T.N., Sudarshan, E.C.G.: Phys. Rev. D **18**, 4580 (1978)
25. Boucher, W., Traschen, J.: Phys. Rev. D **37**, 3522 (1988)
26. Aleksandrov, I.V.: Z. Naturforsch. **36A**, 902 (1981)
27. Peres, A., Terno, D.R.: Phys. Rev. A **63**, 022101 (2001)
28. Diósi, L., Gisin, N., Strunz, W.T.: Phys. Rev. A **61**, 02108 (2000)
29. Hall, M.J.W., Reginatto, M.: Phys. Rev. A **72**, 062109 (2005)
30. Salcedo, L.L.: Phys. Rev. A **85**, 022127 (2012)
31. Barceló, C., Carballo-Rubio, R., Garay, L.J., Gómez-Escalante, R.: Phys. Rev. A **86**, 042120 (2012)
32. Doebner, H.D.: Phys. Lett. A **301**, 139 (2002)
33. Diósi, L.: J. Phys. Conf. Ser. **306**, 012006 (2011)
34. Burić, N., Popović, D.B., Radonjić, M., Prvanović, S.: Phase space hybrid theory of quantum measurement with nonlinear and stochastic dynamics. Available as: arXiv:1307.8424
35. Elze, H.-T.: Int. J. Quantum Inf. **10**, 1241012 (2012)

Phys. Scr. **T157** (2013) 014019 (4pp) doi:10.1088/0031-8949/2013/T157/014019

Effects of laser beam diameter on electromagnetically induced transparency due to Zeeman coherences in Rb vapor

S N Nikolić, A J Krmpot, N M Lučić, B V Zlatković, M Radonjić and B M Jelenković

Institute of Physics, University of Belgrade, Pregrevica 118, 11080 Belgrade, Serbia

E-mail: stankon@ipb.ac.rs

Received 19 August 2012
Accepted for publication 12 December 2012
Published 15 November 2013
Online at stacks.iop.org/PhysScr/T157/014019

Abstract

We experimentally studied the effects of laser beam diameter on electromagnetically induced transparency (EIT) due to Zeeman coherences induced by a laser resonant with the hyperfine transition $F_g = 2 \rightarrow F_e = 1$ of ^{87}Rb in a rubidium buffer gas cell. We use two laser beams of Gaussian intensity radial profile for laser beam diameters of 6.5 and 1.3 mm, laser intensities in the range of 0.1–35 mW cm^{-2} and cell temperatures between 60 and 82 °C. The results show that the amplitude of the normalized EIT resonance has a maximum at a laser intensity which depends on laser beam diameter and cell temperature. The laser intensity corresponding to the maximum EIT amplitude is higher for a smaller laser beam and higher cell temperature. The linewidth of Zeeman EIT resonance varies nearly linearly with laser intensity, almost independent of cell temperature and laser beam diameter.

PACS numbers: 03.65.Fd, 03.65.Sq

(Some figures may appear in colour only in the online journal)

1. Introduction

Electromagnetically induced transparency (EIT) is a coherence phenomenon characterized by narrow transmission resonance of a laser beam through alkali atom vapor [1]. It is essential for fields such as slow and stored light [2], lasing without inversion [3], frequency mixing [4], etc. Important devices such as atomic frequency standards [5] and magnetometers [6] are based on EIT. The optimization of all these processes and devices is therefore directly conditioned on achieving better EIT properties.

The average time-of-flight of an atom through the laser beam limits the EIT amplitudes and linewidths. In order to prolong interaction time and thus the dark states lifetime, an inert buffer gas is added to atomic vapor to slow down the diffusion of the coherently prepared atoms through the laser beam. The linewidth, governed by the ground state relaxation and laser power, is reduced by several orders of magnitude due to the Dicke effect [7]. Linewidths as narrow as 30 Hz are obtained [8].

Hyperfine EIT resonance is formed as a coherent superposition of two ground hyperfine levels while EIT resonance in the Hanle configuration is based on Zeeman coherences between magnetic sublevels of a given hyperfine state of the alkali atom electronic ground state. Cell temperature affects differently hyperfine coherences than Zeeman coherences. For the former, it is found that linewidths vary inversely with density [9, 10]. The linewidth is a linear function of laser intensity and the slope of the linear curve decreases as the cell temperature increases. At lower temperatures than in [9, 10], in the range 30–60 °C, linewidth can be independent on cell temperature, as shown in [11]. On the other hand, EIT resonances due to Zeeman coherence are nearly independent of cell temperature [10]. In addition, the behavior of EIT as a function of laser beam diameter [12], optical depth [13], laser intensity [14, 15] and laser beam profile [16, 17] was investigated.

In this paper, we analyze the properties of Zeeman EIT resonances under different parameters in order to obtain optimum EIT contrast and linewidths, which is essential

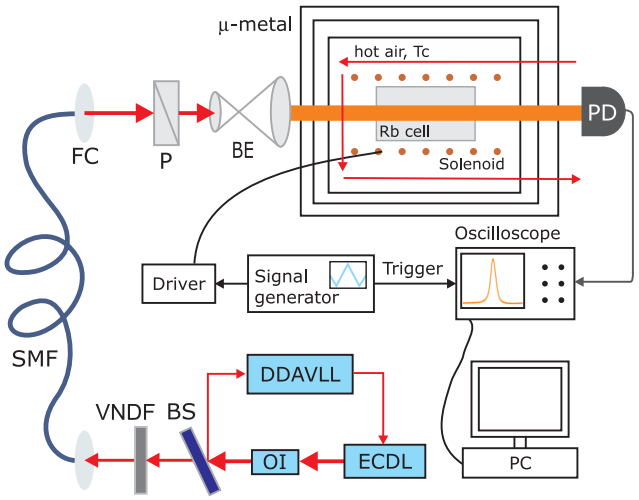

Figure 1. Experimental setup: ECDL—external cavity diode laser; OI—optical insulator; DDAVLL—Doppler-free dichroic atomic vapor laser lock; BS—beam splitter; VNDF—variable neutral density filter; SMF—single-mode fiber; FC—fiber coupler; P—polarizer; BE—beam expander; PD—large-area photodiode. Hot air is used for heating the cell.

for application of Zeeman coherences, like efficient slowing down of light pulses in the cell [18] as well as their storage. Zeeman coherences were induced by the laser locked to the $F_g = 2 \rightarrow F_e = 1$ transition in ^{87}Rb, contained in the cell with 30 Torr of Ne. We analyze EIT for two laser beam diameters and a wide range of laser intensity and cell temperature. Unlike the hyperfine EIT, there are no detailed studies on the behavior of Zeeman EIT when the main experimental parameters vary.

2. Experimental setup

The experimental setup is shown in figure 1. The external cavity diode laser is frequency locked to the hyperfine $F_g = 2 \rightarrow F_e = 1$ transition of the D_1 line in ^{87}Rb by using the Doppler-free dichroic atomic vapor laser lock method [19, 20]. Gaussian distribution of laser intensity radial dependence is achieved by the single-mode optical fiber. For adjusting the laser beam diameter, a beam expander is used. The linear polarization of laser light is ensured by a high-quality polarizer. Laser beam intensity is controlled by the variable neutral density filter. A Rb cell with 30 Torr of Ne as the buffer gas is 8 cm long and 25 mm in diameter. The Rb vapor is shielded from external magnetic fields by the triple layer of μ-metal which reduces stray magnetic fields below 10 nT. In order to obey two-photon detuning in the Hanle experiment, a long solenoid placed around the Rb cell produces a controllable longitudinal magnetic field in the range of $\pm 20\,\mu$T. The intensity of transmitted laser light as a function of applied magnetic field was monitored by the photodiode and recorded by the storage oscilloscope. The Rb cell was heated up to a certain temperature by using circulating hot air around the cell. The advantage of this system in comparison with electrical heating is avoiding the stray magnetic field inside the μ-metal that is inevitably introduced by heating current.

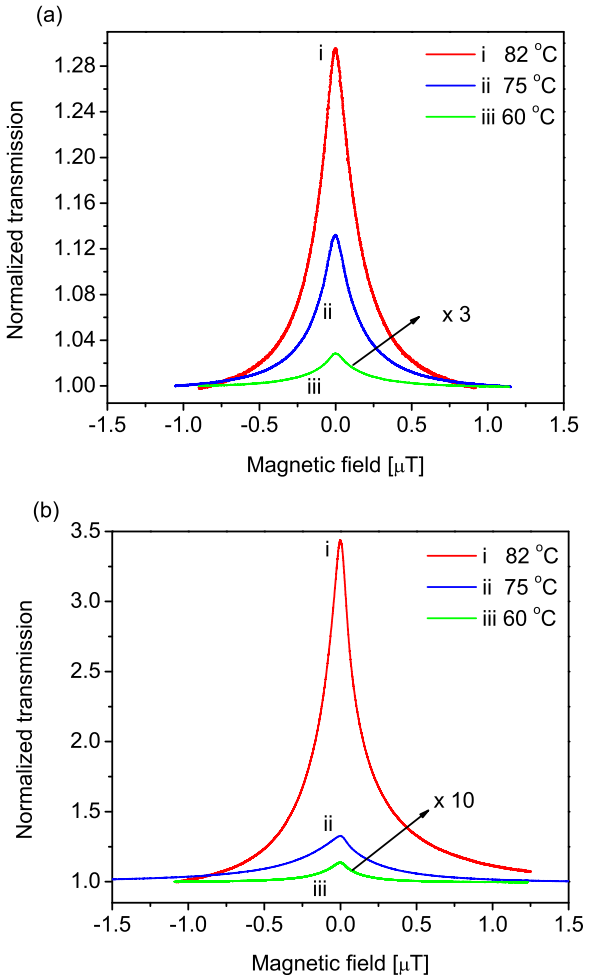

Figure 2. Measured EIT resonances for Gaussian laser beams of diameter (a) $D = 6.5$ mm and (b) $D = 1.3$ mm. Resonances are measured for an overall laser beam intensity of 3.3 mW cm^{-2} at temperatures of 60, 75 and 82 °C.

3. Results and discussions

We present measured EIT resonances in the Hanle configuration obtained with laser beams of Gaussian radial intensity profile for cell temperatures of 60, 75 and 82 °C and laser beam diameters of 1.3 and 6.5 mm. The intensity range covered in the experiment was 0.1–10 mW cm^{-2} for wide and 0.1–35 mW cm^{-2} for narrow laser beams. EIT resonances presented in this paper are obtained after normalizing measured resonances to the transmission signal away from Raman resonance. Examples of experimentally obtained EIT resonances for wide and narrow Gaussian laser beams at three temperatures are given in figure 2.

As can be seen in figure 2, the amplitudes of Zeeman EIT increase with cell temperature, and this effect is particularly strong for narrower laser beams.

The EIT amplitude dependence on overall laser beam intensity measured at different temperatures, for wide and narrow laser beams, is shown in figures 3(a) and (b), respectively. As can be seen, the highest cell temperature with the smaller laser beam diameter gives the strongest EIT resonances. Higher temperatures mean larger atomic density and number of atoms coherently prepared in the dark state. As the laser beam diameter gets smaller, the contribution of wings

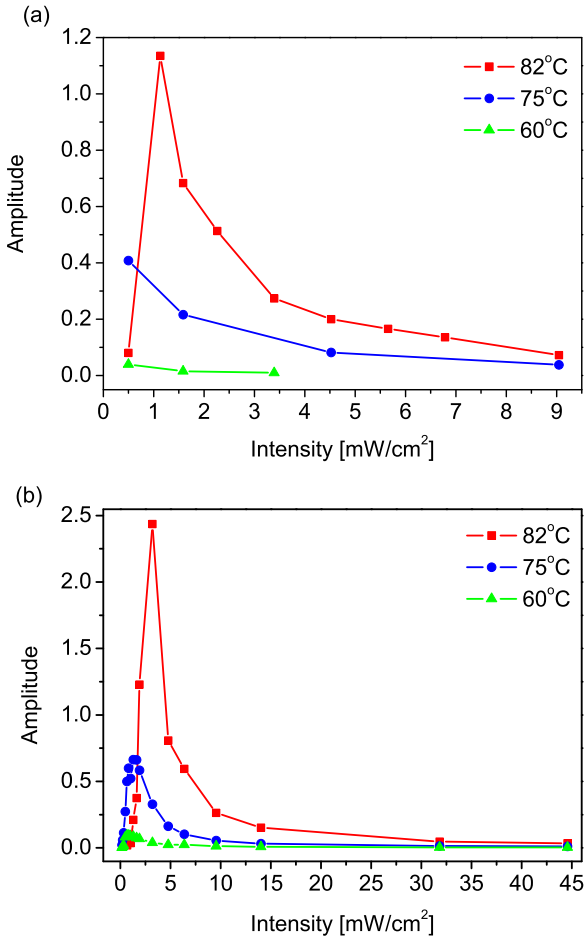

Figure 3. Experimental dependences of EIT amplitudes on overall light intensity for Gaussian laser beams of diameter (a) 6.5 mm and (b) 1.3 mm at temperatures of 60, 75 and 82 °C.

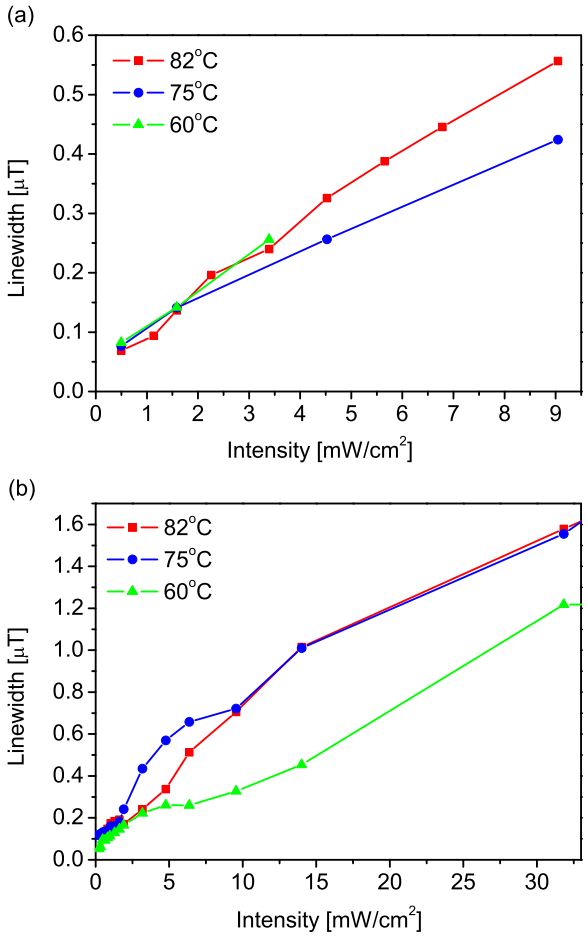

Figure 4. Experimental dependences of EIT linewidth on overall laser beam intensity for Gaussian laser beams of diameter (a) 6.5 mm and (b) 1.3 mm at three different temperatures.

of the Gaussian laser beam to two-photon type resonance like EIT is enhanced.

In figure 4 the EIT linewidth as a function of laser intensity at three different cell temperatures is shown for two Gaussian laser beam diameters. The dependence of EIT linewidths on laser intensity, for either wide or narrower laser beams, is apparently independent of cell temperature. Such behavior of Zeeman EIT with cell temperature is shown in the pump–probe laser configuration in [10]. Ultra narrow Zeeman EIT resonances with linewidths below 100 nT were achieved because of careful elimination of stray magnetic fields inside the triple antimagnetic shielding surrounding the Rb buffer gas cell.

4. Summary

We carried out an experimental study of the behavior of EIT resonances due to Zeeman coherences among sublevels of the ^{87}Rb hyperfine state $F_g = 2$ in a Rb buffer gas cell of 8 cm length, 25 mm diameter and 30 Torr of Ne buffer gas. The dependence of EIT on laser beam diameter (6.5 and 1.3 mm), laser intensity (0.1–35 mW cm^{-2}) and Rb cell temperature (60–82 °C) reveals that the highest contrast and amplitude to linewidth ratios are obtained with the narrower laser beam at about 5 mW cm^{-2}.

Acknowledgments

The authors acknowledge funding from grant numbers 45016 and 171038 of the Ministry of Education and Science of the Republic of Serbia and Scopes JRP IZ7370_127942.

References

[1] Fleischhauer M, Imamoglu A and Marangos J P 2005 *Rev. Mod. Phys.* **77** 633–73
[2] Phillips D F, Fleischhauer A, Mair A, Walsworth R L and Lukin M D 2001 *Phys. Rev. Lett.* **86** 783–6
[3] Scully M O, Zhu S and Gavrielides A 1989 *Phys. Rev. Lett.* **62** 2813–6
[4] Harris S E, Field J E and Imamoğlu A 1990 *Phys. Rev. Lett.* **64** 1107–10
[5] Knappe S, Shah V, Schwindt P D, Holberg L, Kitching J, Liew L A and Moreland J 2004 *Appl. Phys. Lett.* **85** 1460–2
[6] Fleischhauer M, Matsko A V and Scully M O 2000 *Phys. Rev.* A **62** 013808
[7] Dicke R H 1953 *Phys. Rev.* **89** 472–3
[8] Erhard M and Helm H 2001 *Phys. Rev.* A **63** 043813
[9] Sautenkov V A, Kash M M, Velichansky V L and Welch G R 1999 *Laser Phys.* **9** 889–93
[10] Figueroa E, Vewinger F, Appel J and Lvovsky A L 2006 *Opt. Lett.* **31** 2625–7
[11] Deng J L, Hu Z F, He H J and Wang Y Z 2006 *Chin. Phys. Lett.* **23** 1745–8
[12] Li L, Peng X, Liu C, Guo H and Chen X 2004 *J. Phys. B: At. Mol. Opt. Phys.* **37** 1873–8

[13] Pack M V, Camacho R M and Howell J C 2007 *Phys. Rev.* A **76** 013801
[14] Javan A, Kocharovskaya O, Lee H and Scully M O 2002 *Phys. Rev.* A **66** 013805
[15] Ye C Y and Zibrov A S 2002 *Phys. Rev.* A **65** 023806
[16] Taichenachev A V, Tumaikin A M, Yudin V I, Stahler M, Wynands R, Kitching J and Hollberg L 2004 *Phys. Rev.* A **69** 024501
[17] Radonjić M, Arsenović D, Grujić Z and Jelenković B M 2009 *Phys. Rev.* A **79** 023805
[18] Nikolić S N, Djokic V, Lučić N M, Krmpot A J, Ćuk S M, Radonjić M and Jelenković B M 2012 *Phys. Scr.* **T149** 014009
[19] Wasik G, Gawlik W, Zachorowski J and Zawadzki W 2002 *Appl. Phys.* B **75** 613–9
[20] Petelski T, Fattori M, Lamporesi G, Stuhler J and Tino G M 2003 *Eur. Phys. J.* D **22** 279–83

IOP PUBLISHING LASER PHYSICS
Laser Phys. **23** (2013) 105202 (7pp) doi:10.1088/1054-660X/23/10/105202

Dark-state polaritons in a degenerate two-level system

A Maggitti, M Radonjić and B M Jelenković

Institute of Physics, University of Belgrade, Pregrevica 118, 11080 Belgrade, Serbia

E-mail: mangelo@ff.bg.ac.rs

Received 26 July 2013
Accepted for publication 23 August 2013
Published 17 September 2013
Online at stacks.iop.org/LP/23/105202

Abstract
We investigate the formation of dark-state polaritons in an ensemble of degenerate two-level atoms admitting electromagnetically induced transparency. Using a generalization of microscopic equation-of-motion technique, multiple collective polariton modes are identified depending on the polarizations of two coupling fields. For each mode, the polariton dispersion relation and composition are obtained in a closed form out of a matrix eigenvalue problem for arbitrary control field strengths. We illustrate the algorithm by considering the $F_g = 2 \rightarrow F_e = 1$ transition of the D_1 line in ^{87}Rb atomic vapor. In addition, an application of dark-state polaritons to the frequency and/or polarization conversion, using D_1 and D_2 transitions in cold Rb atoms, is given.

(Some figures may appear in colour only in the online journal)

1. Introduction

At the end of the past century, the novel mechanism of electromagnetically induced transparency (EIT) [1, 2] and its many important applications drew a lot of attention. Nonlinearity of EIT media enables slow, stored and stationary light [3–5]. Mazets and Matisov were the first to introduce the concept of adiabatic Raman polaritons that represent a mixture of photon and collective atomic excitations [6]. Subsequently, Fleischhauer and Lukin further extended the concept to dark-state polaritons (DSPs) in a Λ-type EIT system [7]. They also developed a quantum memory technique [8] in order to transfer quantum states of photon wavepackets onto collective Raman excitations in a loss-free and reversible manner. DSPs in more sophisticated schemes have been studied, e.g. double-Λ [9–11], dual-V [12], inverted-Y [13], four-level [14], tripod [15], M-type [16], cyclic three-level [17] and multi-Λ [18, 19]. Collapses and revivals of the DSP number in an atomic ensemble with ground state degeneracy were found in [20]. Resonance beating of light stored using spinor DSPs in a multilevel-tripod scheme was investigated in [21]. Slow light propagation in a degenerate two-level system was experimentally investigated in [22]. DSPs in these various schemes may find applications in quantum information processing, quantum memory and quantum repeaters. Furthermore, degenerate atomic systems, due to their inherent complexity, could lead to new features of DSPs and building blocks for quantum information and quantum computation.

Most of the works treat DSPs using the perturbative approach to the field operator equations of motion, followed by the adiabatic approximation, which was introduced by Fleischhauer and Lukin. In addition, Zimmer *et al* [12] also used the Morris–Shore transformation [23]. Alternatively, Juzeliunas and Carmichael applied a Bogoliubov-type transformation for exact diagonalization of the model Hamiltonian [24]. Chong and Soljacic [9] elegantly derived the properties of the DSPs in single- and double-Λ systems using the Sawada–Brout technique [25]. In this work, we extend the Sawada–Brout–Chong technique to a degenerate two-level system, having a ground state manifold g and an excited state manifold e, that admits the appearance of EIT, i.e. (multiple) dark states exist within g. We present a general algorithm to identify multiple DSP modes that works for an arbitrary number of degenerate states within manifolds g and e and arbitrary polarizations of two coupling fields. The approach is illustrated by finding DSPs at D_1 line transition $F_g = 2 \rightarrow F_e = 1$ in atomic vapor of ^{87}Rb. It is shown

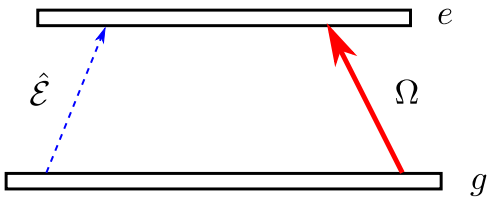

Figure 1. Schematic of a degenerate two-level system, having a ground state manifold g and an excited state manifold e, driven by a strong classical control field (thick line) of Rabi frequency Ω and by a weak quantum probe field $\hat{\mathcal{E}}$ (dashed line) of different polarizations.

that depending on the polarizations of the coupling fields, one or two DSP modes can be determined. In addition, it is shown how DSP modes, originating from different ^{87}Rb transitions, can be utilized for frequency and/or linear polarization conversion.

2. Degenerate two-level system

In this section, we present a general formalism of dark-state polaritons in a degenerate two-level system. It is a generalization of the neat approach of [9]. We consider a gas sample of N atoms, where N is large. Let us denote by $\mathcal{H}_\mathrm{g}$ the Hilbert space of the atomic states in the ground state manifold g and let $\mathcal{H}_\mathrm{e}$ be the Hilbert space of atomic excited states in the manifold e. The corresponding ground- and excited-state energies are denoted by $\hbar\omega_\mathrm{g}$ and $\hbar\omega_\mathrm{e}$, respectively. A strong classical control field of Rabi frequency Ω and a weak quantum probe field $\hat{\mathcal{E}}$, which differ in polarizations and both propagate along the z axis, couple the transition g → e (see figure 1). The corresponding raising and lowering operators of the control (probe) field, $\hat{V}_\mathrm{c}^\dagger$ and $\hat{V}_\mathrm{c}$ ($\hat{V}_\mathrm{p}^\dagger$ and $\hat{V}_\mathrm{p}$), connect the states in manifold g to the states in manifold e and vice versa. We assume that $\dim\mathcal{H}_\mathrm{g} \geq \dim\mathcal{H}_\mathrm{e}$ holds, so that the system admits EIT [26]. This assures the existence of the Hilbert space $\mathcal{H}_\mathrm{g}^\mathrm{d}$ of the states in manifold g that are dark to the g → e transition for the control field [27, 28]. Formally, we can view the raising operator $\hat{V}_\mathrm{c}^\dagger$ as a linear mapping $\hat{V}_\mathrm{c}^\dagger$: $\mathcal{H}_\mathrm{g} \to \mathcal{H}_\mathrm{e}$. The space $\mathcal{H}_\mathrm{g}^\mathrm{d}$ is then the null space of the mapping $\hat{V}_\mathrm{c}^\dagger$

$$\mathcal{H}_\mathrm{g}^\mathrm{d} = \{|g\rangle \in \mathcal{H}_\mathrm{g} \mid \hat{V}_\mathrm{c}^\dagger|g\rangle = 0\}. \tag{1}$$

2.1. Model Hamiltonian

We will now present the model Hamiltonian and the dynamics of the lowest energy excitations of the ensemble of degenerate two-level atoms. The free atomic Hamiltonian has the form

$$\hat{H}_\mathrm{at} = \sum_r (\hbar\omega_\mathrm{g}\hat{\mathbb{I}}_\mathrm{g}(r) + \hbar\omega_\mathrm{e}\hat{\mathbb{I}}_\mathrm{e}(r)), \tag{2}$$

where the summation index r counts the atomic positions, while $\hat{\mathbb{I}}_\mathrm{g}$ and $\hat{\mathbb{I}}_\mathrm{e}$ are the projection operators onto the states in the manifolds g and e, respectively. The free photon Hamiltonian, including multiple quantum probe field modes, is

$$\hat{H}_\mathrm{ph} = \sum_k \hbar\omega_k \hat{a}_k^\dagger \hat{a}_k, \tag{3}$$

where $\hat{a}_k^\dagger$ and $\hat{a}_k$ are the creation and annihilation operators of the probe photons with the wavevector k and frequency $\omega_k = c|k| \sim \omega_\mathrm{eg} \equiv \omega_\mathrm{e} - \omega_\mathrm{g}$. The atom interaction with the probe field is given through the minimal coupling Hamiltonian

$$\hat{H}_\mathrm{p} = -\sum_k \sum_r \hbar g_k \hat{a}_k \exp(\mathrm{i}kr)\hat{V}_\mathrm{p}^\dagger(r) + \mathrm{H.c.} \tag{4}$$

with coupling constant $\hbar g_k = \sqrt{\frac{\hbar\omega_k}{2\epsilon_0 V}}\, d_{ge}$, where d_{ge} is the effective electric dipole moment of the g → e transition, ϵ_0 is the vacuum permittivity and V is the quantization volume. The interaction of the atomic ensemble with the classical control field of the carrier frequency $\omega_\mathrm{c} \sim \omega_\mathrm{eg}$ and the wavevector k_c is of the form

$$\hat{H}_\mathrm{c}(t) = -\sum_r \hbar\Omega \exp[-\mathrm{i}(\omega_\mathrm{c}t - k_\mathrm{c}r)]\hat{V}_\mathrm{c}^\dagger(r) + \mathrm{H.c.} \tag{5}$$

For simplicity, we have used the rotating-wave approximation. In addition, for an atomic operator $\hat{A}(r)$ we define a Fourier-transformed operator $\hat{A}(k) = \sum_r \hat{A}(r)\exp(\mathrm{i}kr)/\sqrt{N}$. Note that $\left(\hat{A}(k)\right)^\dagger = \hat{A}^\dagger(-k)$. Especially, one has $\sum_r \hat{A}(r) = \sqrt{N}\hat{A}(k=0)$. In terms of the Fourier-transformed operators, various Hamiltonian parts are

$$\hat{H}_\mathrm{at} = \hbar\omega_\mathrm{g}\sqrt{N}\,\hat{\mathbb{I}}_\mathrm{g}(k=0) + \hbar\omega_\mathrm{e}\sqrt{N}\,\hat{\mathbb{I}}_\mathrm{e}(k=0), \tag{6a}$$

$$\hat{H}_\mathrm{p} = -\sum_k \hbar g_k \sqrt{N}\,\hat{a}_k \hat{V}_\mathrm{p}^\dagger(k) + \mathrm{H.c.}, \tag{6b}$$

$$\hat{H}_\mathrm{c}(t) = -\hbar\Omega\sqrt{N}\mathrm{e}^{-\mathrm{i}\omega_\mathrm{c}t}\hat{V}_\mathrm{c}^\dagger(k_\mathrm{c}) + \mathrm{H.c.} \tag{6c}$$

The entire Hamiltonian of the ensemble of degenerate two-level atoms interacting with the probe and the control field is $\hat{H}(t) = \hat{H}_\mathrm{at} + \hat{H}_\mathrm{ph} + \hat{H}_\mathrm{p} + \hat{H}_\mathrm{c}(t)$.

2.2. Dark-state polaritons

Now, we focus on the dark-state polaritons in an ensemble of degenerate two-level atoms. Various features of the method in [9], which are obvious *per se* in the case of a simple Λ system, need to be properly adapted to the degenerate two-level system. The additional complexity of the system we investigate also yields some new inherent requirements.

First of all, we remove the time dependence from the Hamiltonian $\hat{H}(t)$ by performing the following unitary gauge transformation:

$$\hat{H}_\mathrm{T} = \hat{U}_\mathrm{c}(t)\hat{H}(t)\hat{U}_\mathrm{c}^\dagger(t) - \hbar\omega_\mathrm{c}\left(\sqrt{N}\hat{\mathbb{I}}_\mathrm{e}(k=0) + \sum_k \hat{a}_k^\dagger\hat{a}_k\right), \tag{7}$$

where

$$\hat{U}_\mathrm{c}(t) = \exp\left[\mathrm{i}\omega_\mathrm{c}t\left(\sqrt{N}\,\hat{\mathbb{I}}_\mathrm{e}(k=0) + \sum_k \hat{a}_k^\dagger\hat{a}_k\right)\right]. \tag{8}$$

Eventually, we restate the time-dependent Schroedinger equation $i\hbar\partial_t|\phi(t)\rangle = \hat{H}(t)|\phi(t)\rangle$ as

$$i\hbar\,\partial_t\big[\hat{U}_c(t)|\phi(t)\rangle\big] = \hat{H}_T\big[\hat{U}_c(t)|\phi(t)\rangle\big]. \tag{9}$$

Solutions of (9) can be obtained by finding the energy eigenstates of the time-independent Hamiltonian $\hat{H}_T$.

Assume that the atomic ensemble is initially prepared in the collective vacuum state with no probe photons $|\boldsymbol{g_0}, 0\rangle = |g_0\rangle \otimes |0\rangle \equiv \otimes_r |g_0\rangle_r \otimes |0\rangle$. Analogously with the Λ system case [8, 9], the atomic ground state $|g_0\rangle$ must be dark with respect to the control field, i.e.

$$\hat{V}_c^\dagger|g_0\rangle = 0, \qquad \text{or equivalently} \qquad |g_0\rangle \in \mathcal{H}_g^d. \tag{10}$$

Additional requirements on the state $|g_0\rangle$ will be specified later.

Dark-state polaritons are particular low energy, single probe photon driven, collective excitations that do not have a contribution of the excited atomic states. To obtain DSPs, we look for a polariton excitation operator $\hat{\phi}_k^\dagger$ such that in the low energy, single excitation case $\hat{\phi}_k^\dagger|\boldsymbol{g_0}, 0\rangle$ is an eigenstate of $\hat{H}_T$ with the energy $\hbar\omega(k)$. This leads to the following relation:

$$\big[\hat{H}_T, \hat{\phi}_k^\dagger\big] = \hbar\omega(k)\hat{\phi}_k^\dagger + \cdots, \tag{11}$$

where dots represent the terms that are omitted in the single excitation case and also terms that give zero when acting on the collective vacuum state $|\boldsymbol{g_0}, 0\rangle$. Note that, for notational simplicity, we keep in mind that all subsequent commutators always act on the state $|\boldsymbol{g_0}, 0\rangle$. In agreement with [8, 9], we neglect Langevin noise effects, which do not influence the adiabatic evolution of the DSPs.

Collective atomic excitations are driven by the probe photons. Hence, we begin by calculating the commutator

$$\big[\hat{H}_T, \hat{a}_k^\dagger\big] = \hbar(\omega_k - \omega_c)\hat{a}_k^\dagger - \hbar g_k\sqrt{N}\,\hat{V}_p^\dagger(k). \tag{12}$$

The states that arise from the interaction with the probe field are the pure photon excitation $\hat{a}_k^\dagger|\boldsymbol{g_0}, 0\rangle$, and the collective atomic excitation $\hat{V}_p^\dagger(k)|\boldsymbol{g_0}, 0\rangle$, up to a normalization constant. Hence, in addition to $\hat{a}_k^\dagger$ the operator $\hat{V}_p^\dagger(k)$ is also a member of the polariton excitation operator $\hat{\phi}_k^\dagger$. Next, we determine the commutation relation

$$\begin{aligned}\big[\hat{H}_T, \hat{V}_p^\dagger(k)\big] = {}& \hbar(\omega_{eg} - \omega_c)\hat{V}_p^\dagger(k) - \hbar\Omega^*(\hat{V}_c\hat{V}_p^\dagger)(k - k_c) \\ & - \sum_{k'} \hbar g_{k'}^*\hat{a}_{k'}^\dagger(\hat{V}_p\hat{V}_p^\dagger)(k - k').\end{aligned} \tag{13}$$

Note that $\sqrt{N}\big[\hat{A}_1(k), \hat{A}_2(k')\big] = \big[\hat{A}_1, \hat{A}_2\big](k + k')$ holds for any two atomic operators $\hat{A}_1$ and $\hat{A}_2$. The new operators, $(\hat{V}_c\hat{V}_p^\dagger)(k - k_c)$ and $\hat{a}_{k'}^\dagger(\hat{V}_p\hat{V}_p^\dagger)(k - k')$, appearing in (13) yield the collective states via stimulated emission. The former can readily be included into the polariton excitation operator $\hat{\phi}_k^\dagger$. It creates the spatially dependent coherence among the atomic ground states $|g_0\rangle$ and $\hat{V}_c\hat{V}_p^\dagger|g_0\rangle$, i.e. the ground state coherence wave. When we commute the latter operator with $\hat{H}_T$, we get the operator $\hat{a}_{k''}^\dagger(\hat{V}_p\hat{V}_p^\dagger)(k - k')(\hat{V}_p\hat{V}_p^\dagger)(k' - k'')$. The emergence of such operators of increasing complexity continues and ends with $\hat{a}_{k^{(N)}}^\dagger\prod_{i=1}^N(\hat{V}_p\hat{V}_p^\dagger)(k^{(i)} - k^{(i-1)})$, where $k^{(0)} = k$. This case corresponds to a formidably complex DSP mode that is not tractable. Tractable modes are obtained by imposing one further requirement on the collective vacuum state. Namely, it is crucial that upon action $\hat{V}_p\hat{V}_p^\dagger|g_0\rangle$ we end up with the state $|g_0\rangle$, i.e.,

$$\hat{V}_p\hat{V}_p^\dagger|g_0\rangle = \lambda_p|g_0\rangle, \tag{14}$$

where $\lambda_p > 0$ is the corresponding eigenvalue. Thus, one obtains $(\hat{V}_p\hat{V}_p^\dagger)(k - k')|\boldsymbol{g_0}, 0\rangle = \lambda_p\sqrt{N}\delta_{k,k'}|\boldsymbol{g_0}, 0\rangle$, so that the relation (13) greatly simplifies to

$$\begin{aligned}\big[\hat{H}_T, \hat{V}_p^\dagger(k)\big] = {}& \hbar(\omega_{eg} - \omega_c)\hat{V}_p^\dagger(k) - \hbar\Omega^*(\hat{V}_c\hat{V}_p^\dagger)(k - k_c) \\ & - \hbar g_k^*\lambda_p\sqrt{N}\hat{a}_k^\dagger.\end{aligned} \tag{15}$$

To proceed further, we define the excited atomic state $|e\rangle = \hat{V}_p^\dagger|g_0\rangle/\sqrt{\lambda_p}$ associated with the action of the probe field. Clearly, it has the property $\hat{V}_p|e\rangle = \sqrt{\lambda_p}|g_0\rangle$ and it is an eigenstate of $\hat{V}_p^\dagger\hat{V}_p$, i.e. $\hat{V}_p^\dagger\hat{V}_p|e\rangle = \lambda_p|e\rangle$. The eigenstates $|g_0\rangle$ and $|e\rangle$ are 'tuned' to the polarization of the probe field. These are so-called polarization-dressed states, first introduced and used in [28, 29] for problems of interaction of resonant elliptically polarized light with atomic and molecular energy levels degenerate in angular momentum projections. Next, let us consider the commutators

$$\big[\hat{H}_T, (\hat{V}_c\hat{V}_p^\dagger)(k - k_c)\big] = -\hbar\Omega(\hat{V}_c^\dagger\hat{V}_c\hat{V}_p^\dagger)(k), \tag{16}$$

and also

$$\begin{aligned}\big[\hat{H}_T, (\hat{V}_c^\dagger\hat{V}_c\hat{V}_p^\dagger)(k)\big] = {}& \hbar(\omega_{eg} - \omega_c)(\hat{V}_c^\dagger\hat{V}_c\hat{V}_p^\dagger)(k) \\ & - \hbar\Omega^*(\hat{V}_c\hat{V}_c^\dagger\hat{V}_c\hat{V}_p^\dagger)(k - k_c) \\ & - \sum_{k'} \hbar g_{k'}^*\hat{a}_{k'}^\dagger(\hat{V}_p\hat{V}_c^\dagger\hat{V}_c\hat{V}_p^\dagger)(k - k').\end{aligned} \tag{17}$$

Similar to the discussion of the relation (13), in order to avoid the appearance of probe photons with all wavevectors, we require that $\hat{V}_p\hat{V}_c^\dagger\hat{V}_c\hat{V}_p^\dagger|g_0\rangle \propto |g_0\rangle$. That can hold provided that

$$\hat{V}_c^\dagger\hat{V}_c\hat{V}_p^\dagger|g_0\rangle = \lambda_c\hat{V}_p^\dagger|g_0\rangle \qquad \text{i.e. } \hat{V}_c^\dagger\hat{V}_c|e\rangle = \lambda_c|e\rangle, \tag{18}$$

where $\lambda_c > 0$ is the corresponding eigenvalue. Thus, the excited atomic state $|e\rangle$ is a common eigenstate of the operators $\hat{V}_p^\dagger\hat{V}_p$ and $\hat{V}_c^\dagger\hat{V}_c$. Under such a condition, the relation (16) becomes

$$\big[\hat{H}_T, (\hat{V}_c\hat{V}_p^\dagger)(k - k_c)\big] = -\hbar\Omega\lambda_c\hat{V}_p^\dagger(k), \tag{19}$$

while (17) turns into

$$\big[\hat{H}_T, (\hat{V}_c^\dagger\hat{V}_c\hat{V}_p^\dagger)(k)\big] = \lambda_c\big[\hat{H}_T, \hat{V}_p^\dagger(k)\big], \tag{20}$$

where the last commutator is found in (15). Hence, under the previous conditions no new components of the polariton excitation operator $\hat{\phi}_k^\dagger$ appear. Stimulated emission, which is driven by the control field, transfers the atoms from the excited state $|e\rangle$ into the ground state $|f\rangle = \hat{V}_c|e\rangle/\sqrt{\lambda_c}$. The states $|g_0\rangle$ and $|e\rangle$ are coupled by the probe field, while the states $|e\rangle$ and $|f\rangle$ are coupled by the control field. Thus, for each eigenvalue pair (λ_p, λ_c) the three states $|g_0\rangle$, $|e\rangle$ and $|f\rangle$ form

an independent Λ system that is related to one independent collective DSP mode. The number of such Λ systems, i.e. tractable DSP modes, can be at most equal to the total number of DSP modes, i.e. to the dimensionality of the dark space $\mathcal{H}_{\rm g}^{\rm d}$.

Now, we collect the necessary commutation relations

$$\left[\hat{H}_{\rm T}, \hat{a}_k^\dagger\right] = \hbar(\omega_k - \omega_{\rm c})\hat{a}_k^\dagger - \hbar g_k\sqrt{N}\hat{V}_{\rm p}^\dagger(k), \tag{21a}$$

$$\left[\hat{H}_{\rm T}, \hat{V}_{\rm p}^\dagger(k)\right] = \hbar(\omega_{\rm eg} - \omega_{\rm c})\hat{V}_{\rm p}^\dagger(k) - \hbar g_k^*\lambda_{\rm p}\sqrt{N}\hat{a}_k^\dagger - \hbar\Omega^*(\hat{V}_{\rm c}\hat{V}_{\rm p}^\dagger)(k-k_{\rm c}), \tag{21b}$$

$$\left[\hat{H}_{\rm T}, (\hat{V}_{\rm c}\hat{V}_{\rm p}^\dagger)(k-k_{\rm c})\right] = -\hbar\Omega\lambda_{\rm c}\hat{V}_{\rm p}^\dagger(k), \tag{21c}$$

so that the polariton excitation operator is of the form

$$\hat{\phi}_{nk}^\dagger = \alpha_{nk}\hat{a}_k^\dagger + \beta_{nk}\frac{\hat{V}_{\rm p}^\dagger(k)}{\sqrt{\lambda_{\rm p}}} + \gamma_{nk}\frac{(\hat{V}_{\rm c}\hat{V}_{\rm p}^\dagger)(k-k_{\rm c})}{\sqrt{\lambda_{\rm p}\lambda_{\rm c}}}, \tag{22}$$

where the band index n enumerates the different polariton species. Orthonormal collective excitations $|\boldsymbol{g_0}, 1_k\rangle$, $|\boldsymbol{e}(k), 0\rangle$ and $|\boldsymbol{f}(k-k_{\rm c}), 0\rangle$ result from the action of the operators $\hat{a}_k^\dagger$, $\hat{V}_{\rm p}^\dagger(k)/\sqrt{\lambda_{\rm p}}$ and $(\hat{V}_{\rm c}\hat{V}_{\rm p}^\dagger)(k-k_{\rm c})/\sqrt{\lambda_{\rm p}\lambda_{\rm c}}$ on the collective vacuum state $|\boldsymbol{g_0}, 0\rangle$, respectively,

$$|\boldsymbol{g_0}, 1_k\rangle = \bigotimes_r |g_0\rangle_r \otimes |1_k\rangle, \tag{23a}$$

$$|\boldsymbol{e}(k), 0\rangle = \frac{1}{\sqrt{N}}\sum_r \mathrm{e}^{\mathrm{i}kr}|e\rangle_r \bigotimes_{r'\neq r} |g_0\rangle_{r'} \otimes |0\rangle, \tag{23b}$$

$$|\boldsymbol{f}(k-k_{\rm c}), 0\rangle = \frac{1}{\sqrt{N}}\sum_r \mathrm{e}^{\mathrm{i}(k-k_{\rm c})r}|f\rangle_r \bigotimes_{r'\neq r} |g_0\rangle_{r'} \otimes |0\rangle. \tag{23c}$$

Note that the collective states $|\boldsymbol{e}(k), 0\rangle$ and $|\boldsymbol{f}(k-k_{\rm c}), 0\rangle$ are entangled. This enables the usage of the polariton state

$$|\phi_{nk}\rangle = \alpha_{nk}|\boldsymbol{g_0}, 1_k\rangle + \beta_{nk}|\boldsymbol{e}(k), 0\rangle + \gamma_{nk}|\boldsymbol{f}(k-k_{\rm c}), 0\rangle \tag{24}$$

as a resource for quantum information processing [2].

We determine the c-numbers α_{nk}, β_{nk} and γ_{nk} by inserting (22) into (11) and make use of (21). This leads to three self-consistency equations that we can represent in the basis $\{|\boldsymbol{g_0}, 1_k\rangle, |\boldsymbol{e}(k), 0\rangle, |\boldsymbol{f}(k-k_{\rm c}), 0\rangle\}$ as

$$\begin{bmatrix} \omega_k - \omega_{\rm c} & -\widetilde{g}_k^*\sqrt{N} & 0 \\ -\widetilde{g}_k\sqrt{N} & \omega_{\rm eg} - \omega_{\rm c} & -\widetilde{\Omega} \\ 0 & -\widetilde{\Omega}^* & 0 \end{bmatrix} \begin{bmatrix} \alpha_{nk} \\ \beta_{nk} \\ \gamma_{nk} \end{bmatrix} = \omega_n(k) \begin{bmatrix} \alpha_{nk} \\ \beta_{nk} \\ \gamma_{nk} \end{bmatrix}, \tag{25}$$

where $\widetilde{g}_k = g_k\sqrt{\lambda_{\rm p}}$ and $\widetilde{\Omega} = \Omega\sqrt{\lambda_{\rm c}}$. Our effective Hamiltonian in (25) is similar to the one in [9], but with a major difference. The effective coupling constant $\widetilde{g}_k$ and the effective Rabi frequency $\widetilde{\Omega}$ differ from the corresponding one in [9] because of the inclusion of the eigenvalues $\lambda_{\rm p}$ and $\lambda_{\rm c}$. The mentioned difference clearly arises as a consequence of the degenerate two-level atomic system.

The dark-state polaritons are obtained as one of the solutions of the eigenproblem (25). The other two solutions are bright-state polaritons, similarly as in [9]. Exactly at the Raman resonance, $\omega_k = \omega_{\rm c}$, there is an eigenvector $\propto \left[-\frac{\widetilde{\Omega}}{\widetilde{g}_k\sqrt{N}}, 0, 1\right]$. This eigenvector has no contribution of the excited atomic states and represents a stable dark-state polariton that is insensitive to incoherent decay processes acting on the excited atoms. Expansion around the resonance $\omega_k \sim \omega_{\rm eg}$ and $\omega_{\rm c} \sim \omega_{\rm eg}$ yields a linearized solution for the dark-state polaritons

$$\omega(k) = \frac{|\widetilde{\Omega}|^2}{|\widetilde{g}_k|^2 N + |\widetilde{\Omega}|^2}(\omega_k - \omega_{\rm c}), \tag{26a}$$

$$\alpha_k = -\frac{\widetilde{\Omega}}{\widetilde{g}_k\sqrt{N}}\gamma_k, \qquad \beta_k = -\frac{\widetilde{\Omega}(\omega_k - \omega_{\rm c})}{|\widetilde{g}_k|^2 N + |\widetilde{\Omega}|^2}\gamma_k. \tag{26b}$$

An interesting property of the DSP solution is that it only depends on the Raman detuning $\omega_k - \omega_{\rm c}$ of the coupling fields and on the coupling parameters $\widetilde{g}_k$ and $\widetilde{\Omega}$. It does not depend on the energy spacing $\omega_{\rm eg}$ of the underlying degenerate two-level system.

The algorithm for finding tractable DSP modes in a degenerate two-level system can be summarized as:

(1) determine the dark space $\mathcal{H}_{\rm g}^{\rm d}$ for the operator $\hat{V}_{\rm c}^\dagger$;
(2) find all states $|g_0\rangle$ from $\mathcal{H}_{\rm g}^{\rm d}$ and pairs of eigenvalues $(\lambda_{\rm p}, \lambda_{\rm c})$ such that $\hat{V}_{\rm p}\hat{V}_{\rm p}^\dagger|g_0\rangle = \lambda_{\rm p}|g_0\rangle$ and $\hat{V}_{\rm c}^\dagger\hat{V}_{\rm c}\hat{V}_{\rm p}^\dagger|g_0\rangle = \lambda_{\rm c}\hat{V}_{\rm p}^\dagger|g_0\rangle$ hold;
(3) for every such pair of eigenvalues obtain DSPs $|\psi_k(\lambda_{\rm p}, \lambda_{\rm c})\rangle$ from (24) and (26).

3. Dark-state polaritons in rubidium vapor

In this section we apply the general formalism to the rubidium vapor. Control and probe fields couple the hyperfine levels $5S_{1/2}, F_{\rm g} = 2$ and $5P_{1/2}, F_{\rm e} = 1$ of ^{87}Rb. The atomic lowering operators of the control and probe fields are, respectively,

$$\hat{V}_{\rm c} = \hat{\mathbf{V}}\cdot\mathbf{e}_{\rm c}, \qquad \hat{V}_{\rm p} = \hat{\mathbf{V}}\cdot\mathbf{e}_{\rm p}, \tag{27}$$

where $\mathbf{e}_{\rm c}$ and $\mathbf{e}_{\rm p}$ are polarizations of the fields. The vector operator $\hat{\mathbf{V}}$ is defined by [28, 30, 31]

$$\hat{\mathbf{V}} = (-1)^{F_{\rm e}+J_{\rm g}+I+1}\sqrt{(2F_{\rm e}+1)(2J_{\rm g}+1)}\begin{Bmatrix} J_{\rm e} & J_{\rm g} & 1 \\ F_{\rm g} & F_{\rm e} & I \end{Bmatrix} \times \sum_{q=-1}^{1}\sum_{m_{\rm g},m_{\rm e}} \langle F_{\rm g}, m_{\rm g}|F_{\rm e}, m_{\rm e}; 1, q\rangle |F_{\rm g}, m_{\rm g}\rangle\langle F_{\rm e}, m_{\rm e}|\mathbf{e}_q^*, \tag{28}$$

where $I = 3/2$ is the nuclear quantum number of ^{87}Rb, $\{:::\}$ is the Wigner $6j$-symbol and $\langle F_{\rm g}, m_{\rm g}|F_{\rm e}, m_{\rm e}; 1, q\rangle$ is the Clebsch–Gordan coefficient that connects the excited level state $|F_{\rm e}, m_{\rm e}\rangle$ to the ground level state $|F_{\rm g}, m_{\rm g}\rangle$ via polarization $\mathbf{e}_q^*$,

$$\mathbf{e}_{\pm1} = \mp\frac{1}{\sqrt{2}}(\mathbf{e}_x \pm \mathrm{i}\,\mathbf{e}_y), \qquad \mathbf{e}_0 = \mathbf{e}_z, \tag{29}$$

given in some orthonormal basis of polarization vectors. We choose the coordinate system such that the fields propagate along the z axis, and define a basis of Zeeman states relative to this quantization axis. The bases of the individual Hilbert spaces $\mathcal{H}_{\rm e}$ and $\mathcal{H}_{\rm g}$ are

$$\mathcal{E} = \{|1, -1\rangle_{\rm e}, |1, 0\rangle_{\rm e}, |1, 1\rangle_{\rm e}\}, \tag{30a}$$

$$\mathcal{G} = \{|2, -2\rangle_{\rm g}, |2, -1\rangle_{\rm g}, |2, 0\rangle_{\rm g}, |2, 1\rangle_{\rm g}, |2, 2\rangle_{\rm g}\}. \tag{30b}$$

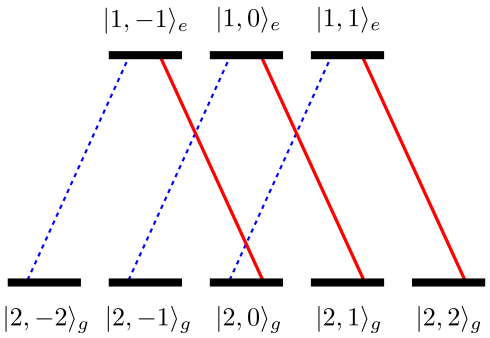

Figure 2. Zeeman sublevel scheme of the transition $F_g = 2 \to F_e = 1$ at the D_1 line of ^{87}Rb. Solid lines denote σ^- transitions coupled by the control field while dashed lines denote σ^+ transitions coupled by the probe field.

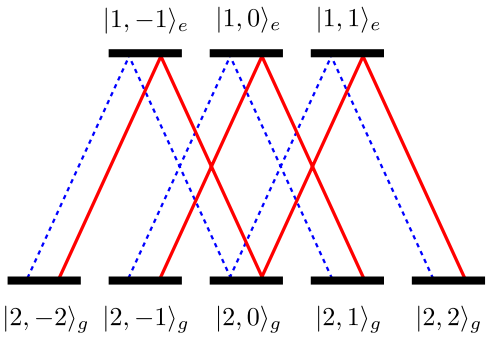

Figure 3. Zeeman sublevel scheme of the transition $F_g = 2 \to F_e = 1$ at the D_1 line of ^{87}Rb. Solid lines denote control field linearly polarized along the y axis while dashed lines denote probe field linearly polarized along the x axis.

We will show that according to the appropriate choice of the polarizations of the coupling fields, one or two DSP modes can be obtained.

3.1. Case of orthogonal circular polarizations

Let the control field couple σ^- transitions, while the probe field couples σ^+ transitions, i.e. $\mathbf{e}_c = \mathbf{e}_{+1}$ and $\mathbf{e}_p = \mathbf{e}_{-1}$ (see figure 2). The lowering operators of the coupling fields, $\hat{V}_c$ and $\hat{V}_p$, are represented in the basis $\mathcal{E} \cup \mathcal{G}$ with the matrices

$$\mathbf{V}_c = \begin{bmatrix} & \mathbf{0}_{3,3} & & \mathbf{0}_{3,5} \\ 0 & 0 & 0 & \\ 0 & 0 & 0 & \\ \frac{1}{2\sqrt{3}} & 0 & 0 & \mathbf{0}_{5,5} \\ 0 & \frac{1}{2} & 0 & \\ 0 & 0 & \frac{1}{\sqrt{2}} & \end{bmatrix}, \tag{31a}$$

$$\mathbf{V}_p = \begin{bmatrix} & \mathbf{0}_{3,3} & & \mathbf{0}_{3,5} \\ \frac{1}{\sqrt{2}} & 0 & 0 & \\ 0 & \frac{1}{2} & 0 & \\ 0 & 0 & \frac{1}{2\sqrt{3}} & \mathbf{0}_{5,5} \\ 0 & 0 & 0 & \\ 0 & 0 & 0 & \end{bmatrix}, \tag{31b}$$

where zeros $\mathbf{0}_{m,n}$ denote rectangular $m \times n$ null matrices. Ground level dark space determined from the null space of $\mathbf{V}_c^\dagger$ is

$$\mathcal{H}_g^d = \{|2,-2\rangle_g, |2,-1\rangle_g\}. \tag{32}$$

Both dark states are appropriate as the initial state $|g_0\rangle$. Below we tabulate the corresponding states and eigenvalues of the Λ system:

	$\lvert g_0\rangle$	$\lvert e\rangle$	$\lvert f\rangle$	λ_p	λ_c
I	$\lvert 2,-2\rangle_g$	$\lvert 1,-1\rangle_e$	$\lvert 2,0\rangle_g$	1/2	1/12
II	$\lvert 2,-1\rangle_g$	$\lvert 1,0\rangle_e$	$\lvert 2,1\rangle_g$	1/4	1/4,

that lead to two DSP modes:

$$\omega^I(k) = \frac{|\Omega|^2}{6\,|g_k|^2 N + |\Omega|^2}(\omega_k - \omega_c), \tag{33a}$$

$$|\psi_k^I\rangle \propto -\frac{\Omega}{\sqrt{6}\,g_k\sqrt{N}}|\boldsymbol{g}_0^I, 1_k\rangle + |\boldsymbol{f}^I(k-k_c), 0\rangle - \frac{2\sqrt{3}\,\Omega\,(\omega_k - \omega_c)}{6\,|g_k|^2 N + |\Omega|^2}|\boldsymbol{e}^I(k), 0\rangle, \tag{33b}$$

$$\omega^{II}(k) = \frac{|\Omega|^2}{|g_k|^2 N + |\Omega|^2}(\omega_k - \omega_c), \tag{34a}$$

$$|\psi_k^{II}\rangle \propto -\frac{\Omega}{g_k\sqrt{N}}|\boldsymbol{g}_0^{II}, 1_k\rangle + |\boldsymbol{f}^{II}(k-k_c), 0\rangle - \frac{2\,\Omega\,(\omega_k - \omega_c)}{|g_k|^2 N + |\Omega|^2}|\boldsymbol{e}^{II}(k), 0\rangle. \tag{34b}$$

We see that for orthogonal circular polarizations of the coupling fields, the maximal number of tractable DSP modes exists. This is the generic case, because relevant independent Λ system(s) can be easily recognized.

3.2. Case of orthogonal linear polarizations

Now we analyze the case of the control field polarization along the y axis and the probe field polarization along the x axis, i.e. $\mathbf{e}_c = \mathbf{e}_y$ and $\mathbf{e}_p = \mathbf{e}_x$ (see figure 3). The matrices representing the atomic lowering operators $\hat{V}_c$ and $\hat{V}_p$ in the basis $\mathcal{E} \cup \mathcal{G}$ are

$$\mathbf{V}_c = i\begin{bmatrix} & \mathbf{0}_{3,3} & & \mathbf{0}_{3,5} \\ \frac{1}{2} & 0 & 0 & \\ 0 & \frac{1}{2\sqrt{2}} & 0 & \\ \frac{1}{2\sqrt{6}} & 0 & \frac{1}{2\sqrt{6}} & \mathbf{0}_{5,5} \\ 0 & \frac{1}{2\sqrt{2}} & 0 & \\ 0 & 0 & \frac{1}{2} & \end{bmatrix}, \tag{35a}$$

$$\mathbf{V}_{\rm p} = \begin{bmatrix} & \mathbf{0}_{3,3} & & \mathbf{0}_{3,5} \\ \frac{1}{2} & 0 & 0 & \\ 0 & \frac{1}{2\sqrt{2}} & 0 & \\ -\frac{1}{2\sqrt{6}} & 0 & \frac{1}{2\sqrt{6}} & \mathbf{0}_{5,5} \\ 0 & -\frac{1}{2\sqrt{2}} & 0 & \\ 0 & 0 & -\frac{1}{2} & \end{bmatrix}. \tag{35b}$$

In this case, the ground level dark space is

$$\mathcal{H}_{\rm g}^{\rm d} = \left\{ -\frac{1}{\sqrt{2}}|2,-1\rangle_{\rm g} + \frac{1}{\sqrt{2}}|2,1\rangle_{\rm g}, \right.$$
$$\left. \frac{1}{\sqrt{8}}|2,-2\rangle_{\rm g} - \frac{\sqrt{3}}{2}|2,0\rangle_{\rm g} + \frac{1}{\sqrt{8}}|2,2\rangle_{\rm g}, \right\}, \tag{36}$$

but only the first dark state satisfies all necessary conditions for the vacuum state of the tractable mode. The states and eigenvalues of the corresponding Λ system are

$$\begin{aligned} |g_0\rangle &= -\frac{1}{\sqrt{2}}|2,-1\rangle_{\rm g} + \frac{1}{\sqrt{2}}|2,1\rangle_{\rm g}, \\ |e\rangle &= |1,0\rangle_{\rm e}, \\ |f\rangle &= \frac{1}{\sqrt{2}}|2,-1\rangle_{\rm g} + \frac{1}{\sqrt{2}}|2,1\rangle_{\rm g}, \\ \lambda_{\rm p} &= 1/4, \qquad \lambda_{\rm c} = 1/4. \end{aligned} \tag{37a}$$

We identify one DSP mode

$$\omega(k) = \frac{|\Omega|^2}{|g_k|^2 N + |\Omega|^2}(\omega_k - \omega_{\rm c}), \tag{38a}$$

$$|\psi_k\rangle \propto -\frac{\Omega}{g_k\sqrt{N}}|\boldsymbol{g}_0, 1_k\rangle + |\boldsymbol{f}(k-k_{\rm c}), 0\rangle$$
$$-\frac{2\,\Omega(\omega_k-\omega_{\rm c})}{|g_k|^2 N + |\Omega|^2}|\boldsymbol{e}(k), 0\rangle, \tag{38b}$$

while the other one is non-tractable.

From the above examples, it can be seen that the choice of the polarization of the coupling fields yields entirely different DSP modes. This is reflected in the composition of the DSP state as well as in the polariton dispersion relation. Note that different polariton dispersion relations would lead to distinct slow light group velocities. In section 4 we outline one possible application of DSP modes in degenerate two-level systems for frequency and/or linear polarization conversion.

4. Frequency and polarization conversion

Let us consider the DSP modes that can be formed from the states within $5S_{1/2}, F_{\rm g} = 1$ hyperfine level of ^{87}Rb atoms, when the control and the probe field have orthogonal linear polarizations. There are three relevant atomic transitions:

(a) $5S_{1/2},\ F_{\rm g} = 1 \rightarrow 5P_{1/2},\ F_{\rm e} = 1,$
(b) $5S_{1/2},\ F_{\rm g} = 1 \rightarrow 5P_{3/2},\ F_{\rm e} = 1,$
(c) $5S_{1/2},\ F_{\rm g} = 1 \rightarrow 5P_{3/2},\ F_{\rm e} = 0.$

The first belongs to the D_1 line. The last two belong to the D_2 line and can be rendered non-overlapping by using ultracold rubidium atoms.

In the case of orthogonal linear polarizations $\mathbf{e}_{\rm c} = \mathbf{e}_x$ and $\mathbf{e}_{\rm p} = \mathbf{e}_y$ of the fields that are resonant to the D_1 line transition (a), we have

$$\begin{aligned} |g_0\rangle &= -\frac{1}{\sqrt{2}}|1,-1\rangle_{\rm g} + \frac{1}{\sqrt{2}}|1,1\rangle_{\rm g}, \\ |e\rangle &= |1,0\rangle_{\rm e}, \\ |f\rangle &= \frac{1}{\sqrt{2}}|1,-1\rangle_{\rm g} + \frac{1}{\sqrt{2}}|1,1\rangle_{\rm g}, \\ \lambda_{\rm p} &= 1/12, \qquad \lambda_{\rm c} = 1/12. \end{aligned} \tag{39a}$$

When considering the D_2 line transition (b) with the same polarizations of the coupling fields as in the previous case, $\mathbf{e}_{\rm c} = \mathbf{e}_x$ and $\mathbf{e}_{\rm p} = \mathbf{e}_y$, we find

$$\begin{aligned} |g_0\rangle &= -\frac{1}{\sqrt{2}}|1,-1\rangle_{\rm g} + \frac{1}{\sqrt{2}}|1,1\rangle_{\rm g}, \\ |e\rangle &= |1,0\rangle_{\rm e}, \\ |f\rangle &= \frac{1}{\sqrt{2}}|1,-1\rangle_{\rm g} + \frac{1}{\sqrt{2}}|1,1\rangle_{\rm g}, \\ \lambda_{\rm p} &= 5/24, \qquad \lambda_{\rm c} = 5/24. \end{aligned} \tag{40a}$$

Finally, for the *swapped linear polarizations*, $\mathbf{e}_{\rm c} = \mathbf{e}_y$ and $\mathbf{e}_{\rm p} = \mathbf{e}_x$, of the fields coupling the D_2 line transition (c), we have

$$\begin{aligned} |g_0\rangle &= -\frac{1}{\sqrt{2}}|1,-1\rangle_{\rm g} + \frac{1}{\sqrt{2}}|1,1\rangle_{\rm g}, \\ |e\rangle &= |0,0\rangle_{\rm e}, \\ |f\rangle &= \frac{1}{\sqrt{2}}|1,-1\rangle_{\rm g} + \frac{1}{\sqrt{2}}|1,1\rangle_{\rm g}, \\ \lambda_{\rm p} &= 1/6, \qquad \lambda_{\rm c} = 1/6. \end{aligned} \tag{41a}$$

Note, if the polarizations of the fields had not been swapped, the states $|g_0\rangle$ and $|f\rangle$ would have been interchanged.

As can be seen from (39) to (41), the DSP modes are formed from the same states $|g_0\rangle$ and $|f\rangle$ in all three cases, but the considered transitions and polarizations of the coupling fields are different. This provides the possibility for frequency [32, 18] and/or polarization conversion [33] of linearly polarized light. First, one can store a pulse of the probe light polarized along the y axis into the atomic coherence among the states $|g_0\rangle$ and $|f\rangle$ using the transition (a) and the control field polarized along the x axis. The retrieval process, using the transition (b) and the control field polarized along the x axis, would release the pulse at a different frequency, but of the same optical quantum state and polarization along the y axis as the original probe pulse. However, the pulse retrieved using the transition (c) and the control field polarized along the y axis would be in the same optical quantum state as the original probe pulse, but of different carrier frequency and linear polarization along the x axis, i.e. *orthogonal to the original one*. Moreover, this realization does not suffer from losses in the retrieved pulse, since the ratios of the probe and control Clebsch–Gordan coefficients are the same among all three transitions [33].

5. Conclusion

To sum up, we have investigated the formation of dark-state polaritons in an ensemble of degenerate two-level atoms with ground state Hilbert space $\mathcal{H}_g$ and excited state Hilbert space $\mathcal{H}_e$, where $\dim \mathcal{H}_g \geq \dim \mathcal{H}_e$ holds. We elaborated an algorithm, which is a generalization of the Sawada–Brout–Chong approach [9, 25]. Under suitable conditions, the polariton mode dispersion relation and composition can be stated in a closed form. Such DSPs do not depend on the energy spacing of the two-level system, but rather on the Raman detuning of the coupling fields. For each polariton mode, the effective field coupling parameters depend on the appropriate eigenvalues of the atomic operators $\hat{V}_p^\dagger \hat{V}_p$ and $\hat{V}_c^\dagger \hat{V}_c$ that determine the eigenproblem for the polariton species. The application of the general procedure is given for ^{87}Rb atomic transition $F_g = 2 \rightarrow F_e = 1$ of the D_1 line. Two cases of polarizations of the control and probe field are analyzed, when the two fields have orthogonal circular polarizations and when both are linearly polarized in the orthogonal directions. In the former case, two DSP modes are identified, while in the latter case, only one DSP mode can be determined. The formation of the modes as well as their dispersion relation critically depend on the polarizations chosen. Possible application of DSP modes in ultracold ^{87}Rb atoms for frequency and/or linear polarization conversion without losses in the retrieved pulse is presented. Our algorithm can be extended to degenerate systems with more levels and might have applications in quantum information processing as a building block for a preparation and read out schemes with the DSPs as qubit states.

Acknowledgments

This work was supported by the Ministry of Education and Science of the Republic of Serbia, under Grants Nos III45016 and OI171038 and also by Scopes JRP IZ7370_127942.

References

[1] Boller K J, Imamoglu A and Harris S E 1991 *Phys. Rev. Lett.* **66** 2593
[2] Fleischhauer M, Imamoğlu A and Marangos J P 2005 *Rev. Mod. Phys.* **77** 633
[3] Kasapi A, Jain M, Yin G Y and Harris S E 1995 *Phys. Rev. Lett.* **74** 2447
Schmidt O, Wynands R, Hussein Z and Meschede D 1996 *Phys. Rev.* A **53** R27
Kash M M, Sautenkov V A, Zibrov A S, Hollberg L, Welch G R, Lukin M D, Rostovtsev Y, Fry E S and Scully M O 1999 *Phys. Rev. Lett.* **82** 5229
Budker D, Kimball D F, Rochester S M and Yashchuk V V 1999 *Phys. Rev. Lett.* **83** 1767
Hau L V, Harris S E, Dutton Z and Behroozi C H 1999 *Nature* **397** 594
Liu C, Dutton Z, Behroozi C H and Hau L V 2001 *Nature* **409** 490
Karpa L and Weitz M 2006 *Nature Phys.* **2** 332
Novikova I, Phillips D F and Walsworth R L 2007 *Phys. Rev. Lett.* **99** 173604
[4] Phillips D F, Fleischhauer A, Mair A, Walsworth R L and Lukin M D 2001 *Phys. Rev. Lett.* **86** 783
Kocharovskaya O, Rostovtsev Y and Scully M O 2001 *Phys. Rev. Lett.* **86** 628
Gao H, Rosenberry M and Batelaan H 2003 *Phys. Rev.* A **67** 053807
Gorshkov A V, Andre A, Fleischhauer M, Sorensen A S and Lukin M D 2007 *Phys. Rev. Lett.* **98** 123601
Novikova I, Gorshkov A V, Phillips D F, Sorensen A D, Lukin M D and Walsworth R L 2007 *Phys. Rev. Lett.* **98** 243602
Hockel D and Benson O 2010 *Phys. Rev. Lett.* **105** 153605
[5] Bajcsy M, Zibrov A S and Lukin M D 2003 *Nature* **426** 638
Andre A, Bajcsy M, Zibrov A S and Lukin M D 2005 *Phys. Rev. Lett.* **94** 063902
Lin Y W, Liao W T, Peters T, Chou H C, Wang J S, Cho H W, Kuan P C and Yu I A 2009 *Phys. Rev. Lett.* **102** 213601
Chen Y H, Lee M J, Hung W, Chen Y C, Chen Y F and Yu I A 2012 *Phys. Rev. Lett.* **108** 173603
[6] Mazets I E and Matisov B G 1996 *JETP Lett.* **64** 515
[7] Fleischhauer M and Lukin M D 2000 *Phys. Rev. Lett.* **84** 5094
[8] Fleischhauer M and Lukin M D 2002 *Phys. Rev.* A **65** 022314
[9] Chong Y D and Soljacic M 2008 *Phys. Rev.* A **77** 013823
[10] Liu X J, Jing H, Zhou X T and Ge M L 2004 *Phys. Rev.* A **70** 015603
[11] Liu Z J, Yan W B and Zhou L 2010 *Eur. Phys. J.* D **57** 111
[12] Zimmer F E, Otterbach J, Unanyan R G, Shore B W and Fleischhauer M 2008 *Phys. Rev.* A **77** 063823
[13] Joshi A and Xiao M 2005 *Phys. Rev.* A **71** 041801
[14] Li Y, Zhang P, Zanardi P and Sun C P 2004 *Phys. Rev.* A **70** 032330
[15] Ruseckas J, Mekys A and Juzeliunas G 2011 *Phys. Rev.* A **83** 023812
[16] Li P, Gu Y, Wang K and Gong Q 2006 *Phys. Rev.* A **73** 032343
[17] Li Y, Zheng L, Liu Y X and Sun C P 2006 *Phys. Rev.* A **73** 043805
[18] Appel J, Marzlin K P and Lvovsky A I 2006 *Phys. Rev.* A **73** 013804
[19] Liu X J, Liu X, Liu Z X, Kwek L C and Oh C H 2007 *Phys. Rev.* A **75** 023809
[20] Jenkins S D, Matsukevich D N, Chaneliere T, Kuzmich A and Kennedy T A B 2006 *Phys. Rev.* A **73** 021803
[21] Karpa L, Vewinger F and Weitz M 2008 *Phys. Rev. Lett.* **101** 170406
[22] Wang L R, Zhao Y T, Ma J, Zhao J M, Xiao L T and Jia S T 2006 *Chin. Phys.* **15** 365
[23] Morris J R and Shore B W 1983 *Phys. Rev.* A **27** 906
[24] Juzeliunas G and Carmichael H J 2002 *Phys. Rev.* A **65** 021601
[25] Sawada K 1957 *Phys. Rev.* **106** 372
[26] Kulshin A M, Barreiro S and Lezama A 1998 *Phys. Rev.* A **57** 2996
Lezama A, Barreiro S, Lipsich A and Akulshin A M 1999 *Phys. Rev.* A **61** 013801
Lipsich A, Barreiro S, Akulshin A M and Lezama A 2000 *Phys. Rev.* A **61** 053803
[27] Taichenachev A V, Tumaikin A M and Yudin V I 2000 *Zh. Eksp. Teor. Fiz.* **118** 77
Taichenachev A V, Tumaikin A M and Yudin V I 2000 *JETP* **91** 67
[28] Taichenachev A V, Tumaikin A M, Yudin V I and Nienhuis G 2004 *Phys. Rev.* A **69** 033410
[29] Prudnikov O N, Taichenachev A V, Tumaikin A M, Yudin V I and Nienhuis G 2004 *Zh. Eksp. Teor. Fiz.* **126** 1303
Prudnikov O N, Taichenachev A V, Tumaikin A M, Yudin V I and Nienhuis G 2004 *JETP* **99** 1137–49
[30] Radonjić M and Jelenković B M 2009 *Phys. Rev.* A **80** 043416
[31] Steck D A 2012 *Quantum and Atom Optics* (http://steck.us/teaching)
[32] Zibrov A S, Matsko A B, Kocharovskaya O, Rostovtsev Y V, Welch G R and Scully M O 2002 *Phys. Rev. Lett.* **88** 103601
Wang B, Li S, Wu H, Chang H, Wang H and Xiao M 2005 *Phys. Rev.* A **72** 043801
[33] Chen Y F, Kuan P C, Wang S H, Wang C Y and Yu I A 2006 *Opt. Lett.* **31** 3511
Guan P C, Chen Y F and Yu I A 2007 *Phys. Rev.* A **75** 013812

J. Phys. B: At. Mol. Opt. Phys. **46** (2013) 175501 (8pp) doi:10.1088/0953-4075/46/17/175501

Influence of a laser beam radial intensity distribution on Zeeman electromagnetically induced transparency line-shapes in the vacuum Rb cell

S M Ćuk, A J Krmpot, M Radonjić, S N Nikolić and B M Jelenković

Institute of Physics, University of Belgrade, Pregrevica 118, 11080 Belgrade, Serbia

E-mail: krmpot@ipb.ac.rs

Received 15 April 2013, in final form 5 July 2013
Published 5 August 2013
Online at stacks.iop.org/JPhysB/46/175501

Abstract

Experimental and theoretical analyses show the effect of laser beam radial intensity distribution on line-shapes and line-widths of the electromagnetically induced transparency (EIT). We used Gaussian and Π (flat top) laser beam profiles, coupling the D_1 transition of ^{87}Rb atoms in the vacuum cell in the Hanle experimental configuration. We obtained non-Lorentzian EIT line-shapes for a Gaussian laser beam, while line-shapes for a Π laser beam profile are very well approximated with Lorentzian. EIT line-widths, lower for Gaussian than for Π, show nonlinear dependence on laser intensity for both laser beam profiles. EIT amplitudes have similar values and dependence on laser intensity for both laser beams, showing the maximum at around 0.8 mW cm^{-2}. Differences between the EIT line-shapes for the two profiles are mainly due to distinct physical processes governing atomic evolution in the rim of the laser beam, as suggested from the EIT obtained from the various segments of the laser beam cross-section.

(Some figures may appear in colour only in the online journal)

1. Introduction

Electromagnetically induced transparency (EIT) [1–3], an effect causing the narrow coherent resonance in a laser transmission through the atomic vapour media, is essential for subjects like slow light and storage of light [4], lasing without inversion [5], frequency mixing [6], Kerr nonlinearities [7], etc. The importance of EIT has become evident after several recent applications, including the development of atomic frequency standards [8, 9] and magnetometers [10, 11]. Prior to EIT, magneto-optical effects, like the ground-state Hanle effect and nonlinear Faraday effect, were studied and their possible application in extremely low magnetic field measurements was shown [12–15]. EIT resonance line-shape and line-width are of interest for many EIT applications. EIT line-shape in alkali vapours contained in gas cells is altered from the fundamental Lorentzian shape of atomic resonances by several factors. In addition to power broadening, thermal motion of atoms in vacuum cells affects the shape of EIT resonance through a transient evolution of the state of the atoms passing through the laser beam [16–18]. The investigation of the temporal evolution of the optical pumping into a dark state in an atomic beam, with special attention given to the influence of the weak external magnetic field, has been performed in [19]. Studies of EIT dependence on laser beam radius [20], laser intensity [21, 22] and radial profile of the laser intensity [16, 23–26] were performed. Recent experiments have shown effects of different laser modes i.e. a Laguerre–Gaussian laser beam gave narrower EIT than a Gaussian laser beam [27]. In buffer gas cells, filled with a mixture of alkali atoms and inert gas at several Torr, EIT line-shapes are influenced by diffusion of the alkali atoms in and out of a laser beam. Such repeated interaction effectively enables Ramsey-induced narrowing and non-Lorentzian EIT line-shape in media where Doppler

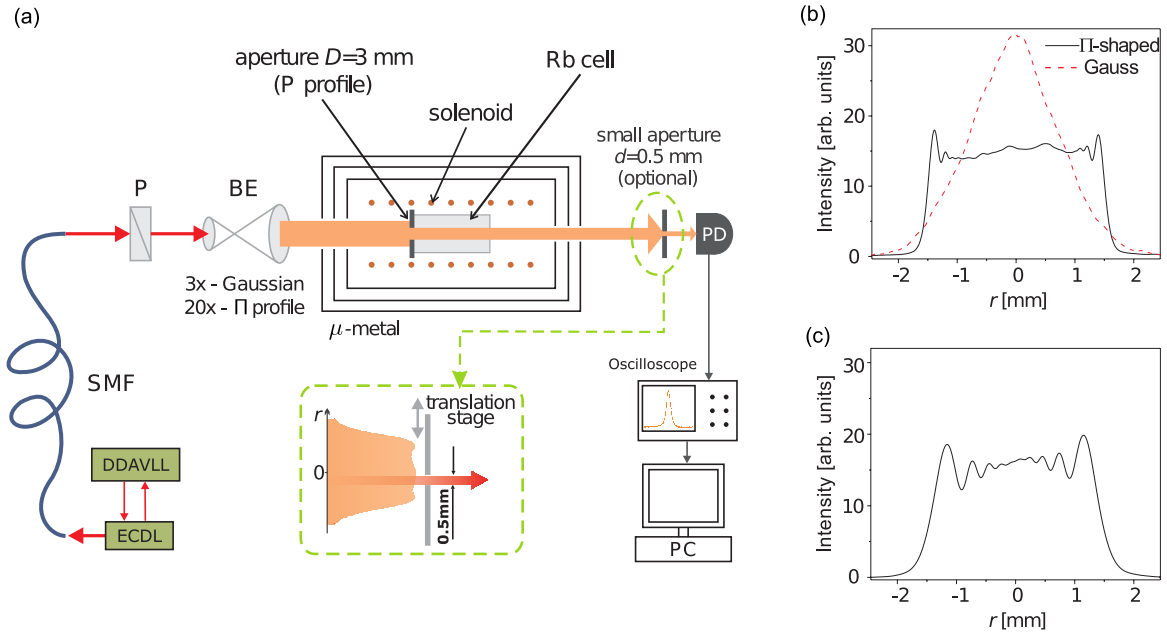

Figure 1. (a) Experimental setup: ECDL—external cavity diode laser; DDAVLL—Doppler-free dichroic atomic vapour laser lock; SMF—single-mode fiber; P—polarizer; BE—beam expander; PD—large area photo diode. For certain measurements the small aperture on the translation stage is placed in the laser beam allowing only a selected part of the laser beam cross-section to reach the detector, while the rest of the laser beam is blocked. Π-shaped beam profiles were recorded by a beam profiler placed at 3 cm (b) and 30 cm (c) from the 3 mm circular aperture. (b) The dashed (red) curve is the profile of the Gaussian laser beam of the same power and diameter as the Π-shaped beam. Note that, in order to have the same overall power of the two laser beams, the peak of the Gaussian beam in the present graph has to have double the value of the flat region of the Π-shaped beam if the diameter of the Gaussian beam is measured at $1/e^2$ of the peak intensity.

broadening is not influential (see [28, 29] and references therein).

Theoretical studies of EIT line-shapes in vacuum cells were mainly carried out assuming a Π (flat top) function for the radial intensity distribution of the laser radiation (see [21] and references therein). Measurements of the EIT line-width as a function of the laser intensity [22], performed with the Gaussian laser beam, show different EIT behaviour with laser intensity than theory [21]— theory predicts wider EIT resonances than experiment, with the discrepancy increasing with the laser intensity. The importance of the laser beam profile on the EIT was indeed demonstrated theoretically for the vacuum [26] and the buffer gas cells [23–25]. Our previous studies have shown that the evolution of the states of the atoms passing through laser beams of different profiles is governed by distinct physical processes [17, 18]. Consequently, line-shapes of EIT resonances obtained from various segments of the laser beam cross-section reflect these differences. It is expected that line-shapes of EIT resonances obtained by detecting whole laser beams of different profiles should also present distinct properties. However, there are no detailed investigations of this kind for vacuum alkali-metal vapour cells. In this work we confirm that the mentioned difference in physical processes significantly affects the overall EIT resonance line-shapes. Besides the results of [17, 18], here we take into account relative amplitudes of EIT resonances from various segments of the laser beam cross-section. The goal of this work is to show how laser intensity affects: (a) differences between the whole beam EIT resonances that are obtained using two laser profiles, (b) contribution of EIT resonances from different parts of the laser beam cross-section to the whole beam EIT and (c) necessity of using a realistic laser beam profile in calculations for proper modelling of experimental results.

The present study is concerned with the radial intensity distribution effects of the laser beam on Zeeman EIT line-shapes in ^{87}Rb contained in a vacuum cell. The study was performed using the Hanle technique. EIT resonances are due to Zeeman coherences developed in the $F_g = 2$ hyperfine level of ^{87}Rb by using resonant laser light that couples the $F_g = 2$ level to the excited hyperfine level $F_e = 1$. We have investigated the dependence of the EIT line-widths and amplitudes on the laser beam profile for a wide range of laser intensities, 0.1–4 mW cm^{-2}. Experimental results are compared with the results of the theoretical model that calculates the density matrix elements by taking into account all of the Rb atomic levels (with Zeeman sublevels) that are resonantly coupled by the laser light.

2. Experiment

The Zeeman EIT experiment employs a single laser whose radiation frequency and polarization are stable and well controlled. Essential for Zeeman EIT measurements is the elimination of laboratory stray magnetic fields, and creation of a variable, homogeneous magnetic field over the entire volume of the Rb cell, directed along the axis of the cell. For the present studies, a careful control of the laser diameter and radial distribution of laser radiation is also necessary. A schematic of the experiment is given in figure 1. We used the extended cavity diode laser whose frequency is stabilized to the $F_g = 2 \rightarrow F_e = 1$ transition of the D_1 line in

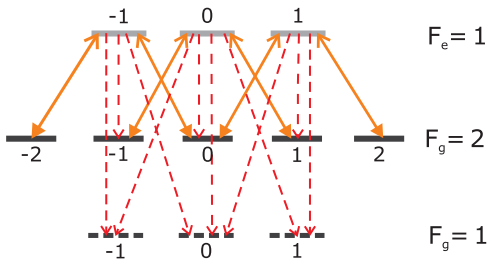

Figure 2. Zeeman sublevels scheme in ^{87}Rb at the D_1 line. The solid lines denote coupling with σ^+ and σ^- components of the linearly polarized laser light. Dashed lines represent spontaneous emission.

^{87}Rb, where F_g and F_e represent the angular momenta of the ground- and excited-state hyperfine levels, respectively. The stabilization scheme is based on the Doppler-free dichroic atomic vapour laser locktechnique [30, 31]. The laser beam is linearly polarized.

The laser beam with Gaussian radial intensity dependence, and 3 mm diameter (measured at $1/e^2$ of the peak intensity), is obtained by the single-mode optical fibre, beam collimator and beam expander. For the Π distribution of the laser beam intensity along its radius, the laser beam behind the fibre is first expanded to about 20 mm, and then the circular diaphragm of 3 mm in diameter is placed over the central part of the laser beam. We used thin foil with a 3 mm hole to obtain the Π profile of laser radiation over the entire length of the Rb cell. The laser beam profile, measured with the commercial beam profilometer, which we consider as the Π radial profile, is given in figures 1(b) and (c), at different distances from the aperture (3 and 30 cm, respectively). In the experiment, this aperture is at the entrance cell window. Laser beam intensity is controlled by the variable neutral density filter. The vacuum Rb vapour cell is 5 cm long and 25 mm in diameter, and is held at room temperature.

The solenoid surrounding the Rb cell produces the magnetic field for the Hanle experiment in the range of $\pm 100\ \mu$T. In order to minimize the stray magnetic fields in the interaction volume, the solenoid and cell are placed inside the triple layered μ-metal. Intensity of the transmitted laser light, as a function of the magnetic field, is detected by the large area photo diode and recorded by the storage oscilloscope. With the small aperture (0.5 mm in diameter) placed in front of the photo diode (with 10 mm in diameter), which we can move along the laser diameter, we were able to obtain EIT resonances only from a small cylindrical segment of the well collimated laser beam.

3. Theoretical model

Zeeman EIT resonances were calculated for the D_1 line transition between hyperfine levels of ^{87}Rb coupled by a linearly polarized laser. The energy level diagram given in figure 2 shows hyperfine levels either coupled to the laser light or populated due to spontaneous emission. The quantization axis is chosen to be parallel to the external magnetic field. The complete magnetic sublevels structure of the transition $F_g = 2 \rightarrow F_e = 1$ is considered in the calculations. The theoretical model is based on time-dependent optical Bloch equations for the density matrix of a moving atom assuming purely radiative relaxation. Equations for density matrix elements related to the ground level $F_g = 1$ are excluded since that level is not coupled by the laser. For additional details about the resulting equations please refer to [18, 26]. It is assumed that after colliding with cell walls, atoms reset into an internal state with equally populated ground magnetic sublevels. Between collisions with cell walls, rubidium atoms interact only with the axially oriented homogeneous magnetic field and spatially dependent laser electric field. Collisions among Rb atoms are negligible due to very low Rb vapour pressure at room temperature, so that an atom moves through the laser beam with constant velocity $\boldsymbol{v} = \boldsymbol{v}_\parallel + \boldsymbol{v}_\perp$, where $\boldsymbol{v}_\parallel$ and $\boldsymbol{v}_\perp$ are longitudinal and transverse velocity components, respectively, with regard to the laser propagation direction. The former affects the longitudinal direction of the atomic trajectory and Doppler shift of the laser frequency seen by a moving atom, while the latter determines the transverse direction of the trajectory and the interaction time. The dependence of the laser intensity on the radial distance r for a Gaussian and Π-shaped profile were modelled using the following equations

$$\begin{aligned} I_{\mathrm{Gauss}}(r) &= 2\bar{I}\exp\left(-2\,r^2/r_0^2\right), \\ I_{\Pi}(r) &= \bar{I}a(1+\mathrm{erf}(p(r_0-r)))^2 \end{aligned} \tag{1}$$

where r_0 is the beam radius, $\bar{I}$ is the beam intensity (total laser power divided by $r_0^2\pi$), a is the normalization constant and p is a positive parameter affecting the steepness of the profile near $r = r_0$. In our calculations we neglect longitudinal changes of the beam profile compared to transverse ones so that only the transverse direction of the trajectory matters. From the reference frame of the moving atom, the electric field varies and the rate of variation depends only on $\boldsymbol{v}_\perp$. Assume that the transverse projection of the atomic trajectory is given by $\boldsymbol{r}_\perp(t) = \boldsymbol{r}_{0\perp} + \boldsymbol{v}_\perp t$, where $\boldsymbol{r}_{0\perp}$ is the perpendicular component of the atom position vector at $t = 0$. The temporal variation of the laser intensity seen by the atom is given by

$$I(t) \equiv I(\boldsymbol{r}_\perp(t)) = I(\boldsymbol{r}_{0\perp} + \boldsymbol{v}_\perp t), \tag{2}$$

representing the spatial laser intensity variation along the trajectory of the atom in the laboratory frame. Additionally, due to the cylindrical symmetry of the beam profile, spatial dependence becomes purely radial dependence.

The observed resonances in EIT experiments are a probabilistic average of the contributions of many individual, mutually non-interacting atoms. Rb atoms traverse the laser beam at different trajectories with different velocities. Maxwell–Boltzmann velocity distribution, diversity of atomic trajectories, the custom cylindrical symmetric radial profile of the laser electric field, effects of the laser propagation along the cell and induced atomic polarization of the Rb vapour are treated similarly as in [18, 26]. The cell temperature was set to room temperature as in the experiment.

4. Results and discussion

In this section we compare EIT resonances obtained with two laser beam profiles in vacuum Rb gas cells. Previous comparisons between the EIT resonances obtained with

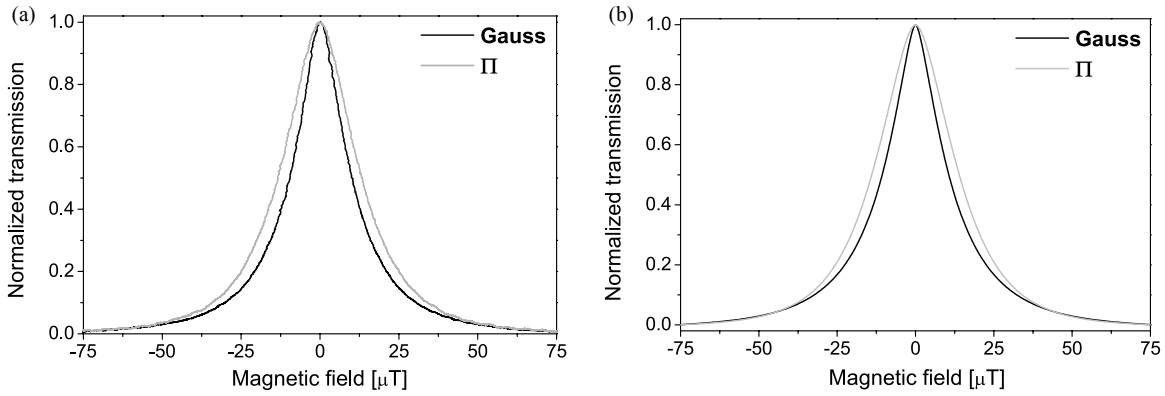

Figure 3. (a) Experimental and (b) theoretical Zeeman EIT resonances obtained by Gaussian and Π laser beam profiles. Laser intensity is 4 mW cm^{-2} and the laser beam diameter is 3 mm for both profiles.

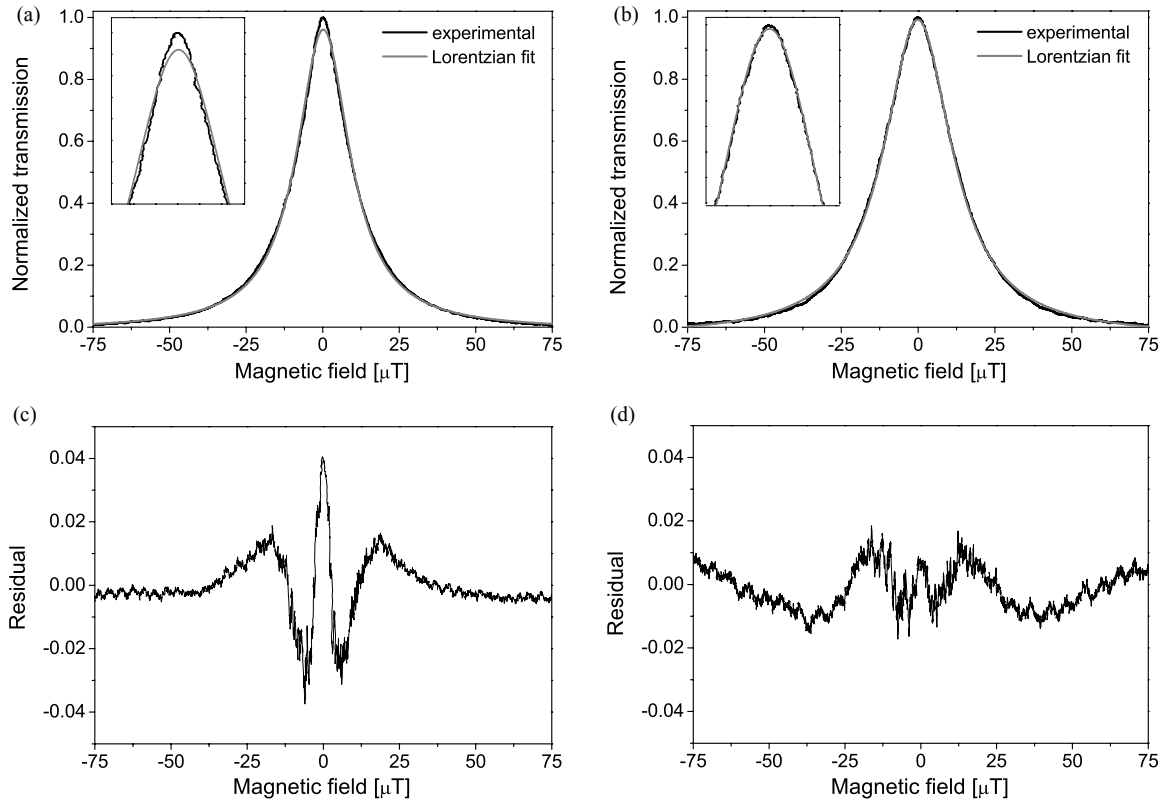

Figure 4. Experimental Zeeman EIT resonances and their Lorentzian fits for the (a) Gaussian and (b) Π laser beam profile. The resonances are obtained under the same conditions like in figure 3(a). Insets show the resonances in the vicinity of their peaks. Residuals, obtained as the difference between the raw data and the corresponding fit, for Gaussian and Π profiles are given in (c) and (d), respectively.

Gaussian and Π laser beam profiles were performed for alkali atoms in buffer gas cells [23–25]. It was calculated, assuming motionless atoms, that EIT line-shapes obtained with a Π laser beam profile are pure Lorentzian. It was also found that the resonances line-shapes are narrower for the Gaussian than for the Π laser beam profile [25]. On the other hand, analysis of the effects of the laser beam shape on EIT in vacuum Rb cells was treated only theoretically [26].

Our EIT resonances were obtained by measuring and calculating the laser transmission as a function of the scanning longitudinal magnetic field, for the Gaussian and the Π laser radial profiles, and for the laser intensity range 0.1–4 mW cm^{-2}. The laser is locked to the $F_g = 2 \rightarrow F_e = 1$ transition of the ^{87}Rb D_1 line. Figure 3 shows measured and calculated resonances for two laser profiles at the laser intensity of 4 mW cm^{-2}. The EIT line-widths and amplitudes, shown and discussed below, were extracted from resonances like these in figure 3, normalized at their maximum values. As seen in figure 3, EIT resonance obtained with the Gaussian laser beam is narrower than the one obtained with the Π laser beam.

If the relaxation of atomic coherences is determined by the radiative decay or by atomic collisions, the line-shapes of the magneto-optical resonances are Lorentzian [16, 23–25, 32]. Experimental resonances and their Lorentzian fits, for the two laser beam profiles, are given in figures 4(a) and (b). It is apparent from these figures, and from residuals between the data and the fits, given in figures 4(c) and (d), that the

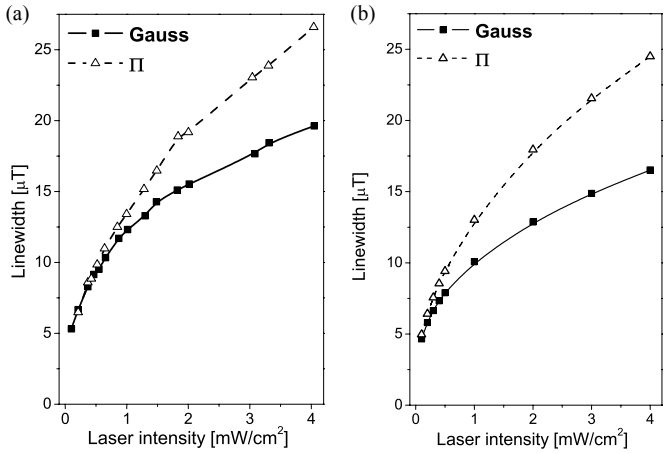

Figure 5. Intensity dependence of (a) experimental and (b) theoretical line-widths of Zeeman EIT resonances for Gaussian and Π laser beam profiles. The beam diameter is 3 mm in both cases. The curves are to guide the eye.

Lorentzian function can better fit the resonance with the Π laser beam profile than with the Gaussian profile. This is particularly the case in the vicinity of a resonance peak, as shown in the insets of figures 4(a) and (b). Corresponding R-square factors, representing the fit goodness, are $R_{\text{Gauss}} = 0.998\ 71$ and $R_{\Pi} = 0.999\ 341$. These differences between the two profiles remain for all laser intensities.

Figure 4 shows that in an effusive regime of the vacuum cell, the Gaussian laser beam profile gives the EIT line-shape that is narrower in the vicinity of the resonance peak than pure Lorentzian. This is in accordance with the previous results [16] and could be attributed to the time of flight and Ramsey-like narrowing during the free atomic passage through the Gaussian laser beam [17]. In buffer gas cells and diffusive regimes, non-Lorentzian shape (similar to figure 4(a)) is also observed due to the Ramsey effect. However, in buffer gas cells, the Ramsey type narrowing occurs because coherently prepared atoms, after leaving the laser beam and spending time outside of the beam, come back into the laser beam [28]. Line-shapes of the EIT resonances obtained with the Π laser beam profile are Lorentzian. In the case of the Π laser beam profile, laser intensity is constant during the atomic passage through the beam and there is no Ramsey-like narrowing like in the case of the Gaussian beam [17]. In figure 5 we present variations of EIT line-widths with the laser intensity for the two laser beam profiles. As the laser intensity increases the difference between the corresponding EIT line-widths also increases. Theoretical results show very good agreement with the experiment, both qualitatively and quantitatively. For the entire range of laser intensities EIT line-width increases nonlinearly with intensity, but the slope decreases at higher laser powers. This increase in line-width is due to power broadening. For the range of laser intensities as in this work, analytical results, based on the three-level atomic system, predicted square root dependence on laser intensity [21]. What we have observed in the vacuum gas cell is different from line-width dependence on laser intensity in buffer gas cells where the linear dependence of line-width on the laser intensity is reported [25, 33–35].

Without entering into details of the atom–laser interaction for particular laser beam profile, one can give a qualitative argument as to why a Π-shaped laser beam yields broader resonances than the Gaussian laser beam. In vacuum cells Rb atoms traverse a laser beam without collisions and along straight lines. During the transit through the laser beam, the atomic state is influenced by both the laser electric field and the external magnetic field. The laser electric field prepares the atoms into a dark state determined by the laser polarization. In such a state, absorption probability of the laser light is minimal—a manifestation of EIT. The external magnetic field introduces oscillations of the atomic Zeeman ground-state coherences at the corresponding Larmor frequencies, and also degrades the dark state. At low laser intensities, the influence of the magnetic field is more significant, and the dark atomic state degrades more easily. The omnichanging electric field of the Gaussian laser beam decreases the robustness of the dark state with respect to the external magnetic field. If the dark state is more robust, the transmission decreases more slowly with the magnetic field. Therefore, greater robustness of the EIT with respect to the external magnetic field requires a larger magnetic field to halve the peak transmission and hence yields larger EIT line-widths for the Π-shaped beam than for the Gaussian beam.

Differences in robustness of dark atomic states for the two beam profiles are illustrated in figure 6. We present

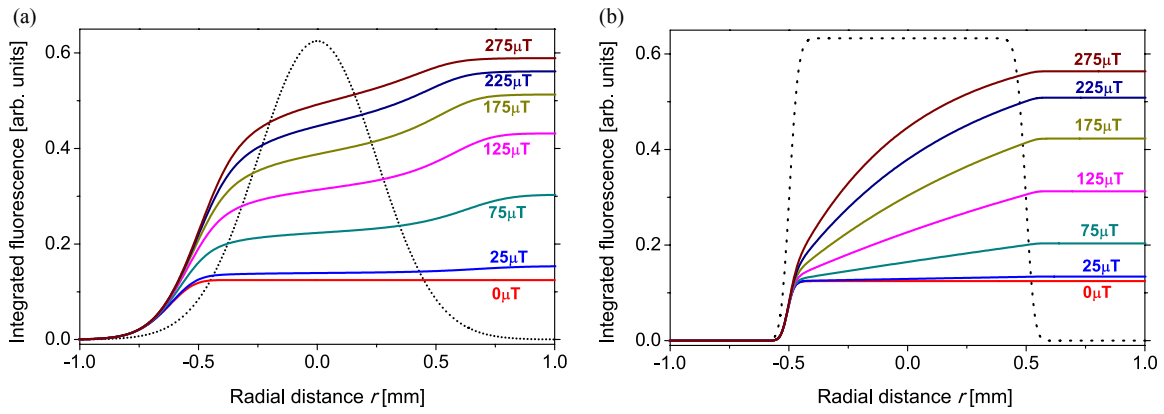

Figure 6. Integrated fluorescence along the atomic trajectory during the atomic passage through (a) Gaussian and (b) Π laser beam at different magnetic fields (given by numbers below each curve). Laser intensity is 4 mW cm^{-2} and radial atomic velocity 180 m s^{-1}.

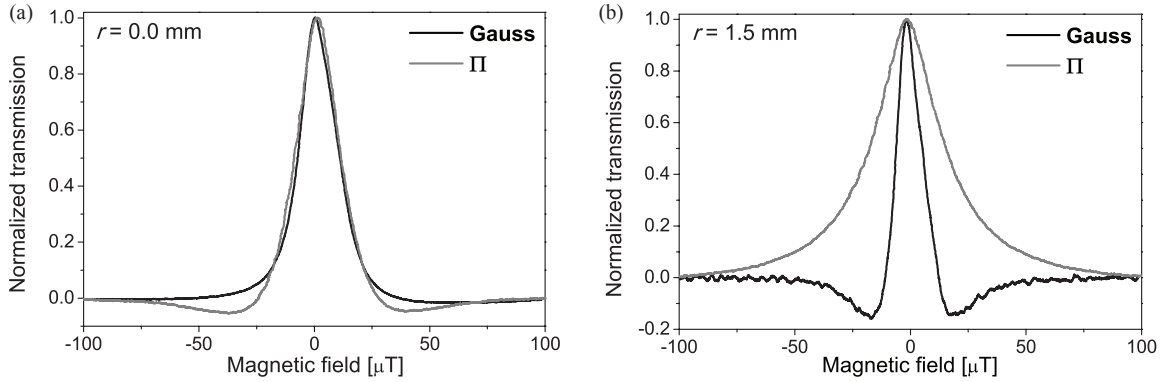

Figure 7. Experimental EIT obtained from only a small circular portion (0.5 mm in diameter) of the laser beam transmitted through the Rb cell when this portion is (a) on the beam axis (r = 0.0 mm) and (b) near the beam edge (r = 1.5 mm).

fluorescence calculated from the total population of excited Zeeman sublevels of the $F_e = 1$ hyperfine level, integrated along the atomic trajectory that passes through the beam centre, for several values of the external magnetic field. We assume that atom enters the laser beam from the left side with a radial atomic velocity of 180 m s^{-1}, which is the most probable in room temperature Rb vapour. From the curves corresponding to the same magnetic fields, it is apparent that the integrated atomic fluorescence, at the exit of an atom from the laser beam, has increased more for the Gaussian profile than for the Π profile.

In figure 7 we show the EIT obtained by detecting only a portion of the laser beam, defined by (movable) aperture placed in front of the large area photo diode (see section 2 for details). This aperture is centred on the beam axis ($r = 0.0$ mm) for the resonances in figure 7(a), and is near the beam edge ($r = 1.5$ mm) for data in figure 7(b). The EIT resonances obtained near the centre of the laser beam are very similar for two laser beam profiles. A large difference exists between EIT measured with the aperture near the beam edges of these two beam profiles. The Gaussian laser beam produces much narrower Zeeman EIT resonances near its edge than the Π-shaped beam.

Further understanding of what causes different EIT line-widths with two laser beam profiles can be obtained from measurements and calculations of EIT amplitudes at various distances from the beam axis, presented in figures 8(a)–(d). Results are given for two laser beam profiles and for two laser intensities. Amplitudes of EIT resonances are increasing with the distance from the beam axis for both beam profiles, which is more pronounced at higher laser intensities. Amplitudes are the highest in the beam segments that have a high geometrical contribution to the total laser beam cross-section. As seen in figure 7, these are also the segments where the resonances for the Gaussian beam are much narrower than for the Π beam profile. Thus, the results of figures 7 and 8 show that the outer parts of the laser beam cross-section are primarily responsible for the observed differences between EIT line-widths obtained with the two laser beam profiles. Physical mechanisms leading to such differences are explained in detail in [17, 18].

Next, we show the behaviour of the EIT amplitudes obtained with the entire Gaussian and Π laser beams. In

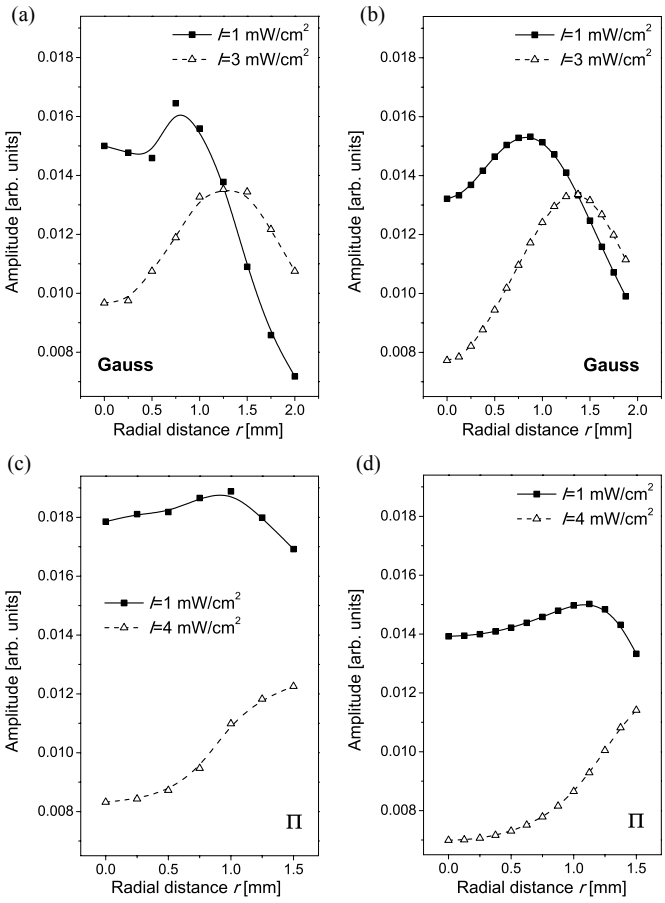

Figure 8. Experimental (a) and (c), and theoretical (b) and (d) amplitudes of the Zeeman EIT resonances obtained at different positions of small aperture along the laser beam radius for the two laser beam profiles.

figure 9 we present measured and calculated EIT amplitudes as a function of the laser intensity. As seen in figure 9, there are no essential differences between EIT amplitudes obtained with the two laser beams. At lower intensities EIT amplitudes show a steep, nearly linear increase with intensity, like in buffer gas cells [36]. The decrease in EIT amplitudes above ∼1 mW cm^{-2} is caused by the increase of the population loss due to optical pumping to the $F_g = 1$ hyperfine level of the Rb ground state, which is not coupled by the laser. Indeed, when the re-pumper

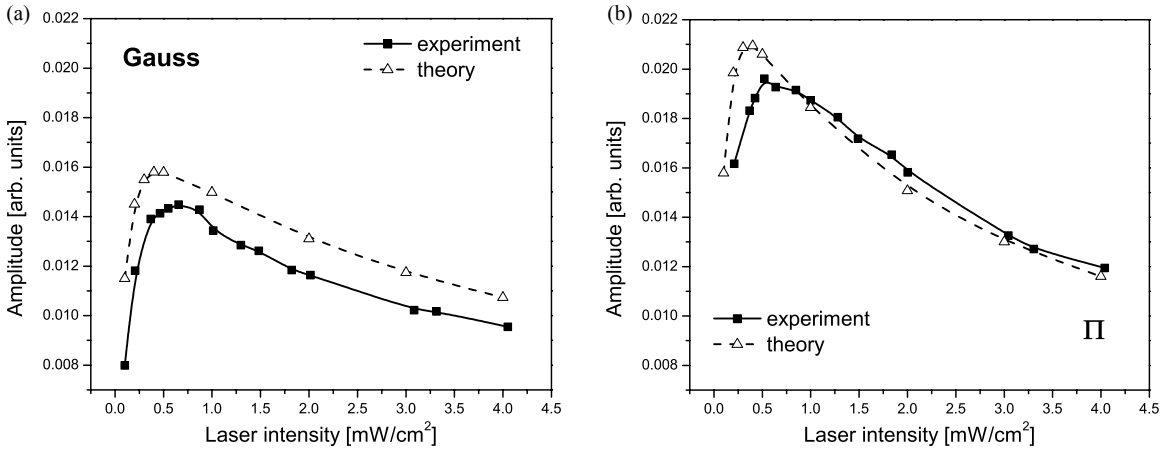

Figure 9. Experimental (solid lines) and theoretical (dashed lines) intensity dependence of Zeeman EIT amplitudes for Gaussian (a) and Π laser beam profile (b). The curves are to guide the eye.

is used to bring the population back to $F_g = 2$ as in [37], the contrast of the amplitudes increases considerably. Figures 9(a) and (b) also show good agreement between experiment and theory.

5. Conclusion

We have demonstrated substantial differences between Zeeman EIT line-shapes and line-widths obtained using two laser radial intensity profiles: Gaussian profile—frequently used in experiments, and Π-shaped laser radial distribution—common in theoretical calculations. Our work is concerned with the effects of these two laser radial profiles on EIT, generated in the Hanle configuration by laser coupling $F_g = 2 \rightarrow F_e = 1$ hyperfine levels in ^{87}Rb atoms in vacuum gas cells. We have shown theoretically and confirmed experimentally the different line-shapes of EIT resonances: those obtained with Π laser beam are very well approximated with Lorentzian, while the Gaussian laser beam profile gives non-Lorentzian Zeeman EIT resonances. EIT resonances are wider for the Π laser beam than for the Gaussian laser beam profile and this difference becomes larger as the laser intensity increases. The study is performed for laser intensities up to 4 mW cm^{-2}. We have shown that major differences in line-widths between two laser profiles are in the regions near the rim of the laser beams. The differences in line-shapes are attributed to different physical processes that Rb atoms undergo during the interaction with the two laser beam profiles. In the wings of the Gaussian laser beam, a Ramsey-like effect can reshape EIT resonances with respect to those near the laser beam centre, as shown in [16, 17]. For the Π profile, optical pumping to the uncoupled ground level dominantly influences the line-shape [18]. The theory demonstrates that the atomic dark state is more sensitive to magnetic field when the atoms are traversing the Gaussian laser beam than when passing through a constant intensity field of the Π laser beam. Larger sensitivity of the atomic dark state to magnetic field variation implies narrower Zeeman EIT line-shapes. The increase of EIT line-widths with the laser intensity is square-root-like for both profiles. Amplitudes of the EIT increase linearly for a laser intensity up to 0.8 mW cm^{-2} for both profiles and decrease at higher intensities due to pumping to the $F_g = 1$ hyperfine level of ^{87}Rb. Observed dependence of line-widths and amplitudes of the EIT with the laser intensity in vacuum gas cells is different from previous results in buffer gas cells.

Acknowledgments

This work was supported by the Ministry of Education and Science of the Republic of Serbia under grant nos 45016 and 171038, and by the Scopes JRP IZ73Z0_127942.

References

[1] Alzetta G, Gozzini A, Moi L and Orriolis G 1976 *Nuovo Cimento* B **36** 5–20
[2] Arimondo E 1996 *Prog. Opt.* **35** 257–354
[3] Fleischhauer M, Imamoğlu A and Marangos J P 2005 *Rev. Mod. Phys.* **77** 633–73
[4] Phillips D F, Fleischhauer A, Mair A, Walsworth R L and Lukin M D 2001 *Phys. Rev. Lett.* **86** 783–6
[5] Scully M O, Zhu S Y and Gavrielides A 1989 *Phys. Rev. Lett.* **62** 2813–6
[6] Harris S E, Field J E and Imamoğlu A 1990 *Phys. Rev. Lett.* **64** 1107–10
[7] Schmidt H and Imamoğlu A 1996 *Opt. Lett.* **21** 1936–8
[8] Knappe S, Shah V, Schwindt P D, Holberg L, Kitching J, Liew L A and Moreland J 2004 *Appl. Phys. Lett.* **85** 1460–2
[9] Affolderbach C, Andreeva C, Cartaleva S, Karaulanov T, Mileti G and Slavov D 2005 *Appl. Phys.* B **80** 841–8
[10] Fleischhauer M, Matsko A B and Scully M O 2000 *Phys. Rev.* A **62** 013808
[11] Belfi J, Bevilacqua G, Biancalana V, Cartaleva S, Dancheva Y and Moi L 2007 *J. Opt. Soc. Am.* B **24** 2357–62
[12] Dupont-Roc J, Haroche S and Cohen-Tannoudji C 1969 *Phys. Lett.* **28** 638–9
[13] Haroche S and Cohen-Tannoudji C 1970 *Phys. Rev. Lett.* **24** 974–8
[14] Weis A, Wurster J and Kanorsky S I 1993 *J. Opt. Soc. Am.* B **10** 716–24
[15] Kanorsky S I, Weis A, Wurster J and Hänsch T W 1993 *Phys. Rev.* A **47** 1220–6
[16] Pfleghaar E, Wurster J, Kanorsky S I and Weis A 1993 *Opt. Commun.* **99** 303–8

[17] Krmpot A J, Ćuk S M, Nikolić S N, Radonjić M, Slavov D G and Jelenković B M 2009 *Opt. Express* **17** 22491–8
[18] Krmpot A J, Radonjić M, Ćuk S M, Nikolić S N, Grujić Z D and Jelenković B M 2011 *Phys. Rev.* A **84** 043844
[19] Korsunsky E A, Maichen W and Windholz L 1997 *Phys. Rev.* A **56** 3908
[20] Li L, Peng X, Liu C, Guo H and Chen X 2004 *J. Phys. B: At. Mol. Opt. Phys.* **37** 1873–8
[21] Javan A, Kocharovskaya O, Lee H and Scully M O 2002 *Phys. Rev.* A **66** 013805
[22] Ye C Y and Zibrov A S 2002 *Phys. Rev.* A **65** 023806
[23] Levi F, Godone A, Vanier J, Micalizio S and Modugno G 2000 *Eur. Phys. J.* D **12** 53–9
[24] Gilles H, Cheron B, Emile O, Bretenaker F and Le Floch A 2001 *Phys. Rev. Lett.* **86** 1175–8
[25] Taïchenachev A V, Tumaikin A M, Yudin V I, Stahler M, Wynands R, Kitching J and Hollberg L 2004 *Phys. Rev.* A **69** 024501
[26] Radonjić M, Arsenović D, Grujić Z and Jelenković B M 2009 *Phys. Rev.* A **79** 023805
[27] Anupriya J, Ram N and Pattabiraman M 2010 *Phys. Rev.* A **81** 043804
[28] Xiao Y, Novikova I, Phillips D F and Walsworth R L 2008 *Opt. Express* **16** 14128–41
[29] Xiao Y, Novikova I, Phillips D F and Walsworth R L 2006 *Phys. Rev. Lett.* **96** 043601
[30] Petelski T, Fattori M, Lamporesi G, Stuhler J and Tino G M 2003 *Eur. Phys. J.* D **22** 279–83
[31] Wasik G, Gawlik W, Zachorowski J and Zawadzki W 2002 *Appl. Phys.* B **75** 613–9
[32] Castagna N and Weis A 2011 *Phys. Rev.* A **84** 053421
[33] Erhard M and Helm H 2001 *Phys. Rev.* A **63** 043813
[34] Sautenkov V A, Kash M M, Velichansky V L and Welch G R 1999 *Laser Phys.* **9** 889–93 www.maik.ru/full/lasphys/99/4/lasphys4_99p889full.pdf
[35] Figueroa E, Vewinger F, Appel J and Lvovsky A I 2006 *Opt. Lett.* **31** 2625–7
[36] Knappe S, Wynands R, Kitching J, Robinson H G and Hollberg L 2001 *J. Opt. Soc. Am.* B **18** 1545–53
[37] Kazakov G, Mosets I, Rozhdestvensky Yu, Mileti G, Delporte J and Matisov B 2005 *Eur. Phys. J.* D **35** 445–8